# CENTER FOR INFRASTRUCTURE ENGINEERING STUDIES

**Experimental Evaluation of FRP Strengthening of Real Size Reinforced Concrete Columns**

By

**Silvia Rocca**
**Nestore Galati**
**Antonio Nanni**

UTC
R142

**Technical Report Documentation Page**

| 1. Report No.<br><br>UTC R142 | 2. Government Accession No. | 3. Recipient's Catalog No. |
|---|---|---|
| 4. Title and Subtitle<br><br>Experimental Evaluation of FRP Strengthening of Real Size Reinforced Concrete Columns | | 5. Report Date<br><br>December 2005 |
| | | 6. Performing Organization Code |
| 7. Author/s<br><br>Silvia Rocca, Nestore Galati, and Antonio Nanni | | 8. Performing Organization Report No.<br><br>00001528 |
| 9. Performing Organization Name and Address<br><br>Center for Infrastructure Engineering Studies/UTC program<br>University of Missouri - Rolla<br>223 Engineering Research Lab<br>Rolla, MO 65409 | | 10. Work Unit No. (TRAIS) |
| | | 11. Contract or Grant No.<br><br>DTRS98-G-0021 |
| 12. Sponsoring Organization Name and Address<br><br>U.S. Department of Transportation<br>Research and Special Programs Administration<br>400 7<sup>th</sup> Street, SW<br>Washington, DC 20590-0001 | | 13. Type of Report and Period Covered<br><br>Final |
| | | 14. Sponsoring Agency Code |
| 15. Supplementary Notes | | |

16. Abstract

In order to analyze the behavior of axially loaded large-size reinforced concrete columns confined by means of Carbon Fiber Reinforced Polymers (CFRP) wrapping, a test matrix was designed to investigate the effect of different variables, such as the geometry of the specimen, the area aspect ratio, the side aspect ratio, and a height-to-width aspect ratio. A total of 22 specimens were divided into six series of three specimens each and two series of two specimens. The largest column tested had a cross-sectional area of 9 ft2 (0.8 m2) and the smallest one and area of 1 ft2 (0.1 m2). Experimental results showed that the size effect is not significant. In addition, between circular and prismatic specimens, the confinement effect of the FRP is less effective for the latter. The strengthening performance of these experiments was also compared with design predictions provided by the current international design guidelines. It is apparent that these predictions differ from one another, in particular for the case of prismatic cross-sections. Additionally, in contrast with the experimental results, for the case of circular cross-sections, most of the guidelines showed to be conservative, on the contrary when referring to the cases of prismatic cross-sections. Therefore a revision of the guidelines is warranted.

| 17. Key Words<br><br>Confinement of Circular and Prismatic Columns, FRP Strengthening, Confining Pressure, Size Effects, Axial Compression | | 18. Distribution Statement<br><br>No restrictions. This document is available to the public through the National Technical Information Service, Springfield, Virginia 22161. | | |
|---|---|---|---|---|
| 19. Security Classification (of this report)<br><br>unclassified | | 20. Security Classification (of this page)<br><br>unclassified | 21. No. Of Pages | 22. Price |

Form DOT F 1700.7 (8-72)

# Acknowledgements

**TABLE OF CONTENTS**

# LIST OF FIGURES

# LIST OF TABLES

## LIST OF NOTATIONS

$A_e$      Effectively confined area (TR 55 guideline)

$A_g$      Total cross-sectional area (TR 55 guideline)

$A_{ol}$      Area of overlap of the parabolas in a prismatic cross-section (TR 55 guideline)

$b$      Short side dimension of prismatic cross-section

$b_f$      Width of FRP strip in partial wrapping

$D$      Diameter of circular cross-section

        Diameter of circular cross-section or least lateral dimension of the prismatic cross-section (CSA-2002 guideline)

$E_0$      Secant modulus of concrete (TR 55 guideline)

$E_2$      Slope of linear portion of confined stress-strain curve (TR 55 guideline)

$E_c$      Initial modulus of elasticity of concrete

$E_f$      Tensile modulus of Elasticity of FRP

$E_{fd}$      Design modulus of elasticity of FRP (TR 55 guideline)

$E_j$      Modulus of elasticity of the FRP jacket (fib guideline)

$E_s$      Tensile modulus of Elasticity of steel reinforcement

$f'_c$      Characteristic concrete compressive strength determined from standard cylinder

$f'_{co}$      Maximum or peak axial compressive stress of unconfined concrete

$f_{co}$      Unconfined concrete compressive strength (TR 55 guideline)

$f'_{cc}$      Maximum or peak axial compressive stress of confined concrete

$f_{cc}$      Confined concrete axial compressive stress (TR 55 and fib guidelines)

$f_{ccd}$      Design or ultimate confined concrete compressive strength (TR 55 guideline)

$f_{cu}$      Characteristic compressive cube concrete strength (TR 55 guideline)

$f_{fe}$      Effective stress in the FRP (ACI 440.2R-02 guideline)

$f_{Fj}$      Stress in the FRP (CSA-2002 guideline)

$f_{Fu}$      Ultimate tensile strength of FRP (CSA-2002 guideline)

$f_{fu}$      Ultimate tensile strength of

$f_l$      Confining pressure due to FRP jacket

$f_r$      Confining pressure due to FRP jacket (TR 55 guideline)

$f_y$      Yield strength of longitudinal steel reinforcement

$f_{yv}$      Yield strength of transverse steel reinforcement

$g_s$      Shape factor for prismatic cross-sections (TR 55 guideline)

$H$      Height of column

$h$      Long side dimensions of prismatic cross-section

$K_{conf}$      Stiffness of the FRP confinement (fib guideline)

$k$      Parameter of CSA-2002 guideline

$k_c$      Confinement parameter (CSA-2002 guideline)

$k_e$      Confinement effectiveness coefficient (fib guideline)

$l_{ol}$      Length of overlapping region (TR 55 guideline)

$n$      Number of FRP plies composing the jacket

$P$      Axial compressive load applied to specimen

$P_{cc}$      Maximum applied axial load

$R_c$      Corner radius (TR 55 guideline)

| | |
|---|---|
| r | Corner radius (ACI 440.2R-02 guideline) |
| $r_c$ | Corner radius (fib guideline) |
| s' | Clear spacing between FRP wraps (fib guideline) |
| s | Pitch in partial wrapping |
| $t_f$ | FRP nominal ply thickness |
| | Thickness of the FRP laminate or jacket (TR 55 guideline) |
| $t_j$ | Total thickness of the FRP jacket based on the nominal fiber thickness or effective area (CSA and fib guidelines) |
| w | width of CFRP tensile coupon |
| | |
| $\beta$ | Parameter of fib guideline |
| $\varepsilon'_{cc}$ | Axial strain corresponding to $f'_{cc}$ (ACI 440.2R-02 guideline) |
| $\varepsilon'_{co}$ | Axial strain corresponding to $f'_{co}$ (ACI 440.2R-02 guideline) |
| $\varepsilon_{fe}$ | FRP effective strain (strain level reached at failure), (ACI 440.2R-02 guideline) |
| $\varepsilon_{fd}$ | Design ultimate strain of FRP (TR 55 guideline) |
| $\varepsilon_{cc}$ | Confined concrete axial strain (TR 55 and fib guidelines) |
| $\varepsilon_{ccu}$ | Confined concrete ultimate axial strain (TR 55 guideline) |
| $\varepsilon_{co}$ | Axial strain in unconfined concrete at peak stress $f_{co}$ (TR 55 and fib guidelines) |
| $\varepsilon_{cu}$ | Ultimate axial strain |
| $\varepsilon_{fu}$ | Ultimate tensile strain of the FRP |
| $\varepsilon_{ju}$ | FRP jacket effective ultimate hoop or circumferential strain (fib guideline) |
| $\varepsilon_t$ | Position of transition region between parabola and straight line (TR 55 guideline) |
| $\varepsilon_{tc}$ | Transverse strain at $f'_{cc}$ |
| $\varepsilon_{ju}$ | Ultimate transverse strain |
| $\phi$ | Strength reduction factor (ACI 440.2R-02 guideline) |
| $\phi_c$ | Resistant factor for concrete (CSA-2002 guideline) |
| $\phi_f$ | Resistant factor for FRP (CSA-2002 guideline) |
| $\phi_s$ | Resistant factor for reinforcing steel (CSA-2002 guideline) |
| $\gamma_{mc}$ | Material safety factor for concrete (TR 55-2005 and fib-2001 guidelines) |
| $\gamma_{ms}$ | Material safety factor for steel (TR 55-2005 and fib-2001 guidelines) |
| $\kappa_a$ | Efficiency factor based on geometry of the cross-section (ACI 440.2R-02 guideline) |
| $\rho_c$ | Specific weight of concrete |
| $\rho_f$ | Ratio of FRP reinforcement |
| $\rho_g$ | Ratio of longitudinal steel reinforcement (ACI 440.2R-02 guideline) |
| $\rho_j$ | FRP volumetric ratio in a circular column (fib guideline) |
| $\rho_l$ | Ratio of longitudinal steel reinforcement |
| $\rho_{sc}$ | Ratio of longitudinal steel reinforcement (TR 55 guideline) |
| $\rho_{sg}$ | Ratio of longitudinal steel reinforcement (fib guideline) |
| $\rho_v$ | Ratio of transverse steel reinforcement |
| $\sigma_l$ | Lateral confining pressure (fib guideline) |

# 1.  INTRODUCTION

Reinforced concrete (RC) columns as vertical structural members that transmit axial compressive loads with or without moments are of critical importance for the performance and the safety of structures.  Nowadays, it is commonly seen the need of strengthening and/or rehabilitating these members due to different reasons, such as: higher loads as a result of the change in the use, more strength code requirements, effects of corrosion of steel reinforcement, need for increased ductility.

Confinement of concrete is an efficient technique used in order to increase the load carrying capacity and/or ductility of a member primarily under compressive loads.  It is precisely the lateral pressure that induces in the concrete a triaxial stress state and consequently an increment of compressive strength and capacity of deformation (Matthys et al. 2005).

Until the beginning of the 1990s, the strengthening of RC columns was conducted by installing a grout injected steel jacket or constructing an additional steel cage (Teng et al. 2002), being the former one the most effective.  But these techniques were limited for both the high labor costs and corrosion.  It is at this stage that the attention was focused in a new emerging strengthening potential technology: the use of fiber reinforced polymers (FRP).  The confinement of a concrete member is accomplished by placing the fibers transverse to the longitudinal axis of the member.   In this direction, the transverse or hoop fibers act similarly to the conventional reinforcing steel ties or spirals (ACI 440.2R-02).  The suitability of FRP materials for strengthening and rehabilitation relies on their intrinsic properties, such as: high strength to weight ratio, good corrosion behavior, simple installation. (De Lorenzis, 2001).   The FRP jackets provide passive confinement to the compression member, which becomes active once the concrete core starts dilating as a result of the internal cracking.

Different methods of FRP strengthening, all of them with their own advantages and disadvantages, have been developed in the last few years, and they are classified as follows: wrapping by manual lay up, filament winding, and prefabricated shell jacketing.  The first one is the most common technique and therefore it will be the focus of this study.  It was first implemented in Japan in the 1980s, and it consists in the resin impregnation of unidirectional fiber plies or woven fabrics and wrapped around the column by the wet lay up process.  The other two techniques have also been widely used (Fardis and Khalili, 1981; Nanni and Bradford, 1995; Xiao and Ma, 1997; Ohno et al., 1997), but their elaboration requires the implementation of automated processes (Teng et al. 2002).

Among the most distinct advantages of the FRP wrapping are (Saadatmanesh et al. 1994):
- Increased ductility: due to the confinement provided by the wrapping, the concrete fails at a larger strain than if it were unconfined
- Increased strength: the lateral pressure given by the wrapping increases the compressive strength of the concrete core resulting in a higher load-carrying capacity. This lateral support also provides stability against probable buckling of the longitudinal reinforcement
- Flexibility and aesthetics: since the wrapping material is very flexible and thin, it is possible to wrap section of different geometry and its use does not alter the appearance of the structures
- Ease of installation: application is easier compared to steel jacketing since its lighter and there is not the need for special equipment or grouting

The wrapping technique may present some disadvantages, such as: lower quality control, and environmental stability (long term performance of certain components of the FRP jacket might not be optimum under different effects like ultraviolet radiation, thermal cycles, and humidity). Regarding the durability of the FRP system, there is still not sufficient experimental data on long-term performance in order to accurately predict service life. Existing design guidelines do account for effects under highly aggressive environments with reduction factors on mechanical properties. Since this area of the research is on going, these factors will be updated and better defined as more data becomes available (ACI 440.2R-02).

The confinement of prismatic columns is generally acknowledged to be less efficient than the confinement of circular columns, since in the latter case, the wrapping provides circumferentially uniform confining pressure to the radial expansion of the compression member. For this reason, FRP wrapping has the fibers aligned in the hoop direction. Contribution of fibers aligned parallel to the longitudinal axis of the member is negligible (ACI 440.2R-02). In columns of prismatic cross-section, the confinement is concentrated at the corners rather than over the entire perimeter. Current research on small-scale columns has shown that the maximum attainable increase in compressive stress for FRP confined prismatic columns with reasonable levels of rounding of corners is about 50 percent, compared with up to 200 percent for circular columns (Kestner et al., 1997; Mirmiran et al., 1998; Rochette and Labossiere, 2000; Cole, 2001; Pessiki et al., 2001; Suter and Pinzelli, 2001; Campione et al., 2003; Chaallal et al., 2003; Mukherjee et al., 2004). For real-size columns, the level of capacity increase may be less than this. The efficiency is further decreased in columns of rectangular cross section with high aspect ratio. The difference in confinement performance between circular and prismatic cross-section columns, is similar to the distinction between the use of continuous spirals and ties in conventional steel reinforced concrete column design (TR 55, 2004).

Several analytical and/or numerical models of the strength enhancement of prismatic columns (Restrepo and De Vino, 1996; La Tegola and Manni, 1998; Vintzileou, 2001; Wang and Restrepo, 2001; Nasrollahzadeh and Yamakawa, 2002; Maalej et al., 2003; Lam and Teng, 2003; Wu et al., 2003; Malvar et al., 2004; Marques et al., 2004) have been proposed and compared with the limited number of experimental results available. Most models are semi-empirical in nature and have been calibrated with small-scale test specimens (in most of the cases calibrated against their own set of specimens). Usually these specimens are $6 \times 6$ in ($150 \times 150$ mm) for square columns and up to $6 \times 9$ in ($150 \times 225$ mm) for rectangular columns (side aspect ratio of 1.5). As rectangular cross-section specimens get bigger in size, the length of the unconfined regions along the sides increases creating a size effect, which is not evident in circular columns. The generally accepted theoretical approach is to develop an area of effective confinement defined by four parabolas within which the concrete is fully confined and outside of which negligible confinement occurs. The shape of the parabolas and the resulting effective confinement area is a function of the dimensions of the column and the radius of the corners (Figure 1-1) (TR 55, 2004). Available literature (Kestner et al., 1997; Tanwongsval et al., 2001; Wang and Restrepo, 2001; Tan 2002; Prota et al., 2003) describes uni-axial compressive tests on rectangular RC specimens with at least one side larger than 12 in (300 mm). Even though this is not to be considered exhaustive evidence, there is really no clear indication that FRP wrapping be ineffective.

The following items are not considered into account in the currently existing models:
- Detrimental effect of longitudinal reinforcement instability
- Transverse steel reinforcement ratio and its contribution to the confinement

- Reduced tensile characteristics of bent FRP: this is closely related to the failure strain, which based on experimental evidence, mostly occurs at strain levels lower than the ultimate strain obtained from standard tensile testing of FRP laminates. This characteristic tensile test does not represent accurately the actual state of stress to which the FRP wrapping is subjected to: tensile stress as a result of the transverse pressure provided by the dilation of the concrete core.
- Size effect: in terms of absolute dimensions of the cross-section
- Concrete dilation controlled by the pseudo-Poisson ratio as a material property of concrete itself
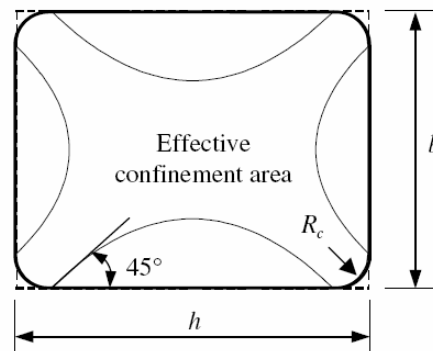


**Figure 1-1  Effectively Confined Concrete in a Rectangular Column (Teng et al., 2002)**

## 2. OBJECTIVE

The principal objective of this research project is to determine if the CFRP confinement of prismatic RC columns is attainable even for the case of large, real-size cross-sections. In order to achieve such purpose this study is divided into two main phases: experimental (I) and analytical (II). This report focuses on Phase I, which includes the design, construction and experimental evaluation of the RC column specimens, as well as comparisons with the predictions of the current available international design guidelines. Three cross-section types compose the test matrix: circular, square, and rectangular with an aspect ratio of 2. The largest cross-section tested has an area of 9 ft$^2$ (0.8 m$^2$), and the smallest one, an area of 1.1 ft$^2$ (0.1 m$^2$). Phase II of this project (to be reported separately) will concentrate on the investigation of the mechanical interaction between the FRP wrapping and the dilatation of concrete, and the development of appropriate methods for the analysis and design of FRP rectangular column strengthening.

The successful completion of this research project will allow the following:
− Validation of design algorithms proposed in international design guidelines such as ACI 440.2R (2002), CSA (2002), TR 55 (2005), and fib (2001)
− Identification of key parameters affecting the performance of RC columns of prismatic cross-section confined by FRP
− Demonstration of the efficiency of the strengthening of prismatic columns with FRP
− Development of a mechanics-based prediction algorithm for analysis and design

# 3. RESEARCH SIGNIFICANCE

The behavior of FRP confined RC columns of circular cross-section has been extensively studied and there is a limited knowledge on the performance of RC columns of prismatic cross-section, in particular of large-size. An explicit and reliable method for the analysis and design of such members is urgently needed.

This research is of practical relevance in that there are thousands of RC structures (bridges and buildings) having prismatic columns that due to increases in loads, changes in use or additions, code updates, require quickly and efficient strengthening, with minimum disruption to users. Wrapping rectangular columns with FRP has the potential to achieve increments in strength and ductility with ease of installation, provided that fundamental behavior is understood.

This research project will contribute to the understanding of the behavior of confined circular and prismatic columns leading to safe, efficient and feasible practice. Each bridge or building which is upgraded and therefore saved from needless demolition, amounts to a significant gain to society. Technology will be transferred to private sector and code writing authorities via publications, presentations, and guideline clause-amendment proposals.

Up to now, the vast majority of tests on rectangular columns has been on small samples. For the reasons stated above, the semi-empirical analysis and design methods based upon these tests may not be reliable in predicting the strength enhancement that might be achieved for larger columns found in practice. A systematic experimental investigation of the effect of column size is carried out, and in the second phase of this project an analytical model will be developed to reflect the size effect and other critical parameters. This research project is now limited to specimens pure axial load (no eccentricity), this is considered the first step to understand the confinement process. Future work should include the effect of flexure and shear in order to develop complete interaction diagrams.

## 4.  REVIEW OF EXPERIMENTS ON LARGE-SIZE RC PRISMATIC COLUMNS

Experimental studies on the enhancement of circular and/or prismatic cross-section RC columns of various scales (mainly small) by means of FRP wrapping have been conducted under two loading conditions: pure axial compressive, and combined axial compressive with bending effects (seismic performance).  Consistent with the experimental test matrix, this review is focused on large-scale RC prismatic columns subject to axial compression only.  Experiments on RC specimens of circular cross-section are also considered for comparisons on level of achieved strengthening capacity.  No studies on environmental performance of RC columns confined with FRP are considered.

Most of the currently available experimental data refers to cylinders and prisms of plain concrete confined with FRP.  Even though such experimental and analytical work is important to the understanding of fundamentals and the proof of concepts, confirming the viability of the wrapping solution, these data were not included in this study since results can not be directly extrapolated for practical design.  Studies on other confinement methods such as FRP shells and filament winding are not considered.  Only specimens where at least one of the dimensions on the cross-section is 12 in (300 mm) were included in this literature review.

Table 4-1 and Table 4-2 summarize different experiments on large-scale prismatic and circular section RC specimens, respectively.  Such data were classified in terms of the following parameters:

- Specimen geometry (lengths of short and long sides $b$ and $h$, diameter $D$, height $H$, side aspect ratio $h/b$)
- FRP layout configuration
- FRP material properties (modulus of elasticity $E_f$, ultimate tensile strain $\varepsilon_{fu}$, nominal ply thickness $t_f$, and number of plies $n$),
- Ratio of longitudinal and transverse steel reinforcement ($\rho_l$ and $\rho_v$),
- Yield strength of steel reinforcement ($f_y$ and $f_{yv}$),
- Characteristic concrete cylinder compressive strength ($f'_c$),
- Maximum axial compressive force $P$
- Increment of confined compressive strength RC column ($f'_{cc}$)with respect to the unconfined ($f'_{co}$), this ratio will be also referred as the strengthening ratio ($f'_{cc}/f'_{co}$)

The test data in Table 4-1 covers square and rectangular RC columns with aspect ratios of 1, 1.5, and 3.7 (the specimens with high aspect ratio are also known as wall-like columns), and corner radius of ¾ in (20 mm), 1.2 in (30 mm), and 1.5 in (38 mm).  It compiles a total of 63 specimens corresponding to six different experimental sets documented by: Kestner et al., 1997; Tanwongsval et al., 2001; Wang and Restrepo, 2001; Tan, 2002; Prota et al., 2003; and Carey and Harries, 2003.  Other research works were identified but not included due to "repetition" or because the specimens were not appropriate. As an example, the work by Kestner et al. was later summarized by Pessiki et al. in 2001, therefore either one of these documents can be used for reference.  The experimental work conducted by Tanwongsval et al. was later used as calibration data for an analytical model to predict the load-displacement response of wall-type RC columns strengthened with FRP by Maalej et al. in 2003.  Although Yeh and Chang (2004) tested specimens whose dimensions fell among the ones of interest of this research, results were not included in this review since specimens were plain concrete elements.  Similarly, the

experiments reported by Campione et al., 2003, were not considered because plain concrete specimens confined by FRP were used.

      Additional information regarding the specimens listed on Table 4-1 include: prior to strengthening, column TA3 was subjected to compressive force of approximately 40 percent of the unstrengthened column carrying capacity (the study included the effects of sustained loading on strengthening efficiency).  Tan (2002) investigated the effect of different fiber types, strengthening schemes and the presence of plaster (specimens TN6, 7, 8, 20, 25, 26, 27, and 29).

      Table 4-2 compiles a total of 23 specimens divided in four sets of studies.  Regarding the specimens from Demers and Neale (1994), four of the eight columns were pre-loaded up to the corresponding peak load and/or to the point where the cracks became visible, before strengthening and re-testing to failure.  The remaining four specimens in this group were undamaged when strengthened.  It should also be noted that specimens DN5 to DN8, presented different characteristics ($f'_c$, $\rho_l$ and $\rho_v$) compared to the control specimens, therefore no values are shown for them under the column corresponding to the compressive strength increment ($f'_{cc}/f'_{co}$).

      Figure 4-1 to Figure 4-5 present the trends on the increment of compressive strength of the experimental database previously introduced.  The parameters selected for the interpretation of the confinement effectiveness for the different sizes of cross-sections in the available literature are: the FRP volumetric ratio, since it encompasses the thickness of the FRP jacket and the geometry of the cross-section, and the relative stiffness of the confining FRP to the axial stiffness of the concrete: $\rho_f * E_f/E_c$, being $\rho_f$ the volumetric ratio of FRP, $E_f$ and $E_c$ the elastic modulus of FRP and concrete, respectively.

      Figure 4-1 corresponds to RC columns of circular cross-section.  In this case both the damaged and undamaged specimens from Demers and Neale (1994) were included.  Note that the latter were compared to the control specimens in spite of the observed difference in the steel reinforcement ratios, and it is of general knowledge that such parameters do affect the performance of the member.   Specimen MA3 and MA7 were not included because they were considered atypical with respect to the rest of the data.  Specimen CH3_C was not considered as well due to the fact that its FRP jacket was unbonded.  In this figure, since all the specimens presented the same trend for the increment of strength, it can be observed that for circular columns there is no significant size effect.

      Figure 4-2 to Figure 4-5 refer to prismatic columns, and they are divided based on the side aspect ratio (1, 1.5, and 3.7).  Figure 4-2 presents the case of square RC columns.  Figure 4-3, Figure 4-4, and Figure 4-5 present the increment of confinement strength in RC columns of rectangular cross-section of ratios of 1.5 for the first one, and 3.7 for the last two figures.  Note that the data presented in Figure 4-4 does not include the specimens strengthened with FRP material in the longitudinal direction, such case is presented in Figure 4-5.

      In Figure 4-2 note that the point corresponding to the highest strengthening ratio is the result of a column specimen whose characteristic concrete cylinder compressive strength was considerably low (2.74 ksi [18.9 MPa]), and a high FRP volumetric ratio (10 percent).  The increase in the confined concrete compressive strength and consequently on the load carrying capacity corresponding to an increment of $\rho_f * E_f/E_c$ tends to be slightly smaller for the specimens presenting a larger cross-section, in particular specimen CH2_S.  In addition, the comparison between Figure 4-1 and Figure 4-2 demonstrates that the effectiveness of the FRP in confining square columns is smaller than for the circular ones.

**Table 4-1 Summary of Tests on FRP-Confined Prismatic-Section RC Columns (at least one side greater than 12 in)**

| Code | b (in) | h (in) | Aspect Ratio | H (ft) | FRP Type | Fiber Configuration | $E_f$ (ksi) | $\varepsilon_{fu}$ (%) | $t_f$ (in) | n | Bars $\rho_1$ (%) | Bars $f_y$ (ksi) | Ties $\rho_v$ (%) | Ties $f_{yv}$ (ksi) | $f'_c$ (ksi) | P (kip) | $[P-A_s f_{yl}]/A_c$ | $f_{cc}/f_{co}$ |
|---|---|---|---|---|---|---|---|---|---|---|---|---|---|---|---|---|---|---|
| **Kestner et al. (1997)** | | | | | | | | | | | | | | | | | | |
| KE1_S | 18 | 18 | 1 | 6 | None | | | | | 0 | 1.48 | 66.3 | 0.105 | 72.7 | 4.57 | 1650 | 4.17 | 1.00 |
| KE2_S | 18 | 18 | 1 | 6 | E-glass | [0°/±45] | 2370 | 2.4 | 0.046 | 3 | 1.48 | 66.3 | 0.105 | 72.7 | 4.57 | 1910 | 4.99 | 1.20 |
| KE3_S | 18 | 18 | 1 | 6 | E-glass | [0°] | 3618 | 1.9 | 0.034 | 3 | 1.48 | 66.3 | 0.105 | 72.7 | 4.57 | 1860 | 4.83 | 1.16 |
| KE4_S | 18 | 18 | 1 | 6 | Carbon | [0°] | 33538 | 1.5 | 0.007 | 3 | 1.48 | 66.3 | 0.105 | 72.7 | 4.57 | 1960 | 5.14 | 1.23 |
| **Tanwongsval et al. (2001)** | | | | | | | | | | | | | | | | | | |
| TA1 | 4.5 | 17 | 3.7 | 5 | None | | | | | 0 | 0.44 | 66.9 | 0.54 | 52.9 | 4.70 | 465 | 5.99 | 1.00 |
| TA2 | 4.5 | 17 | 3.7 | 5 | GFRP | [90°/90°/0°/0°] | 3785 | 2.24 | 0.043 | 4 | 0.44 | 66.9 | 0.54 | 52.9 | 4.70 | 597 | 7.78 | 1.30 |
| TA3 | 4.5 | 17 | 3.7 | 6 | GFRP | [90°/90°/0°/0°] | 3785 | 2.24 | 0.043 | 4 | 0.44 | 66.9 | 0.54 | 52.9 | 4.70 | 563 | 7.32 | 1.22 |
| **Wang and Restrepo (2001)** | | | | | | | | | | | | | | | | | | |
| WR1_S | 12 | 12 | 1.00 | 3 | None | | | | | 0 | 1.50 | 63.7 | 0.54 | 52.9 | 2.74 | 472 | 2.36 | 1.00 |
| WR2_S | 12 | 12 | 1.00 | 3 | GFRP | [0°] | 2970 | 0.02 | 0.050 | 2 | 1.50 | 63.7 | 0.54 | 52.9 | 2.74 | 562 | 2.99 | 1.27 |
| WR3_S | 12 | 12 | 1.00 | 3 | GFRP | [0°] | 2970 | 0.02 | 0.050 | 6 | 1.50 | 63.7 | 0.54 | 52.9 | 2.74 | 900 | 5.38 | 2.28 |
| WR1_R | 12 | 18 | 1.48 | 3 | None | NA | | | | | 1.50 | 63.7 | 0.46 | 52.9 | 2.74 | 764 | 2.67 | 1.00 |
| WR2_R | 12 | 18 | 1.48 | 3 | GFRP | [0°] | 2970 | 0.02 | 0.050 | 2 | 1.50 | 63.7 | 0.46 | 52.9 | 2.74 | 809 | 2.89 | 1.08 |
| WR3_R | 12 | 18 | 1.48 | 4 | GFRP | [0°] | 2970 | 0.02 | 0.050 | 6 | 1.50 | 63.7 | 0.46 | 52.9 | 2.74 | 1012 | 3.85 | 1.44 |
| **Tan (2002)** | | | | | | | | | | | | | | | | | | |
| TN1 | 4.5 | 17 | 3.7 | 5 | None | | | | | 0 | 2.2 | 73.2 | 0.56 | 47.1 | 2.44 | 284 | 2.26 | 1.00 |
| TN2 | 4.5 | 17 | 3.7 | 5 | None | | | | | 0 | 2.2 | 73.2 | 0.56 | 47.1 | 2.54 | 309 | 2.61 | 1.00 |
| TN3 | 4.5 | 17 | 3.7 | 5 | GFRP₁ | [0°] | 3785 | 2.24 | 0.039 | 2 | 2.2 | 73.2 | 0.56 | 47.1 | 3.40 | 394 | 3.78 | 1.67 |
| TN4 | 4.5 | 17 | 3.7 | 5 | GFRP₁ | [90°/0°] | 3785 | 2.24 | 0.039 | 2 | 2.2 | 73.2 | 0.56 | 47.1 | 3.79 | 372 | 3.47 | 1.54 |
| TN5 | 4.5 | 17 | 3.7 | 5 | GFRP₁ | [90°/0°/0°] | 3785 | 2.24 | 0.039 | 3 | 2.2 | 73.2 | 0.56 | 47.1 | 3.35 | 413 | 4.03 | 1.79 |
| TN6 | 4.5 | 17 | 3.7 | 5 | GFRP₁ | [0°] | 3785 | 2.24 | 0.039 | 2 | 2.2 | 73.2 | 0.56 | 47.1 | 3.77 | 443 | 4.46 | 1.97 |
| TN7 | 4.5 | 17 | 3.7 | 5 | GFRP₁ | [90°/0°] | 3785 | 2.24 | 0.039 | 2 | 2.2 | 73.2 | 0.56 | 47.1 | 3.76 | 428 | 4.25 | 1.88 |
| TN8 | 4.5 | 17 | 3.7 | 5 | GFRP₁ | [90°/0°/0°] | 3785 | 2.24 | 0.039 | 3 | 2.2 | 73.2 | 0.56 | 47.1 | 3.91 | 426 | 4.22 | 1.87 |
| TN9 | 4.5 | 17 | 3.7 | 5 | None | | | | | 0 | 2.2 | 68.6 | 0.56 | 87.3 | 1.78 | 227 | 1.58 | 1.00 |
| TN10 | 4.5 | 17 | 3.7 | 5 | None | | | | | 0 | 2.2 | 68.6 | 0.56 | 87.3 | 1.97 | 241 | 1.77 | 1.00 |
| TN11 | 4.5 | 17 | 3.7 | 5 | GFRP₁ | [0°] | 3785 | 2.24 | 0.039 | 3 | 2.2 | 68.6 | 0.56 | 87.3 | 1.76 | 271 | 2.19 | 1.38 |
| TN12 | 4.5 | 17 | 3.7 | 5 | GFRP₁ | [0°] | 3785 | 2.24 | 0.039 | 3 | 2.2 | 68.6 | 0.56 | 87.3 | 1.95 | 286 | 2.39 | 1.51 |
| TN13 | 4.5 | 17 | 3.7 | 5 | GFRP₁ | [90°/90°/0°/0°] | 3785 | 2.24 | 0.039 | 4 | 2.2 | 68.6 | 0.56 | 87.3 | 1.85 | 286 | 2.39 | 1.51 |

| | | | | | | | | | | | | | | | | | | |
|---|---|---|---|---|---|---|---|---|---|---|---|---|---|---|---|---|---|---|
| TN14 | 4.5 | 17 | 3.7 | 5 | GFRP$_1$ | [90°/90°/0°/0°] | 3785 | 2.24 | 0.039 | 4 | 2.2 | 68.6 | 0.56 | 87.3 | 2.41 | 239 | 1.74 | 1.10 |
| TN15 | 4.5 | 17 | 3.7 | 5 | GFRP$_1$ | [90°/90°/0°/0°] | 3785 | 2.24 | 0.039 | 5 | 2.2 | 68.6 | 0.56 | 87.3 | 1.73 | 283 | 2.36 | 1.49 |
| TN16 | 4.5 | 17 | 3.7 | 5 | GFRP$_1$ | [90°/90°/0°/0°] | 3785 | 2.24 | 0.039 | 5 | 2.2 | 68.6 | 0.56 | 87.3 | 1.90 | 296 | 2.53 | 1.60 |
| TN17 | 4.5 | 17 | 3.7 | 5 | None | | | | | 0 | 2.2 | 71.8 | 0.56 | 52.9 | 2.68 | 321 | 2.81 | 1.00 |
| TN18 | 4.5 | 17 | 3.7 | 5 | CFRP$_1$ | [0°] | 33069 | 1.50 | 0.006 | 1 | 2.2 | 71.8 | 0.56 | 52.9 | 3.13 | 368 | 3.45 | 1.23 |
| TN19 | 4.5 | 17 | 3.7 | 5 | CFRP$_1$ | [90°/0°] | 33069 | 1.50 | 0.006 | 2 | 2.2 | 71.8 | 0.56 | 52.9 | 2.26 | 326 | 2.87 | 1.27 |
| TN20 | 4.5 | 17 | 3.7 | 5 | CFRP$_1$ | [0°] | 33069 | 1.50 | 0.006 | 2 | 2.2 | 71.8 | 0.56 | 52.9 | 2.81 | 417 | 4.13 | 1.83 |
| TN21 | 4.5 | 17 | 3.7 | 5 | GFRP$_2$ | [90°/0°] | 10501 | 2.00 | 0.014 | 3 | 2.2 | 71.8 | 0.56 | 52.9 | 3.03 | 374 | 3.54 | 1.57 |
| TN22 | 4.5 | 17 | 3.7 | 5 | GFRP$_2$ | [90°/90°/0°/0°] | 10501 | 2.00 | 0.014 | 4 | 2.2 | 71.8 | 0.56 | 52.9 | 2.26 | 414 | 4.08 | 1.81 |
| TN23 | 4.5 | 17 | 3.7 | 5 | GFRP$_2$ | [90°/0°/0°] | 10501 | 2.00 | 0.014 | 4 | 2.2 | 71.8 | 0.56 | 52.9 | 2.94 | 352 | 3.23 | 1.43 |
| TN24 | 4.5 | 17 | 3.7 | 5 | GFRP$_2$ | [90°/90°/0°/0°/0°] | 10501 | 2.00 | 0.014 | 5 | 2.2 | 71.8 | 0.56 | 52.9 | 2.89 | 401 | 3.91 | 1.73 |
| TN25 | 4.5 | 17 | 3.7 | 5 | GFRP$_2$ | [90°/90°/0°] | 10501 | 2.00 | 0.014 | 3 | 2.2 | 71.8 | 0.56 | 52.9 | 2.83 | 375 | 3.56 | 1.57 |
| TN26 | 4.5 | 17 | 3.7 | 5 | GFRP$_2$ | [90°/90°/0°/0°] | 10501 | 2.00 | 0.014 | 4 | 2.2 | 71.8 | 0.56 | 52.9 | 2.85 | 383 | 3.65 | 1.62 |
| TN27 | 4.5 | 17 | 3.7 | 5 | GFRP$_2$ | [90°/90°/0°/0°/0°] | 10501 | 2.00 | 0.014 | 5 | 2.2 | 71.8 | 0.56 | 52.9 | 2.94 | 420 | 4.17 | 1.85 |
| TN28 | 4.5 | 17 | 3.7 | 5 | CFRP$_1$ & GFRP$_2$ | [90°/0°] | | | | 3 | 2.2 | 71.8 | 0.56 | 52.9 | 3.11 | 372 | 3.50 | 1.55 |
| TN29 | 4.5 | 17 | 3.7 | 5 | CFRP$_1$ & GFRP$_2$ | [90°/0°] | | | | 3 | 2.2 | 71.8 | 0.56 | 52.9 | 2.74 | 425 | 4.24 | 1.88 |
| TN30 | 4.5 | 17 | 3.7 | 5 | None | | | | | 0 | 2.2 | 71.8 | 0.56 | 52.9 | 1.97 | 275 | 2.17 | 1.00 |
| TN31 | 4.5 | 17 | 3.7 | 5 | CFRP$_2$ | [90°/0°/0°] | 33360 | 1.50 | 0.004 | 3 | 2.2 | 71.8 | 0.56 | 52.9 | 3.06 | 355 | 3.27 | 1.51 |
| TN32 | 4.5 | 17 | 3.7 | 5 | CFRP$_2$ | [90°/0°/0°/0°] | 33360 | 1.50 | 0.004 | 4 | 2.2 | 71.8 | 0.56 | 52.9 | 3.35 | 357 | 3.30 | 1.52 |
| TN33 | 4.5 | 17 | 3.7 | 5 | CFRP$_3$ | [0°] | 33360 | 1.50 | 0.007 | 2 | 2.2 | 71.8 | 0.56 | 52.9 | 2.11 | 308 | 2.63 | 1.21 |
| TN34 | 4.5 | 17 | 3.7 | 5 | CFRP$_3$ | [90°/90°/0°] | 33360 | 1.50 | 0.007 | 3 | 2.2 | 71.8 | 0.56 | 52.9 | 2.64 | 311 | 2.67 | 1.23 |
| TN35 | 4.5 | 17 | 3.7 | 5 | CFRP$_3$ | [90°/90°/0°] | 33360 | 1.50 | 0.007 | 3 | 2.2 | 71.8 | 0.56 | 52.9 | 2.56 | 337 | 3.03 | 1.40 |
| TN36 | 4.5 | 17 | 3.7 | 5 | CFRP$_3$ | [90°/90°/0°] | 33360 | 1.50 | 0.007 | 3 | 2.2 | 71.8 | 0.56 | 52.9 | 2.72 | 339 | 3.05 | 1.41 |
| TN37 | 4.5 | 17 | 3.7 | 5 | GFRP$_3$ | [90°/90°/0°/0°/0°] | 1465 | 4.60 | 0.030 | 5 | 2.2 | 71.8 | 0.56 | 52.9 | 2.70 | 445 | 4.51 | 2.08 |
| TN38 | 4.5 | 17 | 3.7 | 5 | None | | | | | 0 | 2.2 | 67.7 | 0.56 | 52.1 | 3.08 | 352 | 3.32 | 1.00 |
| TN39 | 4.5 | 17 | 3.7 | 5 | GFRP$_1$ | [0°] | 3785 | 2.24 | 0.039 | 2 | 2.2 | 67.7 | 0.56 | 52.1 | 3.12 | 365 | 3.50 | 1.05 |
| TN40 | 4.5 | 17 | 3.7 | 5 | None | | | | | 0 | 2.2 | 67.7 | 0.56 | 52.1 | 2.76 | 258 | 2.03 | 1.00 |
| TN41 | 4.5 | 17 | 3.7 | 5 | CFRP$_1$ | [90°/0°] | 33069 | 1.50 | 0.006 | 2 | 2.2 | 67.7 | 0.56 | 52.1 | 2.44 | 292 | 2.49 | 1.23 |
| TN42 | 4.5 | 17 | 3.7 | 5 | CFRP$_1$ | [90°/0°/0°] | 33069 | 1.50 | 0.006 | 3 | 2.2 | 67.7 | 0.56 | 52.1 | 3.80 | 361 | 3.45 | 1.70 |
| TN43 | 4.5 | 17 | 3.7 | 5 | CFRP$_1$ | [90°/0°/0°] | 33069 | 1.50 | 0.006 | 3 | 2.2 | 67.7 | 0.56 | 52.1 | 3.41 | 311 | 2.76 | 1.36 |

**Prota et al. (2003)**

| Code | | | | | FRP | Fiber Direction | $E_f$ (ksi) | $\varepsilon_{fu}$ (%) | $t_f$ (in) | n | $\rho_l$ (%) | $f_y$ (ksi) | $\rho_v$ (%) | $f_{yv}$ (ksi) | | | | $f_{cc}/f_{cO}$ |
|---|---|---|---|---|---|---|---|---|---|---|---|---|---|---|---|---|---|---|
| PR1 | 4.5 | 17 | 3.7 | 5 | None | | | | | 0 | 2.21 | 61.0 | 0.51 | 61.0 | 1.74 | 241 | 1.94 | 1.00 |
| PR2 | 4.5 | 17 | 3.7 | 6 | None | | | | | 0 | 2.21 | 61.0 | 0.51 | 61.0 | 1.74 | 240 | 1.93 | 1.00 |
| PR3 | 4.5 | 17 | 3.7 | 7 | CFRP | [0°] | 10590 | 4.66 | NR | 3 | 2.21 | 61.0 | 0.51 | 61.0 | 1.74 | 314 | 2.95 | 1.53 |
| PR4 | 4.5 | 17 | 3.7 | 8 | CFRP | [0°] | 10590 | 4.66 | NR | 3 | 2.21 | 61.0 | 0.51 | 61.0 | 1.74 | 312 | 2.92 | 1.51 |
| PR5 | 4.5 | 17 | 3.7 | 9 | CFRP | [0°] | 10590 | 4.66 | NR | 3 | 2.21 | 61.0 | 0.51 | 61.0 | 1.74 | 303 | 2.79 | 1.45 |

**Carey and Harries (2003)**

| Code | | | | | FRP | Fiber Direction | $E_f$ (ksi) | $\varepsilon_{fu}$ (%) | $t_f$ (in) | n | $\rho_l$ (%) | $f_y$ (ksi) | $\rho_v$ (%) | $f_{yv}$ (ksi) | | | | $f_{cc}/f_{cO}$ |
|---|---|---|---|---|---|---|---|---|---|---|---|---|---|---|---|---|---|---|
| CH1_S | 21.25 | 21.25 | 1.0 | 5.3 | None | | | | | 0 | 1.40 | 60.0 | 0.17 | 64.0 | 4.86 | 3190 | 6.31 | 1.00 |
| CH2_S | 21.25 | 21.25 | 1.0 | 5.3 | CFRP | [0°] | 10516 | 1.21 | 0.039 | 3 | 1.40 | 60.0 | 0.17 | 64.0 | 4.86 | 3312 | 6.59 | 1.04 |

<u>Notes</u>: NR = Not Reported; 1 in = 25.4 mm; 1 ft = 30.5 cm; 1 ksi = 6.9 MPa; 1 kip = 4.4 KN

Prior to testing, specimen TA3 was subjected to vertical loads from prestressing cables simulating service loads.

**Table 4-2  Summary of Tests on FRP-Confined Circular-Section RC Columns (Minimum diameter 12 in)**

| Code | D (in) | H (ft) | FRP | Fiber Direction | $E_f$ (ksi) | $\varepsilon_{fu}$ (%) | $t_f$ (in) | n | Bars | | Spiral | | P (kip) | $f_c$ (ksi) | $[P-A_s f_y]/A_c$ | $f_{cc}/f_{cO}$ |
|---|---|---|---|---|---|---|---|---|---|---|---|---|---|---|---|---|
| | | | | | | | | | $\rho_l$ (%) | $f_y$ (ksi) | $\rho_v$ (%) | $f_{yv}$ (ksi) | | | | |
| Demers and Neale (1994) | | | | | | | | | | | | | | | | |
| DN1 | 12 | 4 | | | | | | 0 | 1.4 | 58 | 0.4 | 58 | 411 | 4.10 | 2.86 | 1.00 |
| | 12 | 4 | CFRP | [0°] | 12183 | 1.50 | 0.012 | 3 | 1.4 | 58 | 0.4 | 58 | 580 | 4.10 | 4.38 | 1.53 |
| DN2 | 12 | 4 | | | | | | 0 | 3.5 | 58 | 0.8 | 58 | 594 | 4.10 | 3.34 | 1.00 |
| | 12 | 4 | CFRP | [0°] | 12183 | 1.50 | 0.012 | 3 | 3.5 | 58 | 0.8 | 58 | 821 | 4.10 | 5.42 | 1.62 |
| DN3 | 12 | 4 | | | | | | 0 | 1.4 | 58 | 0.8 | 58 | 773 | 6.30 | 6.11 | 1.00 |
| | 12 | 4 | CFRP | [0°] | 12183 | 1.50 | 0.012 | 3 | 1.4 | 58 | 0.8 | 58 | 962 | 6.30 | 7.80 | 1.28 |
| DN4 | 12 | 4 | | | | | | 0 | 3.5 | 58 | 0.4 | 58 | 933 | 6.30 | 6.45 | 1.00 |
| | 12 | 4 | CFRP | [0°] | 12183 | 1.50 | 0.012 | 3 | 3.5 | 58 | 0.4 | 58 | 910 | 6.30 | 6.23 | 0.97 |
| DN5 | 12 | 4 | CFRP | [0°] | 12183 | 1.50 | 0.012 | 3 | 1.4 | 58 | 0.8 | 58 | 663 | 4.10 | 5.12 | NA |
| DN6 | 12 | 4 | CFRP | [0°] | 12183 | 1.50 | 0.012 | 3 | 3.5 | 58 | 0.4 | 58 | 791 | 4.10 | 5.15 | NA |
| DN7 | 12 | 4 | CFRP | [0°] | 12183 | 1.50 | 0.012 | 3 | 1.4 | 58 | 0.4 | 58 | 908 | 6.30 | 7.32 | NA |
| DN8 | 12 | 4 | CFRP | [0°] | 12183 | 1.50 | 0.012 | 3 | 3.5 | 58 | 0.8 | 58 | 1045 | 6.30 | 7.47 | NA |

| | | | | | | | | | | | | | | | |
|---|---|---|---|---|---|---|---|---|---|---|---|---|---|---|---|
| **Kestner et al. (1997)** | | | | | | | | | | | | | | | |
| KE1_C | 20 | 6 | none | | | | 0 | 1.53 | 66.3 | 0.185 | 72.7 | 1680 | 4.57 | 4.40 | 1.00 |
| KE2_C | 20 | 6 | GFRP | [0°/±45] | 2370 | 2.40 | 0.046 | 3 | 1.53 | 66.3 | 0.185 | 72.7 | 1940 | 4.57 | 5.24 | 1.19 |
| KE3_C | 20 | 6 | GFRP | [0°] | 3618 | 1.90 | 0.034 | 3 | 1.53 | 66.3 | 0.185 | 72.7 | 2030 | 4.57 | 5.53 | 1.26 |
| KE4_C | 20 | 6 | CFRP | [0°] | 33538 | 1.50 | 0.0065 | 3 | 1.53 | 66.3 | 0.185 | 72.7 | 2530 | 4.57 | 7.15 | 1.62 |
| **Carey and Harries (2003)** | | | | | | | | | | | | | | | |
| CH1_C | 24 | 6 | | | | | | | | | | 3008 | 4.86 | 5.89 | 1.00 |
| CH2_C | 24 | 6 | CFRP | [0°] | 10615 | 1.21 | 0.039 | 3 | 1.4 | 60.0 | 0.14 | 64.0 | 4784 | 4.86 | 9.87 | 1.68 |
| CH3_C | 24 | 6 | CFRP | [0°] | 10615 | 1.21 | 0.039 | 3 | 1.4 | 60.0 | 0.14 | 64.0 | 3780 | 4.86 | 7.62 | 1.29 |
| **Matthys et al. (2005)** | | | | | | | | | | | | | | | |
| MA1 | 15.75 | 6.5 | 0 | | | | | 0 | 0.90 | 89.9 | 0.33 | 81.2 | 1053 | 4.61 | 4.64 | 1.00 |
| MA2 | 15.75 | 6.5 | CFRP | [0°] | 28717 | 1.19 | 0.005 | 5 | 0.90 | 89.9 | 0.33 | 81.2 | 1677 | 4.97 | 7.87 | 1.70 |
| MA3 | 15.75 | 6.5 | CFRP | [0°] | 69618 | 0.22 | 0.009 | 4 | 0.90 | 89.9 | 0.33 | 81.2 | 1684 | 4.97 | 7.90 | 1.70 |
| MA4 | 15.75 | 6.5 | GFRP | [0°] | 8702 | 1.30 | 0.012 | 6 | 0.90 | 89.9 | 0.33 | 81.2 | 1704 | 5.70 | 8.01 | 1.73 |
| MA5 | 15.75 | 6.5 | GFRP | [0°] | 8702 | 1.30 | 0.012 | 2 | 0.90 | 89.9 | 0.33 | 81.2 | 1197 | 5.70 | 5.38 | 1.16 |
| MA6 | 15.75 | 6.5 | GFRP | [0°] | 8702 | 1.30 | 0.012 | 4 | 0.90 | 89.9 | 0.33 | 81.2 | 1124 | 5.19 | 5.01 | 1.08 |
| MA7 | 15.75 | 6.5 | GFRP | Spiral | 8702 | 1.30 | 0.012 | 4 | 0.90 | 89.9 | 0.33 | 81.2 | 1081 | 5.19 | 4.78 | 1.03 |
| MA8 | 15.75 | 6.5 | HFRP | [0°] | 17405 | 0.96 | 0.005 | 4 | 0.90 | 89.9 | 0.33 | 81.2 | 1401 | 5.67 | 6.44 | 1.39 |

Notes: NA = Not Applicable; 1 in = 25.4 mm; 1 ft = 30.5 cm; 1 ksi = 6.9 MPa; 1 kip = 4.4 KN

Specimen DN4, 40 percent of the section had to be replaced.

The FRP jacket of specimen CH3_C was not bonded.

Specimens MA6 and MA7 were partially wrapped with 8 in (200 mm) strips and 16 in (400 mm) pitch.

The comparison between Figure 4-1 and Figure 4-2 confirms that the effectiveness of the FRP in confining columns of square cross-section is less than for circular ones.  A similar observation is noted for the case of columns rectangular cross-section with respect to the ones of square cross-section (Figure 4-3 and Figure 4-4).  With regards to Figure 4-4 and Figure 4-5, which are limited to columns having an aspect ratio of 3.7 ("wall-type columns"), definite concluding remarks from these last two figures can not be done at this moment due to the high scattering of the data.
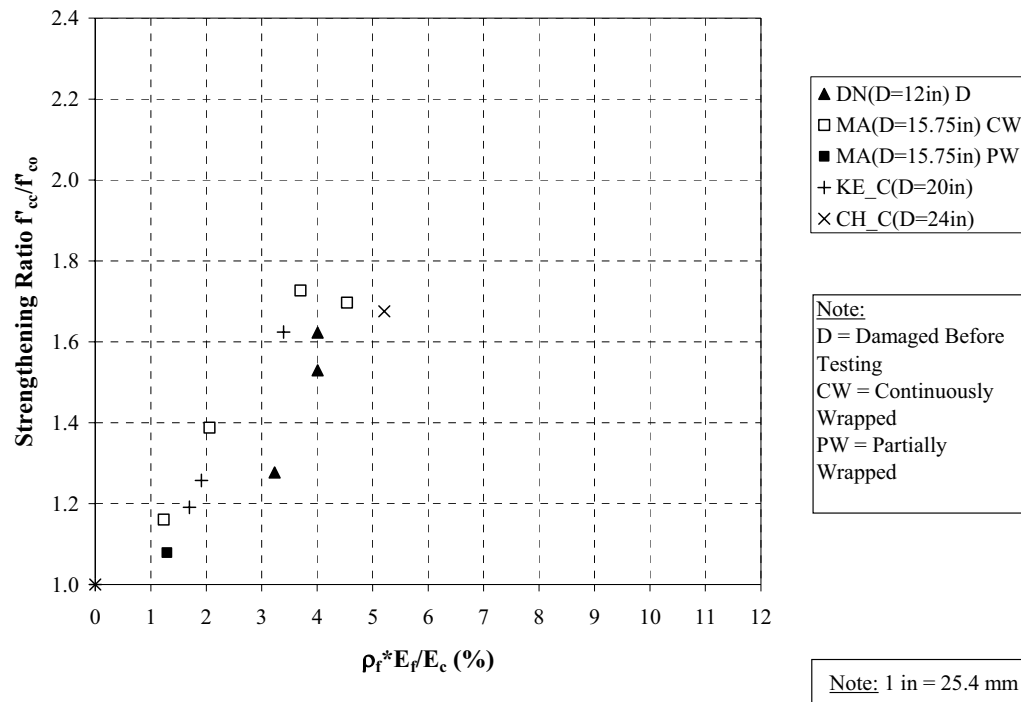
**Figure 4-1  Compressive Strength Increment of Specimens of Circular Cross-Section**
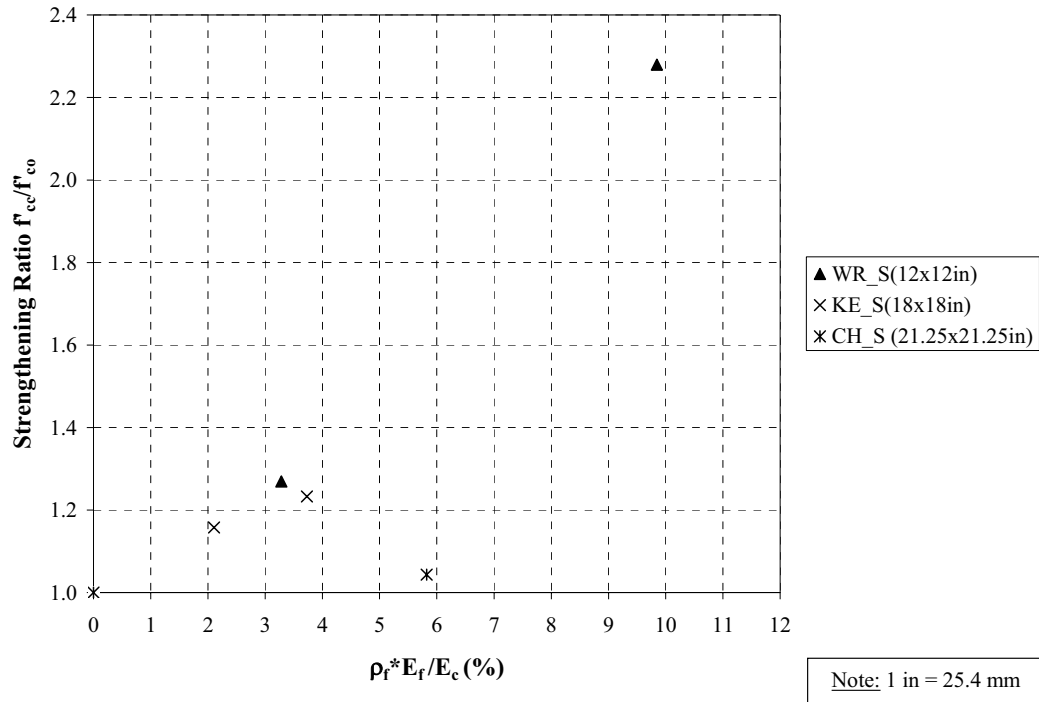
**Figure 4-2  Compressive Strength Increment of Specimens of Square Cross-Section**
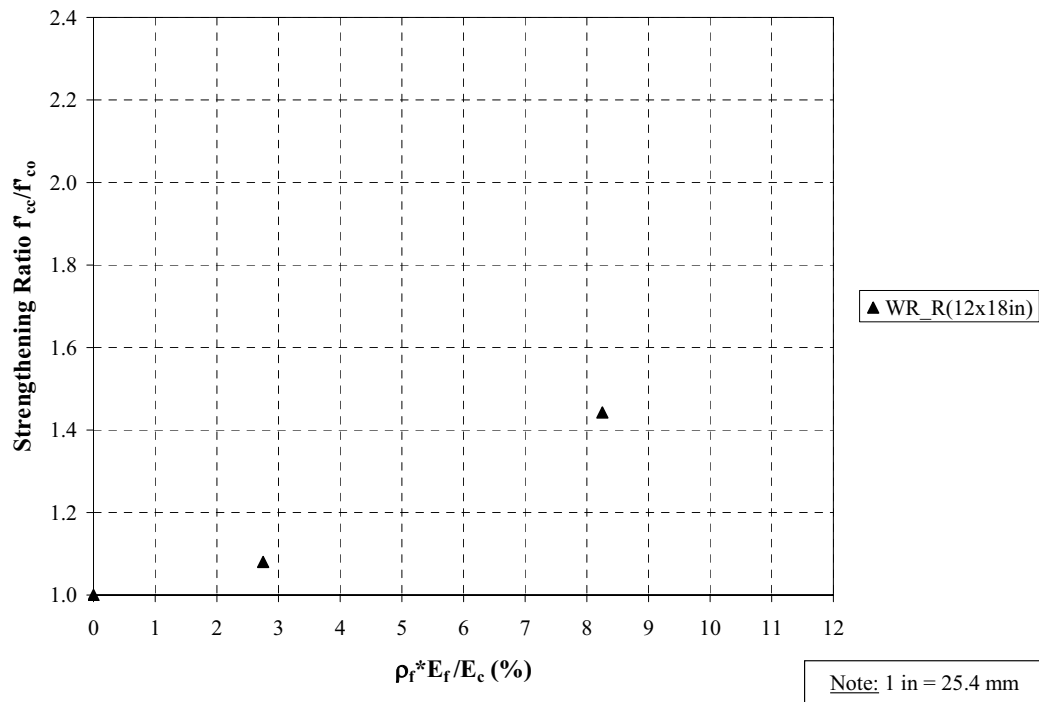


**Figure 4-3  Compressive Strength Increment of Specimens of Rectangular Cross-Section (Side Aspect Ratio of 1.5)**
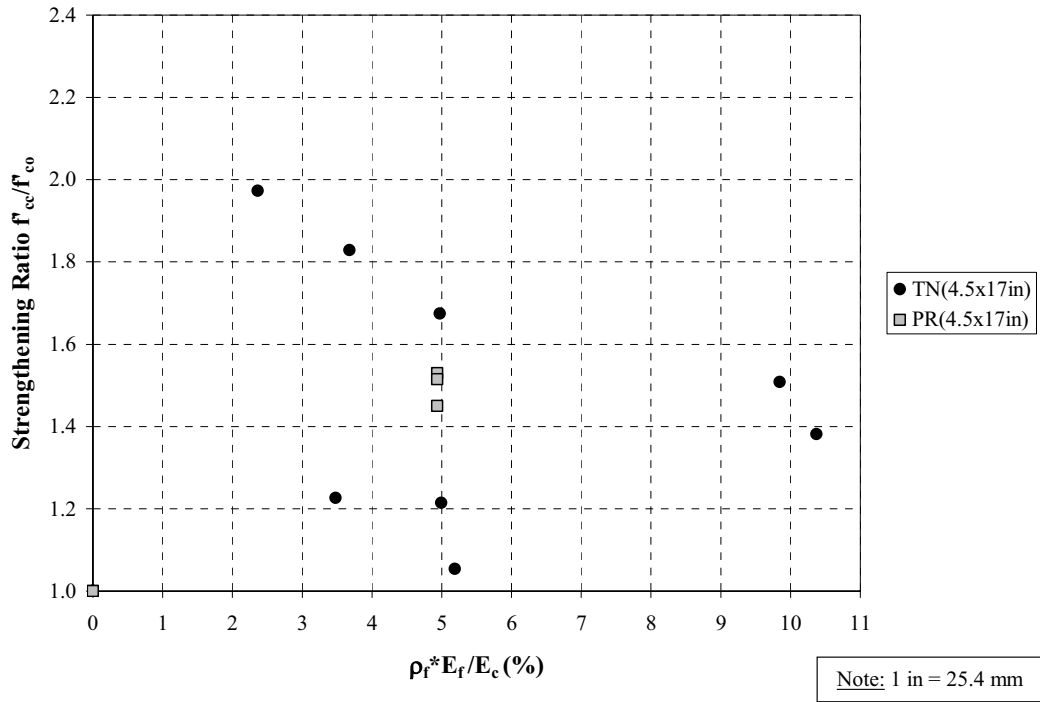
**Figure 4-4  Compressive Strength Increment of Specimens of Rectangular Cross-Section (Side Aspect Ratio of 3.7)**
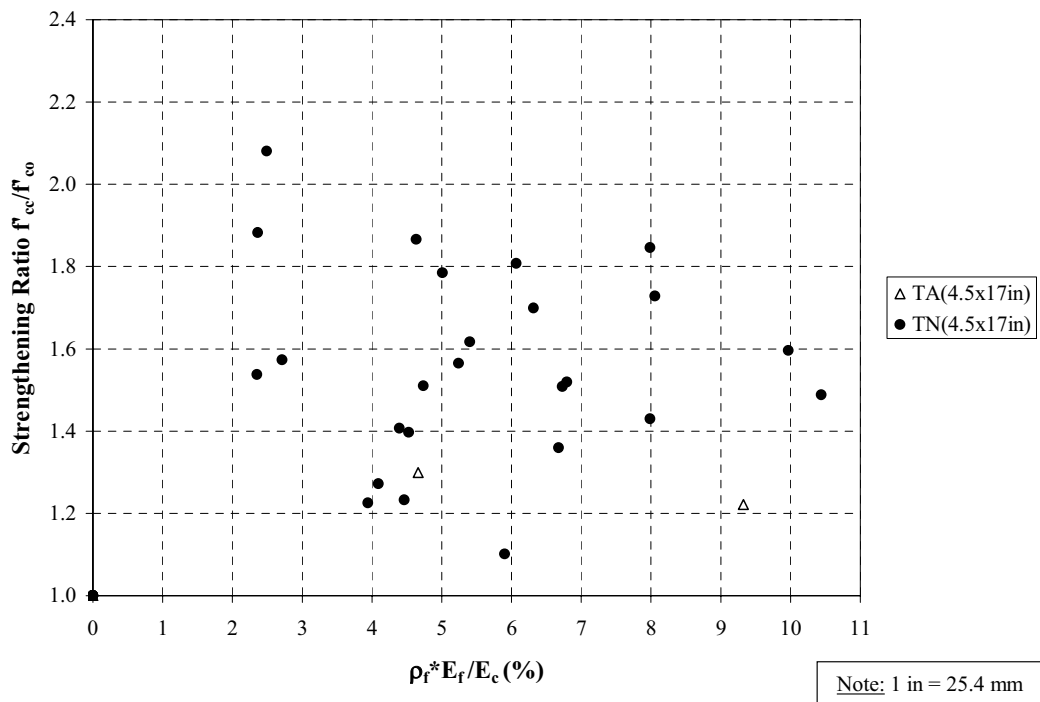


**Figure 4-5  Compressive Strength Increment of Specimens of Rectangular Cross-Section (Side Aspect Ratio of 3.7 and Partial Longitudinal FRP Reinforcement)**

# 5. REVIEW OF INTERNATIONAL GUIDELINES

Part of the objective of this research study is to provide a comparison of the values predicted by currently available design guidelines and the results obtained from the experiments. The documents considered in this study are: "Guide for the Design and Construction of Externally Bonded FRP Systems for Strengthening Concrete Structures" reported by the American Concrete Institute (ACI Committee 440.2R-02), "Design and Construction of Building Components with Fibre-Reinforced Polymers" S806-02 Canadian Standard Association (2002), "Design Guidance for Strengthening Concrete Structures Using Fibre Composite Material" (TR 55), by the Concrete Society Technical Report 55 (2005), and "Externally Bonded FRP Reinforcement for RC Structures" Technical Report, by the fédération internationale du béton (*fib*), (2001). No design guideline or recommendation from the Japan Concrete Institute (JCI) or the Japan Society of Civil Engineers (JSCE) is included in this discussion for the reason that the case of pure axial strengthening of columns is not addressed, in fact, the available documents only refer to enhancement of ductility in terms of deformation under seismic loads.

Regarding the design philosophies adopted by each of these codes, the recommendations for the design of RC members strengthened with FRP are based on limit states design principles, which provide acceptable levels of safety against ultimate (i.e. collapse) and serviceability (i.e. control of deflections) limit states. The combinations of loads to be considered for the determination of the nominal capacity of a structural member are affected by amplifications factors (greater than one), which account for the probability of the loading being larger than the computed one. The nominal capacity is also affected by reduction factors that take into consideration the possibility of the resistances being less than calculated (MacGregor, 1997). These effects are addressed in two different ways by the current available guidelines: for ACI, the strength reduction factors (less than the value of 1) multiply the computed nominal capacity; and for the other guidelines, material safety factors are applied individually to each of the material components of the member in analysis (concrete, steel reinforcement, and FRP when applicable) during the computation of the resistance. For the case of the use of FRP material, all the guidelines consider material reduction factors to be applied individually and they vary basically on the type of material and the exposure condition (environmental).

Table 5-1 shows the reduction factors and material safety factors used by the different guidelines. Note that the subscript "c" refers to concrete and "s" refers to non-prestressing reinforcing steel. Since ACI 440.2R-02 is based on the requirements of ACI 318-99, the reduction factors presented in the table below correspond to such edition, for the case of axial loading.

The design methodologies for each of the guidelines previously introduced are presented from Section 5.1 to Section 5.4, and a comparison in terms of the theoretical increment of concrete compressive strength by means of FRP confinement determined by each of the guidelines, is shown in Section 5.5.

**Table 5-1  Reduction and Material Safety Factors for Different Guidelines**

| Code | Factors |
|---|---|
| ACI 440.2R – 2002 | $\phi = 0.70$ (spiral) <br> $\phi = 0.75$ (ties) |
| CSA S806 – 2002 | $\phi_c = 0.60$ <br> $\phi_s = 0.85$ |
| TR 55 – 2005 | $\gamma_{mc} = 1.50$ <br> $\gamma_{ms} = 1.15$ |
| fib – 2001 | $\gamma_{mc} = 1.50$ <br> $\gamma_{ms} = 1.15$ |

## 5.1. "GUIDE FOR THE DESIGN AND CONSTRUCTION OF EXTERNALLY BONDED FRP SYSTEMS FOR STRENGTHENING CONCRETE STRUCTURES", ACI 440.2R (2002)

ACI Committee 440 provides design equations for the confinement of circular non-slender RC columns with a FRP confinement wrapping.  The apparent compressive strength of confined concrete $f'_{cc}$ is given by the Equation 5-1, which was originally developed for confinement provided by steel jacketing (Mander et al. 1988) (Figure 5-1), but later on proved to be applicable to FRP-confined concrete (Spoelstra and Monti, 1999).
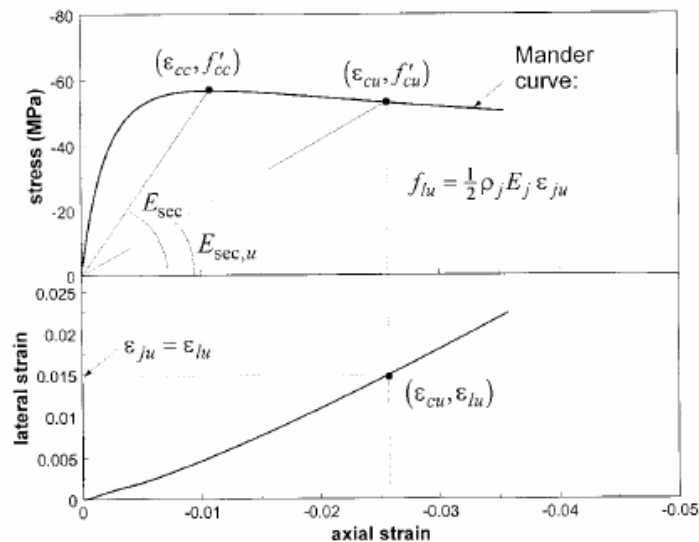


**Figure 5-1  Stress Strain Model for Confined Concrete (Spoelstra and Monti, 1999)**

$$f'_{cc} = f'_c \left[ 2.25\sqrt{1 + 7.9\frac{f_l}{f'_c}} - 2\frac{f_l}{f'_c} - 1.25 \right]$$ 5-1

Where:

$f'_c$ = Specified unconfined concrete compressive strength

$f_l$ = Confining pressure due to FRP jacket and it is given by:

$$f_l = \frac{\kappa_a \rho_f f_{fe}}{2} = \frac{\kappa_a \rho_f \varepsilon_{fe} E_f}{2}$$ 5-2

Where:

$\kappa_a$ = Efficiency factor based on geometry of the cross-section (1 for circular sections)

$\rho_f$ = FRP reinforcement ratio

$f_{fe}$ = Effective stress in the FRP

$\varepsilon_{fe}$ = FRP effective strain (strain level reached at failure). It is specified that for members subjected to combined compression and shear, this strain can not exceed the smaller of these two thresholds: 0.004 and 0.75* $\varepsilon_{fu}$

$\varepsilon_{fu}$ = Ultimate FRP strain

$E_f$ = Tensile modulus of elasticity of FRP

For the case of strength enhancement of compression members of non-circular sections, this guideline does not provide specific recommendations at this time due to the many unknowns for this type of application; in fact, this area is highlighted as a topic for further research. According to this guideline, while the confinement of a non-circular section may not be effective in increasing the axial capacity, it is however recognized to improve the ductility. The maximum usable axial strain for prismatic members can be computed as:

$$\varepsilon'_{cc} = \frac{1.71(5f'_{cc} - 4f'_c)}{E_c}$$ 5-3

Where $f'_{cc}$ is obtained from Equations 5-2 and 5-1. The FRP reinforcement ratio $\rho_f$ is defined as follows:

Circular cross-section: $\rho_f = \dfrac{4nt_f}{D}$

Prismatic cross-section: $\rho_f = \dfrac{2nt_f(b+h)}{bh}$

Where:

n = Number of plies composing the FRP jacket

$t_f$ = Nominal thickness of one ply of the FRP jacket

D = Diameter of the circular cross-section

b = Width of rectangular cross-section

h = Height of rectangular cross-section

The efficiency factor $\kappa_a$ is 1 for the case of circular cross-section and for prismatic ones is given by:

$$\kappa_a = 1 - \frac{(b-2r)^2 + (h-2r)^2}{3bh(1-\rho_g)}$$

5-4

Where:

r = Corner radius; minimum recommended value of ½ in (13 mm)

$\rho_g$ = Longitudinal steel reinforcement ratio

This guideline recommends that the confinement effect for rectangular sections with aspect ratios b/h greater than 1.5, or side dimensions, "b" or "h", greater than 36 in (900 mm), should be neglected, unless demonstrated by experimental testing.

## 5.2. "DESIGN AND CONSTRUCTION OF BUILDING COMPONENTS WITH FIBRE-REINFORCED POLYMERS", CSA-S806 (2002)

According to this document, RC columns of circular and rectangular cross-sections where the ratio of longer side (h) to shorter side (b) dimension is less than 1.5, may have their axial compression capacity enhanced by the confining effect of a FRP jacket with fibers mainly oriented in the hoop direction. It is recommended to round the corners to a radius not less than 0.8 in (20 mm). Specified confined compressive strength of concrete $f'_{cc}$ is given by the following expression:

$$f'_{cc} = f'_c + k_1 + k_c + f_1$$

5-5

Where:

$k_1 = 6.7 (k_c f_1)^{-0.17}$

$k_c = 1 =$ Confinement coefficient for circular cross-sections

$k_c = 0.25 =$ Confinement coefficient for prismatic cross-sections

The confining pressure for circular and prismatic cross-sections is given by Equations 5-6 and 5-7, respectively:

$$f_1 = \frac{2t_j f_{Fj}}{D}$$

5-6

Where:

$t_j =$ Total thickness of the FRP jacket (based on the nominal fiber thickness or effective area)

$D =$ Diameter of the circular cross-section or the least lateral dimension of the prismatic cross-section (CSA A23.3-94)

$f_{Fj} =$ Stress in the FRP, it is the lesser of $0.004*E_F$ and $\phi_F*f_{Fu}$

$\phi_F = 0.75 =$ Resistance factor of FRP

$f_{Fu}$ = Ultimate tensile strength of FRP

$E_F$ = Modulus of elasticity of FRP

Note that no expression for the ultimate axial strain is provided.

## 5.3.  "DESIGN GUIDANCE FOR STRENGTHENING CONCRETE STRUCTURES USING FIBRE COMPOSITE MATERIAL", TR 55, 2005

As for the previous section, it will be first summarized the approach for circular cross-sections and then for non-circular ones.

The model developed by Lam and Teng (2003) was adopted by this technical committee for its simplicity and accuracy in representing the behavior of FRP confined circular columns. This model has been calibrated against all the current available data up to the date of its publication.  As it can be seen in Figure 5-2, the model is basically composed of an initial parabolic portion followed by a linear portion with a smooth transition at the strain $\varepsilon_t$.  This model is defined as follows:

$$f_{cc} = E_c \varepsilon_{cc} - \frac{(E_c - E_2)^2}{4f_{co}} (\varepsilon_{cc})^2 \qquad\qquad 0 \le \varepsilon_{cc} \le \varepsilon_t$$

$$f_{cc} = f_{co} + E_2 \varepsilon_{cc} \qquad\qquad \varepsilon_t < \varepsilon_{cc} \le \varepsilon_{ccu}$$
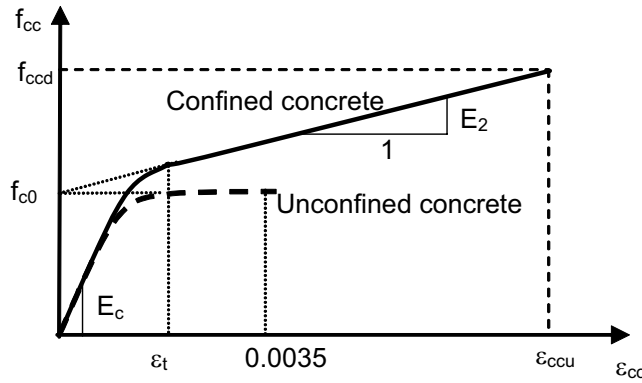


**Figure 5-2  Lam and Teng's Stress-Strain Model for FRP Confined Concrete**

Where:

$f_{cc}$ = Confined concrete axial compressive strength

$E_c = 5.5 \sqrt{\dfrac{f_{cu}}{\gamma_{mc}}} [KN/mm^2]$ = Initial modulus of elasticity of concrete

$\varepsilon_{cc}$ = Confined concrete axial strain

$E_2 = \dfrac{f_{cc} - f_{co}}{\varepsilon_{ccu}}$ = Slope of linear portion of stress-strain confined concrete curve

$f_{co}$ = Unconfined compressive concrete strength $= \dfrac{0.67f_{cu}}{\gamma_{mc}}$

$f_{cu}$ = Characteristic compressive cube concrete strength

$\gamma_{mc}$ = Partial safety factor for concrete

$\varepsilon_t = \dfrac{2f_{co}}{E_c - E_2}$ = Position of transition region between parabola and straight line for confined concrete

$f_{ccd}$ = Design or ultimate confined concrete compressive strength

$\varepsilon_{ccu}$ = Confined concrete ultimate axial strain

This model is only applicable when for increments of confined compressive strength there is also an increment of the axial strain; therefore the fulfillment of a condition for the application of the model is noted in this technical report:

$$\frac{2t_f E_{fd}}{D(f_{co})^2} > 0.183 \quad \left[ mm^2/N \right]$$

Where:

$t_f$ = Thickness of the FRP laminate or jacket (mm)

$E_{fd}$ = Design modulus of elasticity of FRP (N/mm$^2$)

$D$ = Diameter of the column (mm)

The definition of the ultimate design failure stress $f_{ccd}$ and the ultimate compressive failure strain $\varepsilon_{ccu}$ are mandatory in order to use this model. The recommended value for the first parameter is:

$$f_{ccd} = f_{co} + 0.05\left(\frac{2t_f}{D}\right)E_{fd}$$

Note that the equation above is based on the concrete cube compressive strength and partial safety factor of 1.5.

Regarding the ultimate axial strain, the following expression was adopted from also the model of Lam and Teng (2003):

$$\varepsilon_{cu} = \varepsilon_{co}\left( 1.75 + 12\left(\frac{2E_{fd}t_f}{E_0 D}\right)\left(\frac{0.6\varepsilon_{fd}}{\varepsilon_{co}}\right)^{1.45} \right)$$

Where:

$E_0 = \dfrac{0.67f_{cu}}{\gamma_{mc}\varepsilon_{co}}$ = Secant modulus of concrete

$\varepsilon_{co} = 2.4 \times 10^{-4} \sqrt{\dfrac{f_{cu}}{\gamma_{mc}}}$ = Axial strain in unconfined concrete at peak stress $f_{co}$

$\varepsilon_{fd}$ = Design ultimate strain of FRP

It is recommended that if the ultimate strain $\varepsilon_{ccu}$ is greater than 0.01, the failure stress should be taken as the value for $f_{ccd}$ corresponding to the value of $\varepsilon_{cc}$ equal to 0.01 from the stress-strain curve, rather than the failure stress at rupture of the FRP.

Regarding the confinement of non-circular cross-section, the approach presented in this technical report follows the generally accepted methodology of the assessment of an effectively confined area defined by four parabolas and affected by the dimensions of the column cross-section and corner radius. This report explicitly does not recommend any state-of-the-art method for analysis of strengthened prismatic columns unless the following conditions are met:

- Loading is mainly concentric
- The smaller side dimension is not greater than about 8 in (200 mm)
- The side aspect ratio is not greater than 1.5
- Minimum corner radius of at least 0.6 in (15 mm)

The model proposed by Lam and Teng (2003) for prismatic columns, although being calibrated only with small-scale specimens, was adopted by this technical committee and in addition to the general approach, introduces the presence of an overlapping area formed by the parabolas that defined the confined area as it can be seen in

Figure 5-3. When the side aspect ratio of the prismatic cross-section increases up to a limit of $2b < (h - 2R_c)$, the longer parabolas overlap creating a non-confined area or area of overlapping ($A_{ol}$) that must be subtracted from the total effective area enclosed by the parabolas themselves ($A_e$).
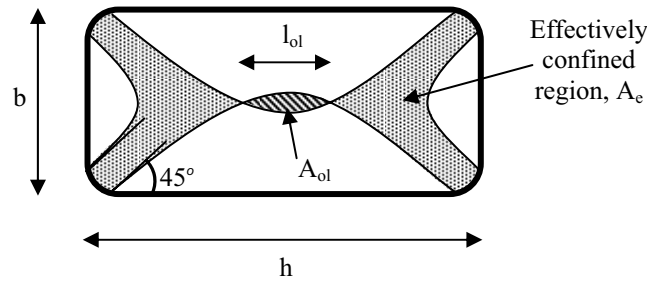


**Figure 5-3 Overlapping Parabolas in Confined Region (TR 55, 2004)**

The confined concrete axial compressive stress is given by:

$$f_{cc} = f_{co} + 2g_s f_r \qquad \textbf{5-7}$$

Where:

$$f_r = \frac{2f_{fd}t_f}{\sqrt{b^2 + h^2}} = \text{Equivalent confinement pressure, where } \sqrt{b^2 + h^2} = D, \text{ the diameter of}$$

an equivalent circular column defined by Lam and Teng as the diagonal distance across the section.

The shape factor $g_s$ is defined as follows:

$$g_s = \frac{b}{h}\frac{A_e}{A_g}$$

5-8

Where, "b" and "h" are the lengths of the short and long side, respectively. The parameter $A_e$ represents the effectively confined area, and $A_g$ the total cross-sectional area: $\left(bh - (4-\pi)(R_c)^2\right)$. The term $R_c$ refers to the corner radius.

$$\frac{A_e}{A_g} = \frac{1 - \dfrac{\left[(h-2R_c)^2 + (b-2R_c)^2 - 3A_{ol}\right]}{3A_g} - \rho_{sc}}{1 - \rho_{sc}}$$

5-9

The term $A_{ol}$ is the overlapping area of the parabolas in Figure 5-3:

$$A_{ol} = \begin{cases} 0 & \text{if } 2b \geq (h-2R_c) \\ \dfrac{4(l_{ol})^3}{3(h-2R_c)} + l_{ol}\left(2b - (h-2R_c)\right) & \text{if } 2b < (h-2R_c) \end{cases}$$

The parameter $l_{ol}$ is the length of the overlapping region in Figure 5-3:

$$l_{ol} = \sqrt{\frac{(h-2R_c)^2}{4} - \frac{b(h-2R_c)}{2}}$$

5-10

Note that for the case of prismatic cross-sections no predictive equations for the ultimate or usable axial strain are provided.

## 5.4. "EXTERNALLY BONDED FRP REINFORCEMENT FOR RC STRUCTURES, FEDERATION INTERNATIONALE DU BETON (fib)", 2001

In this document it is highlighted that the hoop failure strain of the FRP jacket, based on experimental evidence, is lower than the ultimate strain obtained by tensile testing of the material (mechanical characterization). It is pointed out that this reduction is due to several reasons, such as: the quality of execution (fibers not perfectly aligned or not appropriate surface preparation), the size effects when applying several layers, the effect of wrapping the material on the corners of low radius in particular, and the state of stress of the FRP wrapping (which refers to the fact that the jacket is not only subjected to axial tensile stresses but also to transverse confinement which is not reflected by the pure tensile testing conducted for characterization). Due to the limited data with regards to these effects, no appropriate reduction factors are currently suggested.

The maximum confinement pressure is given by the following equation:

$$f_l = K_{conf}\varepsilon_{ju} = \frac{1}{2}k_e\rho_j E_j\varepsilon_{ju}$$ 
**5-11**

Where:

$K_{conf}$ = Stiffness of the FRP confinement

$k_e$ = Confinement effectiveness coefficient for the case of circular cross-section and

partial wrapping = $k_e = \left(1 - \dfrac{s'}{2D}\right)^2$

$D$ = Diameter of circular cross-section

s' = Clear spacing between FRP wraps

$\rho_j$ = FRP volumetric ratio in a circular column

$E_j$ = Modulus of elasticity of the FRP jacket

$\varepsilon_{ju}$ = FRP jacket effective ultimate hoop or circumferential strain

The confined concrete strength and the corresponding axial strain can be determined as follows:

$$f_{cc} = f_{co}\left[2.254\sqrt{1 + 7.94\frac{f_l}{f_{co}}} - 2\frac{f_l}{f_{co}} - 1.254\right]$$ 
**5-12**

$$\varepsilon_{cc} = \varepsilon_{co}\left[1 + 5\left(\frac{f_{cc}}{f_{co}} - 1\right)\right]$$ 
**5-13**

Where:

$f_{co}$ = Unconfined concrete strength

$\varepsilon_{co}$ = Unconfined concrete strain corresponding to $f_{co}$

The ultimate confined concrete strength and ultimate axial strain are given by the following "exact" equations:

$$f_{cu} = \frac{E_c\varepsilon_{cu}}{1 + 2\beta\varepsilon_{ju}}$$ 
**5-14**

$$\varepsilon_{cu} = \varepsilon_{cc}\left(\frac{2\beta\varepsilon_{ju}E_{cc}}{E_c - E_{cc}}\right)^{1 - E_{cc}/E_c}$$ 
**5-15**

Alternative to the equations above "practical" design equations are also provided in this document:

$$f_{cu} = f_{co}\left(0.2 + 3\sqrt{\frac{f_l}{f_{co}}}\right)$$ 
**5-16**

$$\varepsilon_{cu} = \varepsilon_{co}\left(2 + 1.25\frac{E_c}{f_{co}}\varepsilon_{ju}\sqrt{\frac{f_l}{f_{co}}}\right)$$ 
**5-17**

Where:

$E_c$ = Initial tangent modulus of elasticity of concrete

$\beta = \dfrac{5700}{\sqrt{|f_{co}|}} - 500$  (The unconfined concrete strength $f_{co}$ is in MPa)

$E_{cc} = \dfrac{f_{cc}}{\varepsilon_{cc}}$

For the case of prismatic cross-sections, the maximum confinement stress $f_l$ is given by the minimum the lateral confining pressures ($\sigma_{lx}$ and $\sigma_{ly}$) which depends on the stiffness of the FRP jacket $K_{conf}$ in the direction of $d$ and $b$ (Figure 5-4).
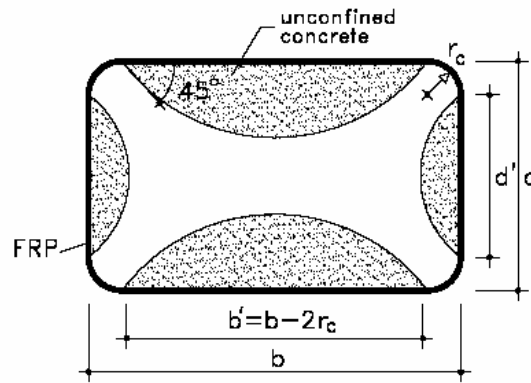


**Figure 5-4  Effectively Confined Core for Non-circular Sections, (*fib*, 2001)**

$$\sigma_{lx} = K_{confx}\varepsilon_{ju} = \left(\rho_{jx}k_e E_j\right)\varepsilon_{ju} \qquad \textbf{5-18}$$

$$\sigma_{ly} = K_{confy}\varepsilon_{ju} = \left(\rho_{jy}k_e E_j\right)\varepsilon_{ju} \qquad \textbf{5-19}$$

The volumetric ratio of the FRP jacket in the directions of "d" and "b" are given by:

$$\rho_{jx} = \frac{2b_f t_j}{sb} \qquad\qquad\qquad \rho_{jy} = \frac{2b_f t_j}{sd}$$

In partial wrapping schemes, $b_f$ is the width of the strip and $s$ is the pitch (s'+ $b_f$). For the case of constantly or fully wrapped, the ratio $b_f$/s equals one. The parameter $t_j$ refers to the total thickness of the FRP jacket.

Accounting for the geometry of the cross section (confinement effectiveness) $k_e$ is expressed by:

$$k_e = 1 - \frac{\left(b - 2r_c\right)^2 + \left(d - 2r_c\right)^2}{3A_g\left(1 - \rho_{sg}\right)} \qquad \textbf{5-20}$$

Where:

$r_c$ = Radius of rounded corner, the suggested range is 0.6 – 1 in (15 – 25 mm) or as recommended by the manufacturer

$A_g$ = Gross area of concrete

$\rho_{sg}$ = Ratio of longitudinal steel reinforcement

The ultimate confining pressure is determined from the lesser of Equation 5-18 and 5-19, then as for the case of circular cross-sections, the parameters $f_{cc}$ and $\varepsilon_{cc}$ are determined using Equations 5-12 and 5-13, and finally the ultimate confinement stress and strain can be computed with either Equations 5-16 and 5-17 or Equations 5-18 and 5-19.

## 5.5. COMPARATIVE STUDY OF GUIDELINES PREDICTIVE EQUATIONS

In order to evaluate the performance and contrast the different approaches from each of the guidelines for the determination of the ultimate confined concrete compressive strength ($f'_{cc}$) and its corresponding axial strain ($\varepsilon'_{cc}$), three specimens from this experimental program of different cross-section type (circular, square, and rectangular) and equal gross area ($A_g$), were selected.  Given an unconfined concrete compressive strength $f'_c$ of 4000 psi (28 MPa) and the following FRP amount and material properties:

- Carbon
- Number of plies: 4
- Nominal thickness of lamina: $t_f$ = 0.0066 in (0.167 mm)
- Ultimate tensile strain: $\varepsilon_{fu}$ = 1.2%
- Modulus of elasticity: $E_f$ = 33360 ksi (230 GPa)

The calculations for each of the cases above can be found in Appendix A.  Table 5-2 presents the results along with the cross-section geometry and longitudinal steel reinforcement ratio $\rho_s$ per each specimen.  As it can be seen in Table 5-2, the results obtained from each of the guidelines are presented as normalized by the compressive strength of unconfined concrete $f'_c$, and the strain of unconfined concrete at peak stress $\varepsilon'_c$, which was assumed as the commonly accepted value of 0.002.

Regarding predictive equations for the maximum usable axial strain $\varepsilon'_{cc}$, not all the guidelines provide expressions for its determination, for that reason such cases are addressed as Not Applicable (NA) in the table of results.

Figure 5-5 and Figure 5-6 show the normalized confined compressive strength and maximum usable axial strain, respectively.  In the first plot, the tendency of the curves from ACI, TR 55, and fib are in agreement with the general acknowledge that for approximately the same FRP volumetric ratio, the increment of confined compressive strength for prismatic cross-section, in particular rectangular, is less efficient than for the case of circular cross-sections.

With regards to the outcomes corresponding to the circular cross-section specimen, it is observed good agreement between TR 55 and fib_practical, meanwhile ACI exhibits a lower strengthening ratio.

Within the prismatic specimens, it can be observed the decline in the gain of confining strength of the specimens of rectangular cross-section with respect to the square.  This is noted for all the cases except the values provided by CSA.  In this particular case, the values corresponding to the specimens of rectangular cross-section show a slightly higher level of strengthening, and this is due to the fact that the computation of the confining pressure is dictated

by the equivalent circular cross-section whose diameter is the minimum dimension of the prismatic cross-section (CSA-A.23.3-94), in other words, it is similar to confining smaller circular cross-sectional columns with the same amount of FRP reinforcement, which explains the increasing tendency of the strengthening ratio.

ACI and fib_exact concur in the case of the rectangular specimen, whilst TR 55 and fib_practical provide lower strengthening ratios. Note that according to the practical equations of fib the four plies of CFRP prescribed in this example do not provide any strengthening.

Regarding the values corresponding to the specimen of square cross-section, most of the guidelines coincide in a strengthening ratio ranging from 1.2 to about 1.4, with the exception of the exact formulas from fib.

With respect to Figure 5-6, only ACI and fib guidelines provide equations for the maximum usable axial strain. Recall that the approach presented by ACI is focused on the maximum compressive strength and its related axial strain, meanwhile fib allows computing the parameters for the ultimate condition, and this is based depending upon the model adopted by each guideline.

**Table 5-2  Performance of Guidelines Predictive Equations for Confined Compressive Strength of RC Columns of Different Cross-Section Shapes**

| Guideline | Circular $D = 20$ in $A_g = 314$ in$^2$ $\rho_s = 1.53\%$ | | Square 18 x 18 in $A_g = 324$ in$^2$ $h/b = 1$ $\rho_s = 1.48\%$ | | Rectangular 12.5 x 25 in $A_g = 313$ in$^2$ $h/b = 2$ $\rho_s = 1.56\%$ | |
|---|---|---|---|---|---|---|
| | $f'_{cc}/f'_{co}$ | $\varepsilon'_{cc}/\varepsilon'_c$ | $f'_{cc}/f'_{co}$ | $\varepsilon'_{cc}/\varepsilon'_c$ | $f'_{cc}/f'_{co}$ | $\varepsilon'_{cc}/\varepsilon'_c$ |
| ACI | 1.50 | 3.35 | 1.30 | 2.35 | 1.22 | 2.00 |
| CSA | 1.33 | NA | 1.37 | NA | 1.39 | NA |
| TR 55 | 2.07 | 5.00 | 1.20 | NA | 1.06 | NA |
| fib_exact | 2.04 | 16.85 | 1.59 | 13.15 | 1.20 | 9.90 |
| fib_practical | 1.74 | 9.00 | 1.34 | 7.00 | 1.00 | 5.50 |

Note: 1 in = 25.4 mm; 1 in$^2$ = 645 mm$^2$
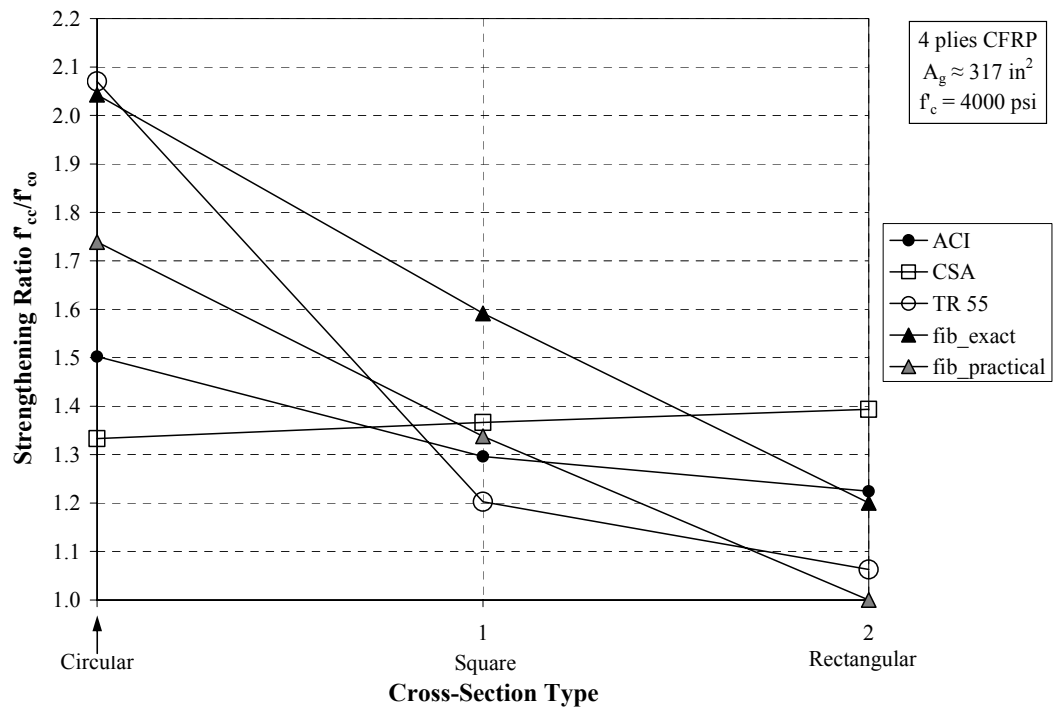
**Figure 5-5  Strengthening Ratio vs. Cross-Section Shape**
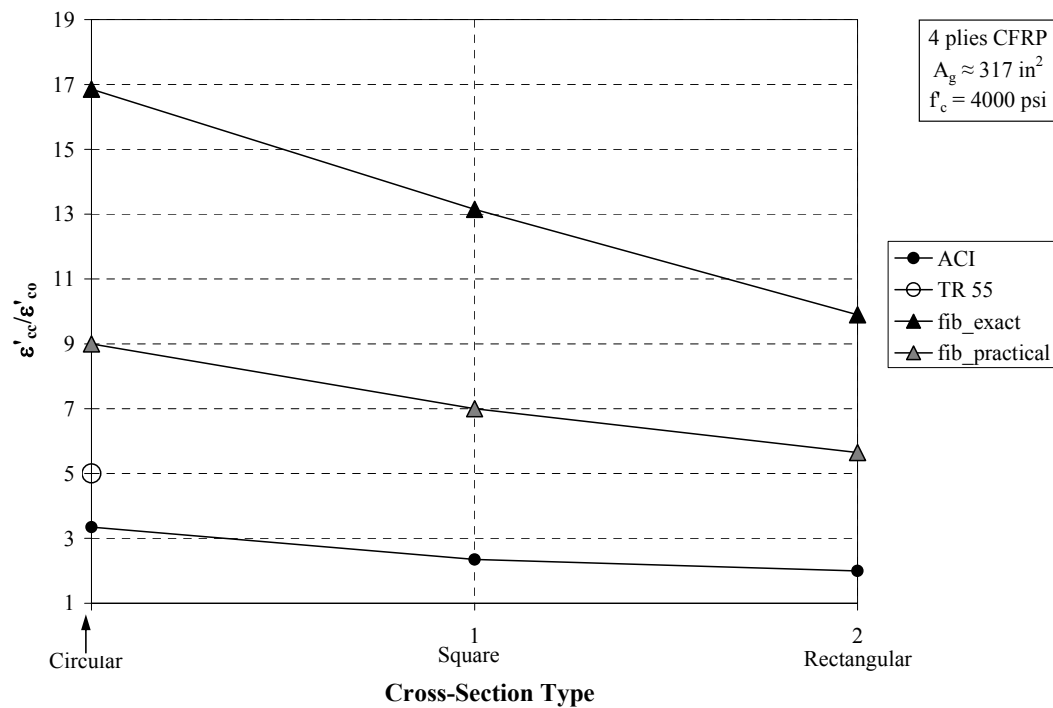


**Figure 5-6  Axial Strain Ratio vs. Cross-Section Shape**

# 6. EXPERIMENTAL PROGRAM

This section describes the experimental program performed on the RC column specimens. Section 6.1 presents the test matrix, Section 6.2 provides technical information regarding the materials used in the experiments, Section 6.3 presents the details of the construction and strengthening of the specimens, and 6.4 refers to the specimens instrumentation and test setup.

## 6.1. TEST MATRIX

The test matrix was designed to investigate the influence of different variables: side aspect ratio (b/h), area aspect ratio (based on an area of 18 x 18 in [460 x 460 mm]), and height-to-side aspect ratio (H/h). The experimental program was divided into two matrices based on the laboratories where the experiments were carried out: CALTRANS Seismic Response Modification Device Testing Laboratory (SRMD) at the University of California San Diego (UCSD) with eighteen specimens (six series of three specimens each: A, B, C, D, E, and F), and the Building and Fire Research Laboratory at the National Institute of Standards and Technology (NIST) with four specimens (two series of two specimens each: G and H).

The total matrix of 22 RC columns consisted of specimens whose dimensions were selected as follows: the testing machine at UCSD dictated a specimen height limitation of 5 ft (1.5 m), therefore a height-to-side ratio of 2:1 was selected, otherwise a higher ratio would have compromised the dimension of the smaller cross-section specimens necessary to the study of the size effect. With this ratio, the largest of the column specimens tested at UCSD featured a 25.5 x 25.5 in (65 x 65 cm) cross-sectional area and 54 in (1.5 m) of height (series D). As already mentioned, to study the confinement effect in prismatic specimens when compared to circular ones, specimens of circular, rectangular, and square geometry, and of gross area section half of the one corresponding to series D, were included in the matrix (series A, B, and C, respectively); note that the same height-to-side ratio was kept constant. To complement the variation on the size of the gross area section, two series of specimens of 12.75 x 12.75 in (324 x 324 mm) were introduced, which are series E and F, respectively; the height-to-side ratio for series F was twice the original value. Finally, the largest specimens of square and rectangular geometry were defined with cross-sectional areas of four times the ones from series B and C, correspondingly; the height-to-side ratio remain constant. Very slight variations in the dimensions of the specimens were considered necessary due to constructability issues, for such reason, for some series of specimens the height-to-side ratio varies in between 2.2 and 2.1.

Each of the series of specimens are depicted in Table 6-1, which in the first and second column presents the specimens geometry, dimensions, longitudinal steel reinforcement ratio $\rho_l$, and the cross-section gross area $A_g$. The third column shows the corresponding side aspect ratio for each series of specimens, this parameter varies between 1 and 1.5. The fourth and fifth columns show the ratio of the gross area section of each specimen to an area base of 18 x 18 in (475 x 475 mm), and the height-to-side aspect ratio, respectively. Finally, the last column, divided in two sub-columns, present the specimens labeling and the corresponding number of CFRP plies applied for the strengthening.

Each series or group of specimens with exception of G and H consists of three specimens. In each of these series of large specimens, a first column (G1 and H1) was considered as control

(no plies) and the second one was strengthened in order to attain a 30 percent increment of the carrying capacity using a full wrapping scheme (G2 and H2).  The specimens in group A (circular specimens) were divided as follows: one as a bench mark or control (A1), a second one strengthened in order to achieve a 30 percent increment of carrying capacity (A2 – full wrapping), and a third one strengthened to achieve the same percentage of increase but with a partial wrapping scheme (A3).  With regards to the rest of the groups (B, C, and D), one specimen for each group was the bench mark (B1, C1, and D1), the number of plies of CFRP in the second specimens varied in order to attain same increment of loading capacity (B2, C2, D2 – all fully wrapped), and the thickness of the FRP jacket of the third specimens was kept constant matching the same number of plies used in the circular specimen A2 (B3, C3, D3 – all fully wrapped).  Concerning groups E and F, their first specimens were control, second and third ones were strengthened to increment their capacity 30 percent as well, with the sole difference of the wrapping format: full for E2 and F2, and partial for E3 and F3.

Regarding the wrapping scheme of all the strengthened specimens, a gap of about ¼ in (6.5 mm) was left at the top and bottom ends between the edge itself and the fabric in order to avoid axial compressive loading of the FRP jacket.  The partially wrapped specimens featured 5.25 in (133.5 mm) strips width and 3 in (76 mm) of clear spacing.

## 6.2.    MATERIALS PROPERTIES

**6.2.1.  Concrete.**  It was considered appropriate a nominal concrete compressive strength of 4,000 psi (28 MPa) for the entire test matrix representing the common strength in current building structures.  Since the specimens were cast at two different locations, the concrete constituents and properties are discussed separately.

All of the specimens at UCSD were built up from one single batch of ready-mix concrete having constituents and mix proportions as follows: Portland cement 478 lb/yd$^3$ (284 kg/m$^3$), fly ash 90 lb/yd$^3$ (53 kg/m$^3$), ½ in (12.5 mm) coarse gravel 1150 lb/yd$^3$, 3/8 in (9.5 mm) coarse gravel 521 lb/yd$^3$ (309 kg/m$^3$), sand 1242 lb/yd$^3$ (737 kg/m$^3$), water 350 lb/yd$^3$ (208 kg/m$^3$), admixture WRDA-64 17 lb/yd$^3$ (10 kg/m$^3$), and 2 percent entrained air.  Standard concrete cylinders 6 x 12 in (152 x 305 mm) were prepared and cured under the same conditions of the columns.  These cylinders were tested according to ASTM C39-04 at 7, 14, 21, 28 days, and at the corresponding age at which the related columns were tested (three cylinders per each case).  The average compressive strength for the characteristic ages were 2.92 ksi (20.1 MPa), 3.44 ksi (23.7 MPa), 3.81 ksi (26.3 MPa), and 4.43 ksi (30.5 MPa), respectively.   These results are shown in Table 6-2 along with the compressive strengths of the cylinders of later ages and their corresponding average, standard deviation (SD), and coefficient of variation (CV) values.  In Figure 6-1 it is shown a plot of the cylinders compressive strength versus their corresponding ages (days), as well as the best fitting curve to be used later for the analysis of experimental results.  The scatter observed for ages beyond 28 days are considered as "natural" for the concrete being a non-homogeneous material and factors as the curing temperature and humidity affect its behavior.  The completion of the testing took approximately two weeks, and in most of the cases, two columns were tested per day.  The order of the testing was dictated only for the height of the specimens that required a slight modification of the test set up (the displacement of the top cross-beam of the testing machine), it started with the tallest specimens (group B) and finished with series E (Table 6-3).

**Table 6-1 - Test Matrix; Total of 22 Specimens**

| Specimen Cross-section Type and Dimension | Height (in) | Side Aspect Ratio (h/b) | Area Aspect Ratio (Area/Area $_{18x18}$) | Height Aspect Ratio (H/b) | Specimens Code & No. Plies | |
|---|---|---|---|---|---|---|
| $\rho_l = 1.53\%$ <br> 20 in circle <br> Area: 314 in$^2$ | 44 (3.7ft) | 0 | 1 | 2.2 | A1 | 0 |
| | | | | | A2 | 2 |
| | | | | | A3* | 4 |
| $\rho_l = 1.56\%$ <br> 12.5 in × 25 in <br> Area: 312 in$^2$ | 54 (4.5ft) | 2 | 1 | 2.2 | B1 | 0 |
| | | | | | B2 | 7 |
| | | | | | B3 | 2 |
| $\rho_l = 1.48\%$ <br> 18 in × 18 in <br> Area: 324 in$^2$ | 40 (3.3ft) | 1 | 1 | 2.2 | C1 | 0 |
| | | | | | C2 | 4 |
| | | | | | C3 | 2 |
| $\rho_l = 1.48\%$ <br> 25.5 in × 25.5 in <br> Area: 650 in$^2$ | 54 (4.5ft) | 1 | 2 | 2.1 | D1 | 0 |
| | | | | | D2 | 5 |
| | | | | | D3 | 2 |
| $\rho_l = 1.53\%$ <br> 12.75 in × 12.75 in <br> Area: 162 in$^2$ | 27 (2.25ft) | 1 | 0.5 | 2.1 | E1 | 0 |
| | | | | | E2 | 2 |
| | | | | | E3* | 4 |
| $\rho_l = 1.53\%$ <br> 12.75 in × 12.75 in <br> Area: 162 in$^2$ | 54 (4.5ft) | 1 | 0.5 | 4.2 | F1 | 0 |
| | | | | | F2 | 2 |
| | | | | | F3* | 4 |
| $\rho_l = 1.50\%$ <br> 36 in × 36 in <br> Area: 1296 in$^2$ | 78 (6.5ft) | 1 | 4 | 2.2 | G1 | 0 |
| | | | | | G2 | 8 |
| $\rho_l = 1.52\%$ <br> 25 in × 50 in <br> Area: 1250 in$^2$ | 108 (9ft) | 2 | 4 | 2.2 | H1 | 0 |
| | | | | | H2 | 19 |

Notes: * Partially wrapped specimens; Groups G and H were tested at NIST and the rest at UCSD; 1 in = 2.54 cm; 1 ft = 0.3 m; 1 in$^2$ = 6.45 cm$^2$

**Table 6-2  Standard Concrete Cylinders Compressive Test Results and Ages; UCSD**

| Days | f'$_c$ (ksi) | | | Mean | SD | CV (%) |
|---|---|---|---|---|---|---|
| | **Cylinder 1** | **Cylinder 2** | **Cylinder 3** | | | |
| **7** | 2.91 | 2.97 | 2.88 | 2.92 | 0.05 | 1.57 |
| **14** | 3.54 | 3.35 | 3.43 | 3.44 | 0.10 | 2.77 |
| **21** | 3.77 | 3.80 | 3.87 | 3.81 | 0.05 | 1.35 |
| **28** | 4.57 | 4.48 | 4.25 | 4.43 | 0.17 | 3.72 |
| **31** | 4.24 | 4.23 | 4.31 | 4.26 | 0.04 | 1.02 |
| **32** | 4.19 | 4.37 | 4.49 | 4.35 | 0.15 | 3.47 |
| **33** | 4.41 | 4.19 | 4.30 | 4.30 | 0.11 | 2.56 |
| **37** | 4.32 | 4.45 | 4.47 | 4.41 | 0.08 | 1.85 |
| **38** | 4.60 | 4.74 | 4.82 | 4.72 | 0.11 | 2.36 |
| **39** | 4.43 | 4.72 | 4.48 | 4.54 | 0.16 | 3.41 |
| **40** | 4.46 | 4.38 | 4.49 | 4.44 | 0.06 | 1.28 |
| **41** | 4.51 | 4.40 | 4.84* | 4.46 | 0.08 | 1.75 |
| **46** | 4.64 | 4.68 | 4.86 | 4.73 | 0.12 | 2.48 |
| **47** | 4.38 | 4.75 | 4.82 | 4.65 | 0.24 | 5.08 |

<u>Note:</u> *Concrete cylinder not considered in the calculations; 1 ksi = 6.9 MPa



Figure 6-1 plot with fitted curve:

$$y = 1\text{E-}05x^3 - 0.0017x^2 + 0.1136x + 2.1884$$
$$R^2 = 0.9234$$
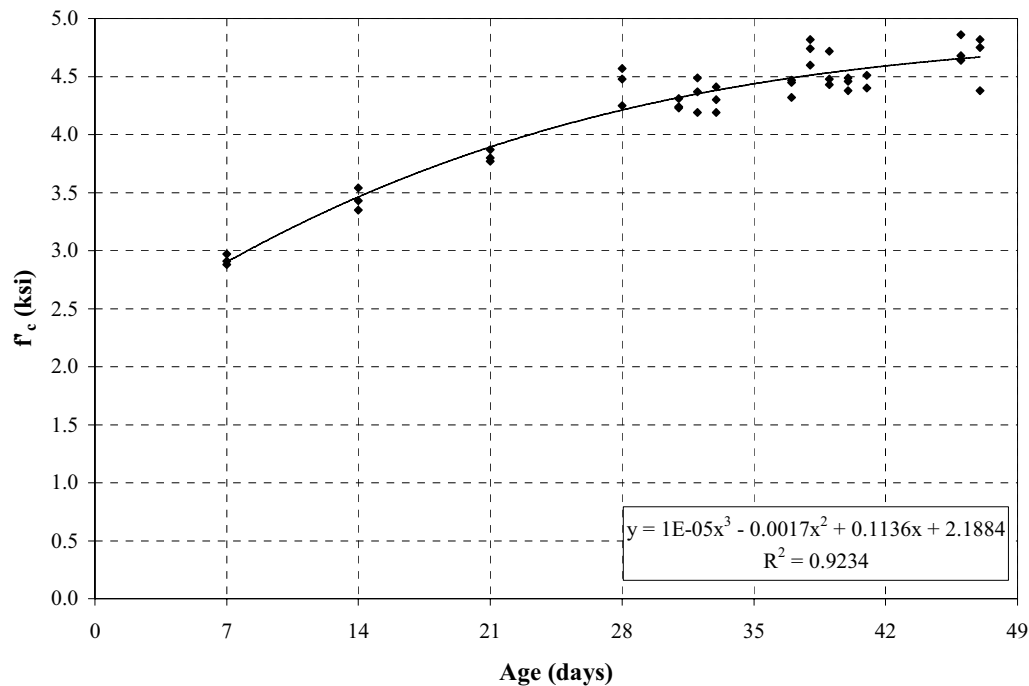
**Figure 6-1  Standard Concrete Cylinders Compressive Test Results vs. Ages; UCSD**

**Table 6-3  UCSD Specimens and Corresponding Testing Age and f'c**

| Age (days) | Specimens | f'c (ksi) |
|---|---|---|
| 31 | B1 | 4.37 |
| 32 | B2, B3 | 4.41 |
| 33 | D1, D3 | 4.45 |
| 34 | D2 | 4.48 |
| 37 | F1, F2 | 4.57 |
| 38 | A1, F3 | 4.60 |
| 39 | A2, A3 | 4.63 |
| 40 | C1, C3 | 4.65 |
| 41 | C2, E1 | 4.68 |
| 46 | E2 | 4.79 |
| 47 | E3 | 4.81 |

Note: 1 ksi = 6.9 MPa

Regarding the concrete for the specimens at NIST, its constituents and mix proportions were as follows: Portland Cement Type I-II 517 lb/yd$^3$ (307 kg/m$^3$), fine aggregate 1664 lb/yd$^3$ (987 kg/m$^3$), coarse aggregate (#8 gravel) 1575 lb/yd$^3$ (934 kg/m$^3$), water 250 lb/yd$^3$ (148 kg/m$^3$), and High-Range Water Reducer (HRWR) 1.29 lb/yd$^3$ (0.77 kg/m$^3$).  Standard concrete cylinders were cast and tested at 7, 28 days (Figure 6-2) and at the time of the actual testing of the columns.  Due to the high congestion of the steel reinforcement at the top and bottom ends of the larger specimens (series G and H), a minimum slump of 8 in (20.3 cm) was considered appropriate for the concrete to flow through the steel grids.  Batch 1 corresponds to the rectangular specimens (Series H) and batch 2 to the square specimens (Series G).  The compressive strengths obtained for these batches along with their corresponding testing ages and statistical parameters (mean, SD, and CV) are presented in Table 6-4.



**(a) Casting of Standard Concrete Cylinders          (b) Compression Test**
**Figure 6-2  Concrete Material Characterization**

**Table 6-4  Standard Concrete Cylinders Compressive Test Results and Ages; NIST**

|  | Days | f'<sub>c</sub> (ksi) | | Mean | SD | CV (%) |
|---|---|---|---|---|---|---|
|  |  | Cylinder 1 | Cylinder 2 |  |  |  |
| Batch 1 (Series H) | 7 | 3752 | 3617 | 3685 | 95 | 2.59 |
|  | 28 | 4067 | 4213 | 4140 | 103 | 2.49 |
|  | 68 | 4439 | 4350 | 4395 | 63 | 1.43 |
| Batch 2 (Series G) | 7 | 3737 | 3891 | 3814 | 109 | 2.86 |
|  | 28 | 4463 | 4137 | 4300 | 231 | 5.36 |
|  | 64 | 4470 | 4710 | 4590 | 170 | 3.70 |

Note: 1 ksi = 6.9 MPa

**6.2.2.  Steel.**  Both UCSD and NIST specimens were designed with a Grade 60 (420 MPa) steel reinforcement at a longitudinal reinforcement ratio of approximately 1.5 percent. Table 6-5 shows the yielding strength of the material used in the specimens and their corresponding values for average, standard deviation (SD) and coefficient of variation (CV). These values were obtained from tensile tests on coupons performed according to ASTM A370.

**Table 6-5  Steel Reinforcement Bars Tensile Tests Results**

|  | Bar Size | f<sub>y</sub> (ksi) | | | Mean | SD | CV (%) |
|---|---|---|---|---|---|---|---|
|  |  | Bar 1 | Bar 2 | Bar 3 |  |  |  |
| UCSD | #3 (#10) | 65.50 | 64.48 | 65.75 | 65.24 | 0.67 | 1.03 |
|  | #5 (#16) | 64.20 | 63.79 | 66.44 | 64.81 | 1.43 | 2.20 |
|  | #7 (#22) | 64.73 | 64.58 | 64.94 | 64.75 | 0.18 | 0.28 |
| NIST | #3 (#10) | 60.88 | 59.95 | 58.80 | 59.88 | 1.04 | 1.74 |
|  | #4 (#13) | 81.50 | 82.84 | 83.50 | 82.61 | 1.02 | 1.23 |
|  | #8 (#25) | 100.00 | N/A | N/A | 100.00 | 0.00 | 0.00 |

Note: 1 ksi = 6.9 MPa

Bars size #3 (#10) were used for the ties along the entire column in UCSD specimens and only in the central part in the NIST specimens, bars #4 (#13) were used as ties and cross-ties only in the NIST specimens at the bottom and top ends and they do not enter in the evaluation of the test performance, finally bars #5 (#16), #7 (#22), and #8 (#25) were used as longitudinal reinforcement.  The steel reinforcement layout for the UCSD and NIST specimens can be found in Appendix B and C, respectively.

**6.2.3.  Carbon FRP.**  The wrapping material for the entire research project was produced and provided my MAPEI S.p.A., Milan, Italy.  The method used for its application is known as wet lay-up, meaning that the dry fabric is placed directly on the concrete surface where a layer of saturant (epoxy resin) has been previously applied, and a second layer of the same saturant is applied on top for a complete impregnation of the fibers.

The materials composing the system are the following (Figure 6-3):

- Mapewrap C UNI-AX 300/40, which is a uni-directional continuous carbon fiber fabric with a high modulus of elasticity and high tensile strength. The designations "300/40" in the trade name of the fibers refer to the weight 300 g/m$^2$ (0.06 lb/ft$^2$), and the height of the roll 40 cm (15.75 in), respectively
- Mapewrap Primer 1, epoxy resin for the treatment of the substrate
- Mapewrap 11, or putty, it is a smoothing compounds to level any rough areas or to seal porous surfaces
- Mapewrap 31, or saturant, this is an impregnating agent for fabrics



**Figure 6-3  Layout of MAPEI FRP Material Components**

Tensile coupon tests were performed in order to determine the mechanical properties of the CFRP material used in the evaluation of the test results.  For the preliminary design, the mechanical properties provided by the manufacturer were used.  This characterization was conducted according to ASTM D3039-00 on a total of 15 specimens of one ply.  The coupons were cut out of a panel after complete curing, they were prepared by manual lay-up technique (as similar as possible to the actual application of the material on the column specimens) and having unidirectional fiber sheets.  These specimens were prepared by the same technician who wrapped the columns.  For the cutting of the specimens, the technique used was high-pressure water-jetting, which allows obtaining accurate dimensions.  Regarding the geometry of the specimens, as suggested by the standard, the coupons featured a final overall length of 10 in (254 mm) and a width of the coupons of 0.5 in (13 mm) (Figure 6-4).



10.0 in

0.5 in
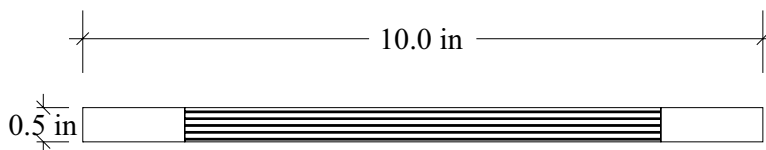
Note: 1 in = 25.4 mm

**Figure 6-4  CFRP Coupon Specimen**

Prior to the actual testing, an average width of each specimen was determined from three measurements at different locations along the gage length. This was done with the use of a caliper of 0.001 in (25 µε) of accuracy and the corresponding values are shown along with the results in Table 6-6.

The instrumentation used to measure the axial deformation of the coupon consisted of an extensometer of 1 in (25.4 mm) gage length, which was clamped to the center part of the coupon for the entire test. All coupons were tested in a 45 kip (200 KN) capacity Instron 4465 Universal Testing Machine. For an appropriate gripping of the specimens to the machine, grinded aluminum tabs were glued to both ends of each coupon using an epoxy based adhesive. Each test was conducted under displacement control at a loading rate of 0.05 in/min (2 mm/min) as suggested by the standard (Figure 6-5).
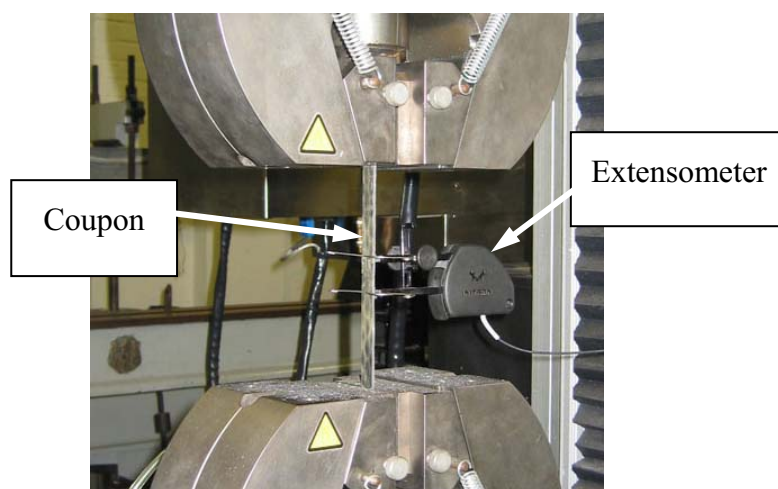


**Figure 6-5  Test Set Up of CFRP Tensile Coupon**

Table 6-6 summarizes the results obtained in terms of ultimate axial strain ($\varepsilon_{fu}$), ultimate tensile strength ($f_{fu}$) and modulus of elasticity ($E_f$). The tensile strength was computed based on the measured average width of the specimen and the nominal ply thickness (0.0066 in [0.167 mm]), which is the value based on the fiber area that is controlled during the manufacturing of the fabric; and the stiffness was computed in a strain range of 0.4 to 0.6 percent (the standard suggests a nominal difference between the two strain points of 0.002). For these parameters, the related average, standard deviation (SD), and coefficient of variation (CV %) values, are also indicated. From this experimental program average values of ultimate tensile strength of 377 ksi (2601 MPa), an ultimate axial strain of 0.93 percent, and a modulus of elasticity of 40.5 msi (280 GPa), were determined.

Regarding the observed failure modes, most of the specimens experienced lateral breakage at two locations, with the exception of specimens 1G where besides the lateral failure, longitudinal splitting was also observed. Only specimen 1J experienced an explosive failure in addition to one lateral breakage (Figure 6-6).

**Table 6-6  CFRP Tensile Mechanical Properties**

| Specimen | w (in) | $\varepsilon_{fu}$ (%) | $f_{fu}$ (ksi) | $E_f$ (msi) |
|---|---|---|---|---|
| 1A | 0.060 | 0.83 | 371.9 | 42.2 |
| 1B | 0.053 | 0.96 | 428.8 | 44.8 |
| 1C | 0.063 | 1.13 | 395.1 | 35.2 |
| 1D | 0.063 | 0.87 | 354.9 | 40.6 |
| 1E | 0.063 | 0.85 | 360.6 | 40.6 |
| 1F | 0.051 | 0.98 | 432.0 | 44.2 |
| 1G | 0.049 | 1.08 | 401.4 | 39.1 |
| 1H | 0.054 | 0.85 | 335.3 | 39.3 |
| 1I | 0.057 | 0.93 | 382.7 | 37.6 |
| 1J | 0.059 | 1.11 | 469.1 | 42.2 |
| 1K | 0.058 | 0.72 | 287.4 | 39.4 |
| 1L | 0.054 | 0.96 | 366.1 | 38.9 |
| 1M | 0.057 | 0.89 | 362.7 | 40.2 |
| 1N | 0.063 | 0.78 | 329.4 | 45.0 |
| 1O | 0.054 | 1.04 | 377.7 | 38.6 |
| Average | | 0.93 | 377.00 | 40.53 |
| SD | | 0.12 | 44.95 | 2.76 |
| CV (%) | | 13.06 | 11.92 | 6.80 |

Notes: 1 in = 25.4 mm; 1 ksi = 6.9 MPa; 1 msi = 6.9 GPa



Lateral          Longitudinal                    Explosive
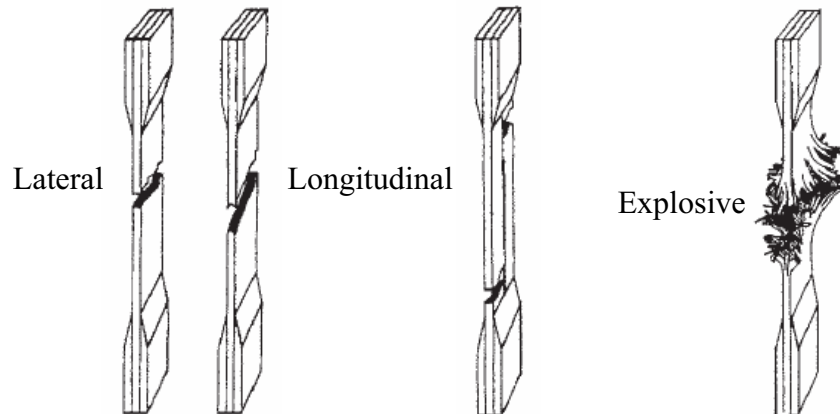
**Figure 6-6  Failure Modes CFRP Tensile Coupons (ASTM D3039)**

## 6.3. COLUMNS CONSTRUCTION AND STRENGTHENING

This section presents the construction (casting and wrapping) of the specimens as well as the instrumentation installed on the steel reinforcement and the FRP jacket.

**6.3.1. Construction.** The detailing (concrete cover, longitudinal bars layout, size, shape and spacing of ties, etc.) of all the specimens was designed according to conventional reinforced concrete practice as per the prescription of the American Concrete Institute (ACI 318-02). In order to prevent premature failure of the specimens at the top and bottom ends, the transverse reinforcement in all the specimens was added to all the specimens at these locations (Table 6-7 and Figure 6-7). All the drawings corresponding to the reinforcement and specimens construction details are available in appendices B and C for UCSD and NIST specimens, respectively.

Each corner of the columns was rounded to exceed the recommended minimum chamfer of ½ in (13 mm) (ACI 440.2R-02). In this research project, the forms of all the prismatic specimens were built so that the columns had a rounded corner with radius equal to 1.2 in (30 mm) as it can be seen in Figure 6-8. This allowed significant labor and time savings.

UCSD specimens (series A through F) were entirely constructed and instrumented (internal and external sensors) at the laboratory of the aforementioned university (Figure 6-9 and Figure 6-10). For details on the location of strain gages on longitudinal and transverse steel, and FRP jacket see Appendix B.

Regarding the larger specimens (series G and H), the steel reinforcement assembling and corresponding instrumentation installation (refer to Appendix C as well for location of strain gages) were performed at the laboratory of the University of Missouri – Rolla (Figure 6-11). The steel cages were transported to the laboratory at NIST for their casting and subsequent testing. Due to the steel layout (fairly congested at the top and bottom ends), as illustrated in Figure 6-7 and Figure 6-11, and the high probability of having large voids in the concrete, these specimens were cast horizontally (Figure 6-12).

**Table 6-7  Steel Reinforcement Bars per Series**

| Series | No. of Longitudinal Steel Bars and Size | No. of Transverse Steel Bars (Ties), Size and Spacing |
|--------|------------------------------------------|--------------------------------------------------------|
| A | 8#7 (8#25) | 2#3 @ 14 in (2#10 @ 35 cm) |
| B | 4#7 + 8#5 (4#22 + 8#16) | 4#3 @ 10 in (4#10 @ 25 cm) |
| C | 8#7 (8#22) | 2#3 @ 14 in (2#10 @ 35 cm) |
| D | 16#7 (16#22) | 2#3 @ 14 in (2#10 @ 35 cm) |
| E | 8#5 (8#16) | 2#3 @ 10 in (2#10 @ 25 cm) |
| F | 8#5 (8#16) | 2#3 @ 10 in (2#10 @ 25 cm) |
| G | 20#9 (20#29) | 3#3 @ 18 in (3#10 @ 46 cm)<br>13#4 @ 2 in (13#13 @ 5 cm)* |
| H | 24#8 (24#25) | 5#3 @ 16 in (5#10 @ 41 cm)<br>15#4 @ 2 in (15#13 @ 5 cm)* |

Note: *Transverse reinforcement at top and bottom ends for the columns. The metric bar size nomenclature is shown in between brackets
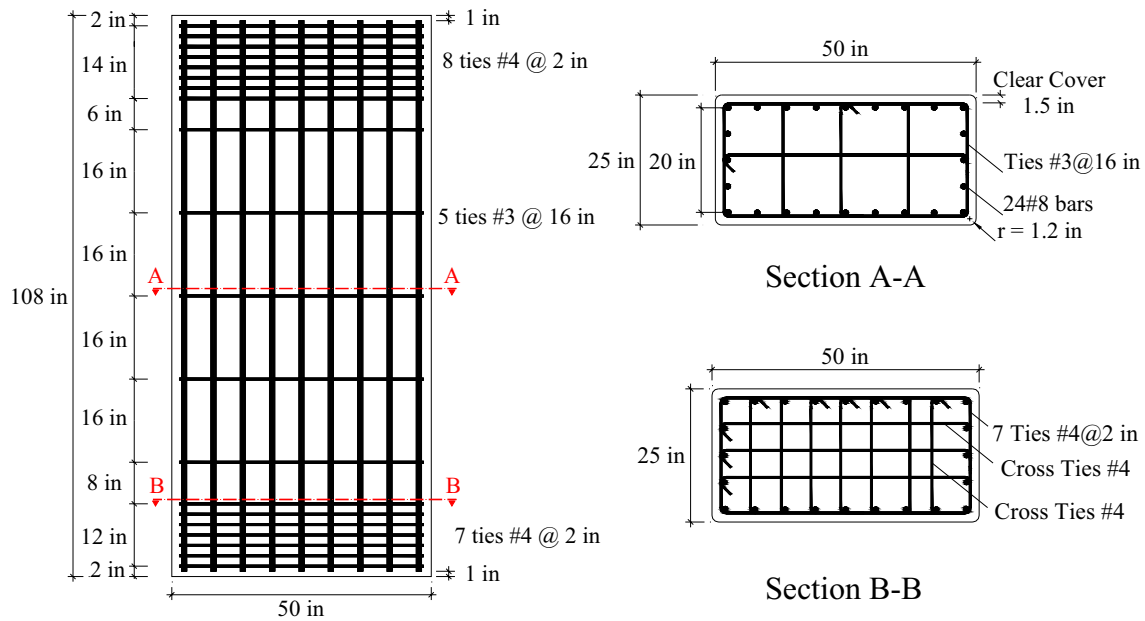
**Figure 6-7 Schematic of Reinforcement Layout; Series H Specimens**
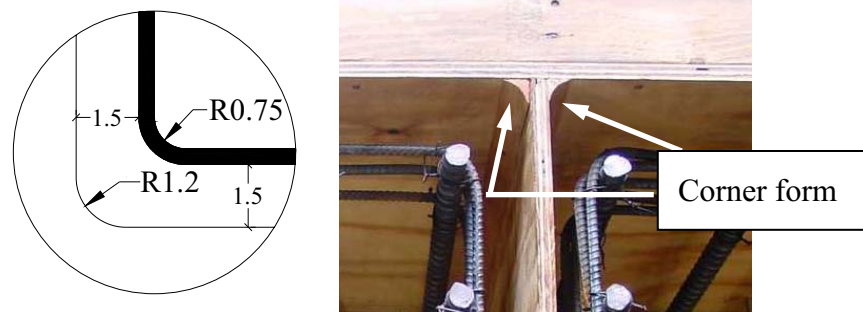


**Figure 6-8 Chamfer Detail for the Corners of All Prismatic Specimens**



**Figure 6-9 Steel Reinforcement for UCSD Specimens**

**Figure 6-10  Casting of Columns and Cylinders at UCSD**



**Figure 6-11  Layout of Steel Reinforcement; NIST Specimens**



**Figure 6-12  Concrete Pouring at NIST**

**6.3.2.  Strengthening.**  About the strengthening of the specimens, from a total of 22, eight specimens were control ones (no CFRP plies), three were partially wrapped (PW), and the remaining were fully wrapped.  The fiber orientation in all the cases was perpendicular to the longitudinal axis of the member.  For details on the wrapping schemes for the partially wrapped specimens see Appendix B.   The procedure followed for the wrapping of the columns is described next.

**6.3.2.1.   Preparation of the Specimens.**  The first step after removal of the forms included the grinding of the concrete surfaces, with leveling of rough areas and imperfections (Figure 6-13).



| (a) UCSD Specimen | (b) NIST Specimen |

**Figure 6-13 - Grinding of Concrete Surface**

Following the grinding, the surfaces of the specimens were cleaned from all loose particles.  Parallel to these activities, the fabric was cut to pre-determined widths (when applicable) and lengths to match the necessary number of plies as prescribed in the design (Figure 6-14).  Specimens for the partial wrapping were marked to indicate the position of the fabric.



**Figure 6-14  Layout and Cutting of the Fibers**

**6.3.2.2.   FRP Material Preparation and Installation.**  Recommendations provided by the manufacturer for this part of the process were followed.  They consisted of the following operational steps:

a. Mixing and application of Mapewrap Primer 1 components (Figure 6-15). The application was performed with a short nap roller on the cleaned concrete surface.

b. Mixing and application of Mapewrap 11 or putty component. The grey paste was spread on the concrete surface where a coat of primer had been previously applied. The purpose of this layer was to seal all the porous areas in the substrate (Figure 6-16).

c. Mixing and application of Mapewrap 31 saturant. A first coat was applied using a short haired roller on the concrete surface following the coats of primer and putty. Right after the first saturant layer, the carbon fabric was placed and flattened minimizing the appearance of wrinkles and bubbles. This was followed by a second coat of saturant over the fabric, using a ribbed roller and assuring the full impregnation of the fibers (Figure 6-17).



**Figure 6-15 Application of Mapewrap 1 Primer to Concrete Surface**



**Figure 6-16 Application of Mapewrap 11 (Putty)**

(a) First coat of saturant

(b) Placing the carbon fabric

(c) Rolling to eliminate bubbles

(d) Second coat of saturant

(e) Specimen near wrapping completion

(f) Specimen Completed

**Figure 6-17  Application of Saturant and Fabric**

## 6.4.    SPECIMEN INSTRUMENTATION AND TEST SETUP

In this section the instrumentation and test setup for each group of specimens are described.  Details regarding the number and location of the sensors on the steel reinforcement and on the FRP jacket are shown in appendices B (UCSD) and C (NIST).  For the actual testing of the specimens, additional external instrumentation such as potentiometers, Linear Variable

Differential Transducers (LVDT) and/or MTS Temposonic Linear Position Sensors, were attached to the sides of the specimens.

**6.4.1. UCSD Specimens.** The experiments were conducted with the SRMD six-degree of freedom shake table for the dynamic testing of full-scale bearings, isolators and dampers. The shake table is powered by computer-controlled hydraulic actuators that can apply up to 12,000 kip (53.4 MN) of vertical force. This machine has a height limitation and for this reason the specimens of series G and H were tested at NIST. The test setup was basically the same for all cases; the only variation was the height of different series of specimens to which the cross beam had to be adjusted, therefore series B, D and F of 54 in height (0.35 m) were tested first, followed by series A (44 in [1.12 m]), C (40 in [1 m]) and finally series E (27 in [0.7 m]).

In all the specimens, besides the strain gages on longitudinal steel bars and ties, and the ones on the FRP jacket, the two linear potentiometers were fixed to two opposite sides of each column (North and South sides) in order to measure the axial shortening. The distances anchor-to-anchor for the brackets of the potentiometers are shown in Table 6-8. Note that only one potentiometer was attached to column C2.

In addition to the potentiometers, four LVDTs were mounted on steel angles on each corner of the testing platen (NE, NW, SE, and SW) in order to record the overall cross-head displacement. A layer of hydrostone plaster (¼ to ½ in [6 to 13 mm]) was used as a self-leveling grout at the top or bottom specimen to reaction plate interface (Figure 6-18).

**Table 6-8 Anchor-to-Anchor Gage Lengths for Side-Attached Potentiometers for UCSD Specimens**

| Specimen | North Side (in) | South Side (in) |
|----------|-----------------|-----------------|
| A1 | 14.01 | 14.14 |
| A2 | 14.14 | 14.02 |
| A3 | 14.08 | 14.04 |
| B1 | 17.38 | 17.38 |
| B2 | 17.38 | 17.38 |
| B3 | 17.38 | 17.38 |
| C1 | 17.88 | 17.64 |
| C2 | 18.35 | N/A |
| C3 | 18.71 | 18.61 |
| D1 | 17.38 | 17.38 |
| D2 | 17.38 | 17.38 |
| D3 | 17.38 | 17.38 |
| E1 | 13.13 | 13.13 |
| E2 | 12.97 | 13.02 |
| E3 | 12.96 | 13.12 |
| F1 | 15.91 | 15.93 |
| F2 | 16.39 | 16.48 |
| F3 | 16.23 | 16.32 |

Note: 1 in = 25.4 mm

The load was applied concentrically under a displacement control rate of 0.001 in/sec (0.025 mm/s). The loading was conducted in five cycles in increments of one fifth of the expected capacity of each specimen; the minimum load level (unloading) corresponded to approximate five percent of the total expected capacity.
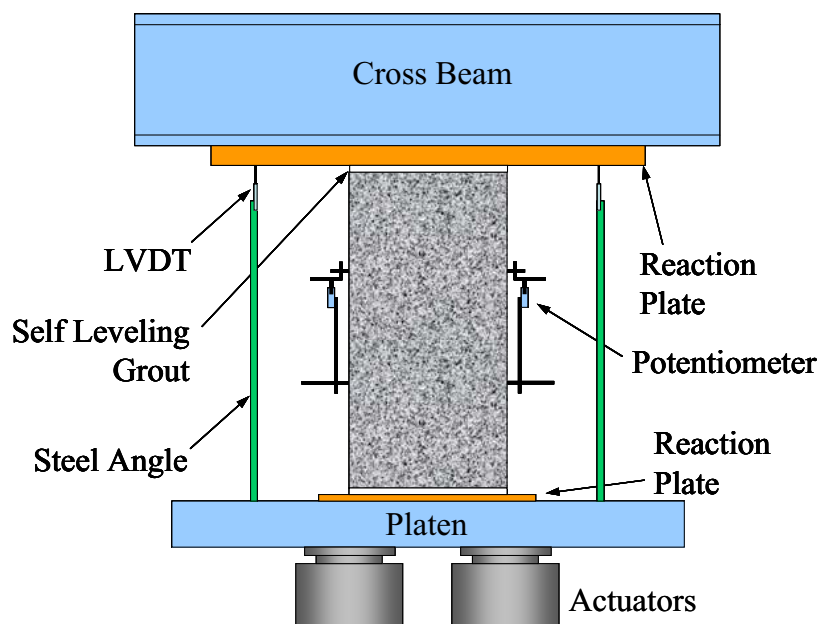


**Figure 6-18 - Instrumentation and Test Setup Schematic for UCSD Specimens**



**Figure 6-19 - Specimen E2 Setup at UCSD**

**6.4.2. NIST Specimens.** The testing of specimens of series G and H was conducted at the testing facility at NIST. The equipment consists of a Universal Testing Machine (UTM), and a 45 ft (13.7 m) high reaction buttress equipped with a horizontal hydraulic ram. A combination of 1012 kip (4.5 MN) horizontal force and 12,000 kip (53 MN) compressive vertical force may be applied to large-scale specimens. The hydraulic-operated UTM is the largest in North America, and is used to test large structural components and to calibrate very large capacity force-measuring devices. It can apply compression forces to column sections or fabricated members up to 59 ft (18 m) of height.

The specimens were centered on the platen and in order to assure leveled bearing surfaces, a ¼ to ½ in (6 to 13 mm) layer of hydrostone plaster was placed between column ends and platens. Linear transducers were mounted on the faces of the specimens and their location was slightly different for each of the columns (schematics of the layout of the linear transducers for these specimens are available in Appendix C). A total of five MTS Temposonic Linear Position Sensors were used to measure the axial shortening and the bulging during loading. The cross-head displacement readings were provided by the machine itself. The gage length for all the cases was 18 in (457 mm). For the case of the control square specimen G1, one sensor in the vertical direction was fixed to each face and one in the horizontal direction was fixed only on the East face. On the wrapped specimen of the same series (G2), three vertical transducers were fixed on East, North and South faces; also on each of the last two sides, one horizontal transducer was mounted. The transducers on the rectangular columns (H1 and H2) were set up the same way as for specimens G1, only the locations within each face varied. Figure 6-20 shows the test setup of specimen H2 as a typical case.

The application of the load was controlled manually in order to attain failure of the specimen within one hour, and the testing protocol consisted on five cycles in increments of one fifth of the expected capacity of each specimen, the minimum load level (unloading threshold) corresponded to approximately five percent of the total capacity or to a level that allowed the machine to remain engaged.
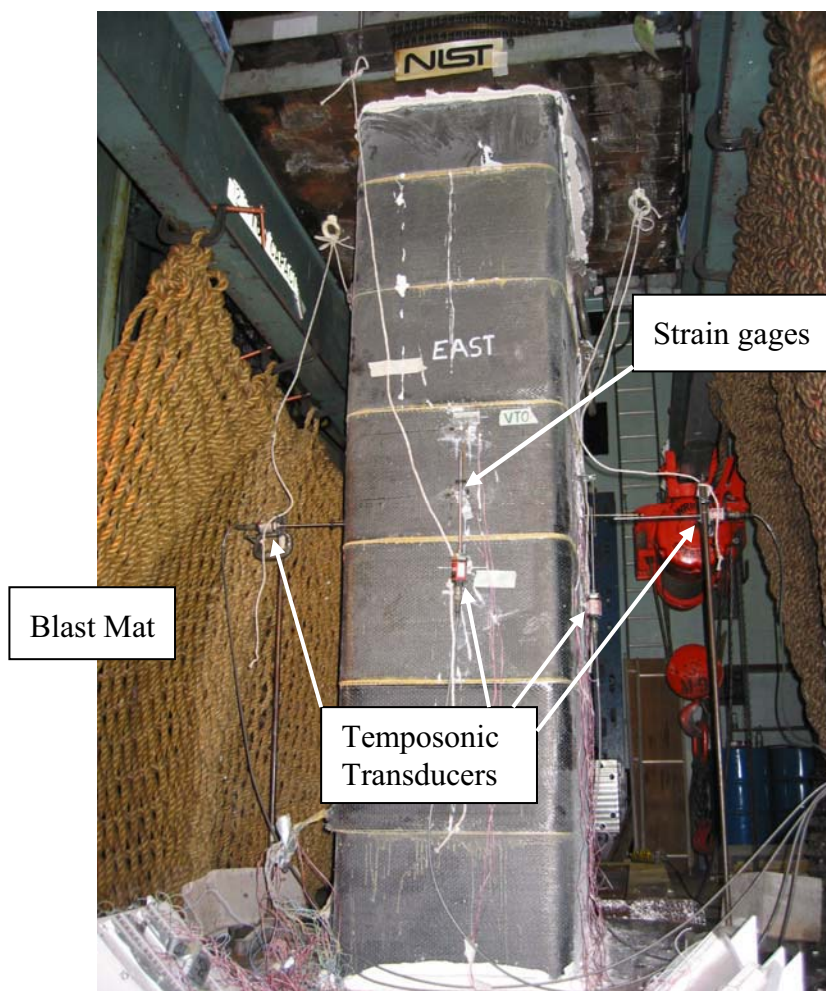
**Figure 6-20  Specimen H2 Set Up at NIST**

# 7. TEST RESULTS

The results from the experimental program are presented in this section. Each series of specimens is addressed individually, and within each group the following items are included:

- A table of key response parameters such as maximum loads, maximum axial compressive strengths, axial and transverse strains at peak stress and/or at failure
- Plots of applied axial load versus the axial deformation provided by the external instrumentation. This deformation is defined as the average displacement measured by the two linear transducers attached to the columns.
- Axial compressive strength versus axial strain and transverse strain provided by the external instrumentation.
- A description of the mode of failure observed for each specimen

Axial compressive strength versus the axial strains on the longitudinal reinforcement, and transverse strains on ties and FRP are shown in Appendix D. The axial compressive stress is defined as the compressive stress in the concrete, and in the plots presented in this section this parameter is approximated using the equivalent or transformed cross-sectional area (Equation 7-1).

$$f_c = \frac{P}{A_{transf}} = \frac{P}{A_c + n*A_s}$$

**7-1**

Where:
$f_c$ = Axial compressive stress
$P$ = Axial compressive load applied to specimen
$A_c$ = Cross-section area of concrete
$A_s$ = Cross-section area of longitudinal steel reinforcement
$n = E_s / E_c$
$E_s$ = Modulus of elasticity of steel = 29,000 ksi (200 GPa)
$E_c$ = Modulus of elasticity of concrete = $33 * \rho_c^{1.5} * \sqrt{f'_{co}}$
$\rho_c$ = Specific weight of normal concrete = 145 lb/ft$^3$ = 2.3 ton/m$^3$

This was done in order to take into consideration the presence of longitudinal steel reinforcement. The authors are aware of the fact that the validity of this equation is within the elastic range, and therefore, from the point where the axial strain in the longitudinal reinforcement reaches approximately 0.2 percent, the concrete compressive strength should be computed as $(P-A_s*f_y)/A_c$. Hence, in order to be consistent with the experimental data presented in Section 4, the maximum stress in the concrete used for comparisons is based in this last formula.

Regarding the axial and transverse or hoop strains, in the case of the control specimens, no transverse measurements were acquired, therefore are not presented. In the case of the strengthened specimens, the transverse strains actually correspond to the strains measured on the FRP jacket at mid-height, but they are interpreted as of transverse strains of the concrete. For the case of the specimens of circular cross-section this hoop strain is defined as the average of the measurements taken along the perimeter, and for the case of the square specimens, as the average

of the readings given by the sensors located at the center of each side. For the case of the specimens of rectangular cross-section, the transverse strain deformation is adopted from the sensors located on the long sides only.

It will be seen that some specimens required an extra sixth cycle to attain failure, in particular the control columns. The reason for this rely on the fact that the load-cycle prediction values were computed with the design nominal concrete compressive strength of 4 ksi (28 MPa), and the actual values of f'c in such specimens were above this value.

It is noted that due to the brittle and explosive nature of the failure of the specimens, it was not possible to closely observe the experiments, therefore all the information is based on videotapes and pictures taken during testing.

## 7.1. SERIES A; D = 20 in; H = 44 in (D = 508 mm; H = 1118 mm)

Table 7-1 presents the basic parameters resulting from the experiments on specimens of circular cross-section. This group was composed of three specimens: A1 (control), A2 (strengthened with two fully wrapped plies), and A3 (strengthened with four partially wrapped plies).

The FRP volumetric ratio ($\rho_f$) is included in the table along with the parameters below. The tables for the remaining series of specimens will have the same format, however a slight addition for the specimens of rectangular cross-section will be observed: the consideration of transverse strain on short and long sides.

| | |
|---|---|
| $P_{cc}$ | = Maximum applied axial load |
| $f'_{co}$ | = Maximum or peak concrete axial compressive stress for control specimens |
| $f'_{cc}$ | = Maximum or peak concrete axial compressive stress for strengthened specimens |
| $\varepsilon'_{co}$ | = Axial strain corresponding to $f'_{co}$ |
| $\varepsilon'_{cc}$ | = Axial strain corresponding to $f'_{cc}$ |
| $\varepsilon_{cu}$ | = Ultimate axial strain |
| $\varepsilon_{tc}$ | = Transverse strain at $f'_{cc}$ |
| $\varepsilon_{tu}$ | = Ultimate transverse strain |

**Table 7-1  Summary of Fundamental Response Parameters; Series A**

| | A1 | A2 | A3 |
|---|---|---|---|
| $\rho_f$ (%) | N/A | 0.26 | 0.34 |
| $P_{cc}$ (kips) | 1493 | 2014 | 2069 |
| $f'_{cc}$ (ksi) | 3.81 | 5.50 | 5.67 |
| $\varepsilon'_{cc}$ (με) | 2600 | 12284 | 7366 |
| $\varepsilon_{cu}$ (με) | 2600 | 12284 | 14692 |
| $\varepsilon_{tc}$ (με) | N/A | 8431 | 6632 |
| $\varepsilon_{ju}$ (με) | N/A | 8808 | 9953 |

Note: 1 kip = 4.45 KN; 1 ksi = 6.9 MPa

**7.1.1.  Specimen A1.**  Figure 7-1 and Figure 7-2 present the applied load versus the axial deformation, and the axial stress-strain behavior, respectively.  For a maximum load of 1493 kips (6641 KN), a compressive stress of 3.81 ksi (26.3 MPa), and a corresponding axial strain of 0.26 percent were achieved.  A sixth cycle was needed in order to attain failure.  No visible significant damage was observed up to the fifth cycle.  Regarding the failure of this column (Figure 7-3), vertical cracking developed running up to the top end.  Spalling of the concrete cover exposed buckled longitudinal reinforcement at the mid-section of the specimen.

**7.1.2.  Specimen A2.**  The applied load versus the axial deformation, and the stress-strain behavior are shown in Figure 7-4 and Figure 7-5, respectively.  For this case, the average transverse or hoop strain was also plotted.  This specimen presented a bi-linear stress-strain response featuring increment of axial deformation along with the carrying capacity.  Axial and transverse strains of 1.23 percent and 0.84 percent were observed at a peak compressive stress of 5.50 ksi (38 MPa).  The failure of the FRP jacket occurred mainly at two locations: on the upper part of the specimen the breakage started near the bracket position on the North side; and at mid-height the failure of the FRP was observed at the South-East side (Figure 7-6).  It is noted as well that the debonding of the FRP jacket occurred almost throughout the entire height of the specimen but for the bottom section (approximately one third of the total height).

**7.1.3.  Specimen A3.**  Figure 7-7 and Figure 7-8 present the axial load versus axial deformation, and the stress-strain (axial and transverse) response, respectively.  This specimen also showed a bi-linear stress-strain behavior, but on the contrary of the previous specimen, the increment was given only on the axial deformation, not on the carrying capacity.  In fact, at a load value of approximately 2000 kip (8900 KN) the axial resistance stabilized and slightly oscillated with the load application until reaching failure.  Axial and transverse strains of 0.74 percent and 0.66 percent were observed at a peak compressive stress of 5.67 ksi (39.1 MPa).  The ultimate measured axial strain was of 1.47 percent. The failure of this column could be classified as gradual, since the rupture of the FRP jacket occurred at different stages throughout the last loading cycle.  In this case, prior to the final breakage of the jacket at mid-height (North side), rupture of small strips was observed at three locations: two of them at about the same height level of the brackets used to fix the linear transducers, and one on the South face.  These premature breakages were followed by slight delaminations of such portions of the jacket at the corresponding locations (Figure 7-9).
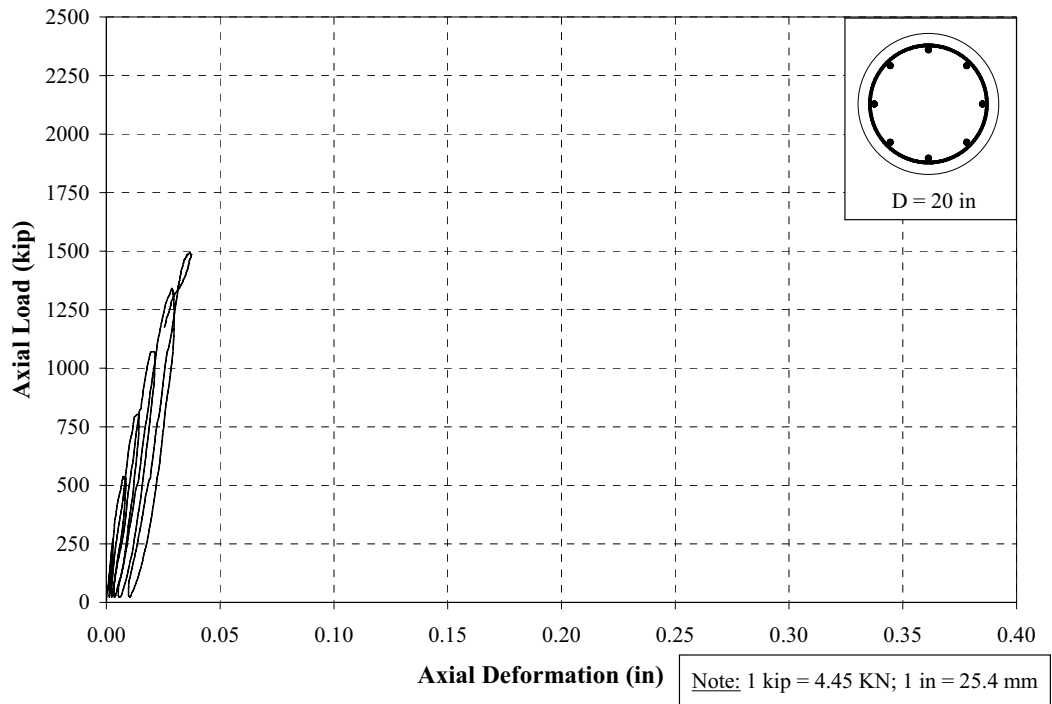
**Figure 7-1 Axial Load vs. Axial Deformation; Specimen A1**

Note: 1 kip = 4.45 KN; 1 in = 25.4 mm
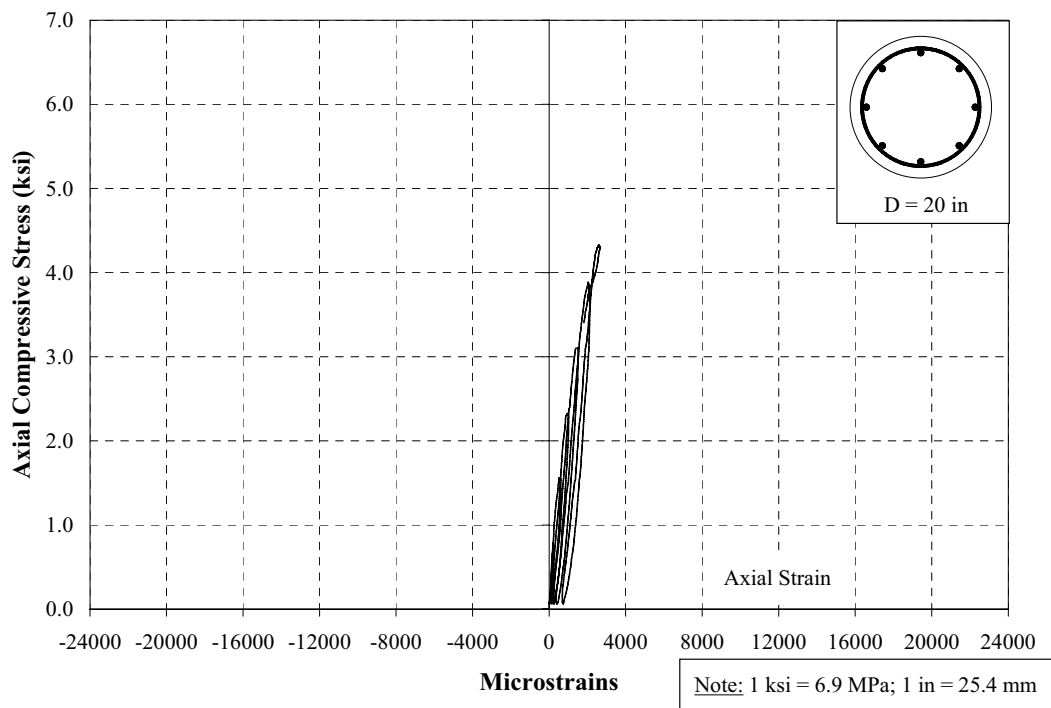


**Figure 7-2  Stress-Strain Behavior; Specimen A1**

Note: 1 ksi = 6.9 MPa; 1 in = 25.4 mm
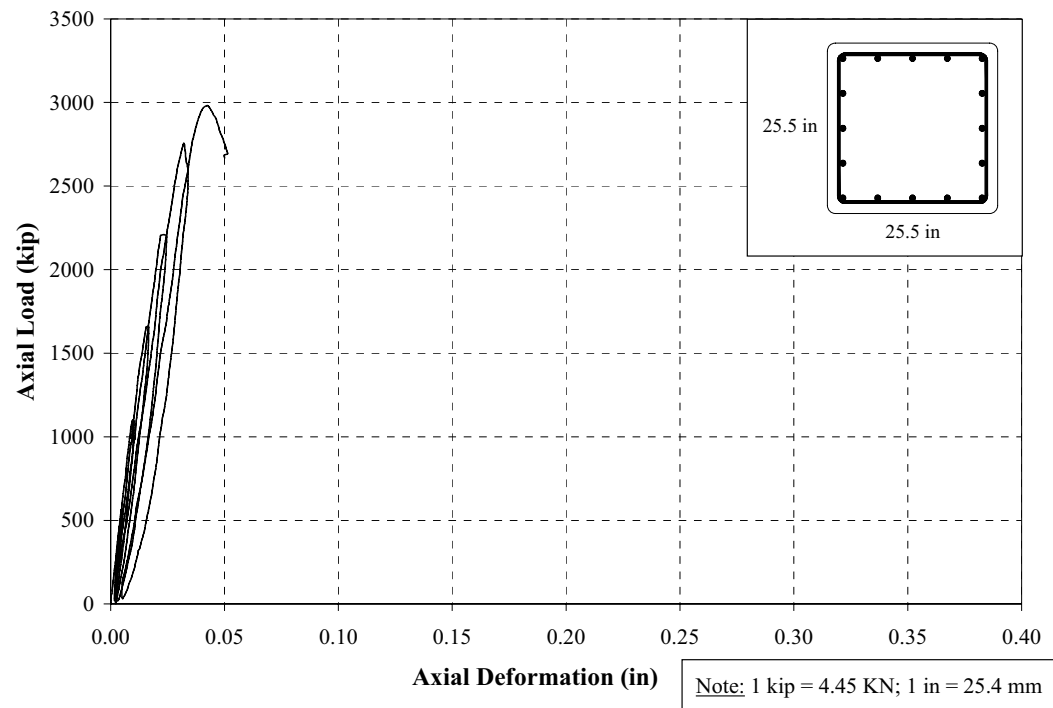
**Figure 7-3  Failure of Specimen A1**
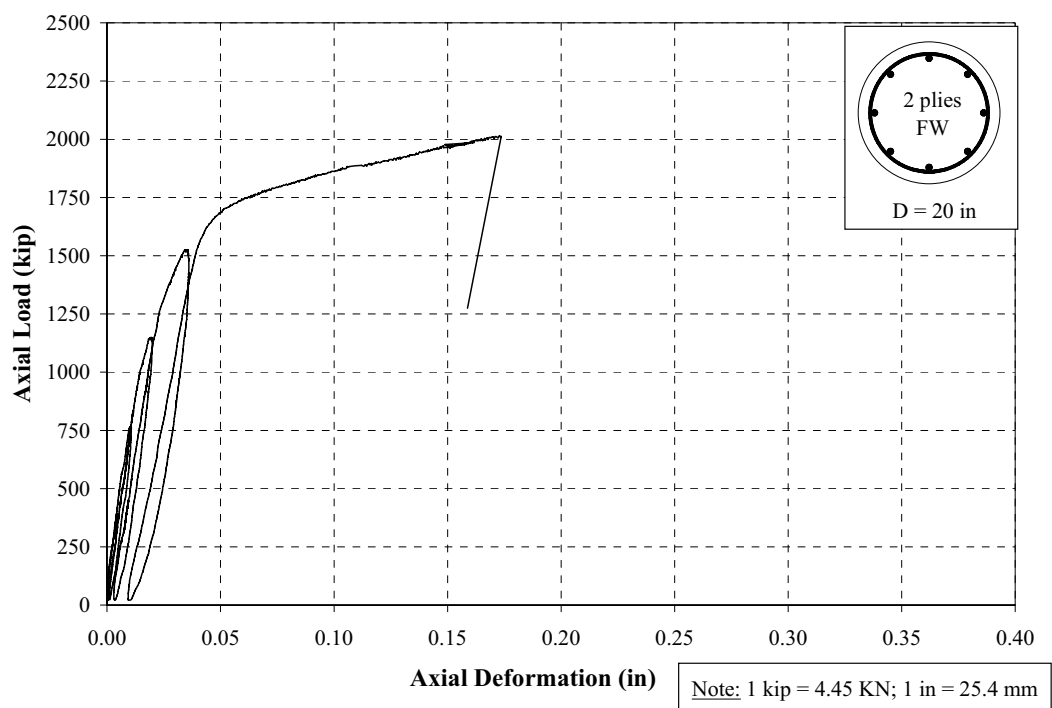


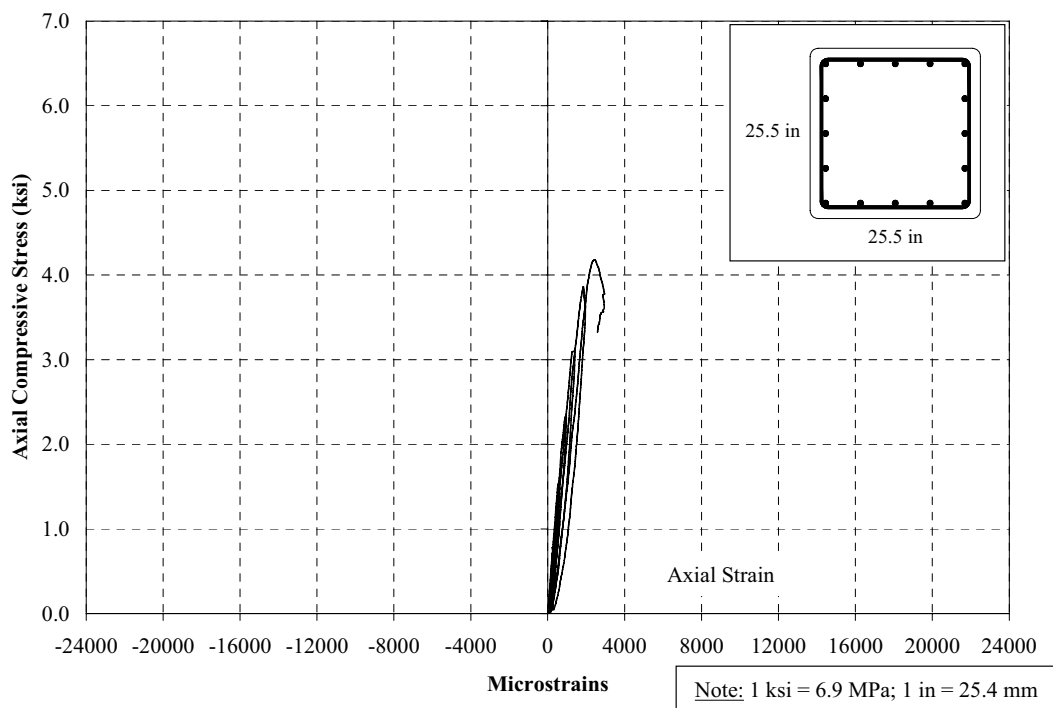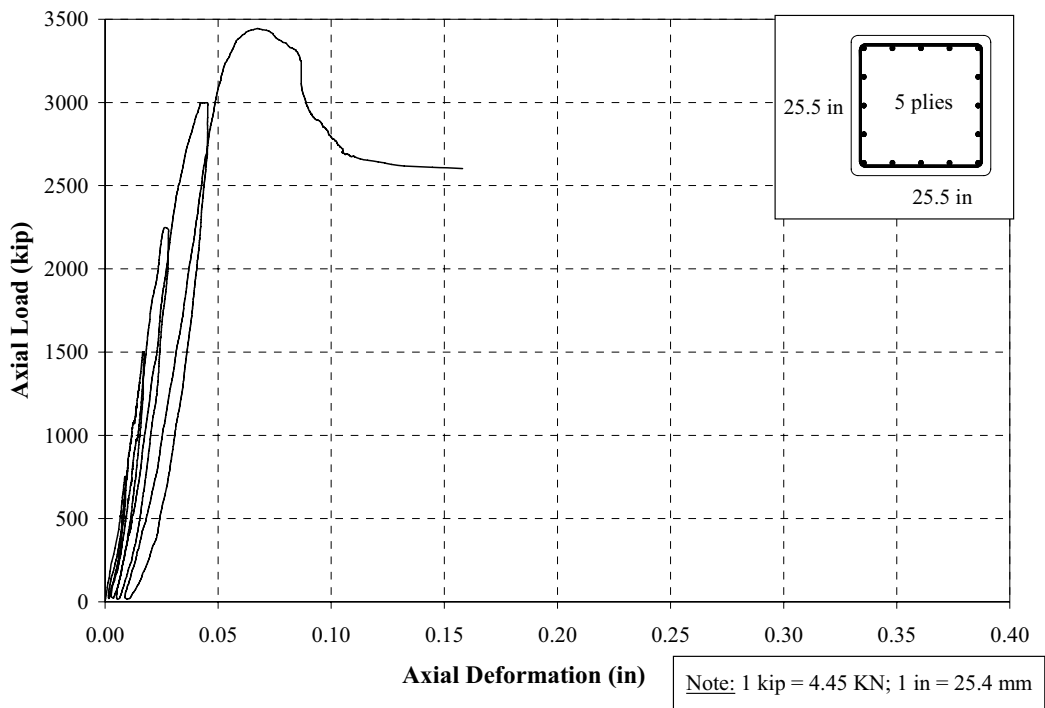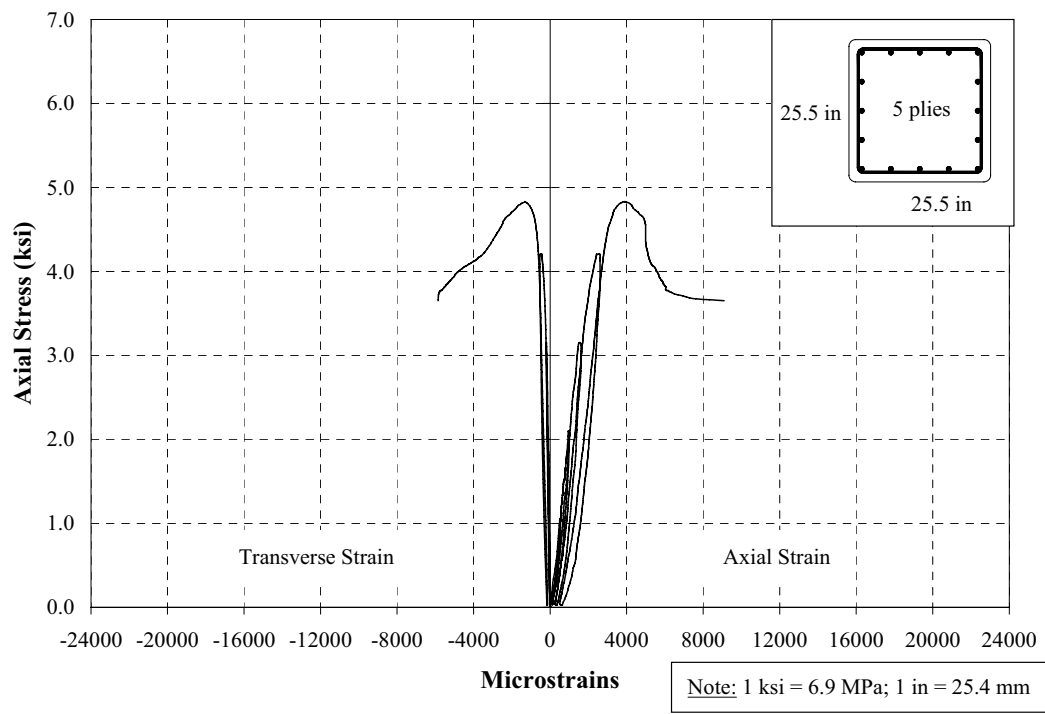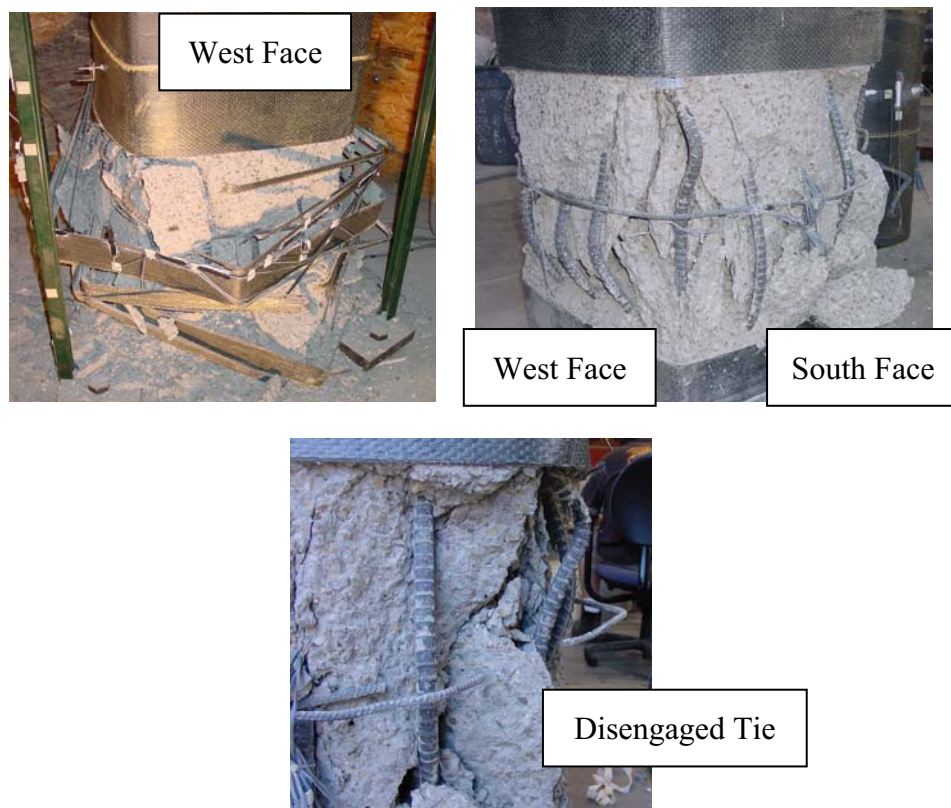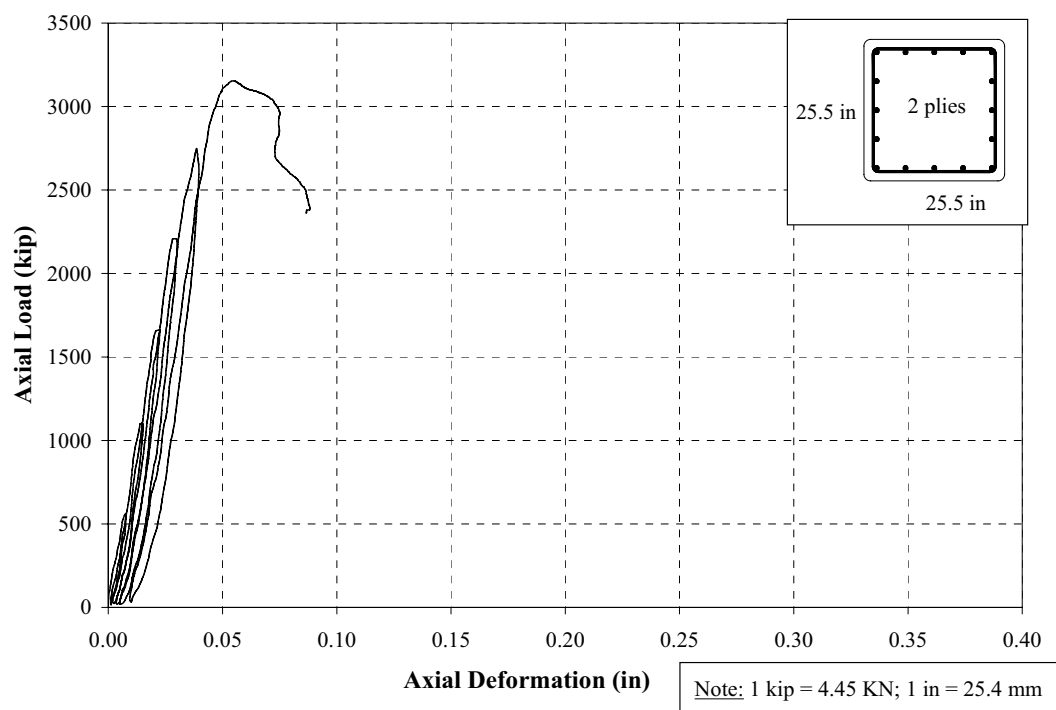**Figure 7-4  Axial Load vs. Axial Deformation; Specimen A2**
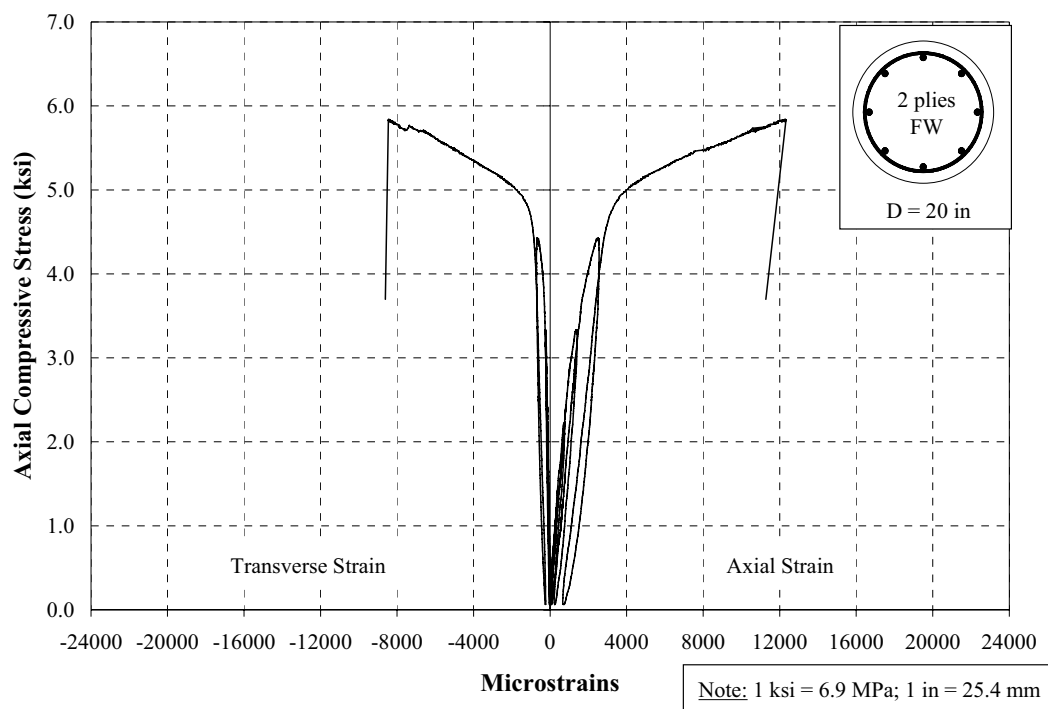
**Figure 7-5  Stress-Strain Behavior; Specimen A2**
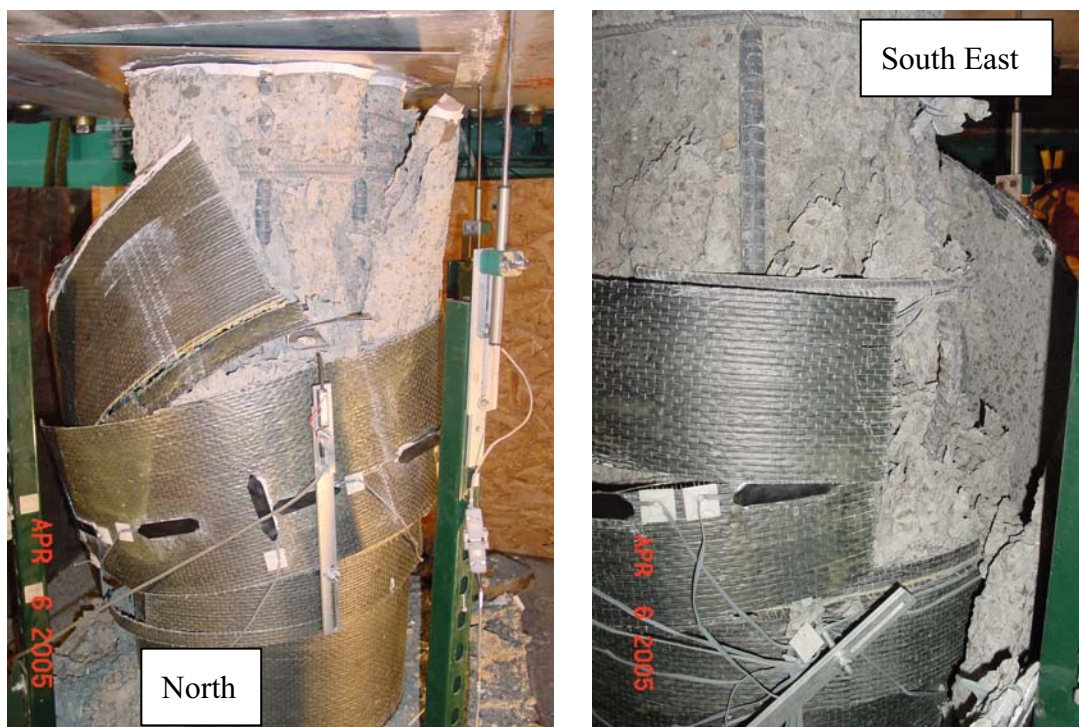


**Figure 7-6  Failure of Specimen A2**
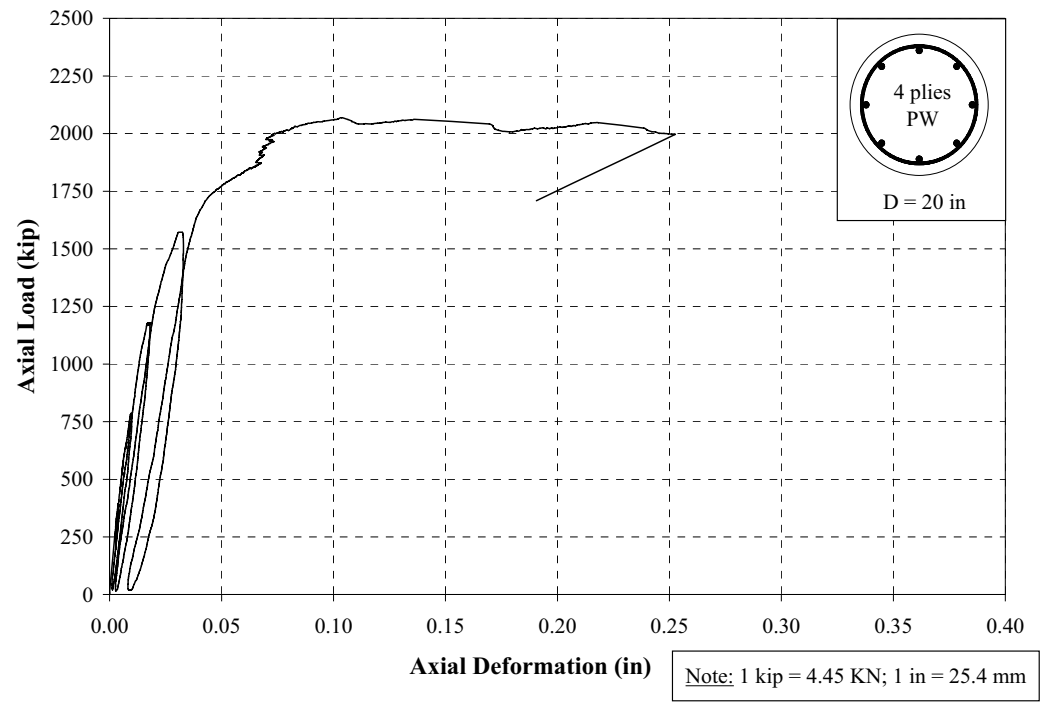
**Figure 7-7  Axial Load vs. Axial Deformation; Specimen A3**
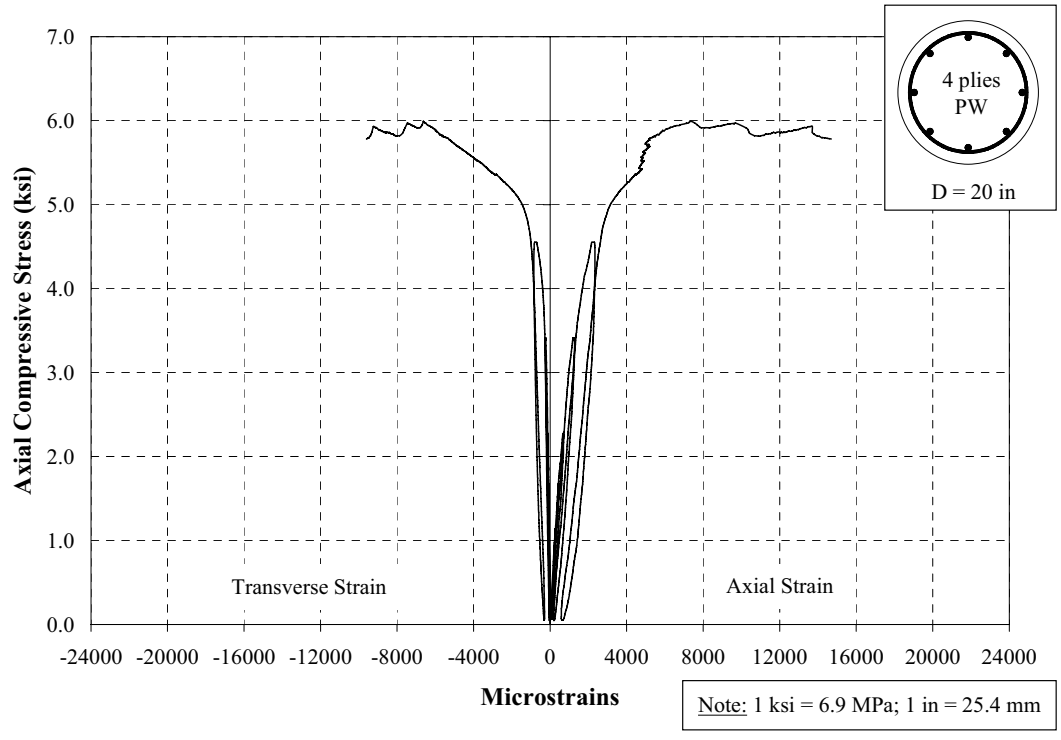


**Figure 7-8  Stress-Strain Behavior; Specimen A3**
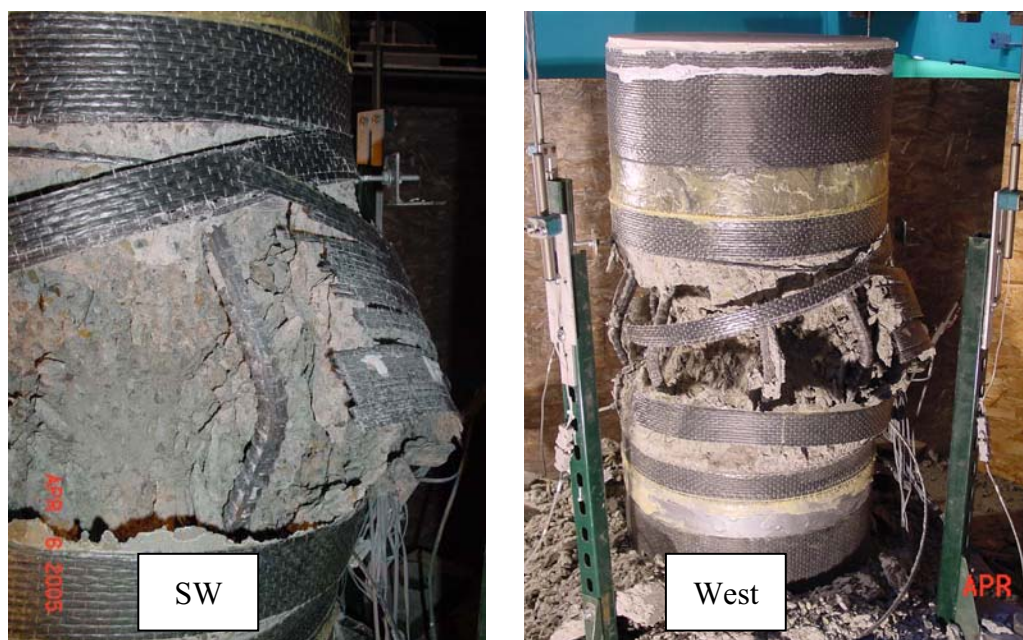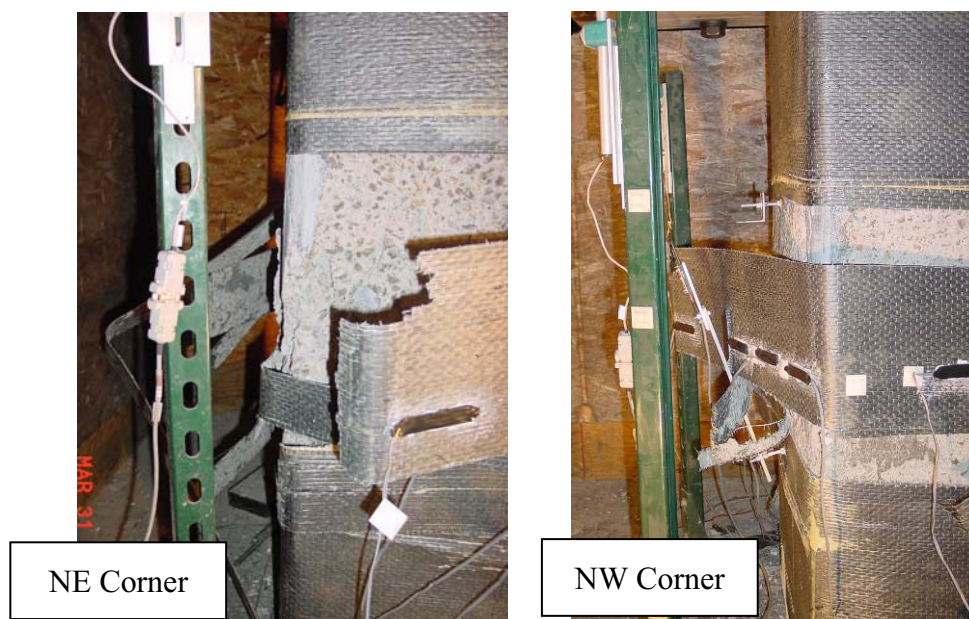
**Figure 7-9  Failure of Specimen A3**

## 7.2.    SERIES B; 12.5 x 25 x 54 in (318 x 635 x 1372 mm)

Table 7-2 presents the basic parameters resulting from the experiments on specimens of rectangular cross-section.  This group was composed of three specimens: B1 (control), B2 (strengthened with seven plies), and B3 (strengthened with two plies).

**7.2.1.  Specimen B1.**  Figure 7-10 and Figure 7-11 present the applied load versus the axial deformation and the axial stress-strain behavior, respectively.  For a maximum load of 1331 kips (5923 KN), a compressive stress of 3.30 ksi (22.8 MPa), and a corresponding axial strain of 0.15 percent were achieved.  Regarding the failure of this column, the spalling of the concrete cover was observed at the lower portion, particularly on the North side extending to the adjacent faces.  Same phenomenon was noticed on the opposite face (South).  Local buckling of the longitudinal steel bars can be seen at these two locations (Figure 7-12).

**7.2.2.  Specimen B2.**  The applied load versus the axial deformation, and the stress-strain (axial and transverse) response are shown in Figure 7-13 and Figure 7-14, respectively.  Axial and transverse strains of 0.29 percent and 0.09 percent were observed at a peak compressive stress of 4.41 ksi (30.4 MPa).  This specimen exhibited good deformation capacity (maximum axial strain of 2.27 percent).  The failure of this column was preceded by a minor breakage of the fibers at the North-East corner at mid-height, and consequently delamination of this portion along the East side.  The final rupture of the jacket was located at mid-height on the South-East corner (Figure 7-15).

**7.2.3.  Specimen B3.**  Figure 7-16 and Figure 7-17 present the applied load versus the axial deformation, and the stress-strain (axial and transverse) behavior, respectively.  On the contrary of the previous specimen, this column showed a poor performance, especially in terms of axial deformability.  For a maximum axial compressive stress of 3.60 ksi (24.8 MPa), an axial and transverse strain of 0.23 percent and 0.12 percent were achieved.  The actual failure of

the jacket was observed at the North-East and South-East corner locations above the mid-height level, 2 in (51 mm) and 6 in (152 mm), respectively (Figure 7-18).

**Table 7-2  Summary of Fundamental Response Parameters; Series B**

|  | B1 | B2 | | B3 | |
|---|---|---|---|---|---|
| $\rho_f$ (%) | N/A | 1.11 | | 0.32 | |
| $P_{cc}$ (kips) | 1331 | 1674 | | 1423 | |
| $f'_{cc}$ (ksi) | 3.30 | 4.41 | | 3.60 | |
| $\varepsilon'_{cc}$ ($\mu\varepsilon$) | 1465 | 2891 | | 2277 | |
| $\varepsilon_{cu}$ ($\mu\varepsilon$) | 1465 | 22724 | | 7507 | |
| $\varepsilon_{tc}$ ($\mu\varepsilon$) | N/A | Long | 840 | Long | 1286 |
|  |  | Short | 826 | Short | 726 |
| $\varepsilon_{ju}$ ($\mu\varepsilon$) | N/A | 8568 | | 2760 | |

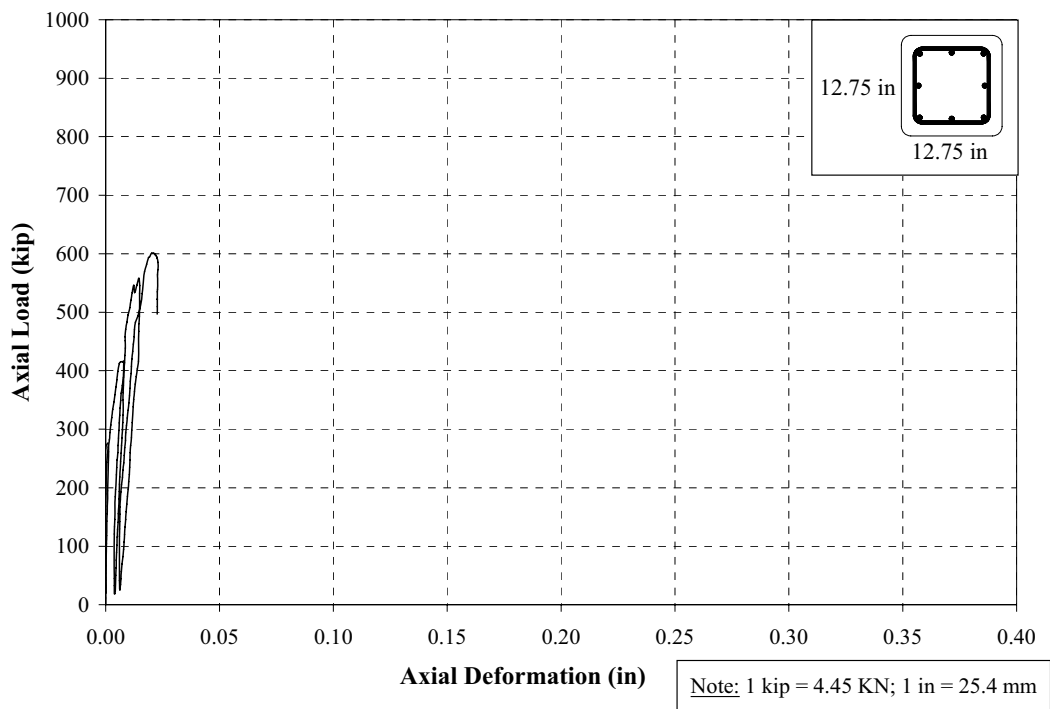Note: 1 kip = 4.45 KN; 1 ksi = 6.9 MPa
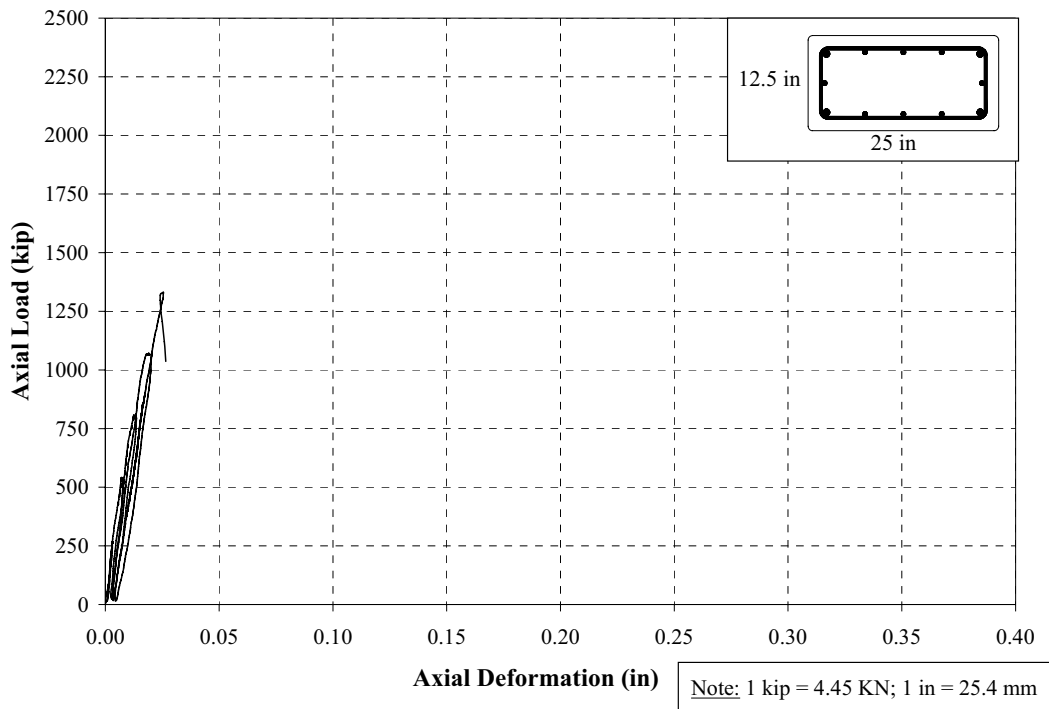


**Figure 7-10  Axial Load vs. Axial Deformation; Specimen B1**
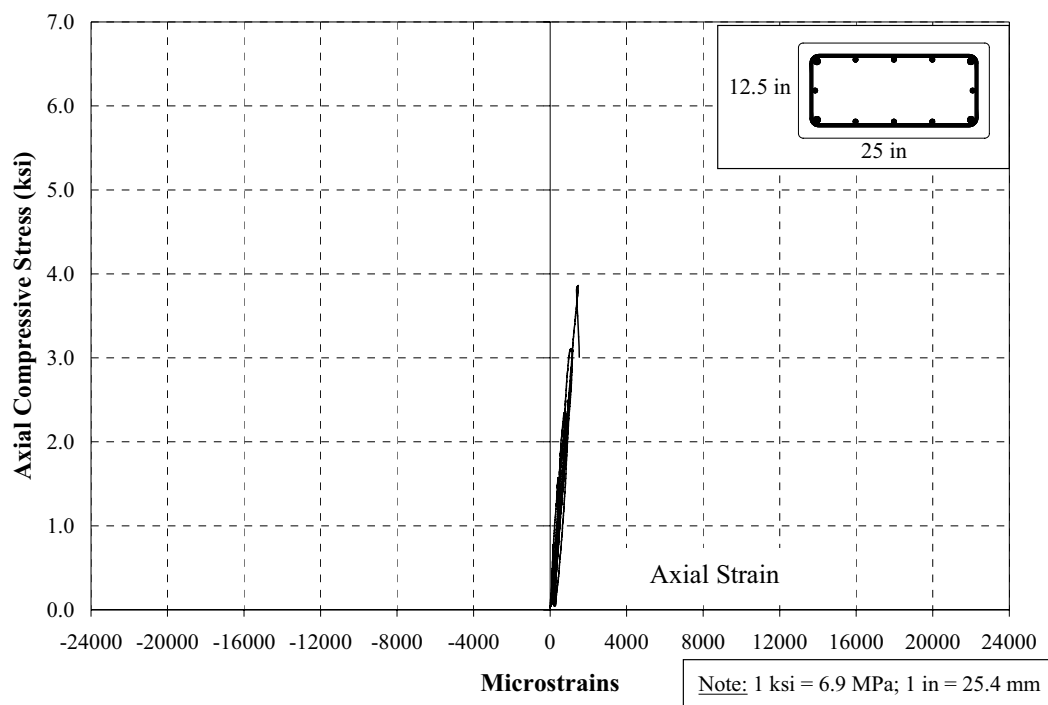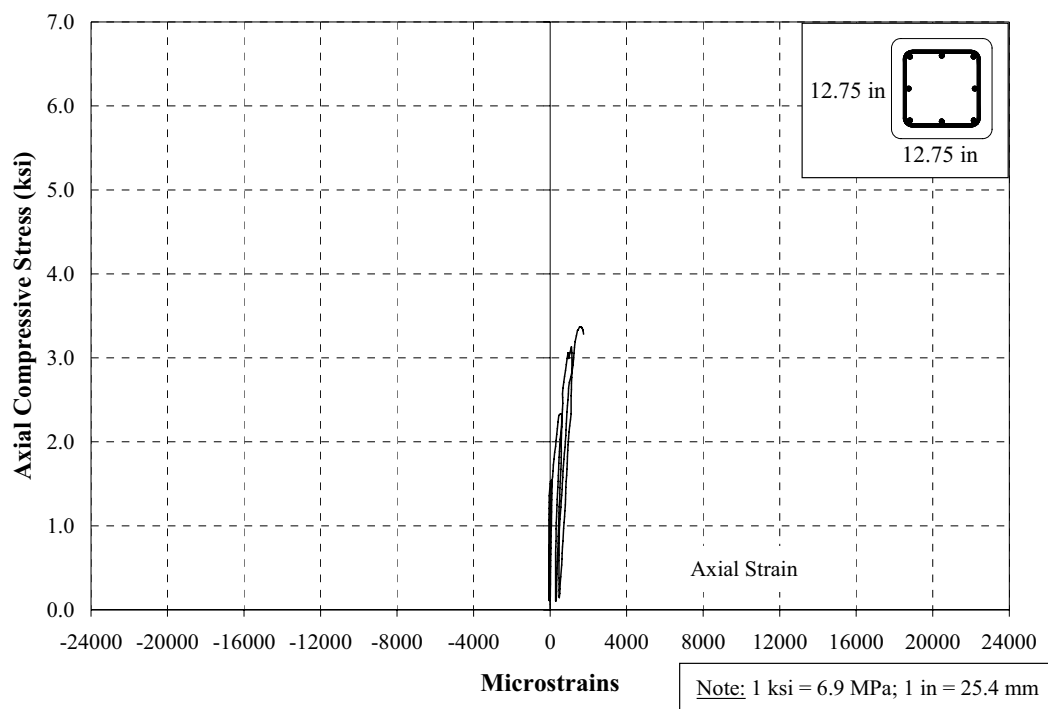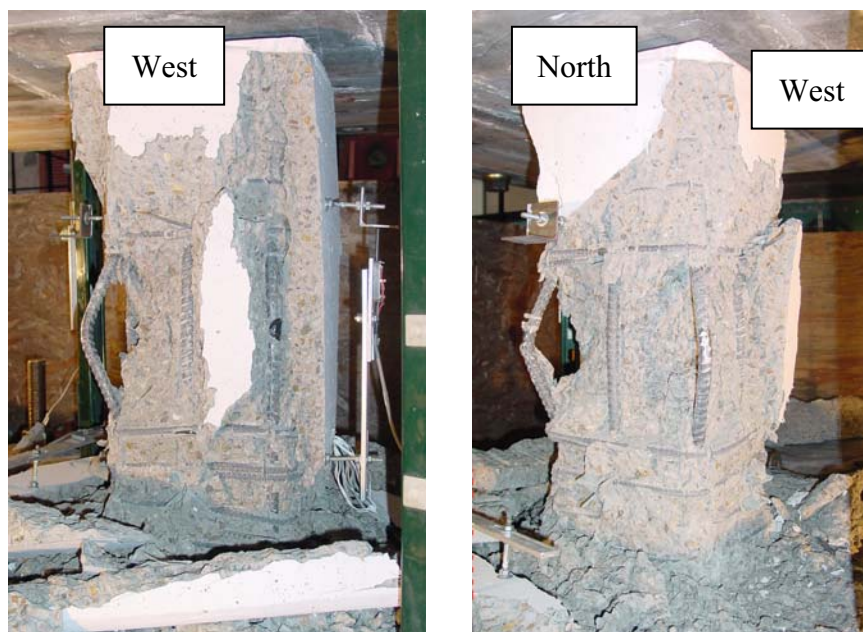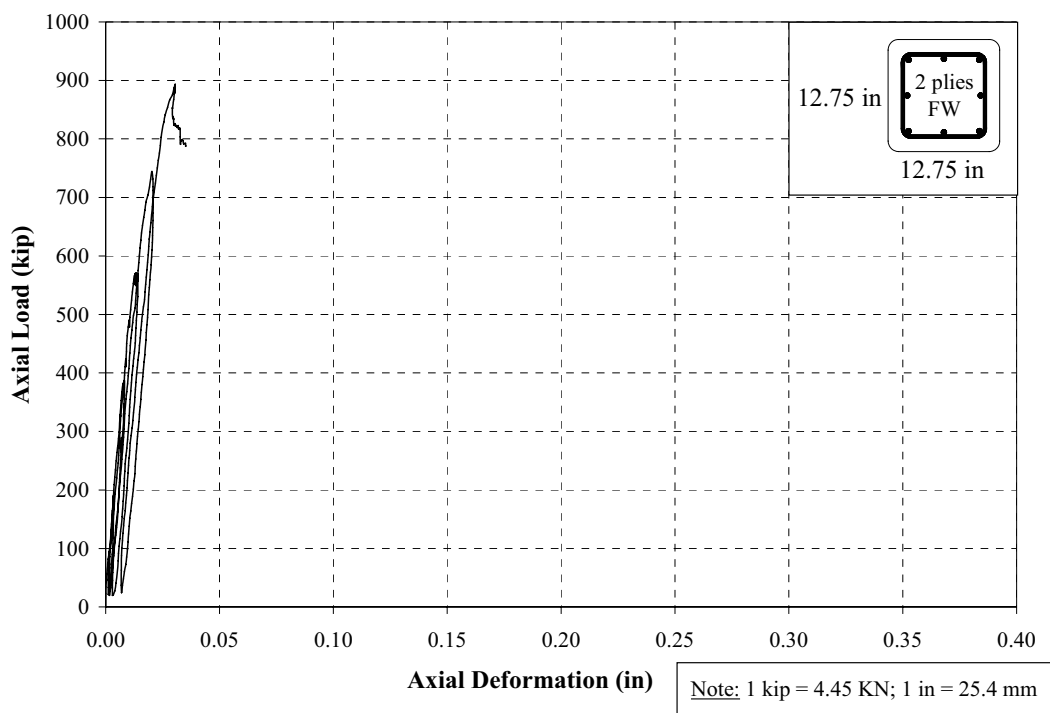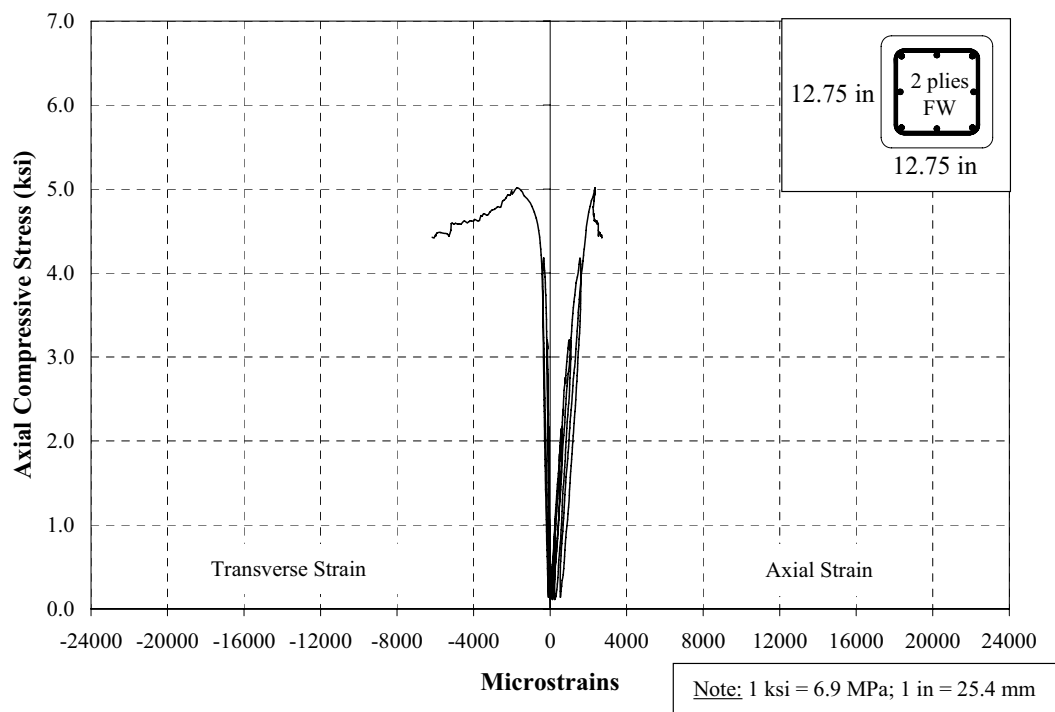
**Figure 7-11  Stress-Strain Behavior; Specimen B1**
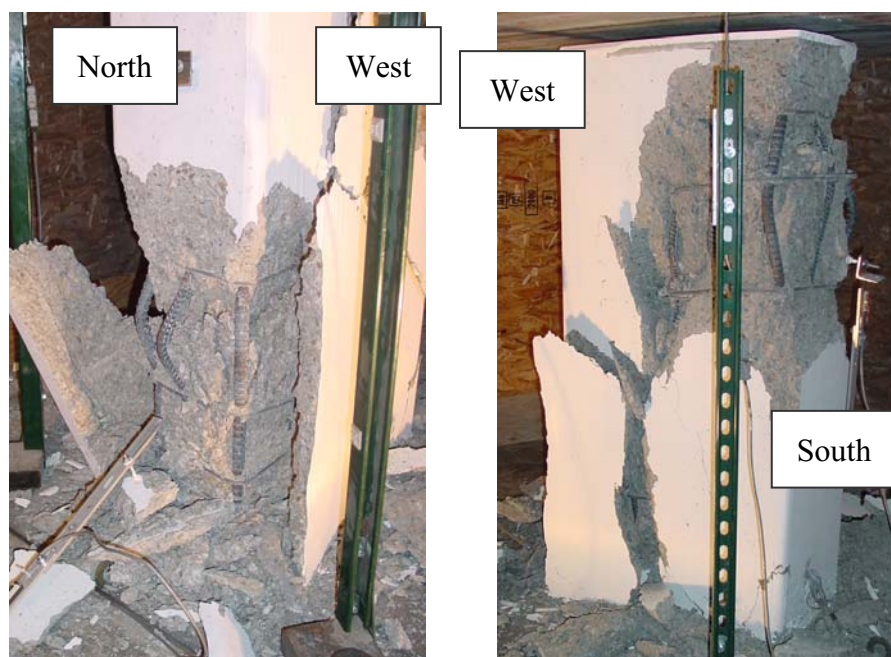


**Figure 7-12  Failure of Specimen B1**
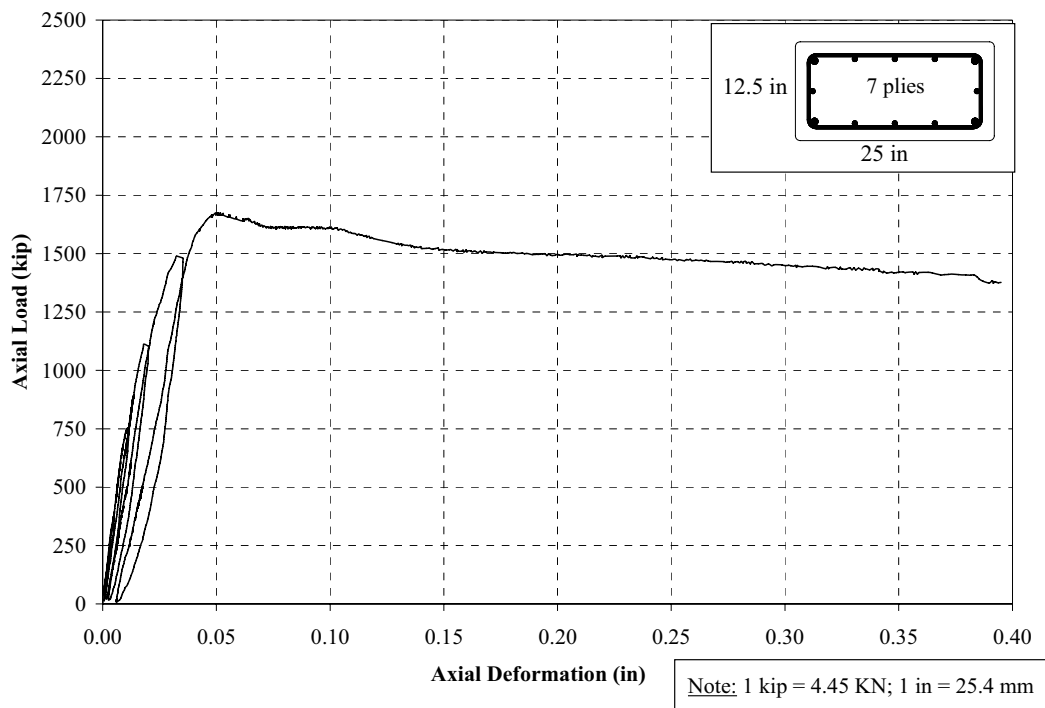
**Figure 7-13  Axial Load vs. Axial Deformation; Specimen B2**
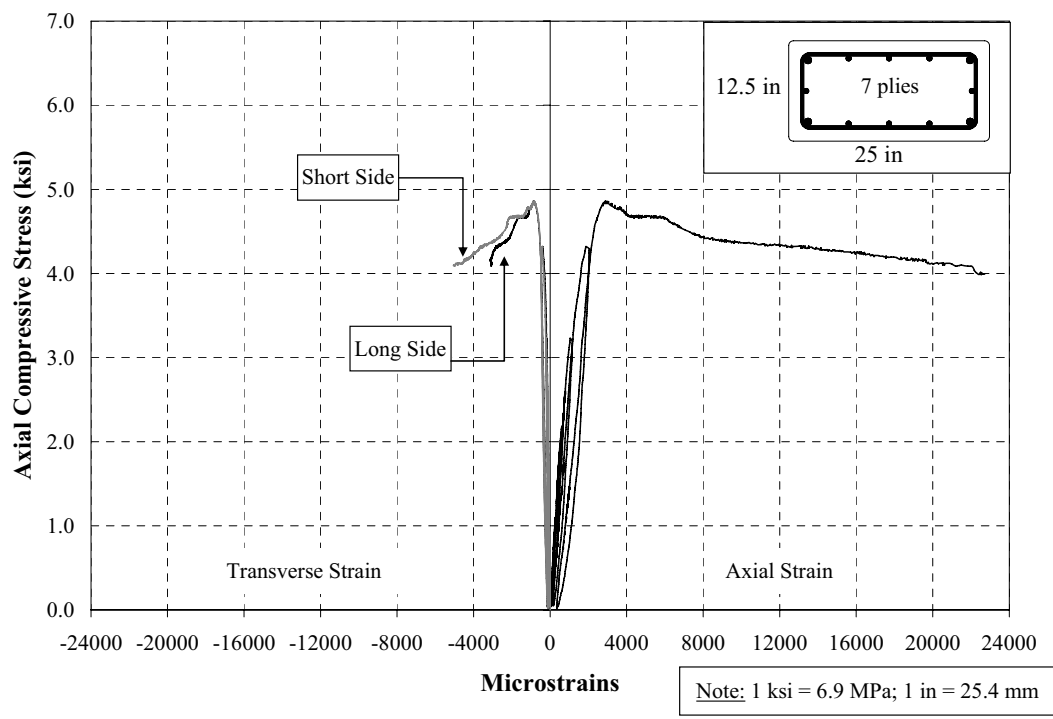


**Figure 7-14  Stress-Strain Behavior; Specimen B2**
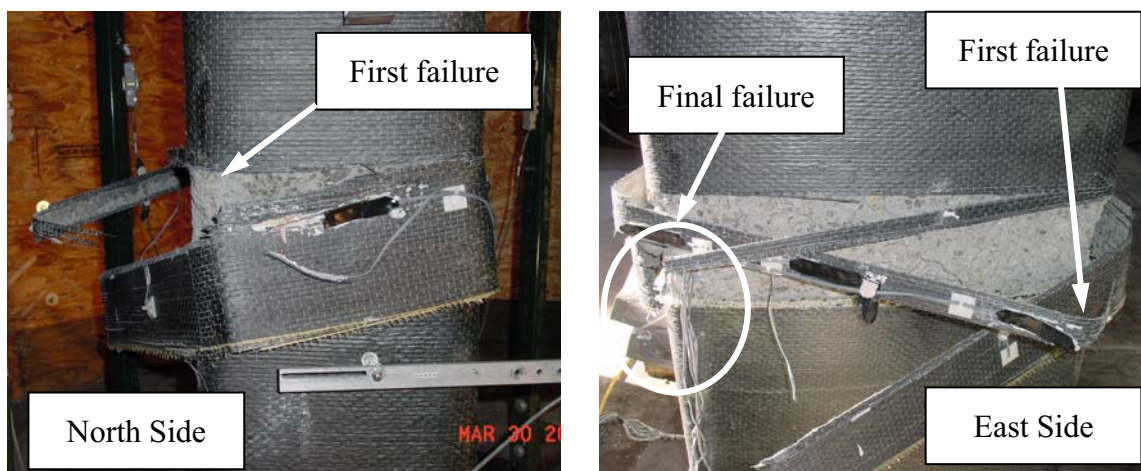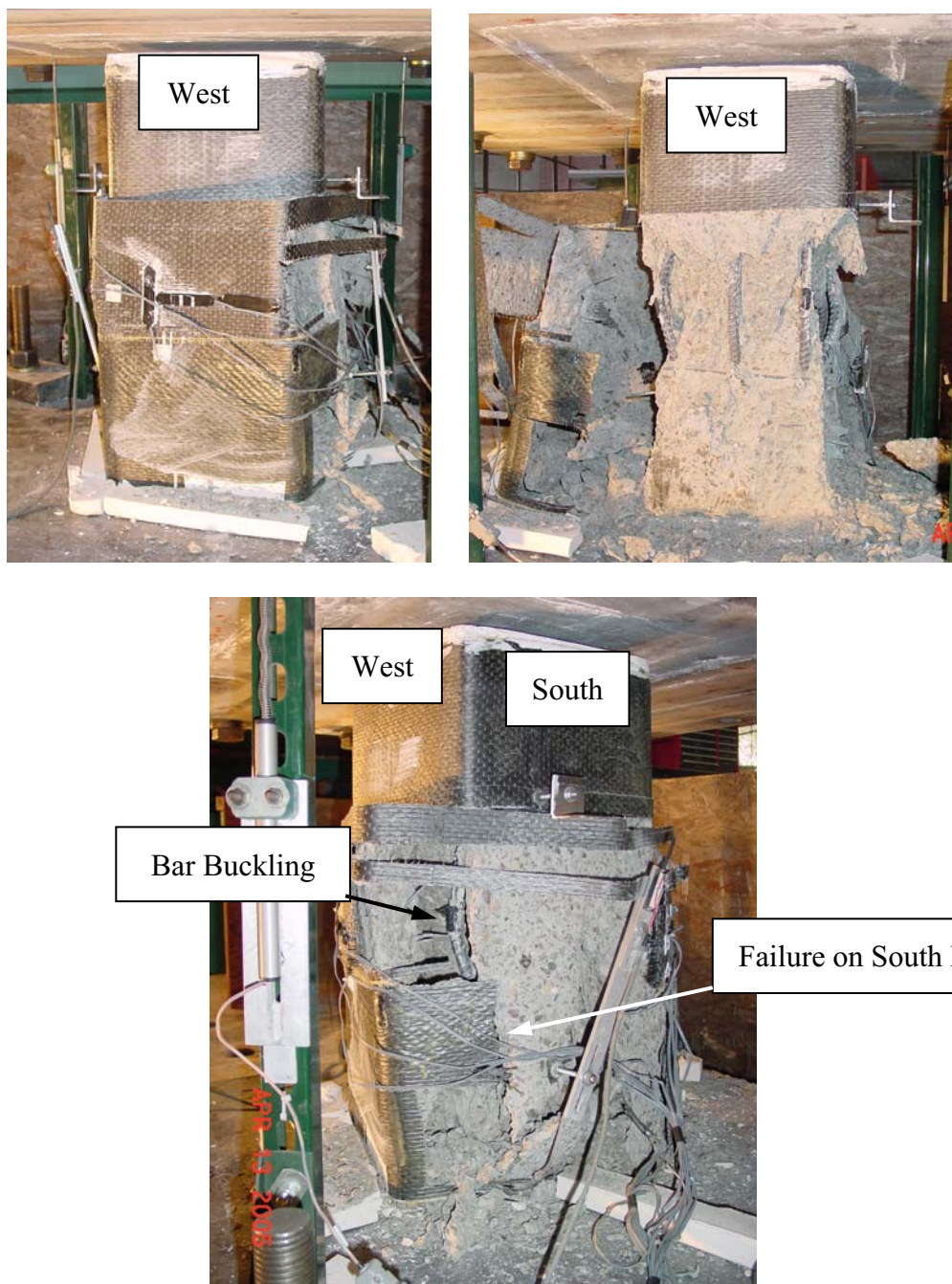
**Figure 7-15  Failure of Specimen B2**
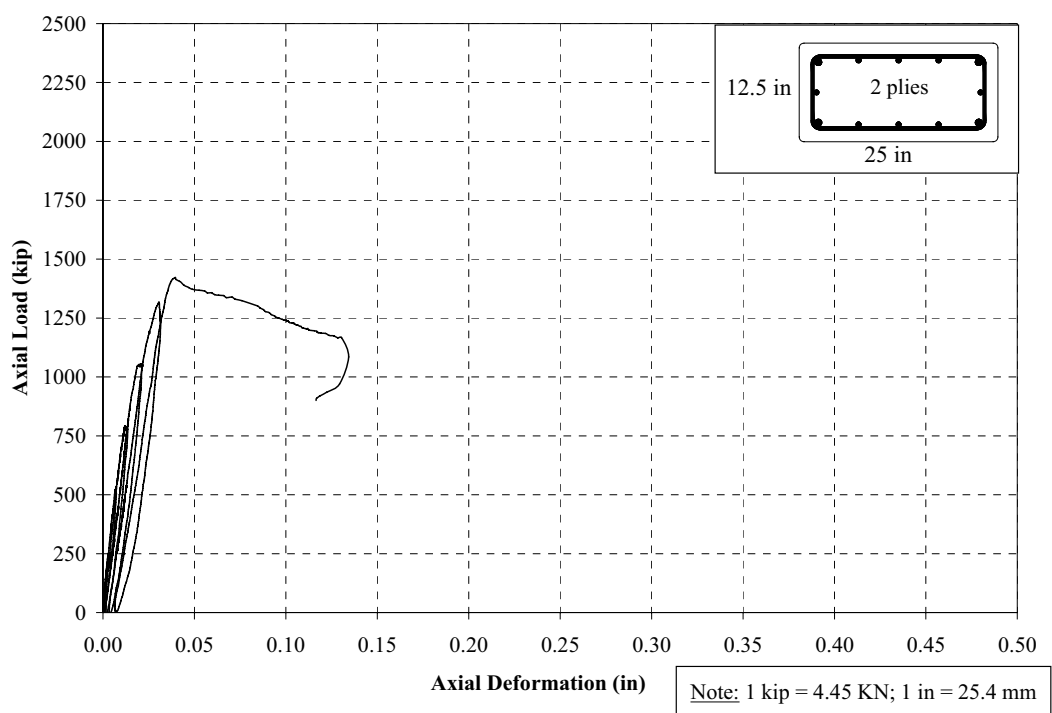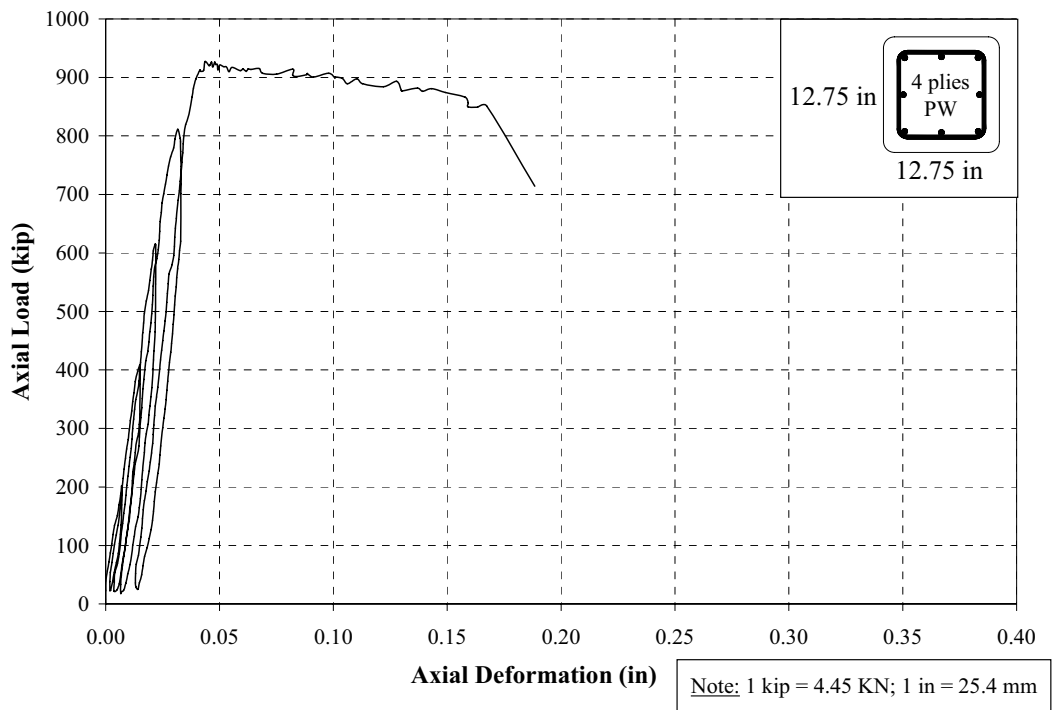


**Figure 7-16  Axial Load vs. Axial Deformation; Specimen B3**
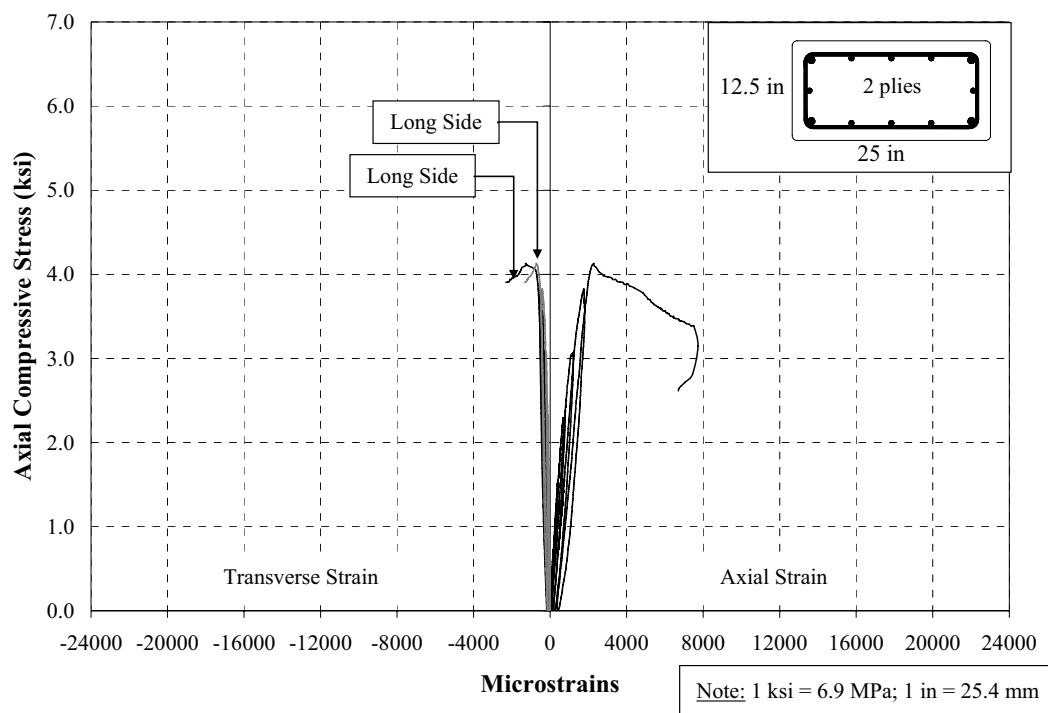
**Figure 7-17  Stress-Strain Behavior; Specimen B3**
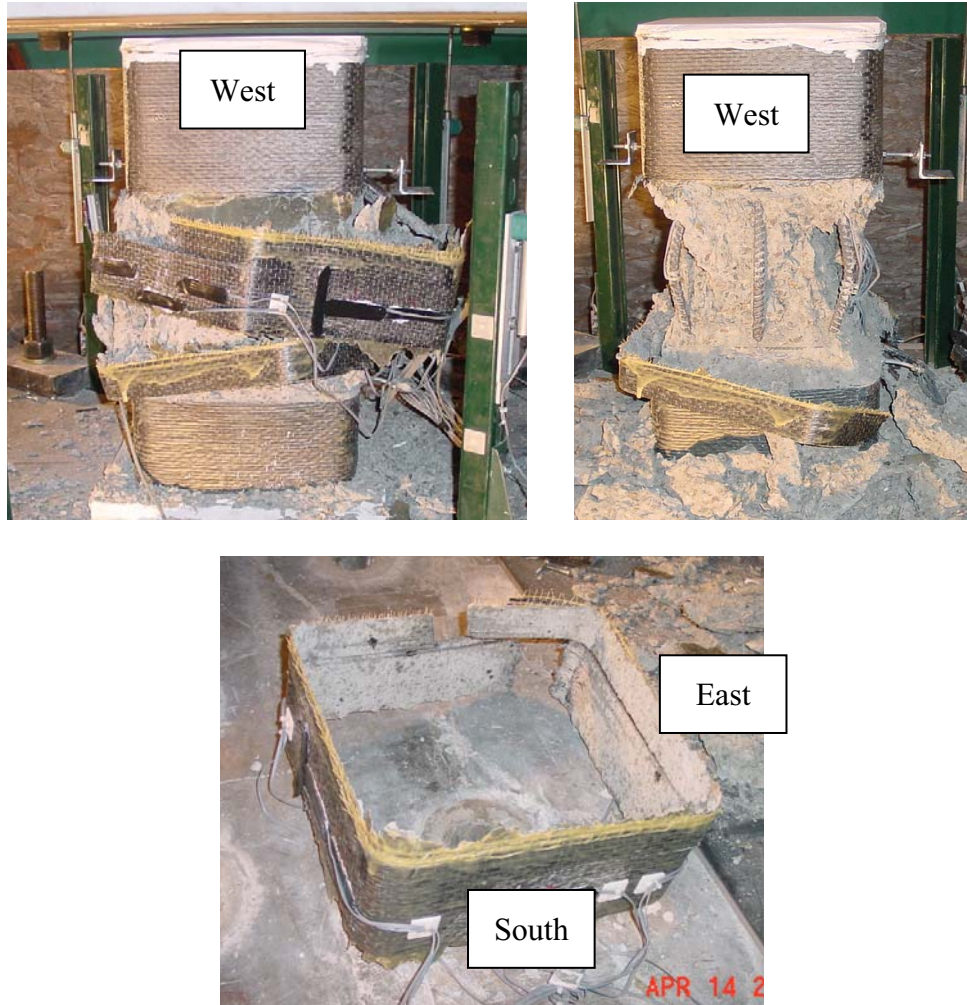
**Figure 7-18 Failure of Specimen B2**

## 7.3. SERIES C; 18 x 18 x 40 in (457 x 457 x 1016 mm)

Table 7-3 presents the basic parameters resulting from the experiments on the specimens of this group. This group was composed of three specimens: C1 (control), C2 (strengthened with four plies), and C3 (strengthened with two plies).

**7.3.1. Specimen C1.** The applied load versus the axial deformation, and the axial stress-strain behavior are shown in Figure 7-19 and Figure 7-20, respectively. For a maximum load of 1515 kips (6742 KN), a compressive stress of 3.77 ksi (26 MPa), and a corresponding axial strain of 0.24 percent were achieved. An extra cycle was necessary to attain the failure of this specimen. Vertical cracking running up to both ends were observed. Buckling of longitudinal reinforcement at mid-height of the specimen, as well as partial disengagement of the center ties was observed (Figure 7-21).

**7.3.2. Specimen C2.** The applied load versus the axial deformation, and the stress-strain response, including both the axial and transverse strains, are presented in Figure 7-22 and Figure 7-23, in that order. The maximum axial compressive stress that was achieved by this specimen was 4.22 ksi (29.1 MPa), and the corresponding axial and hoop strains were 0.51 percent and 0.23 percent. Note that the ultimate axial deformation was of about 1.06 percent. This specimen exhibit a gradual failure: it first started with the rupture of a small jacket strip at mid-height on the North-West corner, as the load kept increasing this strip delaminated along the West face; at the failure of the specimen, the FRP jacket broke at different locations and in portions, the North-West corner at mid-height among them (Figure 7-24).

**7.3.3. Specimen C3.** Figure 7-25 and Figure 7-26 present the applied load versus the axial deformation, and the stress-strain behavior (including both the axial and hoop strains), respectively. For a maximum axial compressive stress of 4.02 ksi (27.7 MPa) the corresponding axial and transverse strains were 0.27 percent and 0.21 percent. The ultimate axial deformation was approximately 0.85 percent. The failure of this column was characterized by rupture and debonding of the FRP jacket at multiple locations (South-East corner at mid-height), and practically along the entire height of the specimen (Figure 7-27).

**Table 7-3  Summary of Fundamental Response Parameters; Series C**

|  | C1 | C2 | C3 |
|---|---|---|---|
| $\rho_f$ (%) | N/A | 0.59 | 0.29 |
| $P_{cc}$ (kips) | 1515 | 1659 | 1593 |
| $f'_{cc}$ (ksi) | 3.77 | 4.22 | 4.02 |
| $\varepsilon'_{cc}$ ($\mu\varepsilon$) | 2365 | 5063 | 2679 |
| $\varepsilon_{cu}$ ($\mu\varepsilon$) | 2423 | 10605 | 8545 |
| $\varepsilon_{tc}$ ($\mu\varepsilon$) | N/A | 2333 | 2090 |
| $\varepsilon_{ju}$ ($\mu\varepsilon$) | N/A | 5966 | 7547 |

Note: 1 kip = 4.45 KN; 1 ksi = 6.9 MPa
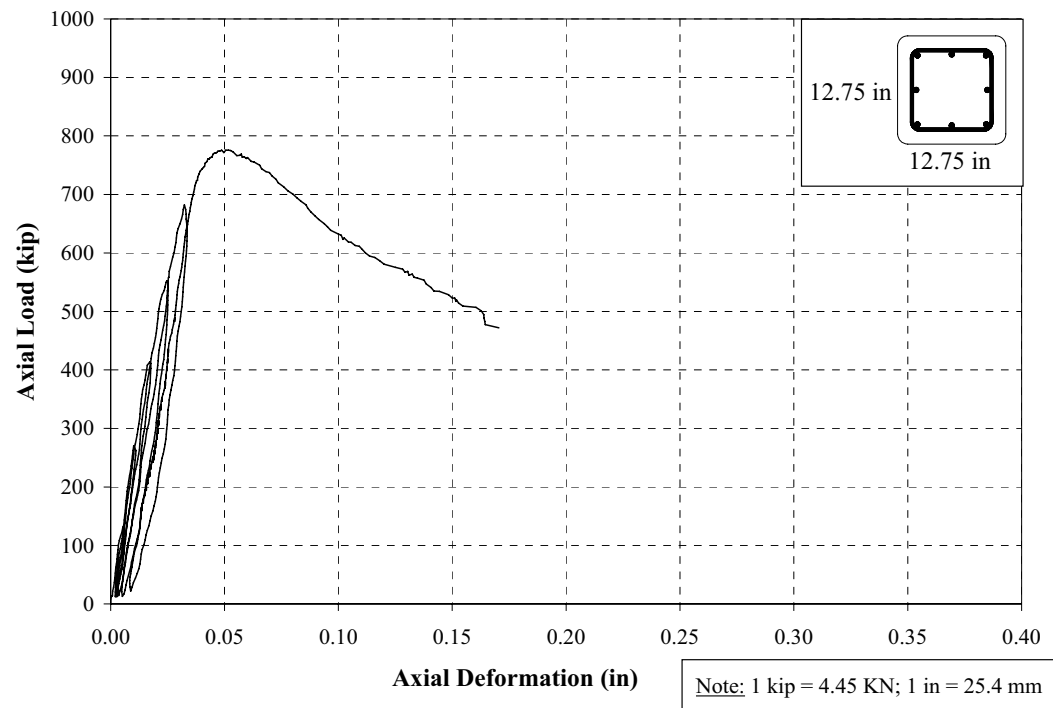


Note: 1 kip = 4.45 KN; 1 in = 25.4 mm
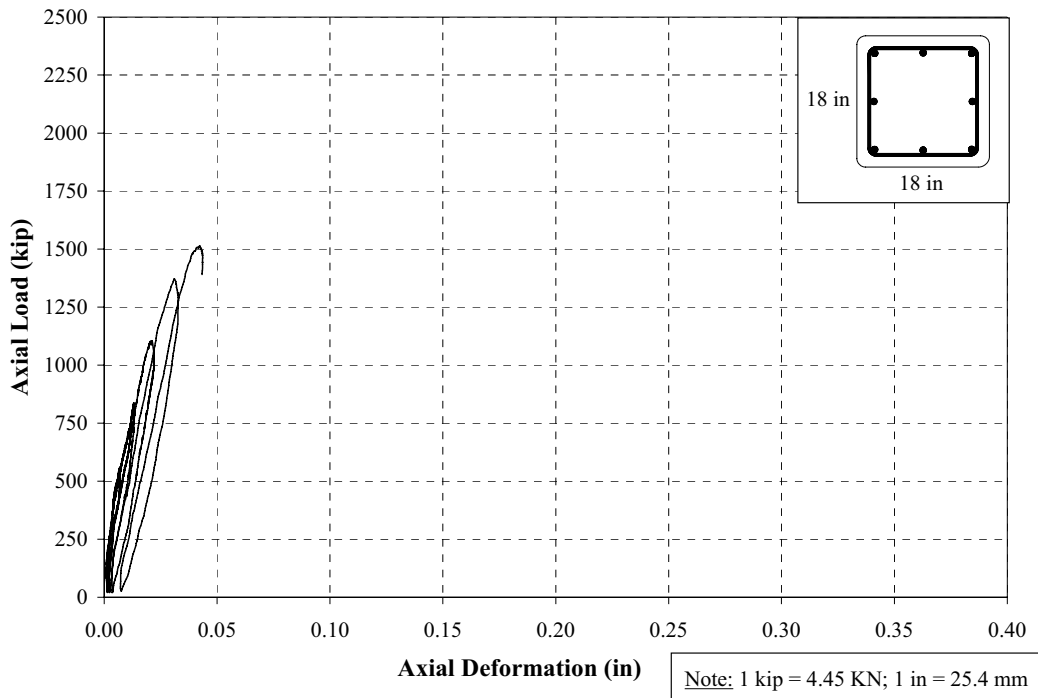
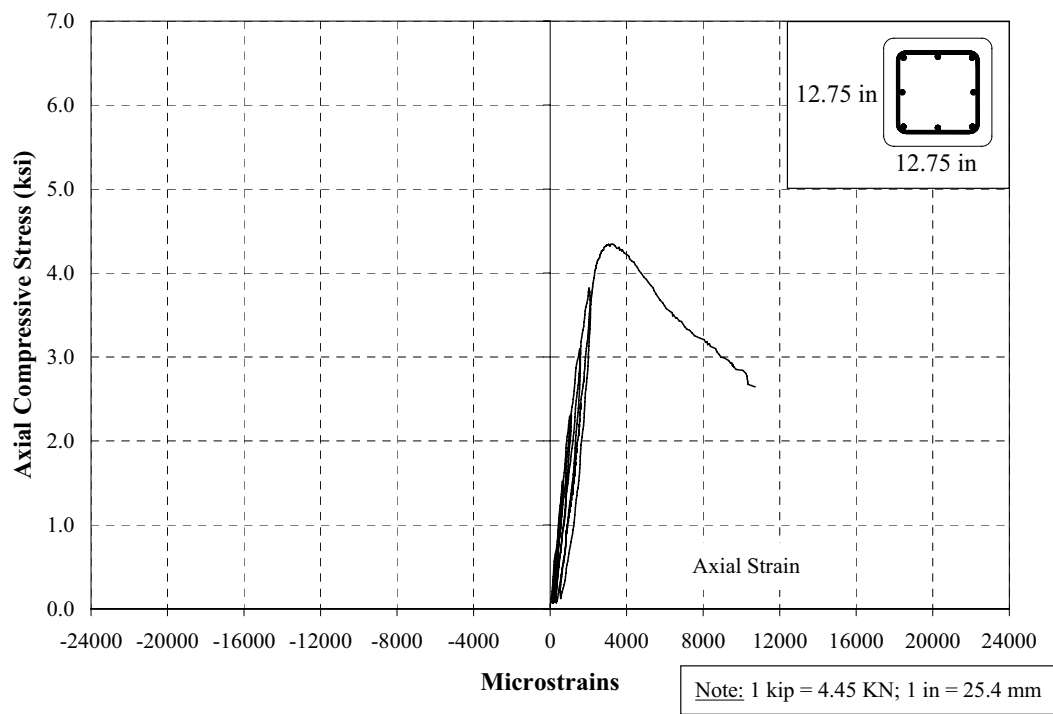**Figure 7-19  Axial Load vs. Axial Deformation; Specimen C1**
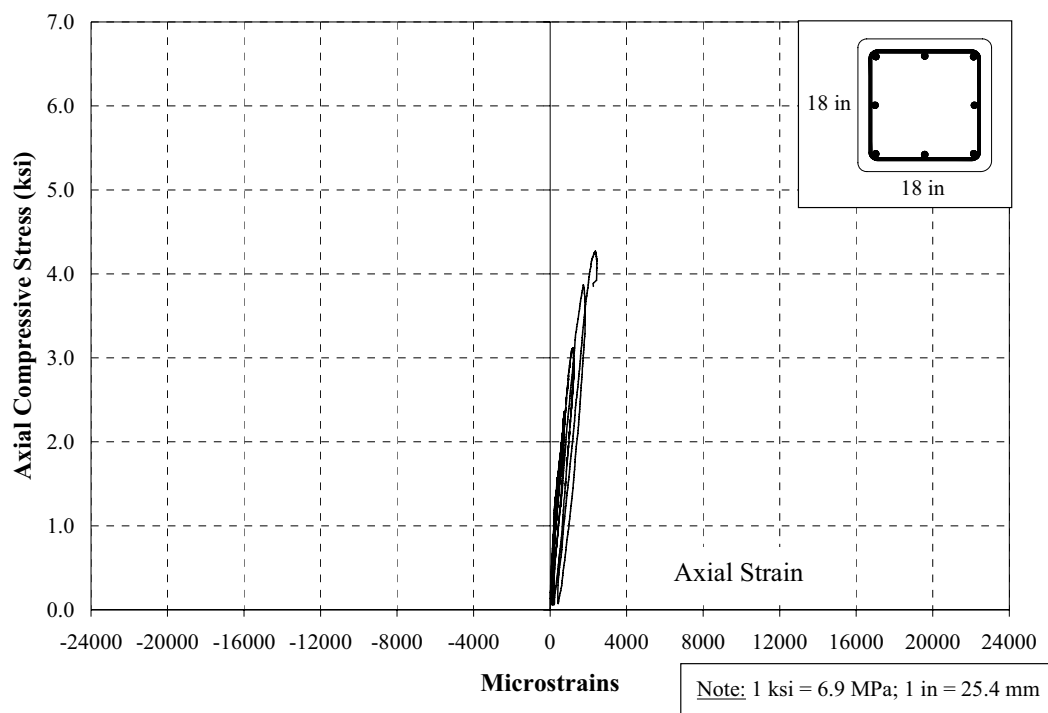
**Figure 7-20  Stress-Strain Behavior; Specimen C1**



**Figure 7-21  Failure of Specimen C1**
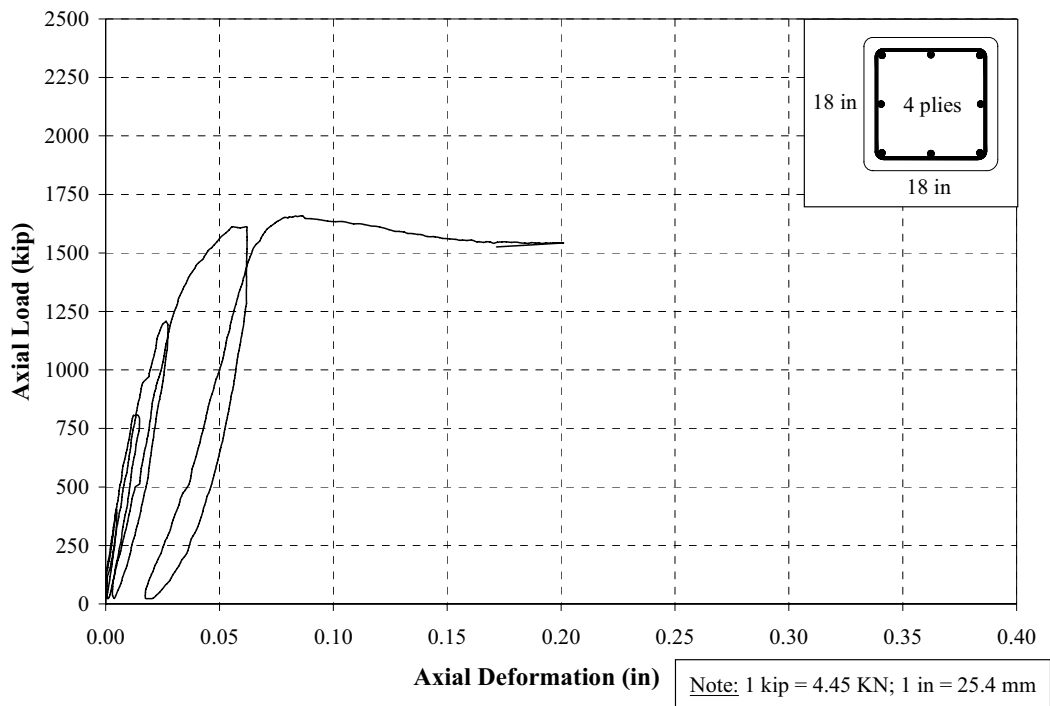
**Figure 7-22  Axial Load vs. Axial Deformation; Specimen C2**
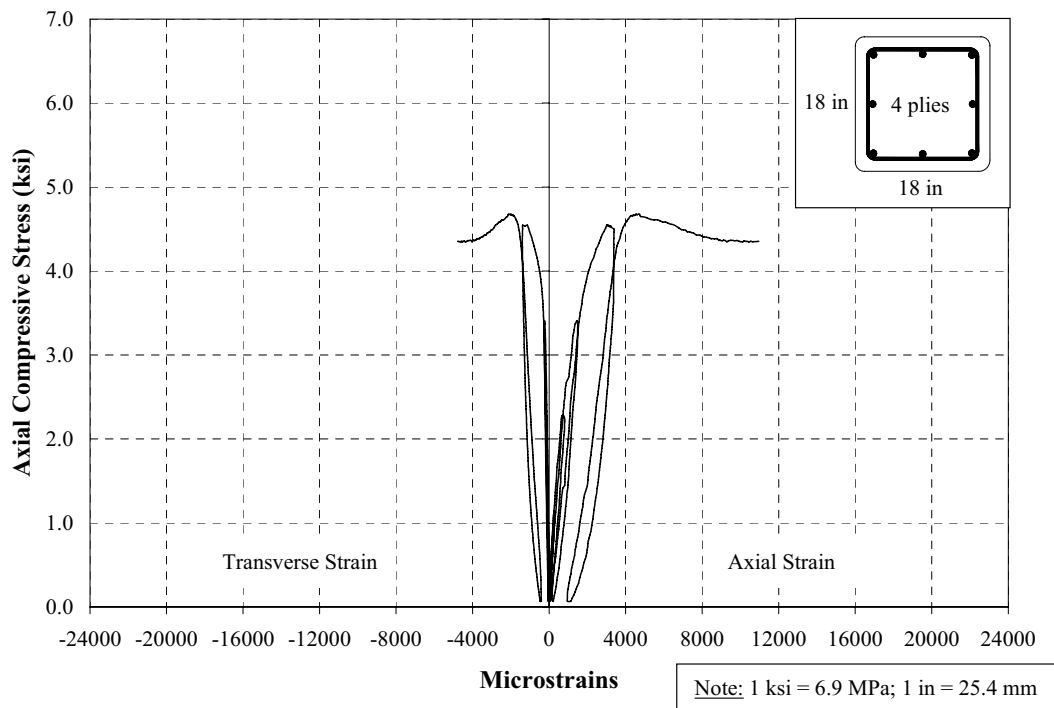


**Figure 7-23  Stress-Strain Behavior; Specimen C2**

West Face

North

NW Corner

Bar Buckling
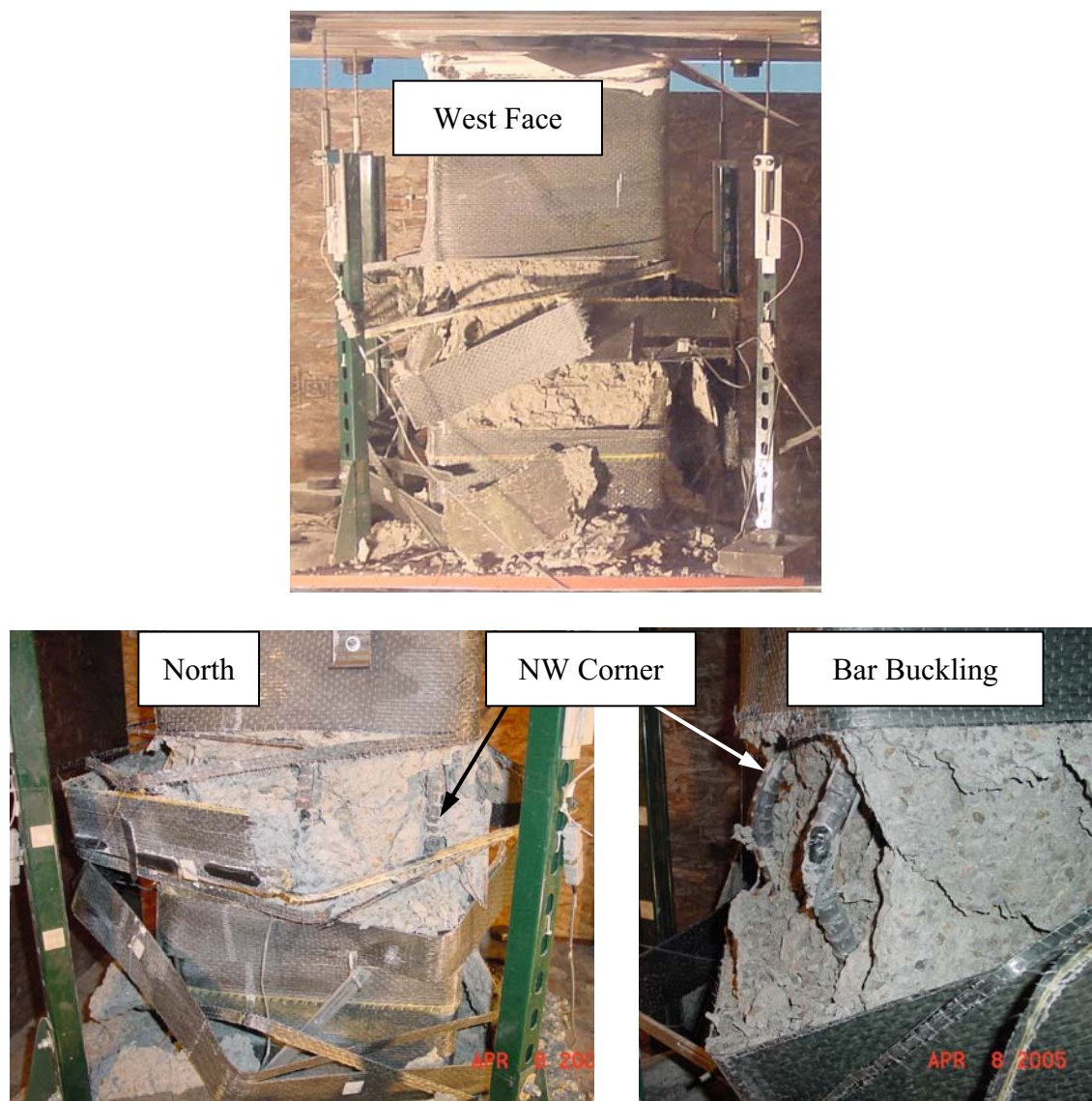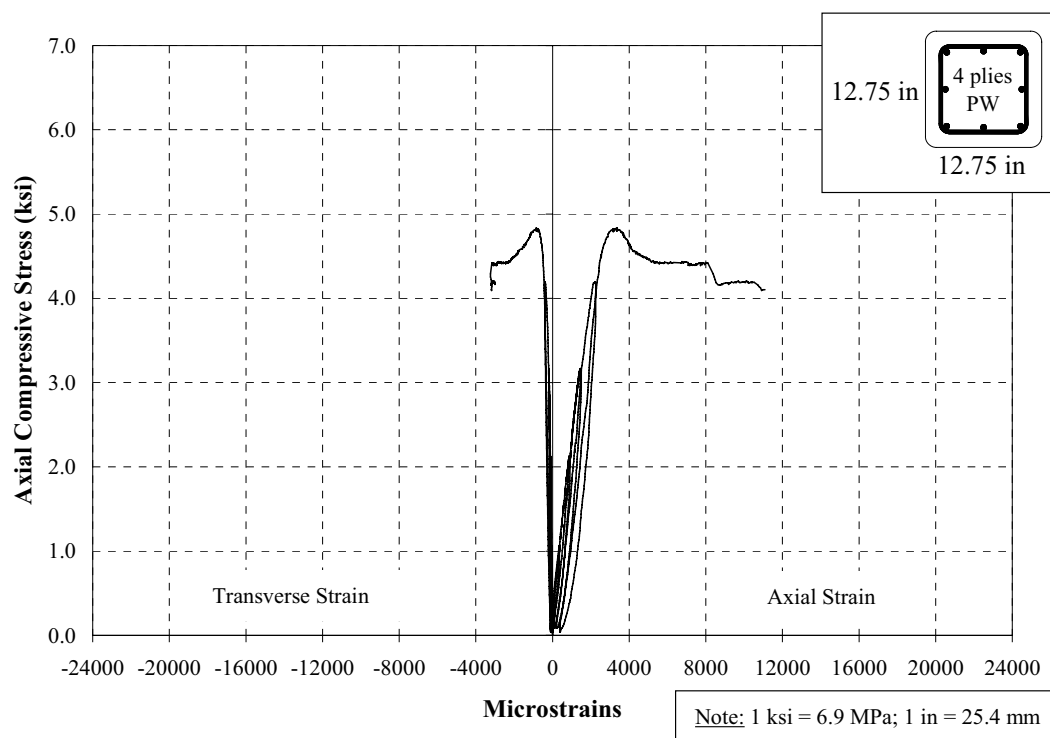
**Figure 7-24 Failure of Specimen C2**
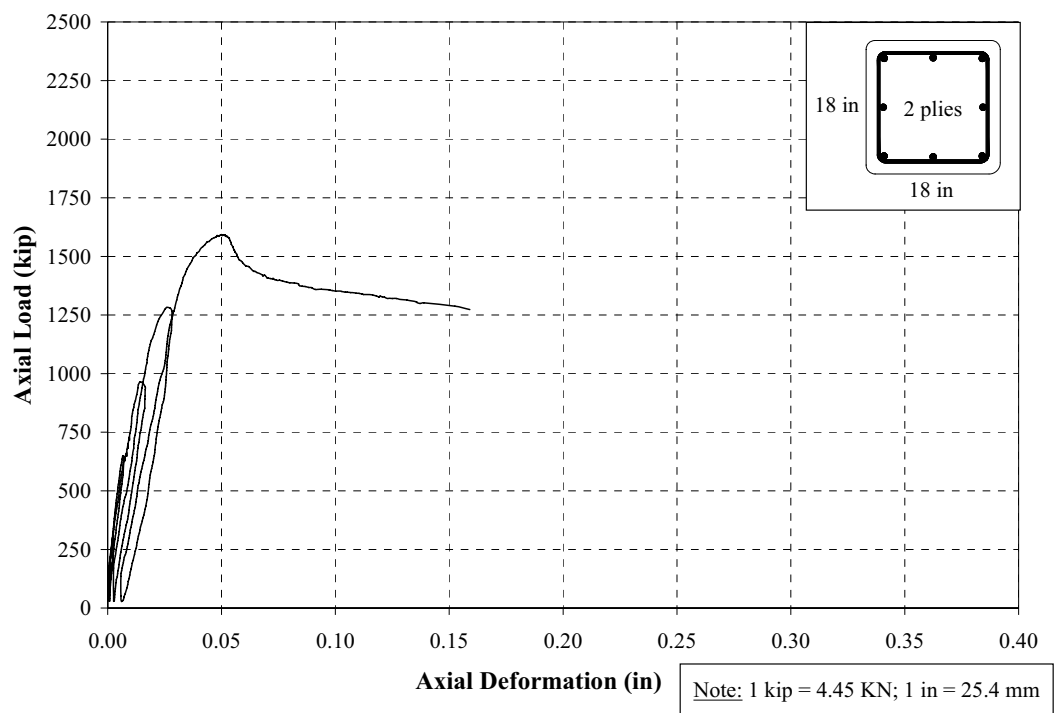
**Figure 7-25 Axial Load vs. Axial Deformation; Specimen C3**
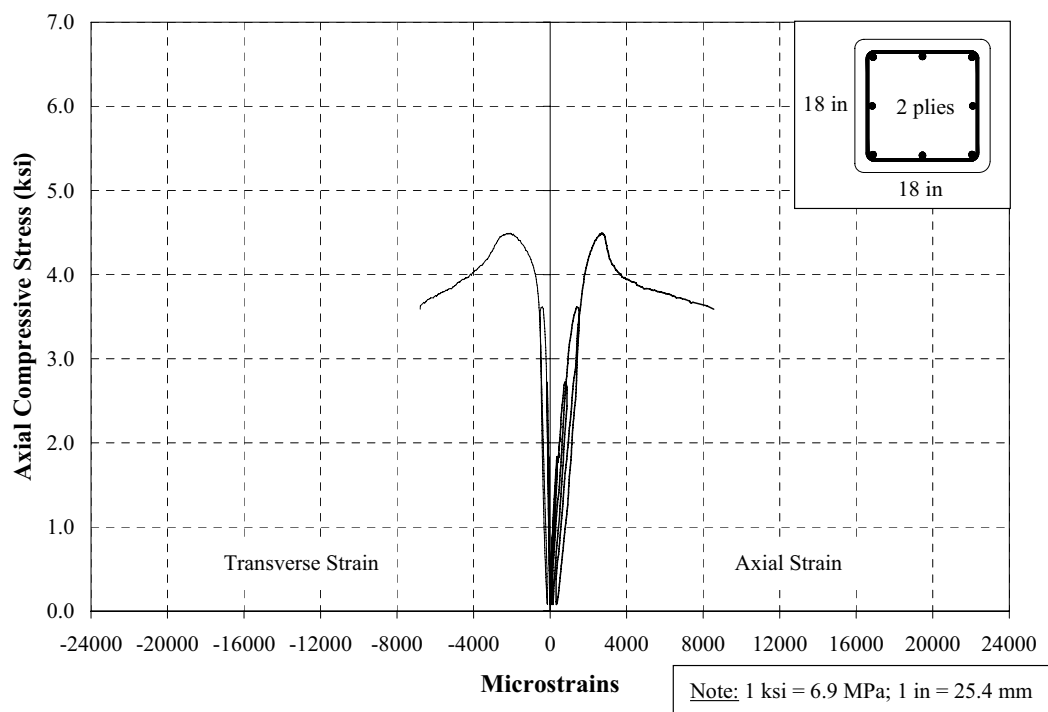


**Figure 7-26 Stress-Strain Behavior; Specimen C3**

West Face

West Face

SE Corner
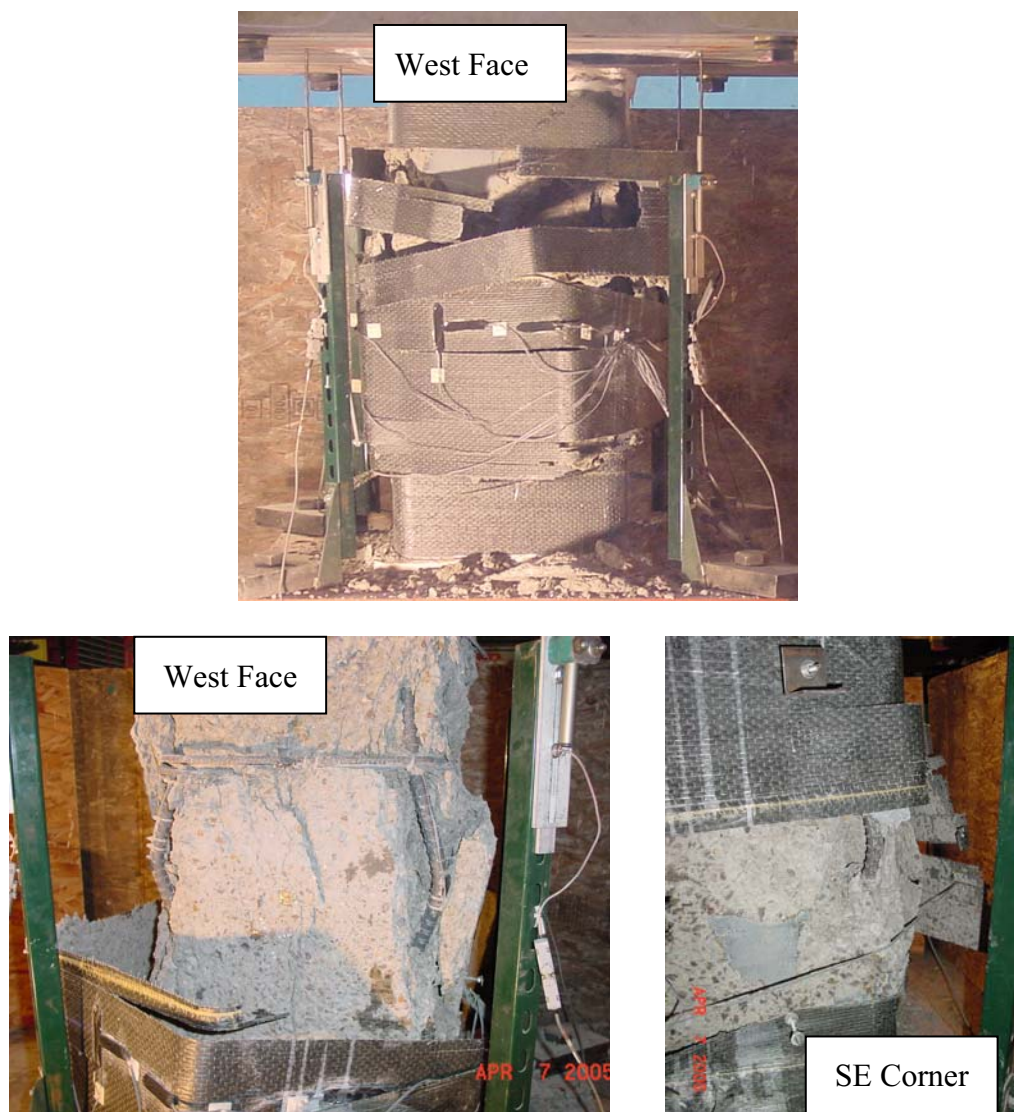
**Figure 7-27  Failure of Specimen C3**

## 7.4.    SERIES D; 25.5 x 25.5 x 54 in (648 x 648 x 1372 mm)

Table 7-4 presents the basic parameters resulting from the experiments on the specimens of this series.  This group was composed of three specimens: D1 (control), D2 (strengthened with five plies), and F3 (strengthened with two plies).

**7.4.1.   Specimen D1.**  For a maximum load of 2981 kips (13,266 KN), a compressive stress of 3.68 ksi (25.4 MPa), and a corresponding axial strain of 0.25 percent were achieved.  Figure 7-28 and Figure 7-29 present the applied load versus the axial deformation and the axial stress-strain behavior, respectively.  A sixth extra cycle was needed in this case in order to attain failure.  About the mode of failure, as for the previously introduced control specimen, this column exhibited vertical cracks along the height.  The spalling of the concrete occurred practically along the entire column, but basically on three sides.  Buckling of longitudinal bars was observed at the mid-height and at the bottom portion of the specimen.  The disengagement of the ties was complete (Figure 7-30).

**7.4.2. Specimen D2.** The applied load versus axial deformation as well as the stress-strain response, including the axial and hoop strains, are presented in Figure 7-31 and Figure 7-32, respectively. An axial strain of 0.39 percent and a hoop strain of 0.13 percent were achieved at the maximum axial compressive stress of 4.40 ksi (30.4 MPa). The maximum axial deformation corresponded to 0.91 percent without carrying capacity increment beyond the peak compressive strength. The failure of this specimen was gradual, which began with the rupture of a very narrow strip occurred at the North-West corner at mid-height, and as the load continued increasing this piece started debonding along the North face. Another small rupture at same corner but below the mid-height level followed up, and scattered horizontal cracks on the North face (bottom part) that had developed throughout the load cycling extended. The ruptures defining the failure of the specimen were at different locations, among them on the North-West corner (bottom) and on the South-East corner at the mid-height level.

**7.4.3. Specimen D3.** The applied load versus the axial deformation, and the stress-strain response (including the axial and hoop strains) are shown in Figure 7-34 and Figure 7-35, respectively. For a peak axial compressive stress of 3.95 ksi (27.3 MPa) the corresponding measured axial and transverse strains were 0.31 percent and 0.1 percent, in that order. As for the previous specimen, this column exhibited a gradual failure described by two premature ruptures of narrow FRP strips on the North-West corner. This was followed by partial delamination along the West face. A definite breakage occurred at the North-East corner at mid-height.

**Table 7-4  Summary of Fundamental Response Parameters; Series D**

|  | D1 | D2 | D3 |
|---|---|---|---|
| $\rho_f$ (%) | N/A | 0.52 | 0.21 |
| $P_{cc}$ (kips) | 2981 | 3444 | 3154 |
| $f'_{cc}$ (ksi) | 3.68 | 4.40 | 3.95 |
| $\varepsilon'_{cc}$ ($\mu\varepsilon$) | 2458 | 3880 | 3122 |
| $\varepsilon_{cu}$ ($\mu\varepsilon$) | 2880 | 9093 | 4990 |
| $\varepsilon_{tc}$ ($\mu\varepsilon$) | N/A | 1323 | 1001 |
| $\varepsilon_{ju}$ ($\mu\varepsilon$) | N/A | 9305 | 7663 |

Note: 1 kip = 4.45 KN; 1 ksi = 6.9 MPa

**Figure 7-28  Axial Load vs. Axial Deformation; Specimen D1**



**Figure 7-29  Stress-Strain Behavior; Specimen D1**

**Figure 7-30  Failure of Specimen D1**

**Figure 7-31  Axial Load vs. Axial Deformation; Specimen D2**
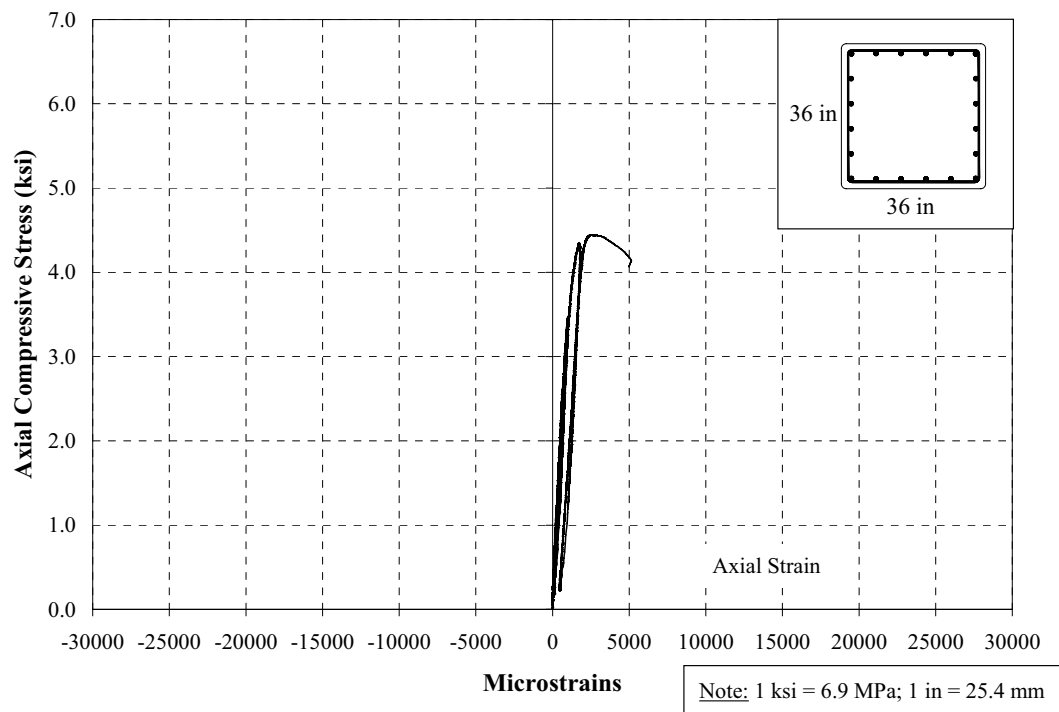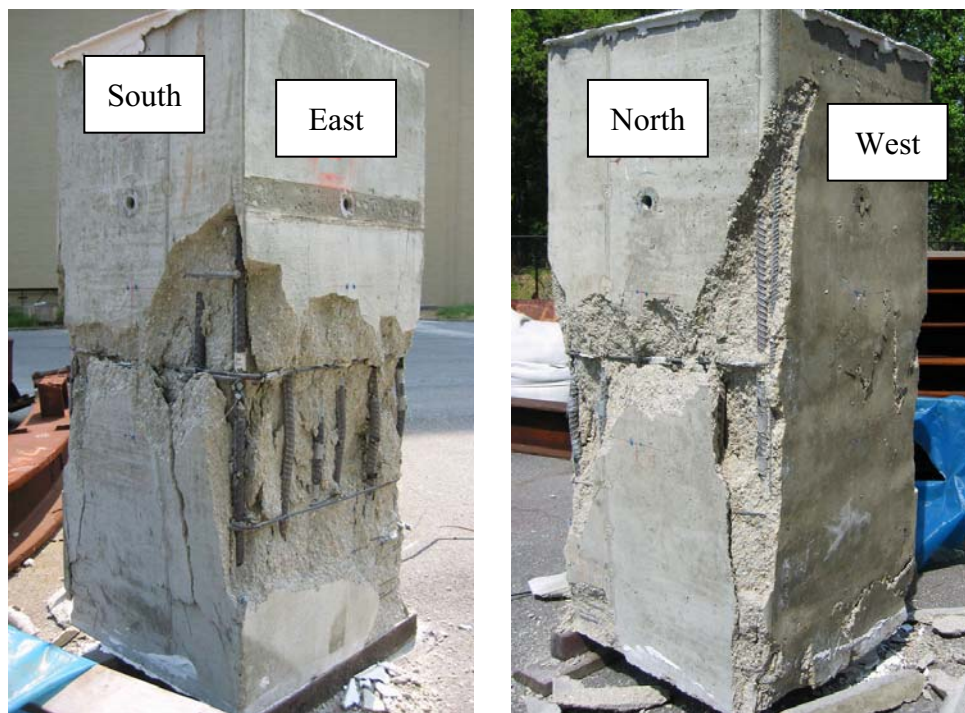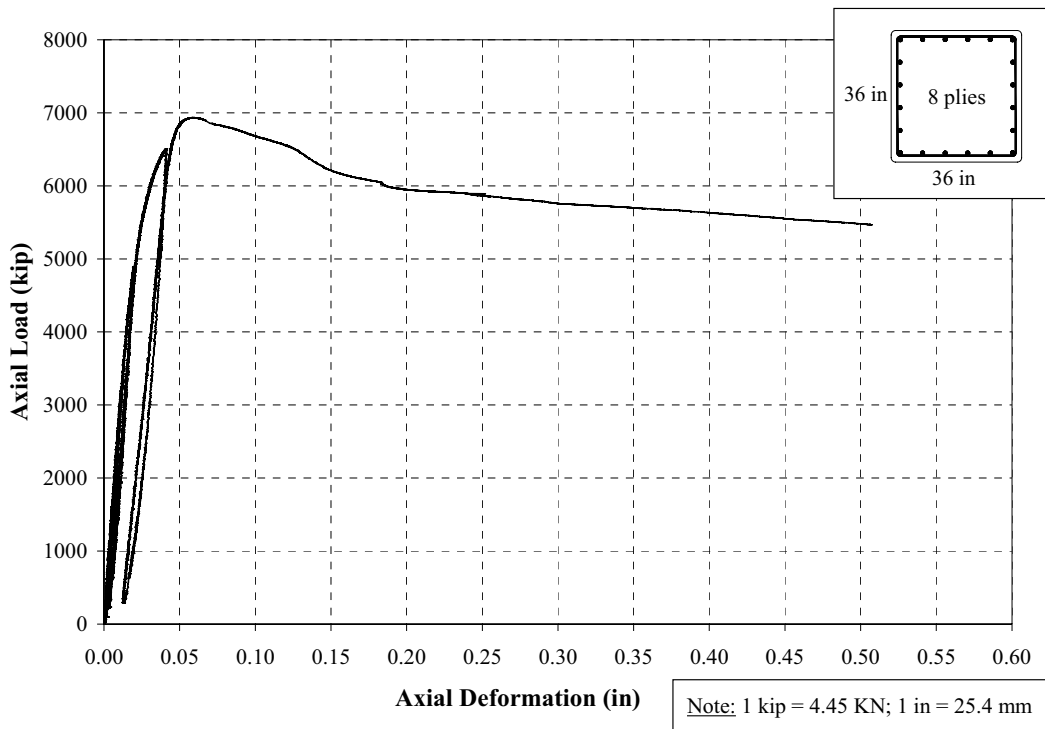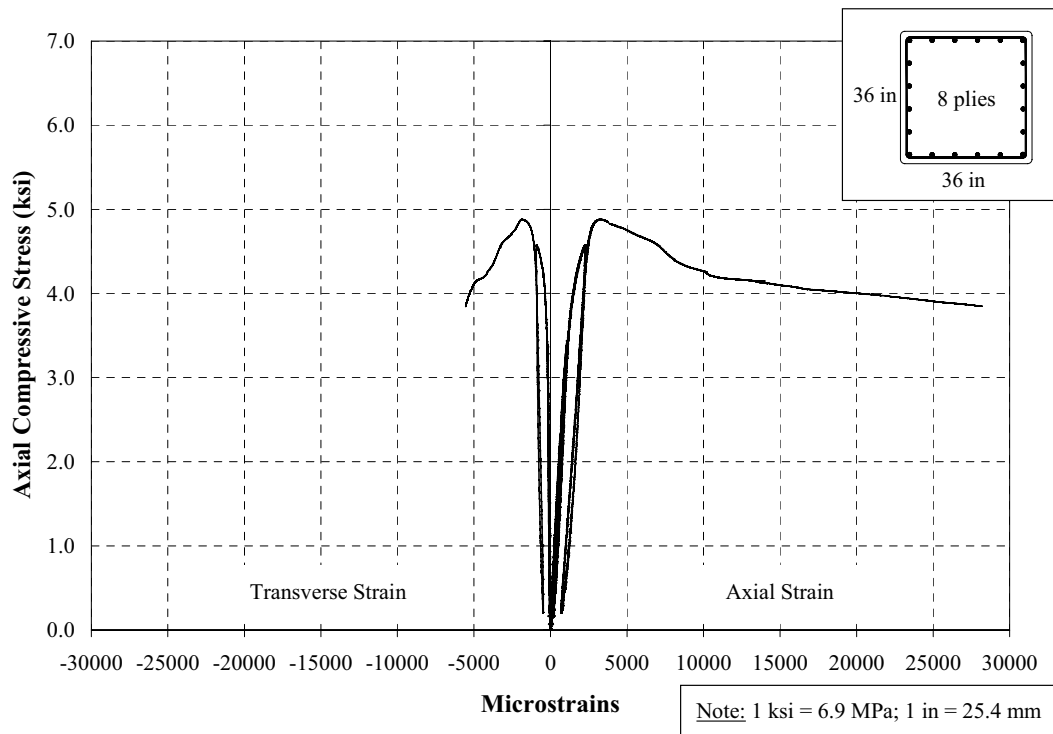


**Figure 7-32  Stress-Strain Behavior; Specimen D2**

Figure 7-33  Failure of Specimen D2
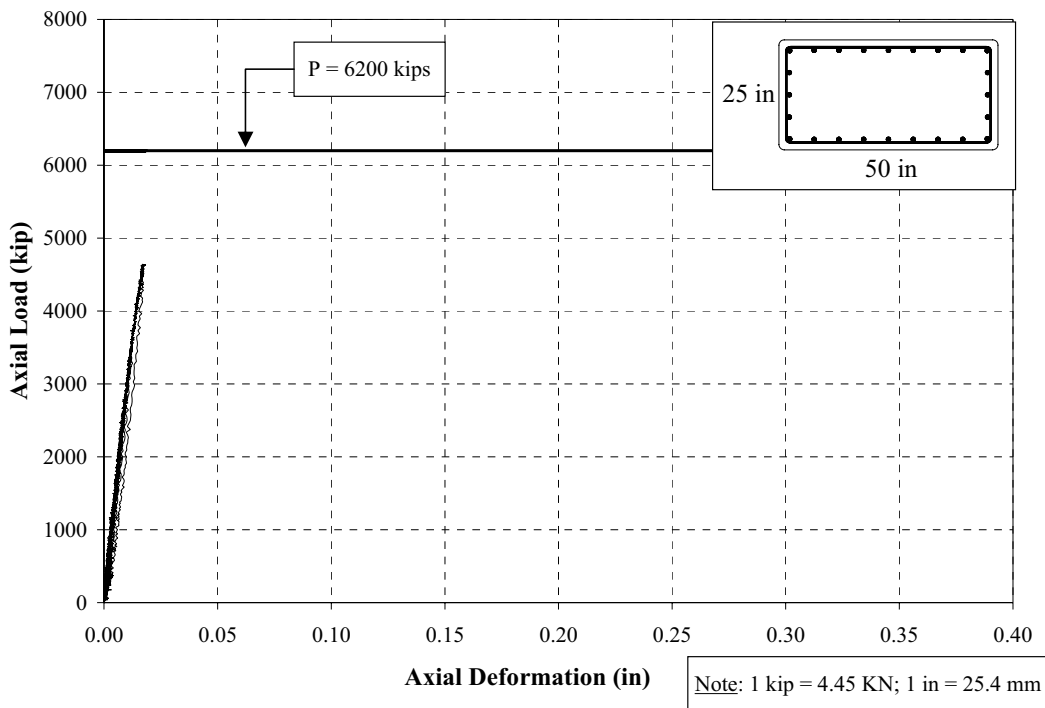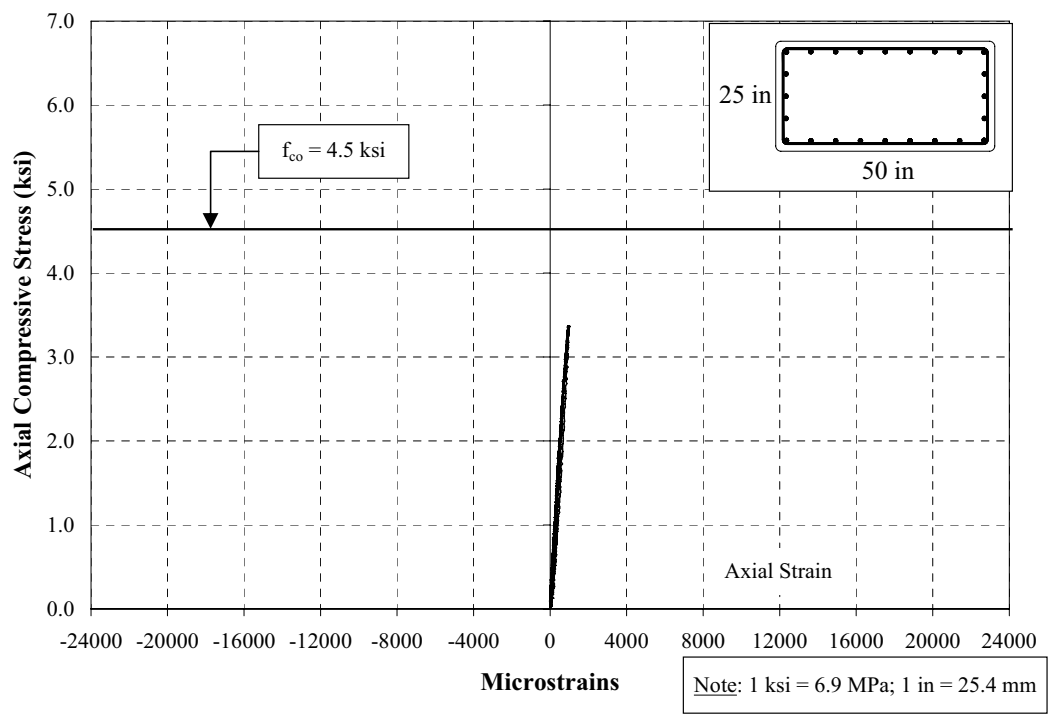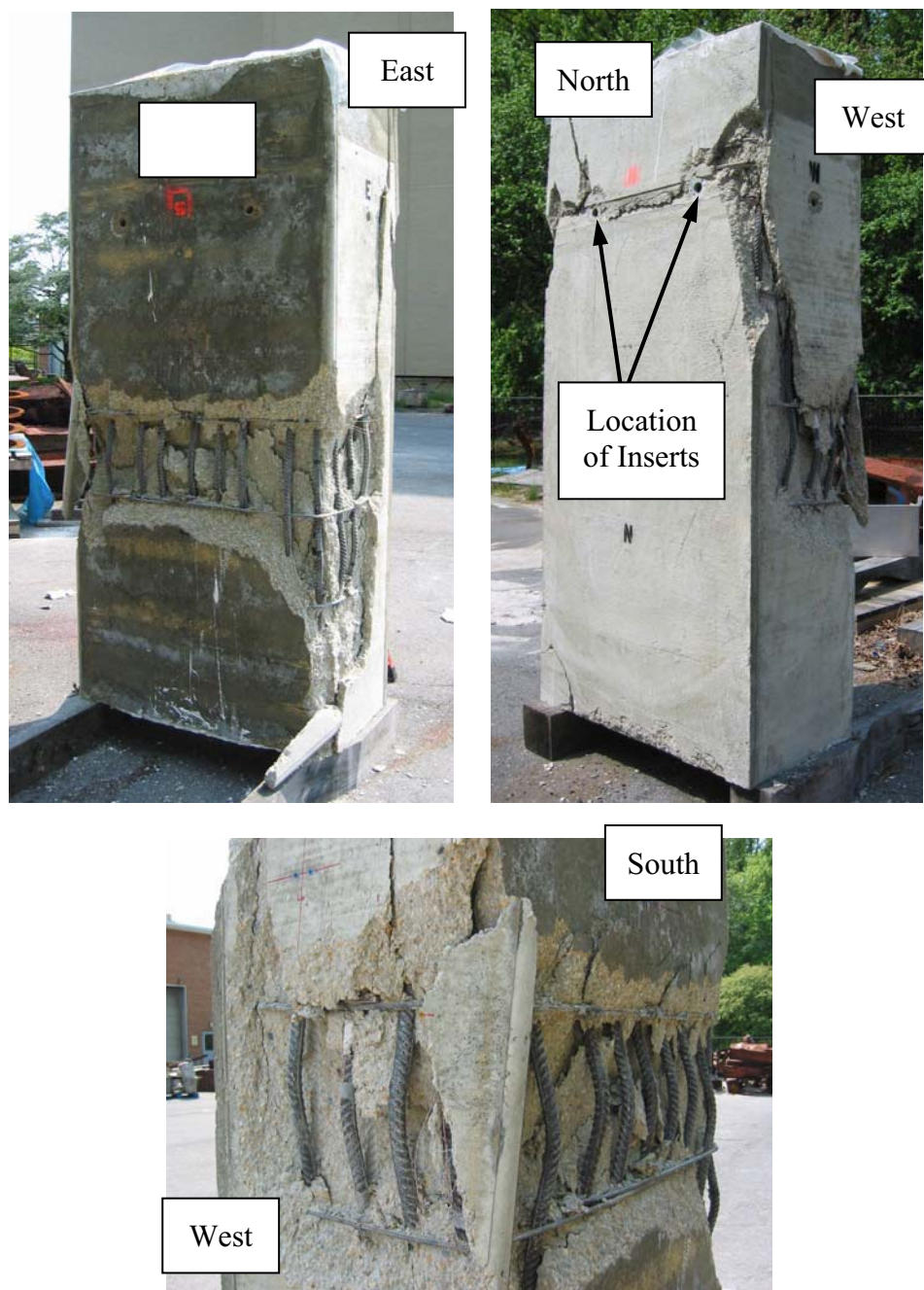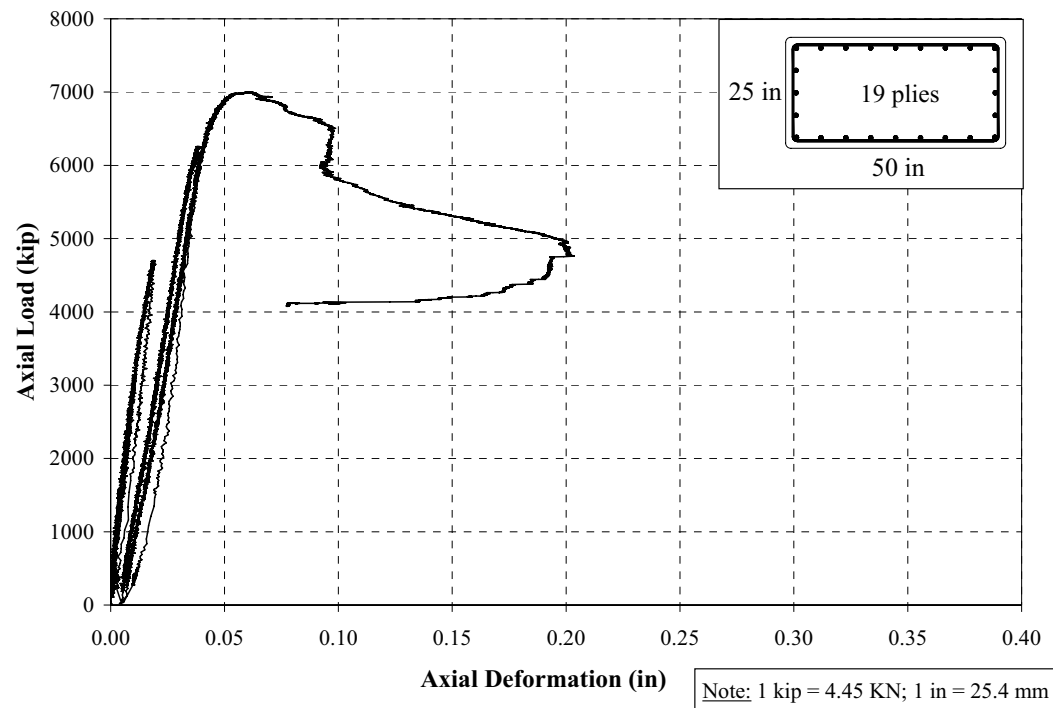


Figure 7-34  Axial Load vs. Axial Deformation; Specimen D3
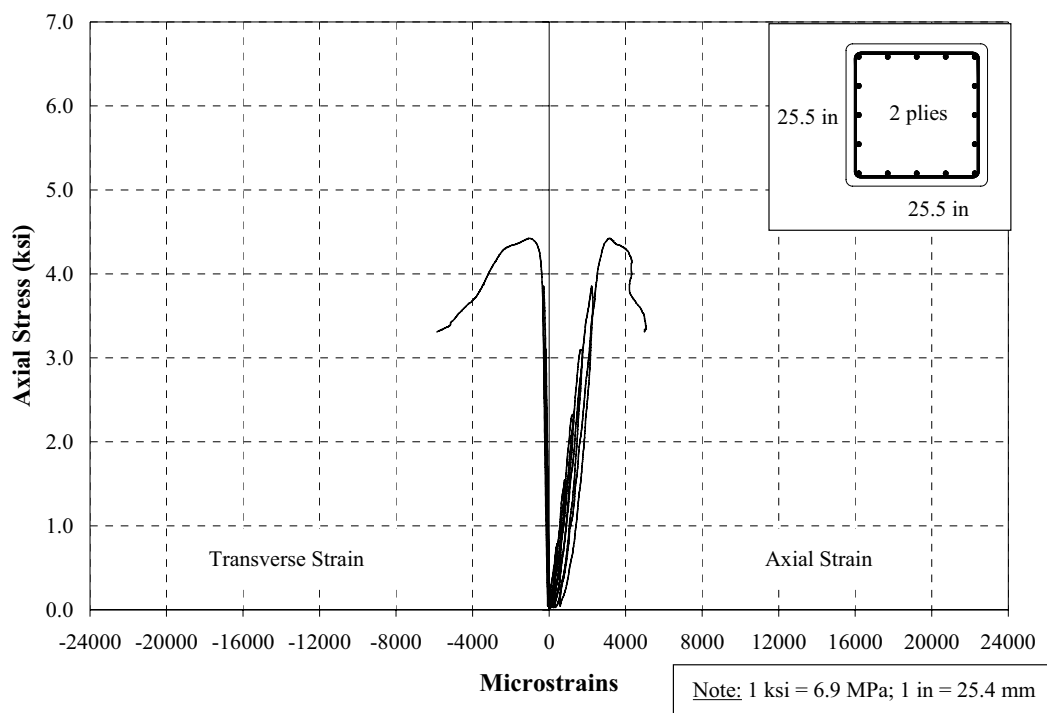
**Figure 7-35  Stress-Strain Behavior; Specimen D3**

**Figure 7-36  Failure of Specimen D3**

### 7.5.    SERIES E; 12.75 x 12.75 x 27 in (324 x 324 x 686 mm)

Table 7-5 presents the results from the experiments on the specimens of this series.  This group was composed of three specimens: E1 (control), E2 (strengthened with two fully wrapped plies), and E3 (strengthened with four partially wrapped plies).

**7.5.1.  Specimen E1.**  This specimen reached failure at an approximate load of 150 kips (668 KN) lower than its actual carrying capacity.  Figure 7-37 and Figure 7-38 present the applied load versus the axial deformation and the axial stress-strain behavior, respectively.  For a maximum load of 601 kips (2675 KN), a compressive stress of 2.75 ksi (19 MPa), and a corresponding axial strain of 0.16 percent, were achieved.  Regarding the failure of the specimen, the vertical cracking started at the bottom end.  The cover spalled on three sides of the column exposing the buckled longitudinal reinforcement at the mid-height (Figure 7-39).

**7.5.2.  Specimen E2.**  Figure 7-40 and Figure 7-41 present the applied load versus the axial deformation, and the stress-strain performance (including both the axial and hoop strains), respectively.  The maximum axial compressive strength achieved by this specimen was of 4.57 ksi (31.5 MPa) with a corresponding axial strain of 0.24 percent and transverse strain of 0.17 percent.  The rupture of the FRP was observed mainly at two locations: at the South-West corner at mid-height and at the bottom of the specimen; at the mid-section on the South face.  The latter was not expected but apparently it was originated at the location of the bracket used to fix the linear transducer on that side.  Unfortunately this took place on a face that was not monitored by the video cameras.  Debonding of the jacket followed its failure, and this occurred approximately along two thirds of the height of the specimen (Figure 7-42)

**7.5.3.  Specimen E3.**  The applied load versus the axial deformation, and the stress-strain behavior are presented in Figure 7-43 and Figure 7-44, respectively.  For a maximum compressive stress of 4.78 ksi (33 MPa) an axial strain of 0.33 percent and a hoop strain of 0.14 percent were achieved.  Regarding the failure of this specimen, a definitive rupture

was observed on the North-East corner at the mid-height level. A breakage of the FRP jacket was also noted at the vertical overlap on the North face (Figure 7-45).

**Table 7-5  Summary of Fundamental Response Parameters; Series E**

|  | E1 | E2 | E3 |
|---|---|---|---|
| $\rho_f$ (%) | N/A | 0.41 | 0.53 |
| $P_{cc}$ (kips) | 601 | 893 | 927 |
| $f'_{cc}$ (ksi) | 2.75 | 4.57 | 4.78 |
| $\varepsilon'_{cc}$ ($\mu\varepsilon$) | 1604 | 2348 | 3327 |
| $\varepsilon_{cu}$ ($\mu\varepsilon$) | 1751 | 2704 | 12030 |
| $\varepsilon_{tc}$ ($\mu\varepsilon$) | N/A | 1732 | 1432 |
| $\varepsilon_{ju}$ ($\mu\varepsilon$) | N/A | 7548 | 7088 |

Note: 1 kip = 4.45 KN; 1 ksi = 6.9 MPa



**Figure 7-37  Axial Load vs. Axial Deformation; Specimen E1**

**Figure 7-38 Stress-Strain Behavior; Specimen E1**



**Figure 7-39 Failure of Specimen E1**

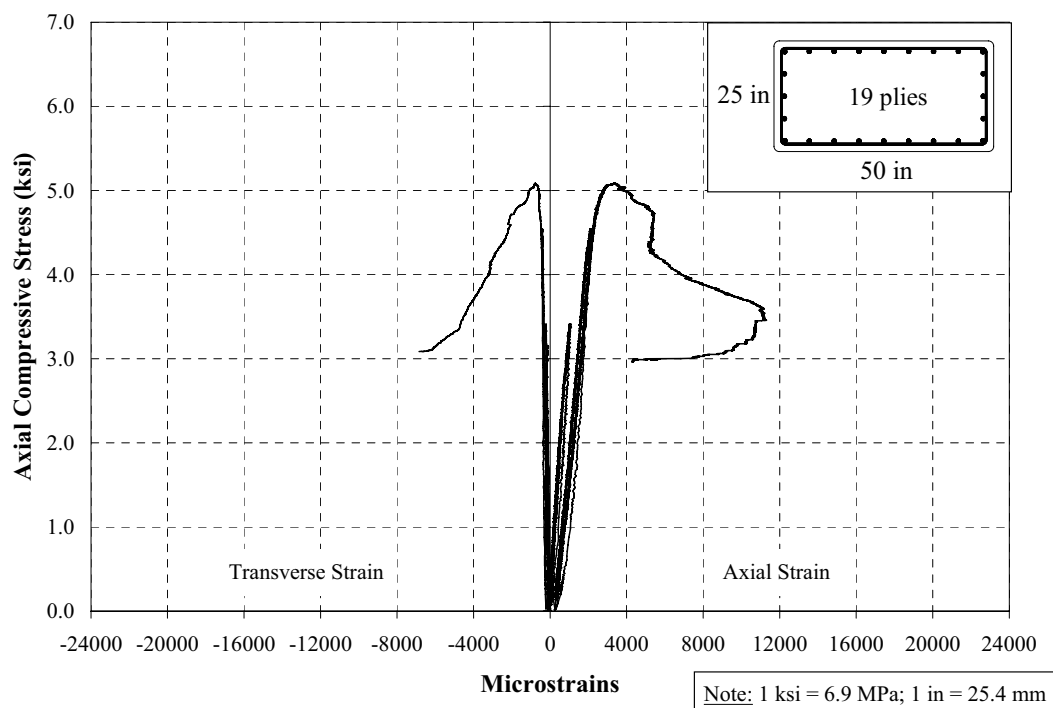**Figure 7-40  Axial Load vs. Axial Deformation; Specimen E2**
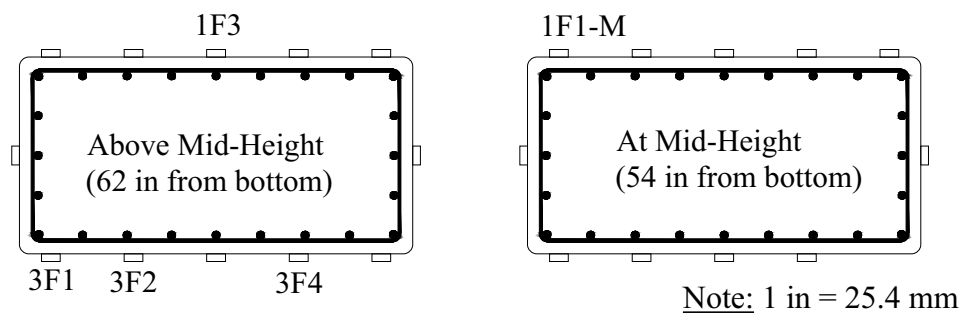


**Figure 7-41  Stress-Strain Behavior; Specimen E2**

**Figure 7-42  Failure of Specimen E2**

**Figure 7-43  Axial Load vs. Axial Deformation; Specimen E3**
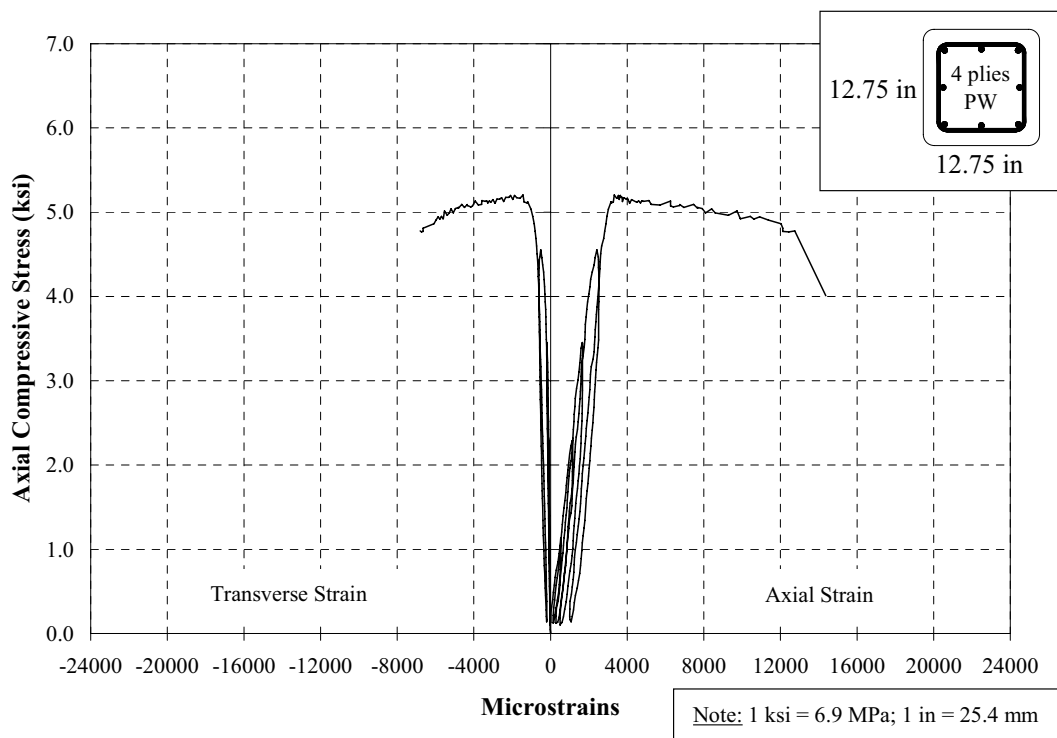


**Figure 7-44  Stress-Strain Behavior; Specimen E3**

**Figure 7-45  Failure of Specimen E3**

## 7.6.    SERIES F; 12.75 x 12.75 x 54 in (324 x 324 x 1372 mm)

Table 7-6 presents the results from the experiments on the specimens of this series.  This group was composed of three specimens: F1 (control), F2 (strengthened with two fully wrapped plies), and F3 (strengthened with four partially wrapped plies).

**7.6.1.   Specimen F1.**  The applied load versus the axial deformation, and the axial stress-strain behavior are shown in Figure 7-46 and Figure 7-47, respectively.  An extra sixth cycle was needed to attain failure.  For a maximum load of 775 kips (3449 KN), a compressive stress of 3.84 ksi (26.5 MPa), and a corresponding axial strain of 0.33 percent were achieved.  About the failure of this specimen, most of the cracking and spalling occurred on the top half of the column, no significant visible damage was observed on the bottom half.  The buckling of the bars was also observed at this location (Figure 7-48).

**7.6.2.   Specimen F2.**  The applied load versus the axial deformation, and the stress-strain behavior are shown in Figure 7-49 and Figure 7-50, respectively.  For a maximum axial compressive stress of 4.39 ksi (30.3 MPa), an axial strain of 0.34 percent and a hoop strain of 0.08 percent were obtained.  The failure of this column was gradual.  On the last stage of the final cycle, the rupture of a narrow strip of FRP jacket on the South-East corner practically at

mid-height was first observed, this was then followed by the rupture of a portion of the jacket at that same corner but extending longitudinally towards the top of the column (Figure 7-51).

**7.6.3. Specimen F3.** Applied load versus axial deformation, and stress-strain behavior corresponding to this column are presented in Figure 7-52 and Figure 7-53, respectively. This column achieved the same peak compressive stress as the previous specimen (4.37 ksi [30.2 MPa]), but the related axial and transverse strain at this level were 0.48 percent and 0.15 percent. This specimen showed ductility enhancement (ultimate axial strain of 1.86 percent) when compared to the two previous specimens in this series. No significant increment of carrying capacity was observed. With regards to the failure of the FRP jacket of this specimen, it occurred on the South. The definitive rupture was preceded by a slight breakage of a small strip on either one of the South corners. There is not certainty of the exact location due to the fact that this side of the column was not directly monitored by the video recording. From the images documentation, it can be observed that the failure took place at the both South corners and above mid-height. The buckling of the longitudinal reinforcement was observed above mid-height level as well (Figure 7-54).

**Table 7-6  Summary of Fundamental Response Parameters; Series F**

|  | F1 | F2 | F3 |
|---|---|---|---|
| $\rho_f (\%)$ | N/A | 0.41 | 0.53 |
| $P_{cc}$ (kips) | 775 | 863 | 861 |
| $f'_{cc}$ (ksi) | 3.84 | 4.39 | 4.37 |
| $\varepsilon'_{cc} (\mu\varepsilon)$ | 3248 | 3380 | 4835 |
| $\varepsilon_{cu} (\mu\varepsilon)$ | 10714 | 11086 | 18648 |
| $\varepsilon_{tc} (\mu\varepsilon)$ | N/A | 842 | 1506 |
| $\varepsilon_{ju} (\mu\varepsilon)$ | N/A | 4848 | 6930 |

Note: 1 kip = 4.45 KN; 1 ksi = 6.9 MPa

**Figure 7-46  Axial Load vs. Axial Deformation; Specimen F1**



**Figure 7-47  Stress-Strain Behavior; Specimen F1**

**Figure 7-48  Failure of Specimen F1**
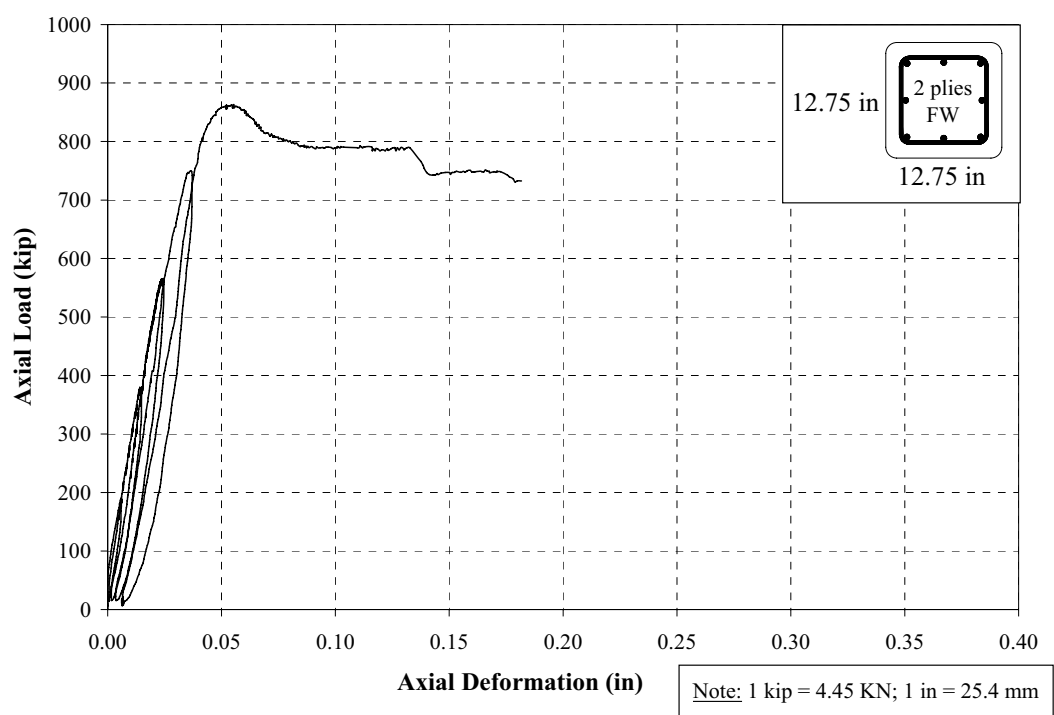


**Figure 7-49  Axial Load vs. Axial Deformation; Specimen F2**

**Figure 7-50  Stress-Strain Behavior; Specimen F2**

**Figure 7-51  Failure of Specimen F2**
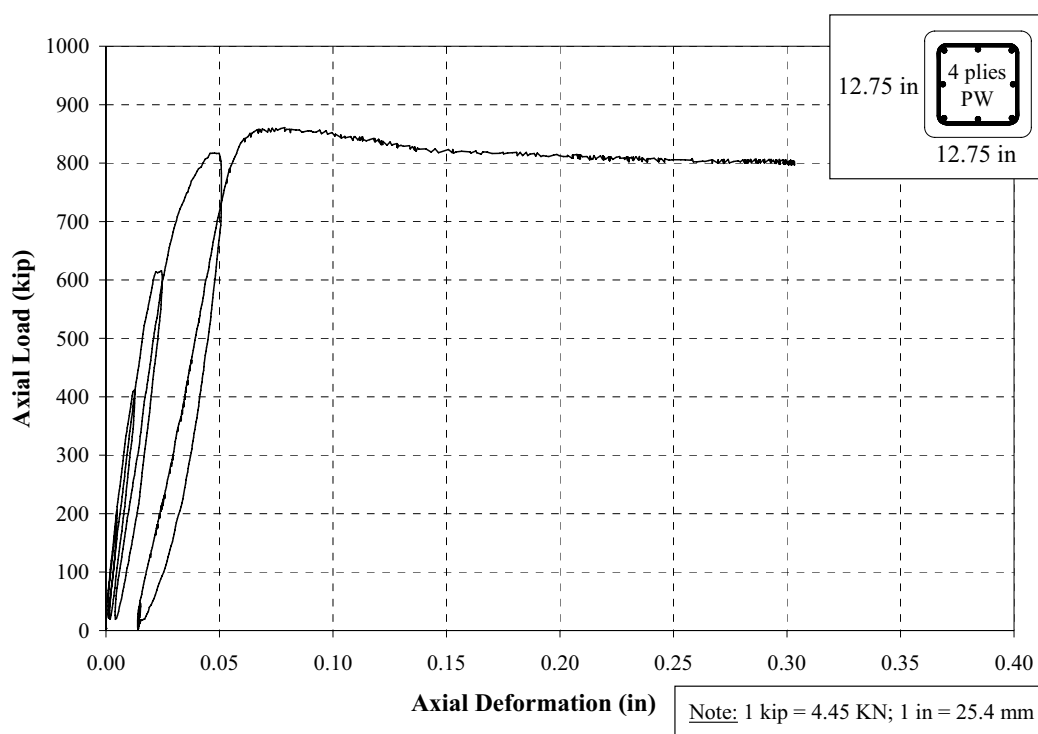


**Figure 7-52  Axial Load vs. Axial Deformation; Specimen F3**
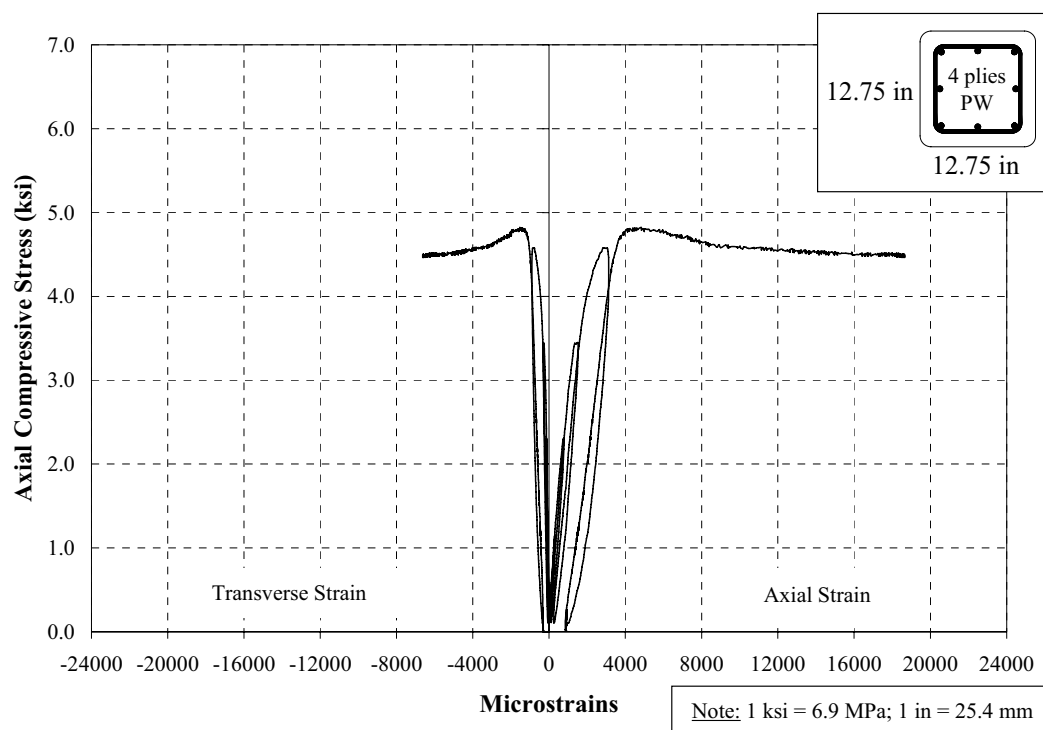
**Figure 7-53  Stress-Strain Behavior; Specimen F3**
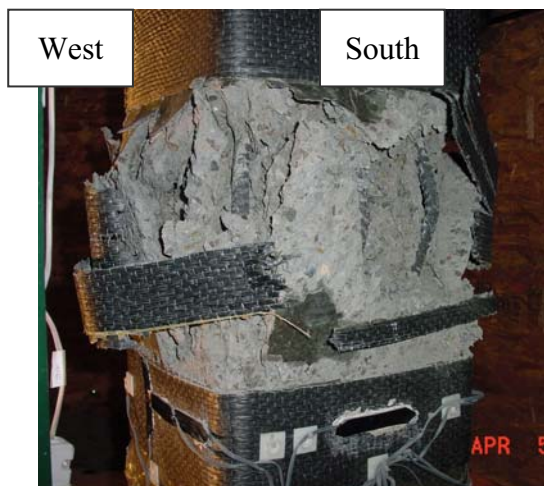
**Figure 7-54  Failure of Specimen F3**


## 7.7.    SERIES G; 36 x 36 x 78 in (915 x 915 x 1981 mm)

Table 7-7 presents the results from the experiments on the specimens of this series.  This group was composed of two specimens: G1 (control), and G2 (strengthened with eight fully wrapped plies).

**7.7.1.   Specimen G1.**  For a maximum load of 6,332 kips (28,177 KN), a compressive stress of 3.40 ksi (23.5 MPa), and a corresponding axial strain of 0.26 percent, were achieved.  Figure 7-55 and Figure 7-56 show the applied load versus the axial deformation, and the stress-strain behavior for this specimen, respectively.  The spalling of the concrete was partial, mainly at mid-height and on three faces of the column.  The exposure of the longitudinal reinforcement was basically observed on only one face of the specimen and right below mid-height (Figure 7-57).

**7.7.2.   Specimen G2.**  For a maximum axial compressive stress of 3.91 ksi (27 MPa) the corresponding axial and transverse strains were 0.33 percent and 0.19 percent, in that order.  The applied load versus the axial deformation and the stress-strain behavior are presented in Figure 7-58 and Figure 7-59, respectively.  Although the increment of axial carrying capacity was not significant with respect to the control specimen, this test unit did show enhancement of ductility in terms of axial deformation (ultimate axial strain of 1.88 percent).  Regarding the failure of this specimen, it was characterized by a single snap at an approximate compressive stress of 3.85 ksi (26.6 MPa).  The rupture of the FRP jacket was mainly on the South-West corner at the mid-height level.  The jacket debonded in portions and different plies along this level on a strip of approximately 16 in wide (406 mm) exposing buckled longitudinal reinforcement (Figure 7-60).

**Table 7-7  Summary of Fundamental Response Parameters; Series G**

|  | **G1** | **G2** |
|---|---|---|
| $\rho_f$ **(%)** | N/A | 0.59 |
| $P_{cc}$ **(kips)** | 6332 | 6935 |
| $f'_{cc}$ **(ksi)** | 3.40 | 3.91 |
| $\varepsilon'_{cc}$ **(με)** | 2566 | 3307 |
| $\varepsilon_{cu}$ **(με)** | 5146 | 28202 |
| $\varepsilon_{tc}$ **(με)** | N/A | 1909 |
| $\varepsilon_{ju}$ **(με)** | N/A | 11130 |

Note: 1 kip = 4.45 KN; 1 ksi = 6.9 MPa
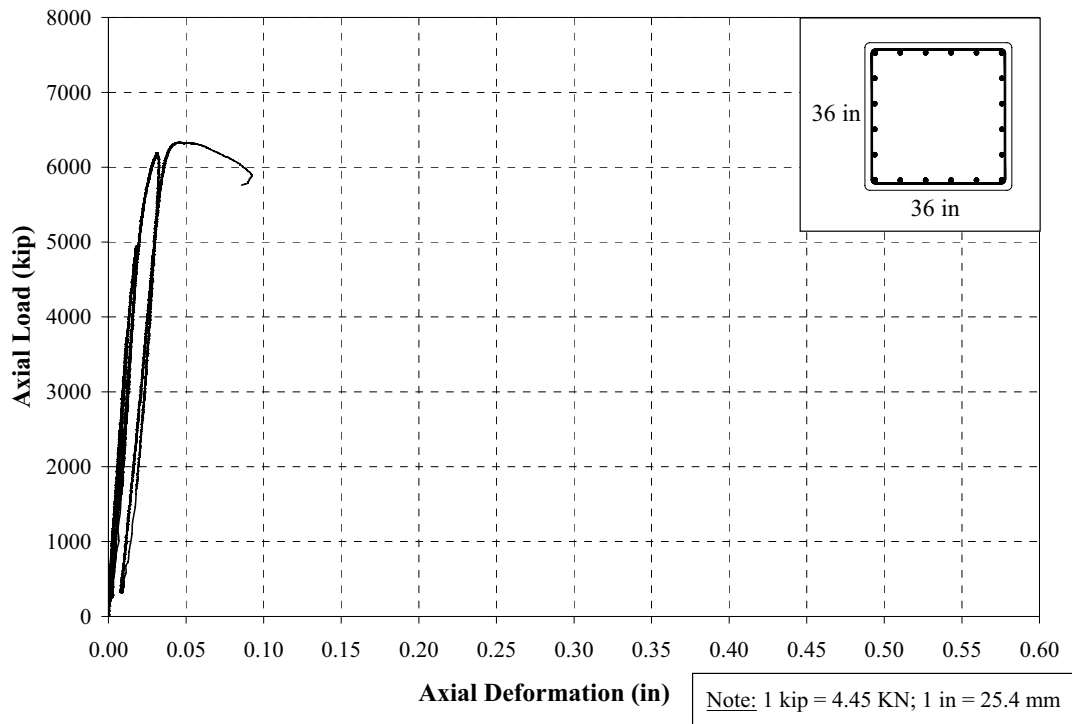


**Figure 7-55  Axial Load vs. Axial Deformation; Specimen G1**

**Figure 7-56  Stress-Strain Behavior; Specimen G1**



**Figure 7-57  Failure of Specimen G1**

**Figure 7-58  Axial Load vs. Axial Deformation; Specimen G2**



**Figure 7-59  Stress-Strain Behavior; Specimen G2**

**Figure 7-60  Failure of Specimen G2**

## 7.8.    SERIES H; 25 x 50 x 108 in (635 x 1270 x 2743 mm)

Table 7-8 presents the results from the experiments on the specimens of this series.  This group was composed of two specimens: H1 (control), and H2 (strengthened with 19 fully wrapped plies).

**7.8.1.  Specimen H1.**  Due to a DAS inconvenience the last load cycle applied to this specimen was lost.  From video tape recording documentation it was possible to learn the load at which this specimen failed, therefore the maximum compressive stress attained was 3.49 ksi (24.1 MPa).  About its failure, the spalling of the cover primarily occurred on three faces and at mid-height.  Concrete cover cracking was also noted on the North face as consequence of the mechanical inserts fixed on the column for transporting.  The buckling of the longitudinal reinforcement was observed at the location right below mid-height level (Figure 7-63).

**7.8.2. Specimen H2.** The applied load versus the axial deformation is presented in Figure 7-64. Figure 7-65 shows the stress-strain response corresponding to this specimen. In this figure are depicted both the axial and the hoop strains, the latter corresponding the longer sides of the cross-section. For a maximum load of 7000 kips (31150 KN) the corresponding compressive stress was 4.14 ksi (28.6 MPa).

Due to problems of the DAS many sensors on the FRP presented highly scatter values and therefore were not considered acceptable. Only five sensors were taken into account: 1F1-M (at mid-height), 1F3, 3F1, 3F2, and 3F4 (at 8 in [203 mm] above mid-height) (Figure 7-66). Regarding the failure of this column, it was characterized by a first rupture of the FRP jacket at the South-West corner slightly above mid-height, this was followed by another breaks at the North-East and North-West corners. The jacket broke and debonded in strips of different widths and number of plies, mainly at the central part of the column revealing buckled longitudinal reinforcement on the four faces of the specimen (Figure 7-67).

**Table 7-8  Summary of Fundamental Response Parameters; Series H**

|  | **H1** | **H2** |
|---|---|---|
| $\rho_f$ **(%)** | N/A | 1.50 |
| $P_{cc}$ **(kips)** | 6200 | 7000 |
| $f'_{cc}$ **(ksi)** | 3.49 | 4.14 |
| $\varepsilon'_{cc}$ **($\mu\varepsilon$)** | * | 3774 |
| $\varepsilon_{cu}$ **($\mu\varepsilon$)** | * | 11270 |
| $\varepsilon_{tc}$ **($\mu\varepsilon$)** | N/A | 785** |
| $\varepsilon_{ju}$ **($\mu\varepsilon$)** | N/A | * |

Note: * Values not provided due to DAS problems; ** Approximate value; 1 kip = 4.45 KN; 1 ksi = 6.9 MPa

**Figure 7-61  Axial Load vs. Axial Deformation; Specimen H1**



**Figure 7-62  Stress-Strain Behavior; Specimen H1**

**Figure 7-63 Failure of Specimen H1**

**Figure 7-64  Axial Load vs. Axial Deformation; Specimen H2**



**Figure 7-65  Stress-Strain Behavior; Specimen H2**

1F3

Above Mid-Height
(62 in from bottom)

3F1    3F2        3F4

1F1-M

At Mid-Height
(54 in from bottom)

Note: 1 in = 25.4 mm

**Figure 7-66  Location of Selected Strain Gages on FRP; Specimen H2**
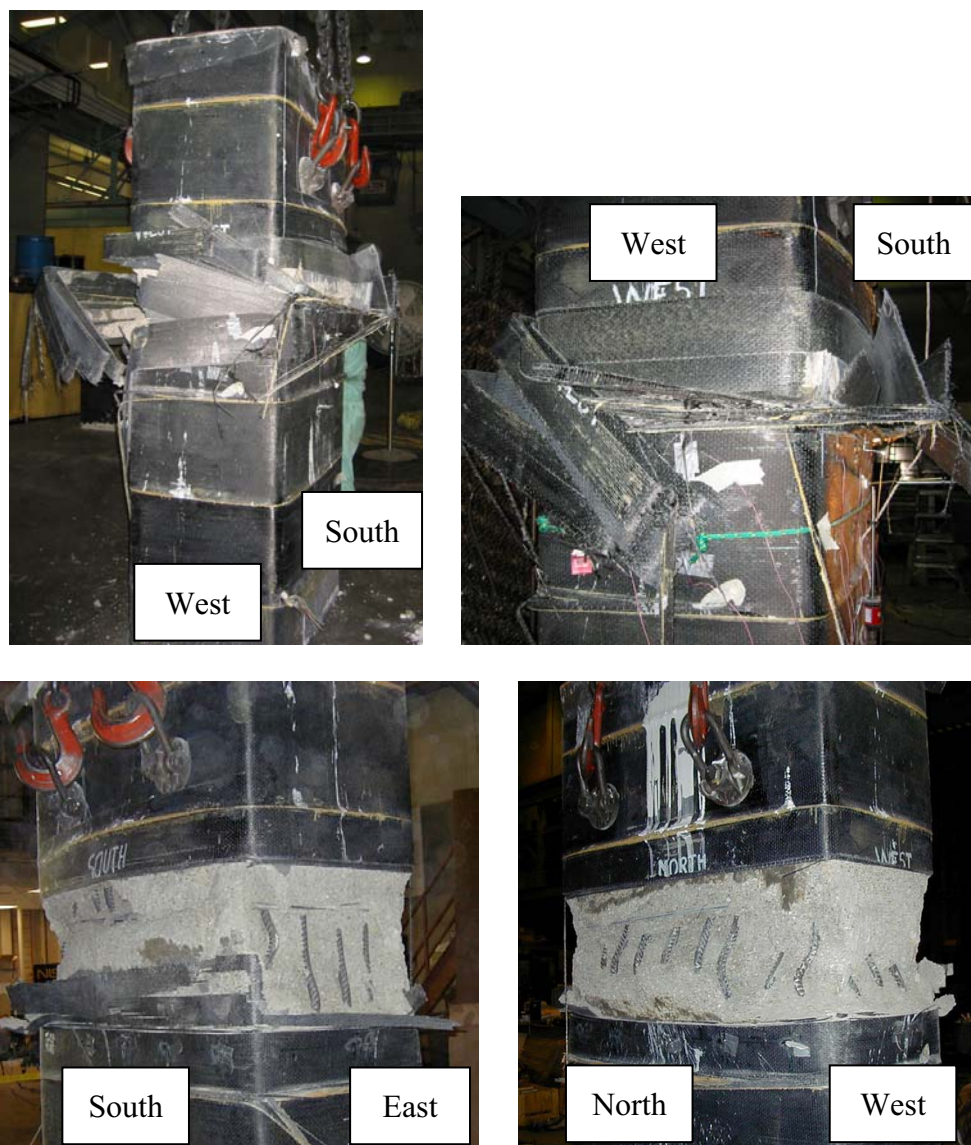


**Figure 7-67  Failure of Specimen H2**

## 8. DISCUSSION OF RESULTS

This chapter discusses the results obtained in the experimental program and their performance with respect to current available data (Section 4). In Section 8.1 each series of specimens is addressed as an individual group. Section 8.2 is divided in two subsections, where the first one presents comparisons of solely the experimental results obtained in this study, and the comparisons in the second subsection include this data along with the collected literature. Section 8.3 shows comparisons of the strengthening ratios obtained experimentally for each specimen against design values provided by the international guidelines previously introduced in Chapter 5.

### 8.1. PERFORMANCE EVALUATION OF INDIVIDUAL SERIES

The following tables present summaries of the basic response parameters per each group of specimens. The comparisons are shown in terms of ratios of the response parameters of the strengthened specimens to the corresponding control unit in each of the series. This assessment is based particularly on the increment of concrete compressive strength (strengthening ratio $f'_{cc}/f'_{co}$) since the test matrix itself was conceived in order to evaluate the performance of specimens strengthened to achieve a 30 percent increment in carrying capacity (reflected in the axial compressive strength), and to observe the effect of prismatic cross-sections when wrapped with the same number of plies that a circular cross-section (uniformly confined) required to attain a 30 percent of increment as well.

From Figure 8-1 to Figure 8-8, the strengthening ratio is plotted versus the same factor used in Section 4 to analyze the up-to-date available data: $\rho_f * E_f/E_c$, being $\rho_f$ the volumetric ratio of FRP, $E_f$ and $E_c$ the elastic modulus of FRP and concrete, respectively.

With regards to the notations used in these plots, note that the numbers labeling each point correspond to the number of plies utilized in the represented specimen.

**8.1.1. Series A.** The performance of these circular specimens was as expected, both strengthened specimens overcame the 30 percent increase of carrying capacity prescribed in the design, as it can be seen in Table 8-1, in fact the levels reached by specimen A2 and A3 in percentages were 35 and 39, respectively. Regarding the concrete compressive strength, specimen A2, fully wrapped with two plies, and specimen A3, partially wrapped with four plies, showed similar increments: 44 and 49, respectively (Figure 8-1).

**8.1.2. Series B.** Regarding the increment of load carrying capacity, in Table 8-2 it can be observed that specimen B2, which was fully wrapped with seven plies, roughly reached the design increment of 30 percent, on the contrary of specimen B3, featuring two plies, that did not have a significant effect (seven percent). About the ductility in terms of axial deformation, both specimens showed good performance, in particular specimen B2.

The strengthening ratios for this series are presented in Figure 8-2. Increments of 34 and nine percent were attained by specimen B2 and specimen B3, respectively.

**8.1.3. Series C.** Regarding the increments of load carrying capacity, in Table 8-3 it can be observed that specimen C2, which was fully wrapped with four plies, and specimen C3, featuring two fully wrapped plies, had both very limited strengthening effect: nine and five percent, respectively. About the ductility in terms of axial deformation, both specimens showed limited improvement.

The strengthening ratios for this series are presented in Figure 8-3. Increments of 12 and seven percent were attained by specimen C2 and specimen C3, respectively.

**8.1.4. Series D.** With regards to the increments of load carrying capacity, in Table 8-4 it can be observed that specimen D2, which was fully wrapped with five plies, and specimen D3, featuring two fully wrapped plies, had both very narrow strengthening effects: 16 and six percent, respectively. About the ductility in terms of axial deformation, both specimens showed limited improvement, in particular specimen D3.

The strengthening ratios for this series are presented in Figure 8-4. Increments of 20 and seven percent were attained by specimens D2 and D3, respectively.

**8.1.5. Series E.** It was previously noted that the control specimen E1 failed prematurely, therefore the ratios presented in Table 8-5 are considered not to be truly representative of the strengthening effect in specimens E2 (two fully wrapped plies) and E3 (four partially wrapped plies). Since series F featured specimens of equal geometrical properties with the exception of the height (double the one of series E), and about the same cylindrical concrete compressive strength; therefore the strengthened specimens E2 and E3 were compared only in terms of axial compressive strength against the control specimen of series F (F1) in order to have a more illustrative trend of the strengthening performance being aware of the possible effect of the different height-to-side ratio. Both comparisons are shown in Figure 8-5. The increment of axial compressive stress of specimens E2 and E3 when compared to F1 are 19 and 24 percent, in that order.

**8.1.6. Series F.** With regards to the increments of load carrying capacity, in Table 8-6 it can be observed that specimen F2, fully wrapped with 2 plies, and specimen F3, featuring four partially wrapped plies, had both the same strengthening level effect: 11 percent. The strengthening ratios were 1.14 for both specimens (Figure 8-6). About the ductility in terms of axial deformation, both specimens showed very small improvement.

**8.1.7. Series G.** As it can be seen in Table 8-7 the improvement of load carrying capacity and concrete compressive strength attained by specimen G2 (eight fully wrapped plies) were 10 percent and 1.15 times the concrete strength from specimen G1. Axial ductility was also enhanced about 5.5 times the maximum axial strain observed in specimen G1.

**8.1.8. Series H.** The load carrying capacity reached by the strengthened specimen was 13 percent higher than the one in the control specimen (Table 8-8). A slightly higher percentage (19) was observed regarding the concrete compressive strength (Figure 8-8).

**Table 8-1  Summary of Specimens Series A**

|  | A1 | A2 | A3 |
|---|---|---|---|
| $\rho_f$ (%) | N/A | 0.26 | 0.34 |
| $P_{cc}$ (kips) | 1493 | 2014 | 2069 |
| $P_{cc}/P_{co}$ | 1.00 | 1.35 | 1.39 |
| $f'_{cc}$ (ksi) | 3.81 | 5.50 | 5.67 |
| $f'_{cc}/f'_{co}$ | 1.00 | 1.44 | 1.49 |
| $\varepsilon'_{cc}$ ($\mu\varepsilon$) | 2600 | 12284 | 7366 |
| $\varepsilon'_{cc}/\varepsilon'_{co}$ | 1.00 | 4.72 | 2.83 |
| $\varepsilon_{cu}$ ($\mu\varepsilon$) | 2600 | 12284 | 14692 |
| $\varepsilon_{cu}/\varepsilon_{cu}$ | 1.00 | 4.72 | 5.65 |

Note: 1 kip = 4.45 KN; 1 ksi = 6.9 MPa
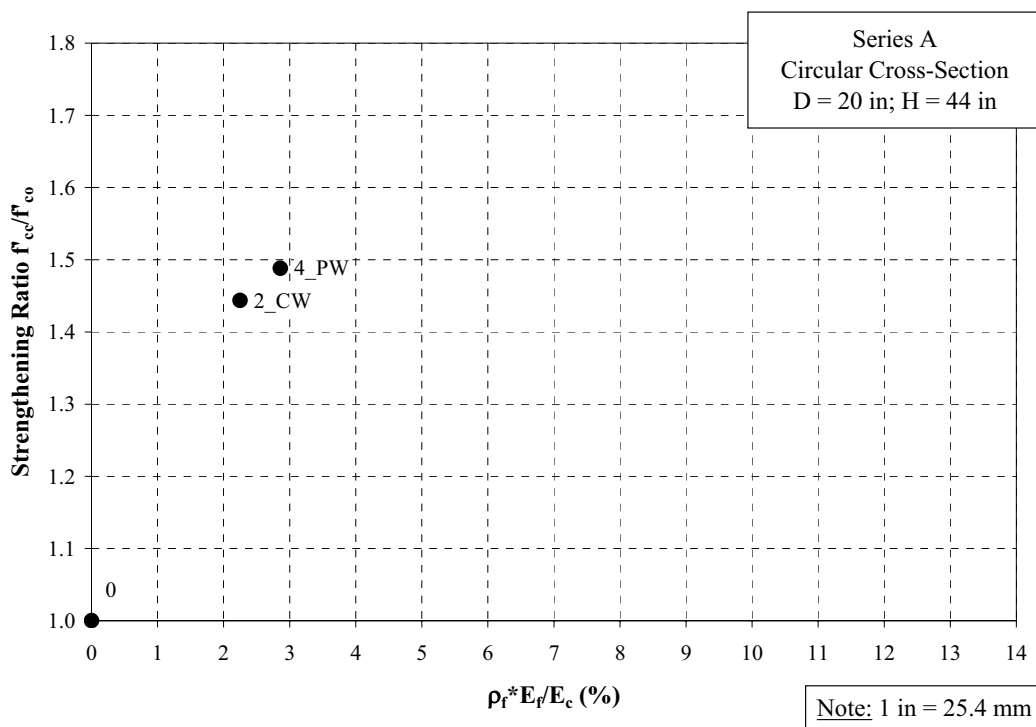


**Figure 8-1  Strengthening Performance; Series A**

**Table 8-2  Summary of Specimens Series B**

|  | **B1** | **B2** | **B3** |
|---|---|---|---|
| $\rho_f$ (%) | N/A | 1.11 | 0.32 |
| $P_{cc}$ (kips) | 1331 | 1674 | 1423 |
| $P_{cc}/P_{co}$ | 1.00 | 1.26 | 1.07 |
| $f'_{cc}$ (ksi) | 3.30 | 4.41 | 3.60 |
| $f'_{cc}/f'_{co}$ | 1.00 | 1.34 | 1.09 |
| $\varepsilon'_{cc}$ ($\mu\varepsilon$) | 1465 | 2891 | 2277 |
| $\varepsilon'_{cc}/\varepsilon'_{co}$ | 1.00 | 1.97 | 1.55 |
| $\varepsilon_{cu}$ ($\mu\varepsilon$) | 1465 | 22724 | 7507 |
| $\varepsilon_{cu}/\varepsilon_{cu}$ | 1.00 | 15.51 | 5.13 |

Note: 1 kip = 4.45 KN; 1 ksi = 6.9 MPa
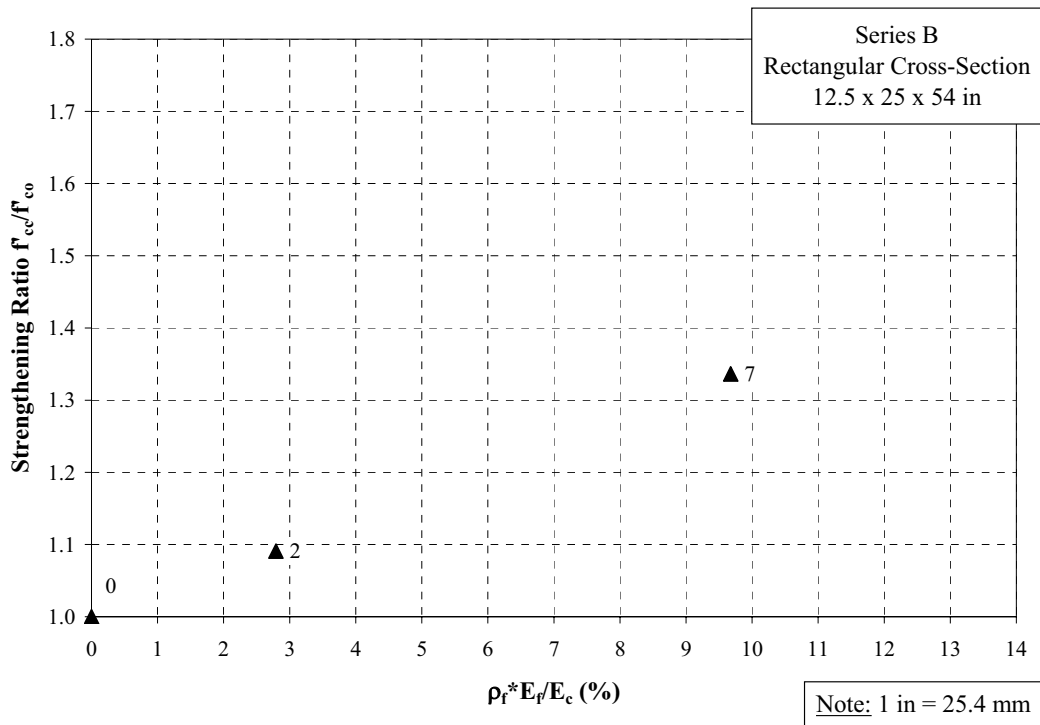


**Figure 8-2  Strengthening Performance; Series B**

**Table 8-3  Summary of Specimens Series C**

|  | C1 | C2 | C3 |
|---|---|---|---|
| $\rho_f$ (%) | N/A | 0.59 | 0.29 |
| $P_{cc}$ (kips) | 1515 | 1659 | 1593 |
| $P_{cc}/P_{co}$ | 1.00 | 1.09 | 1.05 |
| $f'_{cc}$ (ksi) | 3.77 | 4.22 | 4.02 |
| $f'_{cc}/f'_{co}$ | 1.00 | 1.12 | 1.07 |
| $\varepsilon'_{cc}$ ($\mu\varepsilon$) | 2365 | 5063 | 2679 |
| $\varepsilon'_{cc}/\varepsilon'_{co}$ | 1.00 | 2.14 | 1.13 |
| $\varepsilon_{cu}$ ($\mu\varepsilon$) | 2423 | 10605 | 8545 |
| $\varepsilon_{cu}/\varepsilon_{cu}$ | 1.00 | 4.38 | 3.53 |

Note: 1 kip = 4.45 KN; 1 ksi = 6.9 MPa
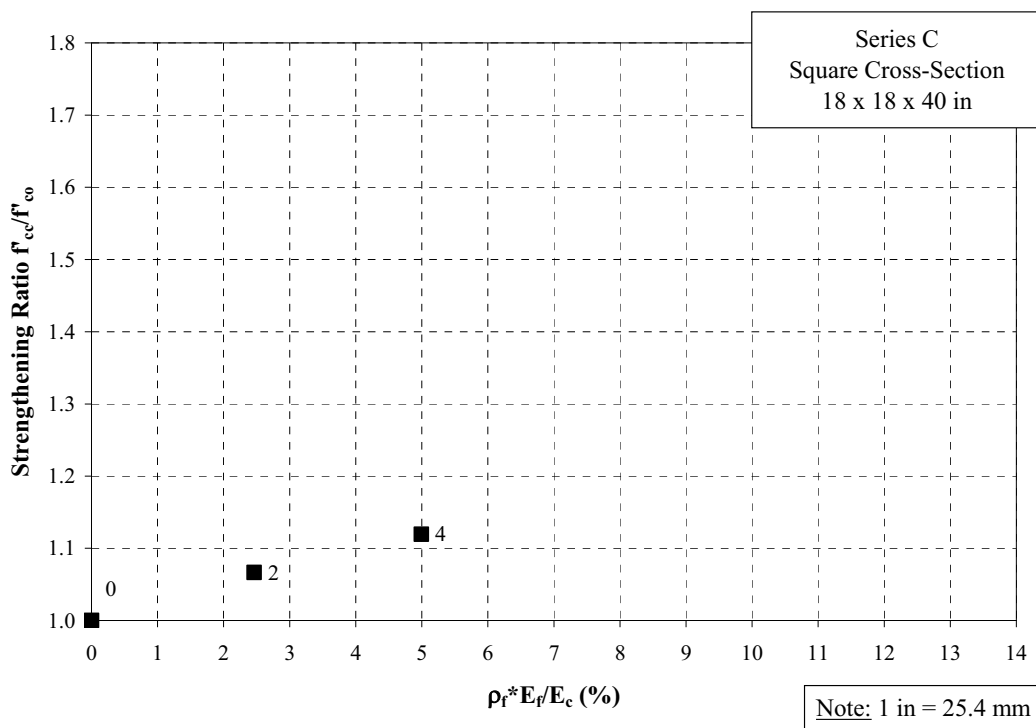


**Figure 8-3  Strengthening Performance; Series C**

**Table 8-4  Summary of Specimens Series D**

|  | D1 | D2 | D3 |
|---|---|---|---|
| $\rho_f$ (%) | N/A | 0.52 | 0.21 |
| $P_{cc}$ (kips) | 2981 | 3444 | 3154 |
| $P_{cc}/P_{co}$ | 1.00 | 1.16 | 1.06 |
| $f'_{cc}$ (ksi) | 3.68 | 4.40 | 3.95 |
| $f'_{cc}/f'_{co}$ | 1.00 | 1.20 | 1.07 |
| $\varepsilon'_{cc}$ ($\mu\varepsilon$) | 2458 | 3880 | 3122 |
| $\varepsilon'_{cc}/\varepsilon'_{co}$ | 1.00 | 1.58 | 1.27 |
| $\varepsilon_{cu}$ ($\mu\varepsilon$) | 2880 | 9093 | 4990 |
| $\varepsilon_{cu}/\varepsilon_{cu}$ | 1.00 | 3.16 | 1.73 |

Note: 1 kip = 4.45 KN; 1 ksi = 6.9 MPa
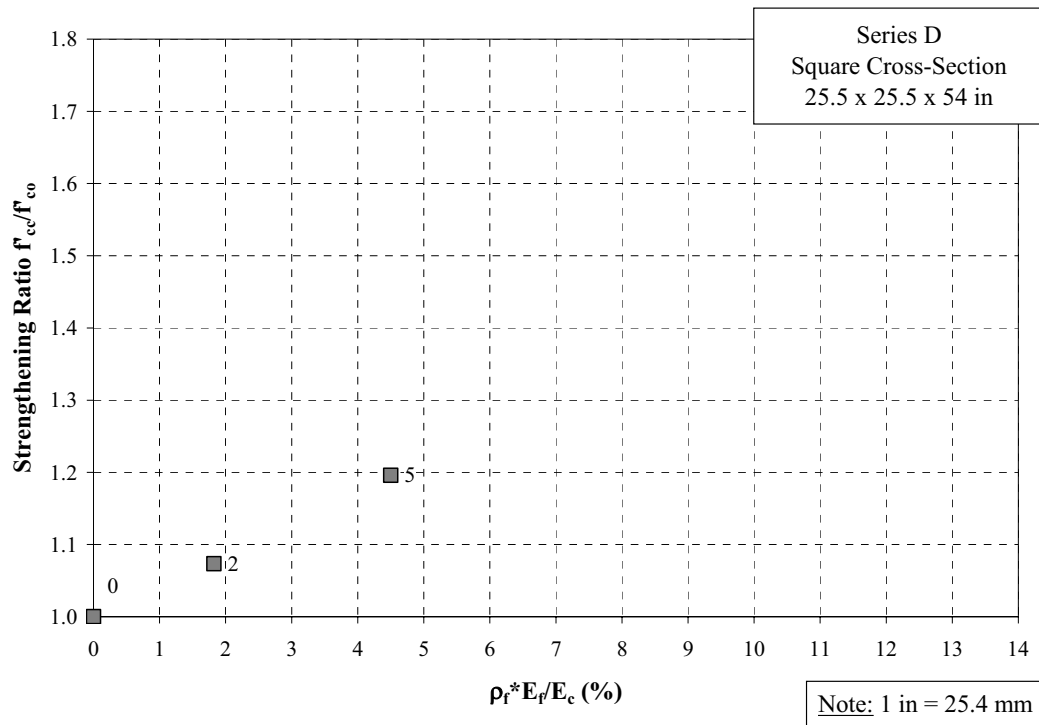


**Figure 8-4  Strengthening Performance; Series D**

**Table 8-5  Summary of Specimens Series E**

|  | E1 | E2 | E3 |
|---|---|---|---|
| $\rho_f$ (%) | N/A | 0.41 | 0.53 |
| $P_{cc}$ (kips) | 601 | 893 | 927 |
| $P_{cc}/P_{coE1}$ | 1.00 | 1.49 | 1.54 |
| $P_{cc}/P_{coF1}$ | N/A | 1.15 | 1.20 |
| $f'_{cc}$ (ksi) | 2.75 | 4.57 | 4.78 |
| $f'_{cc}/f'_{coE1}$ | 1.00 | 1.66 | 1.74 |
| $f'_{cc}/f'_{coF1}$ | N/A | 1.19 | 1.24 |
| $\varepsilon'_{cc}$ ($\mu\varepsilon$) | 1604 | 2348 | 3327 |
| $\varepsilon'_{cc}/\varepsilon'_{co}$ | 1.00 | 1.46 | 2.07 |
| $\varepsilon_{cu}$ ($\mu\varepsilon$) | 1751 | 2704 | 12030 |
| $\varepsilon_{cu}/\varepsilon_{cu}$ | 1.00 | 1.54 | 6.87 |

<u>Note:</u> 1 kip = 4.45 KN; 1 ksi = 6.9 MPa
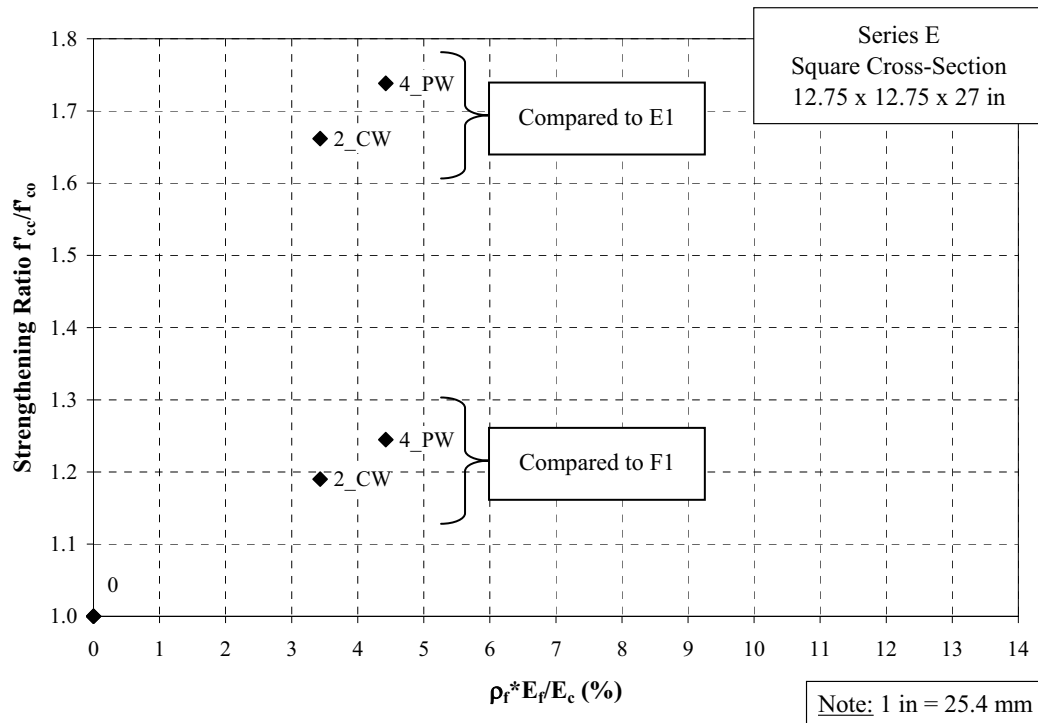


**Figure 8-5  Strengthening Performance; Series E**

**Table 8-6  Summary of Specimens Series F**

|  | F1 | F2 | F3 |
|---|---|---|---|
| $\rho_f$ (%) | N/A | 0.41 | 0.53 |
| $P_{cc}$ (kips) | 775 | 863 | 861 |
| $P_{cc}/P_{co}$ | 1.00 | 1.11 | 1.11 |
| $f'_{cc}$ (ksi) | 3.84 | 4.39 | 4.37 |
| $f'_{cc}/f'_{co}$ | 1.00 | 1.14 | 1.14 |
| $\varepsilon'_{cc}$ ($\mu\varepsilon$) | 3248 | 3380 | 4835 |
| $\varepsilon'_{cc}/\varepsilon'_{co}$ | 1.00 | 1.04 | 1.49 |
| $\varepsilon_{cu}$ ($\mu\varepsilon$) | 10714 | 11086 | 18648 |
| $\varepsilon_{cu}/\varepsilon_{cu}$ | 1.00 | 1.03 | 1.74 |

Note: 1 kip = 4.45 KN; 1 ksi = 6.9 MPa
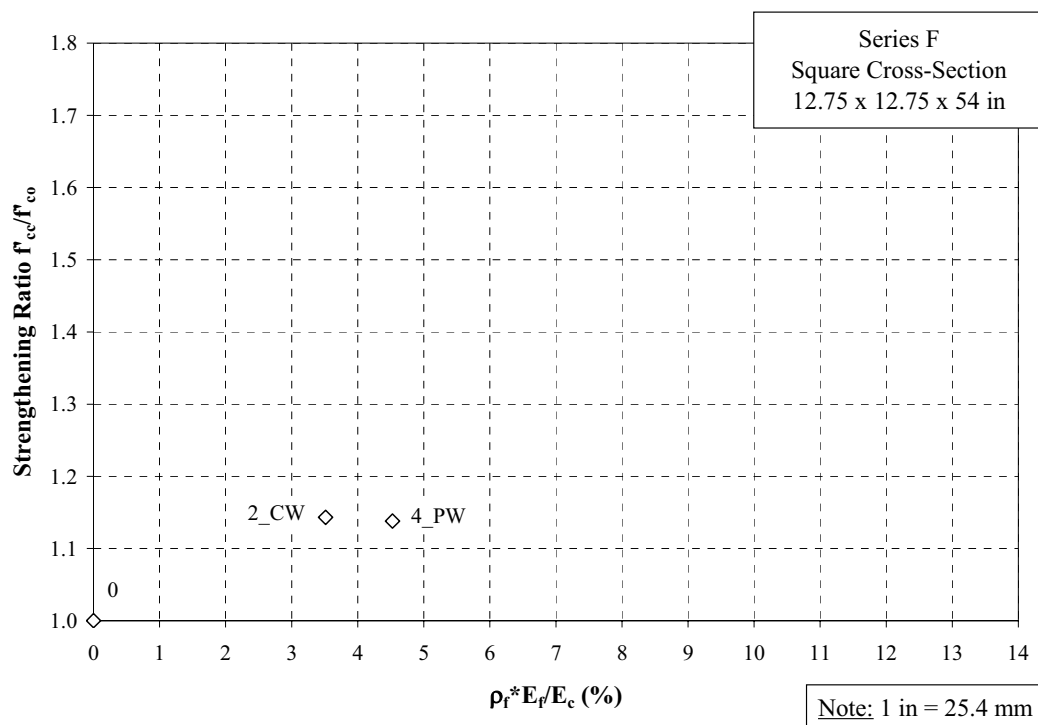


**Figure 8-6  Strengthening Performance; Series F**

**Table 8-7  Summary of Specimens Series G**

|  | G1 | G2 |
|---|---|---|
| $\rho_f$ (%) | N/A | 0.59 |
| $P_{cc}$ (kips) | 6332 | 6935 |
| $P_{cc}/P_{cc}$ | 1.00 | 1.10 |
| $f'_{cc}$ (ksi) | 3.40 | 3.91 |
| $f'_{cc}/f'_{co}$ | 1.00 | 1.15 |
| $\varepsilon'_{cc}$ ($\mu\varepsilon$) | 2566 | 3307 |
| $\varepsilon'_{cc}/\varepsilon'_{co}$ | 1.00 | 1.29 |
| $\varepsilon_{cu}$ ($\mu\varepsilon$) | 5146 | 28202 |
| $\varepsilon_{cu}/\varepsilon_{cu}$ | 1.00 | 5.48 |

Note: 1 kip = 4.45 KN; 1 ksi = 6.9 MPa
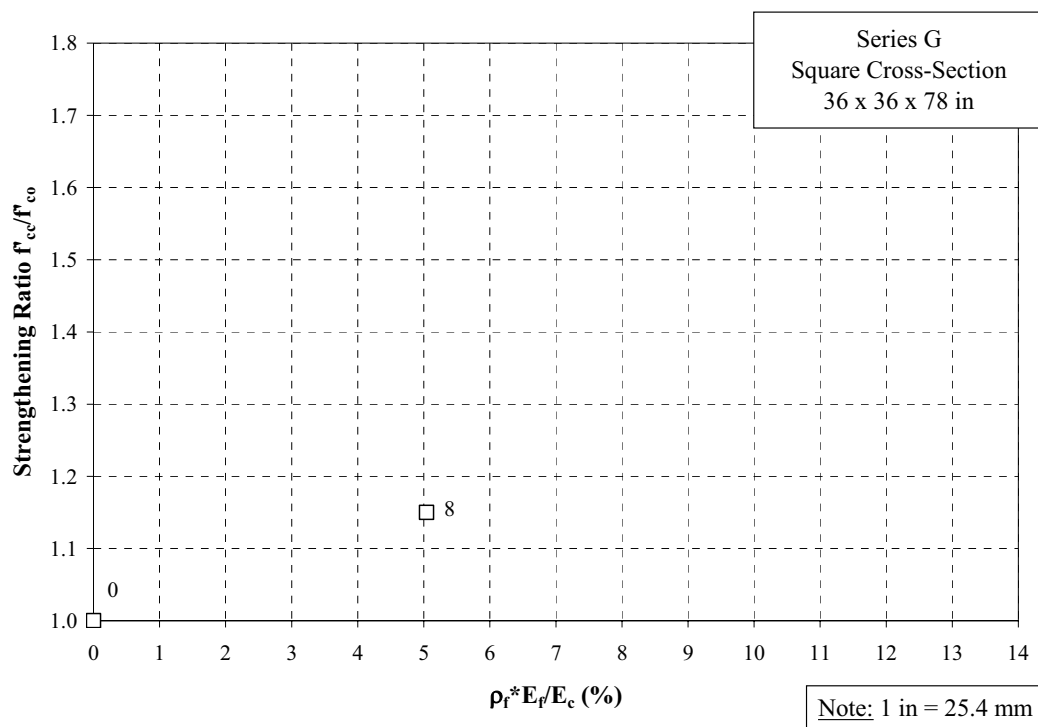


**Figure 8-7  Strengthening Performance; Series G**

**Table 8-8  Summary of Specimens Series H**

|  | H1 | H2 |
|---|---|---|
| $\rho_f$ (%) | N/A | 1.50 |
| $P_{cc}$ (kips) | 6200 | 7000 |
| $P_{cc}/P_{co}$ | 1.00 | 1.13 |
| $f'_{cc}$ (ksi) | 3.49 | 4.14 |
| $f'_{cc}/f'_{co}$ | 1.00 | 1.19 |
| $\varepsilon'_{cc}$ ($\mu\varepsilon$) | * | 3774 |
| $\varepsilon'_{cc}/\varepsilon'_{co}$ | NA | NA |
| $\varepsilon_{cu}$ ($\mu\varepsilon$) | * | 11270 |
| $\varepsilon_{cu}/\varepsilon_{cu}$ | NA | NA |

Note: * Data not available; 1 kip = 4.45 KN; 1 ksi = 6.9 MPa
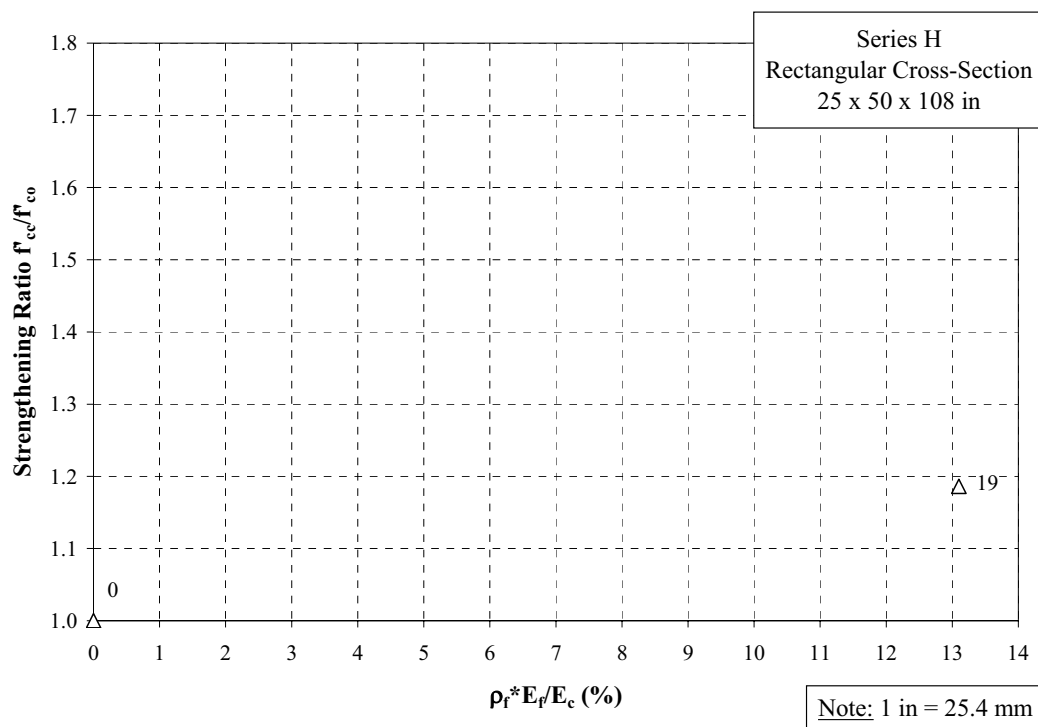


**Figure 8-8  Strengthening Performance; Series H**

## 8.2.    STRENGTHENING PERFORMANCE EVALUATION

**8.2.1.    Comparison within Test Matrix.**  Since this research study is focused on the investigation of size effect in the strengthening of RC columns, and for that reason the test matrix was precisely conceived with a variety of cross-section shapes and area-size (medium and full size), different comparisons based on these variations are presented in this section.  The matrix-scheme shown in Figure 8-9 is to aid the reader visualizing the order on which the comparisons are made.  The cross-section area taken as a base (A) is the one corresponding to series C: 18 x 18 in (457 x 457 mm).

All the series featured an approximate height-to-width (or diameter for series A) ratio of 2.1 to 2.2, with the exception of group F, whose related ratio was 4.2.  Therefore, no distinction in this ratio was made among all the series, but for group F.

Regarding Figure 8-9, specimens within each of the columns present the same cross-section geometry: rectangular, square, and circular for column 1, 2, and 3, respectively.  Specimens within each of the rows depict equal cross-sectional area size: four times the base area (4xA), two times the base area (2xA), specimens with the area base (A), and specimens of half the area base (0.5xA) for row 1, 2, 3, and 4, respectively.

Then, the comparisons are made in following order: along row 3, along column 2, along column 1, and finally within specimens E and F.

Figure 8-10 shows the influence of the cross-section shape to the strengthening performance for a constant cross-sectional area.  It can be observed among the specimens strengthened with the same amount of FRP (two plies) and therefore approximately same FRP volumetric ratio, that there is not shape effect for the case of square (C) and rectangular (B) cross-sections.  It is also confirmed that between specimens of circular cross-section and prismatic cross-section and of similar characteristics, including the amount of FRP, the FRP confinement is less effective for the latter.

Figure 8-11 and Figure 8-12 show the strengthening ratios for specimens of square cross-section geometry and varied cross-sectional area (from 0.5A to 4A).  The strengthening of specimens of area aspect ratio less than one (group E) showed to be more effective than in the other cases.  The specimens strengthened with two plies and area aspect ratio greater or equal than one, seem to have similar performance leading to believe on the lack of size effect, in particular for the case of specimen from group D (about 40 percent less FRP volumetric ratio).  With regards to specimen from group G, which is equivalent to specimen C (with four plies) in the FRP volumetric ratio, shows no significant degradation on strengthening ratio.

Similarly to the previous figures, Figure 8-13 and Figure 8-14 present the case for specimens of rectangular cross-section and varied cross-sectional area.  Based on these data point, it could be noted that there is a size effect, however, not a general conclusion could be drawn since it would be based on a single specimen data point (group H).

In Figure 8-15 and Figure 8-16 the strengthening performance of specimens E and F is presented.  At this point it is recalled the premature failure of the control specimen of group E, and since the capacity of the fully wrapped specimens of both groups were sufficiently similar, it was decided to compare the strengthened specimens of group E to the control unit of series F.  Based on this, the shorter specimens (E) showed a better performance than specimens F.

| | 1 | 2 | 3 |
|---|---|---|---|
| 1 | Series H<br>4xA<br>H/b ≈ 2.2 | Series G<br>4xA<br>H/b ≈ 2.2 | |
| 2 | | Series D<br>2xA<br>H/b ≈ 2.1 | |
| 3 | Series B<br>A<br>H/b ≈ 2.2 | Series C<br>A<br>H/b ≈ 2.2 | Series A<br>A<br>H/b ≈ 2.2 |
| 4 | | Series E    Series F<br>0.5xA<br>H/b ≈ 2.1    H/b ≈ 4.2 | |

**Figure 8-9  Matrix Scheme**
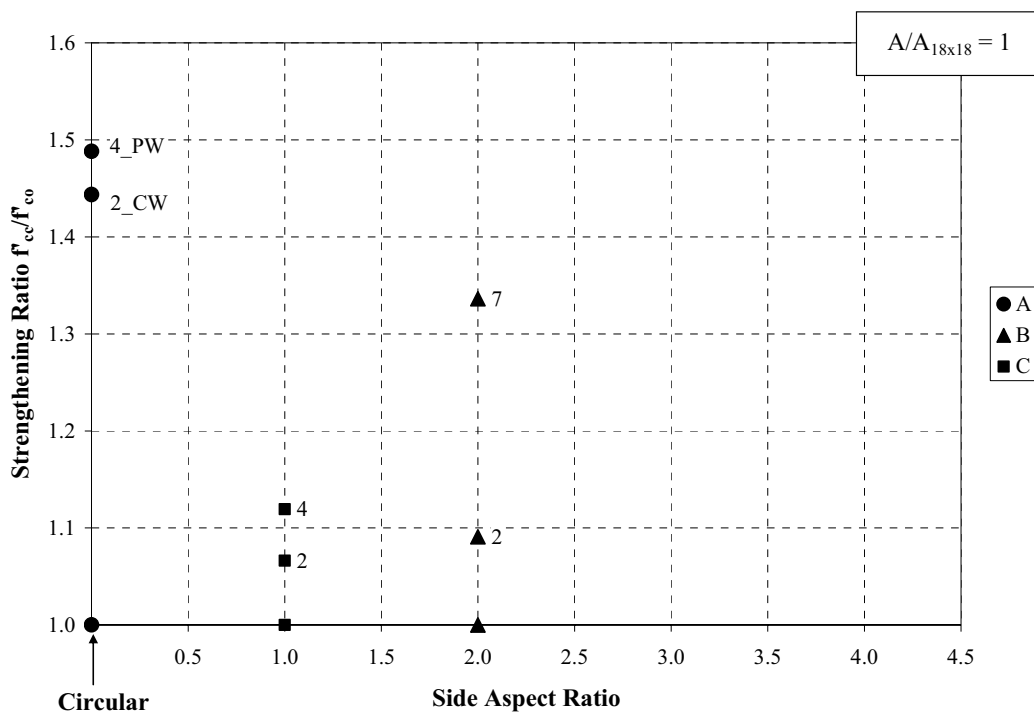


**Figure 8-10  Strengthening Ratio vs. Side Aspect Ratio; Series A, B, C; Constant Area Section**
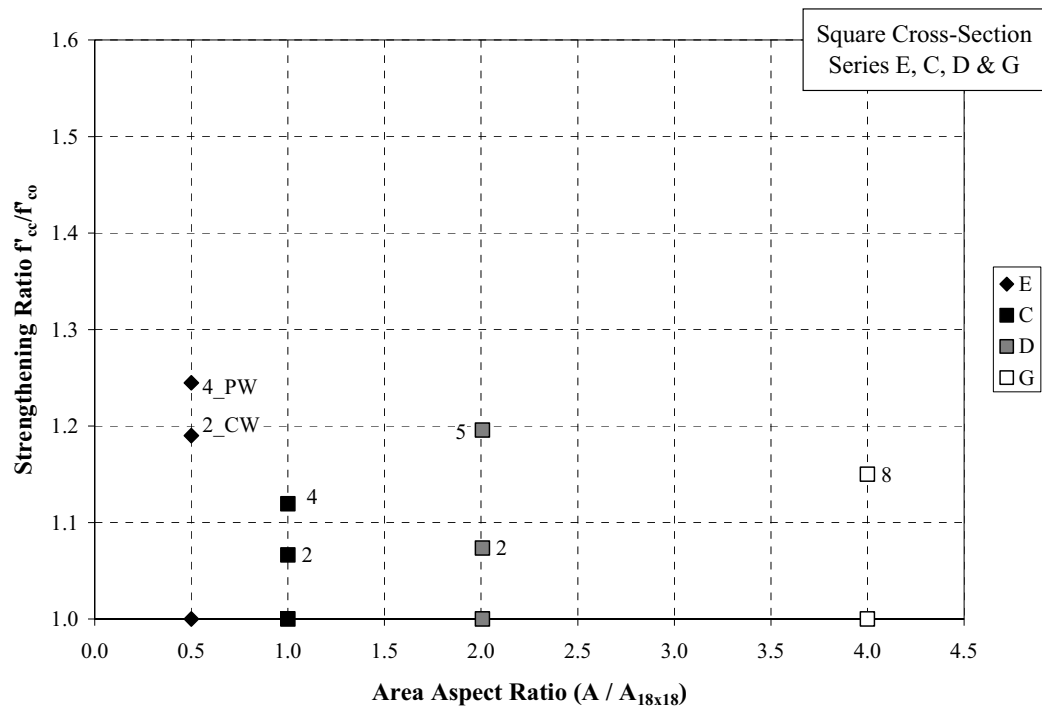
**Figure 8-11  Strengthening Ratio vs. Area Aspect Ratio; Series E, C, D, and G; Square Cross-Sections**
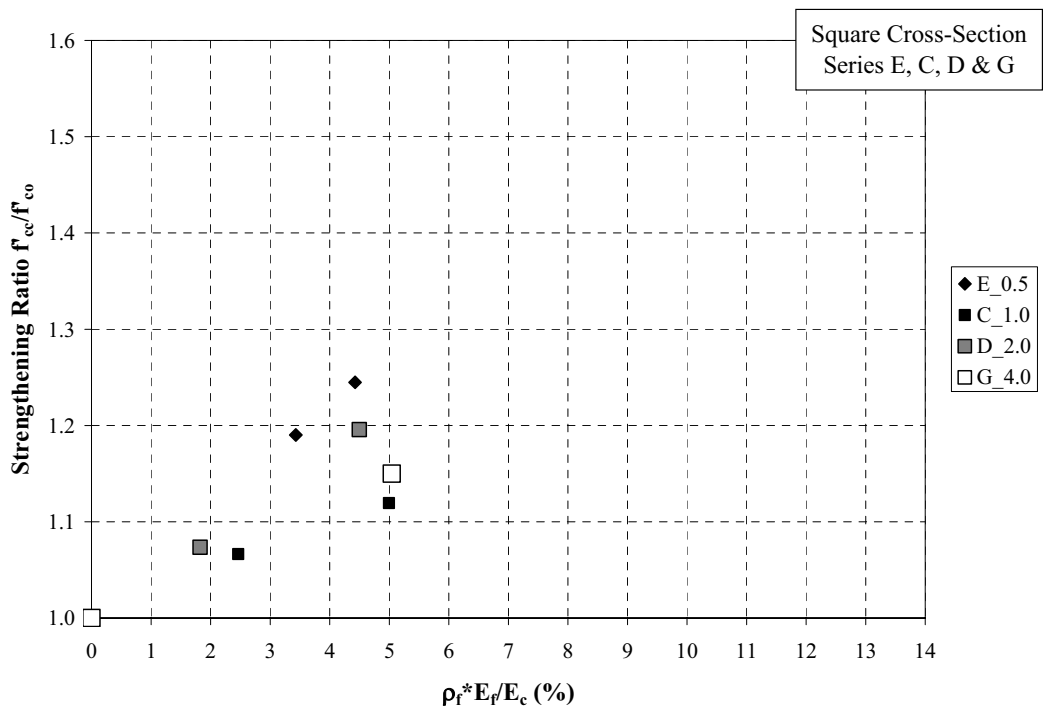


**Figure 8-12  Strengthening Performance; Series E, C, D, and G; Square Cross-Sections**
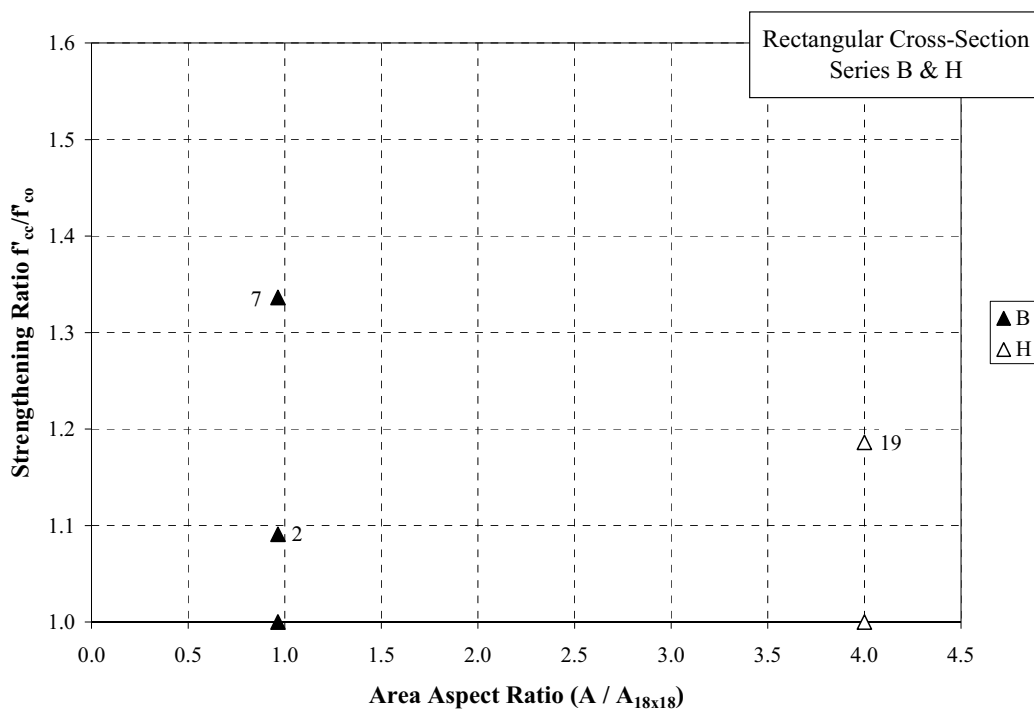
**Figure 8-13  Strengthening Ratio vs. Area Aspect Ratio; Series B and H; Rectangular Cross-Sections**
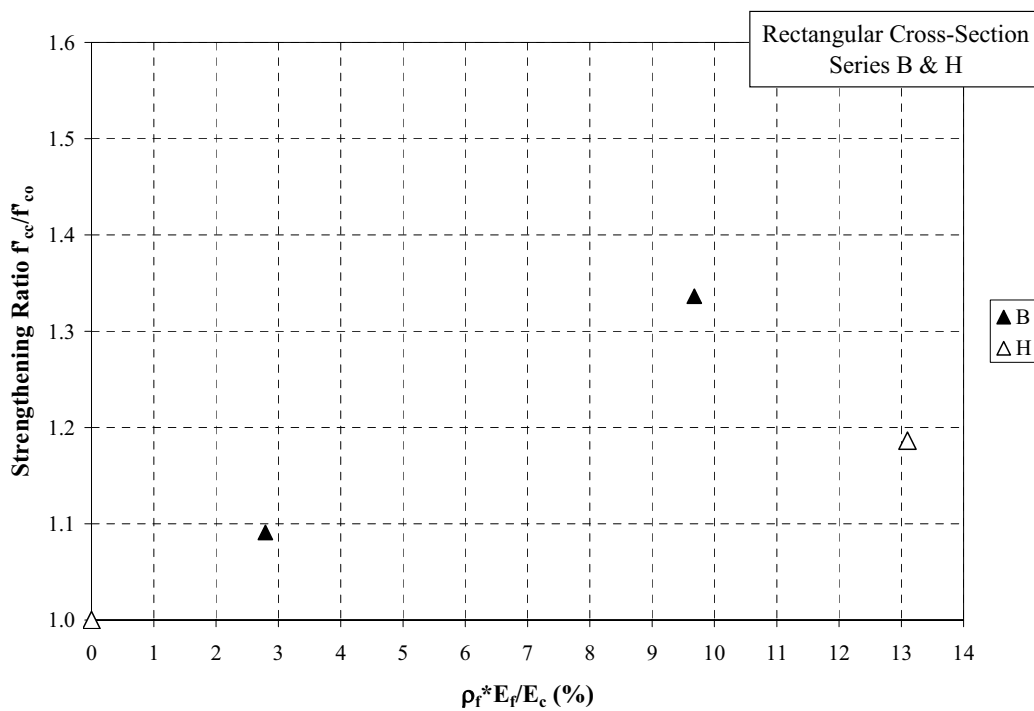


**Figure 8-14  Strengthening Performance; Series B and H; Rectangular Cross-Sections**
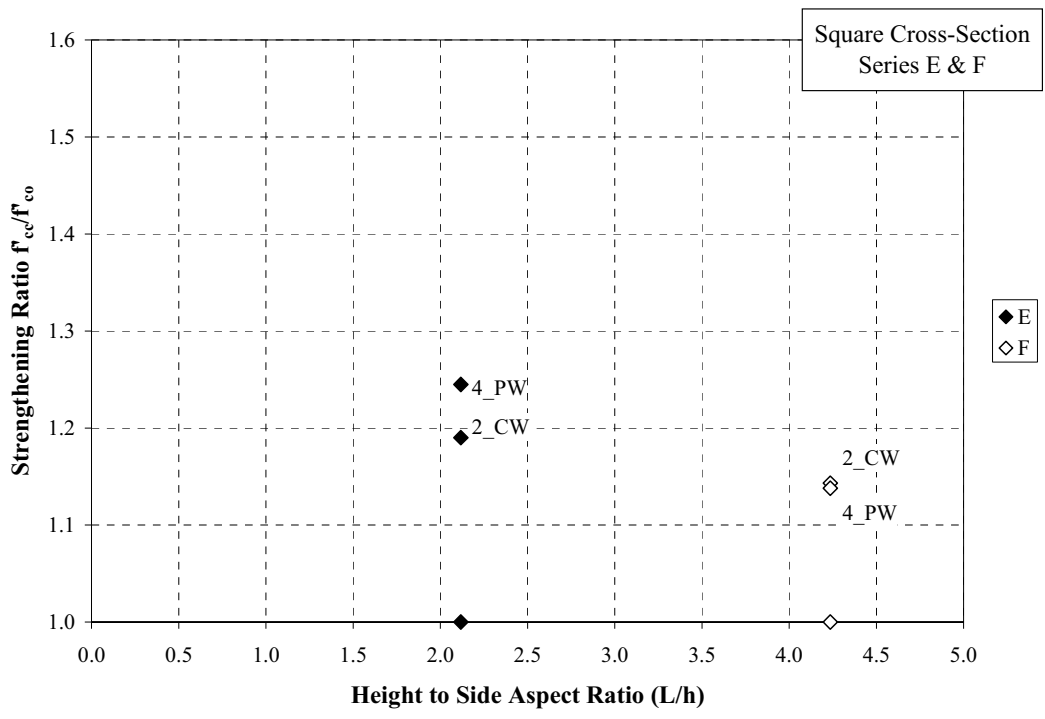
**Figure 8-15  Strengthening Ratio vs. Height to Length Aspect Ratio; Series E and F**
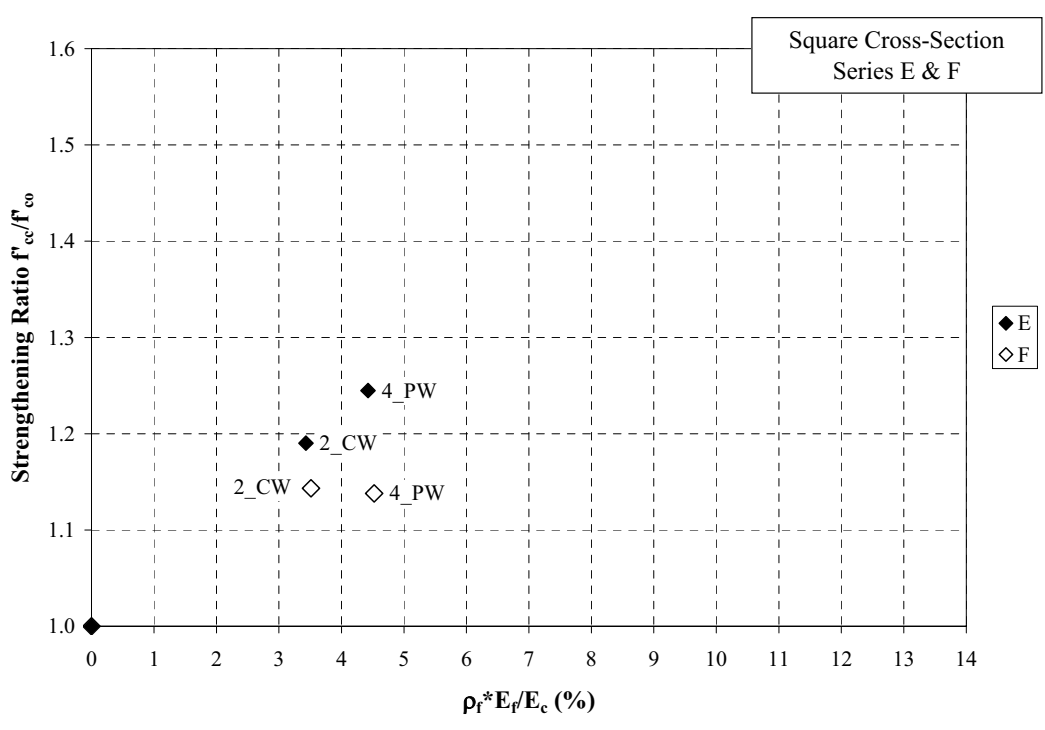


**Figure 8-16  Strengthening Performance; Series E and F; Square Cross-Sections**

**8.2.2. Comparison with Available Literature.** The purpose is to determine the effect of the size of the cross-sectional area from a much broader scope, therefore results of both the existing data and the new tests conducted in this research project were grouped according to cross-section shape and plotted in terms of the strengthening ratio ($f'_{cc}/f'_c$) versus $\rho_f*E_f/E_c$ (%) in Figure 8-17 to Figure 8-19. The same notation used for the specimens in Section 4 (Table 4-1 and Table 4-2) is used for the legend in these graphs. The new tests are labeled as "RO".

Figure 8-17, Figure 8-18, and Figure 8-19 refer to the cases of specimens of circular, square and rectangular (h/b ≤ 2) cross-section, respectively. With respect to the first figure, circular cross-section data set, the increment of concrete compressive strength ranges in between 10 percent and 75 percent among cross-sections of diameters varying from 12 in (305 mm) to 24 in (610 mm). The new tests fit within the tendency of the rest of the data; note the uniformity of the trend and minor scattering. No pattern reflecting the effect of cross-sectional area size is identified leading to establish the lack of such effect on this type of specimens.

Among the specimens of square cross-section (Figure 8-18), the isolated data point corresponding to specimen WR3_S (Table 4-1 and Figure 4-2) was not included due to the fact that its extreme strengthening ratio when compared to the rest of the data was a result of having a $f'_c$ considerably low and a very high FRP volumetric ratio. The performance of the specimens of this type of cross-section shape is noticeable less effective than in the case of the circular type, which confirms the generally accepted notion of confinement of different cross-section shapes. The strengthening ratio varies in between four and about 30 percent. The scatter of data is more pronounced in this case, it is unclear the deficient performance of specimen CH_S data point (farthest right on plot). No size effect is observed in these set of data.

Regarding Figure 8-19, this data set is composed of five data points, on the contrary of the two previous cases composed of 14 and 13 data points, respectively. Effect of cross-sectional area size seems to be not significant for this case as well.

Figure 8-20 presents the linear trends and their reliability indexes obtained by regression analysis corresponding to each data set of specimens. These tendencies reflect the level of effectiveness of the FRP confinement in the axial strengthening of the selected RC specimens. It is noted that the slope of the trends corresponding to the prismatic specimens is about the same, although the reliability index is much greater for the set of specimens of rectangular cross-section (smallest data set). This similarity leads to establish that in prismatic specimens featuring a side aspect ratio less or equal than 2, the size effect is not significant and their level of confinement effectiveness is approximately 30 percent of the one corresponding to specimens of circular cross-section.
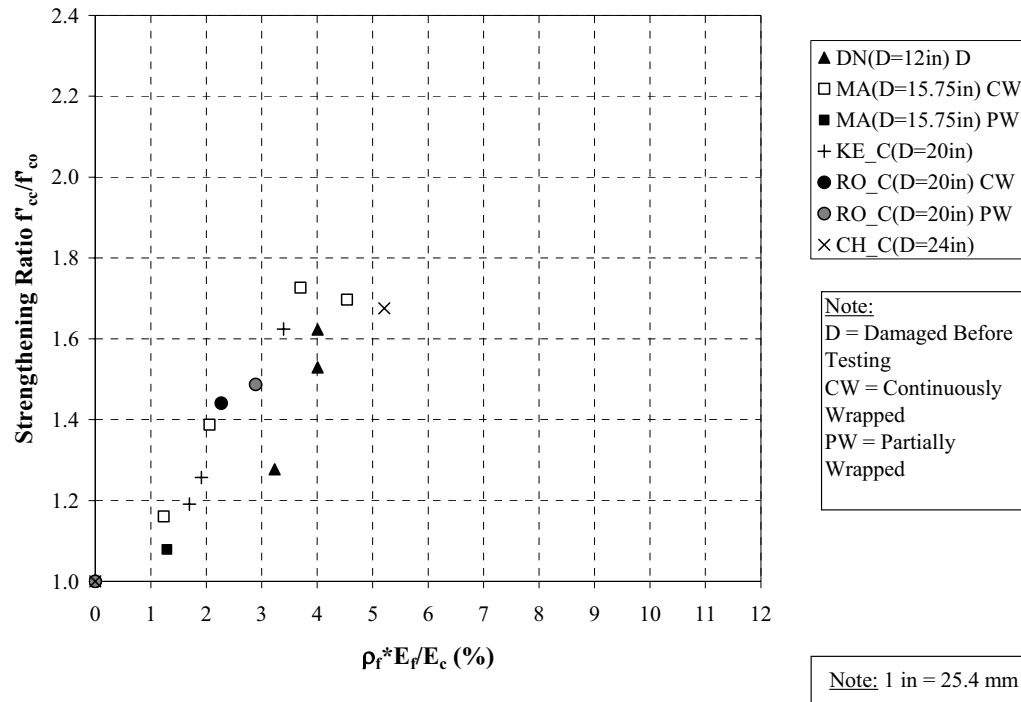
**Figure 8-17 Global Strengthening Performance of Specimens of Circular Cross-Section**
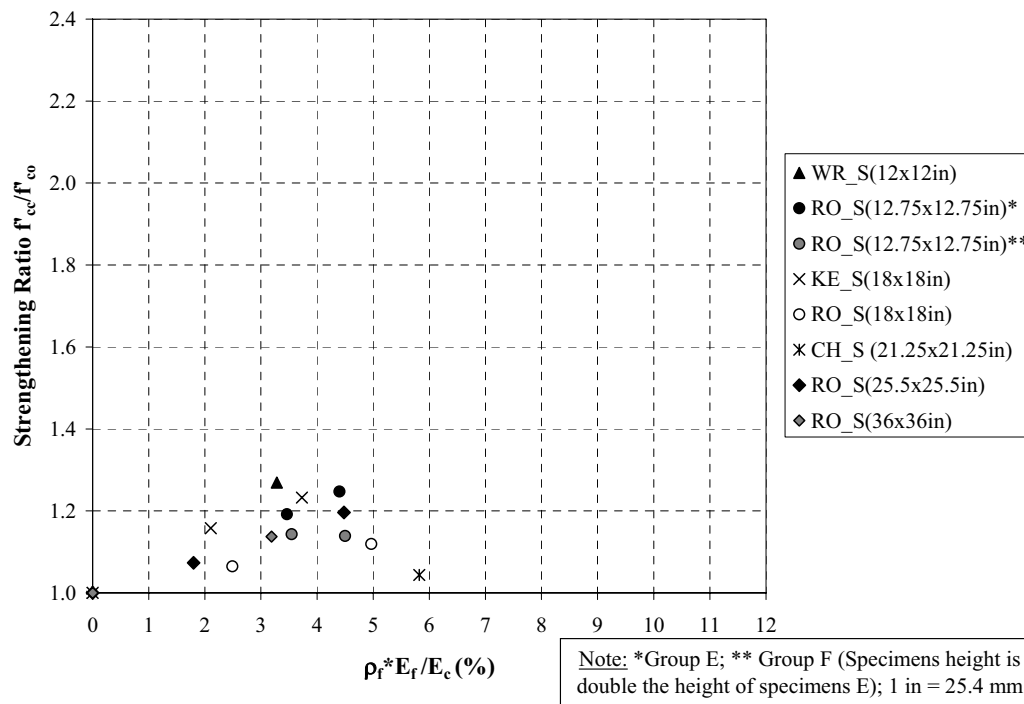


**Figure 8-18 Global Strengthening Performance of Specimens of Square Cross-Section**
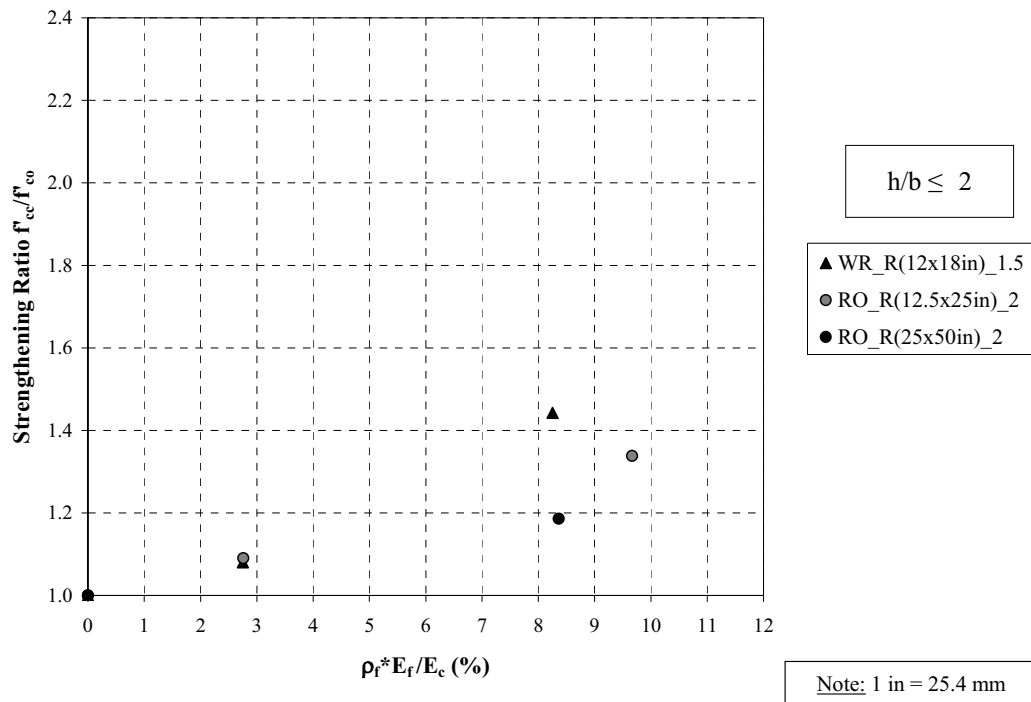
**Figure 8-19.  Global Strengthening Performance of Specimens of Rectangular Cross-Section**
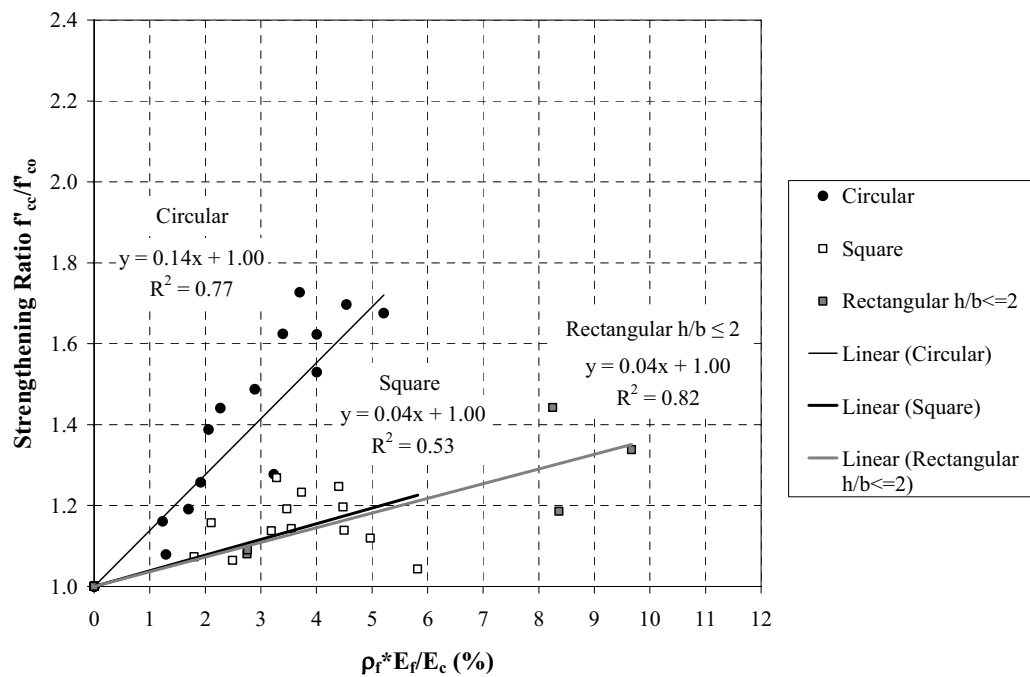


**Figure 8-20. Global Strengthening Performance of Specimens of Varied Cross-Section Shape; Linear Trends**

## 8.3. VALIDATION OF DESIGN PREDICTIONS

This evaluation was focused only on the experiments conducted in this research project and that were strengthened seeking a 30 percent increment of their original load carrying capacity. The experimental values for the strengthening ratio ($f'_{cc}/f'_c$) were compared to the design ones computed using the international guidelines presented in Section 5 of this report: ACI 440.2R – 2002, CSA S806 – 2002, TR 55 – 2005, and fib – 2001.

Figure 8-21 presents the specimens of series of equal cross-sectional area and different shape (row 3 in Figure 8-9): A (circular), C (square), and B (rectangular). With respect to specimen A2 (fully wrapped), TR 55 and the "exact" predictive equations provided by fib yield the best fit, and regarding specimen A3 (partially wrapped), the same approach from fib predicted it most accurately. For the case specimen C2 (four plies), TR 55 and CSA were the most approximated. About specimen B2 (seven plies) and ACI and CSA exhibit the best estimate, followed by fib "practical".

For the square specimens (column 2 in Figure 8-9), Figure 8-22 shows that all the approaches with the exception of the "exact" formulas from fib are sufficiently close to the experimental results in the cases of series E, F, D, and G.

Figure 8-23 illustrates the data corresponding to the specimens of rectangular cross-section (column 1 in Figure 8-9). It can be observed that the "practical" approach from fib yields the best approximation followed by TR 55, and that the remaining guidelines overvalue the experimental results.
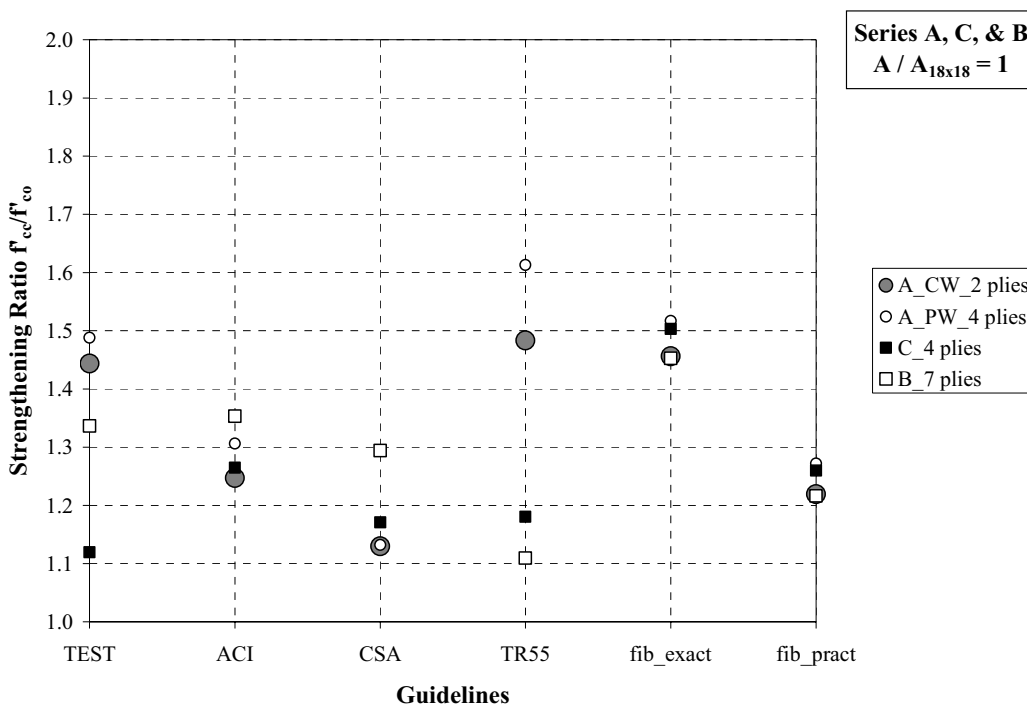


**Figure 8-21  Experimental vs. Theoretical Strengthening Performance; Constant Cross-Sectional Area; Series A, C & B**
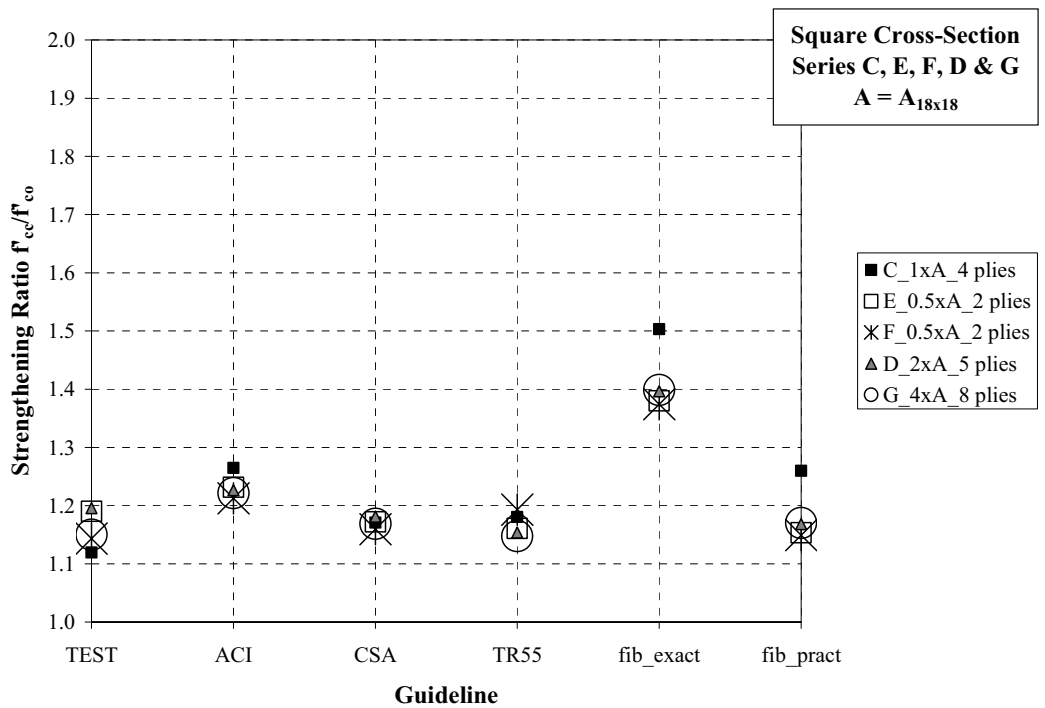
**Figure 8-22  Experimental vs. Theoretical Strengthening Performance; Square Cross-Section; Series C, E, D & G**
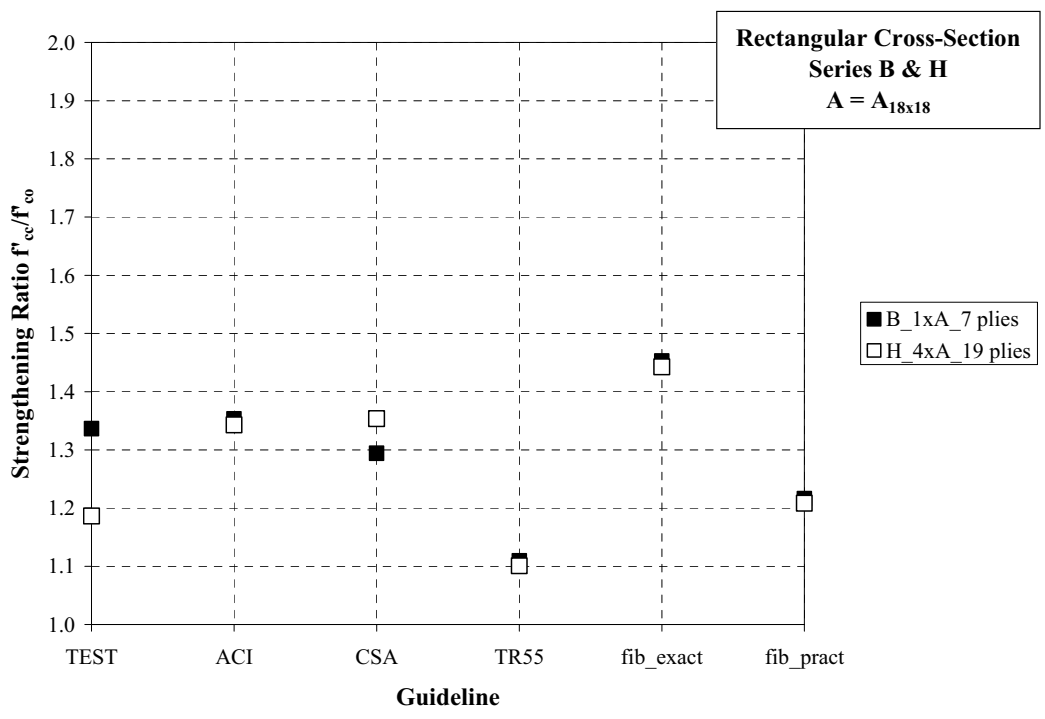


**Figure 8-23  Experimental vs. Theoretical Strengthening Performance; Rectangular Cross-Section; Specimen B & H**

## 9.  SUMMARY AND CONCLUSIONS


The first phase of this research program, which is presented in this report, was focused on the experimental performance of strengthening of reinforced concrete columns having circular and prismatic cross-sections with minimum and maximum cross-sectional area of 163 in$^2$ (0.1 m$^2$) and 1296 in$^2$ (0.84 m$^2$).  Their strengthening performance compared to those of current available data and contrasted against design guidelines provides a reference in the state-of-the-art with respect to the strength enhancement of RC columns oriented to practical applications.

A test matrix composed of a total of 22 reinforced concrete columns divided in six series of three specimens each and two series of two specimens each, was developed to study the effects of variable cross-sectional area, shape (circular, square, and rectangular), side aspect ratio, and height to side aspect ratio.  These specimens were tested under pure axial loading.

The following preliminary conclusions are based on the experiments carried out in this research project:

- Among specimens of the same cross-sectional area and confined with the same amount of FRP reinforcement, those of circular cross-section have a better performance compared to those of prismatic cross-section, as expected.  Additionally, prismatic specimens of side aspect ratio less to or equal to 2 showed similar performance.
- With respect to the specimens of square cross-section and varied size, the specimens of minimum cross-sectional area showed slightly higher strengthening ratios than the rest.  Among the remaining specimens, those of approximately the same FRP volumetric ratio exhibit similar performance, implying no size effect.
- The strengthening ratios showed by the two groups of specimens of rectangular cross-section lead to conclude the slight effect of cross-sectional size.  However, this preliminary conclusion was later weakened when a global comparison was conducted, which included specimens of available literature.

Concluding remarks based on the performance of all the current available data including the new experiments are as follows:

- Specimens of circular cross-section, showed the highest effectiveness of FRP confinement in axial strengthening.  The recent tests fit properly within the tendency of the rest of the experiments.  Minor scattering is noted in the trend.  No pattern reflecting the effect of cross-sectional area size was identified leading to establish the lack of such effect on this type of specimens.
- The performance of the specimens of square cross-section is noticeable less effective than in the case of the circular type, which confirms the generally accepted notion of confinement of different cross-section shapes.  No size effect is observed in these sets of data.
- In the data set corresponding to specimens of rectangular cross-section, the effect of cross-sectional area size seems to be not significant as well.
- The slope of the linear trends, which reflect the level of effectiveness of the FRP confinement in the axial strengthening corresponding to the prismatic specimens, is about the same for both sets of prismatic specimens, although the reliability index is much greater for the set of rectangular cross-section (smallest data set).  This similarity leads to establish that in prismatic specimens featuring a side aspect ratio

less than or equal to 2, the size effect is not significant and their level of confinement effectiveness is approximately 30 percent of the one corresponding to specimens of circular cross-section.

The validation of available guidelines was only conducted with data from this experimental program. It is apparent that these predictions differ from one another, in particular for the case of prismatic cross-sections. Additionally, for the case of circular cross-sections, most of the guidelines showed to be conservative, on the contrary when referring to the cases of prismatic cross-sections. Therefore a revision of the guidelines is warranted. A comparative study including all the data available, representing the complete evidence for the appropriate recommendations is currently being conducted and will be reported on the second phase of this project.

The evaluation presented in the first phase of this project was carried out basically in terms of the increment of axial compressive stress attained by the specimens confined by means of CFRP with respect to homologous control specimens. It is acknowledged by the authors that besides the variables considered in these comparisons, there are other key parameters in the strengthening performance such as: the corner radius of the specimens of prismatic cross-section, ultimate effective FRP hoop strain, and the amount of transverse steel reinforcement, among others. This is considered for the second phase of this research project, where in a broader fashion all the physical parameters will complement an analysis on the interaction of the concrete dilation and the FRP wrapping, yielding to the development of appropriate methods for the design of FRP column strengthening, in particular of prismatic cross-section.

# 10. REFERENCES

American Concrete Institute, ACI 440.2R-02., "Guide for the Design and Construction of Externally Bonded FRP Systems for Strengthening of Concrete Structures," American Concrete Institute, Farmington Hills, MI.

ASTM., 2000, "Standard Test Method for Tensile Properties of Polymer Matrix Composite Materials," ASTM D 3039, West Conshohocken, PA.

ASTM., 2003, "Standard Test Methods and Definitions for Mechanical Testing of Steel Products," ASTM A 370, West Conshohocken, PA.

ASTM., 2004, "Standard Test Method for Compressive Strength of Cylindrical Concrete Specimens," ASTM C 39, West Conshohocken, PA.

Campione, G., Miraglia, N., and Papia, M., 2003, "Influence of Section Shape and Wrapping Technique on the Compressive Behaviour of Concrete Columns Confined with CFRP Sheets," Proceedings of the International Conference Composites in Construction, University of Calabria, Cosenza, Italy, September, pp. 301-306.

Canadian Standards Association, CSA-S806-02, "Design and Construction of Building Components with Fibre-Reinforced Polymers," Ontario, Canada, 2002.

Canadian Standards Association, CSA A23.3-94, "Design of Concrete Structures," Ontario, Canada, 1994.

Chaallal, O., Shahawy, M., and Hassan, M., 2003, "Performance of Axially Loaded Short Rectangular Columns Strengthened with Carbon Fiber-Reinforced Polymer Wrapping," Journal of Composites for Construction, Vol. 7, No. 3, pp. 200-208.

Carey, S. and Harries, K., 2003, "The Effects of Shape, 'Gap', and Scale on the Behavior and Modeling of Variably Confined Concrete", University of South Carolina, Report No. ST03-05.

Chaallal, O., Hassan, M., and Shahawy, M., 2003, "Performance of Axially Loaded Short Rectangular Columns Strengthened with Carbon Fiber-Reinforced Polymer Wrapping," ASCE Journal of Composites for Construction, Vol. 7, No. 3, pp. 215-221.

Cole, C. B., 2001, "Performance of FRP-Jacketed Reinforced Concrete Columns Subjected to Uniaxial Compression," MS Thesis, University of Missouri – Rolla, Rolla, MO.

De Lorenzis, L. and Tepfers, T., 2001, "A Comparative Study of Models on Confinement of Concrete Cylinders with FRP Composites," Chalmers University of Technology, Division of Building Technology, Sweden.

Fardis, M. N. and Khalili, H., 1982, "Concrete Encased in Fiberglass Reinforced Plastic," ACI Journal, Vol. 78, pp. 440-445.

fédération internationale du béton (fib), Externally Bonded FRP Reinforcement for RC Structures , Technical Report, Lausanne, 2001.

Hosny, A., Shahin, H., Abdelrahman, A., and El-Afandy, T., 2001, "Strenthening of Rectangular RC Columns Using CFRP," Proceedings of the Fifth International Conference on Fibre-Reinforced Plastics for Reinforced Concrete Structures, Cambridge, UK, 16-18 July, pp. 773-782.

Kestner, J. T., Harries, K. A., Pessiki, S. P., Sause, R., and Ricles, J. M., 1997, "Rehabilitation of Reinforced Concrete Columns using Fiber Reinforced Polymer Composite Jackets," ATLSS Rep. No. 97-07, Lehigh University, Bethlehem, PA.

Lam, L., and Teng, J., 2003, "Design-oriented Stress-Strain Model for FRP-confined Concrete", Construction and Building Materials, Vol. 17, pp. 471-489.

Lam, L., and Teng, J., 2003, "Design-oriented Stress-Strain Model for FRP-confined Concrete in Rectangular Columns," Journal of Reinforced Plastics and Composites, Vol. 22, No. 13, pp. 1149-1186.

La Tegola, A., and Manni, O., 1998, "Structural Behaviour of Concrete Elements Confined with FRP Jackets," European Conference on Composites Materials. Science, Technology and Applications, Vol. 2, Naples, Italy, pp. 323-330.

MacGregor, J., 1997, "Reinforced Concrete Mechanics and Design," Third Edition, Prentice Hall, Inc., New Jersey.

Maalej, M., Tanwongsval, S., and Paramasivam, P., 2003, "Modelling of Rectangular RC Columns Strengthened with FRP," Cement and Concrete Composites, Vol. 25, pp. 263-276.

Malvar, L. J., Morril, K. B., and Crawford, J. E., 2004, "Numerical Modeling of Concrete Confined by Fiber-Reinforced Composites," Journal of Composites for Construction, Vol. 8, No. 4, pp. 315-322.

Mander, J. B.; Priestley, M. J. N.; and Park, R., 1988, "Theoretical Stress-Strain Model for Confined Concrete," Journal of Structural Engineering, Vol. 114, No. 8, pp. 1804-1826.

Marques, S., Marques, D., Silva, J., and Cavalcante, M., 2004, "Model for Analysis of Short Columns of Concrete Confined by Fiber-Reinforced Polymer," Journal of Composites for Construction, Vol. 8, No. 4, pp. 332-340.

Matthys, S., Toutanji, H., Audenaert, K., and Taerwe, L., 2005, "Axial Load Behavior of Large-Scale Columns Confined with Fiber-Reinforced Polymer Composites," ACI Structural Journal, Vol. 102, No. 2, pp. 258-267.

Mirmiran, A., Shahawy, M., Samaan, M., El Echary, E., Mastrapa, J. C., and Pico, O., 1998, "Effect of Column Parameters on FRP-Confined Concrete," Journal of Composites for Construction, Vol. 2, No. 4, pp. 175-185.

Mukherjee, A., Boothby, T. E., Bakis C. E., Joshi, M. V., and Maitra, S. R., 2004, "Mechanical Behavior of Fiber-Reinforced Polymer-Wrapped Concrete Columns-Complicating Effects," Journal of Composites for Construction, Vol. 8, No. 2, pp. 97-103.

Nanni, A. and Bradford, N. M., 1995, "FRP Jacketed Concrete under Uni-axial Compression," Construction and Building Materials, Vol. 9, No. 2, pp. 115-124.

Nasrollahzadehnesheli, N., and Yamakawa, T., 2002, "FEM-Based Confinement Model for Axially Loaded Columns Retrofitted by Prestressed Aramid Fibre Belts," Proceedings of the Japan Concrete Institute, Vol. 24, No. 2, pp. 115-120.

Ohno, S., Miyauchi, Y., Kei, T. and Higashibata, Y., 1997, "Bond Properties of CFRP Plate Joint," Non-Metallic (FRP) Reinforcement for Concrete Structures, Proceedings of the Third International Symposium, Sapporo, Japan, pp. 241-248.

Pessiki, S., Harries, K. A., Kestner, J. T., Sause, R., and Ricles, J. M., 2001, "Axial Behavior of Reinforced Concrete Columns Confined with FRP Jackets," Journal of Composites for Construction, Vol. 5, No. 4, pp. 237-245.

Prota, A., Manfredi, G., and Cosenza, E., 2003, "Confinement of RC Rectangular Columns Using GFRP," Proceedings of the Sixth International Conference on Fibre-Reinforced Plastics for Reinforced Concrete Structures, Singapore, 8-10 July, pp. 653-662.

Restrepol, J., and De Vino, B., 1996, "Enhancement of the Axial Load Carrying Capacity of Reinforced Concrete Columns by Means of Fiberglass-Epoxy Jacket," Second

International Conference Advanced Composite Materials in Bridges and Structures, Quebec, Canada, 11-14 August, pp. 547-553.

Rochette, P., and Labossiere, P., 2000, "Axial Testing of Rectangular Column Models Confined with Composites," Journal of Composites for Construction, Vol. 4, No. 3, pp. 129-136.

Saadatmanesh, H., Ehsani, M. R., and Li, M. W., 1994, "Strength and Ductility of Concrete Columns Externally Reinforced with Fiber Composite Straps," ACI Structural Journal, Vol. 91, No. 4, pp. 434-447.

Spoelstra, M. R., and Monti, G., 1999, "FRP-Confined Concrete Model," Journal of Composites for Construction, Vol. 3, No. 3, pp. 143-150.

Suter, R., and Pinzelli, R., 2001, "Confinement of Concrete Columns with FRP Sheets," Proceedings of the Fifth International Conference on Fibre-Reinforced Plastics for Reinforced Concrete Structures, Cambridge, UK, 16-18 July, 793-802.

Tan, K. H., 2002, "Strength Enhancement of Rectangular Reinforced Concrete Columns Using Fiber-Reinforced Polymer," Journal of Composites for Construction, Vol. 6, No. 3, pp. 175-183.

Tanwongsval, S., Maalej, M., and Paramasivam, P., 2001, "Strengthening of RC Wall-Like Columns," International Conference on Recent Advances in Concrete Technology, Fifth CANMET/ACI, V. M. Malhotra, ACI SP-200, 2001, pp. 663-676.

Teng, J. G., Chen, J. F., Smith, S. T., and Lam, L., 2002, "FRP-Strengthened RC Structures," John Wiley & Sons, Ltd., England.

Vintzileou, E., 2001, "An Empirical Model for Predicting the Properties of Concrete Confined by Means of Composite Materials," Proceedings of the Fifth International Conference on Fibre-Reinforced Plastics for Reinforced Concrete Structures, Cambridge, UK, 16-18 July, 845-853.

Wang, Y. C., and Restrepo, J. I., 2001, "Investigation of Concentrically Loaded Reinforced Concrete Columns Confined with Glass Fiber-Reinforced Polymer Jackets," ACI Structural Journal, V. 98, No. 3, pp. 377-385.

Wu, G., Wu, Z., and Lu, Z., 2003, "Stress-Strain Relationship for FRP-Confined Concrete Prisms," Proceedings of the Sixth International Conference on Fibre-Reinforced Plastics for Reinforced Concrete Structures, Singapore, 8-10 July, pp. 561-570.

Xiao, Y. and Ma, R., 1997, "Seismic Retrofit of RC Circular Columns using Prefabricated Composite Jacketing," Journal of Structural Engineering, ASCE, Vol. 123, No. 10, pp. 1357-1364.

**APPENDIX A**

**INTERNATIONAL GUIDELINES ALGORITHMS**

**ACI 440.2R – 2002 Circular Cross-Section**
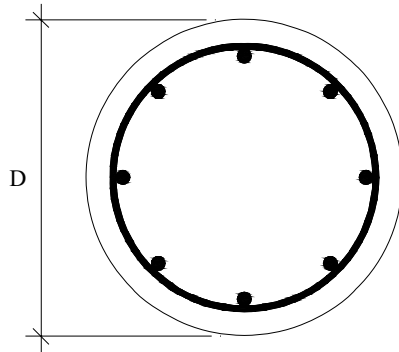


## Section Properties:

Column Diameter: $D := 20 \text{in}$

Gross Section Area: $A_g := \pi \cdot \dfrac{D^2}{4}$

$$A_g = 314 \, \text{in}^2$$

## Material Properties:

### Longitudinal Steel Reinforcement:

Steel Yield Strength: $f_y := 64.75 \text{ksi}$

Reinforcement Ratio: $\rho_{sg} := 0.0153$

Total area of longitudinal steel $A_s := \rho_{sg} \cdot A_g$

$$A_s = 4.81 \, \text{in}^2$$

*Concrete*

Cylindrical Concrete Compressive Strength: $f_c := 4000\,psi$

Concrete Density$(lb / ft^3)$:    $\rho_c := 145$

Modulus of Elasticity: $E_c := \rho_c^{1.5} \cdot 33 \cdot psi^{0.5} \cdot \sqrt{f_c}$

**Strengthening**

FRP Properties (manufacturer):

Ultimate Tensile Strength: $\quad f'_{fu} := 2700 \text{MPa}$

Ultimate Rupture Strain: $\quad \varepsilon'_{fu} := 0.012$

Tensile Modulus of Elasticity:$E_f := 230000 \text{MPa}$

Nominal Thickness of One Ply of FRP Reinforcement:$t_f := 0.167 \text{mm}$

Environmental reduction factor: $C_E := 1$

Then,

$$f_{fu} := C_E \cdot f'_{fu}$$

$$\varepsilon_{fu} := C_E \cdot \varepsilon'_{fu}$$

Number of Plies: $\quad n := 4$

Efficiency factor for FRP reinforcement (based on section geometry):

$$\kappa_a := 1 \qquad \text{For circular column}$$

Width of FRP Strip $\qquad b_f := 5.25 \text{in}$

Spacing (pitch) of FRP Strips: $\quad s := 5.25 \text{in} + 0 \text{in}$

Clear spacing in between FRP wraps: $\quad s' := s - b_f$

FRP reinforcement ratio: $\quad \rho_f := \dfrac{4 \cdot n \cdot t_f}{D} \cdot \dfrac{b_f}{s}$

Effective strain in the FRP attained at failure:

$$\varepsilon_{fe} := \min\left(0.004, 0.75 \varepsilon_{fu}\right)$$

$$\varepsilon_{fe} = 0.004$$

Confining pressure due to FRP jacket:  $f_l := \dfrac{\kappa_a \cdot \rho_f \cdot \varepsilon_{fe} \cdot E_f}{2}$

$$f_l = 351\,\text{psi}$$

Compressive strength of confined concrete  $f'_{cc} := f'_c \cdot \left( 2.25 \cdot \sqrt{1 + 7.9 \cdot \dfrac{f_l}{f'_c}} - 2 \cdot \dfrac{f_l}{f'_c} - 1.25 \right)$

$$f'_{cc} = 6009\,\text{psi}$$

Maximum Usable Compressive Strain
of FRP Confined Concrete:  $\varepsilon'_{cc} := \dfrac{1.71 \cdot \left( 5 \cdot f'_{cc} - 4 \cdot f'_c \right)}{E_c}$

$$\varepsilon'_{cc} = 0.0066$$

### ACI 440.2R – 2002 Prismatic Cross-Section



Corner radius: r
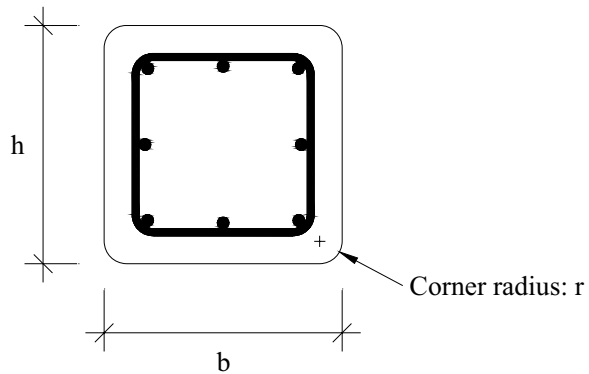
## Section Properties:

$b := 12.5\text{in}$

$h := 25\text{in}$

$r := 1.2\text{in}$

Gross Area Section: $\quad A_g := b \cdot h$

$$A_g = 313\,\text{in}^2$$

## Material Properties:

### *Longitudinal Steel Reinforcement*

Steel Yield Strength: $\quad f_y := 64.78\text{ksi}$

Reinforcement Ratio: $\rho_{sg} := 0.0156$

Total Area of Longitudinal Steel: $A_s := \rho_{sg} \cdot A_g$

$$A_s = 4.88\,\text{in}^2$$

*Concrete*

Cylindrical Concrete Compressive Strength: $f_c := 4000 \text{psi}$

Concrete Density (lb/ft³): $\rho_c := 145$

Modulus of Elasticity: $E_c := \rho_c^{1.5} \cdot 33 \cdot \text{psi}^{0.5} \cdot \sqrt{f_c}$

## **Strengthening**

FRP Properties (manufacturer)

Ultimate Tensile Strength: $f'_{fu} := 2700 \text{MPa}$

Ultimate Rupture Strain: $\varepsilon'_{fu} := 0.012$

Tensile Modulus of Elasticity: $E_f := 230000 \text{MPa}$

Nominal Thickness of One Ply of FRP Reinforcement: $t_f := 0.167 \text{mm}$

Environmental reduction factor: $C_E := 1$

Then,

$$f_{fu} := C_E \cdot f'_{fu}$$

$$\varepsilon_{fu} := C_E \cdot \varepsilon'_{fu}$$

Number of Plies: $n := 4$

Width of FRP Strip $b_f := 5.25 \text{in}$

Spacing (pitch) of FRP Strips: $s := 5.25 \text{in} + 0 \text{in}$

Clear spacing in between FRP wraps: $s' := s - b_f$

Efficiency factor for FRP reinforcement (based on section geometry, aspect ratio, steel reinforcement layout):

$$\kappa_a := 1 - \frac{(b - 2 \cdot r)^2 + (h - 2 \cdot r)^2}{3 \cdot b \cdot h \cdot \left(1 - \rho_{sg}\right)}$$

$$\kappa_a = 0.336$$

FRP reinforcement ratio: $\rho_f := \dfrac{2 \cdot n \cdot t_f (b + h)}{b \cdot h} \cdot \dfrac{b_f}{s}$

$$\rho_f = 0.006$$

Effective strain in the FRP attained at failure:

$$\varepsilon_{fe} := \min\left(0.004, 0.75\varepsilon_{fu}\right)$$

$$\varepsilon_{fe} = 0.004$$

Confining pressure due to FRP jacket: $f_l := \dfrac{\kappa_a \cdot \rho_f \varepsilon_{fe} \cdot E_f}{2}$

$$f_l = 142\,\text{psi}$$

Compressive strength of confined concrete:

$$f'_{cc} := f'_c \cdot \left(2.25 \cdot \sqrt{1 + 7.9 \cdot \frac{f_l}{f'_c}} - 2 \cdot \frac{f_l}{f'_c} - 1.25\right)$$

$$f'_{cc} = 4897\,\text{psi}$$

Maximum usable compressive strain: $\varepsilon'_{cc} := \dfrac{1.71 \cdot \left(5 \cdot f'_{cc} - 4 \cdot f'_c\right)}{E_c}$

$$\varepsilon'_{cc} = 0.004$$

## CSA-S806-2002 Circular Cross-Section
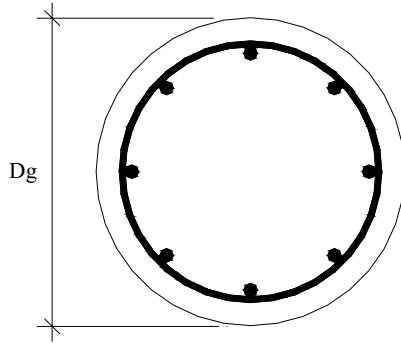


### Section Properties:

Diameter of the column: $D_g := 20\text{in}$

Gross section area: $A_g := \pi \cdot \dfrac{D_g^2}{4}$

### Material Properties:

*Longitudinal Steel Reinforcement*

Steel yield strength: $f_y := 64.75\text{ksi}$

Resistance factor for steel reinforcing bar: $\phi_s := 1$

Longitudinal reinforcement ratio: $\rho_s := 0.0153$

Total area of longitudinal steel: $A_{st} := \rho_s \cdot A_g$

*Concrete*

Cylindrical Concrete Compressive Strength: $f_c := 4000\text{psi}$

Resistance factor for concrete: $\phi_c := 1$

Density of the concrete $\gamma_c := 145\,\dfrac{\text{lb}}{\text{ft}^3}$

Strength reduction factor applied for unexpected eccentricities: $k_e := 1$

**Strengthening**

FRP Properties (manufacturer):

Tensile Modulus of Elasticity: $E_F := 230000 \text{MPa}$

Ultimate Rupture Strain: $\varepsilon_{Fu} := 0.012$

Ultimate tensile strength: $f_{Fu} := 2700 \text{MPa}$

Nominal Thickness of One Ply of FRP Reinforcement $t_F := 0.167 \text{mm}$

Number of plies: $N_b := 4$

Thickness of the FRP jacket: $t_j := N_b \cdot t_F$

Partial safety factor: $\phi_F := 1$

Stress in the jacket: $f_{Fj} := \min\left(0.004 \cdot E_F, \phi_F \cdot f_{Fu}\right)$

$$f_{Fj} = 133.43 \, \text{ksi}$$

Average confining stress of concrete:

$b_f := 5.25 \text{in}$

In case of partial wrapping:
"$b_f$" is the width of the strip in case of partial wrapp
"$s'$" is the clear spacing between strips

$s' := 0 \text{in}$

$s := b_f + s'$

$$f_l := \frac{2 \cdot t_j \cdot f_{Fj}}{D_g} \cdot \frac{b_f}{s}$$

$f_l = 351 \, \text{psi}$

Confinement Coefficient for Circular Cross-Sections $k_c := 1$

$$k_l := 6.7 \cdot \left( k_c \cdot \frac{f_l}{MPa} \right)^{-0.17}$$

$$k_l = 5.766$$

Compressive strength of confined concrete:

$$f'_{cc} := \left( k_e \cdot \frac{f'_c}{MPa} + k_l + k_c + \frac{f_l}{MPa} \right) \cdot MPa$$

$$f'_{cc} = 5332 \, psi$$

## CSA-S806-2002 Prismatic Cross-Sections
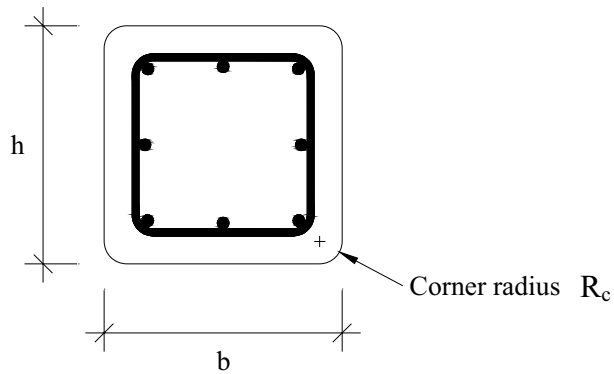


Corner radius $R_c$

### Section Properties:

Length of short side: $b := 12.5\text{in}$

Length of the long side: $h := 25\text{in}$

Corner radius: $R_c := 1.2\text{in}$

Gross section area: $A_g := b \cdot h$

### Material Properties:

***Longitudinal Steel Reinforcement***

Steel yield strength: $f_y := 64.78\text{ksi}$

Partial safety factor: $\phi_s := 1$

Longitudinal reinforcement ratio: $\rho_s := 0.0156$

Total area of longitudinal steel: $A_s := \rho_s \cdot A_g$

***Concrete***

Unconfined concrete strength $f'_c := 4000\text{psi}$

Partial safety factor: $\phi_c := 1$

**Strengthening**

FRP Properties (manufacturer):

Tensile Modulus of Elasticity: $E_{frp} := 230000 MPa$

Ultimate Rupture Strain: $\varepsilon_{frp} := 0.012$

Ultimate tensile strength: $f_{fu} := 2700 MPa$

Nominal Thickness of One Ply of FRP Reinforcement: $t_{frp} := 0.167 \cdot mm$

Number of plies: $N_b := 4$

Thickness of the FRP jacket: $t_j := N_b \cdot t_{frp}$

Partial safety factor: $\phi_{frp} := 1$

Performace coefficient for a rectangular section $\alpha_{pr} := 1$   This value is function of the quality of application and fiber-resin-concrete bond, and it is suggested as 1 at the present time.

Stress in the FRP: $f_{Fj} := min\left(0.004 \cdot E_{frp}, \phi_{frp} \cdot f_{fu}\right)$

$$f_{Fj} = 133 \, ksi$$

Average confining stress of concrete:

Width of the FRP strip: $b_f := 5.25 in$

Clear spacing: $s' := 0 in$

Pitch or spacing: $s := b_f + s'$

$D_g := min(b, h)$

$$f_l := \frac{2 \cdot t_j \cdot f_{Fj}}{D_g} \cdot \frac{b_f}{s}$$

$$f_l = 561 \, psi$$

Confinement Coefficient for Prismatic Cross-Sections: $k_c := 0.25$

$$k_l := 6.7 \cdot \left( k_c \cdot \frac{f_l}{MPa} \right)^{-0.17}$$

$$k_l = 6.737$$

Compressive Strength of Confined Concrete:

$$f'_{cc} := \left( \frac{f'_c}{MPa} + k_l + k_c + \frac{f_l}{MPa} \right) \cdot MPa$$

$$f'_{cc} = 5575 \, psi$$

**TR 55 – 2005 Circular Cross-Section**
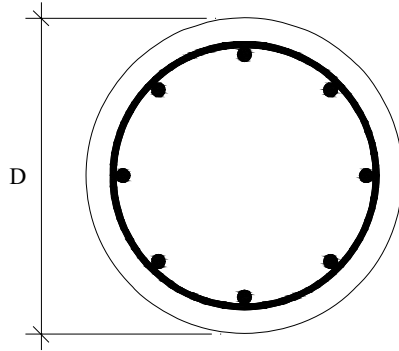


## Section Properties:

Diameter: $D := 20\text{in}$

Gross section area: $A_g := \pi \cdot \dfrac{D^2}{4}$

## Material Properties:

### *Longitudinal Steel Reinforcement*

Steel Yield Strength: $f_y := 64.75\text{ksi}$

Steel Material Factor: $\gamma_s := 1$

Design Steel yield strength: $f_{yd} := \dfrac{f_y}{\gamma_s}$

Longitudinal reinforcement ratio: $\rho_{sc} := 0.0153$

Total area of longitudinal steel: $A_s := \rho_{sc} \cdot A_g$

### *Concrete*

Concrete Material Factor: $\gamma_{mc} := 1$

Characteristic Compressive Cylinder Strength of Concrete: $f_c := 4000 \text{psi}$

Characteristic Compressive Cube Strength of Concrete: $f_{cu} := \dfrac{f_c}{0.8}$

Unconfined concrete strength: $f_{co} := f_c$

Axial strain in unconfined concrete at peak stress: $\varepsilon_{co} := 0.002$

Density of the concrete (lb/ft³): $\rho_c := 145$

Secant Modulus of Elasticity: $E_o := \dfrac{f_{co}}{\left( \gamma_{mc} \cdot \varepsilon_{co} \right)}$

Initial Modulus of elasticity: $E_c := \rho_c^{1.5} \cdot 33 \cdot \text{psi}^{0.5} \cdot \sqrt{f_c}$

**Strengthening**

FRP Properties (manufacturer):

Characteristic failure strain of FRP: $\varepsilon_{fk} := 0.012$

Partial safety factor for strain in FRP: $\gamma_\varepsilon := 1$

Partial safety factor for manufacture of FRP: $\gamma_{mm} := 1$

Design partial safety factor for strain of FRP: $\gamma_{m\varepsilon} := \gamma_\varepsilon \cdot \gamma_{mm}$

$$\gamma_{m\varepsilon} = 1$$

Design ultimate strain of FRP: $\varepsilon_{fd} := \dfrac{\varepsilon_{fk}}{\gamma_{m\varepsilon}}$

$$\varepsilon_{fd} = 0.012$$

Characteristic modulus of elasticity of FRP: $E_{fk} := 230000 \, MPa$

Partial safety factor for modulus of elasticty in FRP: $\gamma_E := 1$

Design partial safety factor for modulus of elasticity of FRP: $\gamma_{mE} := \gamma_E \cdot \gamma_{mm}$

$$\gamma_{mE} = 1$$

Design modulus of elasticity of FRP: $E_{fd} := \dfrac{E_{fk}}{\gamma_{mE}}$

$$E_{fd} = 230000 \, MPa$$

Design tensile strength on FRP: $f_{fd} := E_{fd} \cdot \varepsilon_{fd}$

$$f_{fd} = 2760 \, MPa$$

Number of Plies: $n := 4$

Nominal Ply Thickness: $t_f := 0.167 \, mm$

Thickness of the Jacket $t := n \cdot t_f$

Designed Confined concrete compressive axial strength:

Width of strip: $b_f := 5.25 \, in$

Clear spacing: $s' := 0 \, in$

Pitch: $s := b_f + s'$

This model is only suitable if the following condition is met:

$$\frac{2 \cdot t \cdot E_{fd}}{D \cdot \left(f_{co}\right)^2} \cdot \frac{b_f}{s} = 0.795 \, \frac{mm^2}{N}$$ This is greater than 0.183, therefore the model can be used

$$f_{ccu} := f_{co} + 0.05 \cdot \left(\frac{2 \cdot t}{D} \cdot \frac{b_f}{s}\right) \cdot E_{fd}$$

$$f_{ccu} = 8387 \, psi$$

Confined Concrete ultimate axial strain:

$$\varepsilon_{ccu} := \varepsilon_{co} \cdot \left[1.75 + 12 \cdot \left(\frac{2 \cdot E_{fd} \cdot t}{E_o \cdot D}\right) \cdot \left(\frac{0.6 \cdot \varepsilon_{fd}}{\varepsilon_{co}}\right)^{1.45}\right]$$

$$\varepsilon_{ccu} = 0.0102$$

Since it is recommended that if the ultimate strain $\varepsilon_{ccu}$ is greater than 0.01, then the failure stress should be taken as the value of $f_{cd}$ corresponding to the value $\varepsilon_{cc} = 0.01$ from the stress-strain curve, rather than the failure stress at rupture of the FRP

$$\varepsilon_{ccd} := min\left(0.01, \varepsilon_{ccu}\right)$$

$$\varepsilon_{ccd} = 0.01$$

Slope of linear portion of confined stress-strain curve: $E_2 := \dfrac{\left(f_{ccu} - f_{co}\right)}{\varepsilon_{ccu}}$

$$E_2 = 428 \, ksi$$

$$f_{ccd} := f_{co} + E_2 \cdot \varepsilon_{ccd}$$

$$f_{ccd} = 8282 \, psi$$

## TR 55 – 2005 Prismatic Cross-Section
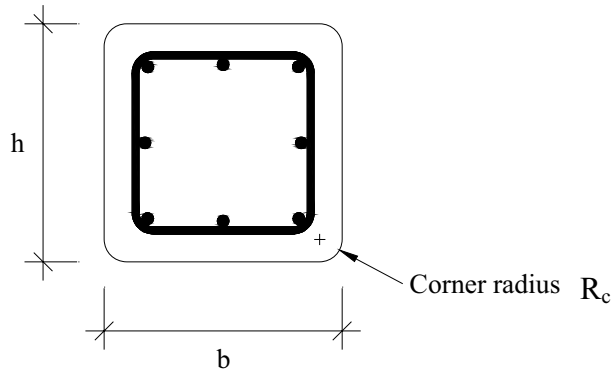


**Section Properties:**

Length of short side: $b := 12.5\text{in}$

Length of the long side: $h := 25\text{in}$

Corner radius: $R_c := 1.2\text{in}$

Gross section area of column with rounded corners: $A_g := b \cdot h - (4 - \pi) \cdot R_c^2$

Area of concrete: $A_c := b \cdot h$

**Material Properties:**

*Longitudinal Steel Reinforcement*

Steel yield strength: $f_y := 64.78\text{ksi}$

Steel material factor: $\gamma_{ms} := 1$

Design yield strength: $f_{yd} := \dfrac{f_y}{\gamma_{ms}}$

Longitudinal reinforcement ratio: $\rho_{sc} := 0.0156$

Total area of longitudinal steel: $A_s := \rho_{sc} \cdot A_g$

*Concrete*

Concrete Material Factor: $\gamma_{mc} := 1$

Characteristic Compressive Cylinder Strength of Concrete $f'_c := 4000\text{psi}$

Characteristic Compressive Cube Strength of Concrete $f_{cu} := \dfrac{f'_c}{0.8}$

Unconfined Concrete Strength $f_{co} := f'_c$

## **Strengthening**

FRP Properties (manufacturer):

Characteristic failure strain of FRP: $\varepsilon_{fk} := 0.012$

Partial safety factor for strain in FRP $\gamma_\varepsilon := 1$

Partial safety factor for manufacture of FRP $\gamma_{mm} := 1$

Design partial safety factor for strain of FRP: $\gamma_{m\varepsilon} := \gamma_\varepsilon \cdot \gamma_{mm}$

Design ultimate strain of FRP: $\varepsilon_{fd} := \dfrac{\varepsilon_{fk}}{\gamma_{m\varepsilon}}$

$$\varepsilon_{fd} = 0.012$$

Characteristic modulus of elasticity of FRP: $E_{fk} := 230000\text{MPa}$

Partial safety factor for modulus of elasticty in FRP: $\gamma_E := 1$

Characteristic modulus of elasticity of FRP: $E_{fk} := 230000\text{MPa}$

Partial safety factor for modulus of elasticty in FRP: $\gamma_E := 1$

Design partial safety factor for modulus of elasticity of FRP: $\gamma_{mE} := \gamma_E \cdot \gamma_{mm}$

Design ultimate strain of FRP: $E_{fd} := \dfrac{E_{fk}}{\gamma_{mE}}$

Design tensile strength on FRP: $f_{fd} := E_{fd} \cdot \varepsilon_{fd}$

Number of Plies: $n := 4$

Nominal Ply Thickness: $t_f := 0.167\,mm$

Thickness of the Jacket $t := n \cdot t_f$

Width of strip: $b_f := 5.25\,in$

Clear spacing: $s' := 0\,in$

Pitch: $s := b_f + s'$

Confinement pressure: $f_r := \dfrac{2 \cdot f_{fd} \cdot t}{\sqrt{b^2 + h^2}} \cdot \dfrac{b_f}{s}$

$$f_r = 753\,psi$$

Length of overlapping region:

$$l_{ol} := \sqrt{\dfrac{\left(h - 2 \cdot R_c\right)^2}{4} - \dfrac{b \cdot \left(h - 2 \cdot R_c\right)}{2}}$$

Area of overlap of the parabolas:

$$A_{ol} := \begin{vmatrix} 0in^2 & \text{if } 2 \cdot b \geq \left(h - 2 \cdot R_c\right) \\ \left[ \dfrac{4 \cdot \left(l_{ol}\right)^3}{3 \cdot \left(h - 2 \cdot R_c\right)} + l_{ol} \cdot \left[2 \cdot b - \left(h - 2 \cdot R_c\right)\right] \right] & \text{if } 2 \cdot b < \left(h - 2 \cdot R_c\right) \end{vmatrix}$$

$$A_{ol} = 0\,in^2$$

Effectively confined area:

$$A_e := A_g \cdot \left[ \dfrac{1 - \dfrac{\left[\left(h - 2 \cdot R_c\right)^2 + \left(b - 2 \cdot R_c\right)^2 - 3 \cdot A_{ol}\right]}{3 \cdot A_g} - \rho_{sc}}{1 - \rho_{sc}} \right]$$

$$A_e = 104\,in^2$$

Shape factor:

$$g_s := \dfrac{b}{h} \cdot \dfrac{A_e}{A_g}$$

$$g_s = 0.167$$

Confined concrete axial compressive stress: $f_{ccd} := f_{co} + 2 \cdot g_s \cdot f_r$

$$f_{ccd} = 4251\,psi$$

**fib – 2001 Circular Cross-Section**
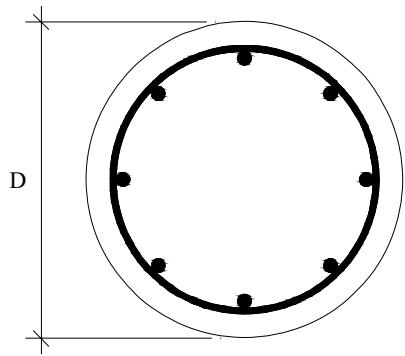


## Section Properties:

Diameter: $D := 20\text{in}$

Gross section area: $A_g := \pi \cdot \dfrac{D^2}{4}$

$$A_g = 314\,\text{in}^2$$

## Material Properties:

### *Longitudinal Steel Reinforcement*

Steel yield strength: $f_y := 64.75\text{ksi}$

Longitudinal reinforcement ratio: $\rho_{sg} := 0.0153$

Total area of longitudinal steel: $A_s := \rho_{sg} \cdot A_g$

$$A_s = 4.81\,\text{in}^2$$

### *Concrete*

Concrete strength: $f_{co} := 4000\text{psi}$

$$\varepsilon_{co} := 0.002$$

Density of the concrete (lb / ft$^3$): $\qquad \rho_c := 145$

Modulus of elasticity: $\quad E_c := \rho_c^{1.5} \cdot 33 \cdot psi^{0.5} \cdot \sqrt{f_{co}}$

$$E_c = 3644 \, ksi$$

## **Strengthening**

FRP Properties (manufacturer):

Ultimate Tensile Strength: $f_{fu} := 2700 MPa$

Ultimate Rupture Strain: $\quad \varepsilon_{fu} := 0.012$

Tensile Modulus of Elasticity: $E_f := 230000 MPa$

Nominal Ply Thickness: $t_f := 0.167 mm$

Number of Plies: $\quad n := 4$

Thickness of the Jacket: $\quad t := n \cdot t_f$

Width of FRP strip: $\quad b_f := 5.25 in$

Clear spacing in between FRP wraps: $\quad s' := 0 in$

Spacing (pitch) of FRP strips: $\quad s := 5.25 in + s'$

Volumetric ratio of the FRP jacket: $\qquad \rho_f := \dfrac{4 \cdot t}{D} \cdot \dfrac{b_f}{s}$

Arching effect (confinement-effectiveness) coefficient K

If the specimen is Partially Wrapped (PW):

$$k_e := \begin{vmatrix} 1 & \text{if } s = b_f \\ \\ \dfrac{\left(1 - \dfrac{s'}{2 \cdot D}\right)^2}{1 - \rho_{sg}} & \text{otherwise} \end{vmatrix}$$

$$k_e = 1$$

Stiffness of the FRP confinement: $K_{conf} := \dfrac{1}{2} k_e \cdot \rho_f E_f$

$$K_{conf} = 87.73 \, ksi$$

Effective confining pressure: $f_l := K_{conf} \cdot \varepsilon_{fu}$

$$f_l = 1053 \, psi$$

**"Exact Formula"**

Confined concrete strength and strain:

$$f_{cc} := f_{co} \cdot \left( 2.254 \cdot \sqrt{1 + 7.94 \cdot \dfrac{f_l}{f_{co}}} - 2 \cdot \dfrac{f_l}{f_{co}} - 1.254 \right)$$

$$f_{cc} = 8726 \, psi$$

$$\varepsilon_{cc} := \varepsilon_{co} \cdot \left[ 1 + 5 \cdot \left( \dfrac{f_{cc}}{f_{co}} - 1 \right) \right]$$

$$\varepsilon_{cc} = 0.0138$$

$$E_{cc} := \frac{f_{cc}}{\varepsilon_{cc}}$$

$$E_{cc} = 632\,\text{ksi}$$

Secant Modulus of Elasticity of Concrete at ultimate:

Modulus of FRP Jacket: $\quad E_j := E_f$

Ultimate Strength of FRP Jacket: $\quad f_j := f_{fu}$

FRP Jacket Effective Ultimate Circumferential Strain: $\varepsilon_{ju} := \varepsilon_{fu}$

Paramater of Damage Law (Property of Concrete):

$$\beta := \frac{5700}{\sqrt{\left|\dfrac{f_{co}}{\text{MPa}}\right|}} - 500$$

Secant Modulus of Elasticity of Concrete at Ultimate:

$$E_{secu} := \frac{E_c}{1 + 2\cdot\beta\cdot\varepsilon_{ju}}$$

$$E_{secu} = 242\,\text{ksi}$$

Ultimate Concrete Strain:

$$\varepsilon_{cu} := \varepsilon_{cc}\cdot\left(\frac{2\cdot\beta\cdot\varepsilon_{ju}\cdot E_{cc}}{E_c - E_{cc}}\right)^{\left(1 - \frac{E_{cc}}{E_c}\right)}$$

$$\varepsilon_{cu} = 0.0337$$

Concrete Strength at Ultimate

$$f_{cu} := \frac{E_c \cdot \varepsilon_{cu}}{1 + 2 \cdot \beta \cdot \varepsilon_{ju}}$$

$$f_{cu} = 8172 \, psi$$

**"Practical Formula"**

Concrete Strength at Ultimate: $\quad f_{cu} := f_{co} \cdot \left( 0.2 + 3 \cdot \sqrt{\frac{f_l}{f_{co}}} \right)$

$$f_{cu} = 6956 \, psi$$

Ultimate Concrete Strain:
$$\varepsilon_{cu} := \varepsilon_{co} \cdot \left( 2 + 1.25 \cdot \frac{E_c}{f_{co}} \cdot \varepsilon_{ju} \cdot \sqrt{\frac{f_l}{f_{co}}} \right)$$

$$\varepsilon_{cu} = 0.018$$

## fib – 2001 Prismatic Cross-Section
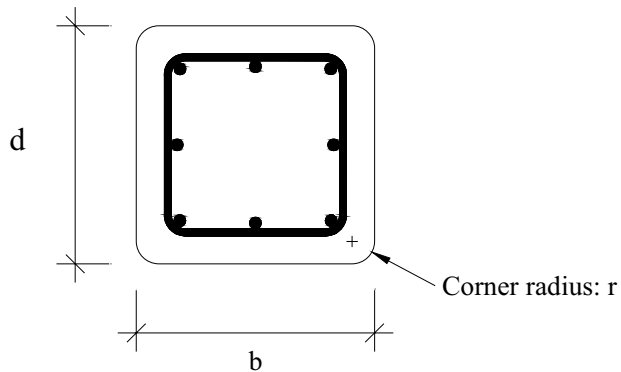


Corner radius: r

### Section Properties:

Dimension short side: $b := 12.5\text{in}$

Dimension long side: $d := 25\text{in}$

Corner radius: $r := 1.2\text{in}$

Gross section area: $A_g := b \cdot d$

### Material Properties:

#### *Longitudinal Steel Reinforcement*

Steel yield strength: $f_y := 64.78\text{ksi}$

Longitudinal reinforcement ratio: $\rho_{sg} := 0.0156$

Total area of longitudinal steel: $A_s := \rho_{sg} \cdot A_g$

#### *Concrete*

Unconfined concrete strength $f_{co} := 4000\text{psi}$

$\varepsilon_{co} := 0.002$

Density of the concrete (lb/ft³) $\rho_c := 145$

Modulus of elasticity: $E_c := \rho_c^{1.5} \cdot 33 \cdot psi^{0.5} \cdot \sqrt{f_{co}}$

$$E_c = 3826 \, ksi$$

## Strengthening

FRP Properties (manufacturer):

Ultimate Tensile Strength: $f_{fu} := 2700 MPa$

Ultimate Rupture Strain: $\varepsilon_{fu} := 0.012$

Tensile Modulus of Elasticity $E_f := 230000 MPa$

Nominal Ply Thickness: $t_f := 0.167 mm$

Number of Plies: $n := 4$

Thickness of the Jacket $t := n \cdot t_f$

Width of FRP Strip: $b_f := 5.25 in$

Clear Spacing: $s' := 0 in$

Pitch: $s := b_f + s'$

$$s = 5.25 \, in$$

Volumetric ratio of the FRP jacket: $\rho_{jx} := \dfrac{2 \cdot t}{b} \cdot \dfrac{b_f}{s}$

$$\rho_{jy} := \dfrac{2 \cdot t}{d} \cdot \dfrac{b_f}{s}$$

*Arching Effect (Confinement - Effectiveness) Coefficient $K_e$:*

Shape Factor

Clear distance between rounded corners:

$b' := b - 2 \cdot r$

$d' := d - 2 \cdot r$

$$k_e := 1 - \frac{b'^2 + d'^2}{3 \cdot A_g \cdot \left(1 - \rho_{sg}\right)}$$

$k_e = 0.336$

Stiffness of the FRP confinement:

$K_{confx} := \rho_{jx} \cdot k_e \cdot E_f$ $\qquad$ $K_{confy} := \rho_{jy} \cdot k_e \cdot E_f$

$K_{confx} = 47167 \, psi$ $\qquad$ $K_{confy} = 23583 \, psi$

Lateral confining pressures:

$\varepsilon_{ju} = \varepsilon_{fu}$ because the orientation of the FRP layers is perpendicular to the long axis of the column

$\sigma_{lx} := K_{confx} \varepsilon_{fu}$ $\qquad$ $\sigma_{ly} := K_{confy} \varepsilon_{fu}$

$\sigma_{lx} = 566 \, psi$ $\qquad$ $\sigma_{ly} = 283 \, psi$

Maximum confining stress:

$f_l := \min\left(\sigma_{lx}, \sigma_{ly}\right)$

$f_l = 283 \, psi$
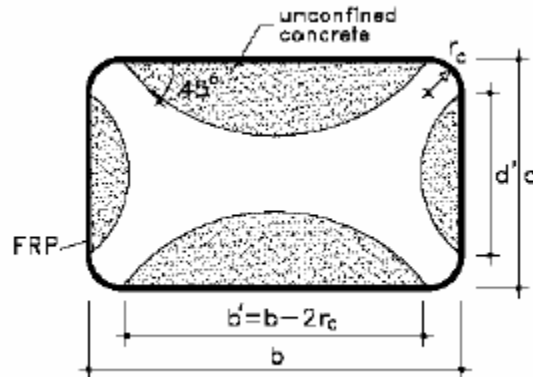
**"Exact Formula"**

Confined concrete strength and strain:

$$f_{cc} := f_{co} \cdot \left( 2.254 \cdot \sqrt{1 + 7.94 \cdot \frac{f_l}{f_{co}}} - 2 \cdot \frac{f_l}{f_{co}} - 1.254 \right)$$

$$f_{cc} = 5.685 \, \text{ksi}$$

$$\varepsilon_{cc} := \varepsilon_{co} \cdot \left[ 1 + 5 \cdot \left( \frac{f_{cc}}{f_{co}} - 1 \right) \right]$$

$$\varepsilon_{cc} = 0.0062$$

$$E_{cc} := \frac{f_{cc}}{\varepsilon_{cc}}$$

$$E_{cc} = 915 \, \text{ksi}$$

Secant Modulus of Elasticity of Concrete at ultimate:

Modulus of FRP Jacket: $\quad E_j := E_f$

Ultimate Strength of FRP Jacket: $\quad f_j := f_{fu}$

FRP Jacket Effective Ultimate Circumferential Strain $\varepsilon_{ju} := \varepsilon_{fu}$

Paramater of Damage Law (Property of Concrete):

$$\beta := \frac{5700 \text{MPa}^{0.5}}{\sqrt{|f_{co}|}} - 500$$

Secant Modulus of Elasticity of Concrete at Ultima

$$E_{secu} := \frac{E_c}{1 + 2 \cdot \beta \cdot \varepsilon_{ju}}$$

Ultimate Concrete Strain:

$$\varepsilon_{cu} := \varepsilon_{cc} \cdot \left( \frac{2 \cdot \beta \cdot \varepsilon_{ju} \cdot E_{cc}}{E_c - E_{cc}} \right)^{\left( 1 - \frac{E_{cc}}{E_c} \right)}$$

$$\varepsilon_{cu} = 0.0198$$

Concrete Strength at Ultimate:

$$f_{cu} := \frac{E_c \cdot \varepsilon_{cu}}{1 + 2 \cdot \beta \cdot \varepsilon_{ju}}$$

$$f_{cu} = 4802 \, psi$$

**"Practical Formula"**

Concrete Strength at Ultimate: $f_{cu} := f_{co} \cdot \left( 0.2 + 3 \cdot \sqrt{\frac{f_l}{f_{co}}} \right)$

$$f_{cu} = 3992 \, psi$$

Ultimate Concrete Strain $\varepsilon_{cu} := \varepsilon_{co} \cdot \left( 2 + 1.25 \cdot \frac{E_c}{f_{co}} \cdot \varepsilon_{ju} \sqrt{\frac{f_l}{f_{co}}} \right)$

$$\varepsilon_{cu} = 0.011$$

**APPENDIX B**

**UNIVERSITY OF CALIFORNIA – SAN DIEGO SPECIMENS FABRICATION & INSTRUMENTATION**

## Table B1 - Specimens Matrix; Total: 18

| Specimen Cross-section Type and Dimension | Height (in) | Side Aspect Ratio (b/h) | Area Aspect Ratio (Area/Area $_{18x18}$) | Height Aspect Ratio (H/h) | Specimens Code & No. Plies | |
|---|---|---|---|---|---|---|
| $\rho_l = 1.53\%$  20 in  Area: 314 in$^2$ | 44 (3.7ft) | 0 | 1 | 2.2 | A1 | 0 |
| | | | | | A2 | 2 |
| | | | | | A3* | 4 |
| $\rho_l = 1.56\%$  12.5 in  25 in  Area: 312 in$^2$ | 54 (4.5ft) | 2 | 1 | 2.2 | B1 | 0 |
| | | | | | B2 | 7 |
| | | | | | B3 | 2 |
| $\rho_l = 1.48\%$  18 in  18 in  Area: 324 in$^2$ | 40 (3.3ft) | 1 | 1 | 2.2 | C1 | 0 |
| | | | | | C2 | 4 |
| | | | | | C3 | 2 |
| $\rho_l = 1.48\%$  25.5 in  25.5 in  Area: 650 in$^2$ | 54 (4.5ft) | 1 | 2 | 2.1 | D1 | 0 |
| | | | | | D2 | 5 |
| | | | | | D3 | 2 |
| $\rho_l = 1.53\%$  12.75 in  12.75 in  Area: 162 in$^2$ | 27 (2.25ft) | 1 | 0.5 | 2.1 | E1 | 0 |
| | | | | | E2 | 2 |
| | | | | | E3* | 4 |
| $\rho_l = 1.53\%$  12.75 in  12.75 in  Area: 162 in$^2$ | 54 (4.5ft) | 1 | 0.5 | 4.2 | F1 | 0 |
| | | | | | F2 | 2 |
| | | | | | F3* | 4 |

Notes: * Partially wrapped specimens; 1 in = 2.54 cm; 1 ft = 0.3 m; 1 in$^2$ = 6.45 cm$^2$

**TableB2 – Distribution and Number of Strain Gages**

| Specimen | Steel | | Subtotal | FRP | | Subtotal | Total |
|---|---|---|---|---|---|---|---|
| | Rebars | Ties | | Horizontal | Vertical | | |
| A0 | 4 | 8 | 12 | N/A | | | 12 |
| A1 | 4 | 8 | 12 | 8 | 4 | 12 | 24 |
| A2 | 4 | 8 | 12 | 8 | 4 | 12 | 24 |
| B0 | 6 | 6 | 12 | N/A | | | 12 |
| B1 | 6 | 6 | 12 | 10 | 2 | 12 | 24 |
| B2 | 6 | 6 | 12 | 10 | 2 | 12 | 24 |
| C0 | 6 | 6 | 12 | N/A | | | 12 |
| C1 | 6 | 6 | 12 | 8 | 2 | 10 | 22 |
| C2 | 6 | 6 | 12 | 8 | 2 | 10 | 22 |
| D0 | 6 | 8 | 14 | N/A | | | 14 |
| D1 | 6 | 8 | 14 | 10 | 2 | 12 | 26 |
| D2 | 6 | 8 | 14 | 10 | 2 | 12 | 26 |
| E0 | 4 | 6 | 10 | N/A | | | 10 |
| E1 | 4 | 6 | 10 | 8 | 2 | 10 | 20 |
| E2 | 4 | 6 | 10 | 8 | 2 | 10 | 20 |
| F0 | 4 | 6 | 10 | N/A | | | 10 |
| F1 | 4 | 6 | 10 | 8 | 2 | 10 | 20 |
| F2 | 4 | 6 | 10 | 8 | 2 | 10 | 20 |
| | | | | | | Total | 342 |

Notes:
1. Design concrete compressive strength $f'_c$ = 4000 psi (28 MPa).
2. Total area of transverse steel (ties only) is as per code requirements
   Steel yield strength: $f_y$ = 60 ksi (420 MPa).
   Steel reinforcement ratio ($\rho_l$) for each type of specimen is detailed in Table B1.
3. One specimen for each group is the bench mark. For a second specimen in each group, the FRP jacket thickness is kept constant (two plies of 300 gr/m2 equivalent UD fabric which corresponds to a 30 percent capacity increase in the circular specimen as per attached design). For the third specimen in each group, the FRP jacket will vary to match the capacity increase obtained in the circular column. In all cases, the FRP plies will be Continuously Wrapped (CW) over the entire column surface with the exception of the third specimen from series A, E, and F, that will be Partially Wrapped (PW).
4. For the strengthened specimens, a gap of ¼ in (6.5 mm) is left in between the top (or bottom) end and the border of the FRP sheet.
5. Table B2 shows the distribution and total number of sensors on the internal reinforcements as well as on the FRP jacket per specimen. Figures illustrating the location of strain gages in each specimen are presented in this document. This instrumentation is placed in the central part of the specimens (at mid-height). For the case of the circular specimens (group A), the total number of gages in the steel is 12; four

of them are attached to four longitudinal bars (every second one – one gage per bar). The remaining eight are placed along the two center ties. A total of four strain gages (horizontal direction) per tie are used. They are placed next to the longitudinal bars where strain gages in the vertical direction are located. For the case of the prismatic specimens, the figures are accompanied of additional notes referring the layout.

6. In all the figures showing location of strain gages on the steel or FRP, the position indicated is with respect to their centers. The strain gages are not in scale with respect to the dimensions shown in the figures. With regards to their labeling see Table B3 and Table B4.

7. The pick up points for the specimens are to be selected and designed by UCSD.

**Table B3 – Rebar Cage Strain Gage Labeling Scheme**

| LNE | | HNU | | |
|---|---|---|---|---|
| L | NE | H | N | U |
| Longitudinal Rebar | Location in Plan (N, S, E, W) | Hoop Rebar | Location in Plan (N, S, E, W) | Upper or Lower Hoop |

**Table B4 – FRP Jacket Strain Gage Labeling Scheme**

| JVNE | | | JHNE | | |
|---|---|---|---|---|---|
| J | V | NE | J | H | NE |
| FRP Jacket | Vertical Position | Location in Plan (N, S, E, W) | FRP Jacket | Horizontal Position | Location in Plan (N, S, E, W) |

# CIRCULAR COLUMN (D=20 in; H = 44 in) – SPECIMENS A1, A2 & A3

¼ in Self leveling grout

2 in
2 in
2 in

1 in

3 ties #3 @ 2in

9 in

A — A

44 in

14 in

B — B

C — C

9 in

2 in
2 in
2 in

3 ties #3 @ 2in

1 in

20 in
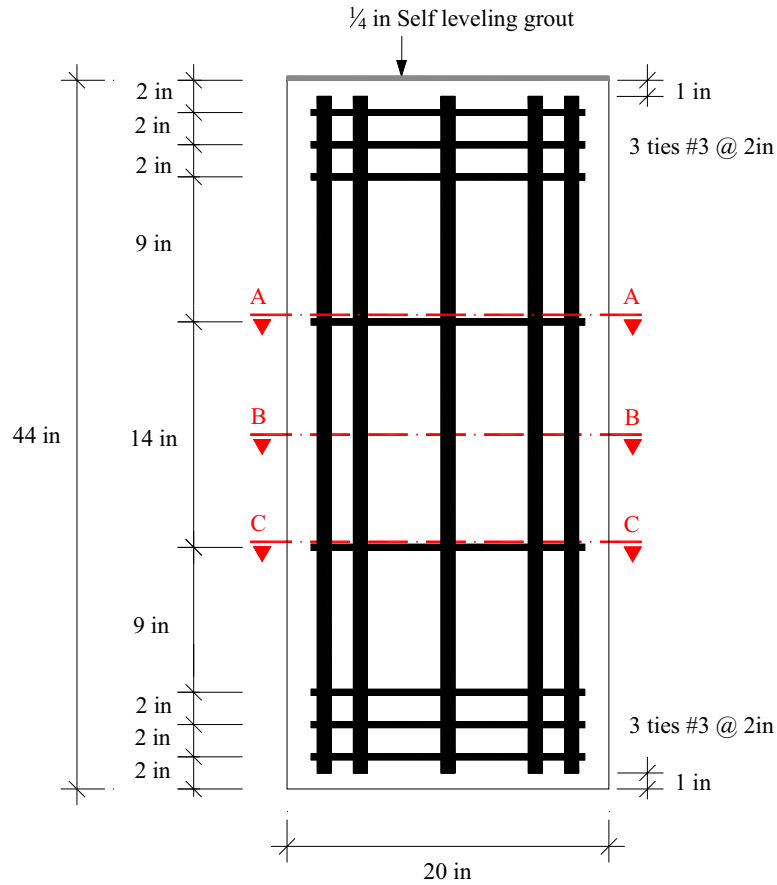
**Figure B1 – Longitudinal Cross Section; Specimens A1, A2 & A3**

Clear Cover 1.5 in

20 in

8#7 rebars

Ties #3@14in
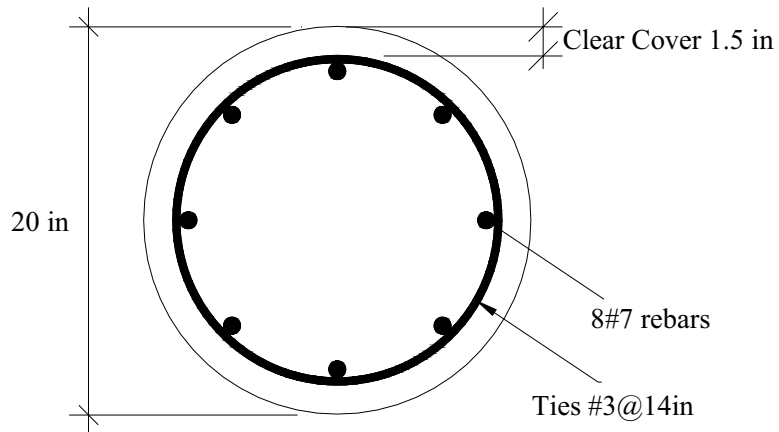
**Figure B2 – Section A-A & C-C; Specimens A1, A2 & A3**

12 in

17 in

**Figure B3 – Tie Detail; Circular Column**

Note:
The splice on the tie is alternated
along the height of the specimen.

LN

LW

LE

20 in

LS

Strain gages (vertical direction)
attached to longitudinal bars.
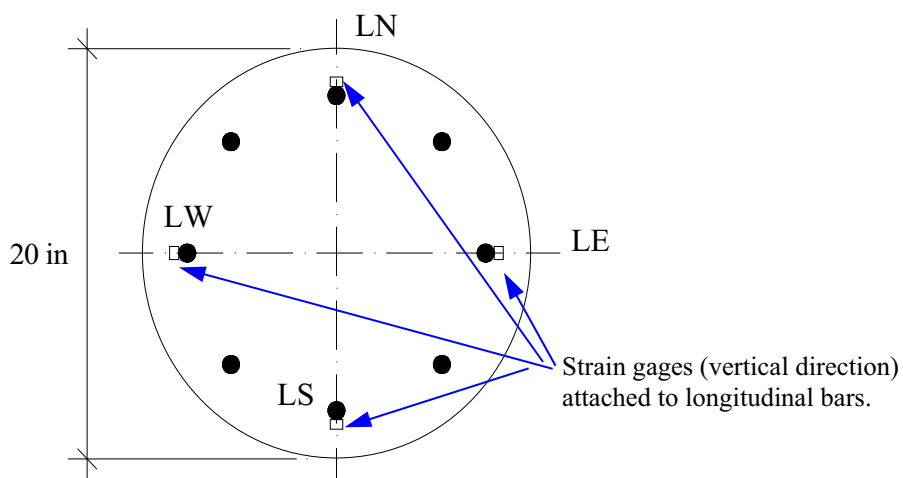
**Figure B4 – Section B-B; Strain Gages Location on Longitudinal Steel; Specimens A1, A2, A3**
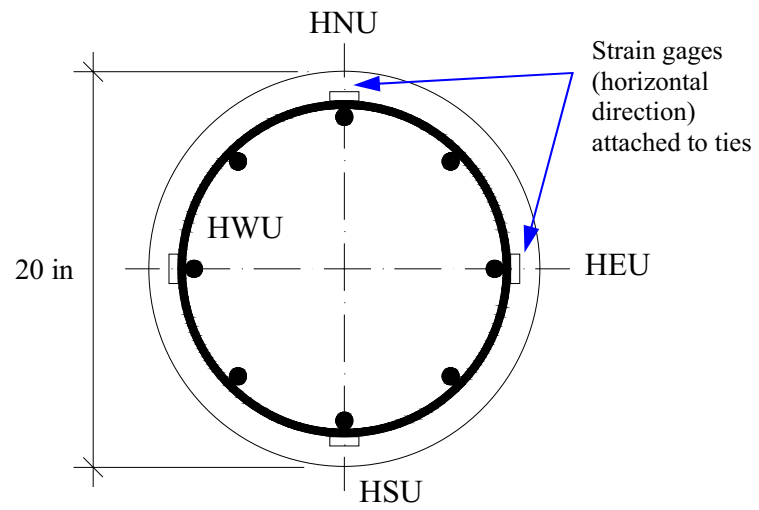
**Figure B5 – Section A-A and C-C; Strain Gages Location on Ties; Specimens A1, A2 & A3**

Strain gages along the two center ties. A total of four strain gages (horizontal direction) per tie are used. They are placed next to the longitudinal bars where strain gages in the vertical direction are located (equally spaced along the tie).

One strain gage (vertical direction) at mid-height of the specimen (22in) in four longitudinal bars (every second bar – 1 gage per bar).

¼ in Self leveling grout

Mid height

1 in

Mid height: 22 in

1 in

20 in

2 in
2 in
2 in

9 in

14 in

9 in

2 in
2 in
2 in

44 in
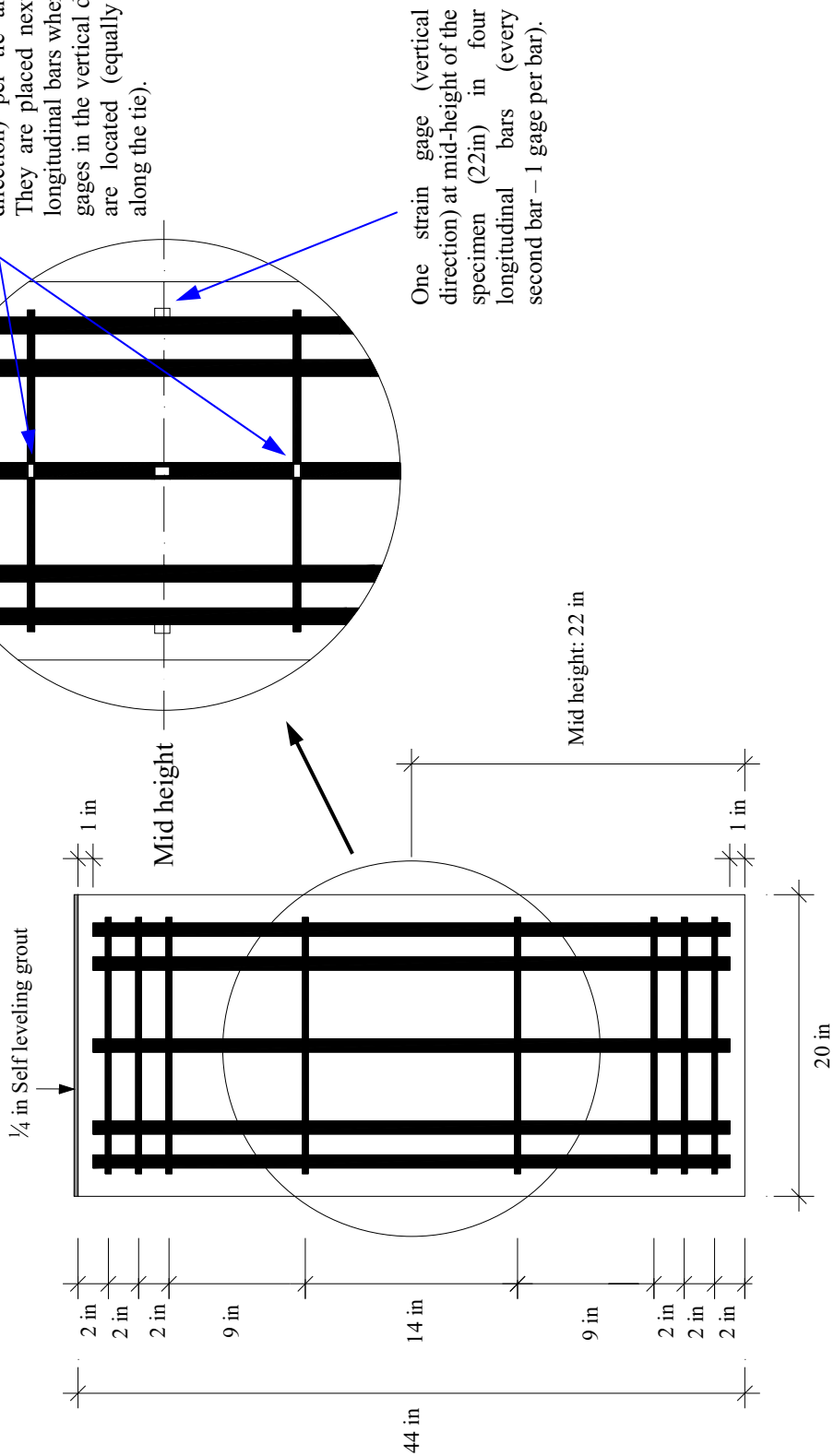
**Figure B6 – Strain Gages Location on the Steel; Specimens A1, A2 & A3**
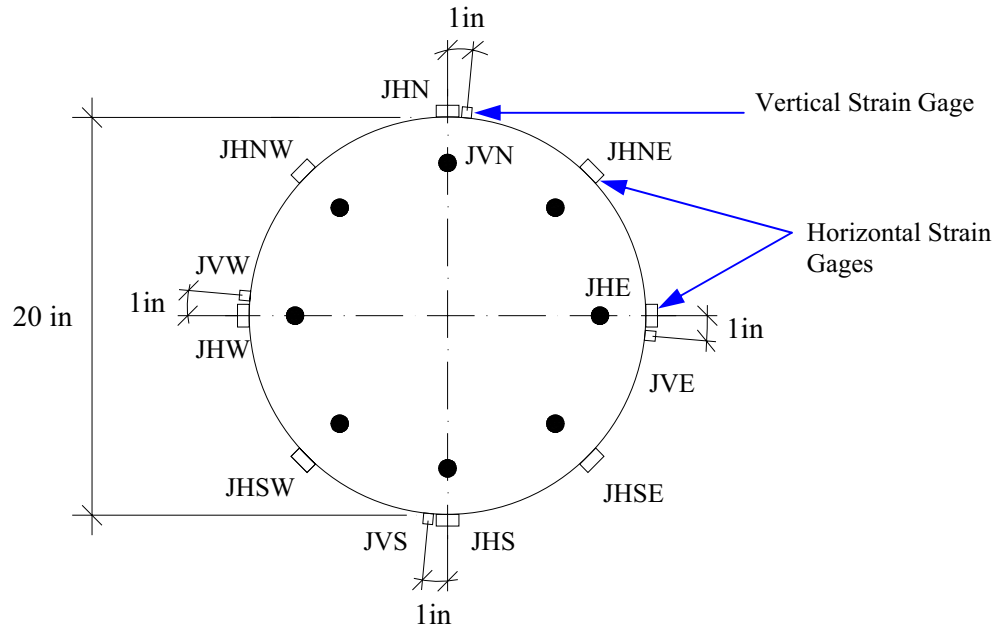
**Figure B7 – Section B-B; Strain Gages Location on FRP; Specimen A2 & A3**
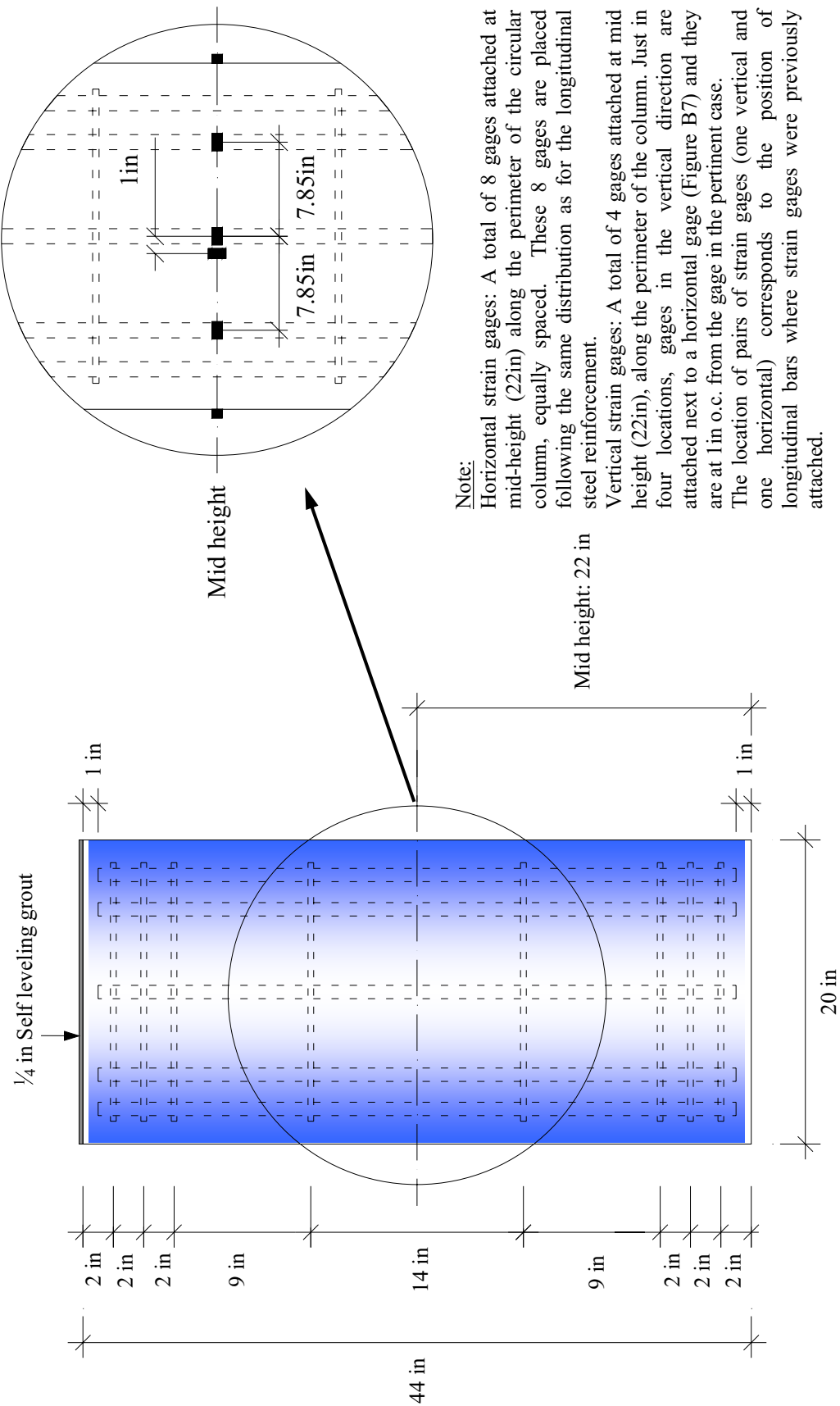
Mid height

Mid height: 22 in

Note:
Horizontal strain gages: A total of 8 gages attached at mid-height (22in) along the perimeter of the circular column, equally spaced. These 8 gages are placed following the same distribution as for the longitudinal steel reinforcement.

Vertical strain gages: A total of 4 gages attached at mid height (22in), along the perimeter of the column. Just in four locations, gages in the vertical direction are attached next to a horizontal gage (Figure B7) and they are at 1in o.c. from the gage in the pertinent case.

The location of pairs of strain gages (one vertical and one horizontal) corresponds to the position of longitudinal bars where strain gages were previously attached.

**Figure B8 – Strain Gages Location on FRP; Specimen A2**

8.5 in

1in

7.85in — 7.85in

Mid height

Note:
Horizontal strain gages: A total of 8 gages attached at mid-height (22in) along the perimeter of the circular column, equally spaced. These 8 gages are placed following the same distribution as for the longitudinal steel reinforcement.
Vertical strain gages: A total of 4 gages attached at mid height (22in), along the perimeter of the column. Just in four locations, gages in the vertical direction are attached next to a horizontal gage (Figure B7), and they are at 1in o.c. from the gage in the pertinent case. The location of pairs of strain gages (one vertical and one horizontal) corresponds to the position of longitudinal bars where strain gages were previously attached.

Mid height: 22 in

$7\frac{7}{8}$in

3in

$5\frac{1}{4}$in

3in

$5\frac{1}{4}$in

3in

$5\frac{1}{4}$in

3in

$7\frac{7}{8}$in

¼ in gap

¼ in gap

¼ in Self leveling grout

20 in

2 in
2 in
2 in

9 in

14 in

9 in

2 in
2 in
2 in

44 in

**Figure B9 – Strain Gages Location on FRP; Specimen A3**

**RECTANGULAR COLUMN 12.5 x 25 x 54 in – SPECIMENS B1, B2, B3**



¼ in Self leveling grout

2 in
2 in
2 in
6 in
10 in
54 in
10 in
10 in
6 in
2 in
2 in
2 in

1 in
3 Ties #3 @ 2in
Tie Type A
Tie Type B

A A
B B
C C
D D

3 Ties #3 @ 2in
1 in

25 in

Note: Two overlapping ties at the top and bottom ends in the first three ties.
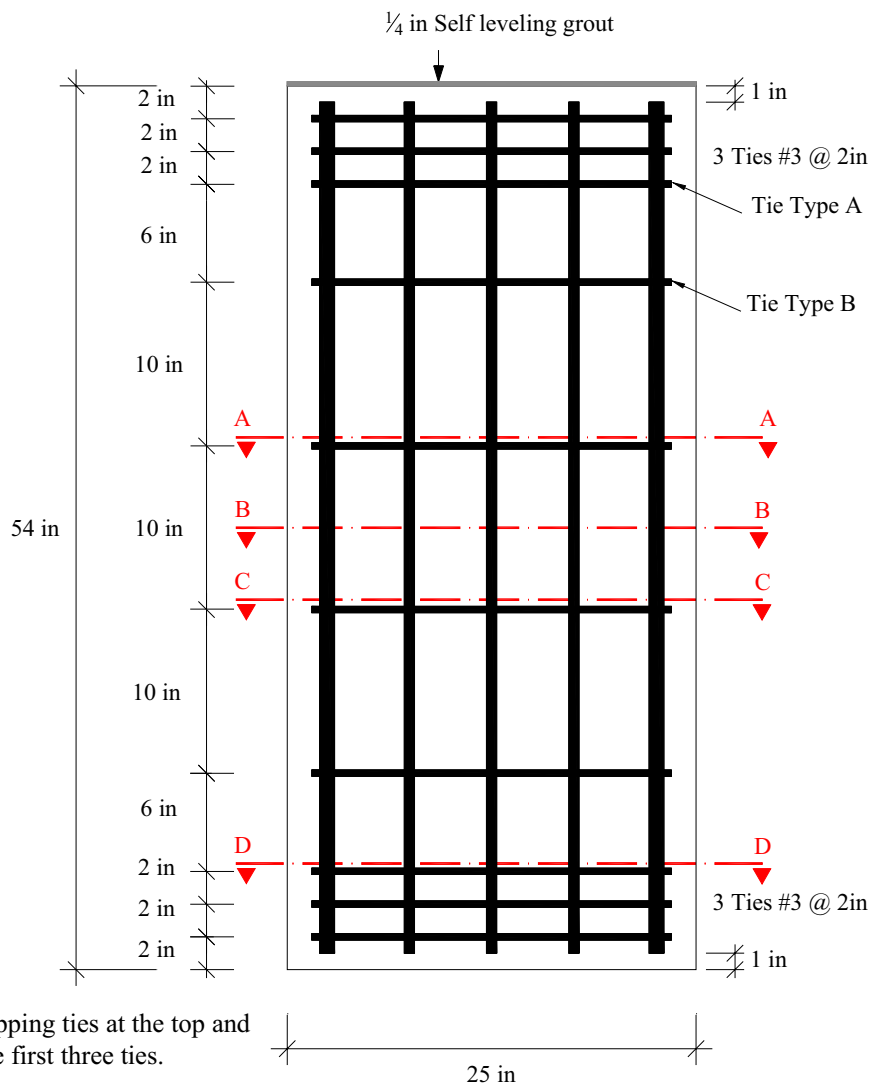
**Figure B10 – Longitudinal Cross Section; Specimens B1, B2 & B3**
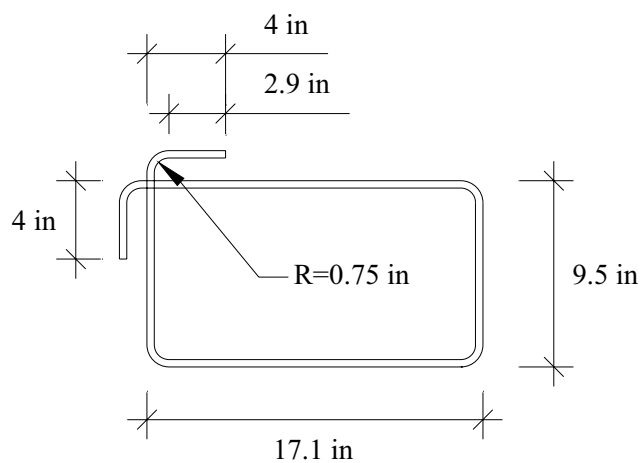
**Figure B11 – Overlapping Tie Type A; Specimens B1, B2 & B3**
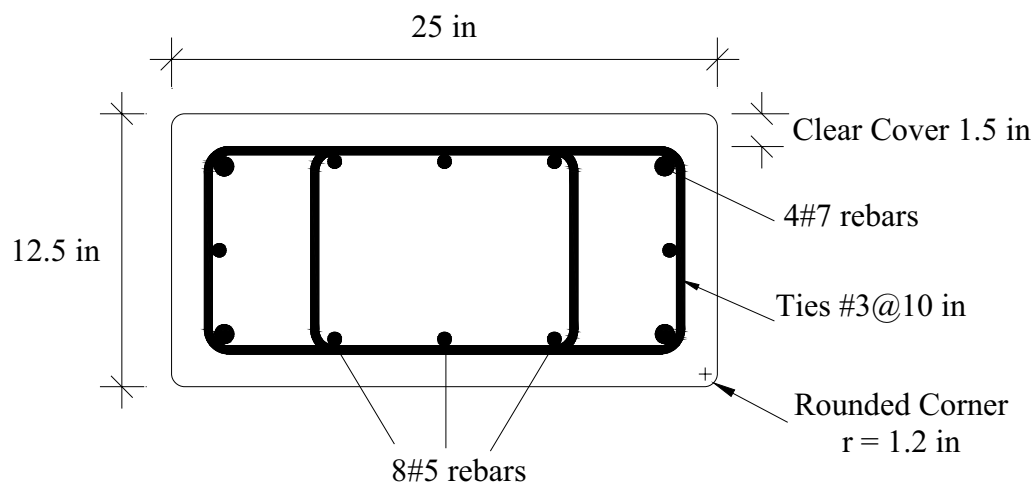


**Figure B12 – Section D-D, Type A Tie Overlapping Detail; Specimens B1, B2 & B3**

166
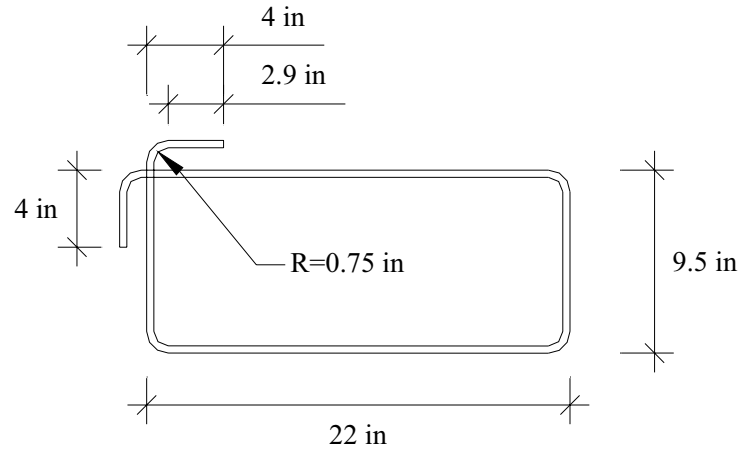


**Figure B13 – Tie Type B; Specimens B1, B2 & B3**
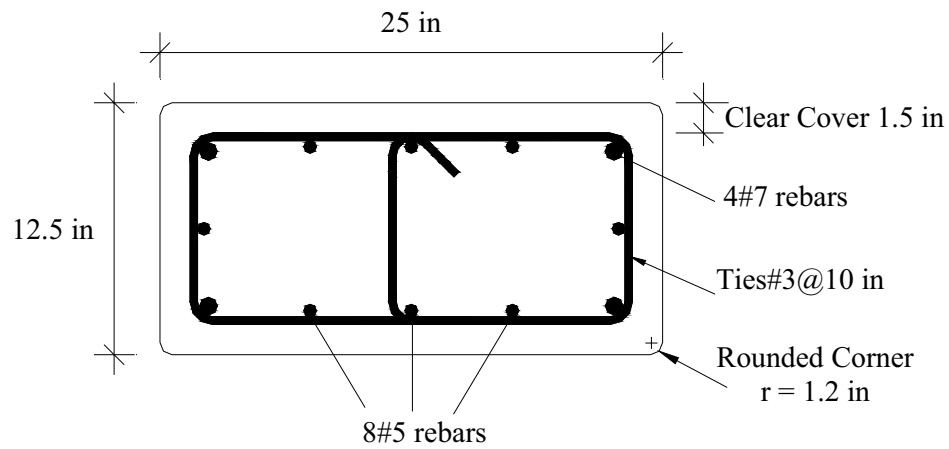


**Figure B14 – Section A-A & C-C; Type B Tie; Specimens B1, B2 & B3**
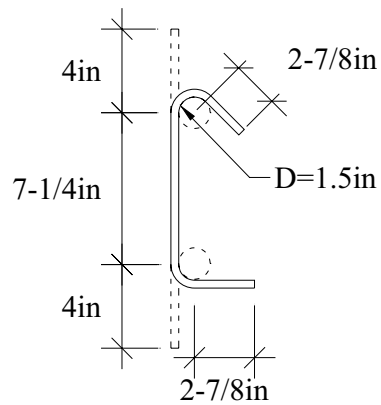


**Figure B15 – Cross Tie Detail; Specimens B1, B2 & B3**
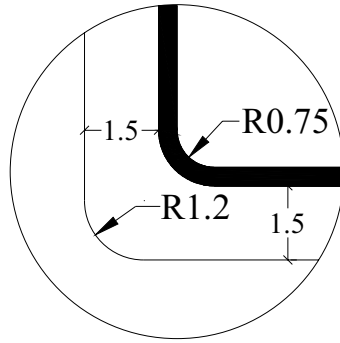
**Figure B16 – Chamfer Detail for the Corners of all the Prismatic Specimens**
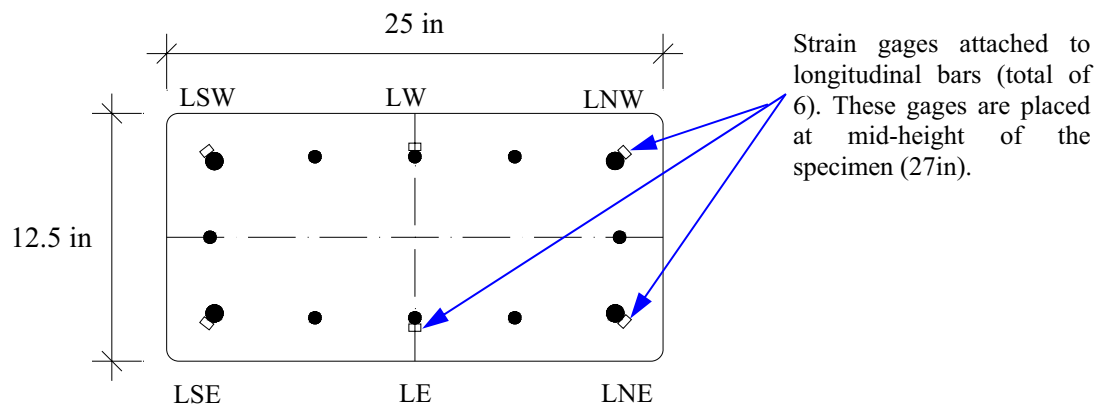


**Figure B17 – Section B-B; Strain Gage Location on Longitudinal Steel; Specimens B1, B2 & B3**
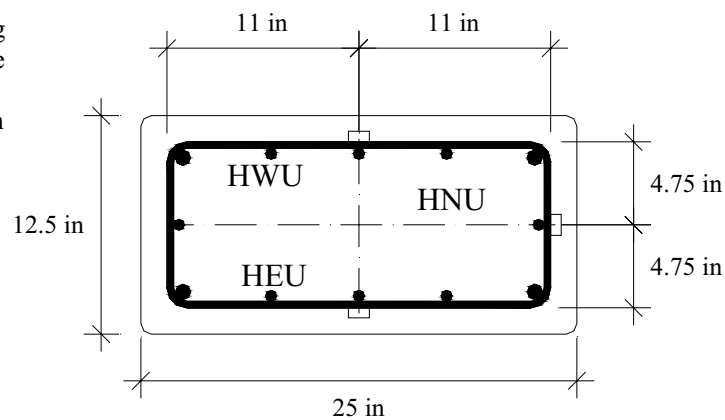


**Figure B18 – Section A-A & C-C; Strain Gages Location on Ties; Specimens B1, B2 & B3**

Three strain gages (horizontal direction) on each of the two center ties. Two of these gages are placed in each of the long sides of the tie and the remaining one in one of the short sides.

A total of 6 strain gages (vertical direction) are placed at mid-height of the specimen (27in). These gages are attached to the four corner longitudinal bars and also the middle bar in both longer sides.

Mid height

Mid height: 27 in

¼ in Self leveling grout

2 in
2 in
2 in
6 in
10 in
10 in
10 in
10 in
6 in
2 in
2 in
2 in

54 in

25 in

**Figure B19 – Strain Gages Location on Steel; Specimens B1, B2 & B3**
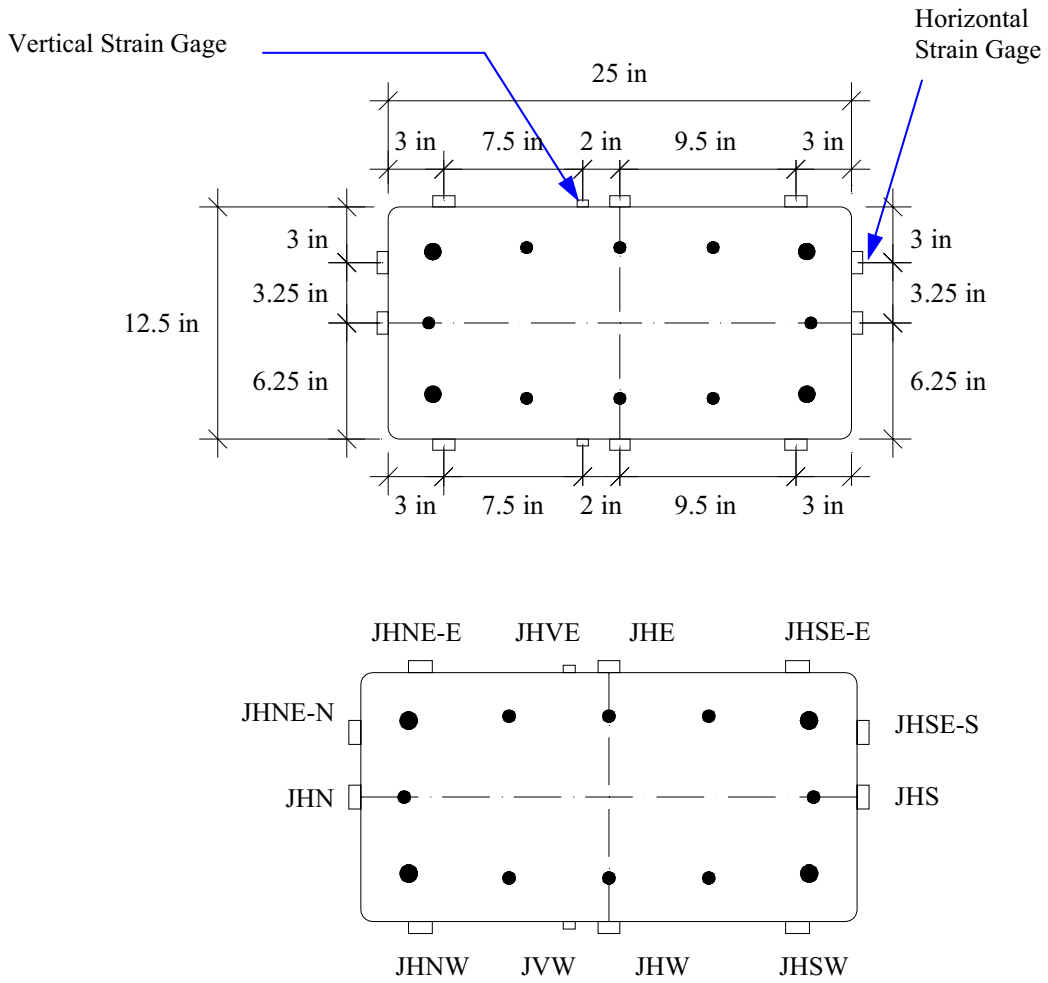
**Figure B20 – Section B-B; Strain Gages Location on FRP; Specimens B2 & B3**
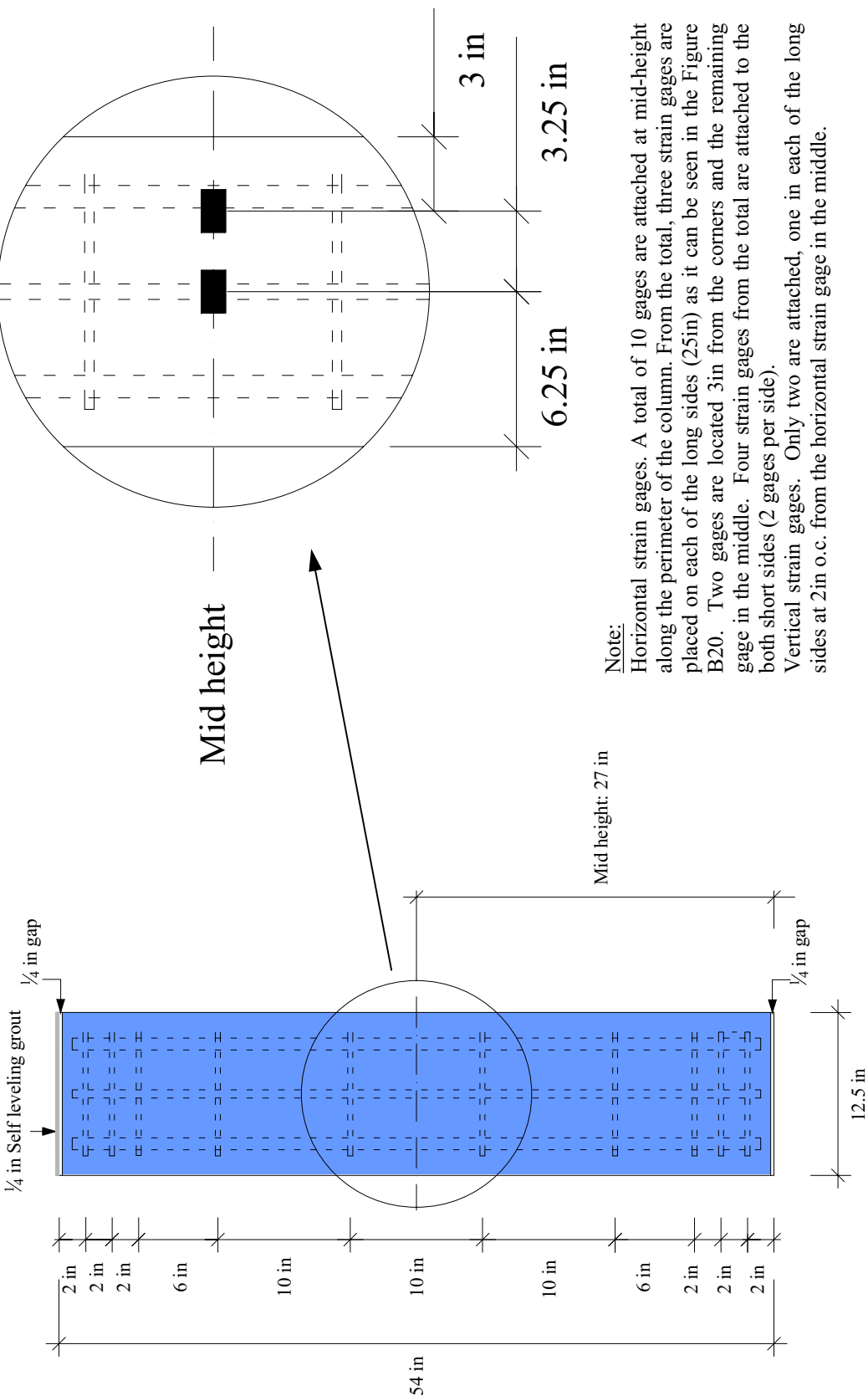
Mid height

Mid height: 27 in

6.25 in   3.25 in   3 in

¼ in gap

¼ in Self leveling grout

¼ in gap

54 in

2 in
2 in
2 in
6 in
10 in
10 in
10 in
6 in
2 in
2 in
2 in

12.5 in

Note:
Horizontal strain gages. A total of 10 gages are attached at mid-height along the perimeter of the column. From the total, three strain gages are placed on each of the long sides (25in) as it can be seen in the Figure B20. Two gages are located 3in from the corners and the remaining gage in the middle. Four strain gages from the total are attached to the both short sides (2 gages per side).
Vertical strain gages. Only two are attached, one in each of the long sides at 2in o.c. from the horizontal strain gage in the middle.

**Figure B21 – Strain Gages Location on FRP – Side 12.5 in; Specimens B2 & B3**

**Figure B22 – Strain Gages Location on FRP - Side 25 in; Specimens B2 & B3**

Note:
Horizontal strain gages. A total of 10 gages are attached at mid-height along the perimeter of the column. From the total, three strain gages are placed on each of the long sides (25in) as it can be seen in the Figure B20. Two gages are located 3in from the corners and the remaining gage in the middle. Four strain gages from the total are attached to the both short sides (2 gages per side).
Vertical strain gages. Only two are attached, one in each of the long sides at 2in o.c. from the horizontal strain gage in the middle.

**COLUMN 18 x 18 x 40 in – SPECIMENS C1, C2 & C3**

¼ in Self leveling grout

2 in
2 in
2 in

7 in

A          A

40 in   14 in   B          B

C          C

7 in

2 in
2 in
2 in

1 in

3 Ties #3 @ 2in

3 Ties #3 @ 2in

1 in

18 in
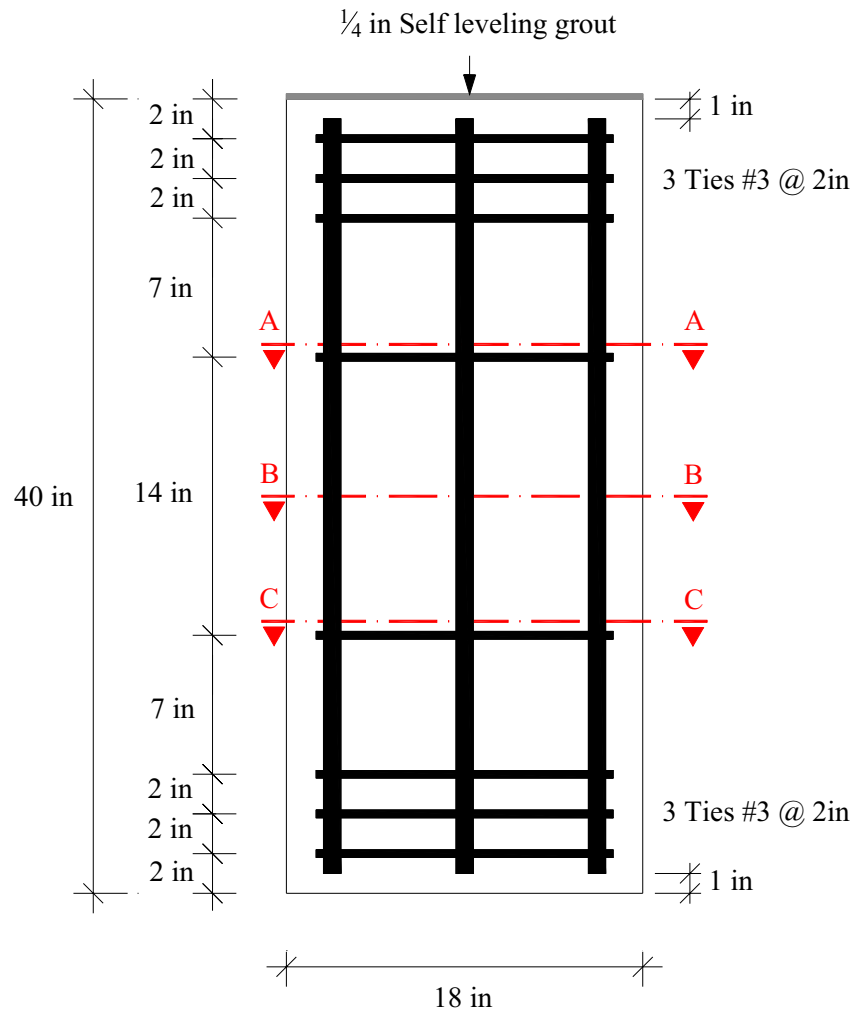
**Figure B23 – Longitudinal Cross Section; Specimens C1, C2 & C3**
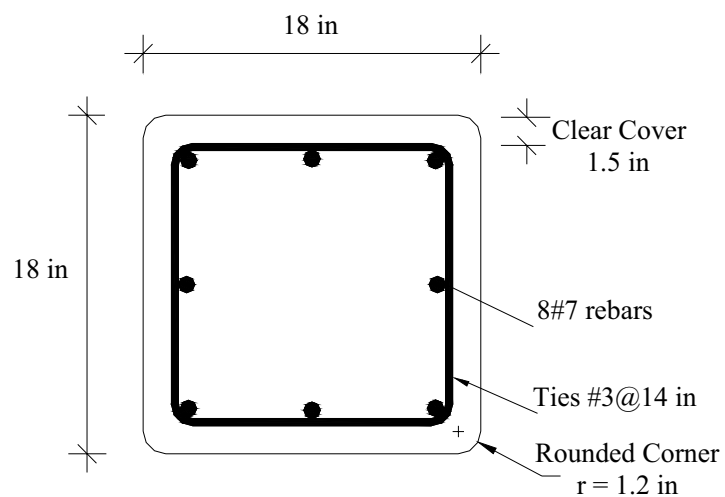
**Figure B24 – Section A-A & C-C; Specimens C1, C2 & C3**
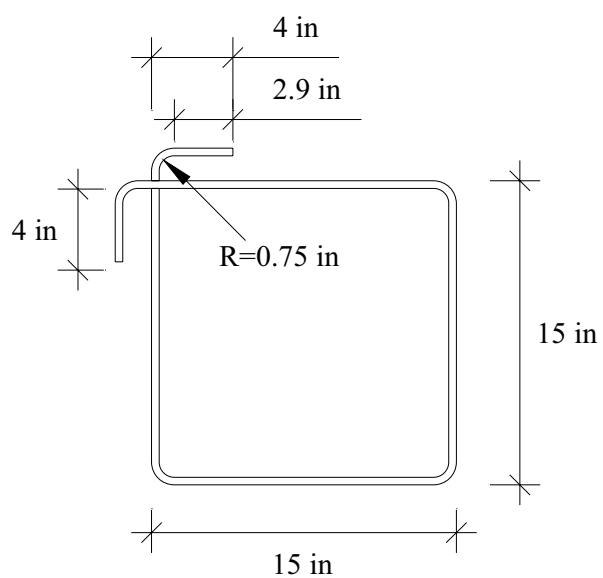


**Figure B25 – Tie Detail; Specimens C1, C2 & C3**

18 in

LN

LNW    LNE

18 in

LW

LSW    LSE

Six strain gages attached to 6 longitudinal bars (one gage per bar). These gages are placed at mid-height of the specimen (20in).
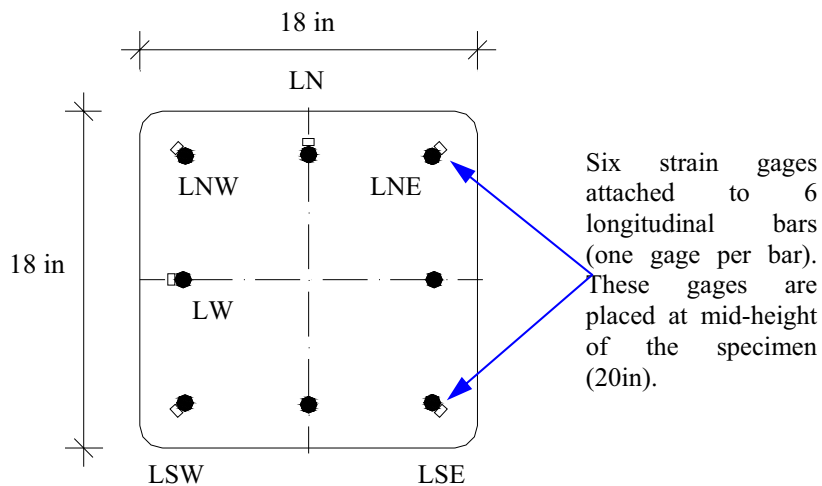
**Figure B26 – Section B-B; Strain Gages Location on Longitudinal Steel; Specimens C1, C2 & C3**

7.5 in    7.5 in

Horizontal Strain Gage

7.5 in

HNU

Note: In the labeling corresponding to the lower tie, the letter "U" is replaced with "L"

18 in

HWU    HEU

7.5 in

18 in
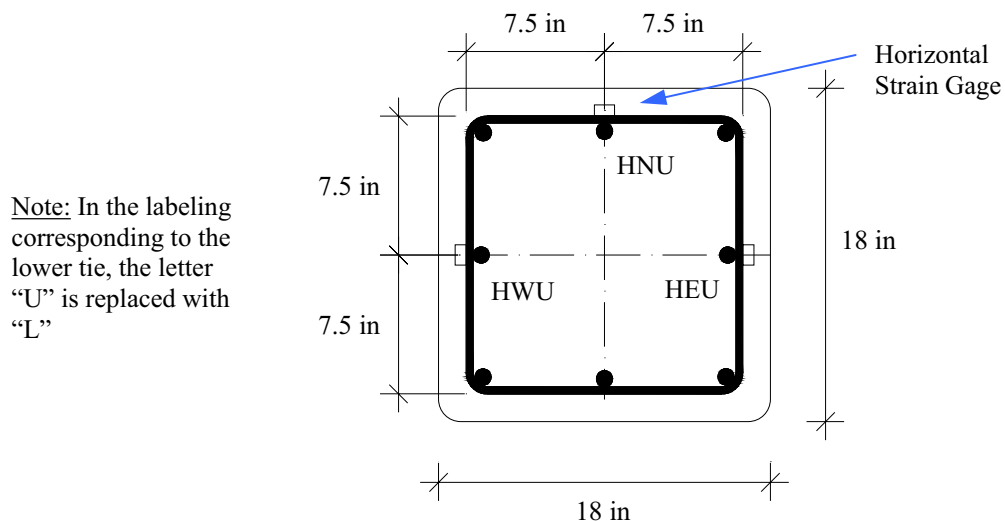
**Figure B27 – Section A-A & C-C; Strain Gages Location on the Tie; Specimens C1, C2 & C3**

**North and West Sides**

Three strain gages (horizontal direction) on each of the two center ties (total of 6 gages). It was considered sufficient to place the instrumentation on just three legs of the tie (one per leg). Note for their position in the previous figure.

A total of 6 strain gages (vertical direction) attached at mid height of the specimen (20in). They are placed on 6 of the longitudinal bars (the four corner bars and the middle bars on 3 sides of the column).

Mid height

Mid height: 20in

Note:
Two sides of the column present 3 strain gages on long bars in addition to the gage on the tie (figure above). On one side of the column there are not strain gages on the tie, but there is one gage in each of the two longitudinal corner bars. On the remaining side, there is one strain gage in each of the two corner bars and one gage on the tie. See Figure B26 and Figure B27 for illustration.

¼ in Self leveling grout

18 in

2 in
2 in
2 in
7 in
14 in
7 in
2 in
2 in
2 in

40 in

**Figure B28 – Strain Gages Location on Steel; Specimens C1, C2 & C3**
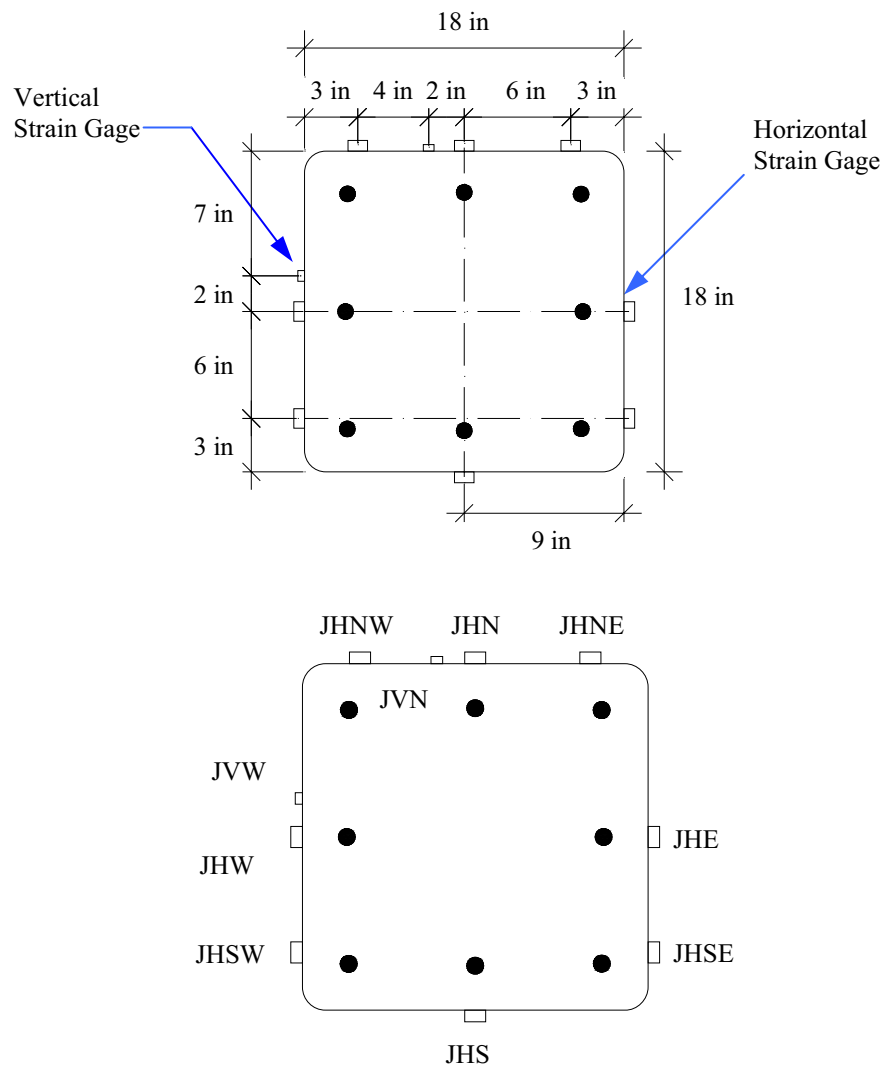
**Figure B29 – Section B-B; Strain Gages Location on FRP; Specimens C2 & C3**
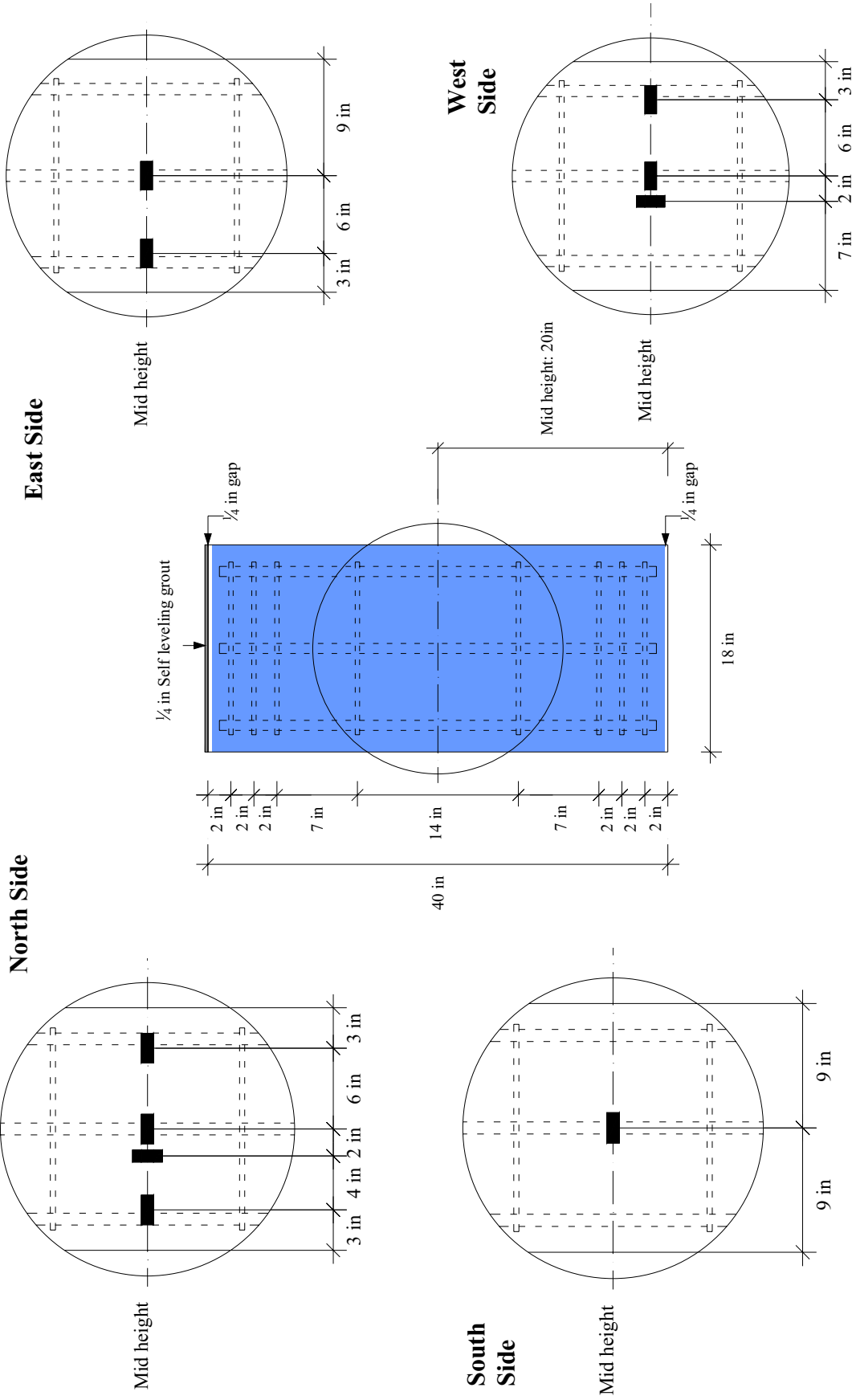
**Figure B30 – Strain Gages Location on the FRP; Specimens C2 & C3**

**COLUMN 25.5 x 25.5 x 54 in – SPECIMENS D1, D2 & D3**

¼ in Self leveling grout

2 in
2 in
2 in

1 in

3 Ties #3 @ 2in

14 in

A — A

54 in

14 in

B — B

C — C

14 in

2 in
2 in
2 in

3 Ties #3 @ 2in

1 in

25.5 in
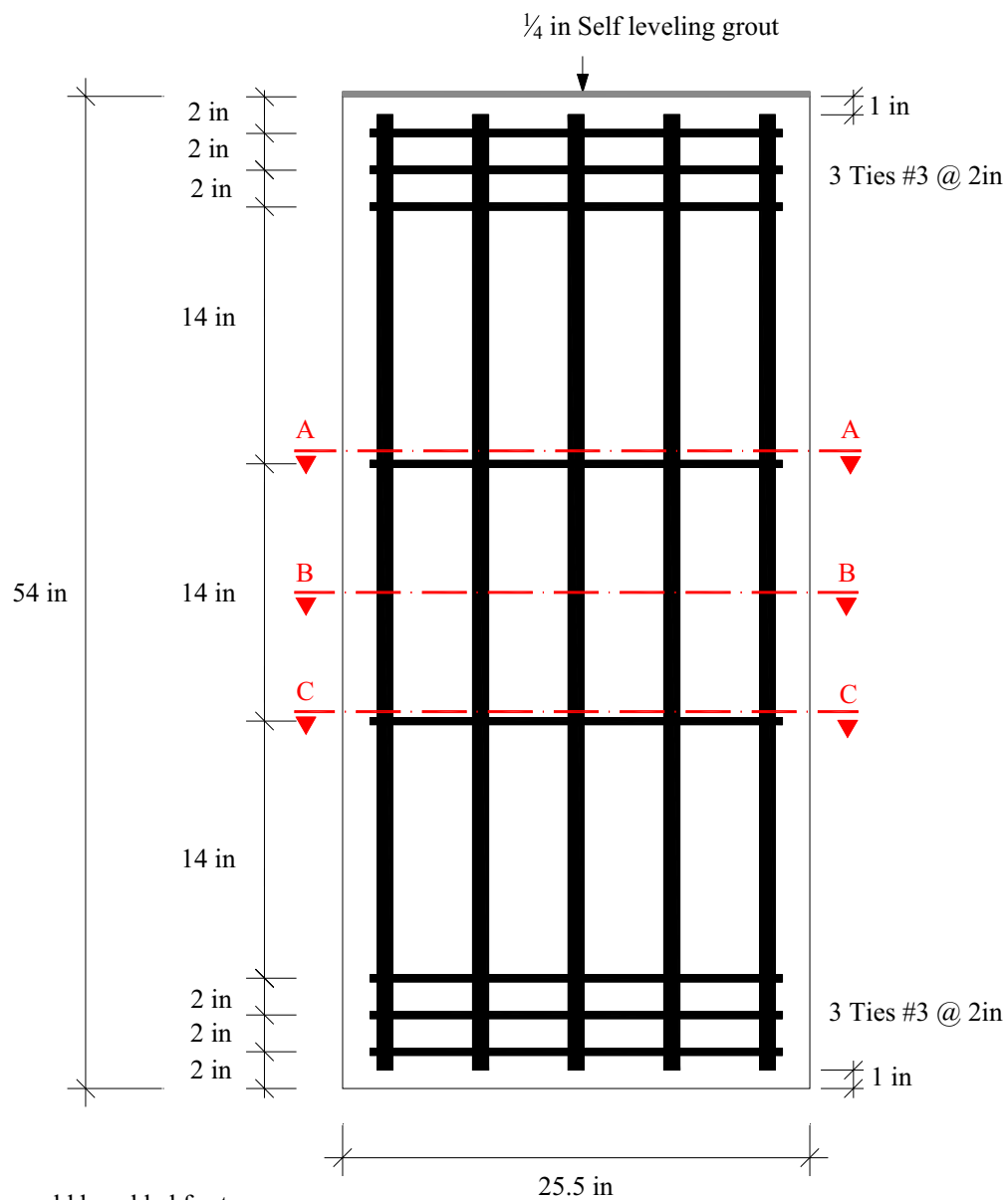
Note: Cross ties could be added for top and bottom ends confinement.

**Figure B31 – Longitudinal Cross Section; Specimens D1, D2 & D3**

25.5 in

Clear Cover
1.5 in

25.5 in

16#7 rebars

Cross Ties #3

Ties #3@14 in

Rounded Corner
r = 1.2 in
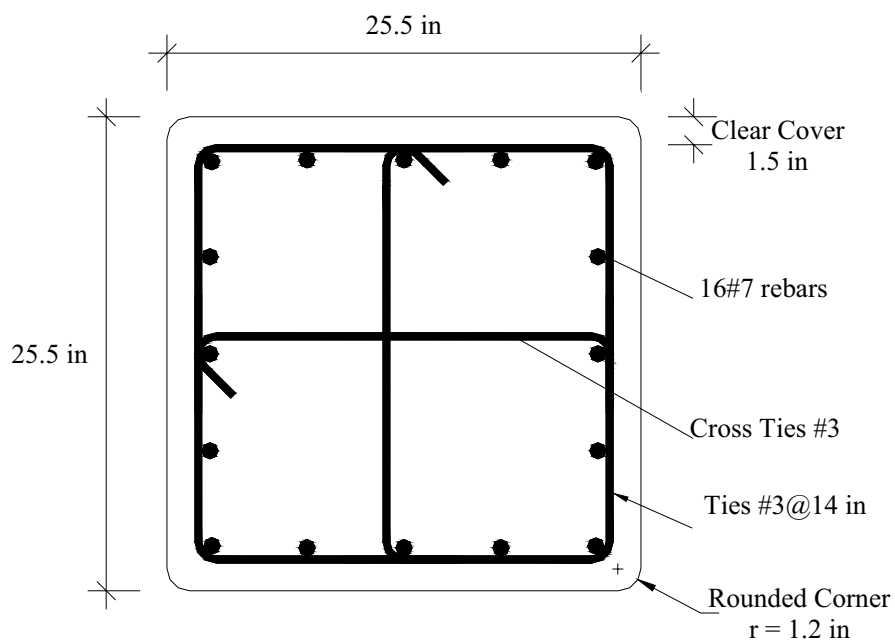
**Figure B32 – Section A-A & C-C; Specimens D1, D2 & D3**

4 in

2.9 in

4 in

R=0.75 in

22.5 in

22.5 in
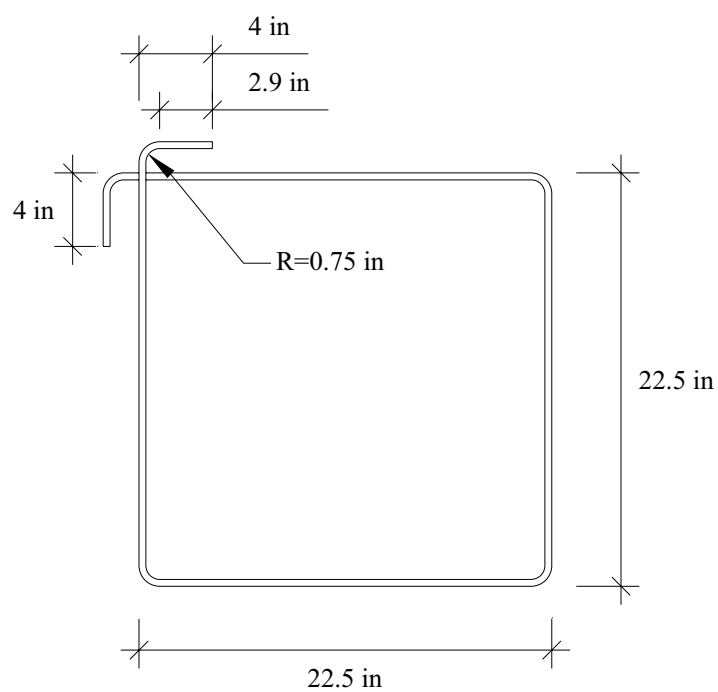
**Figure B33 – Tie Detail; Specimens D1, D2 & D3**
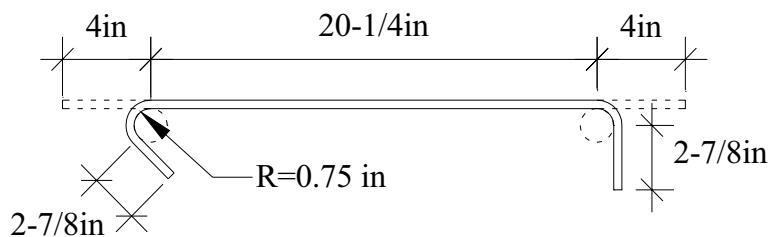
**Figure B34 – Cross Tie Detail; Specimens D1, D2 & D3**



Only on six longitudinal bars of the column one strain gage is attached. This instrumentation in the vertical direction is placed at mid-height of the specimen (27in).

**Figure B35 – Section B-B; Strain Gage Location on Longitudinal Steel; Specimens D1, D2 & D3**

Figure B36 – Section A-A & C-C; Strain Gages Location on Tie; Specimens D1, D2 & D3

**East & South Sides**

**North & West Sides**

Horizontal Strain Gages

Vertical Strain Gages

Mid height

Mid height

¼ in Self leveling grout

Mid height: 27 in

25.5 in

54 in

2 in
2 in
2 in

13 in

16 in

13 in

2 in
2 in
2 in
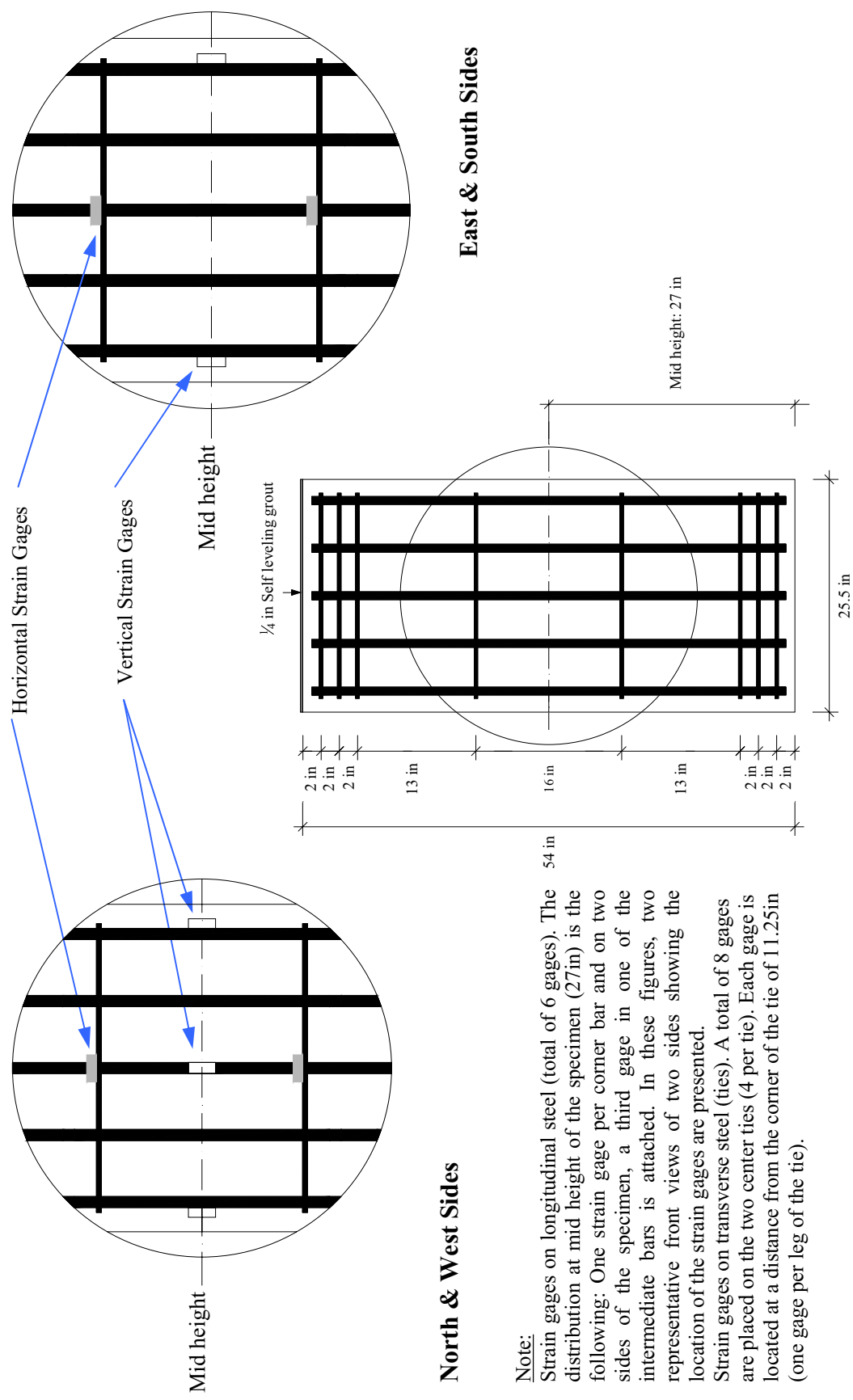
Note:
Strain gages on longitudinal steel (total of 6 gages). The distribution at mid height of the specimen (27in) is the following: One strain gage per corner bar and on two sides of the specimen, a third gage in one of the intermediate bars is attached. In these figures, two representative front views of two sides showing the location of the strain gages are presented.
Strain gages on transverse steel (ties). A total of 8 gages are placed on the two center ties (4 per tie). Each gage is located at a distance from the corner of the tie of 11.25in (one gage per leg of the tie).

**Figure B37 – Strain Gages Location on Steel; Specimens D1, D2 & D3**
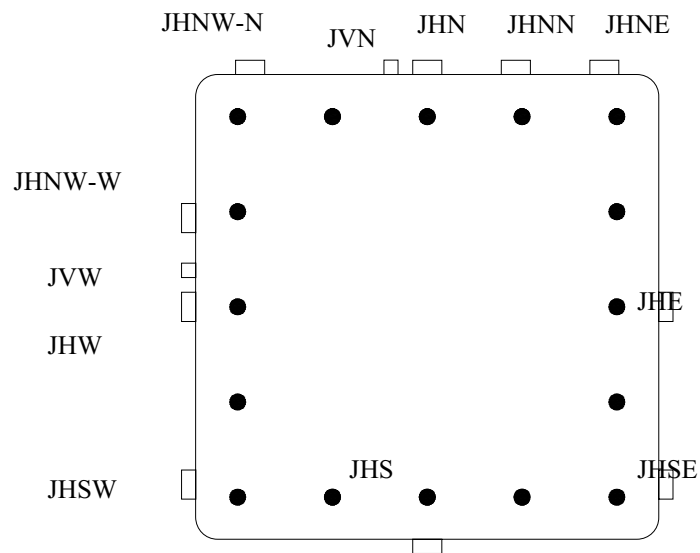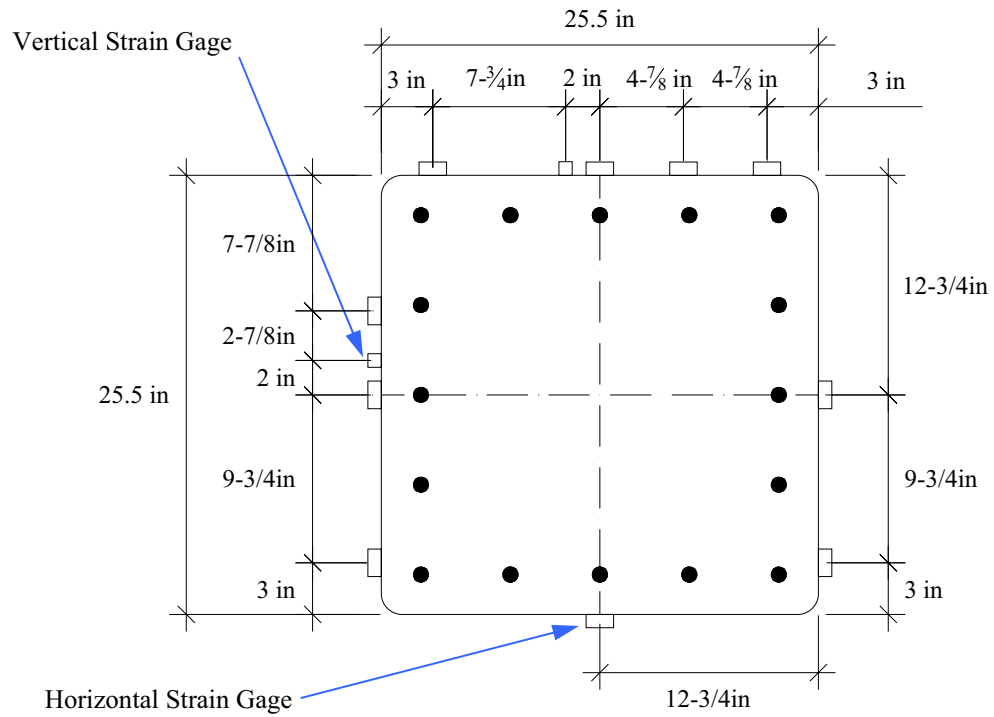
**Figure B38 – Section B-B; Strain Gages Location on FRP; Specimens D2 & D3**

**North Side**

**East Side**

**South Side**

**West Side**

**Figure B39 – Strain Gages Location on the FRP; Specimens D2 & D3**

**COLUMN 12.75 x 12.75 x 27 in – SPECIMENS E1, E2 & E3**

¼ in Self leveling grout

2in
2in
2in
2.5in
A    A
27in    10in
B    B
C    C
2.5in
2in
2in
2in

1 in

3 Ties #3 @ 2in

3 Ties #3 @ 2in

1 in

12.75 in
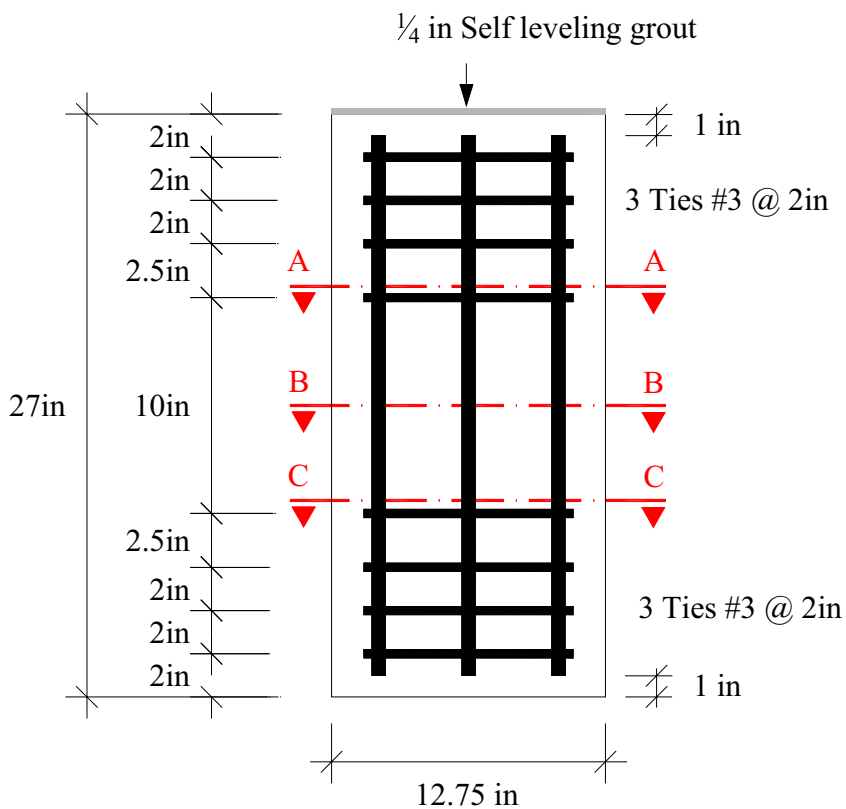
**Figure B40 – Longitudinal Cross Section; Specimens E1, E2 & E3**

12.75 in

12.75 in

Clear Cover
1.5 in

8#5 rebars

Ties #3@10 in

Rounded Corners
r = 1.2 in
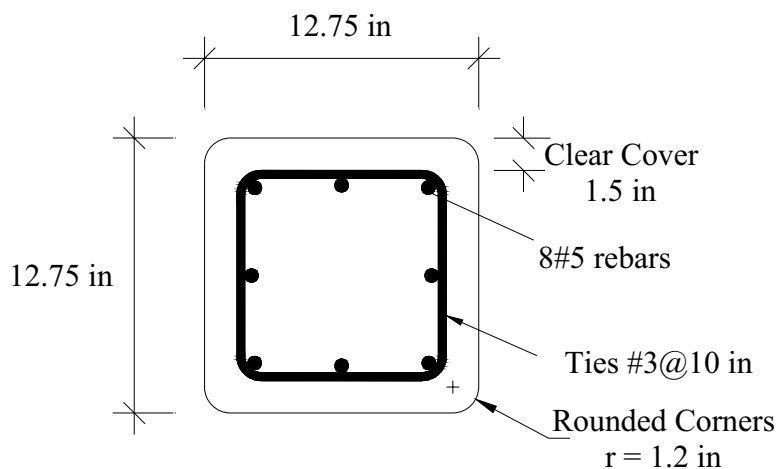
**Figure B41 – Section A-A & C-C; Specimens E1, E2 & E3**

4 in

2.9 in

4 in

R=0.75 in

9.75 in

9.75 in
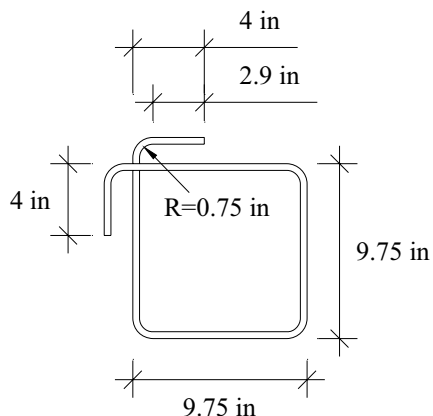
**Figure B42 – Tie Detail; Specimens E1, E2 & E3**

12.75 in

12.75 in

LNW    LNE

LSW    LSE

A total of four strain gages (vertical direction) attached to the corner longitudinal bars (one gage per bar) at mid height of the specimen (13.5in)
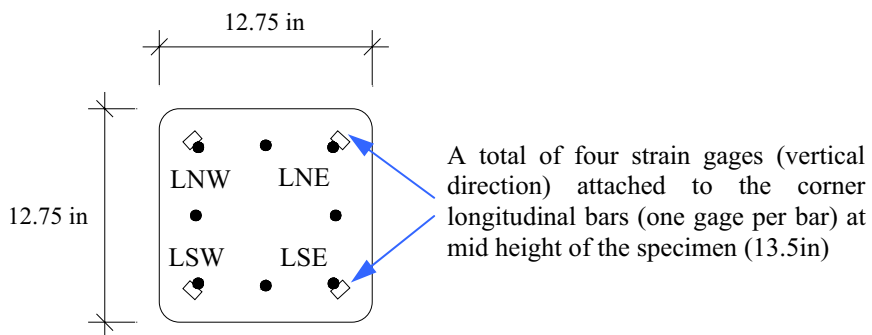
**Figure B43 – Section B-B; Strain Gages Location on Longitudinal Steel; Specimens E1, E2 & E3**

12.75 in

4-7/8in

Horizontal Strain Gage

HNU

HEU

4-7/8in

12.75 in

HWU

Note: In the labeling corresponding to the lower tie, the letter "U" is replaced with "L"
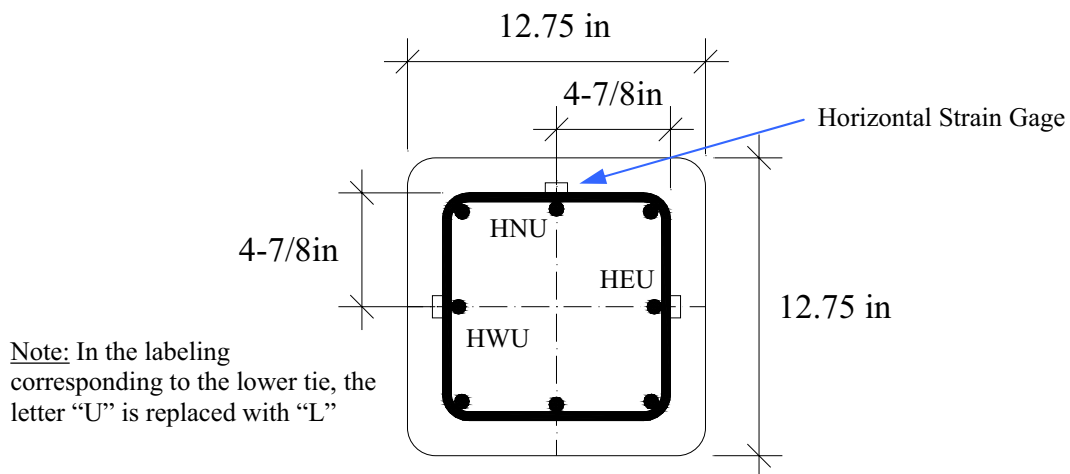
**Figure B44 – Section A-A & C-C; Strain Gages Location on the Tie; Specimens E1, E2 & E3**

**South Side**

Mid height

Horizontal Strain Gage

Vertical Strain Gages

¼ in Self leveling grout

Mid height: 13.5in

12.75 in

2in
2in
2in
2.5in

10in

27in

2.5in
2in
2in
2in
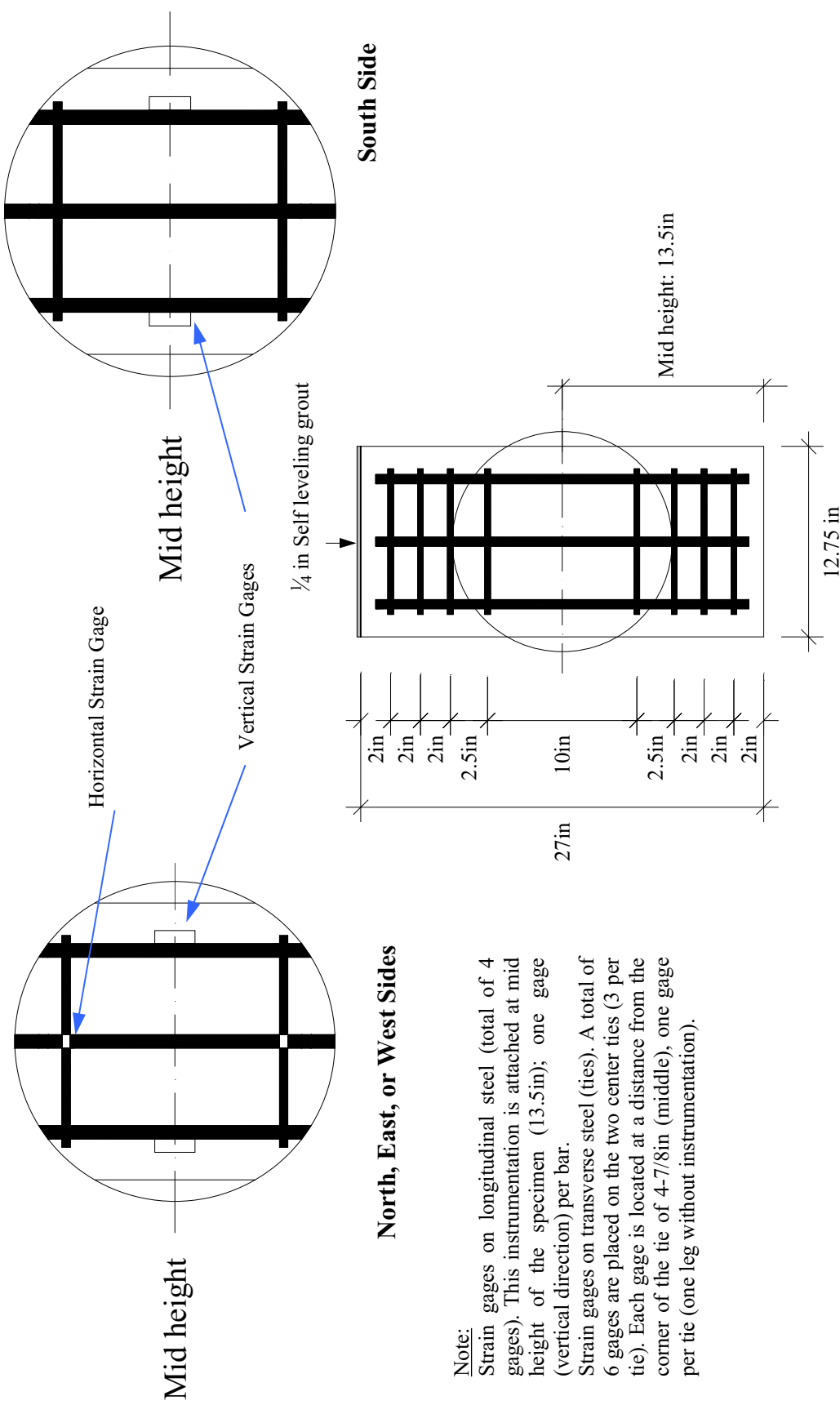
**North, East, or West Sides**

Mid height

Note:
Strain gages on longitudinal steel (total of 4 gages). This instrumentation is attached at mid height of the specimen (13.5in); one gage (vertical direction) per bar.
Strain gages on transverse steel (ties). A total of 6 gages are placed on the two center ties (3 per tie). Each gage is located at a distance from the corner of the tie of 4-7/8in (middle), one gage per tie (one leg without instrumentation).

**Figure B45 – Strain Gages Location on Steel; Specimens E1, E2 & E3.**

2-3/8in

1in

3-3/8in

Horizontal
Strain Gage

Vertical Strain Gage

3in

3in

5-3/8in

6-3/8in

12.75in

1in

3-3/8in

3-3/8in

3in

3in

6-3/8in

12.75in

JHNW    JHN    JNE

JVN

JVW

JHW    JHE

JHSW    JHSE

JHS
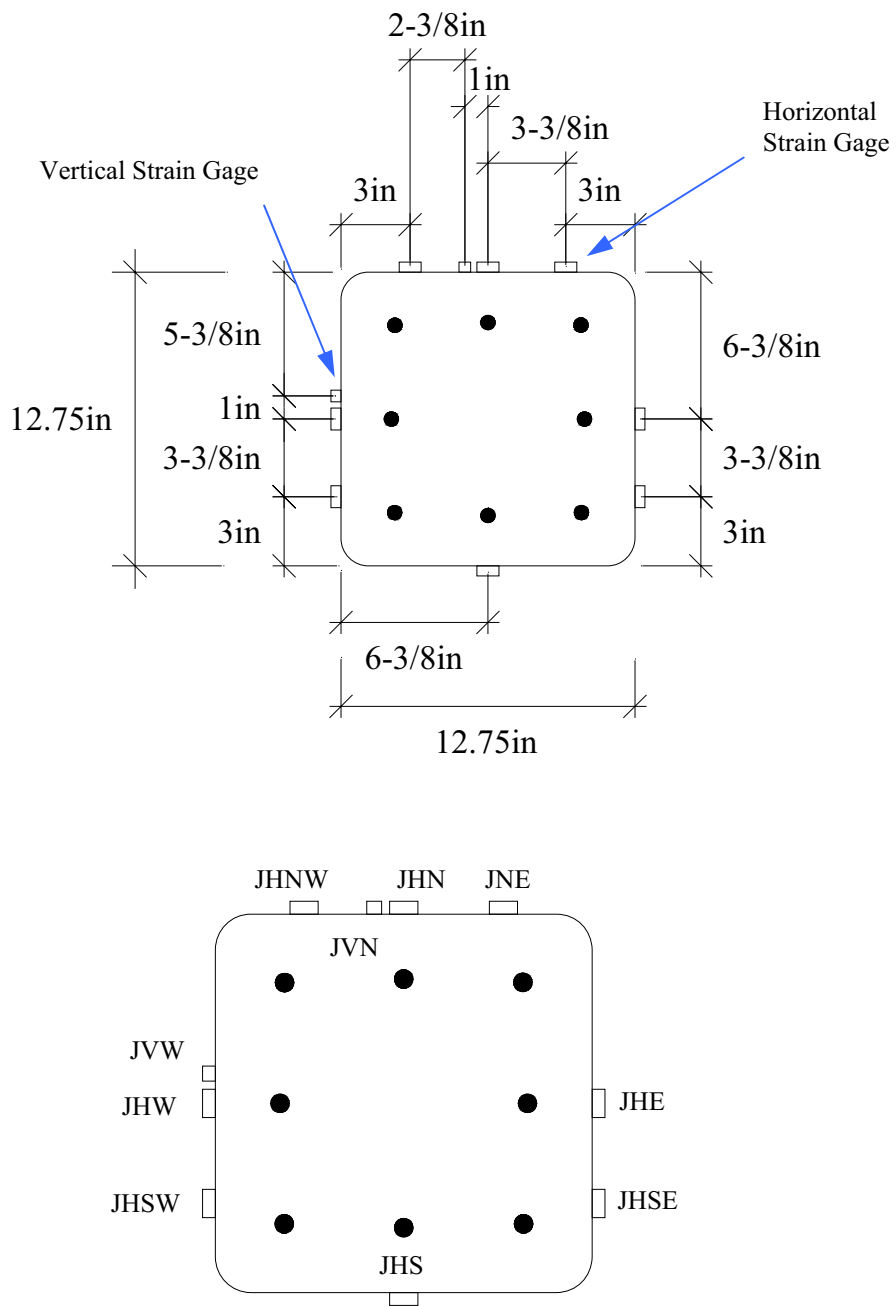
**Figure B46 – Section B-B; Strain Gages Location on FRP; Specimens E2 & E3**

**East Side**

Mid height

6-3/8in

3-3/8in

3in

**North Side**

5-3/8in

Mid height

3in

3-3/8in

3-3/8in

3in

**South Side**

Mid height

6-3/8in

6-3/8in

**West Side**

5-3/8in

Mid height

3in

3-3/8in

6-3/8in

Mid height: 13.5in

¼ in Self leveling grout

¼ in gap

¼ in gap

¼ in gap

12.75 in

2in
2in
2in
2.5in

10in

2.5in
2in
2in
2in
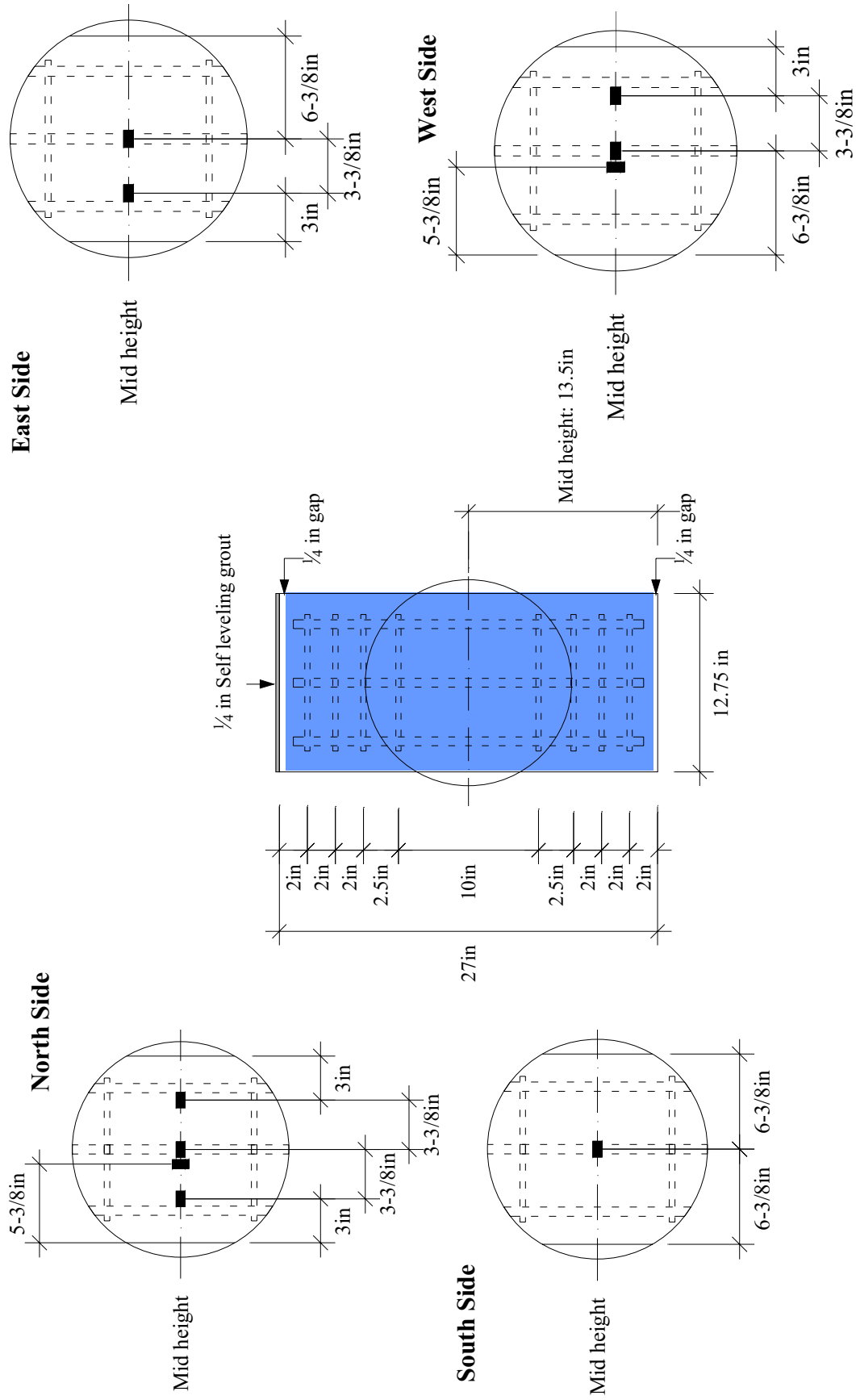
27in

**Figure B47 – Strain Gages Location on FRP; Specimens E2**

**East Side**

Mid height

6-3/8in

3-3/8in

3in

**West Side**

3in

3-3/8in

6-3/8in

5-3/8in

Mid height: 13.5in

Mid height

¼ in gap

7⅝in

3in

5¼in

3in

7⅝in

¼ in gap

12.75 in

¼ in Self leveling grout

2in
2in
2in
2.5in

10in

2.5in
2in
2in
2in

27in

**North Side**

5-3/8in

3in

3-3/8in

3-3/8in

3in

**South Side**

Mid height

6-3/8in

6-3/8in
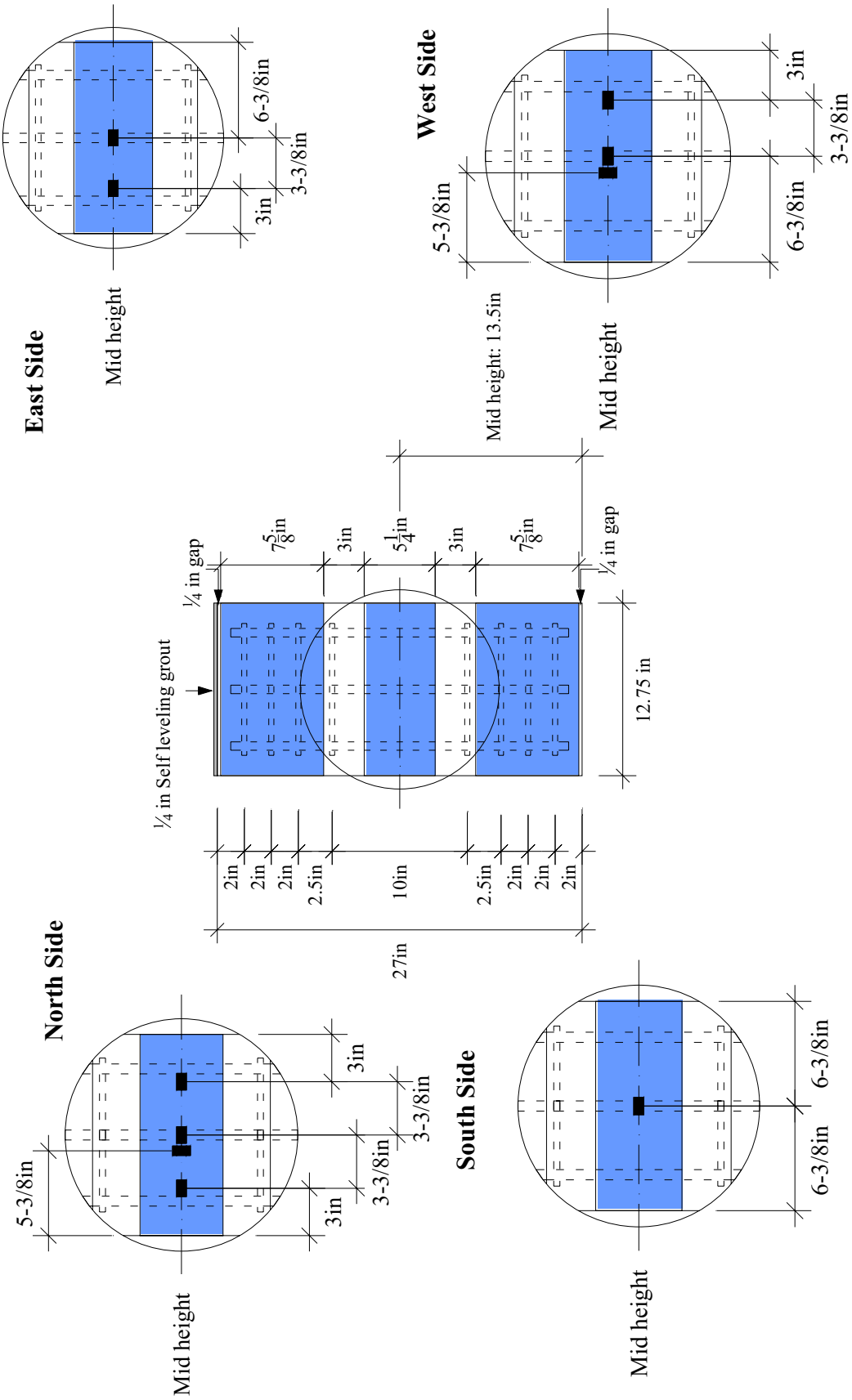
Mid height

**Figure B48 – Strain Gages Location on FRP; Specimens E3**

## COLUMN 12.75 x 12.75 x 54 in – SPECIMENS F1, F2 & F3

The layout of the instrumentation at mid height (27 in from the base) in these specimens is identical to the one in specimens from group E. Specimen F2 is continuously wrapped and F3 is partially wrapped. It is shown below the longitudinal cross section to illustrate the arrangement of the ties and the partial wrapping detail for specimen F3.



¼ in Self leveling grout

1in

2in
2in
2in

3 Ties #3 @ 2in

6in

10in

A — — — A

B — — — B

54 in    10in

C — — — C

10in

6in

2in

3 Ties #3 @ 2in

2in

2in    1in

Note:
For sections A-A, B-B, and C-C please see corresponding figures for specimens from group E.

12.75 in
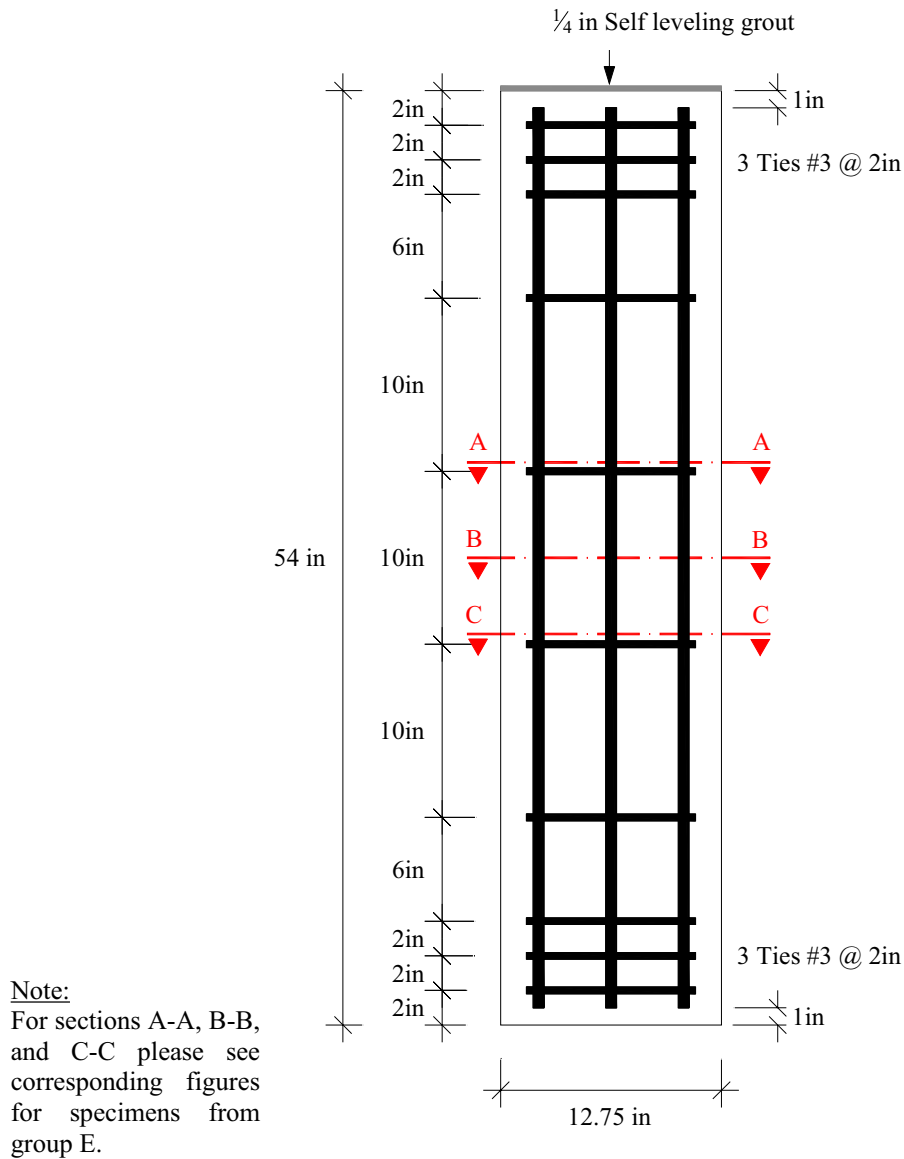
**Figure B49 – Longitudinal Cross Section; Specimens F1, F2 & F3**
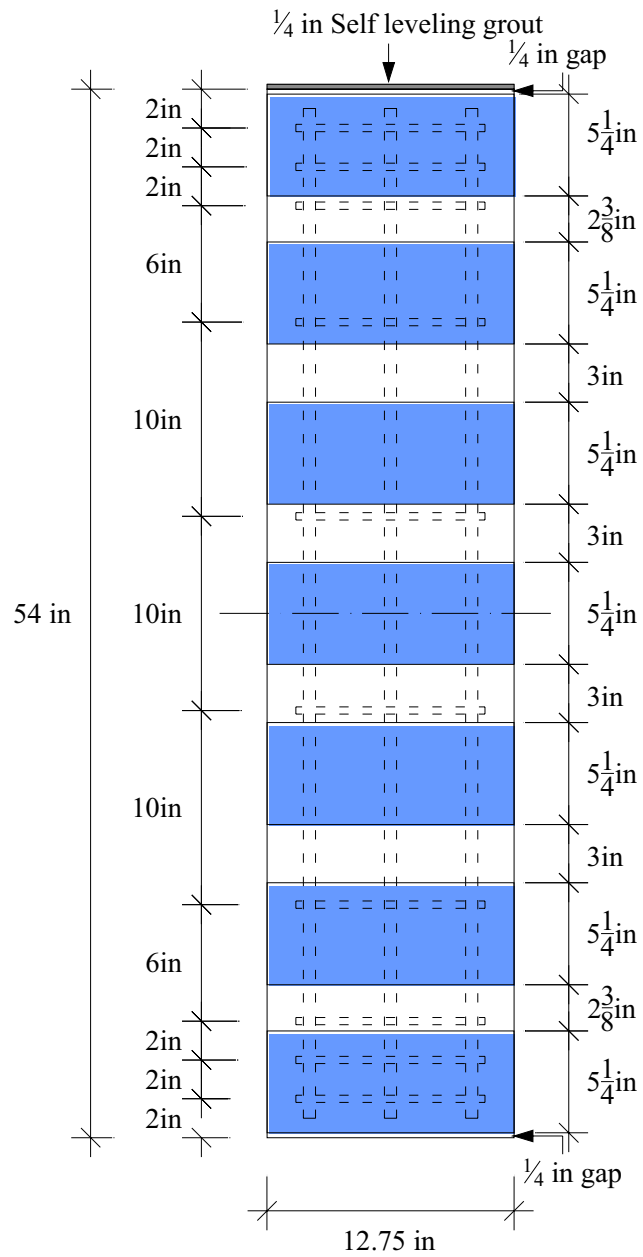
**Figure B50 – Longitudinal Cross Section; Wrapping Detail; Specimens F3**

**APPENDIX C**

**NATIONAL INSTITUTE OF STANDARDS AND TECHNOLOGY SPECIMENS
FABRICATION & INSTRUMENTATION**

**Table C1. Specimens Matrix; Total: 4**

| Specimen Cross-section Type and Dimension | Height (in) | Side Aspect Ratio (b/h) | Area Aspect Ratio (Area/Area $_{18x18}$) | Height Aspect Ratio (H/h) | Specimens Code & No. Plies | |
|---|---|---|---|---|---|---|
| $\rho_l = 1.50\%$ <br> 36 in <br> Area: 314 in$^2$  36 in | 78 (6.5 ft) | 1 | 4 | 2.2 | G1 | 0 |
| | | | | | G2 | 8 |
| $\rho_l = 1.52\%$ <br> 25 in <br> Area: 312 in$^2$  50 in | 108 (9 ft) | 2 | 4 | 2.2 | H1 | 0 |
| | | | | | H2 | 19 |

Note: 1 in = 2.54 cm; 1 ft = 0.3 m; 1 in$^2$ = 6.45 cm$^2$

**Table C2. Distribution and Number of Strain Gages**

| Specimen | | Steel | | Subtotal | FRP | | Subtotal | Total |
|---|---|---|---|---|---|---|---|---|
| | | Rebars | Ties | | Horizontal | Vertical | | |
| Square | G1 | 12 | 12 | 24 | N/A | N/A | N/A | 24 |
| | G2 | 12 | 12 | 24 | 24 | 4 | 28 | 52 |
| Rectangular | H1 | 12 | 12 | 24 | N/A | N/A | N/A | 24 |
| | H2 | 12 | 12 | 24 | 24 | 4 | 28 | 52 |
| | | | | | | | Total | 152 |

Notes:
1. One specimen for each group is the bench mark. For a second specimen in each group, the FRP will vary in order to attain a 30 percent increase in nominal capacity. In this case the FRP will be continuously wrapped (CW) over the entire column surface leaving a ¼ in (6 mm) gap in between the top (or bottom) end and the border of the FRP sheet.
2. The total area of transverse steel (ties only) is as per code requirements.
   Steel yield strength: $f_y$ = 60 ksi (400 MPa)
   Steel reinforcement ratio for each group of specimens is detailed in Table C1
3. Design concrete compressive strength: $f'_c$ = 4000 psi (28 MPa)
4. Figures showing the location of the strain gages on the steel reinforcement as well as on the FRP material are presented for each specimen. This instrumentation is placed at three locations in the central part of the specimens (mid height and at the level of the center ties)
5. In all the figures showing the location of strain gages on the steel and FRP, the position indicated is regarding their centers. The strain gages are not to scale with respect to the dimensions shown in the figures.

**SQUARE COLUMN 36 x 36 x 78 in – SPECIMENS G1 & G2**
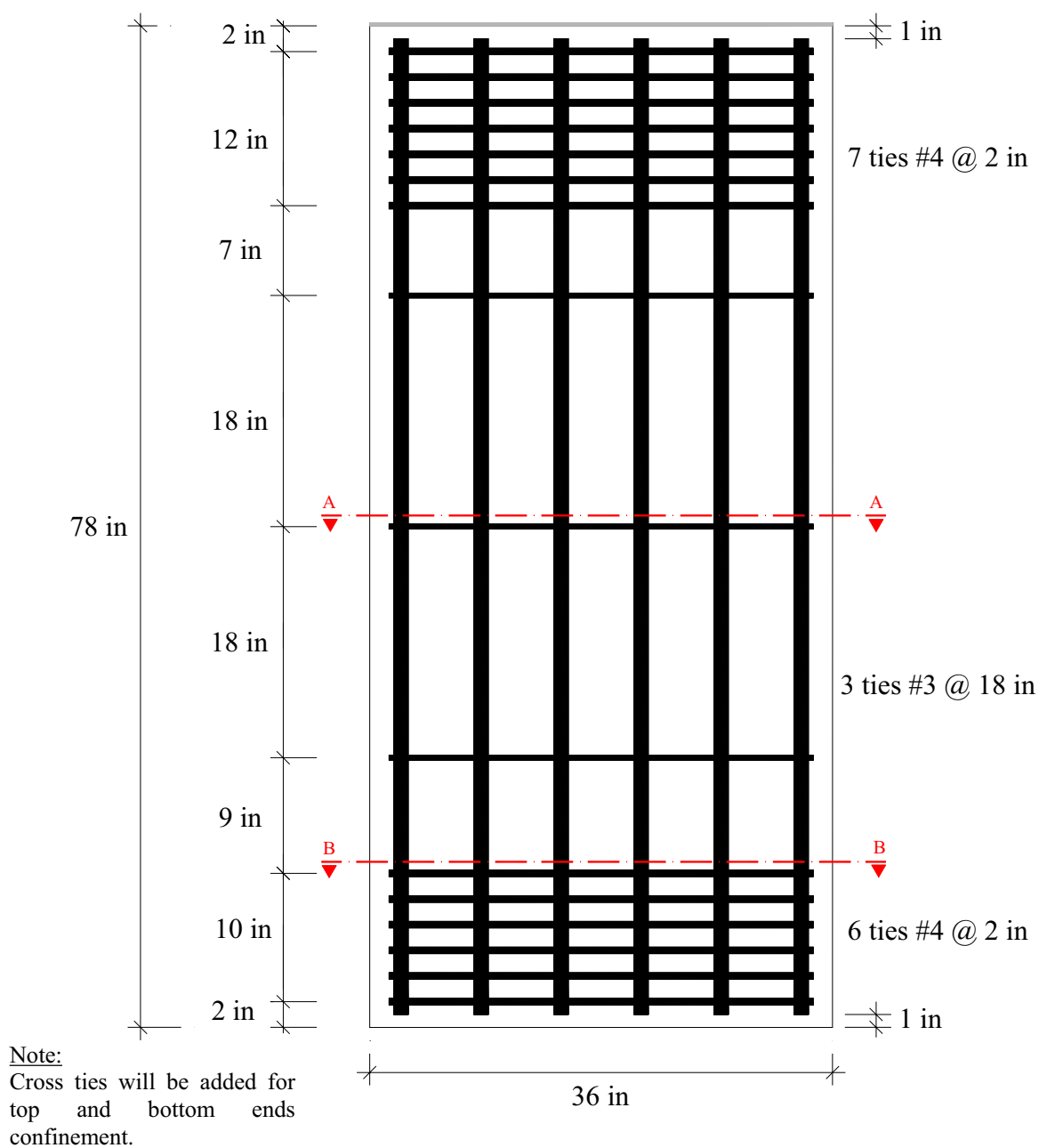


**Figure C1. Longitudinal Cross Section; Specimens G1 & G2**

36 in

Clear Cover
1.5 in

20#9 bars

Ties #3@18 in

Cross ties (A) #3

36 in

Rounded Corner
r = 1.2 in
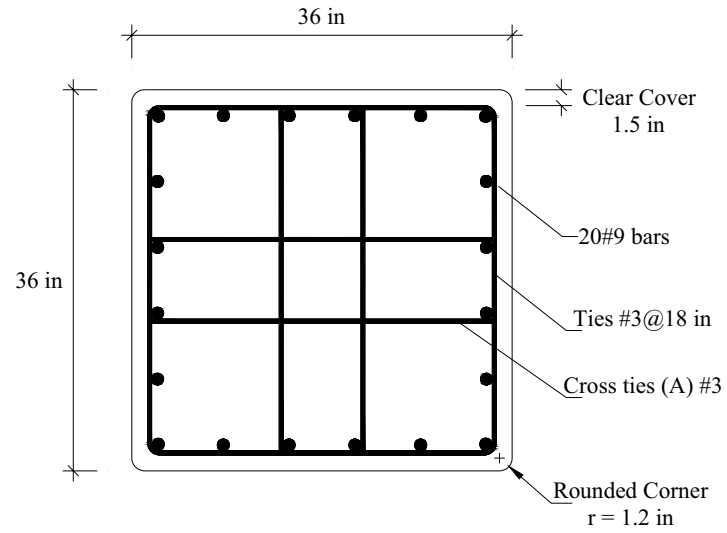
**Figure C2. Section A-A; Specimens G1 & G2**

4 in

4 in

D =1.5 in

33 in

33 in
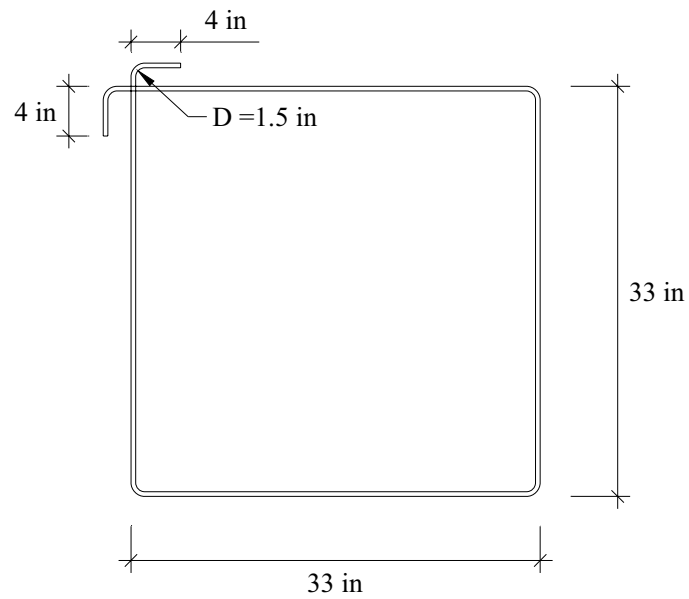
**Figure C3. Section A-A; Tie #3 Detail; Specimens G1 &G2**
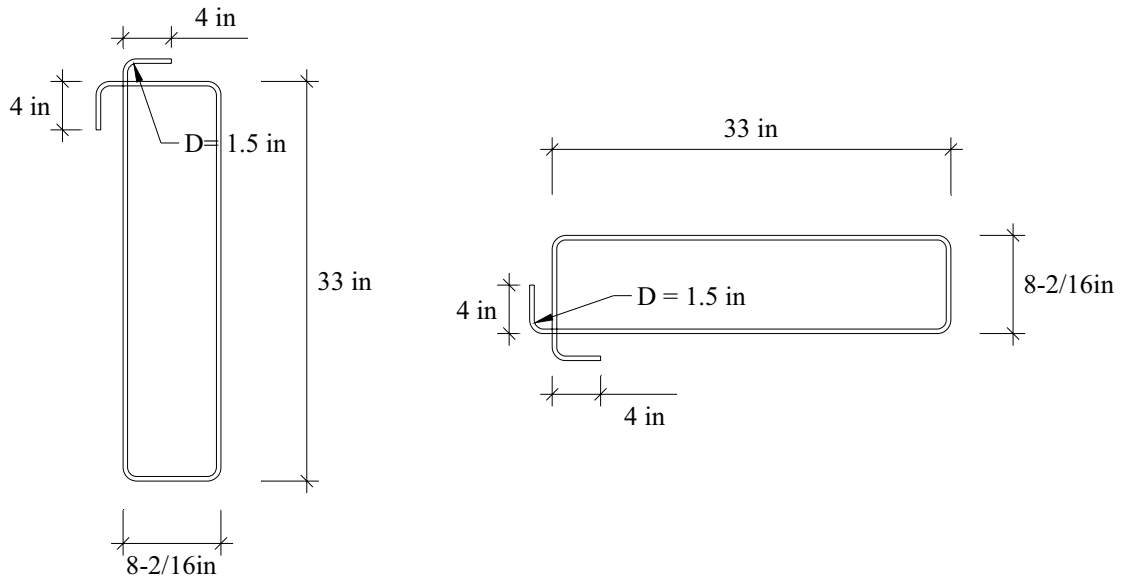
**Figure C4. Section A-A; Cross Ties (A) #3 Details; Specimens G1 & G2**
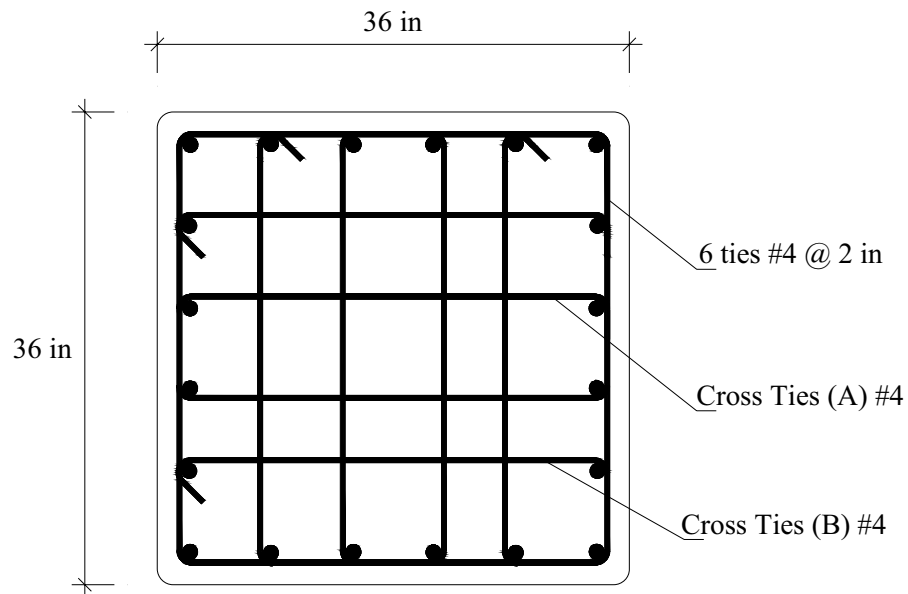


**Figure C5. Section B-B; Cross Ties #4 (Top and Bottom Ends); Specimens G1 & G2**

4.5 in

4.5 in

D =2 in

33 in

33 in
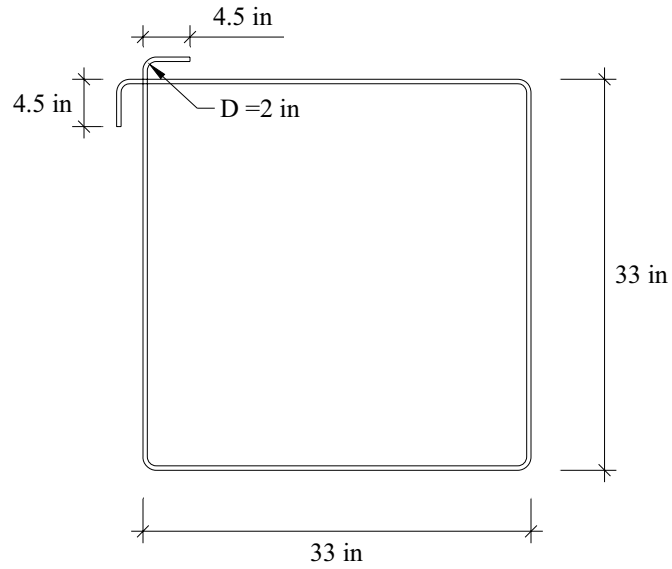
**Figure C6. Section B-B; Tie #4 Detail; (Top and Bottom Ends); Specimens G1 &G2**

4.5 in

4.5 in

D= 2 in

33 in

8-2/16in

33 in

4.5 in

D = 2 in

8-2/16in

4.5 in
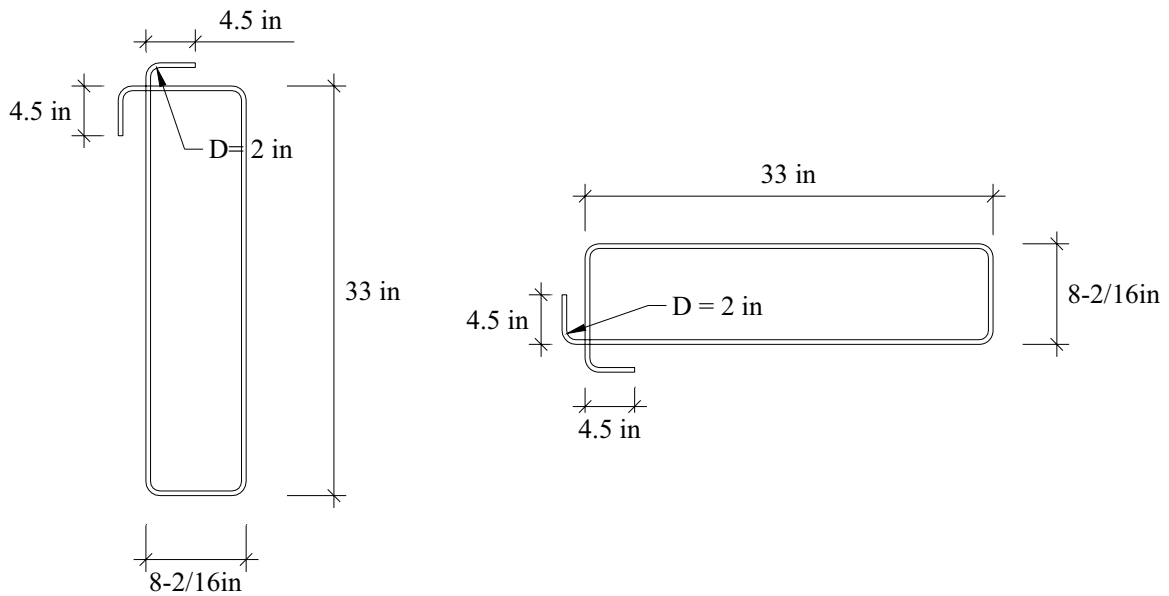
**Figure C7. Section B-B; Cross Ties (A) #4 Details; Specimens G1 & G2**
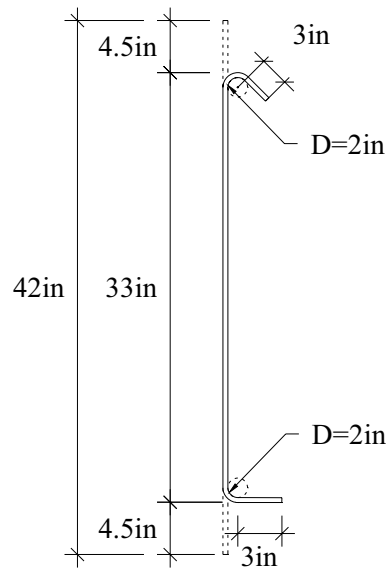
**Figure C8. Section B-B; Cross Tie (B) #4 Detail; Specimens G1 & G2**
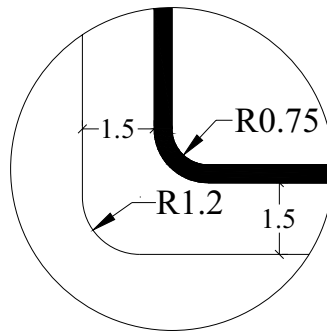


**Figure C9. Chamfer Detail for the Corners of all the Specimens**
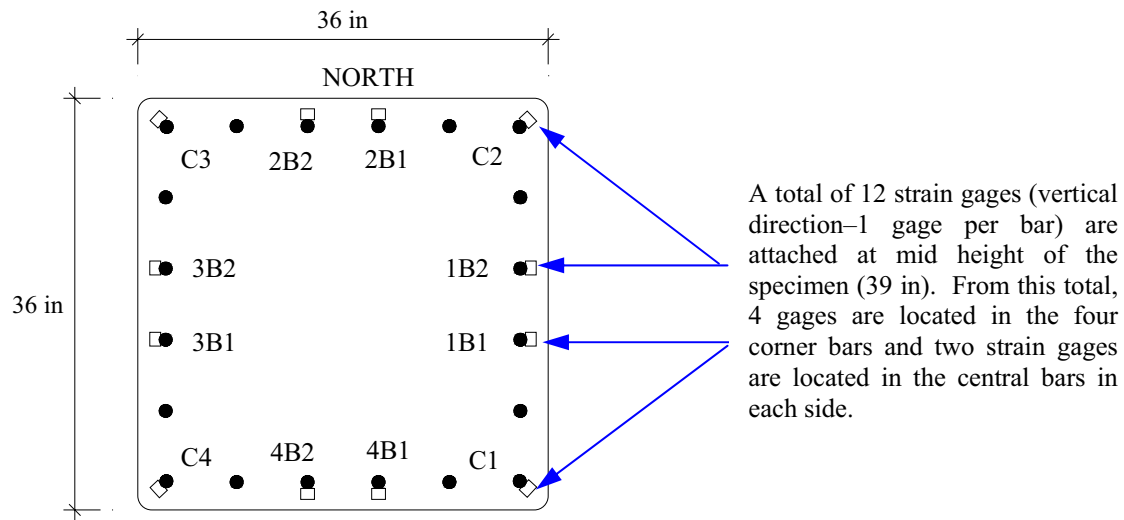
**Figure C10. Section B-B; Strain Gages Location on Longitudinal Steel; Specimens G1 & G2**

A total of 12 strain gages (vertical direction–1 gage per bar) are attached at mid height of the specimen (39 in). From this total, 4 gages are located in the four corner bars and two strain gages are located in the central bars in each side.
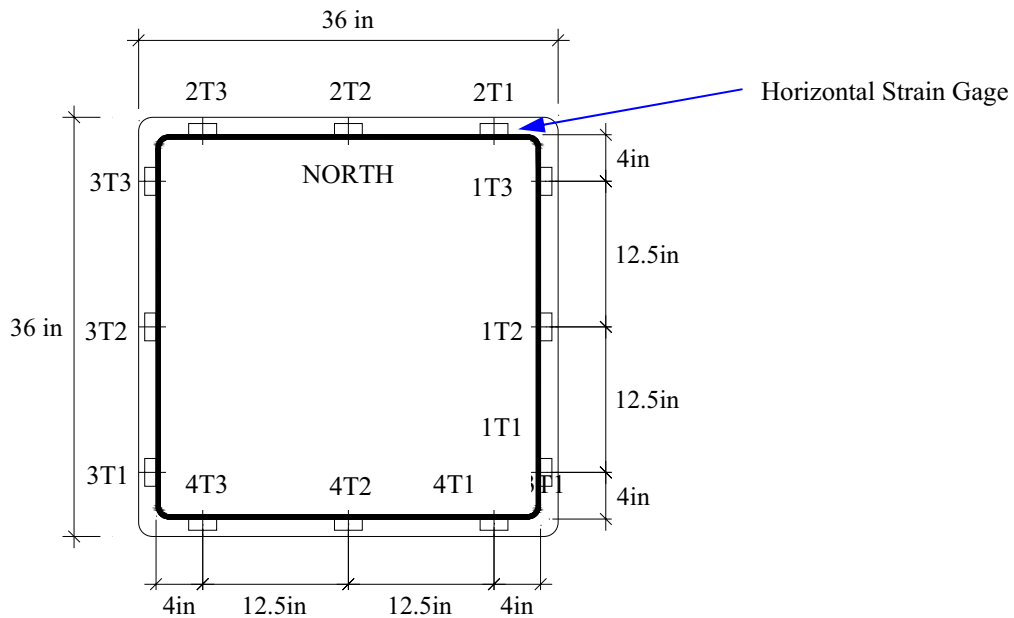


**Figure C11.  Section C-C; Strain Gages Location on Tie; Specimens G1 & G2**
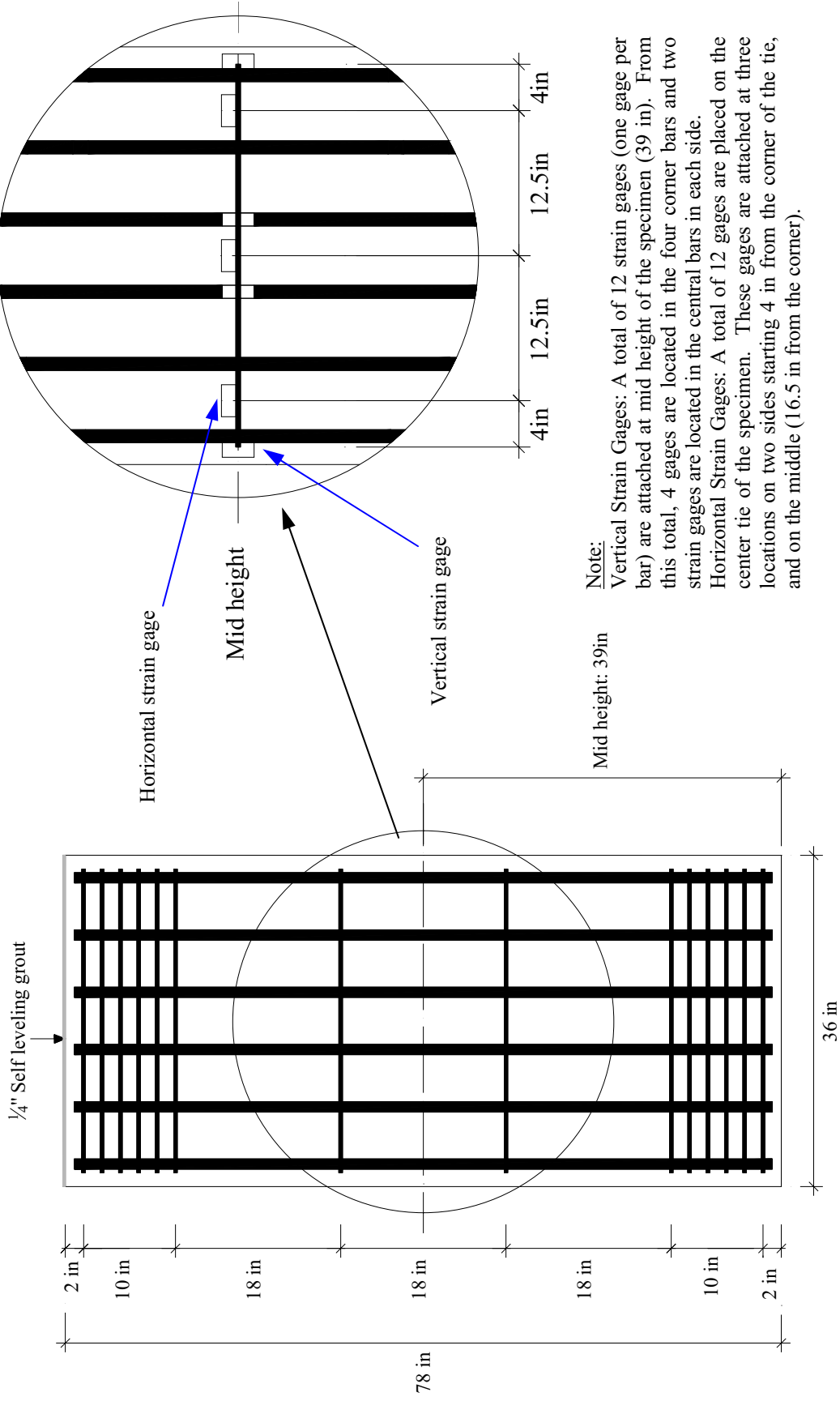
½" Self leveling grout

2 in
10 in
18 in
18 in
18 in
10 in
2 in

78 in

36 in

Mid height: 39in

Horizontal strain gage

Mid height

Vertical strain gage

4in
12.5in
12.5in
4in

Note:

Vertical Strain Gages: A total of 12 strain gages (one gage per bar) are attached at mid height of the specimen (39 in). From this total, 4 gages are located in the four corner bars and two strain gages are located in the central bars in each side.

Horizontal Strain Gages: A total of 12 gages are placed on the center tie of the specimen. These gages are attached at three locations on two sides starting 4 in from the corner of the tie, and on the middle (16.5 in from the corner).

**Figure C12. Strain Gages Location on Steel; Specimens G1 & G2**
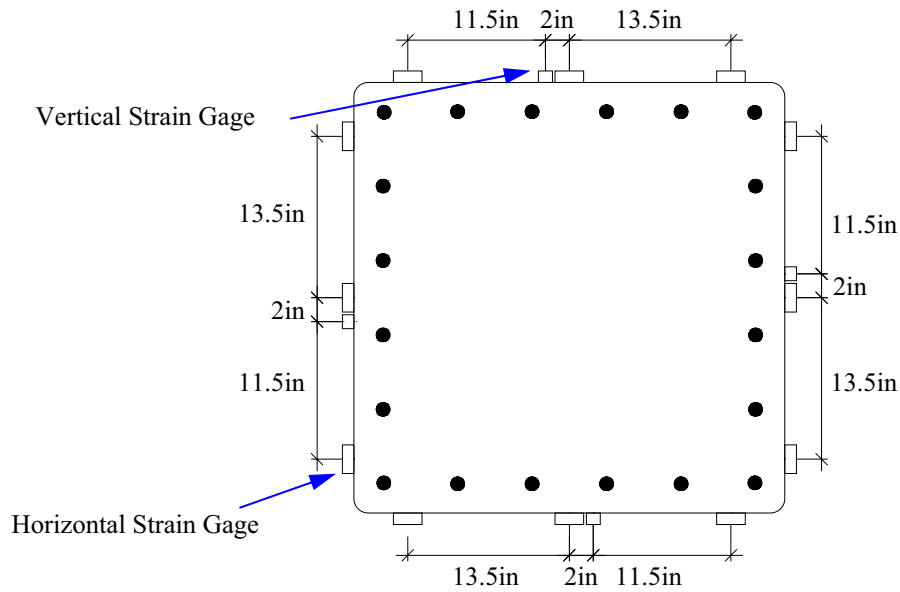
11.5in　2in　13.5in

Vertical Strain Gage

13.5in

2in

11.5in

Horizontal Strain Gage

11.5in

2in

13.5in

13.5in　2in　11.5in

Note:

Horizontal strain gages: They are attached to the specimen at two locations: at mid height (39 in), and a distance of 48 in from the bottom. A total of 12 gages are placed along the perimeter of the column per level. They are distributed at three locations per side starting at 4.5 in from the corner of the column.

Vertical strain gages: A total of 4 gages are placed on the column, one gage per side, and they are attached at 2 in o.c. from the central gage. This instrumentation is only applied at the mid-height of the specimen (39 in).



4F3-M　4FV　4F2-M　4F1-M

3F1-M　　　　NORTH　　　　1F1-M

3FV

3F2-M

1FV

1F2-M

3F3-M

1F3-M

2F3-M　2FV　2F2-M　2F1-M
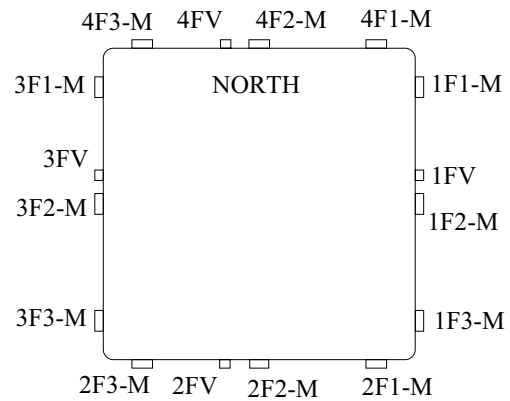
**Figure C13. Section B-B; Strain Gages Location on FRP; Specimen G2**

1F1

1F1-M

9in

4.5in

13.5in

2in

13.5in

4.5in

1F2

1F3

Mid height

1F3-M

1F2-M

Note:
Horizontal strain gages: They are attached to the specimen at two locations: at mid height (39 in), and a distance of 48 in from the bottom. A total of 12 gages are placed along the perimeter of the column per level. They are distributed at three locations per side starting at 4.5 in from the corner of the column.

Vertical strain gages: A total of 4 gages are placed on the column, 1 gage per side, and they are attached at 2 in o.c. from the central gage. This instrumentation is only applied at the mid-height of the specimen (39 in).

¼" Self leveling grout

¼ in gap

¼ in gap

Mid height: 39in

36 in

2 in
10 in
18 in
18 in
18 in
10 in
2 in

78 in

**Figure C14. Strain Gages Location on FRP; Specimen G2**
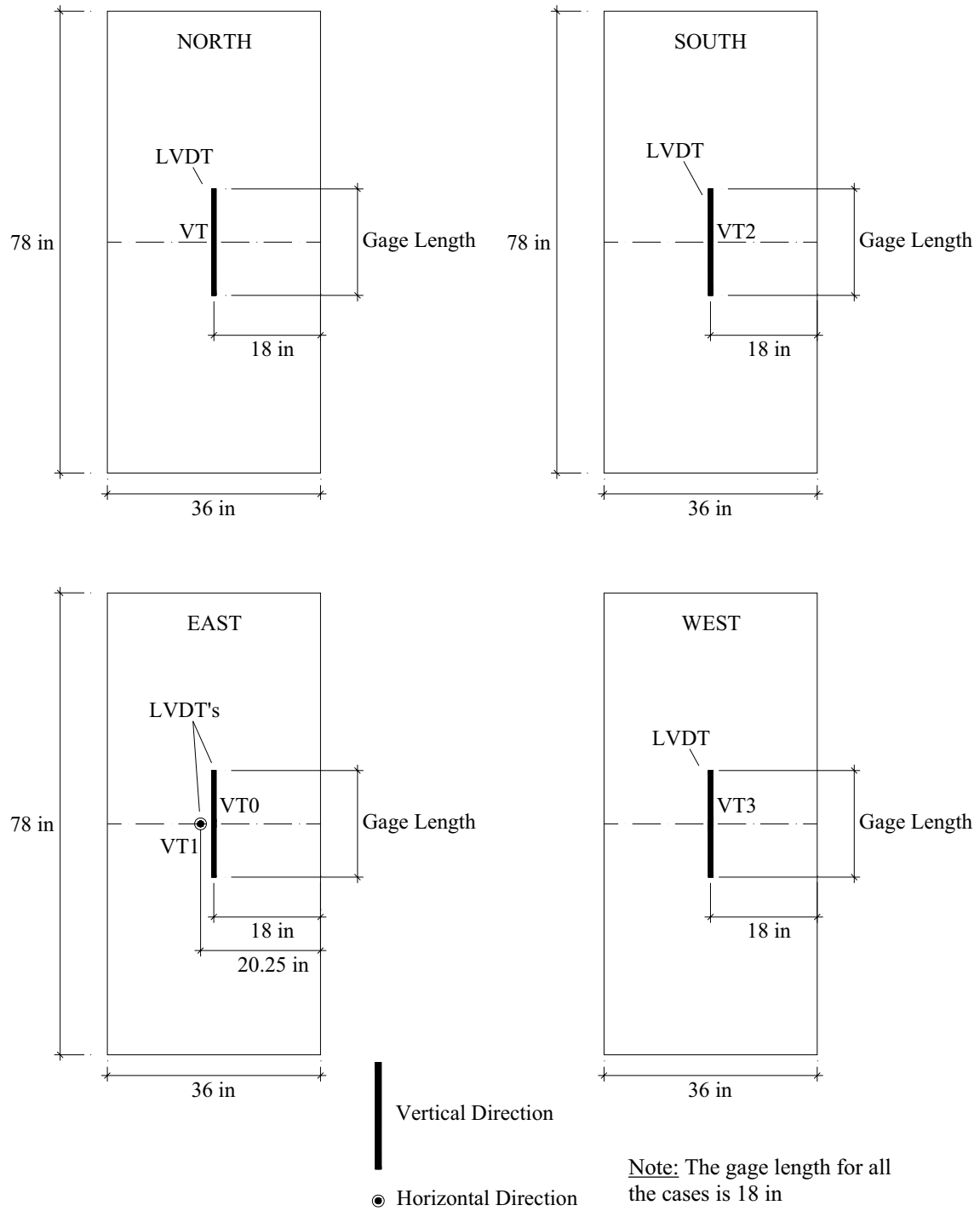
**Figure C15. Layout of Linear Transducers; Specimen G1**

**NORTH**

Gage Length

78 in

VT  VT3

18 in

20 in

41 in

50.5 in

36 in

**SOUTH**

VT1  VT2

Gage Length

50.75 in

40 in

18 in

20.5 in

36 in

**EAST**

Gage Length

78 in

VT0

18 in

50.5 in

36 in

**WEST**

36 in

Vertical Direction

⊙ Horizontal Direction

Note: The gage length for all the cases is 18 in
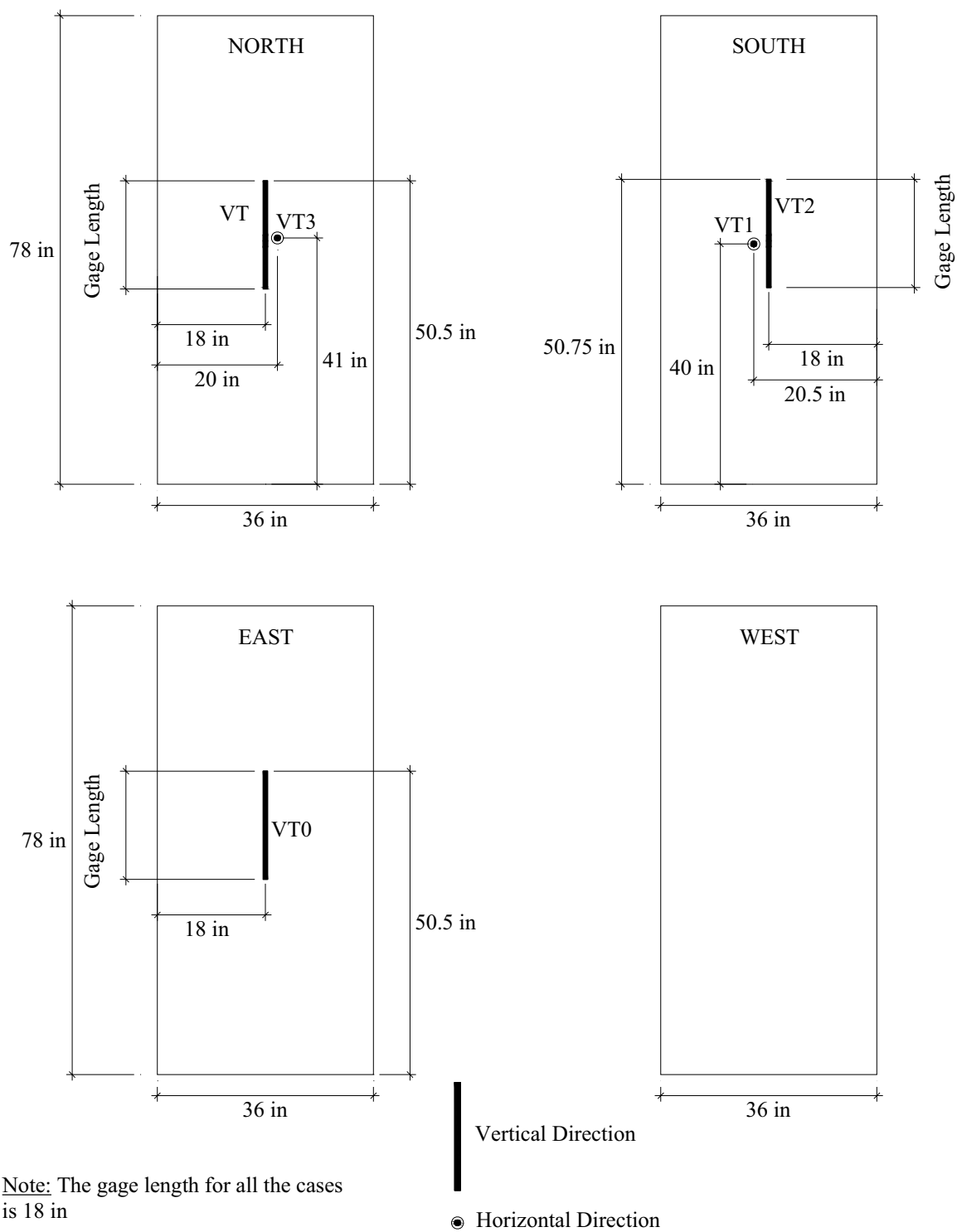
**Figure C16. Layout of Linear Transducers; Specimen G2**

**RECTANGULAR COLUMN 25 x 50 x 108 in – SPECIMENS H1 & H2**
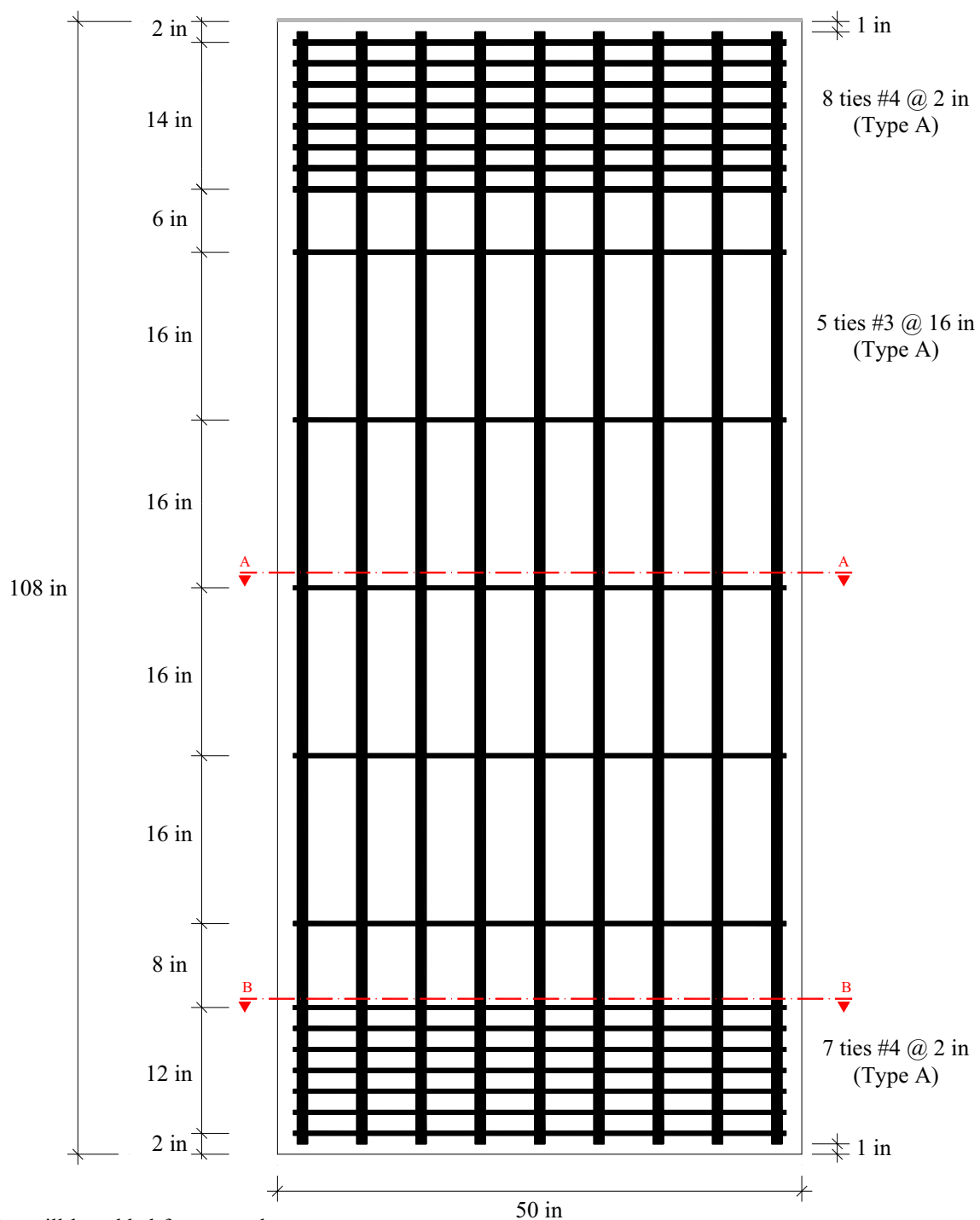


**Figure C17. Longitudinal Cross Section; Specimens H1 & H2**
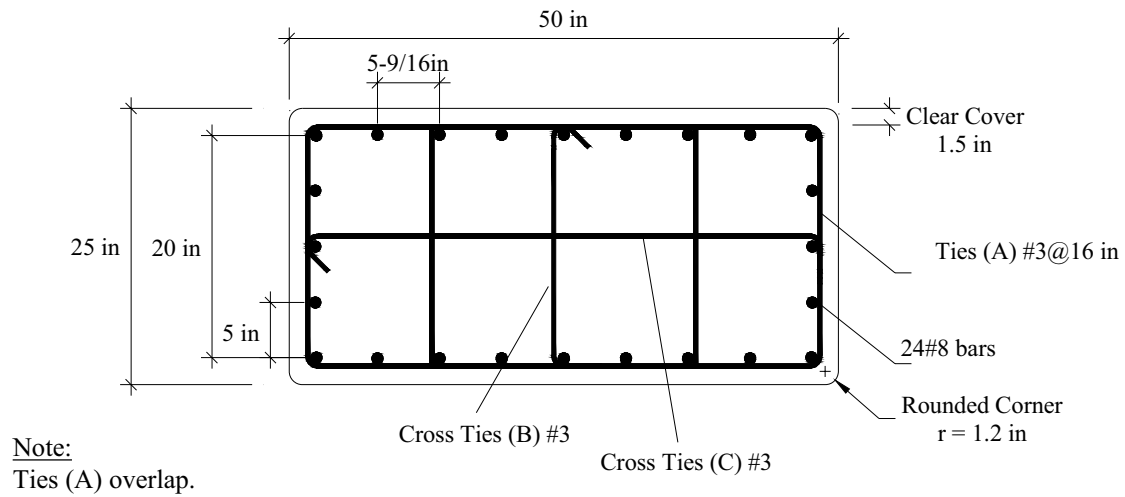
**Figure C18. Section A-A; Specimens H1 & H2**
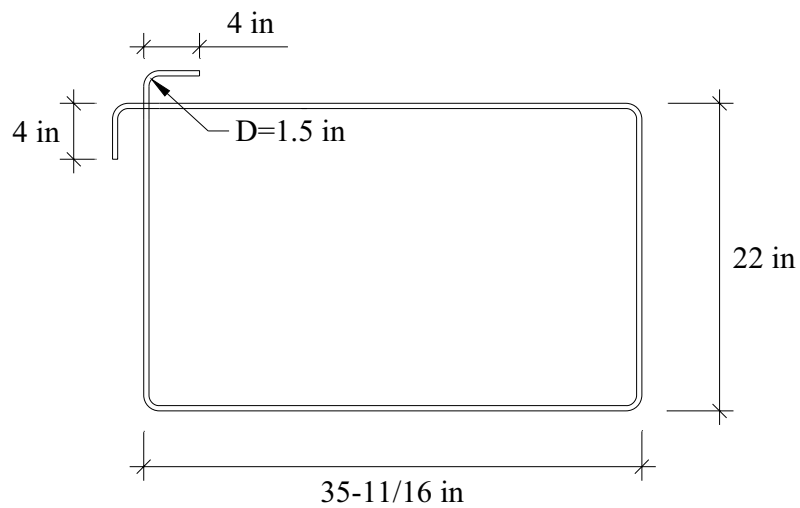


**Figure C19. Section A-A; Detail Overlapping Tie (A) #3; Specimens H1 & H2**
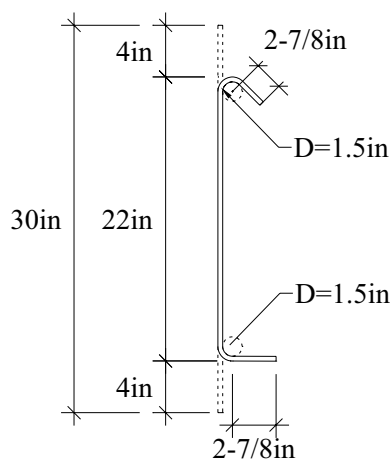
**Figure C20. Section A-A; Cross Tie (B) #3 - Side 25 in; Specimens H1 & H2**
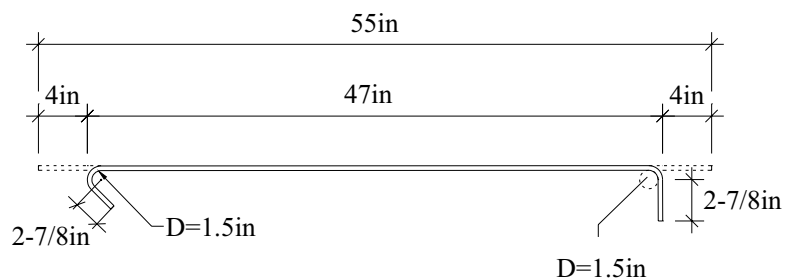
**Figure C21. Section A-A; Cross Tie (C) #3 - Side 50in; Specimens H1 & H2**
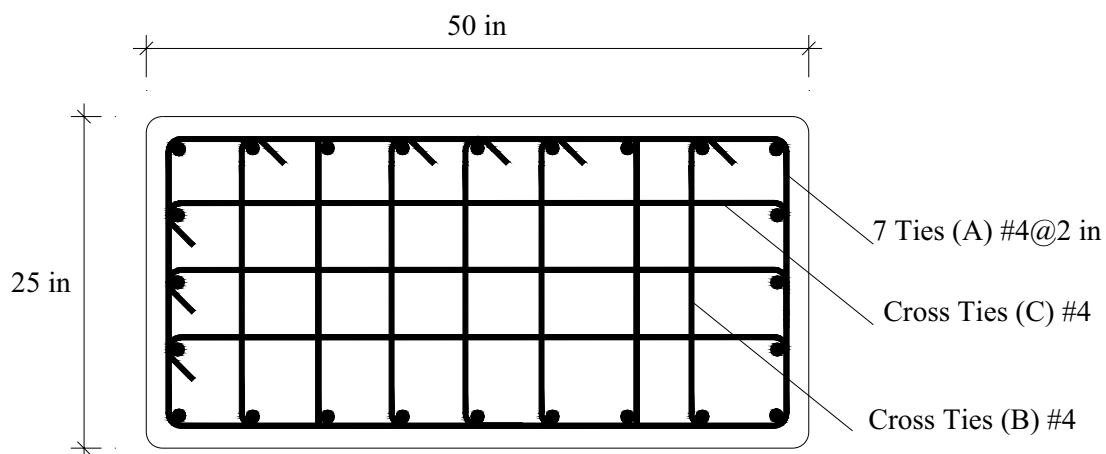
**Figure C22. Section B-B; Cross Ties #4 (Top and Bottom Ends); Specimens H1 & H2**
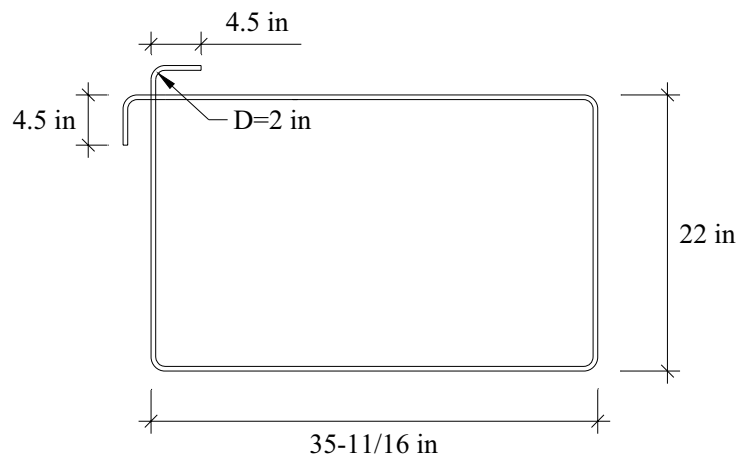
**Figure C23. Section B-B; Detail Overlapping Tie (A) #4; Specimens H1 & H2**
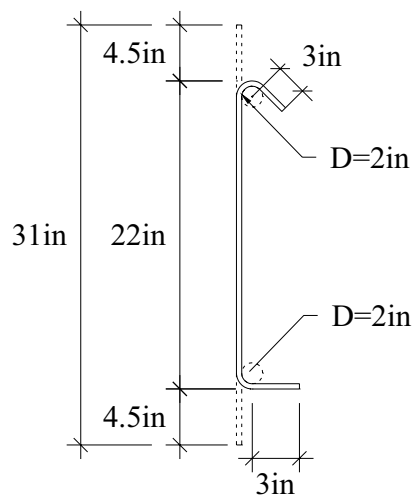


**Figure C24. Section B-B; Cross Tie (B) #4 - Side 25 in; Specimens H1 & H2**
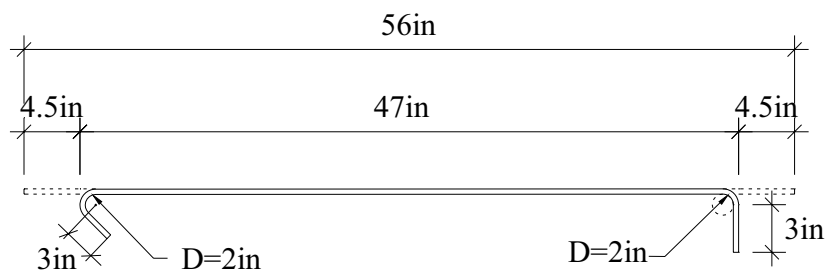


**Figure C25. Section B-B; Cross Tie (C) #4 - Side 50 in; Specimens H1 & H2**
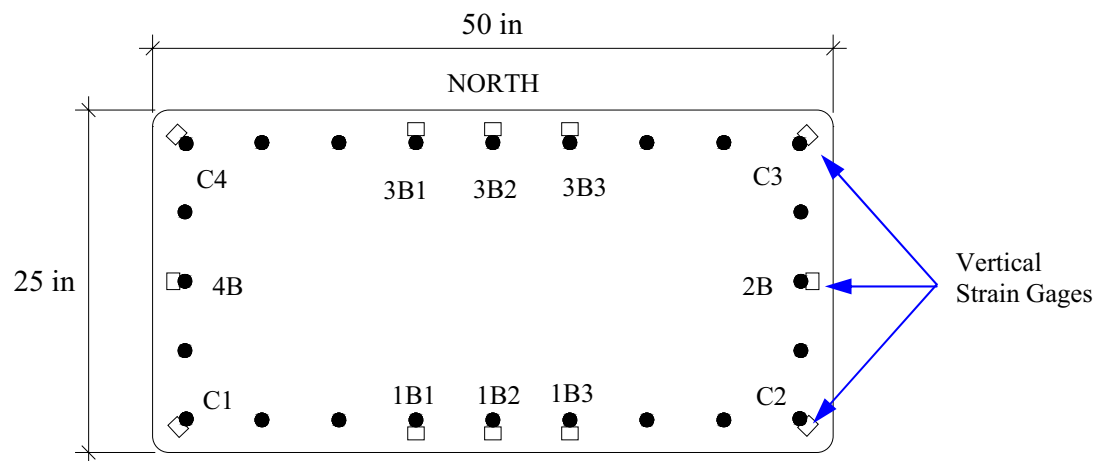
**Figure C26. Section A-A; Strain Gages Location on Longitudinal Steel; Specimens H1 & H2**
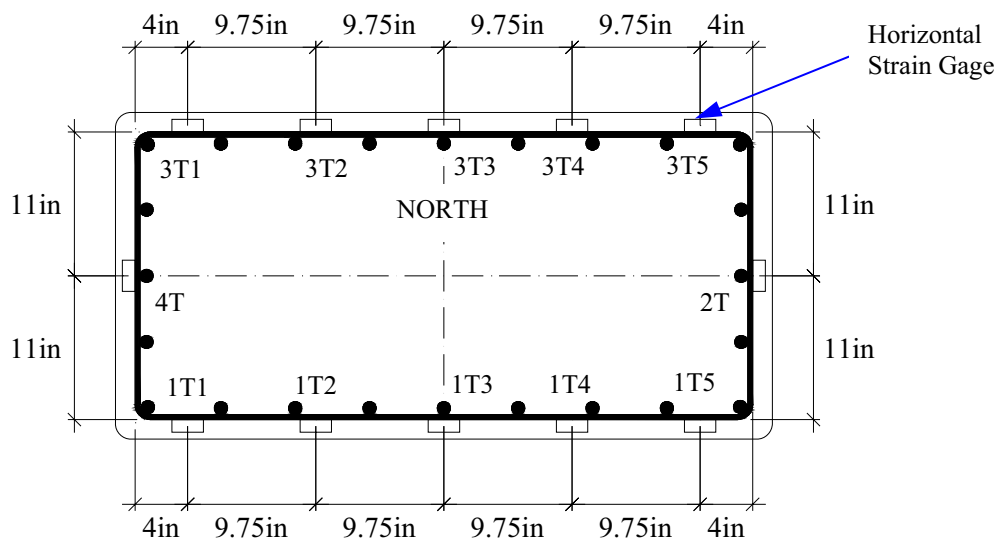


**Figure C27. Section A-A; Strain Gages on Tie; Specimens H1 & H2**

Horizontal Strain Gage

Vertical Strain Gage

11in

11in

Mid height

Note:
Vertical Strain Gages: A total of 12 strain gages (one gage per bar) are attached at mid height of the specimen (54 in). From this total, four gages are located in the four corner bars, three gages on the bars on the long side (central), and one strain gage is placed in each central bar on the short side.
Horizontal Strain Gages: A total of 12 strain gages are attached to the center tie. They are placed at one location per short side (middle), and at five locations per long side (starting 4 in from the corner).

Mid height: 54in

25in

2 in

14 in

6 in

16 in

16 in

16 in

16 in

8 in

12 in

2 in

108 in

**Figure C28. Strain Gages Location on Steel; Side 25 in; Specimens H1 & H2**
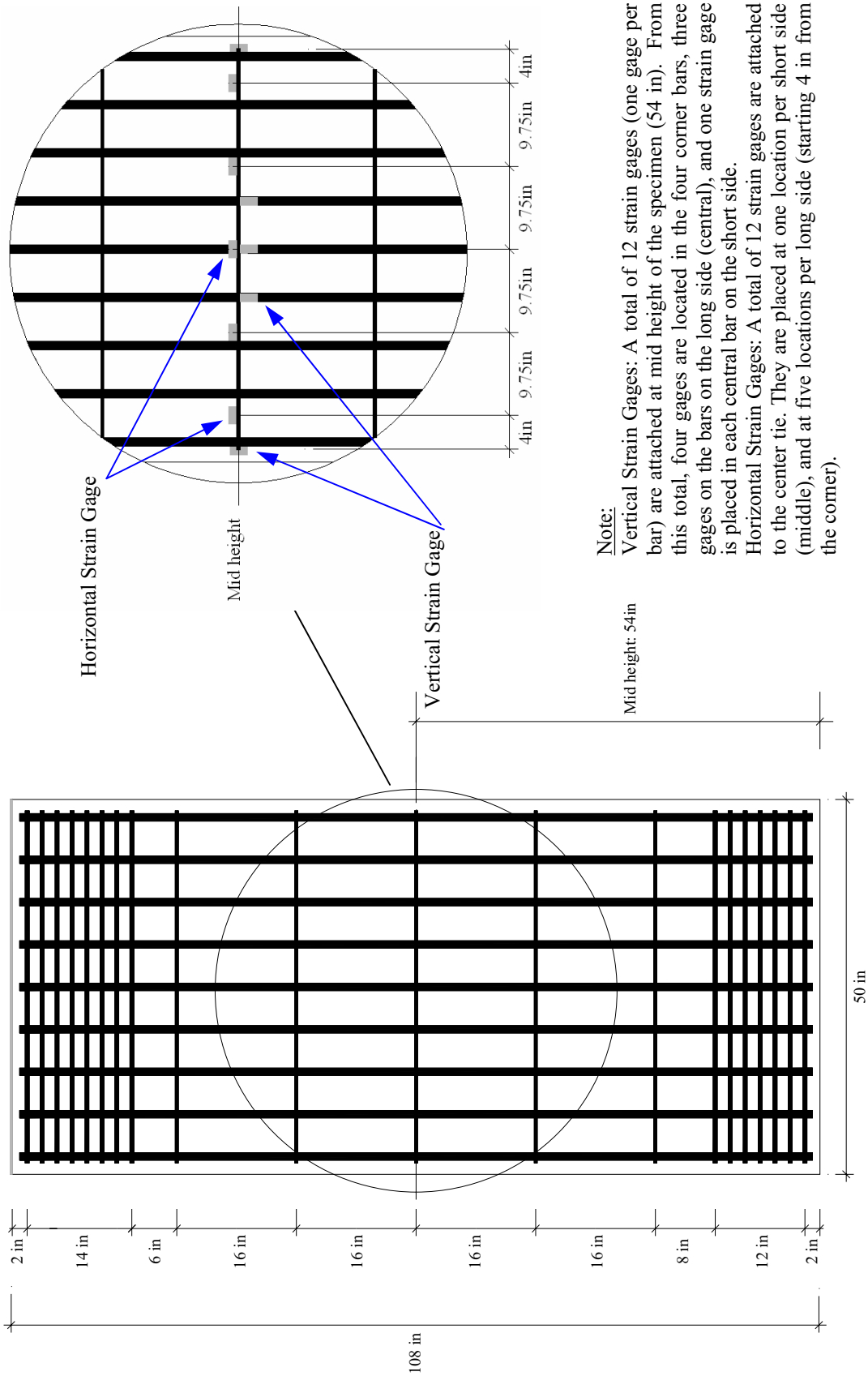
Horizontal Strain Gage

Mid height

Vertical Strain Gage

4in

9.75in

9.75in

9.75in

9.75in

4in

Mid height: 54in

Note:
Vertical Strain Gages: A total of 12 strain gages (one gage per bar) are attached at mid height of the specimen (54 in). From this total, four gages are located in the four corner bars, three gages on the bars on the long side (central), and one strain gage is placed in each central bar on the short side.

Horizontal Strain Gages: A total of 12 strain gages are attached to the center tie. They are placed at one location per short side (middle), and at five locations per long side (starting 4 in from the corner).

2 in

14 in

6 in

16 in

16 in

16 in

16 in

8 in

12 in

2 in

108 in

50 in

**Figure C29. Strain Gages Location on Steel; Side 50 in; Specimens H1 & H2**

Vertical Strain Gage

50 in

2in

$12\frac{1}{2}$in

$10\frac{1}{2}$in

25 in

2in

2in

$10\frac{1}{2}$in

$12\frac{1}{2}$in

Horizontal Strain Gage

$5\frac{1}{2}$in  $9\frac{3}{4}$in  $9\frac{3}{4}$in  2in  $7\frac{3}{4}$in  $9\frac{3}{4}$in  $5\frac{1}{2}$in

3F5-M   3F4-M   3FV  3F3-M   3F2-M   3F1-M

NORTH

4FV

2F-M

4F-M

2FV

1F5-M   1F4-M   1F3-M  1FV   1F2-M   1F1-M
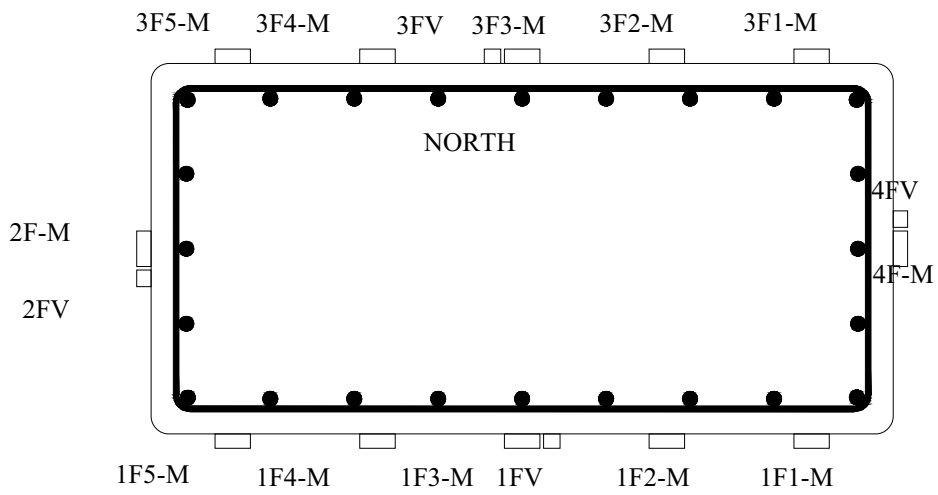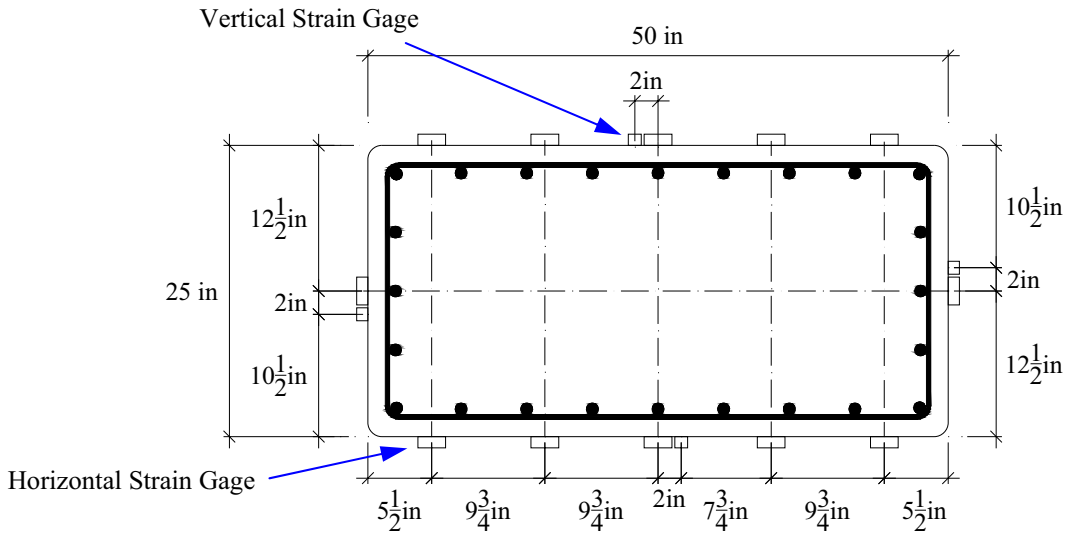
**Figure C30. Section A-A; Strain Gages Location on FRP; Specimen H2**
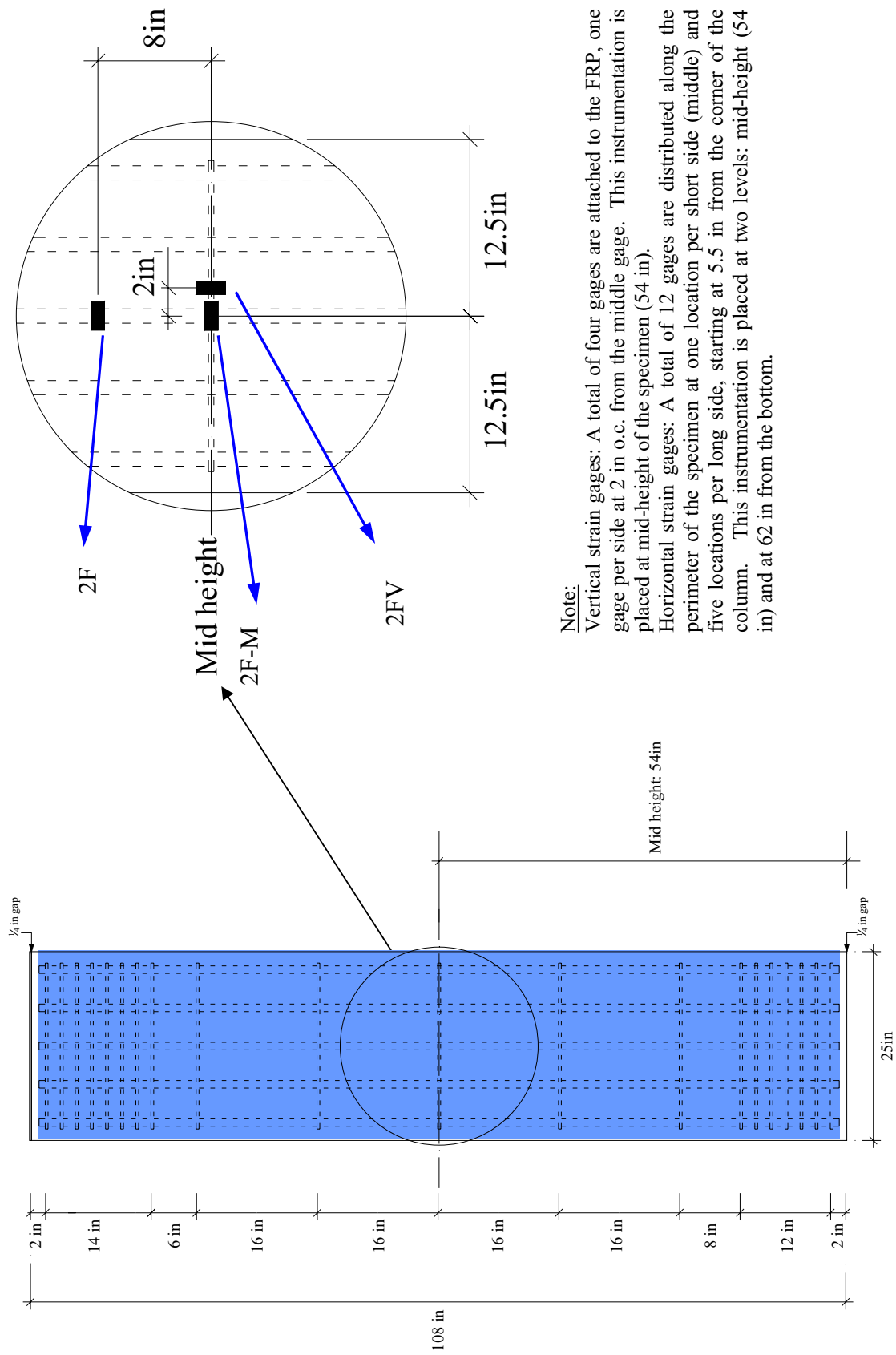
8in

2in

12.5in

12.5in

2F

Mid height

2F-M

2FV

Note:
Vertical strain gages: A total of four gages are attached to the FRP, one gage per side at 2 in o.c. from the middle gage. This instrumentation is placed at mid-height of the specimen (54 in).
Horizontal strain gages: A total of 12 gages are distributed along the perimeter of the specimen at one location per short side (middle) and five locations per long side, starting at 5.5 in from the corner of the column. This instrumentation is placed at two levels: mid-height (54 in) and at 62 in from the bottom.

Mid height: 54in

25in

¼ in gap

¼ in gap

2 in
14 in
6 in
16 in
16 in
16 in
16 in
8 in
12 in
2 in

108 in

**Figure C31. Strain Gages Location on FRP; Side 25 in; Specimen H2**

**Note:**

Vertical strain gages: A total of four gages are attached to the FRP, one gage per side at 2 in o.c. from the middle gage. This instrumentation is placed at mi-height of the specimen (54 in). Horizontal strain gages: A total of 12 gages are distributed along the perimeter of the specimen at one location per short side (middle) and five locations per long side, starting at 5.5 in from the corner of the column. This instrumentation is placed at two levels: mid-height (54 in) and at 62 in from the bottom.

**Figure C32. Strain Gages on FRP; Side 50 in; Specimen H2**
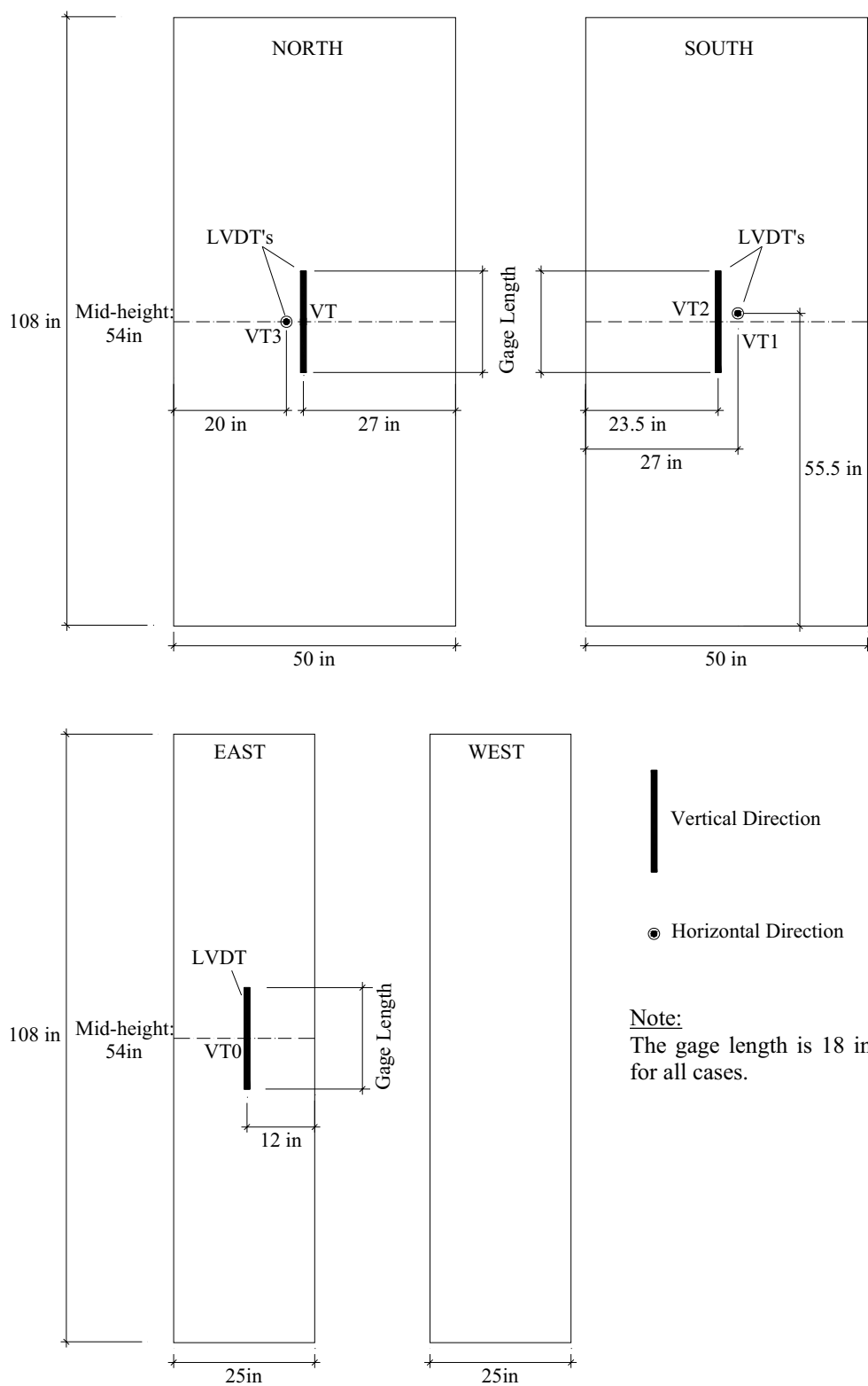
**Figure C33. Layout of Linear Transducers; Specimen H1**
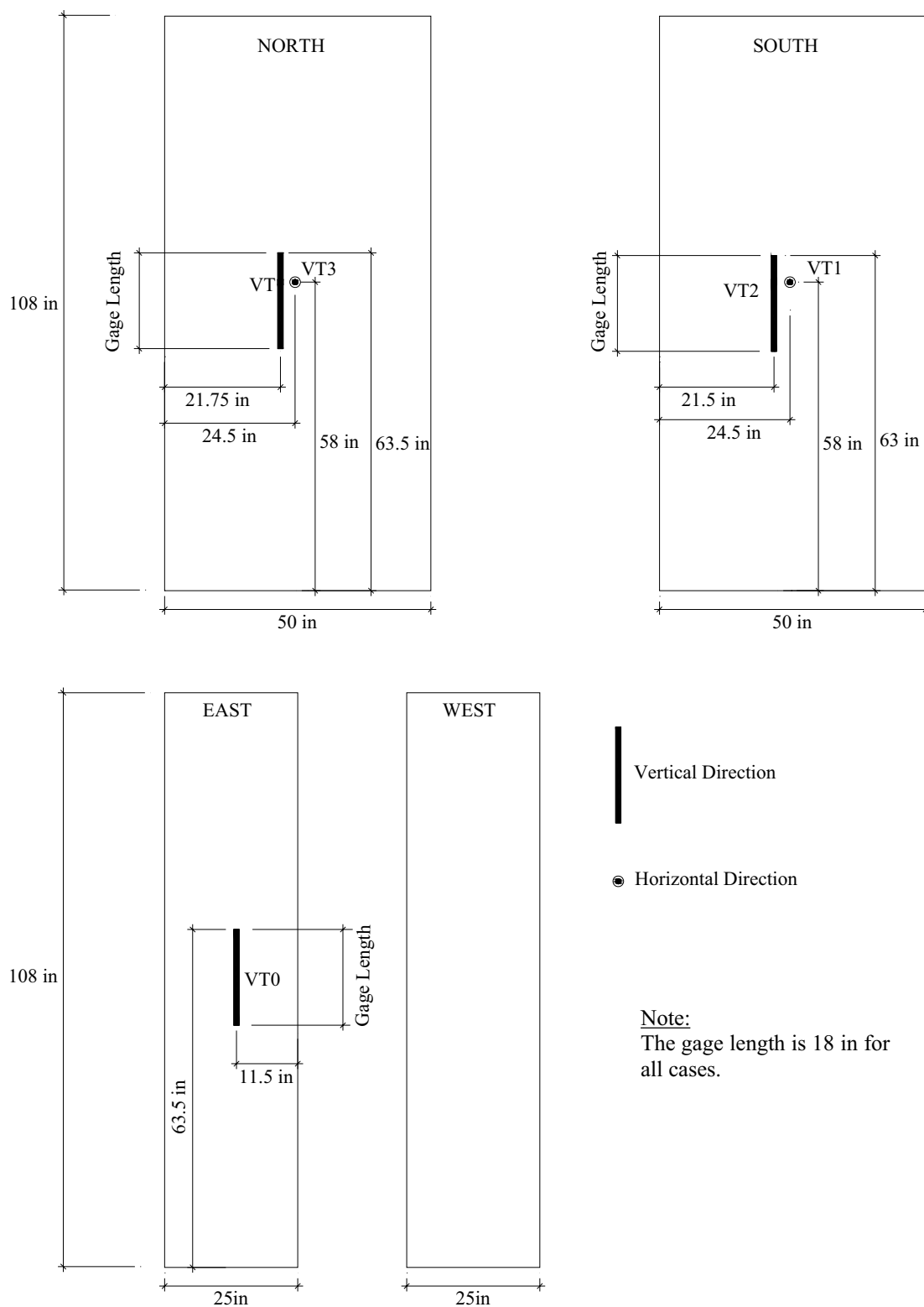
**Figure C34. Layout of Linear Transducers; Specimen H2**
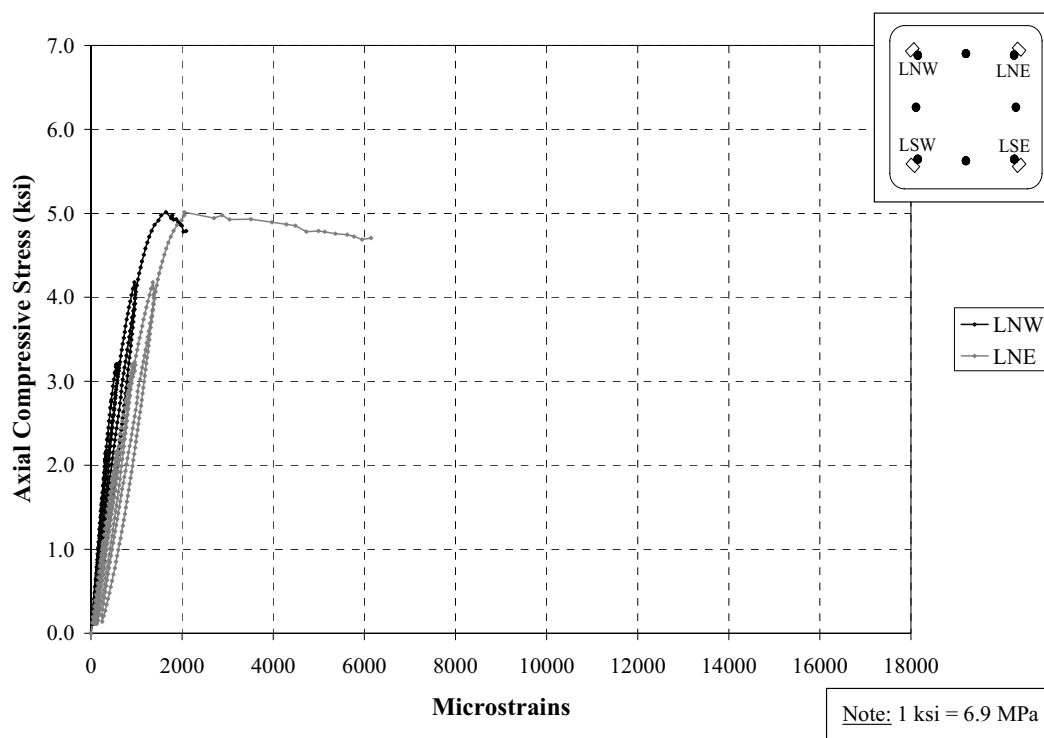
# APPENDIX D

# RAW DATA
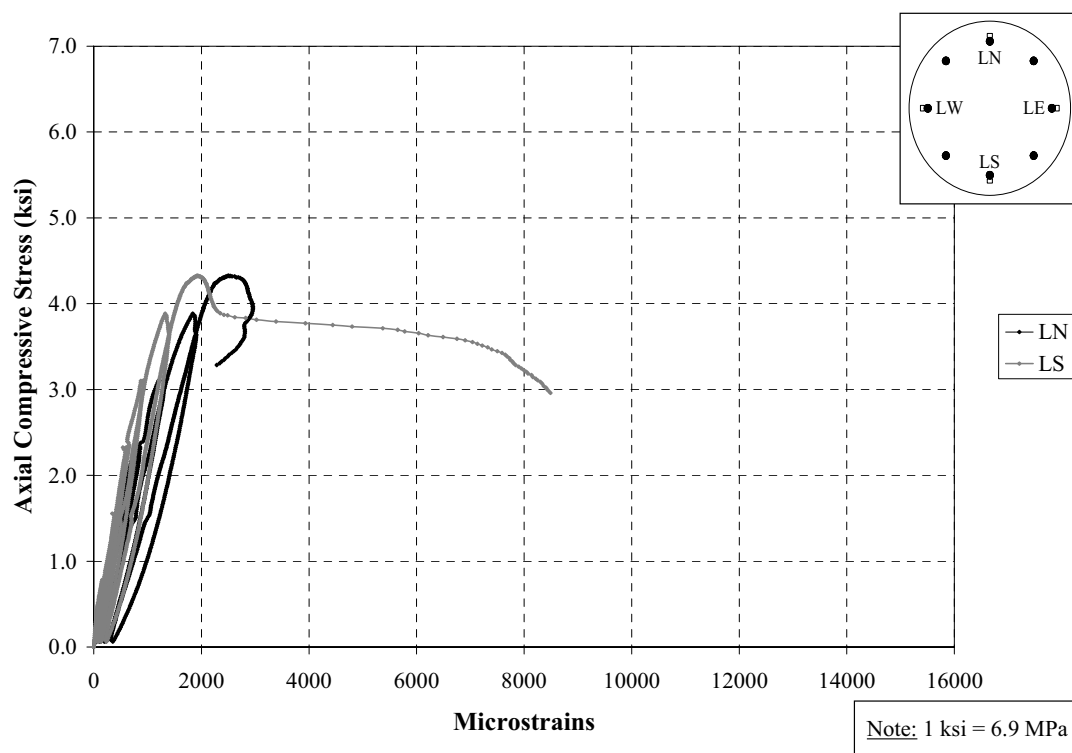
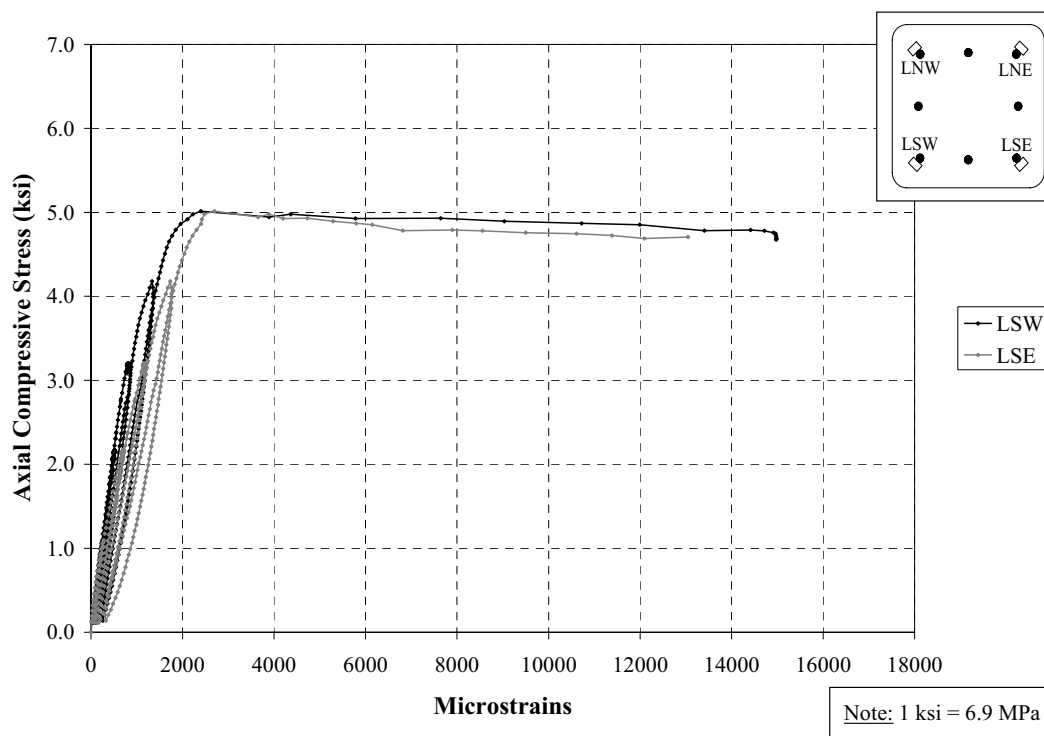**Figure D1.  Axial Stress vs. Axial Strain on Longitudinal Bars (LN & LS); Specimen A1**
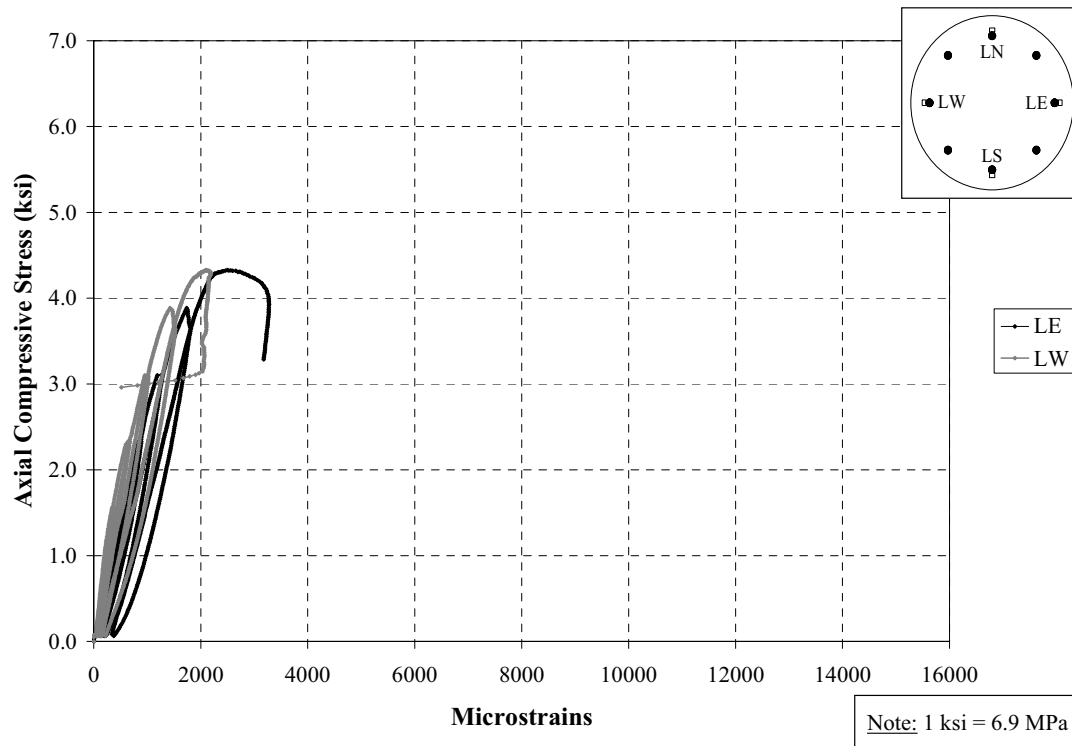


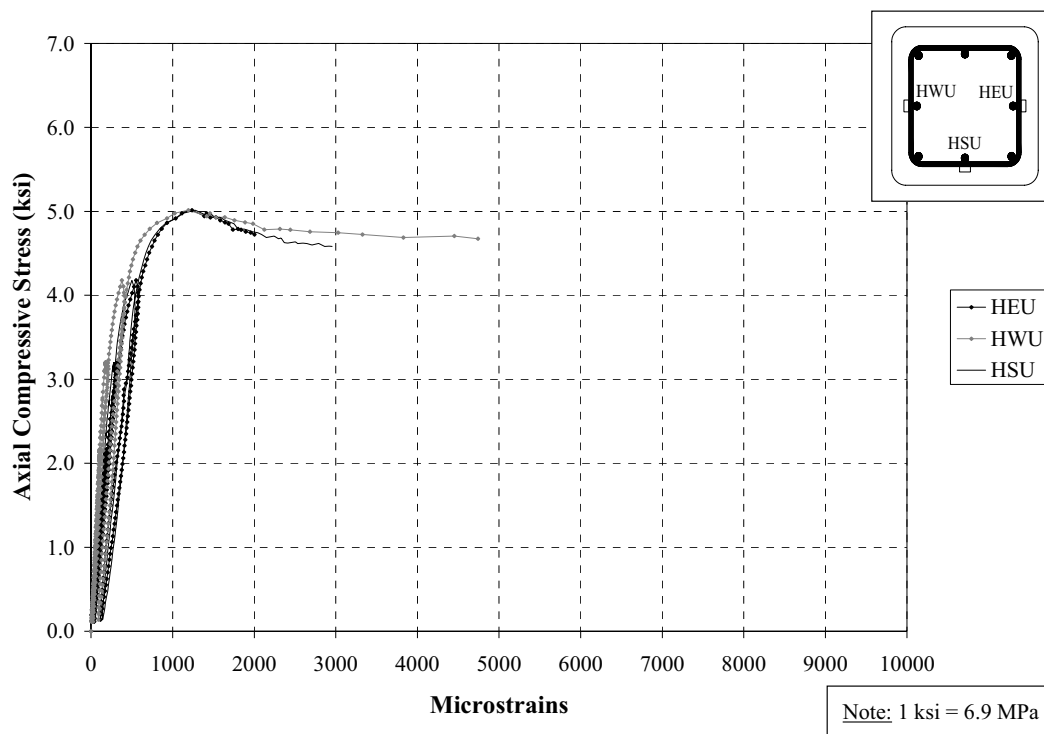**Figure D2.  Axial Stress vs. Axial Strain on Longitudinal Bars (LE & LW); Specimen A1**
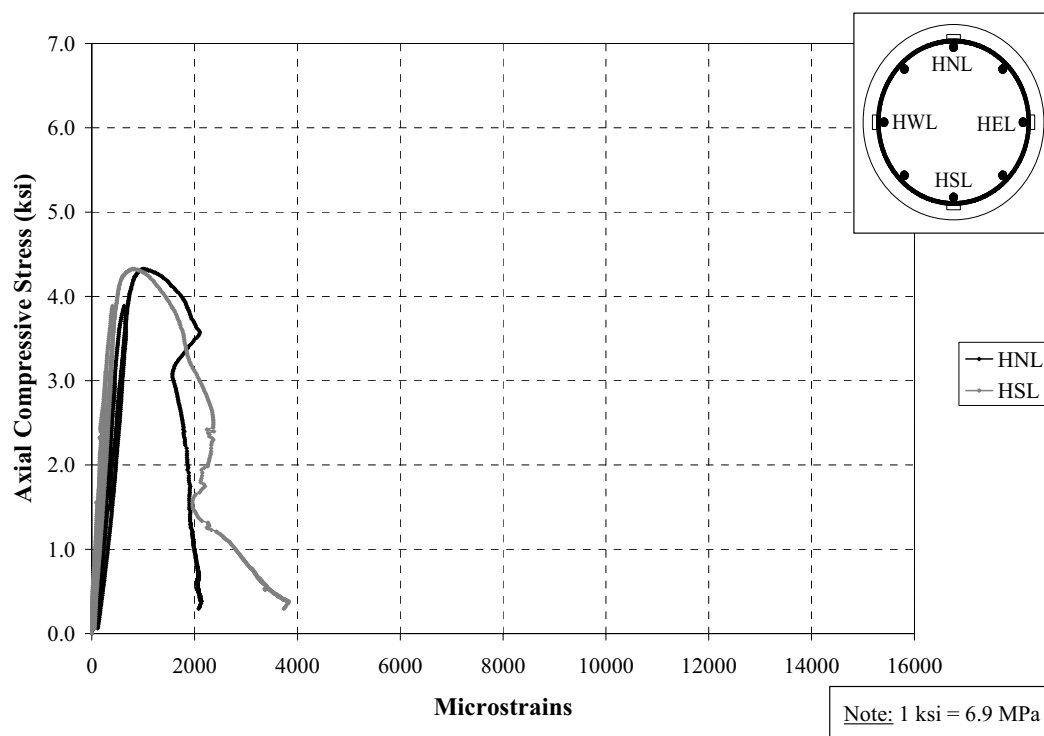
**Figure D3. Axial Stress vs. Transverse Strain on Lower Tie (HNL & HSL); Specimen A1**
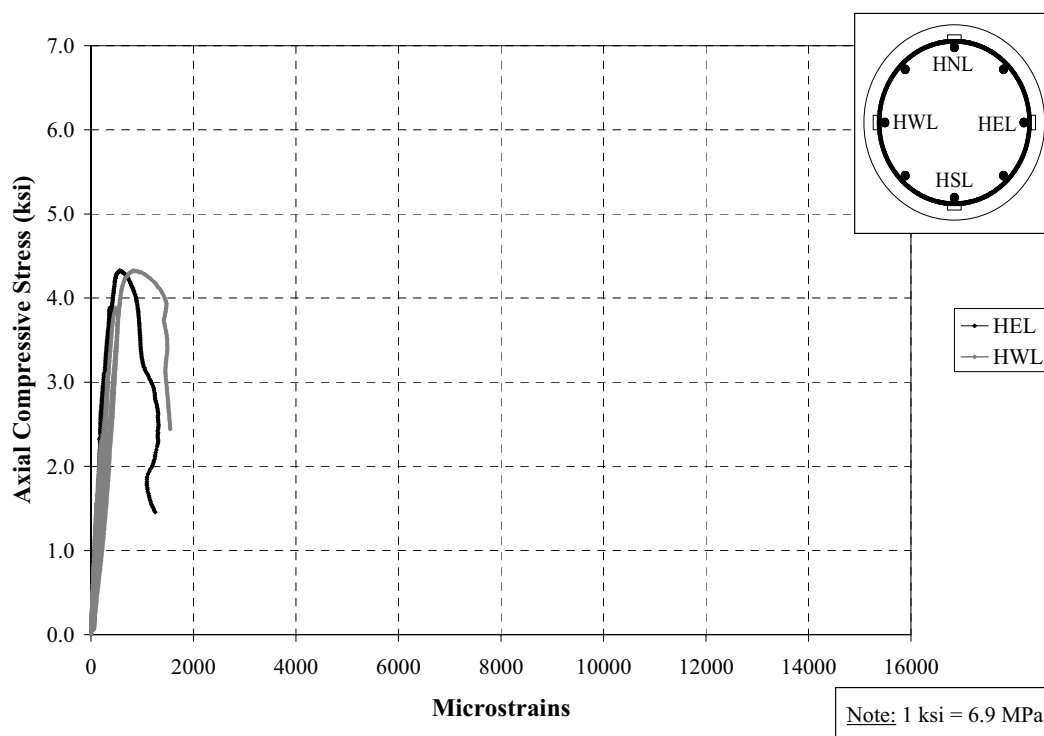


**Figure D4. Axial Stress vs. Transverse Strain on Lower Tie (HEL & HWL); Specimen A1**
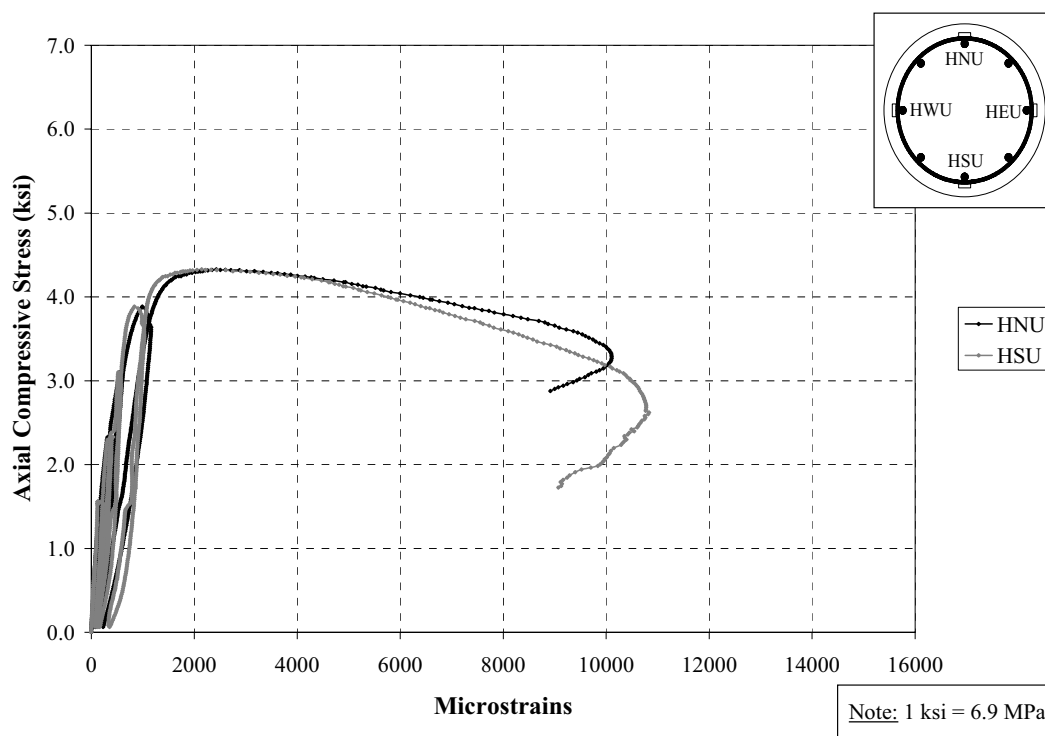
**Figure D5.  Axial Stress vs. Transverse Strain on Upper Tie (HNU & HSU); Specimen A1**
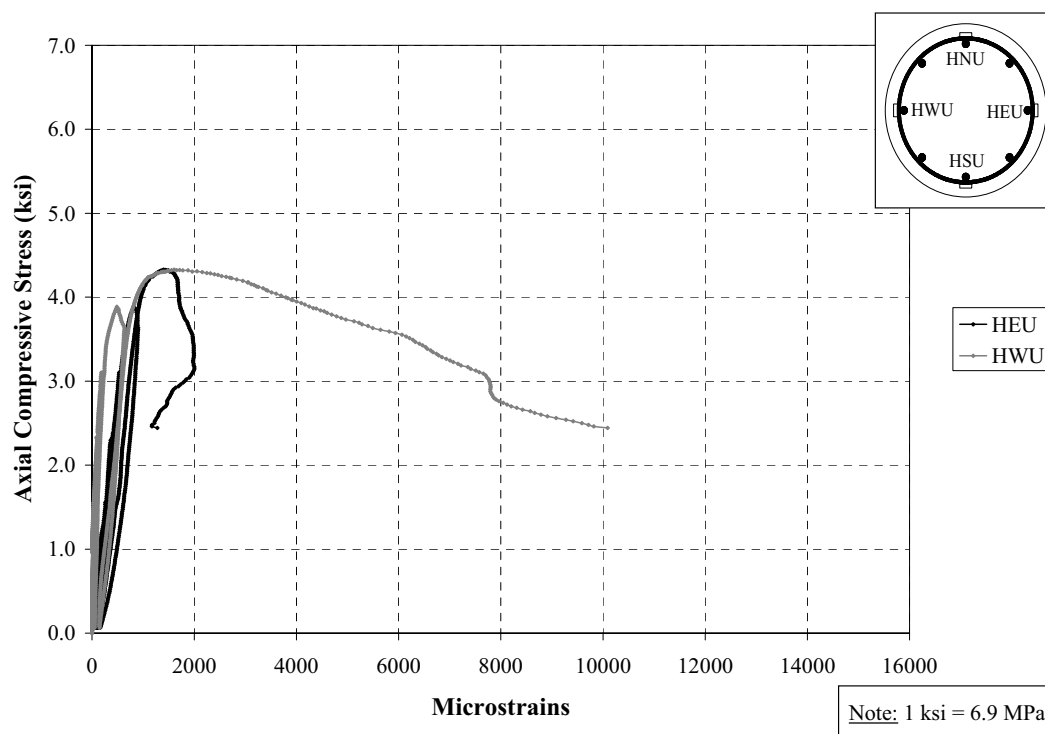


**Figure D6.  Axial Stress vs. Transverse Strain on Upper Tie (HEU & HWU); Specimen A1**
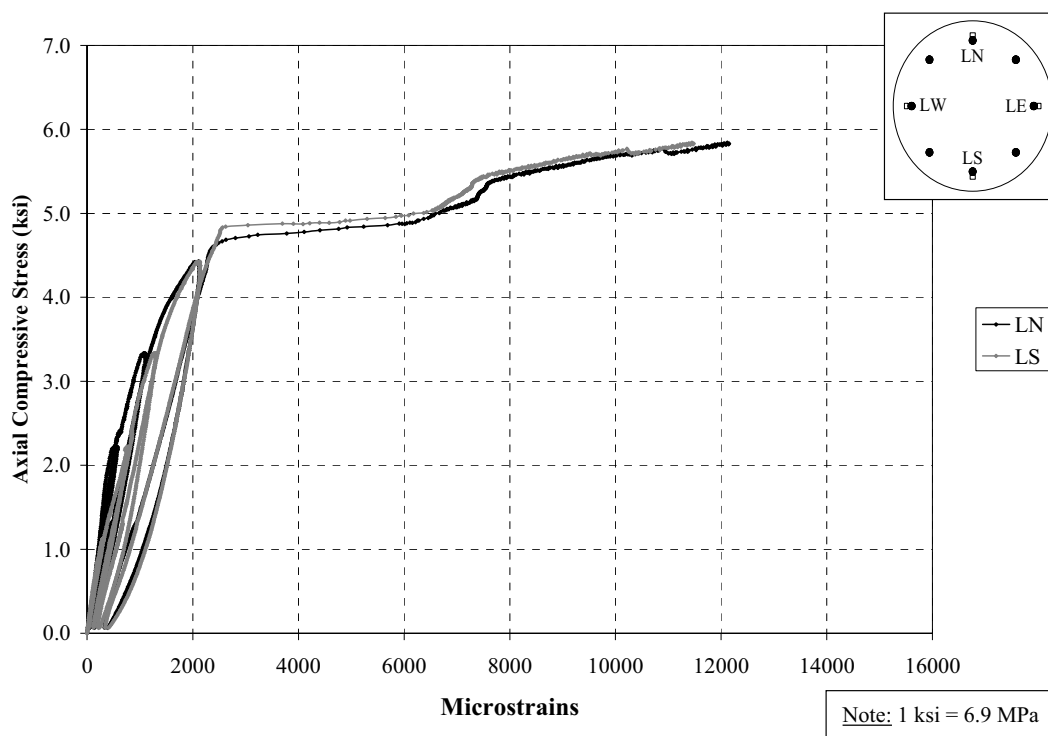
**Figure D7.  Axial Stress vs. Axial Strain on Longitudinal Bars (LN & LS); Specimen A2**
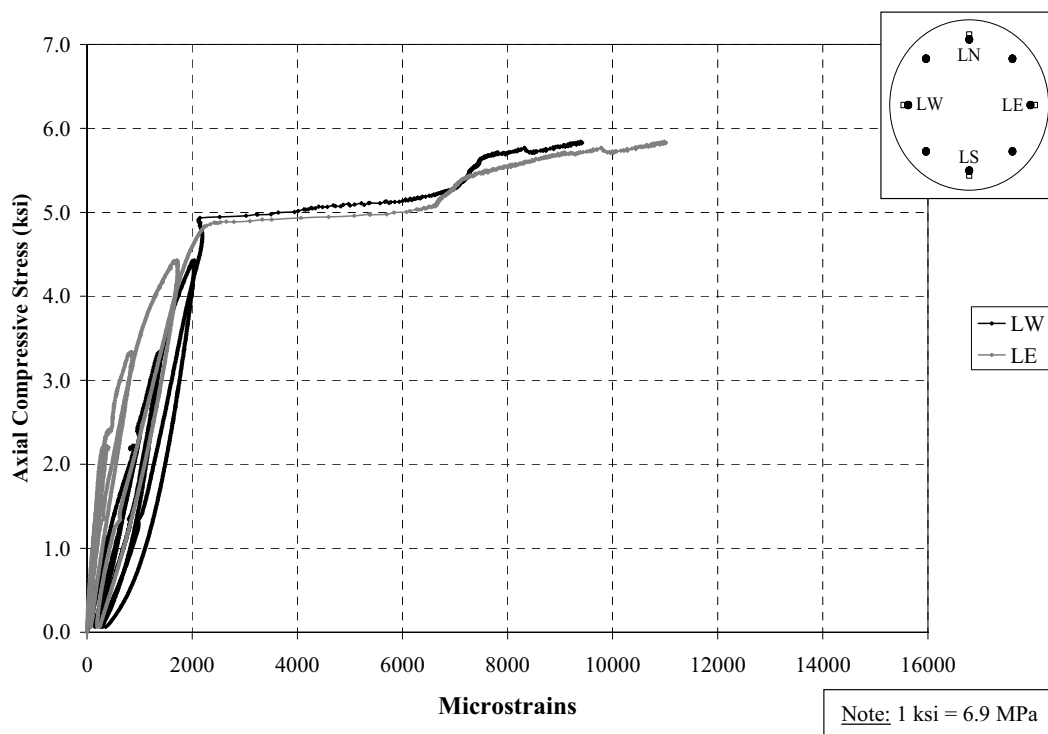


**Figure D8.  Axial Stress vs. Axial Strain on Longitudinal Bars (LE & LW); Specimen A2**
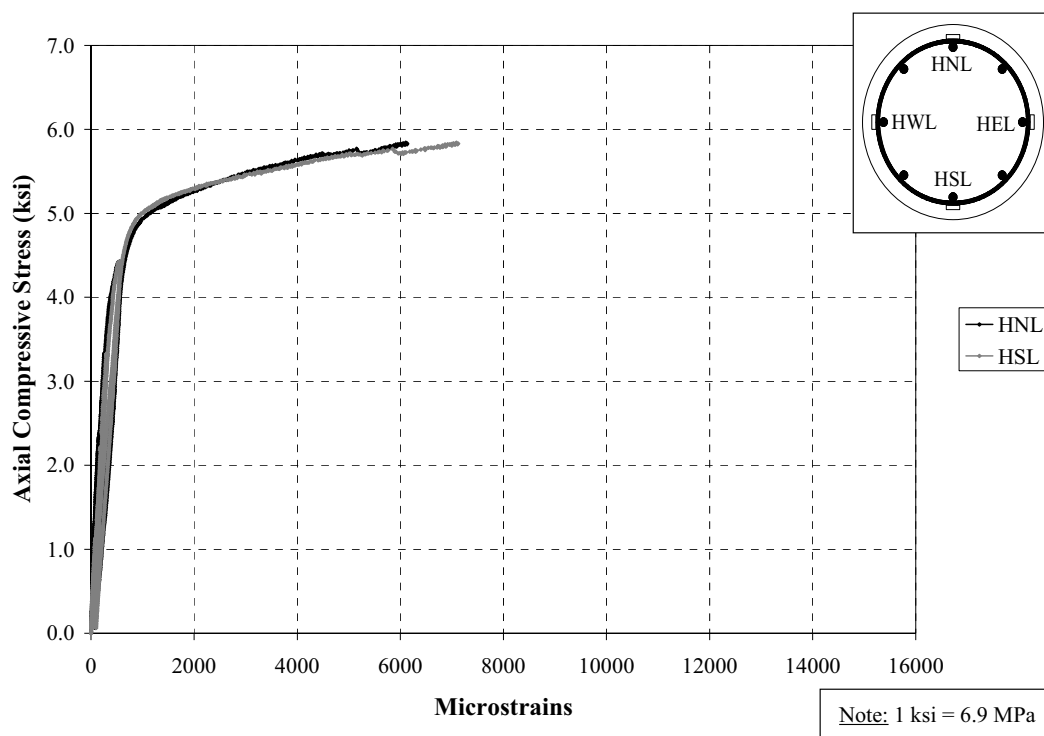
**Figure D9. Axial Stress vs. Transverse Strain on Lower Tie (HNL & HSL); Specimen A2**
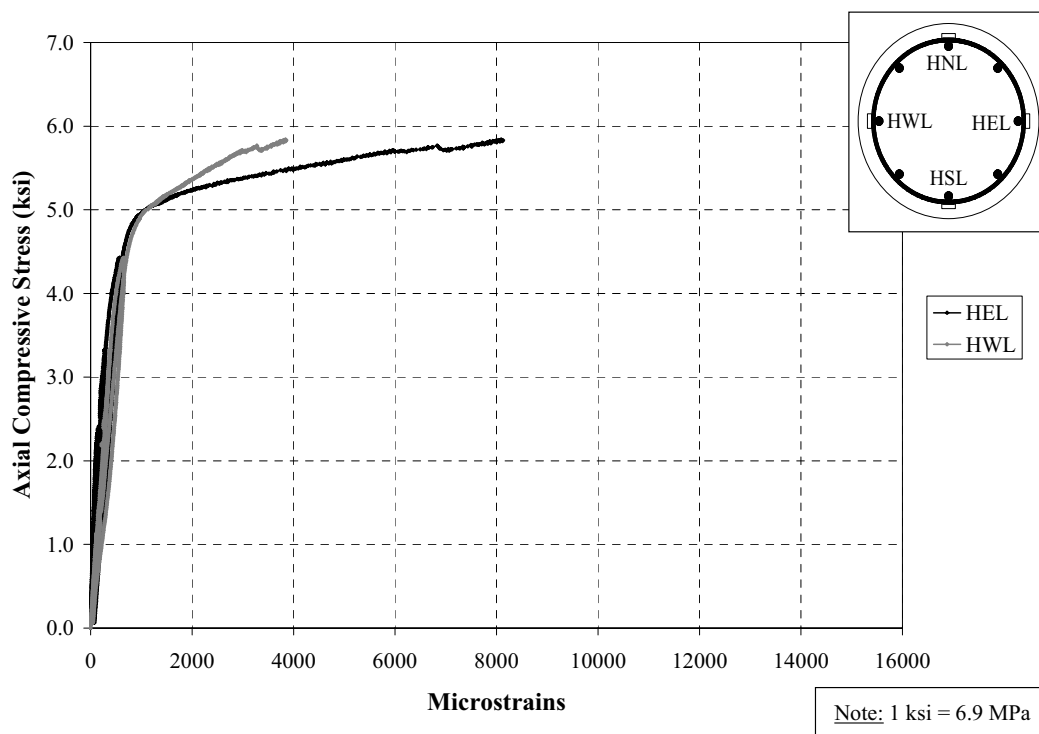


**Figure D10. Axial Stress vs. Transverse Strain on Lower Tie (HEL & HWL); Specimen A2**
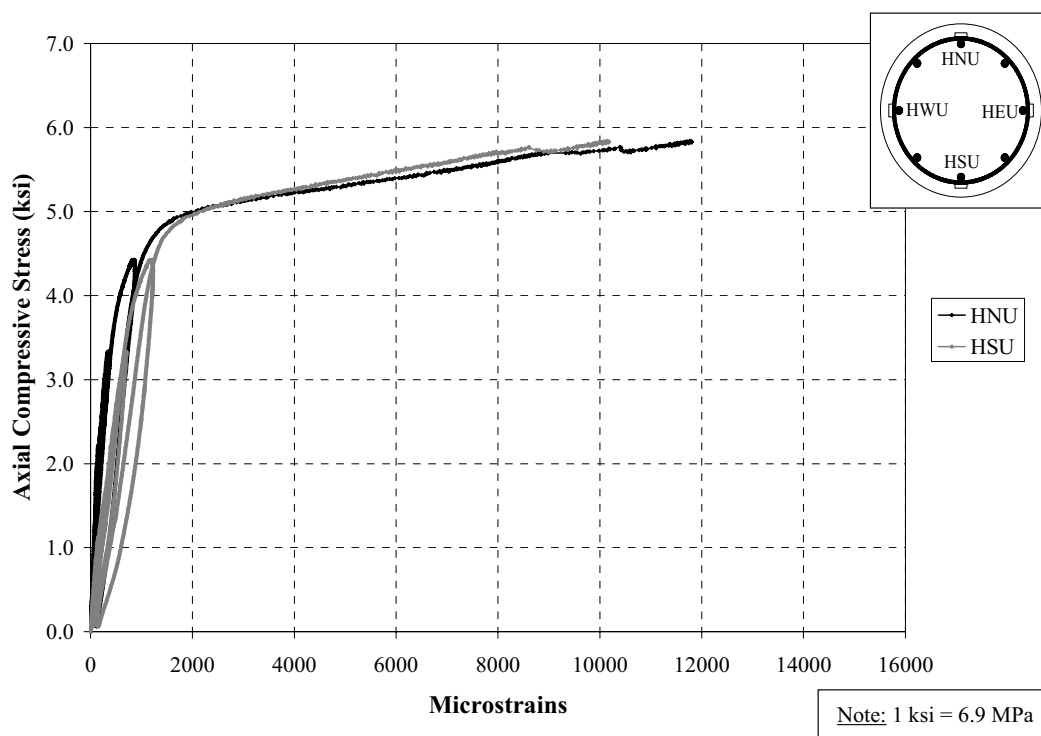
**Figure D11. Axial Stress vs. Transverse Strain on Upper Tie (HNU & HSU); Specimen A2**
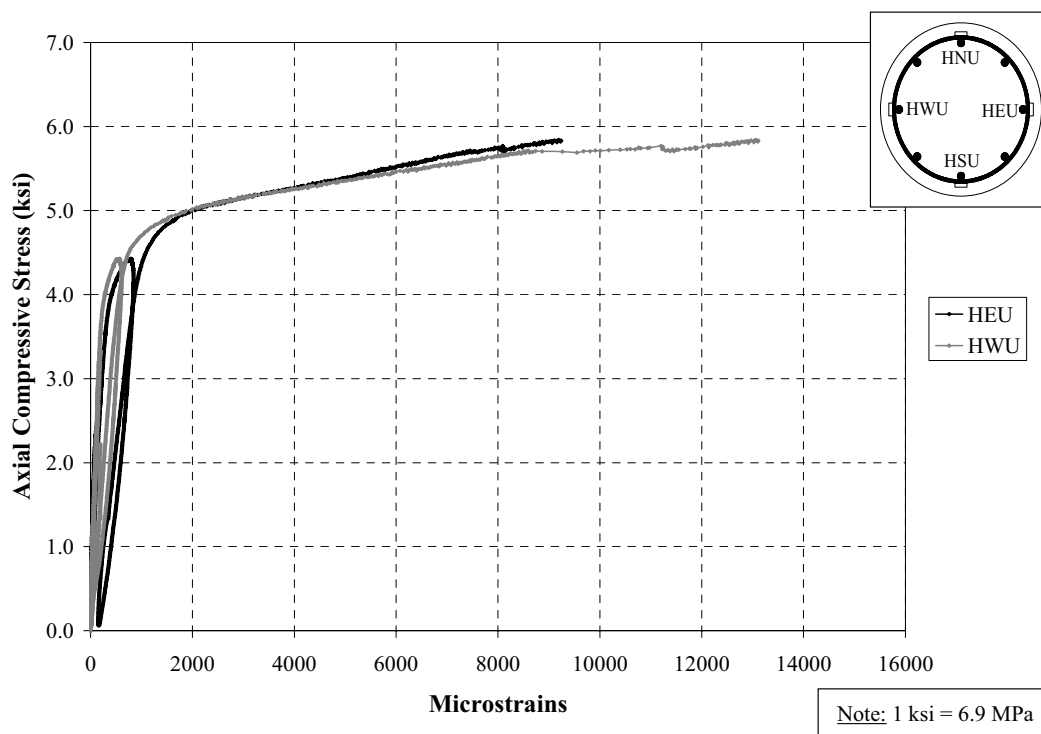


**Figure D12. Axial Stress vs. Transverse Strain on Upper Tie (HEU & HWU); Specimen A2**
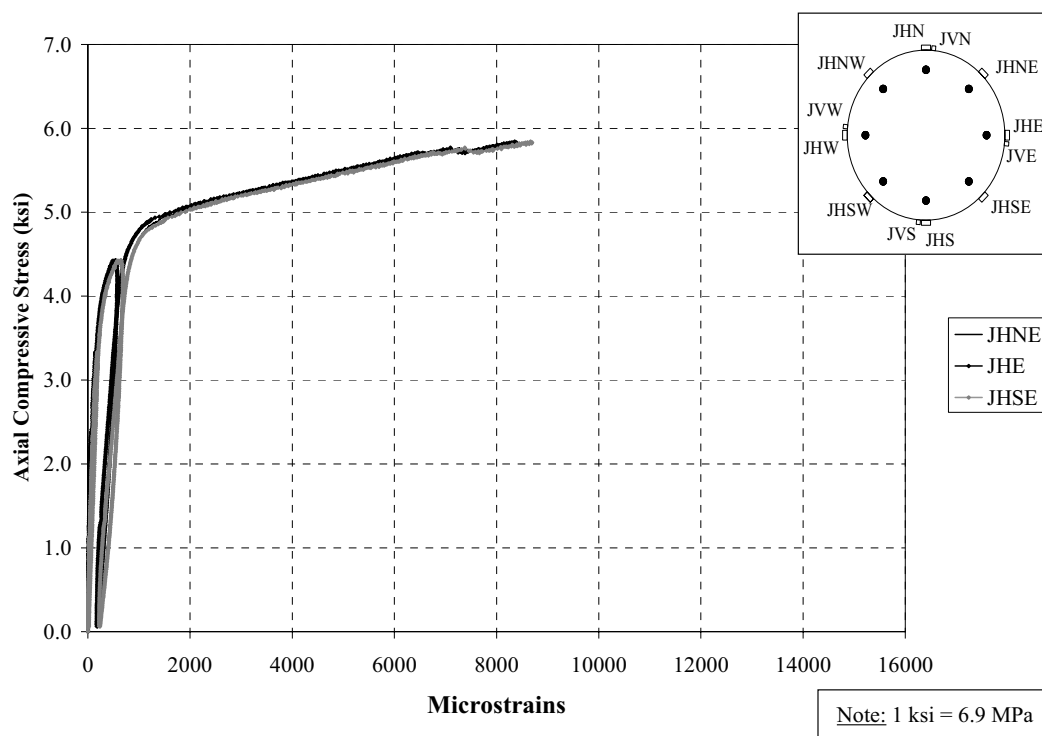
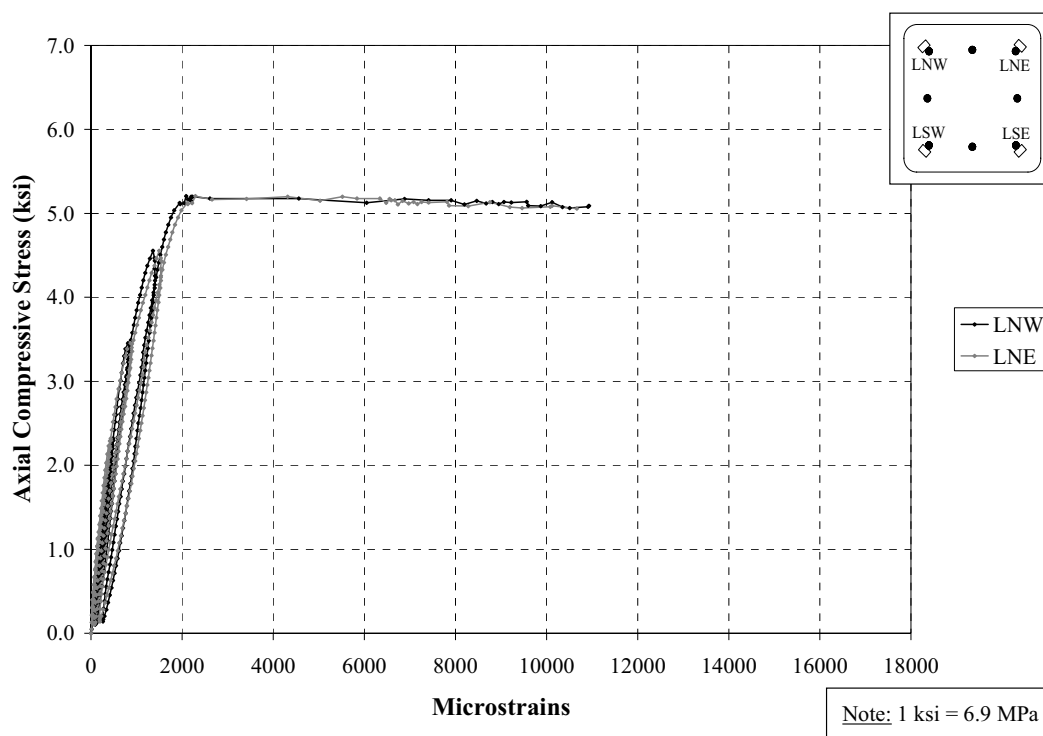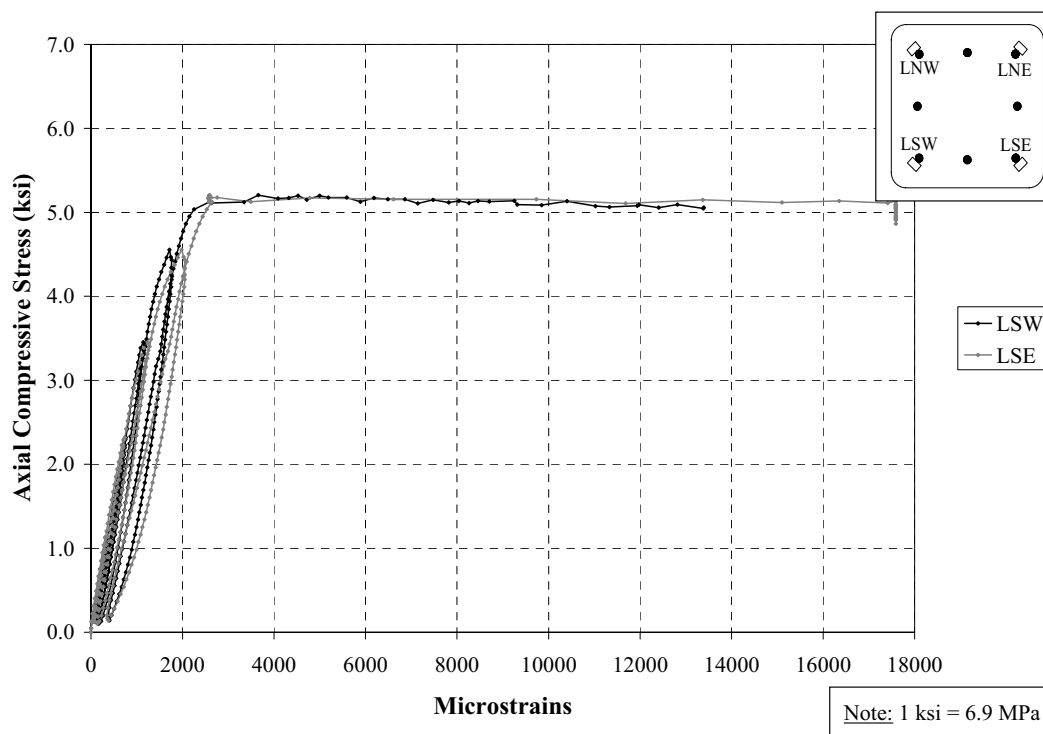**Figure D13.  Axial Stress vs. Transverse Strain on FRP (East); Specimen A2**
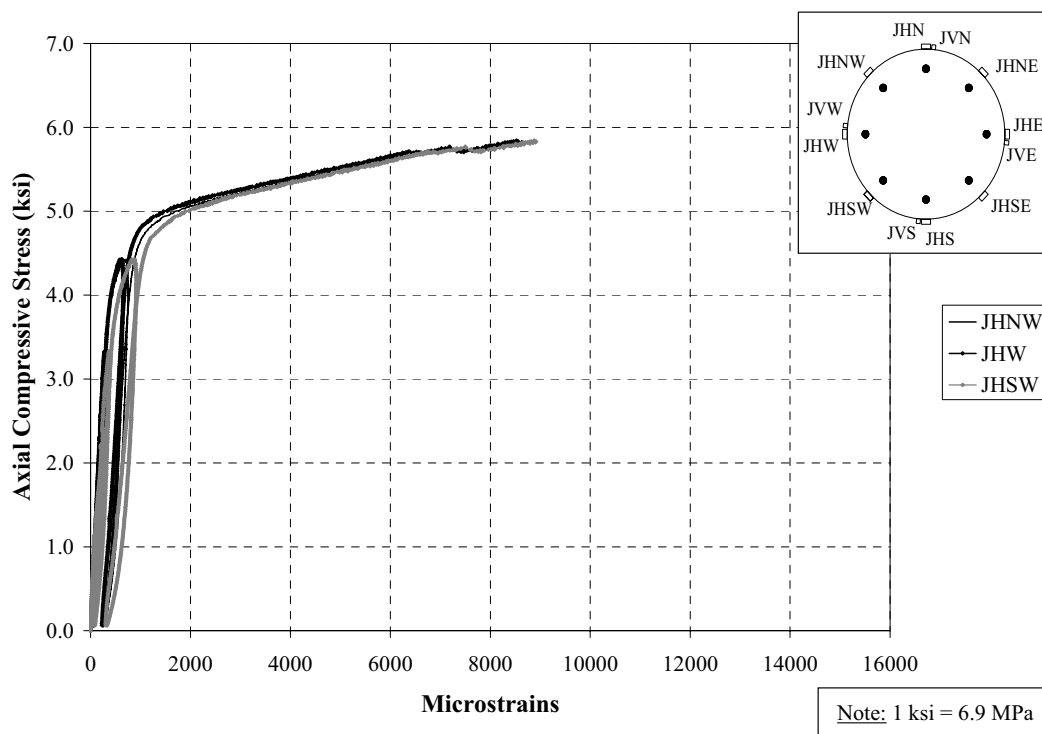


**Figure D14.  Axial Stress vs. Transverse Strain on FRP (West); Specimen A2**
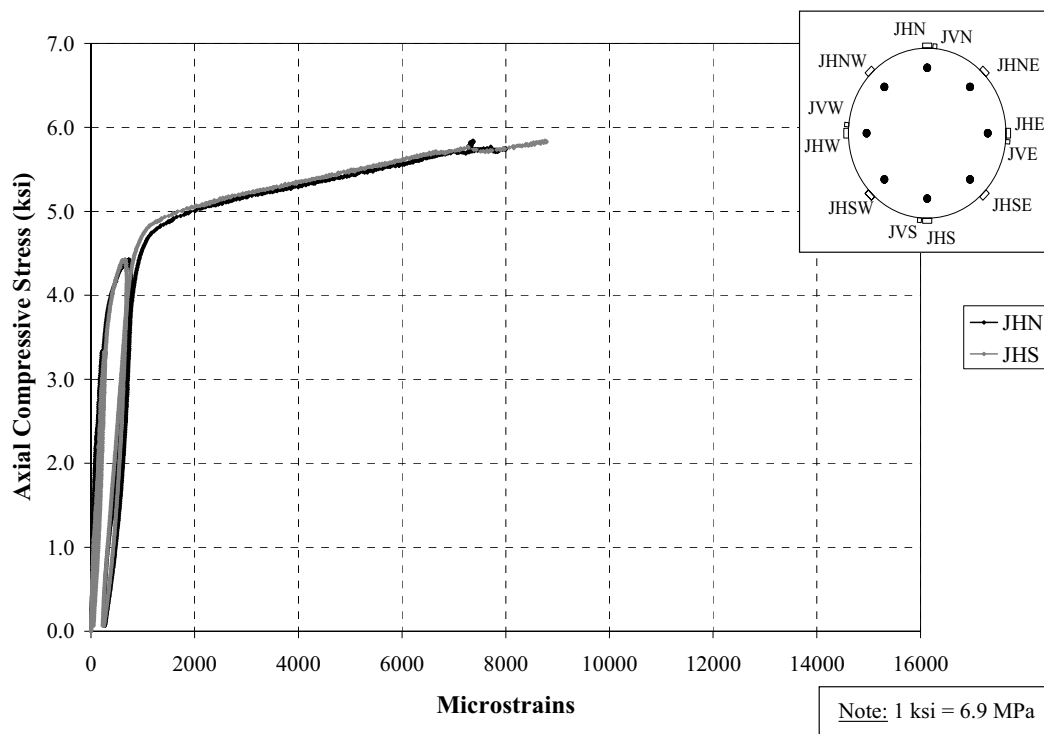
**Figure D15.  Axial Stress vs. Transverse Strain on FRP (N & S); Specimen A2**
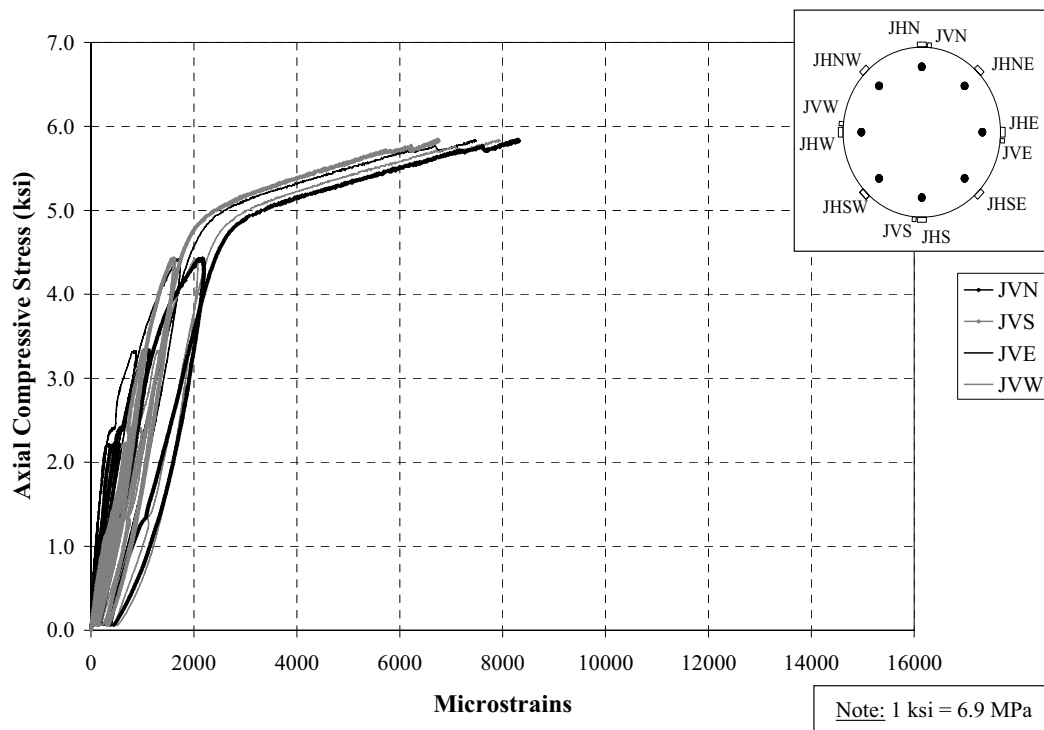


**Figure D16.  Axial Stress vs. Axial Strain on FRP (Sensors on Vertical Direction); Specimen A2**
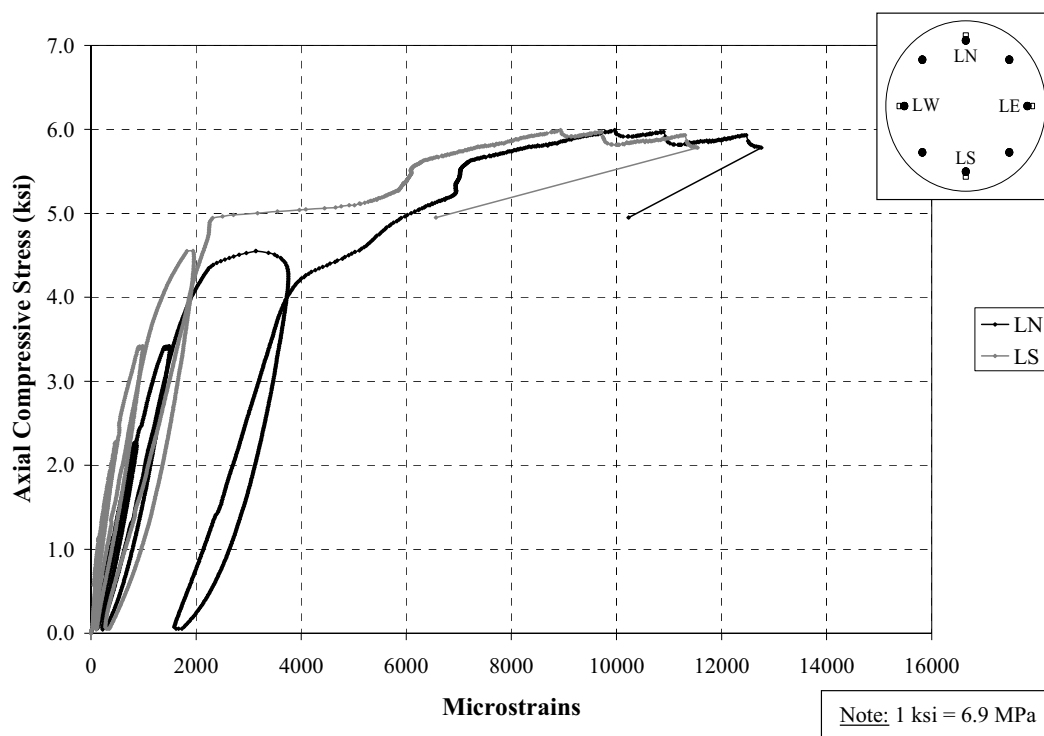
**Figure D17. Axial Stress vs. Axial Strain on Longitudinal Bars (LN & LS); Specimen A3**
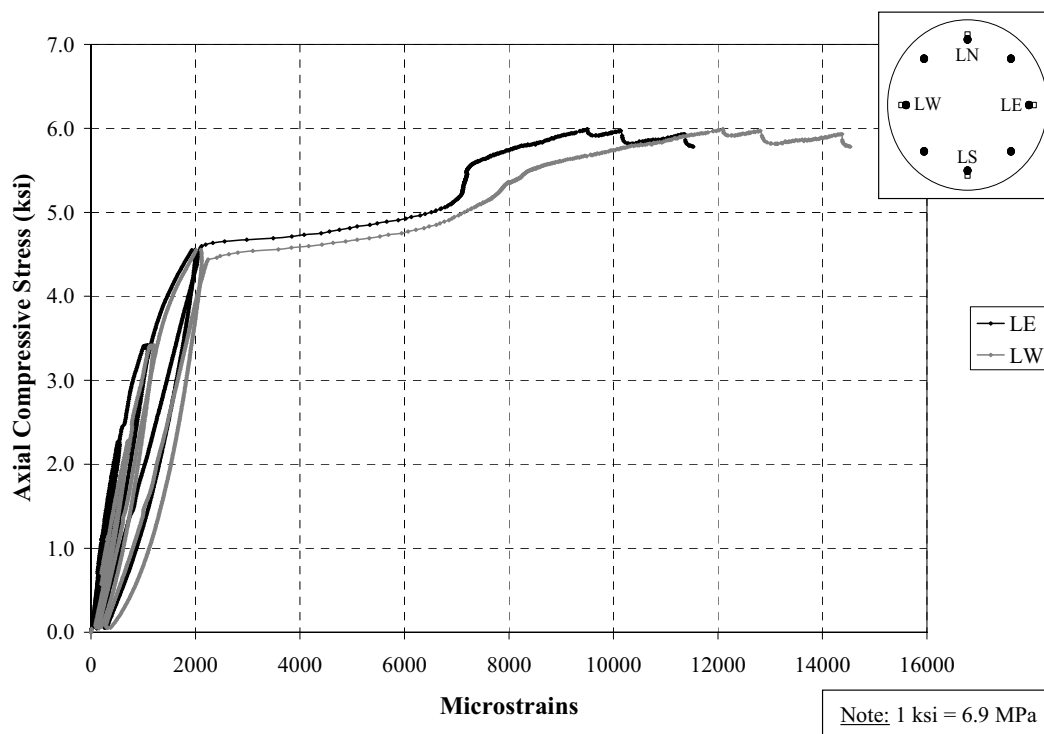


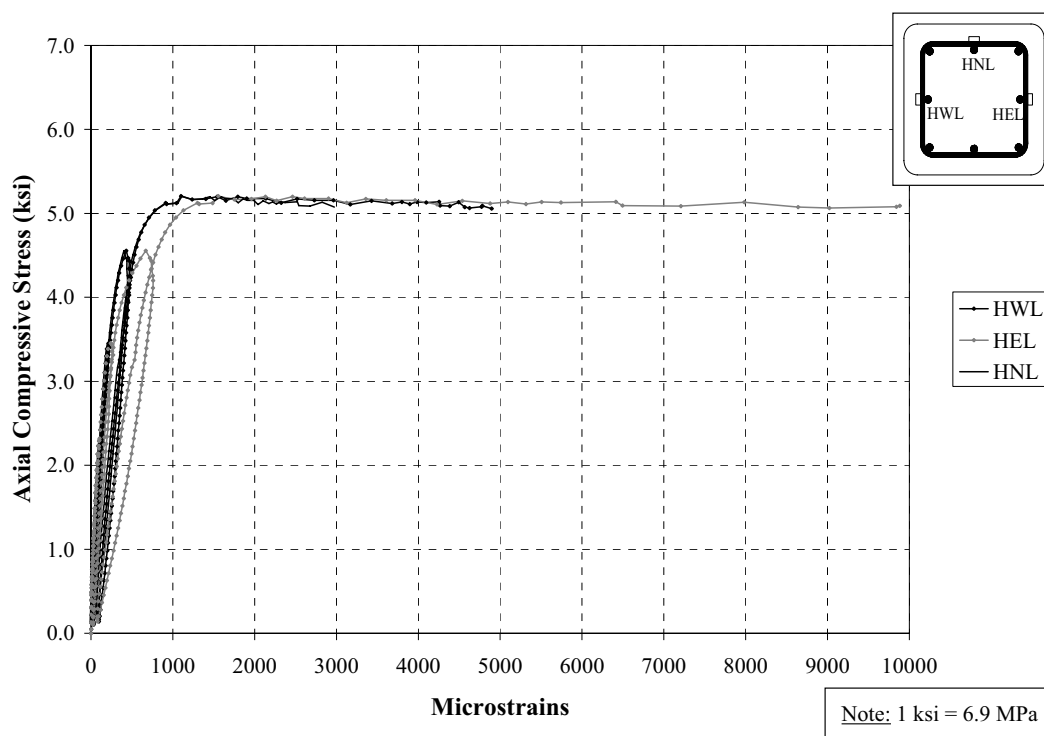**Figure D18. Axial Stress vs. Axial Strain on Longitudinal Bars (LE & LW); Specimen A3**
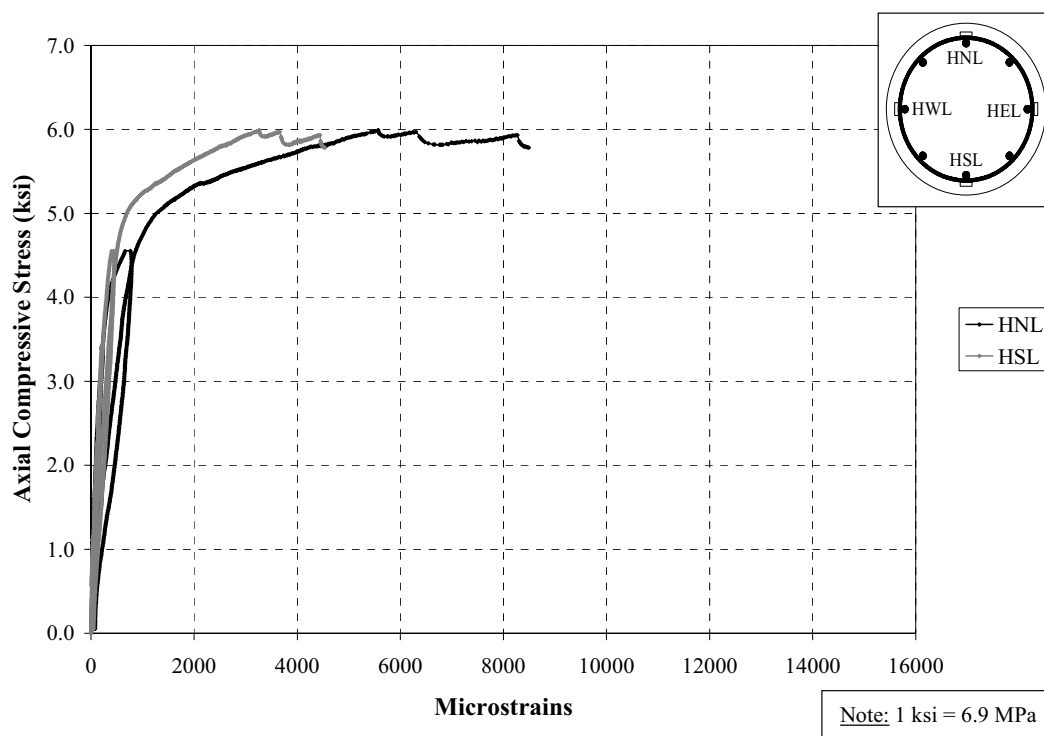
**Figure D19.  Axial Stress vs. Transverse Strain on Lower Tie (HNL & HSL); Specimen A3**
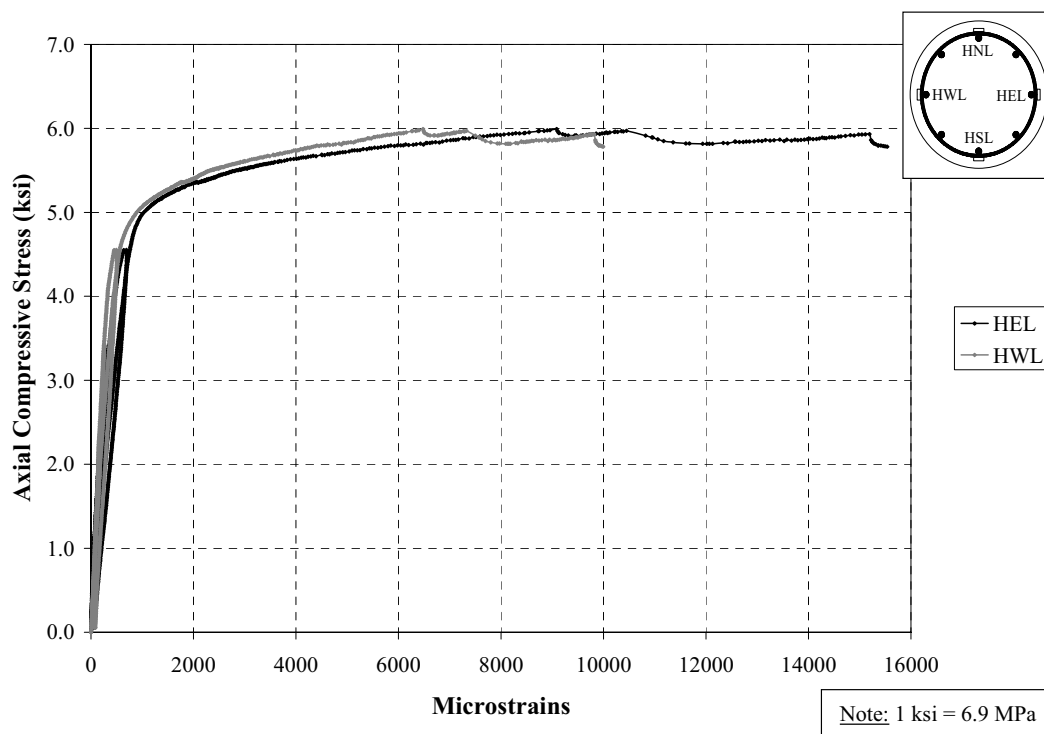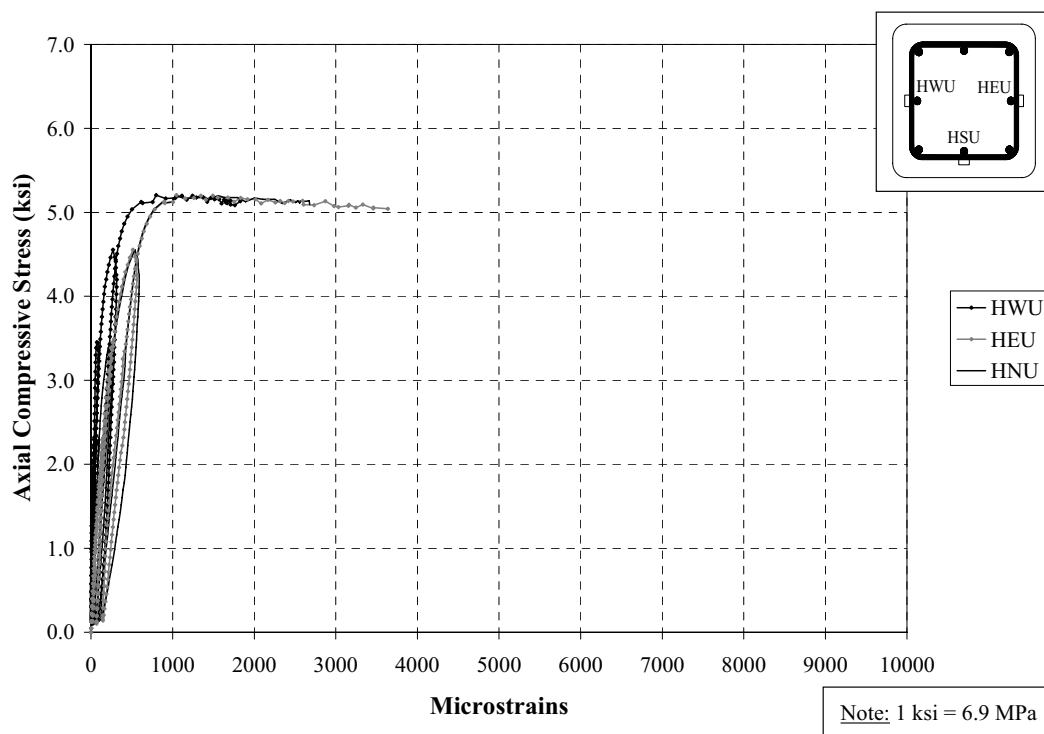


**Figure D20.  Axial Stress vs. Transverse Strain on Lower Tie (HEL & HWL); Specimen A3**
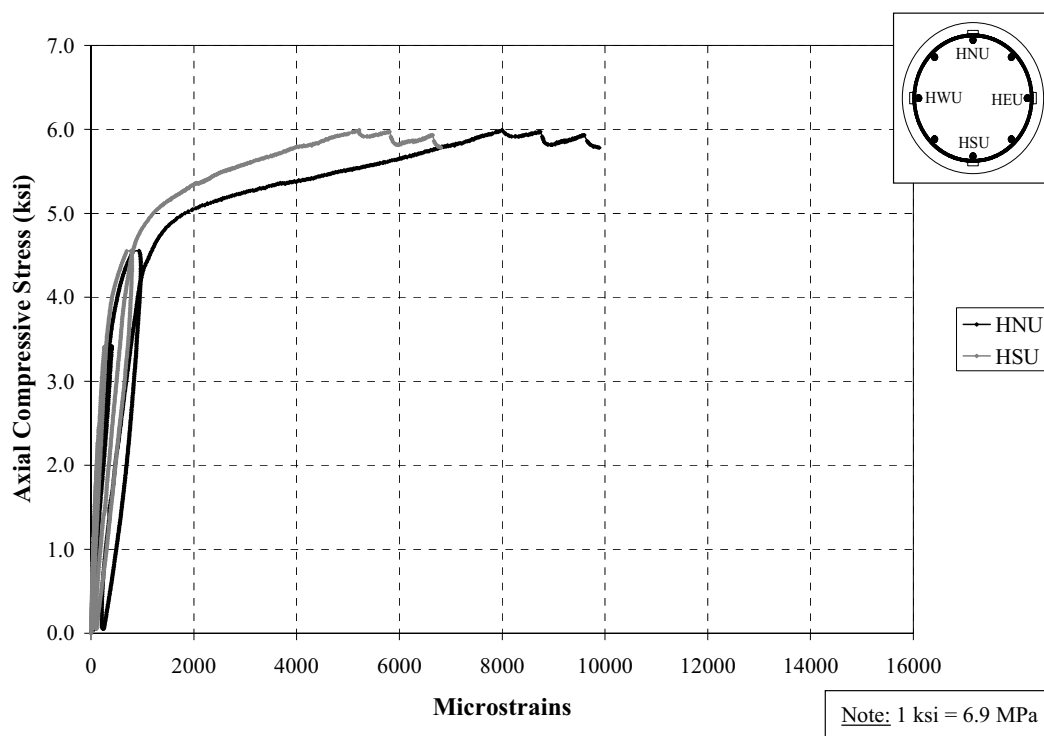
**Figure D21.  Axial Stress vs. Transverse Strain on Upper Tie (HNU & HSU); Specimen A3**
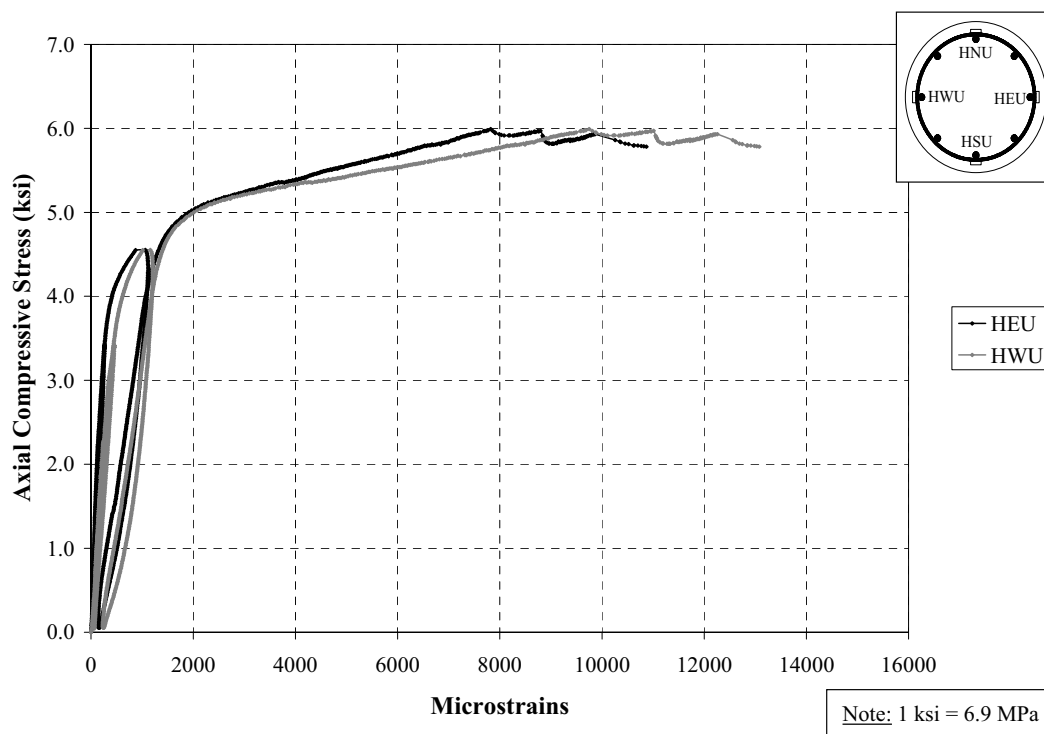


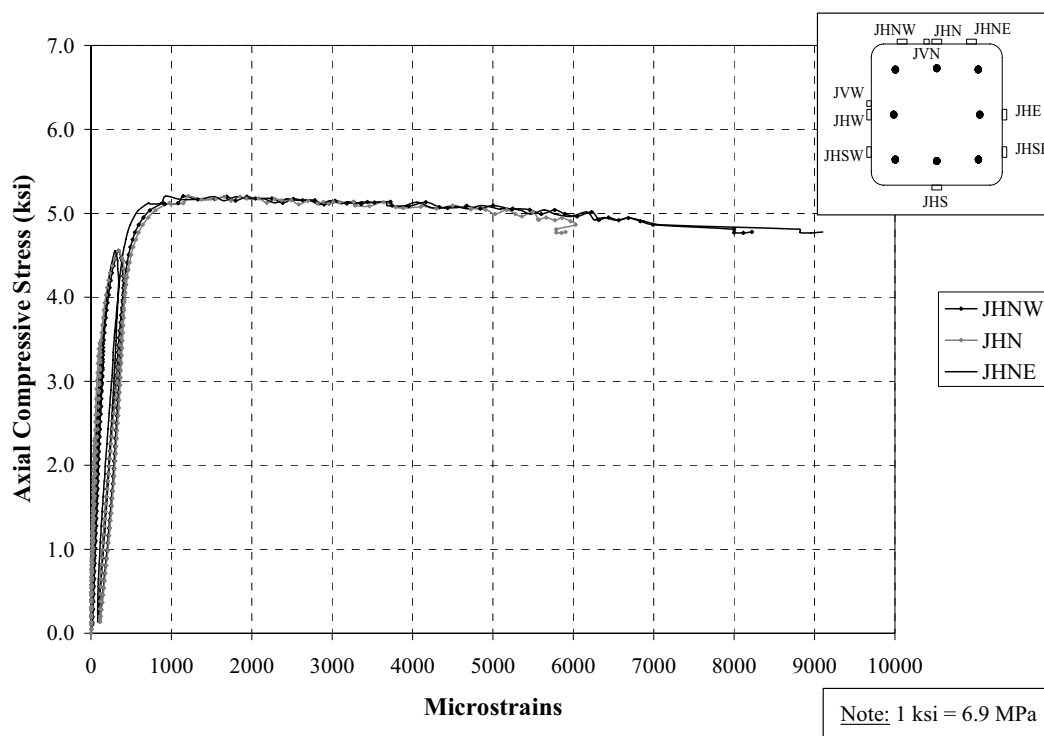**Figure D22.  Axial Stress vs. Transverse Strain on Upper Tie (HEU & HWU); Specimen A3**
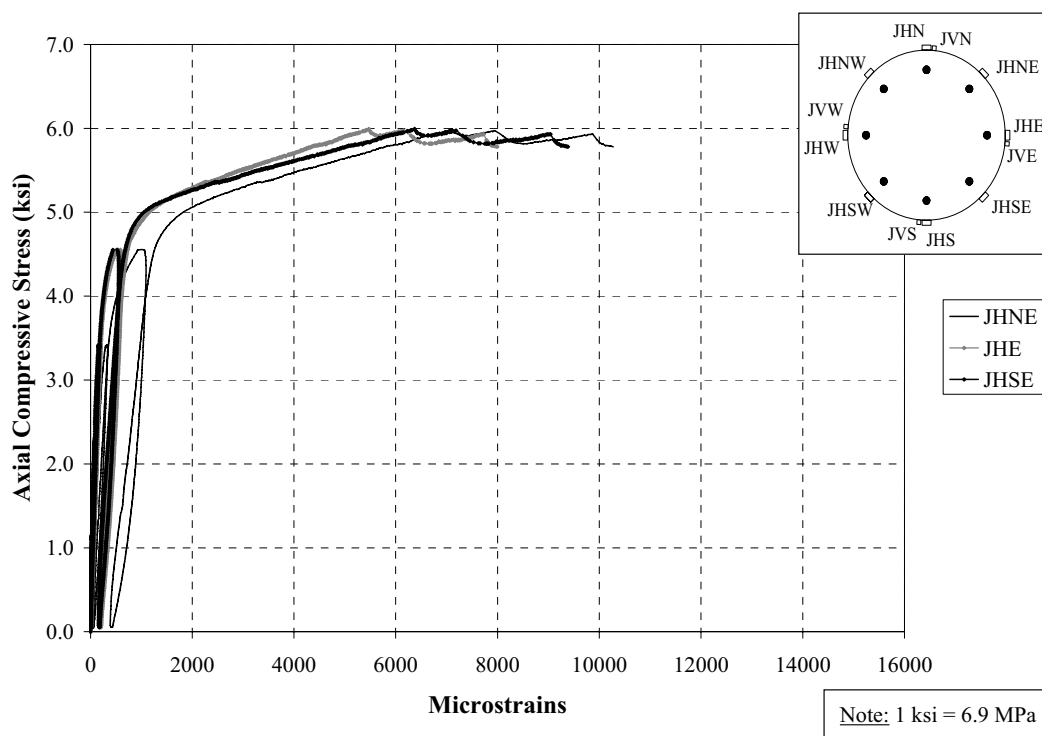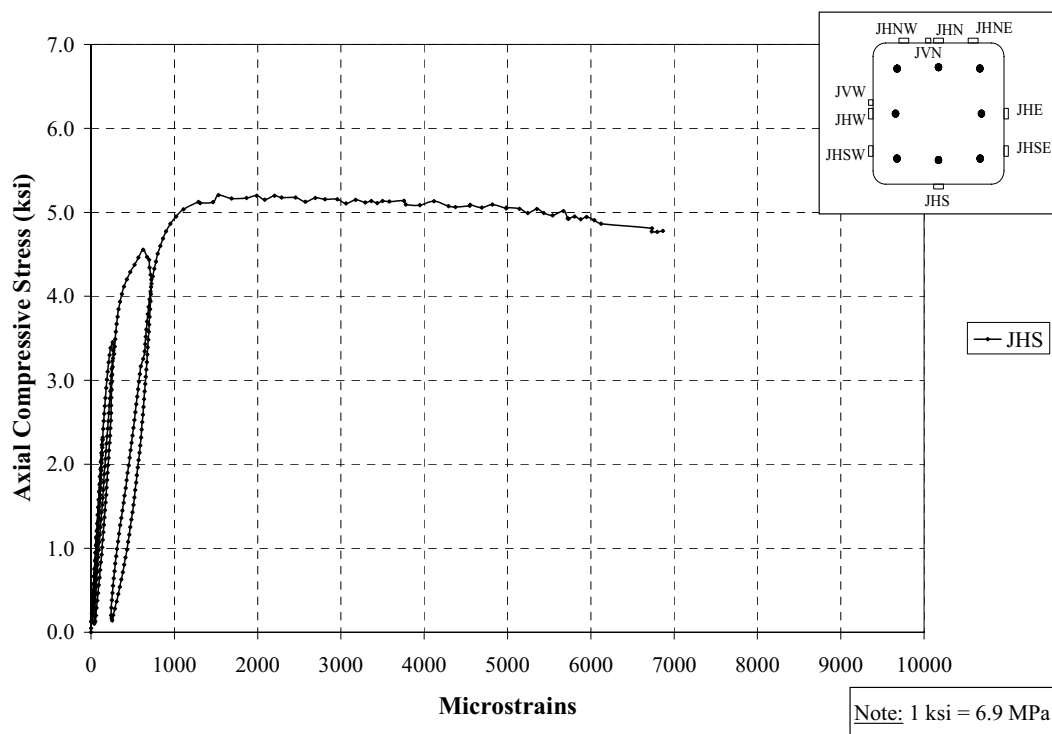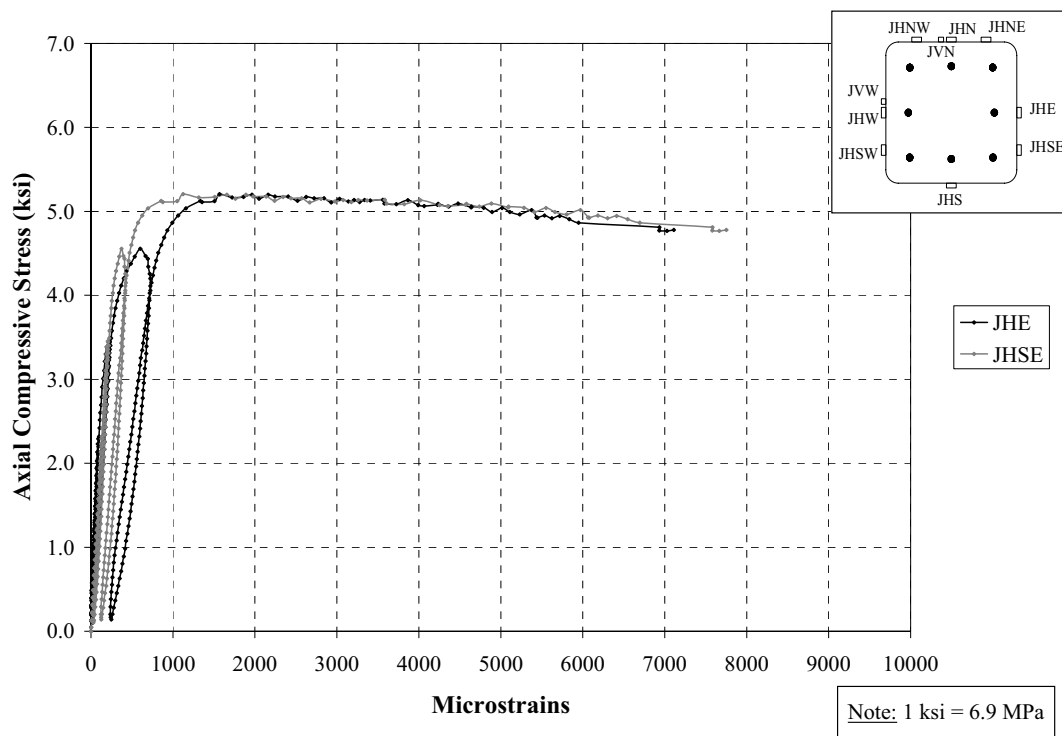
**Figure D23. Axial Stress vs. Transverse Strain on FRP (East); Specimen A3**
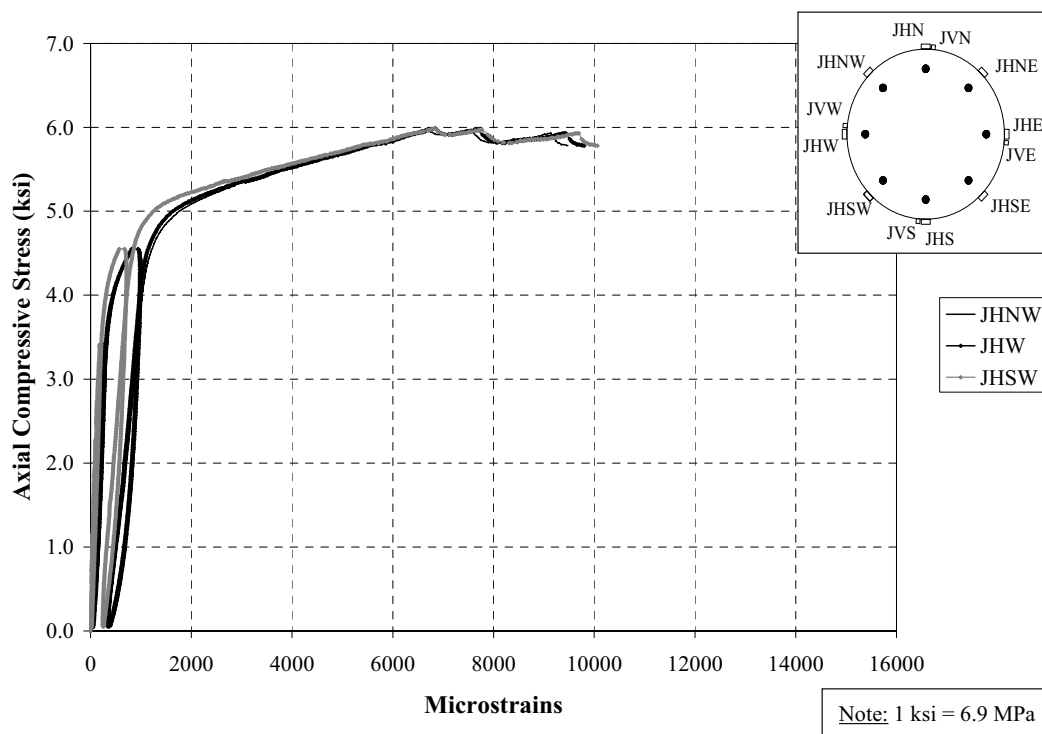


**Figure D24. Axial Stress vs. Transverse Strain on FRP (West); Specimen A3**
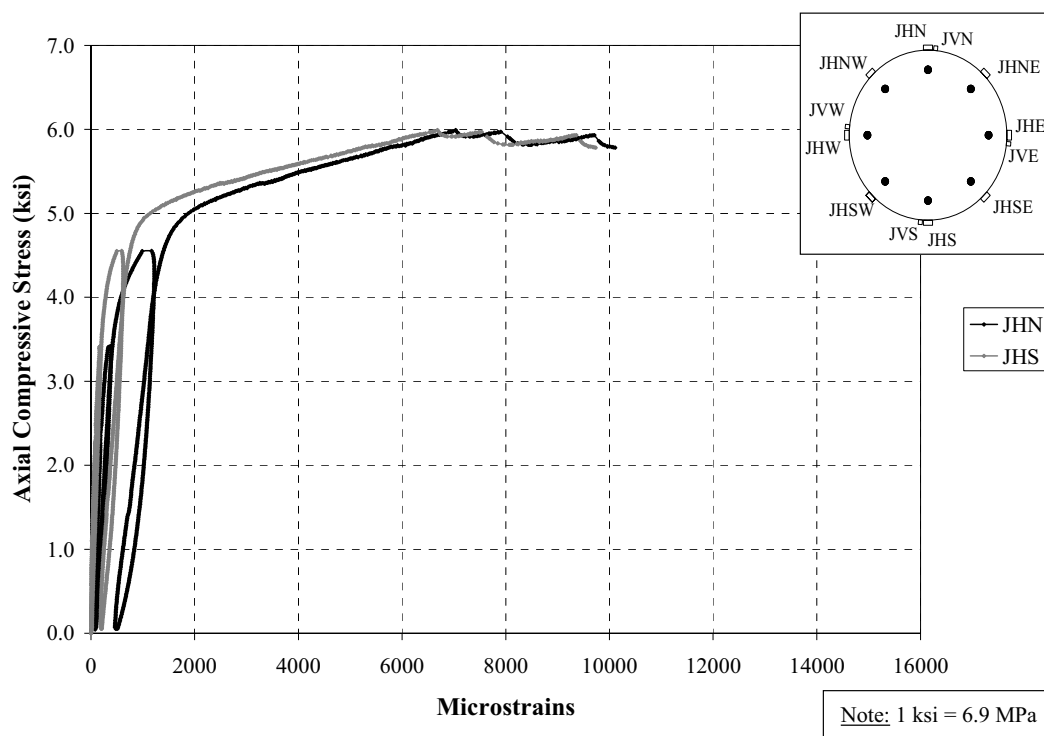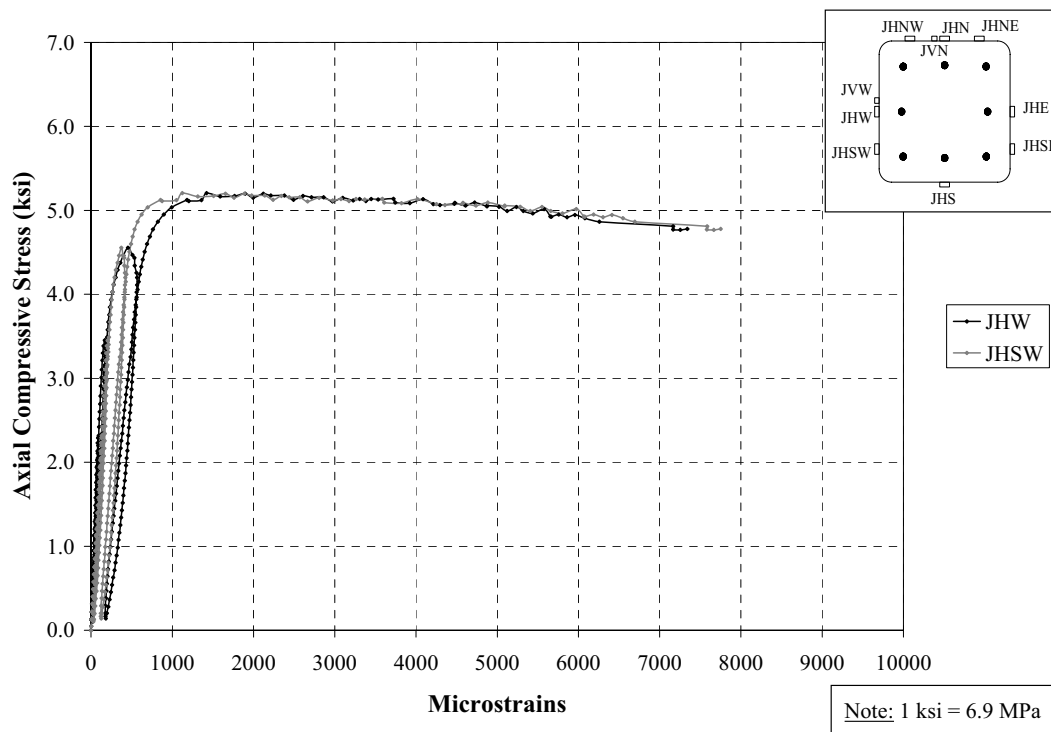
**Figure D25.  Axial Stress vs. Transverse Strain on FRP (N & S); Specimen A3**
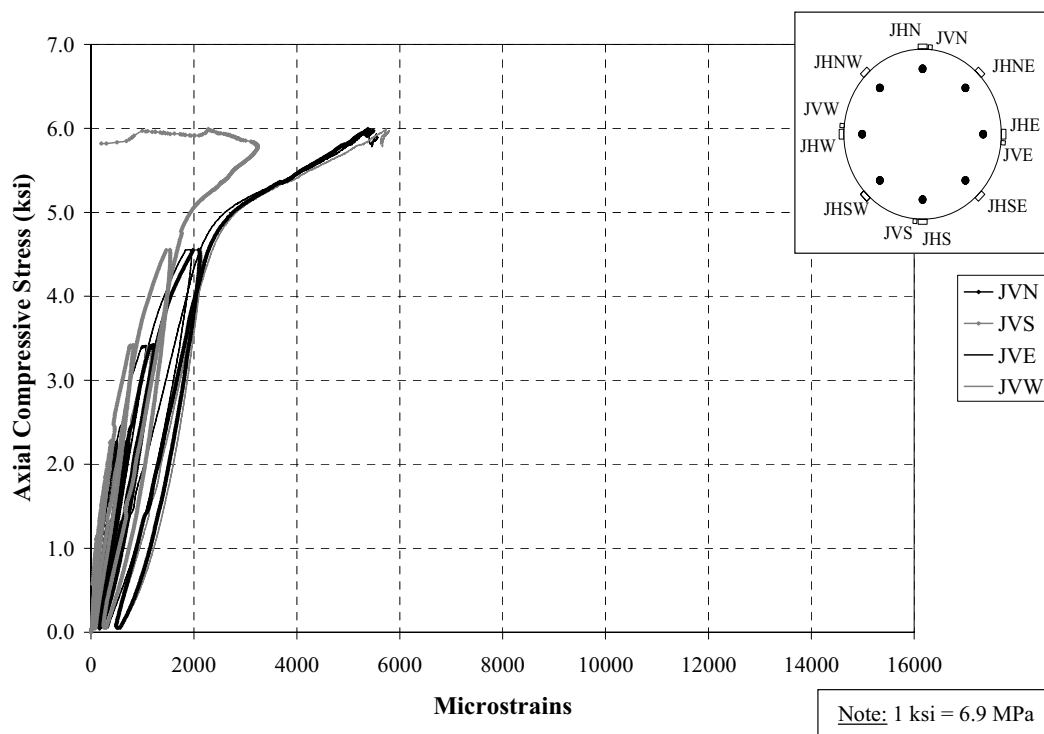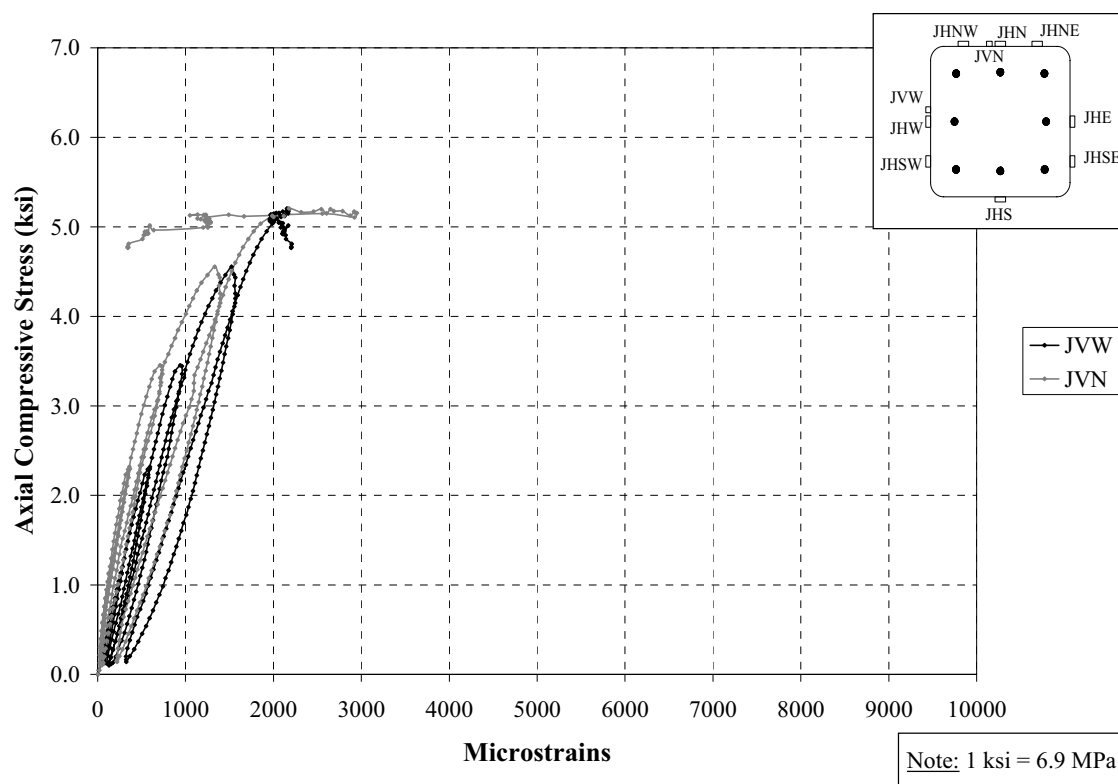


**Figure D26.  Axial Stress vs. Axial Strain on FRP (Sensors on Vertical Direction); Specimen A3**
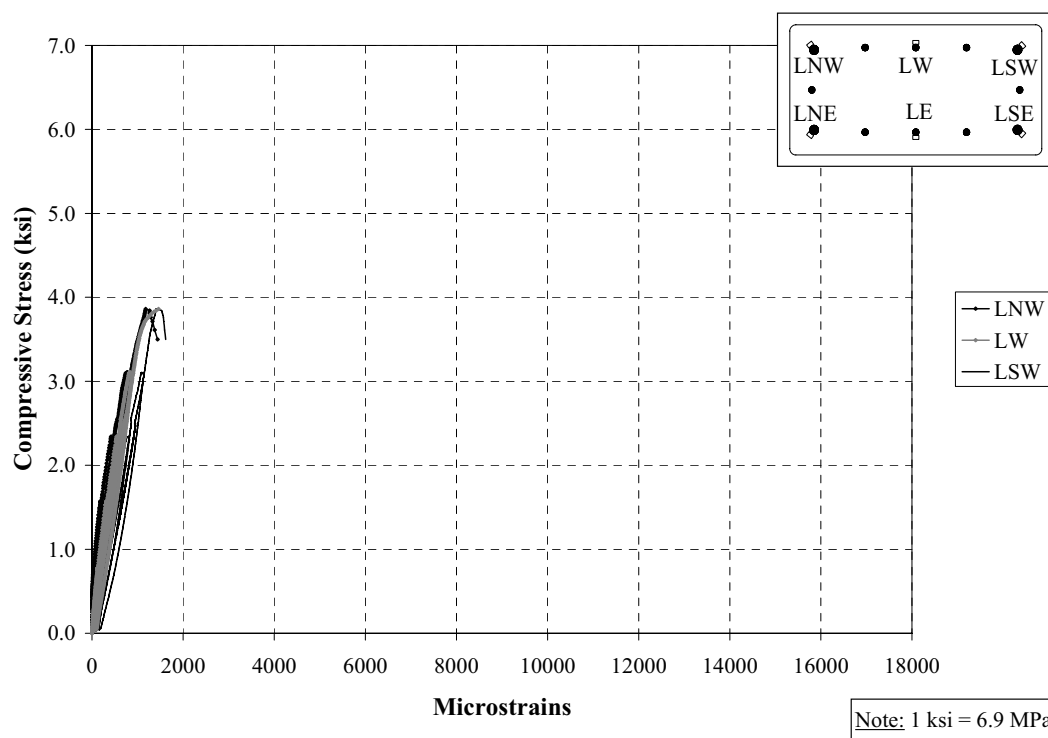
**Figure D27.  Axial Stress vs. Axial Strain on Longitudinal Bars (West); Specimen B1**
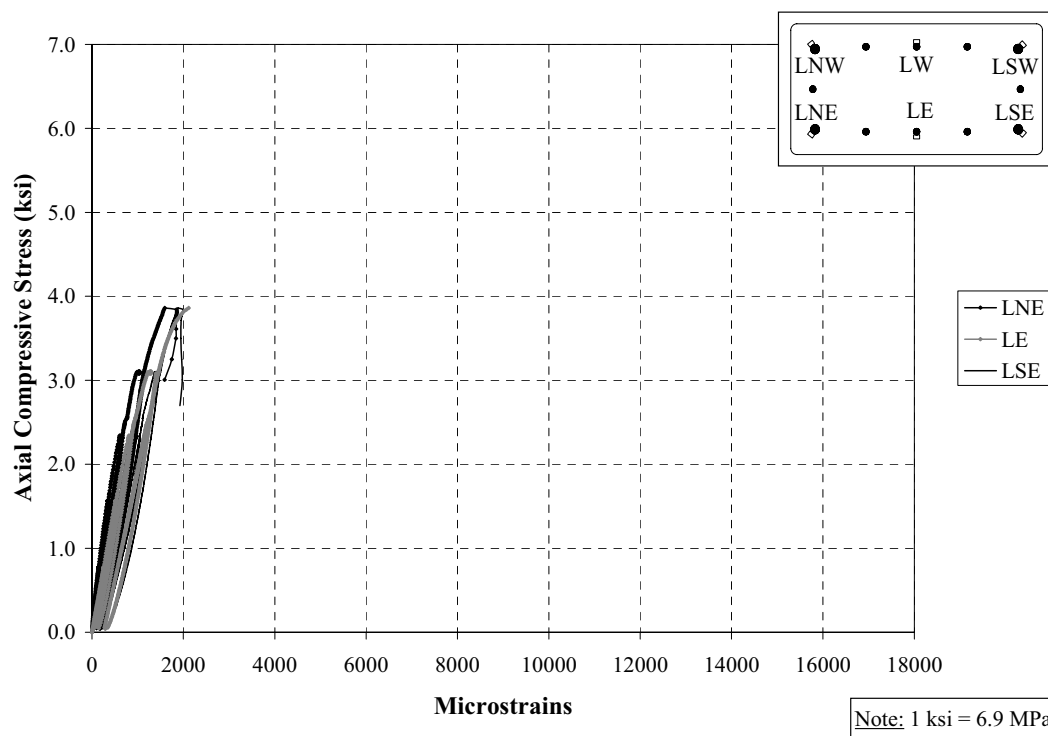


**Figure D28.  Axial Stress vs. Axial Strain on Longitudinal Bars (East); Specimen B1**
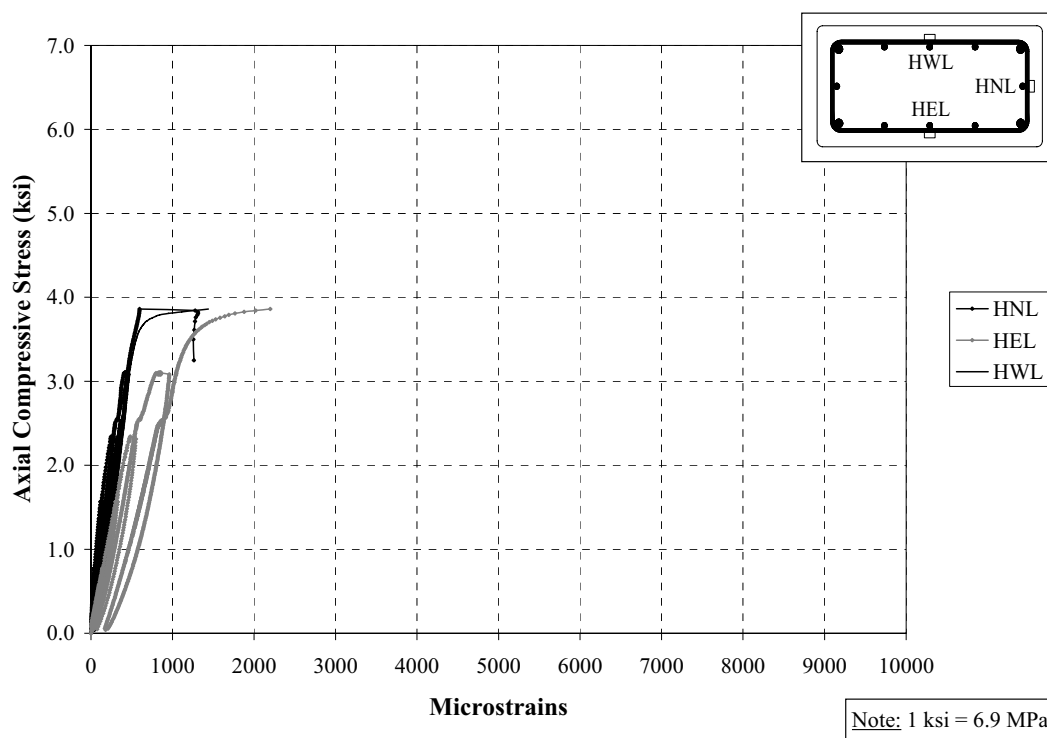
**Figure D29. Axial Stress vs. Transverse Strain on Lower Tie; Specimen B1**
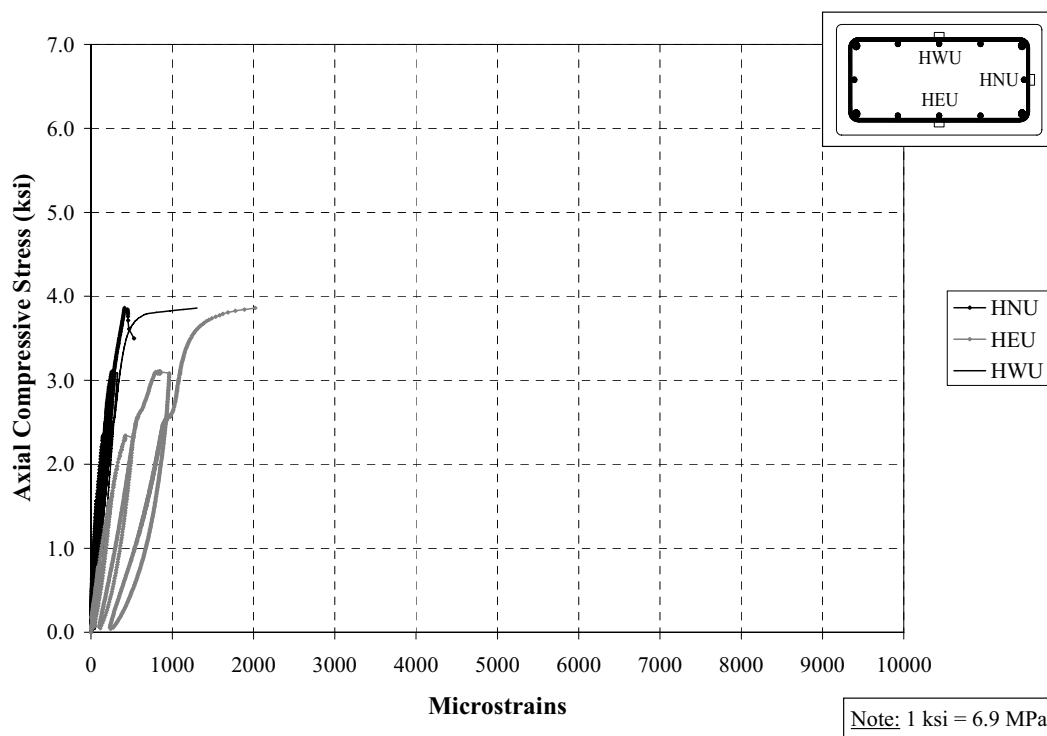


**Figure D30. Axial Stress vs. Transverse Strain on Upper Tie; Specimen B1**
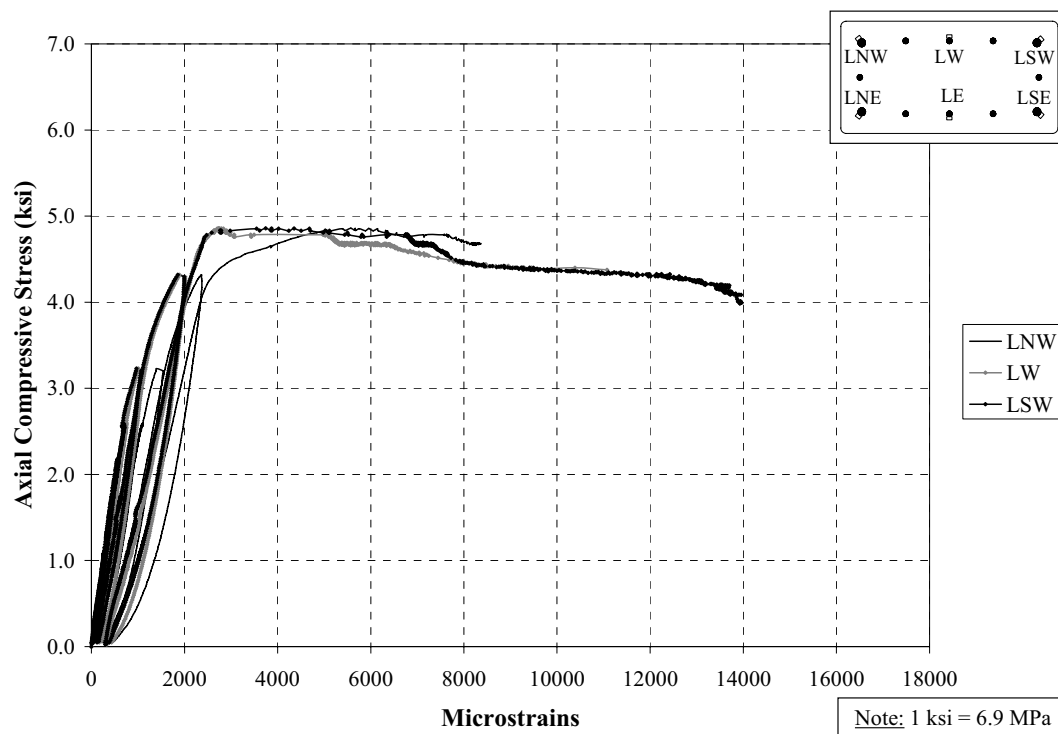
**Figure D31. Axial Stress vs. Axial Strain on Longitudinal Bars (West); Specimen B2**
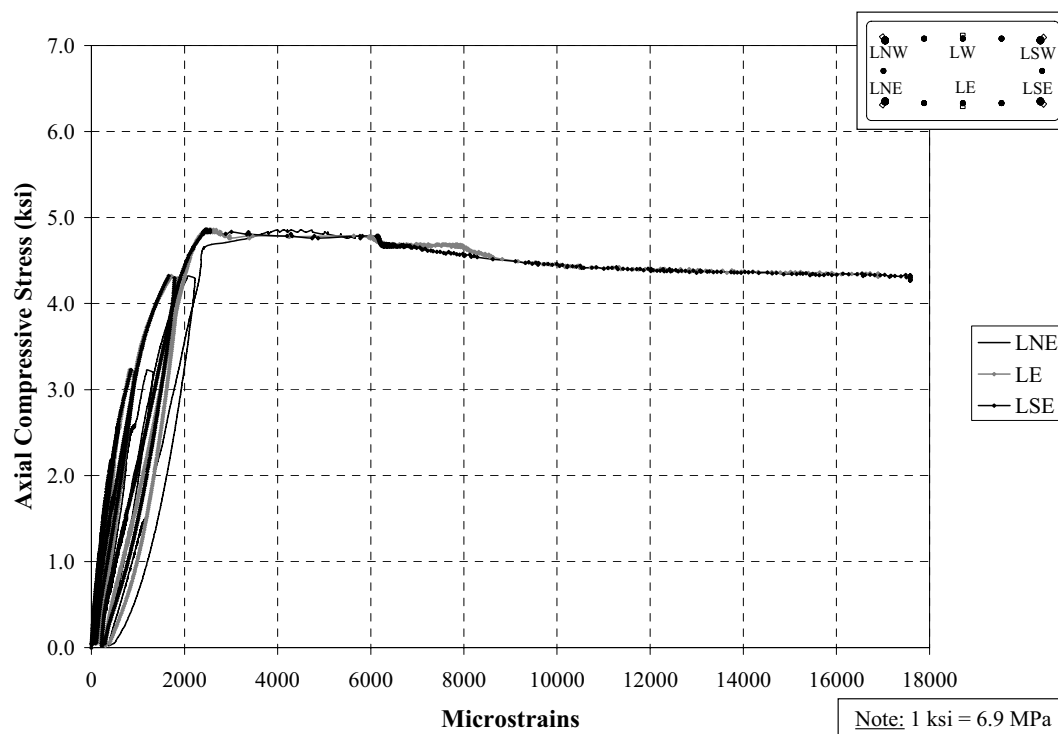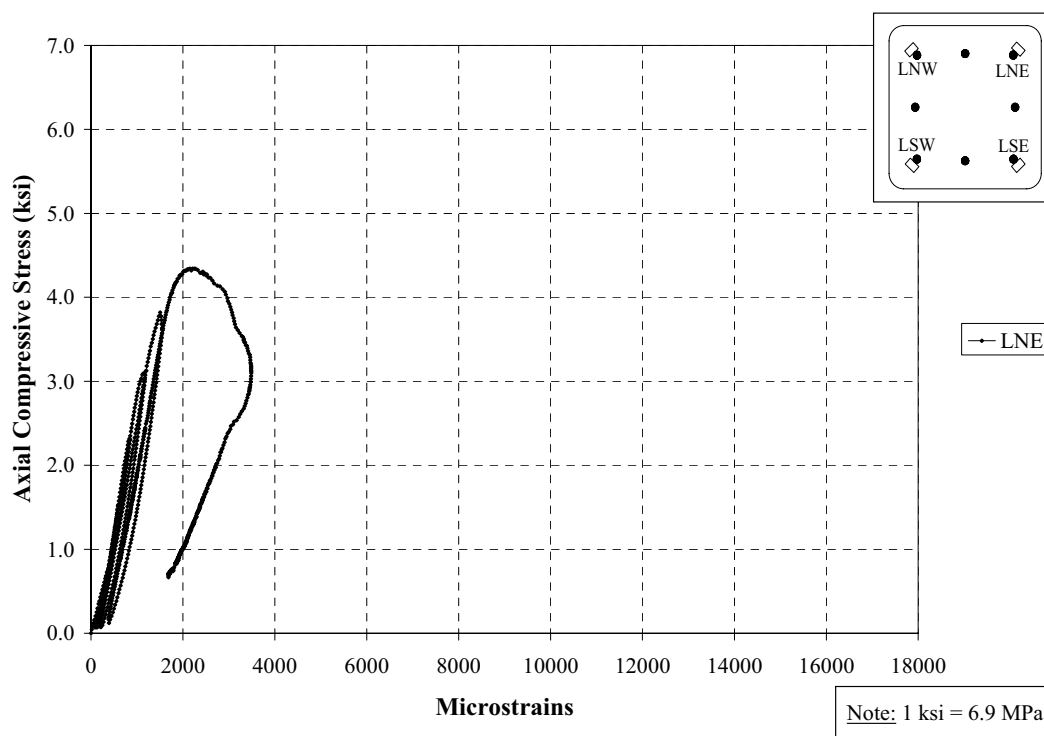


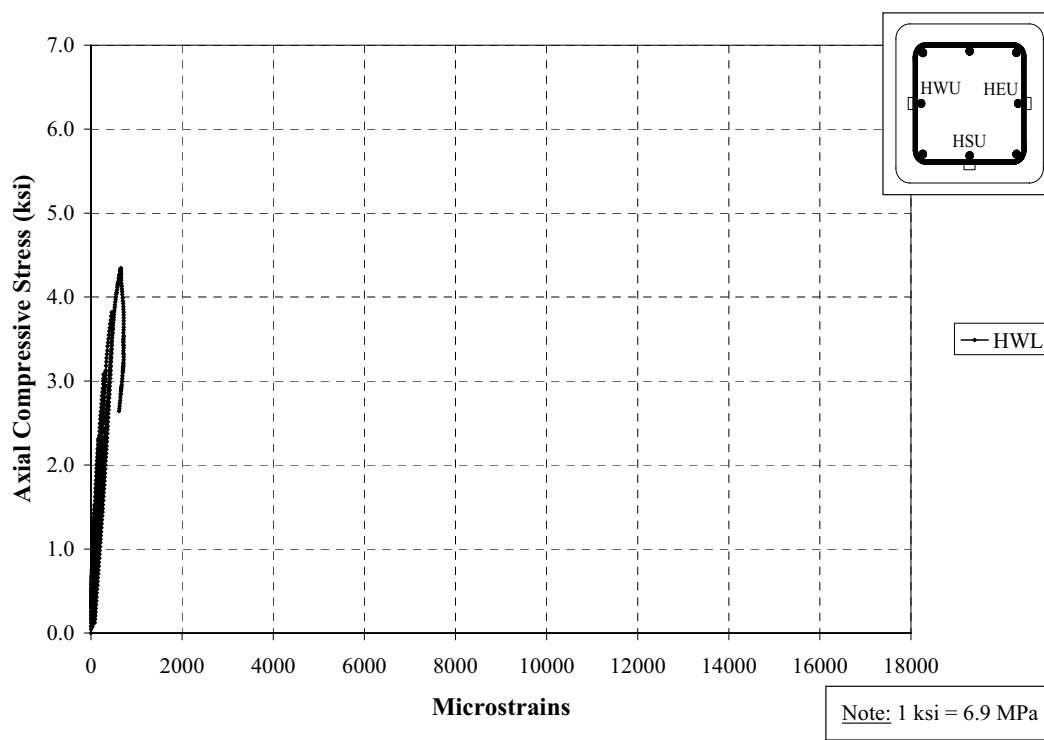**Figure D32. Axial Stress vs. Axial Strain on Longitudinal Bars (East); Specimen B2**
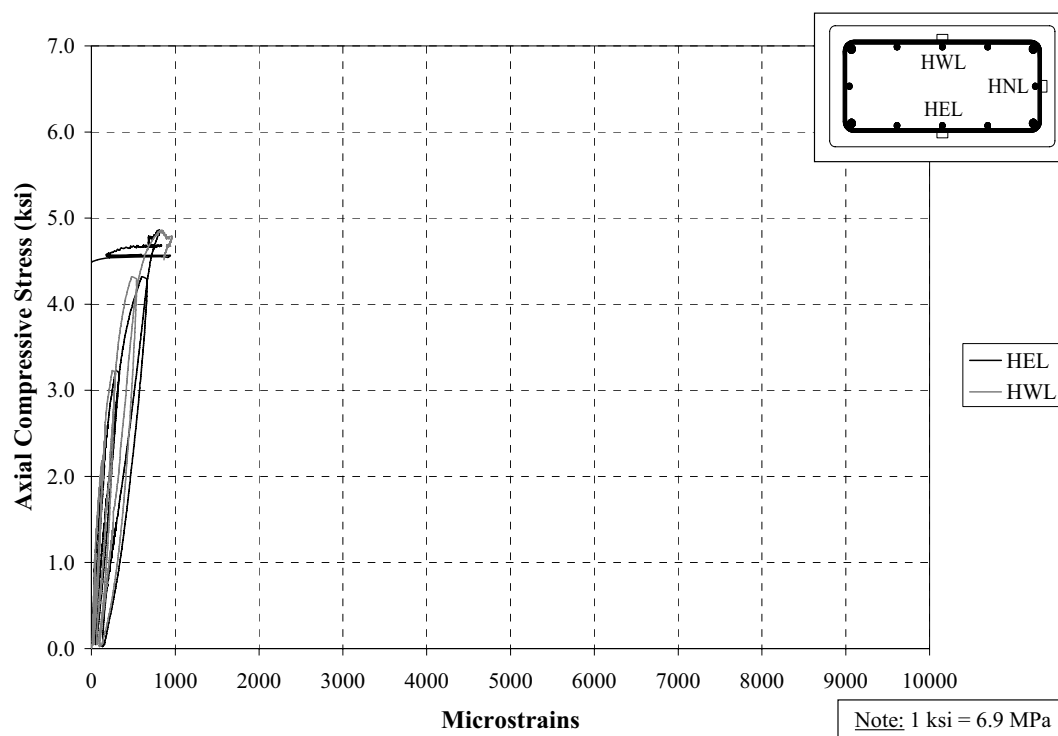
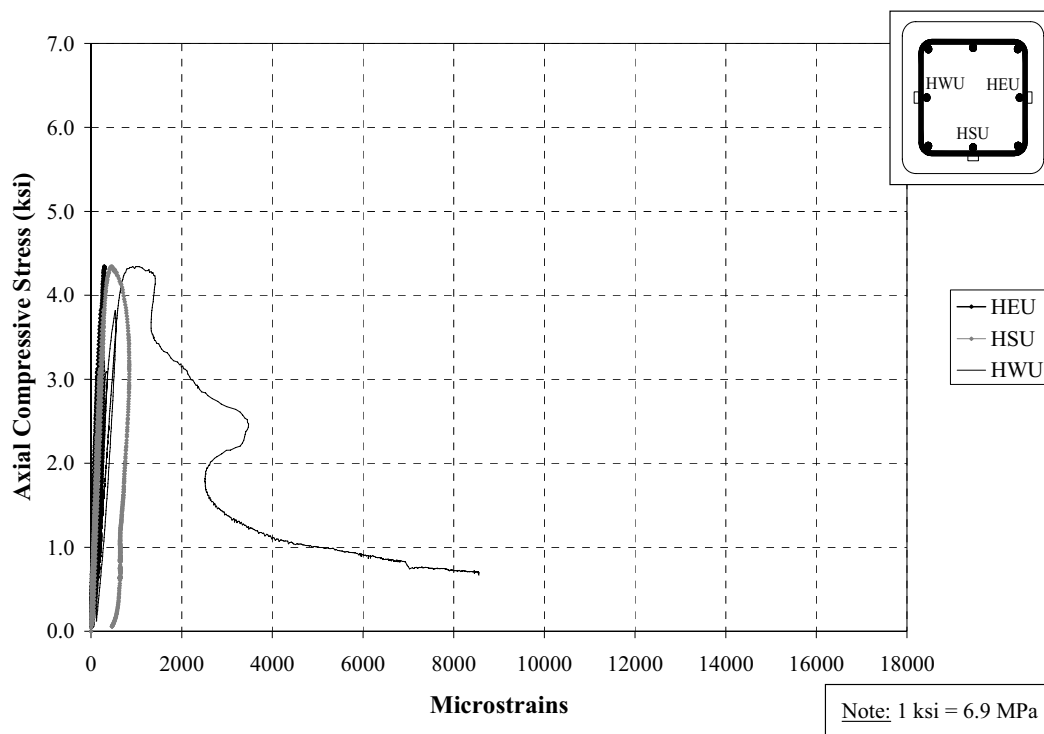**Figure D33.  Axial Stress vs. Transverse Strain on Lower Tie; Specimen B2**
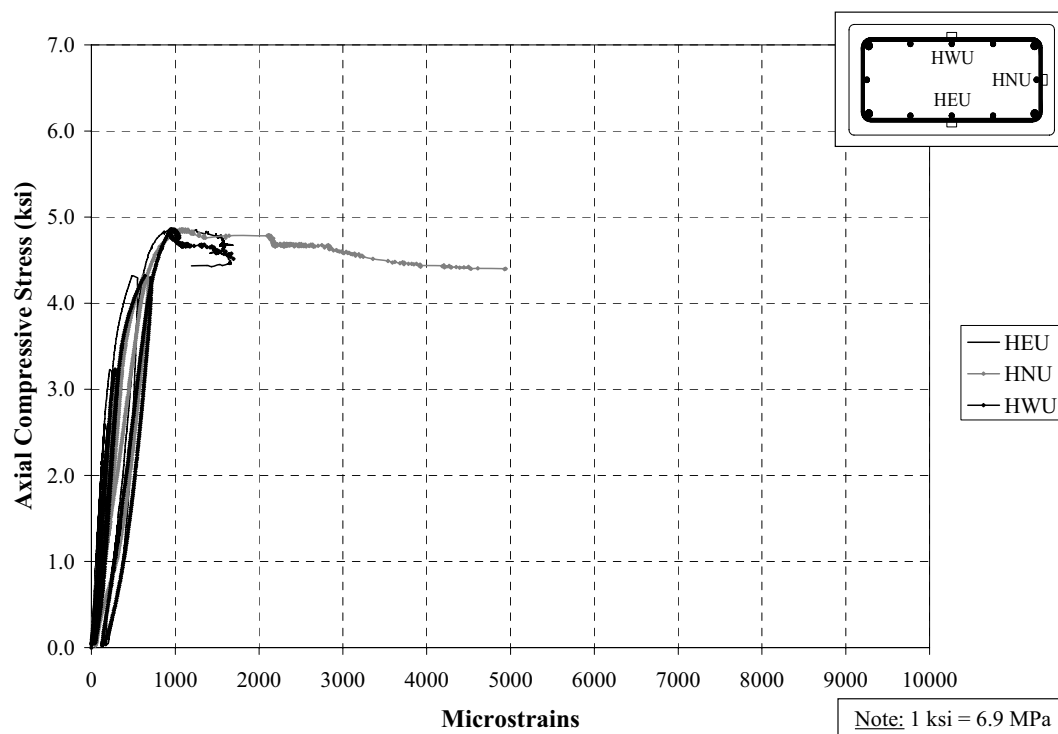


**Figure D34.  Axial Stress vs. Transverse Strain on Upper Tie; Specimen B2**
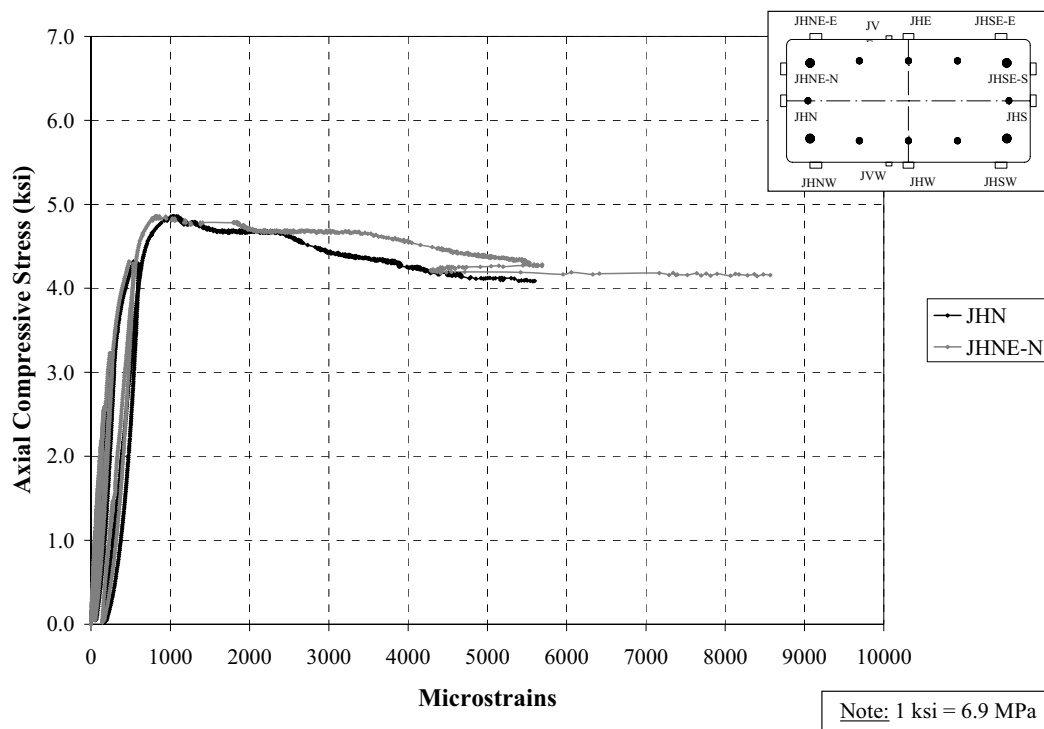
**Figure D35.  Axial Stress vs. Transverse Strain on FRP (North); Specimen B2**
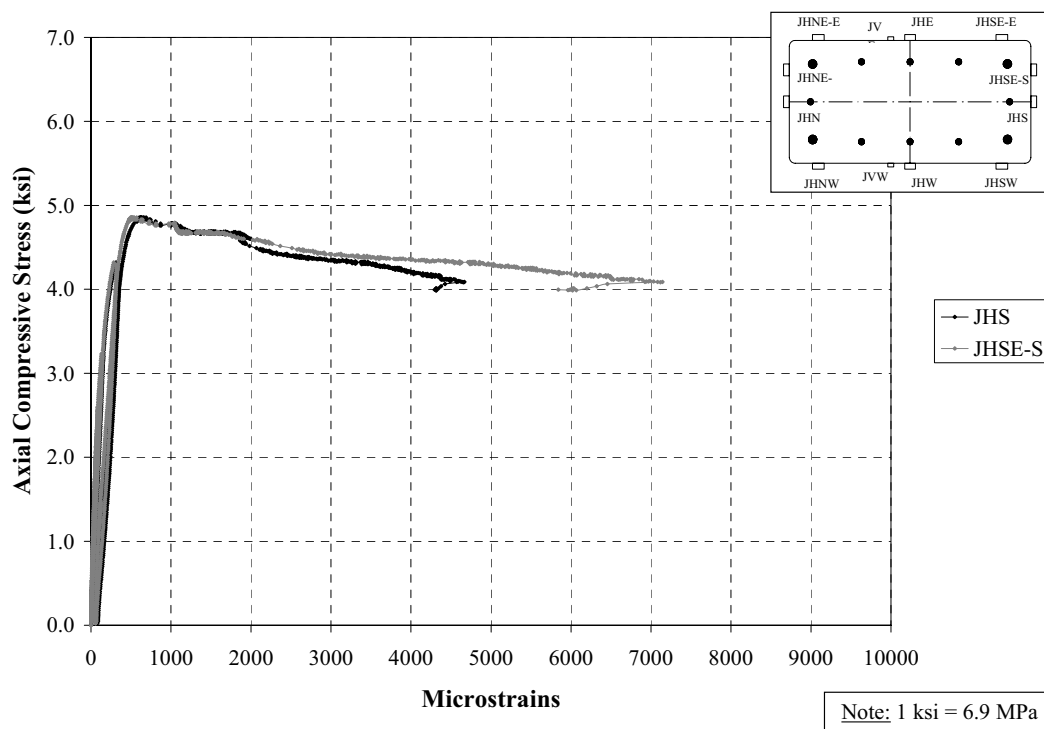


**Figure D36.  Axial Stress vs. Transverse Strain on FRP (South); Specimen B2**
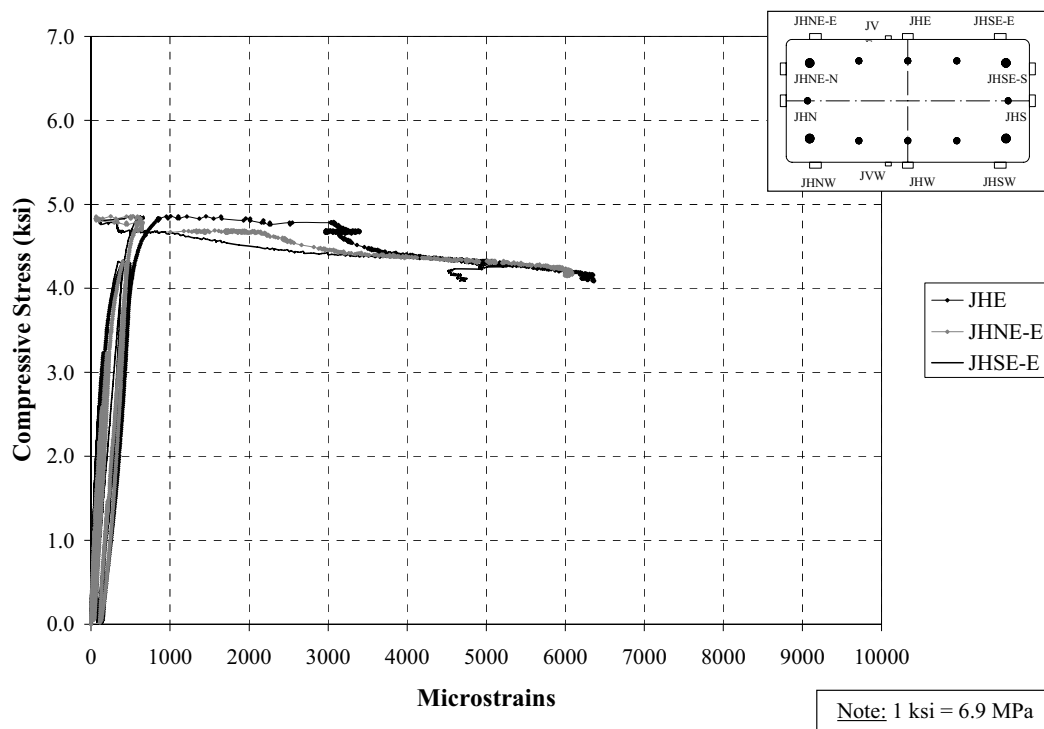
**Figure D37. Axial Stress vs. Transverse Strain on FRP (East); Specimen B2**
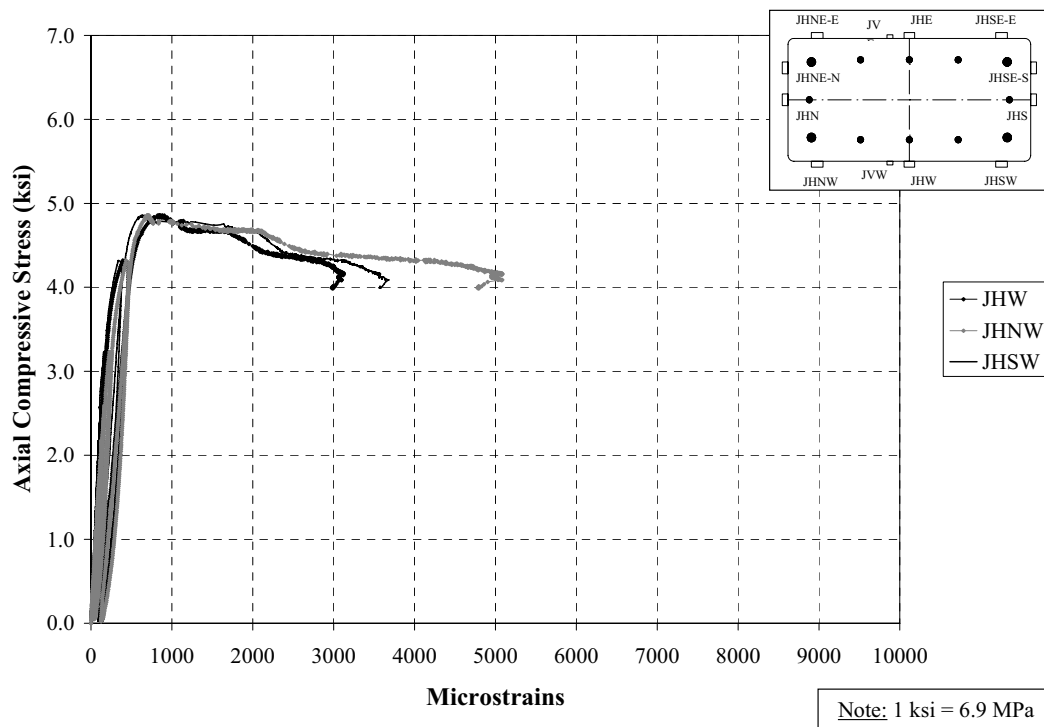


**Figure D38. Axial Stress vs. Transverse Strain on FRP (West); Specimen B2**
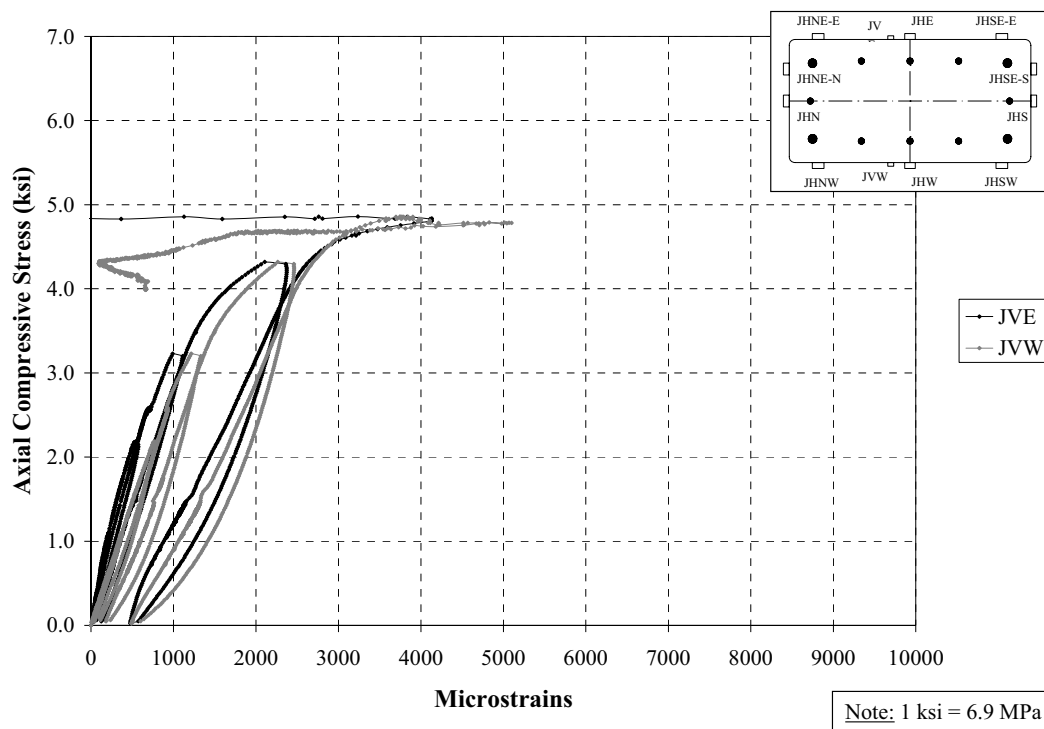
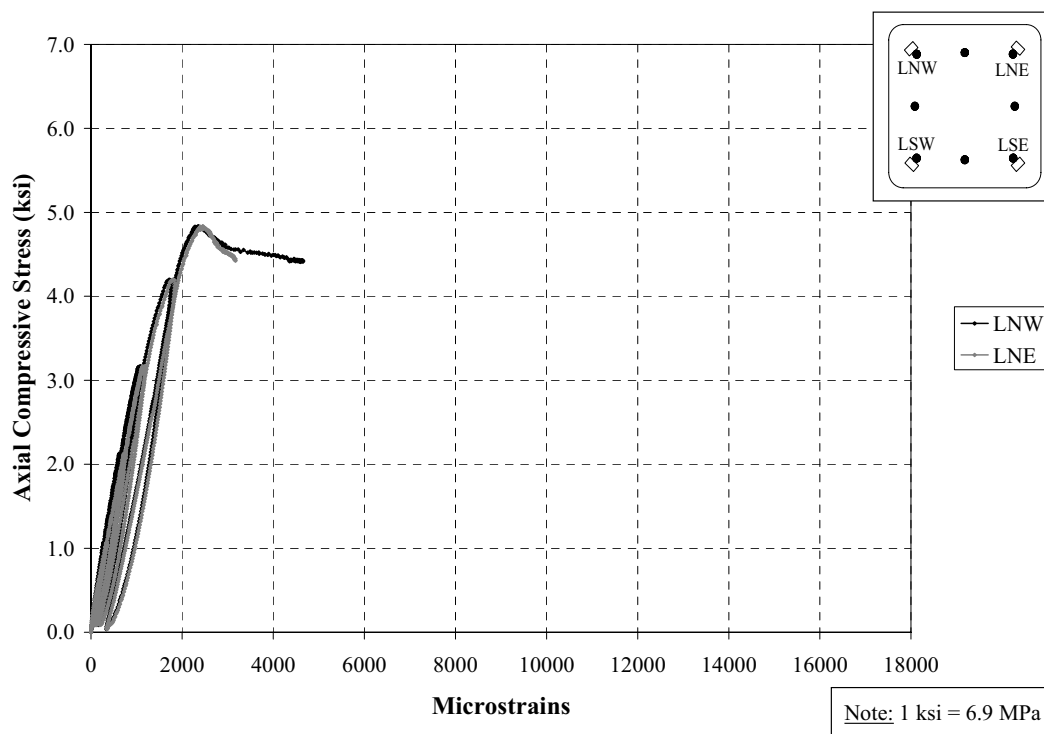**Figure D39.  Axial Stress vs. Axial Strain (Sensors on Vertical Direction); Specimen B2**
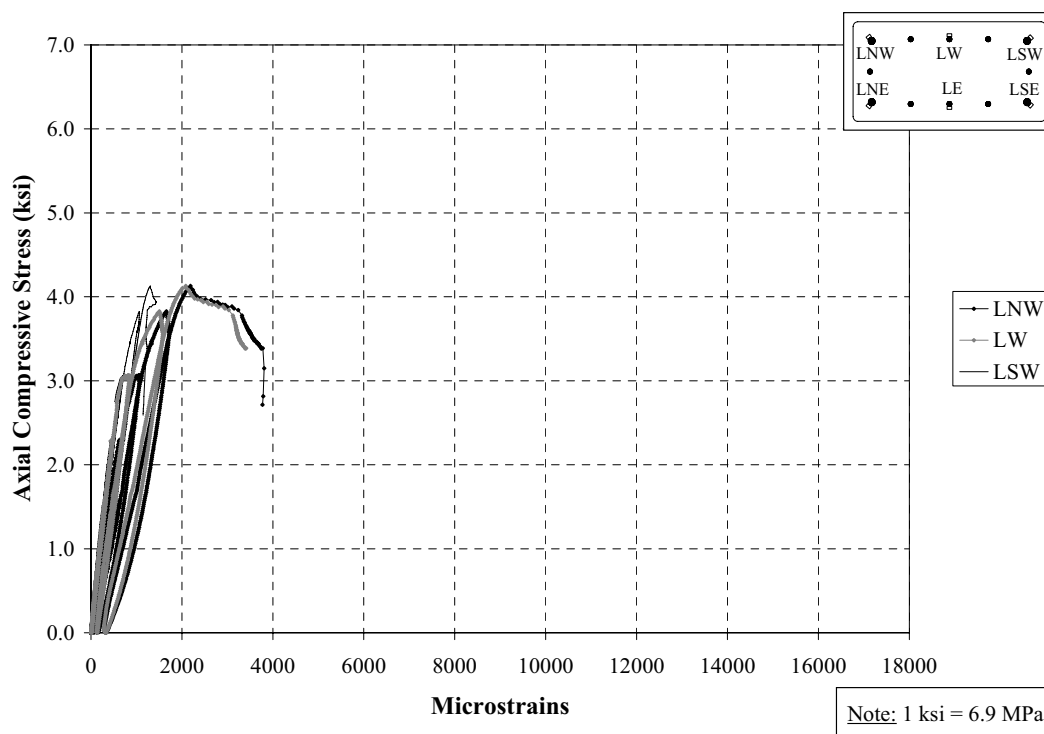


**Figure D40.  Axial Stress vs. Axial Strain on Longitudinal Bars (West); Specimen B3**
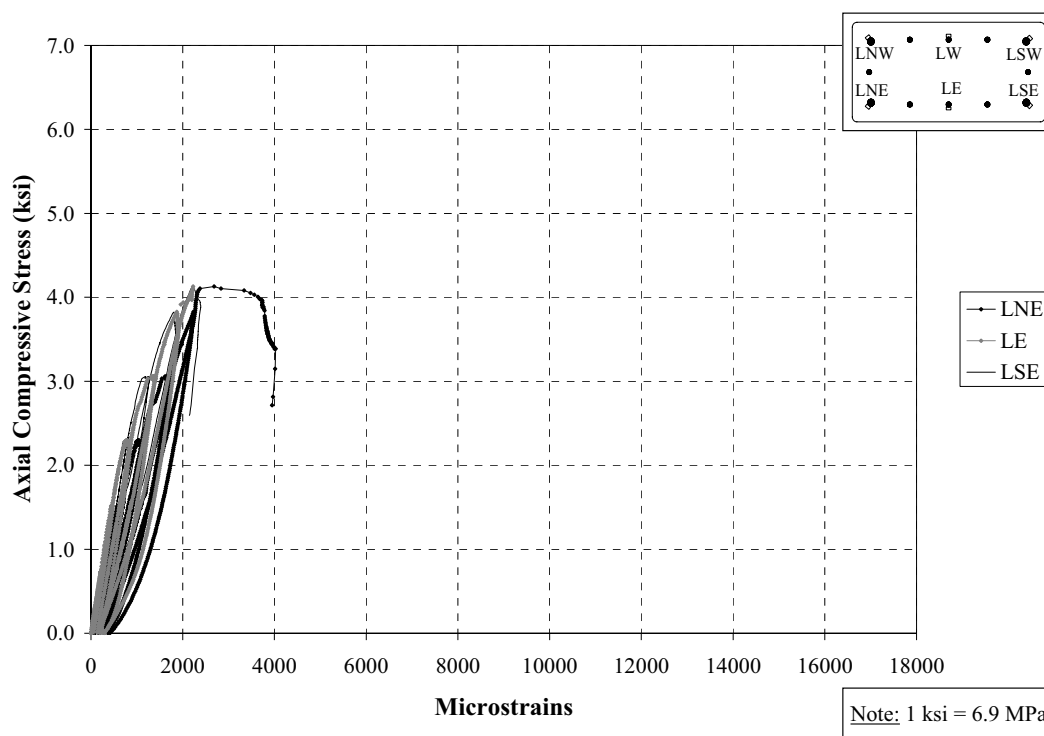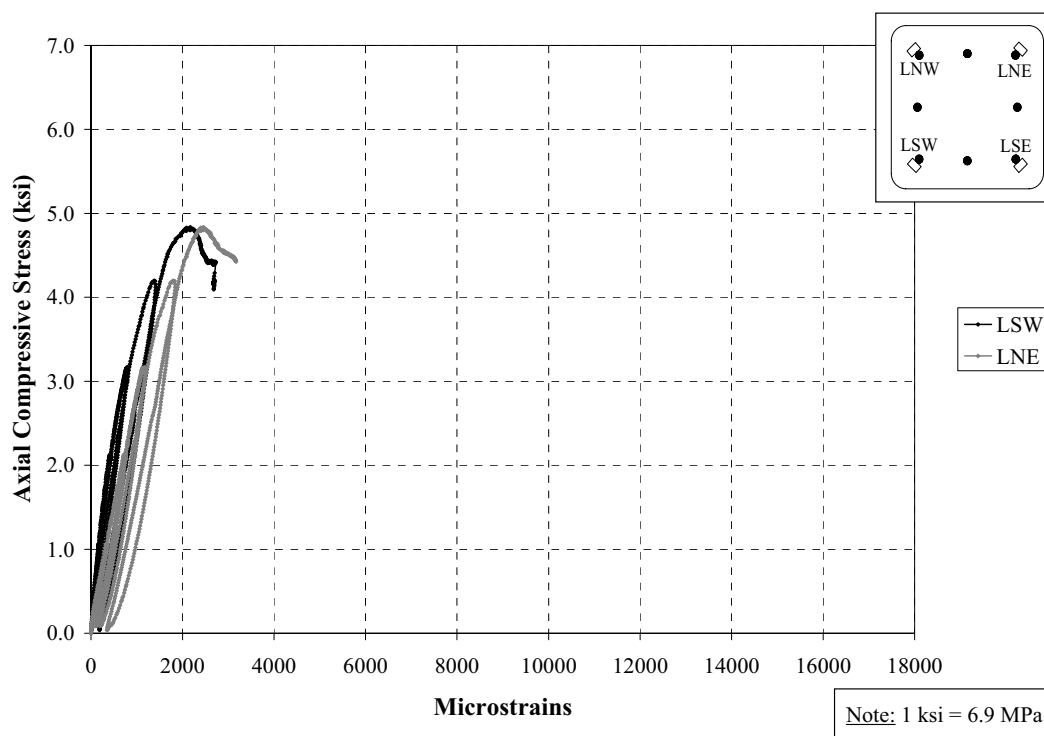
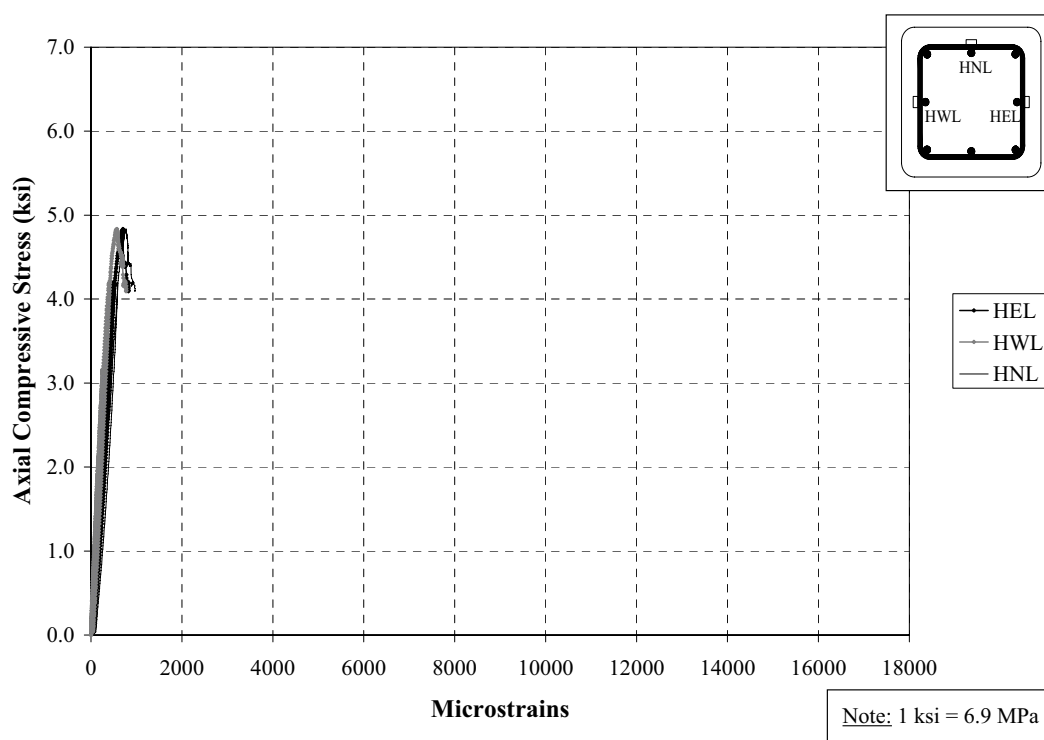**Figure D41. Axial Stress vs. Axial Strain on Longitudinal Bars (East); Specimen B3**
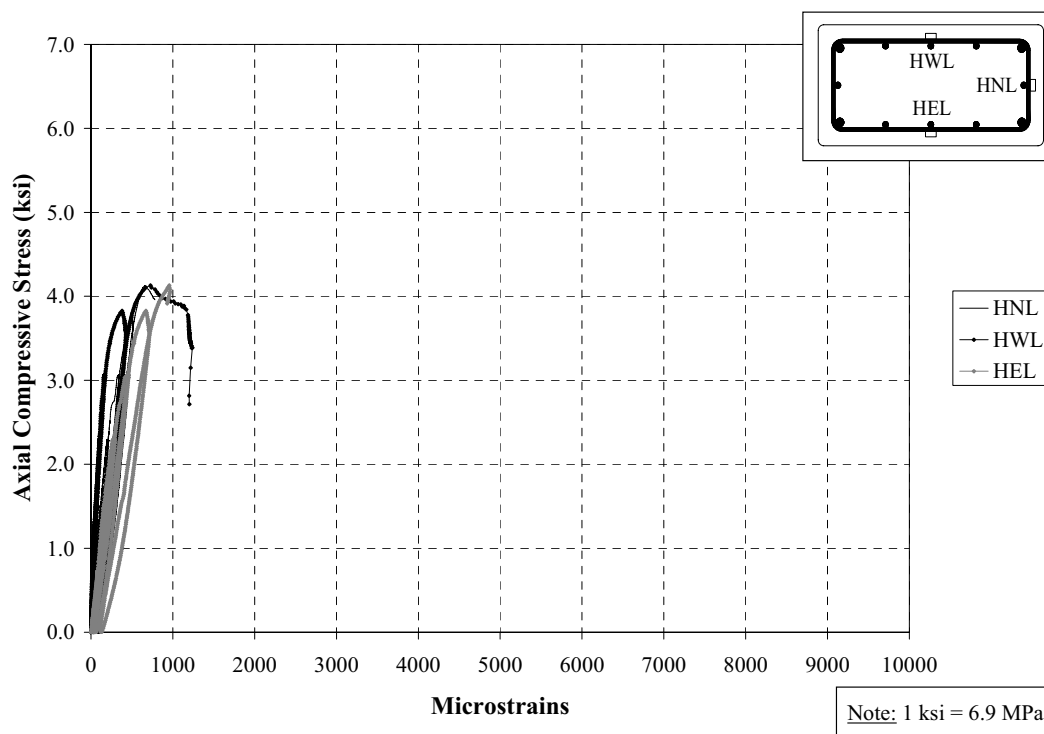


**Figure D42. Axial Stress vs. Transverse Strain on Lower Tie; Specimen B3**
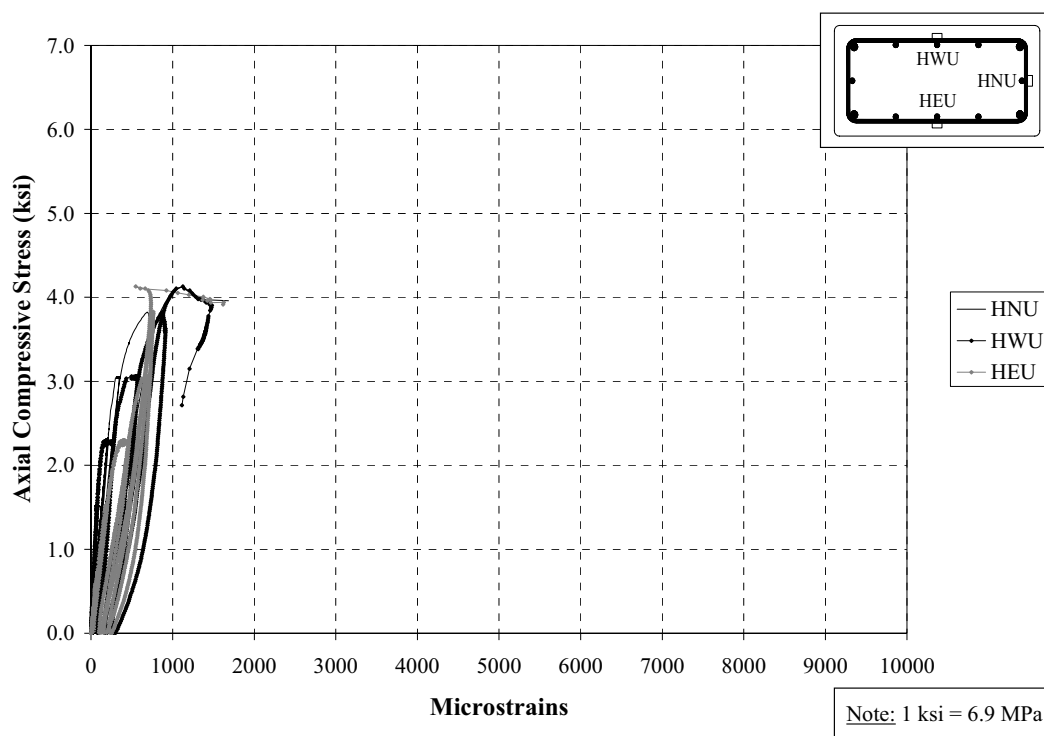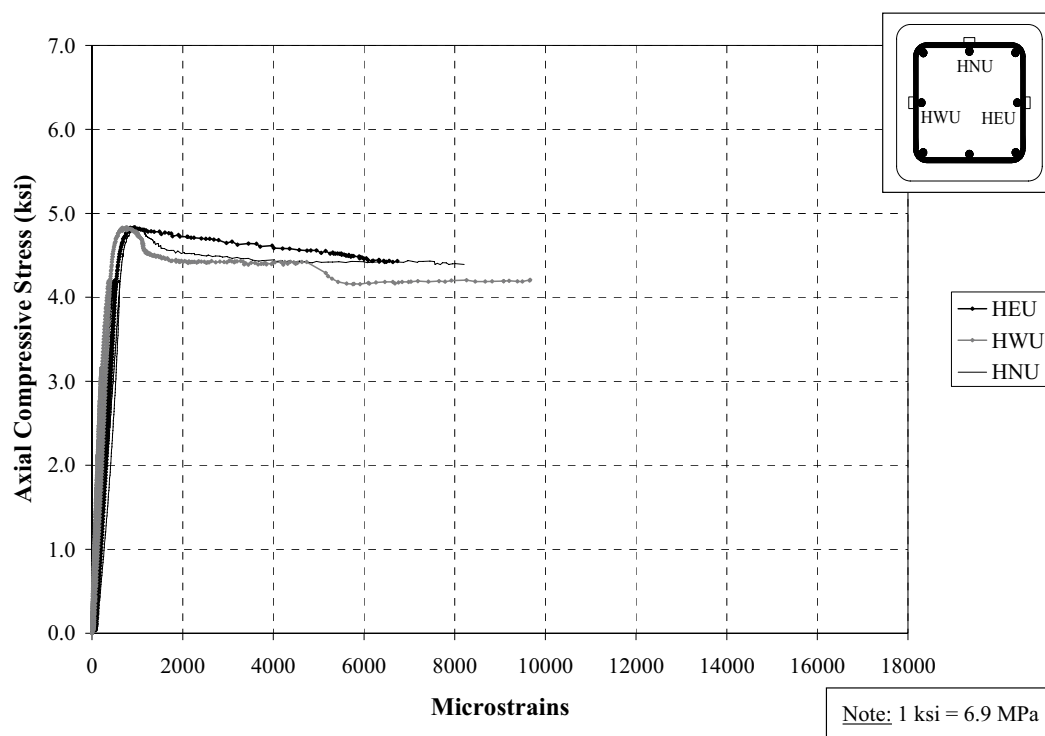
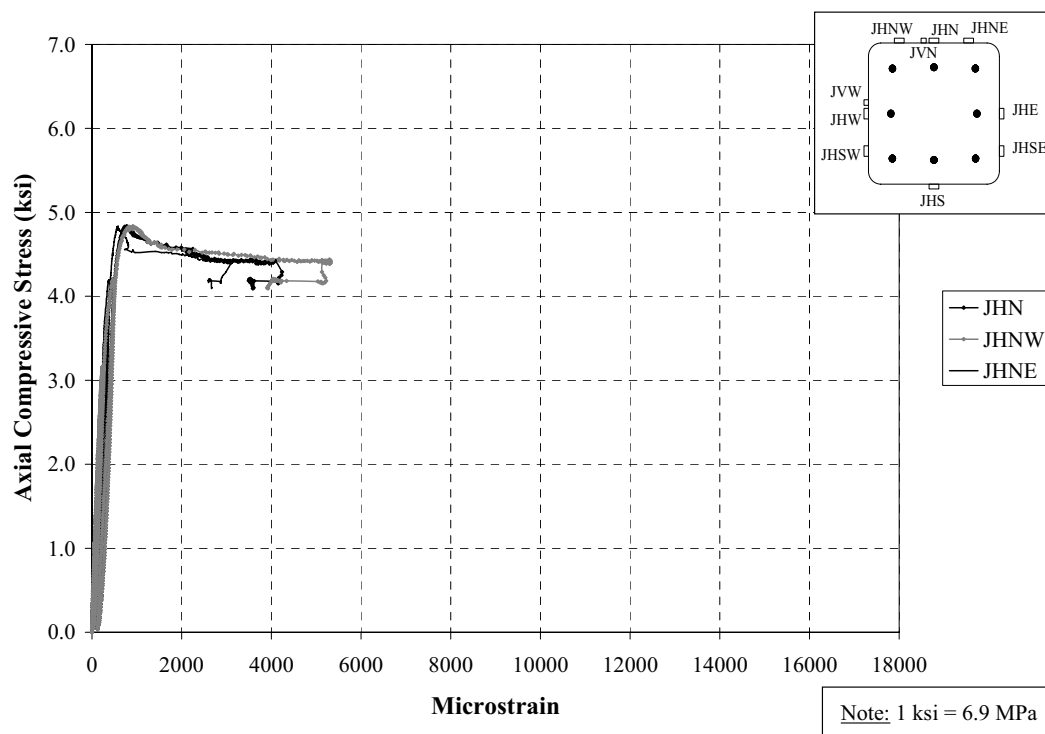**Figure D43.  Axial Stress vs. Transverse Strain on Upper Tie; Specimen B3**
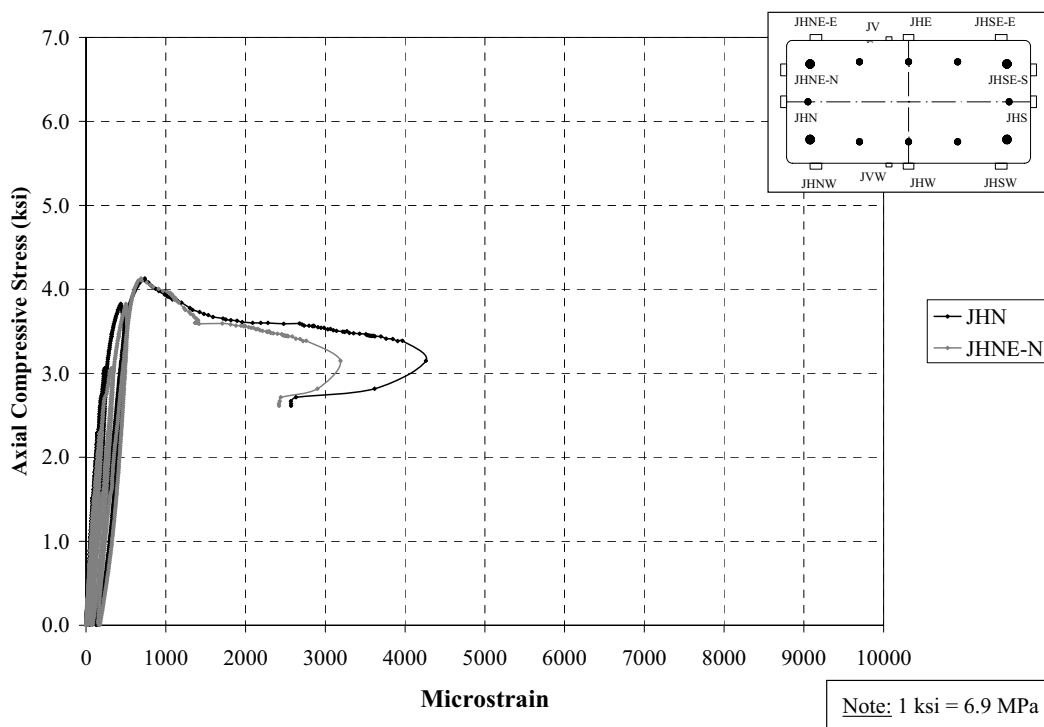


**Figure D44.  Axial Stress vs. Transverse Strain on FRP (North); Specimen B3**
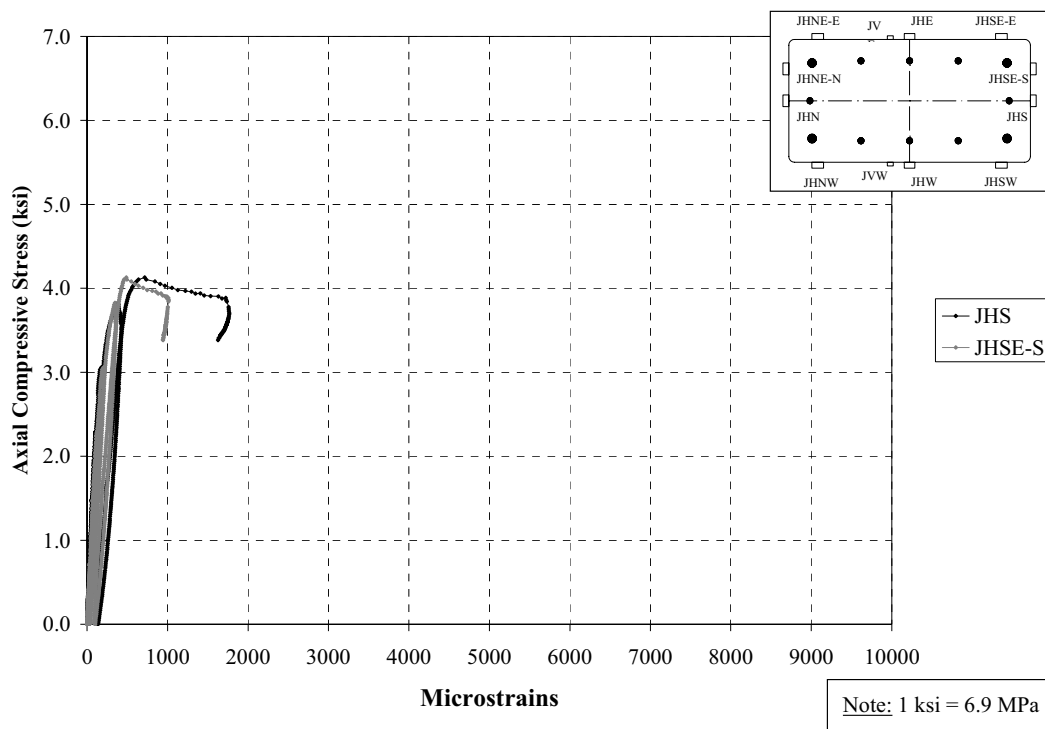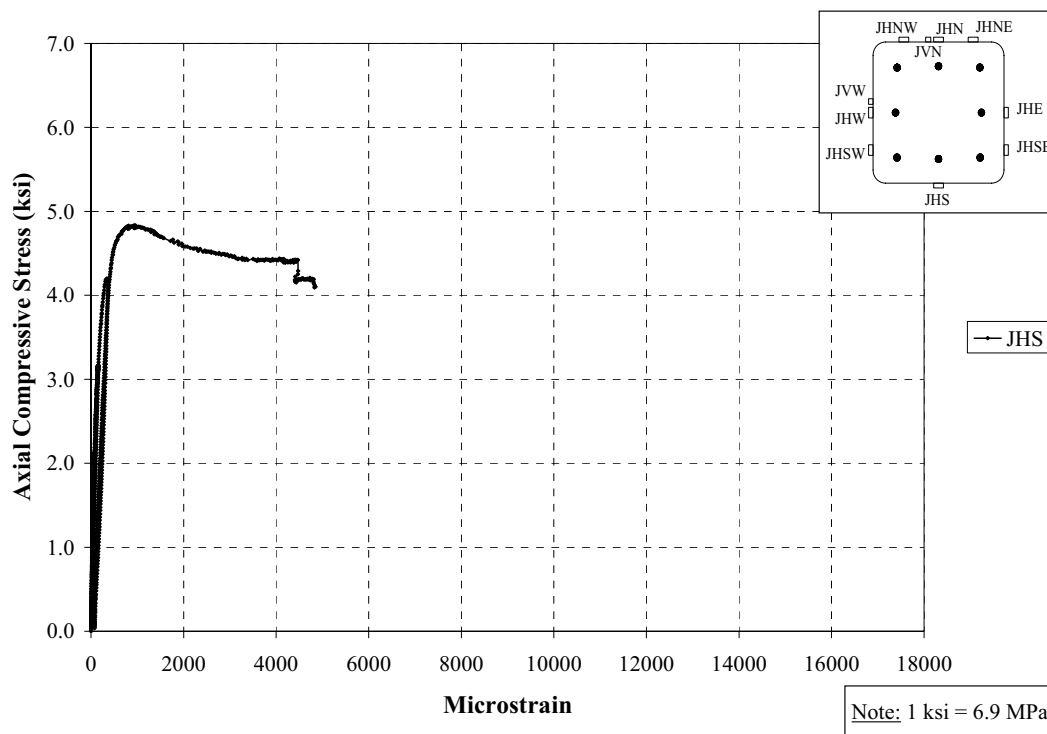
Figure D45.  Axial Stress vs. Transverse Strain on FRP (South); Specimen B3
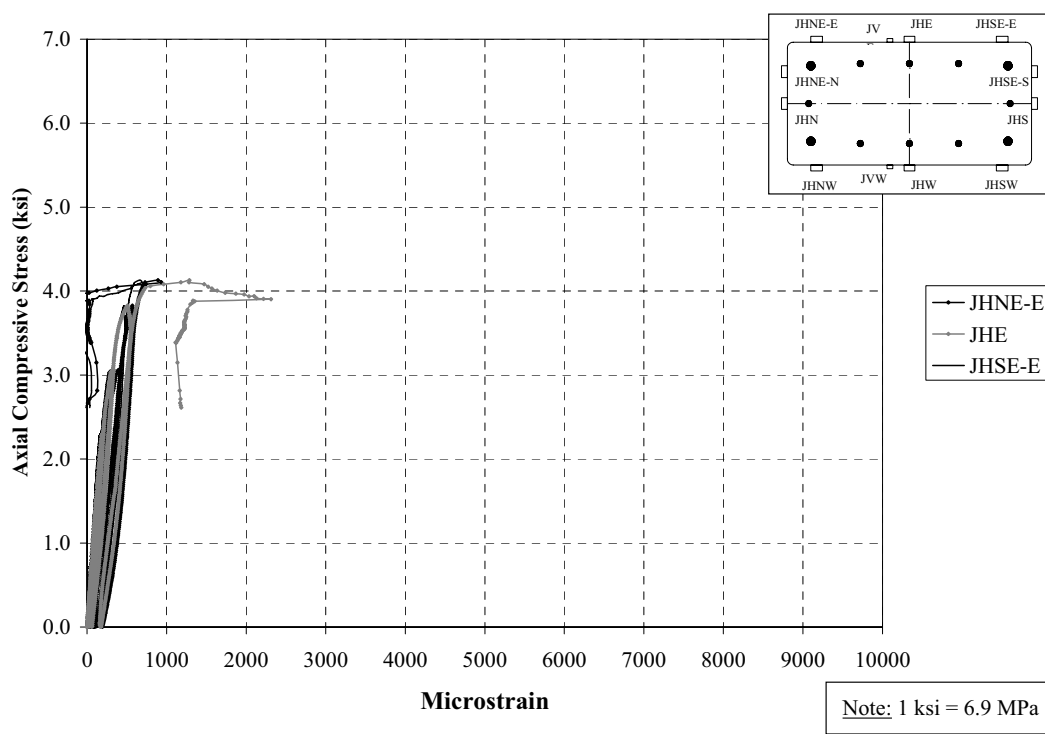


Figure D46.  Axial Stress vs. Transverse Strain on FRP (East); Specimen B3
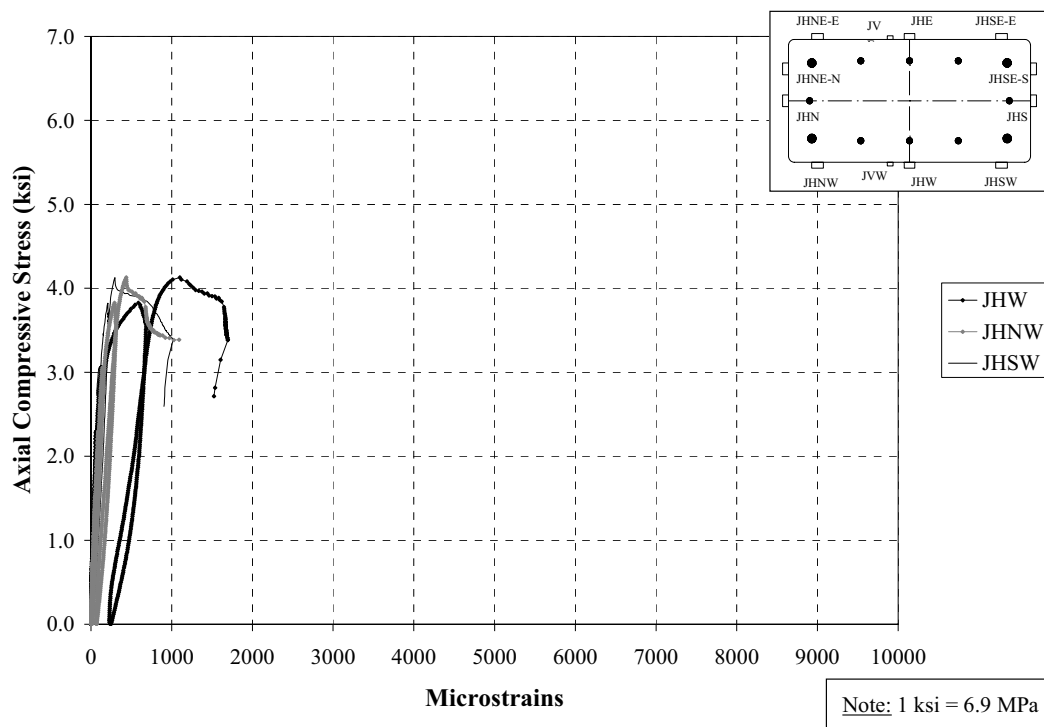
**Figure D47.  Axial Stress vs. Transverse Strain on FRP (West); Specimen B3**
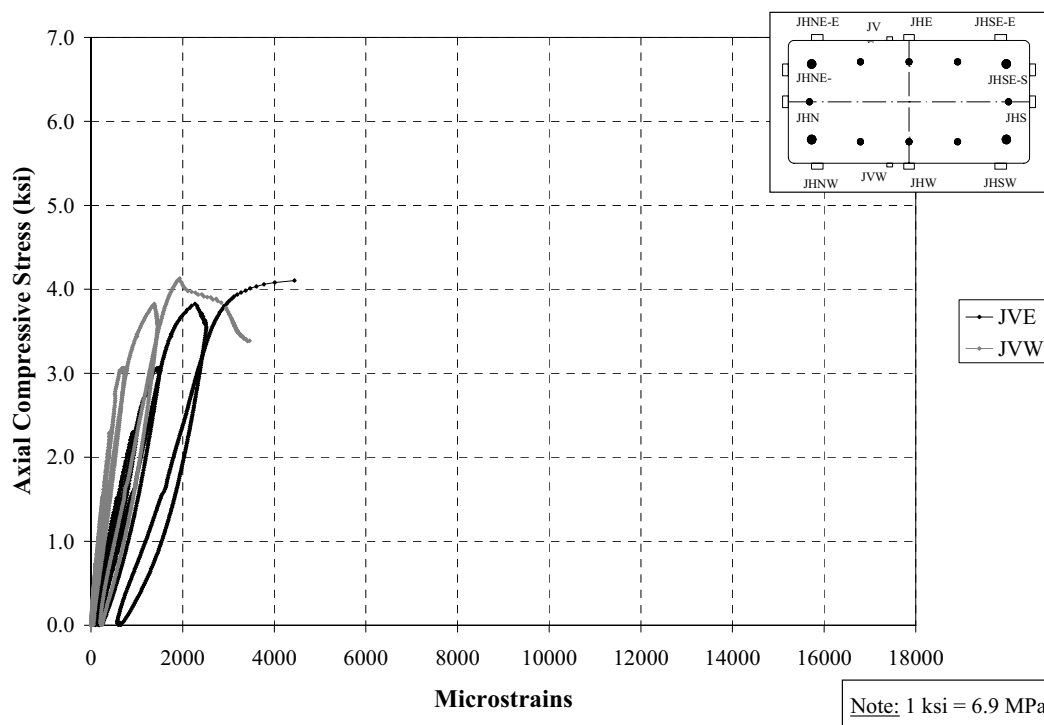


**Figure D48.  Axial Stress vs. Axial Strain on FRP (Sensors on Vertical Direction); Specimen B3**
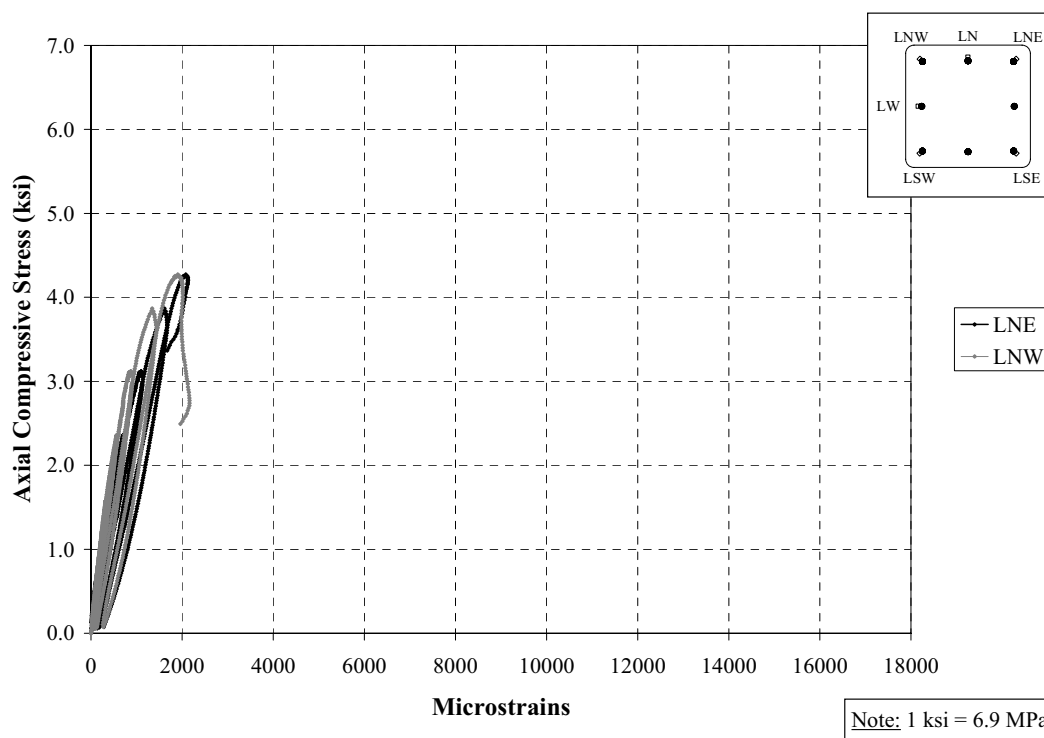
**Figure D49. Axial Stress vs. Axial Strain on Longitudinal Bars (North); Specimen C1**
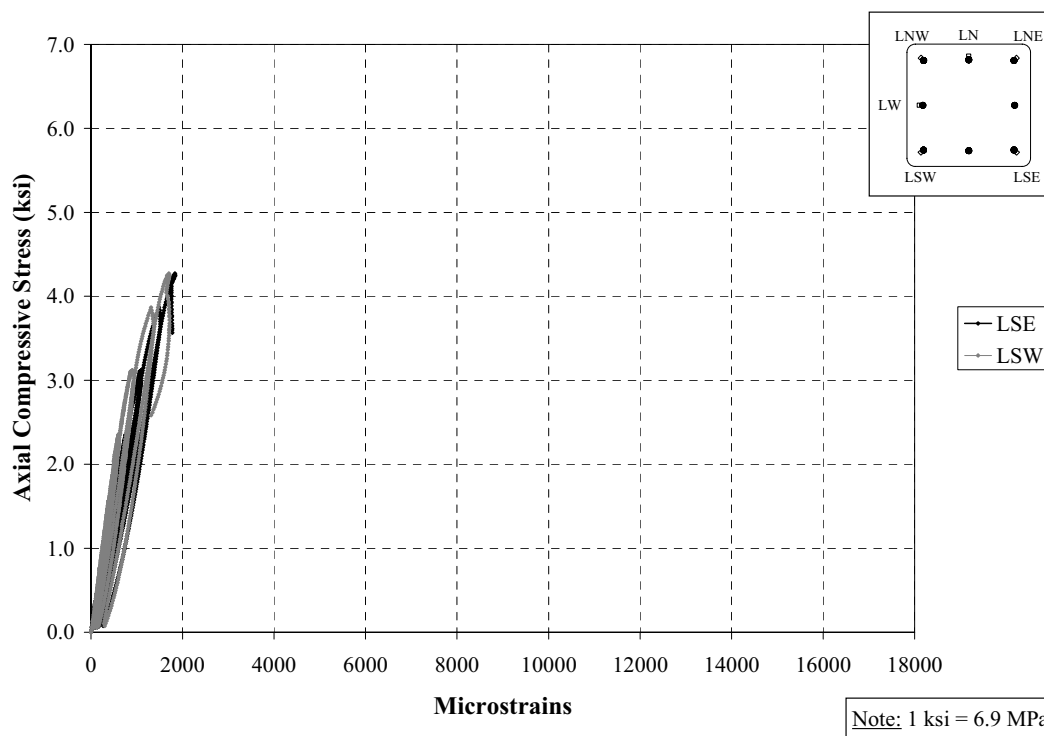


**Figure D50. Axial Stress vs. Axial Strain on Longitudinal Bars (South); Specimen C1**
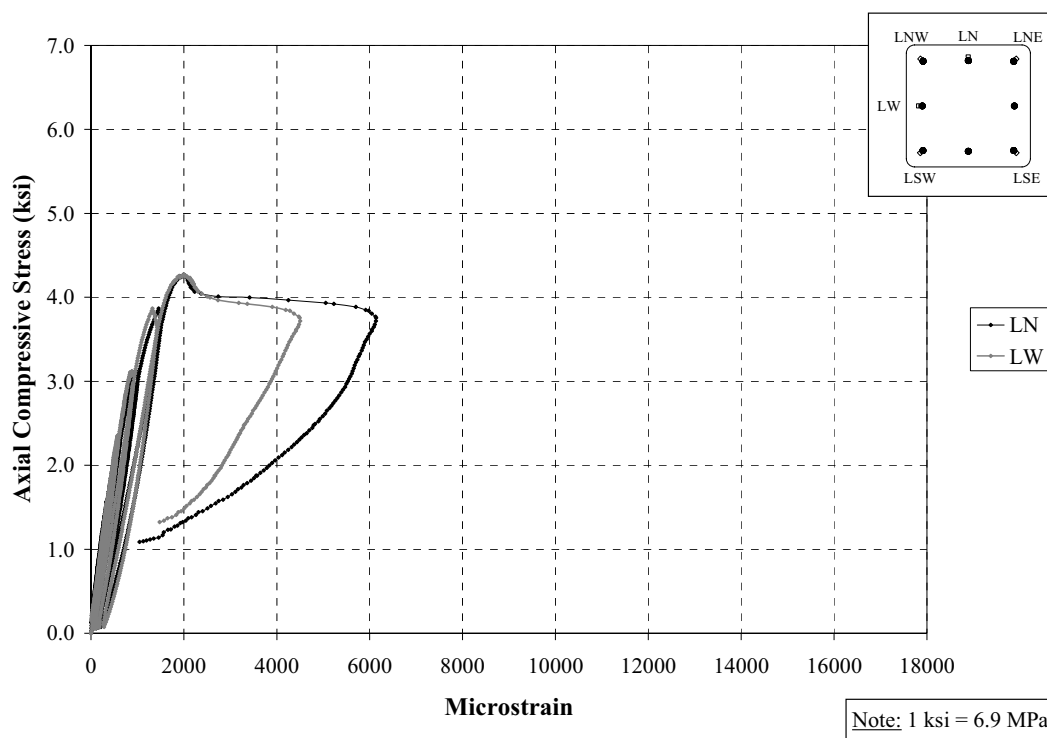
**Figure D51.  Axial Stress vs. Axial Strain on Longitudinal Bars (LN & LW); Specimen C1**
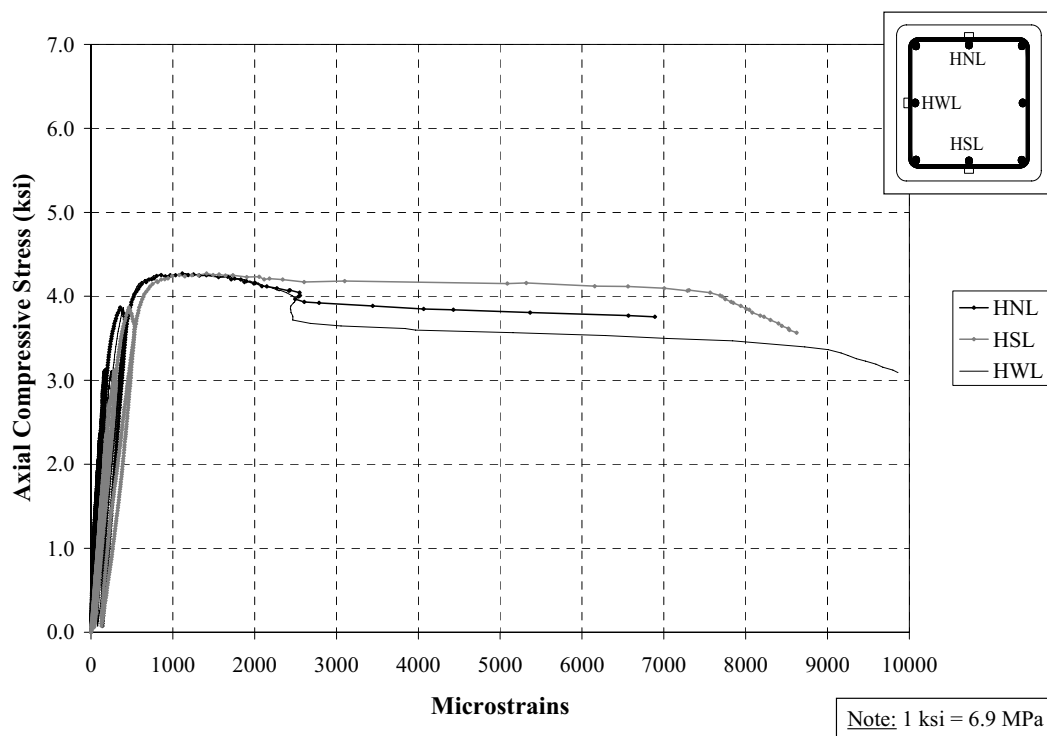


**Figure D52.  Axial Stress vs. Transverse Strain on Lower Tie; Specimen C1**
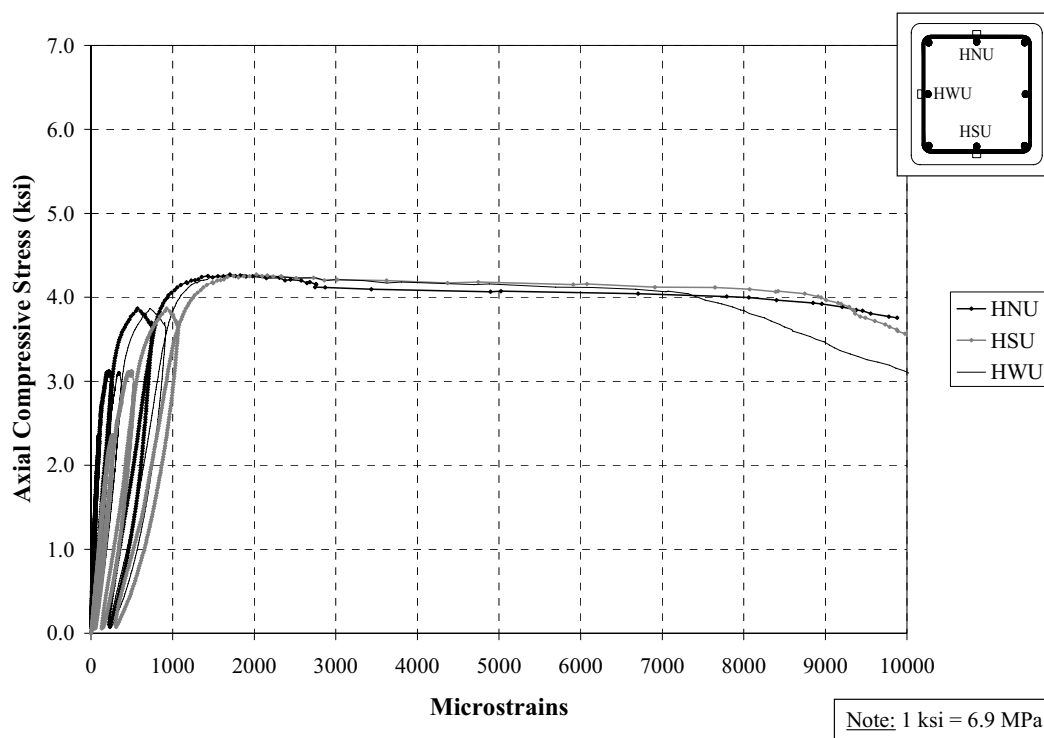
**Figure D53. Axial Stress vs. Transverse Strain on Upper Tie; Specimen C1**
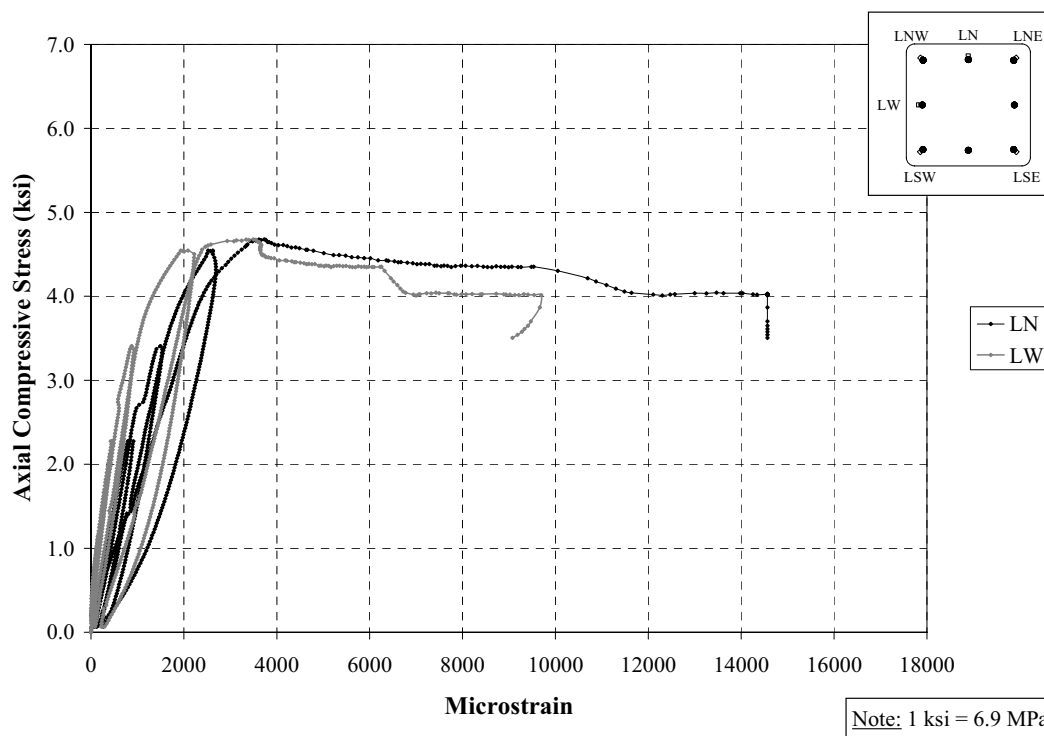


**Figure D54. Axial Stress vs. Axial Strain on Longitudinal Bars (LN & LW); Specimen C2**
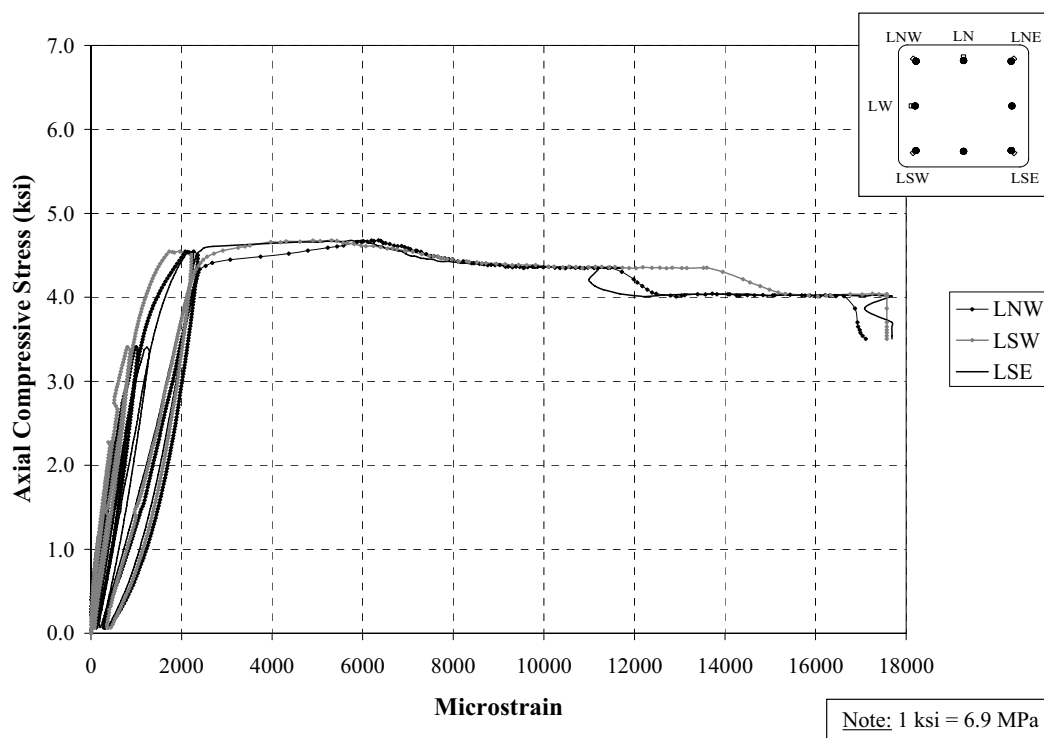
**Figure D55.  Axial Stress vs. Axial Strain on Longitudinal Bars (Corners); Specimen C2**
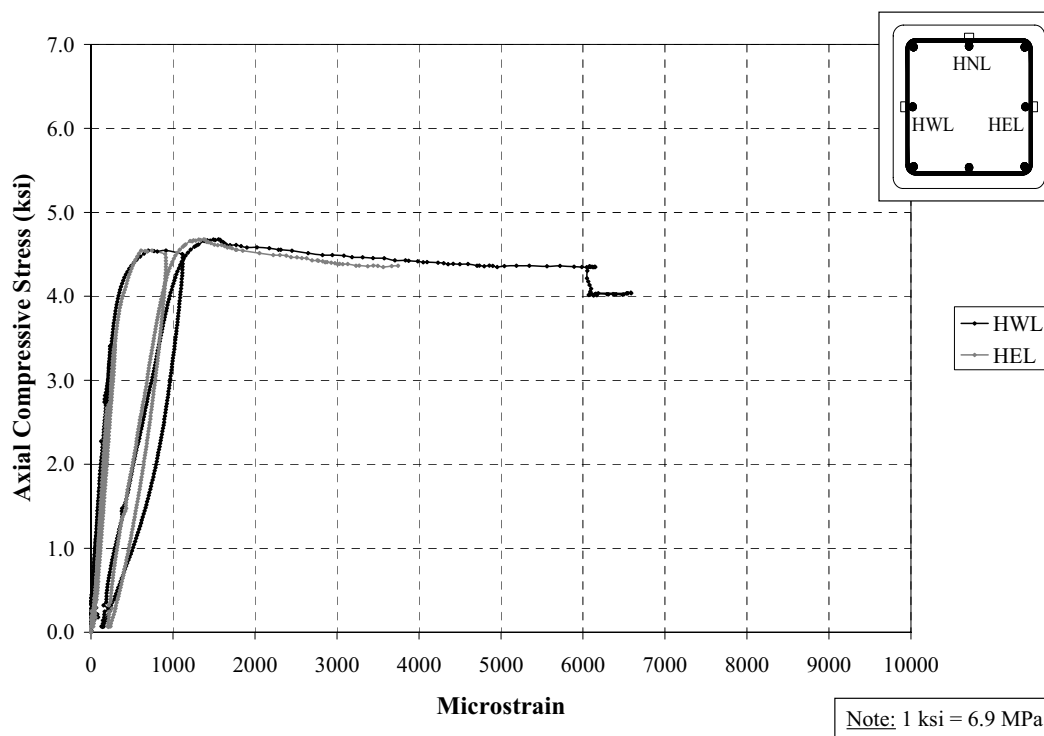


**Figure D56.  Axial Stress vs. Transverse Strain on Lower Tie; Specimen C2**
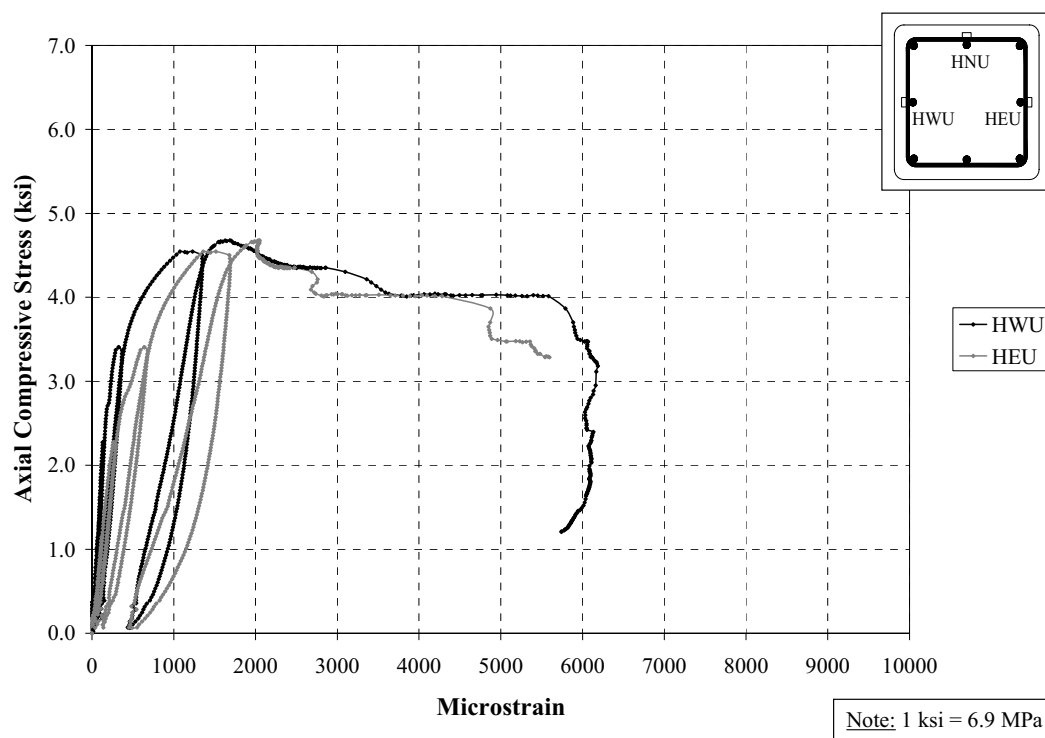
**Figure D57. Axial Stress vs. Transverse Strain on Upper Tie; Specimen C2**
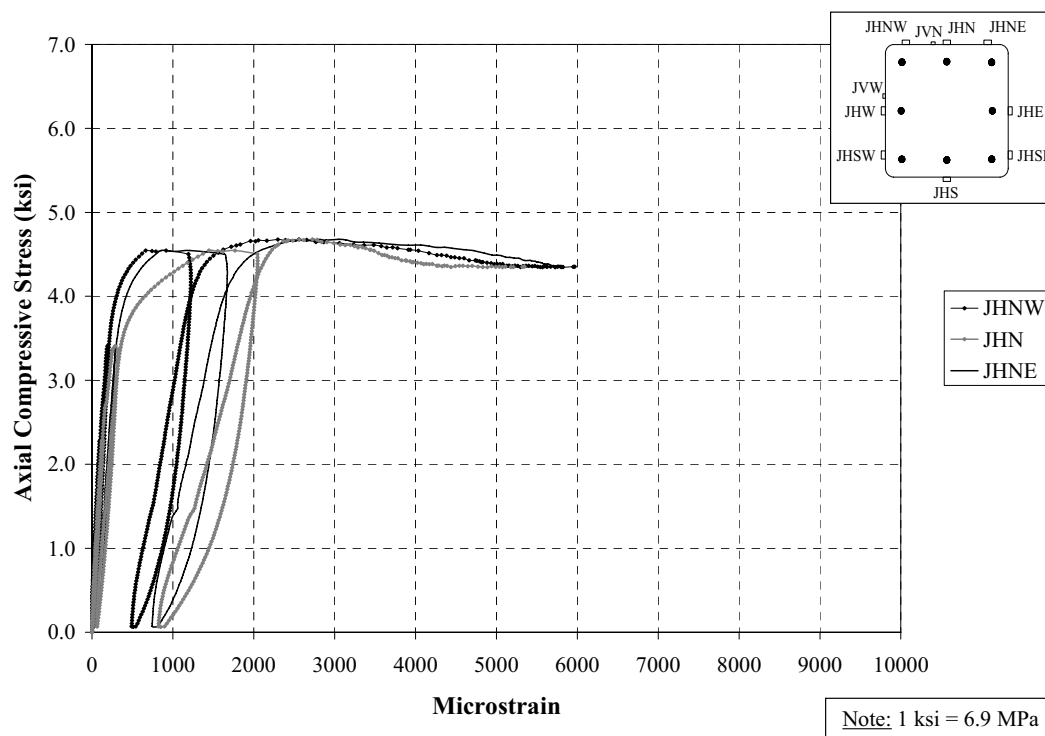


**Figure D58. Axial Stress vs. Transverse Strain on FRP (North); Specimen C2**
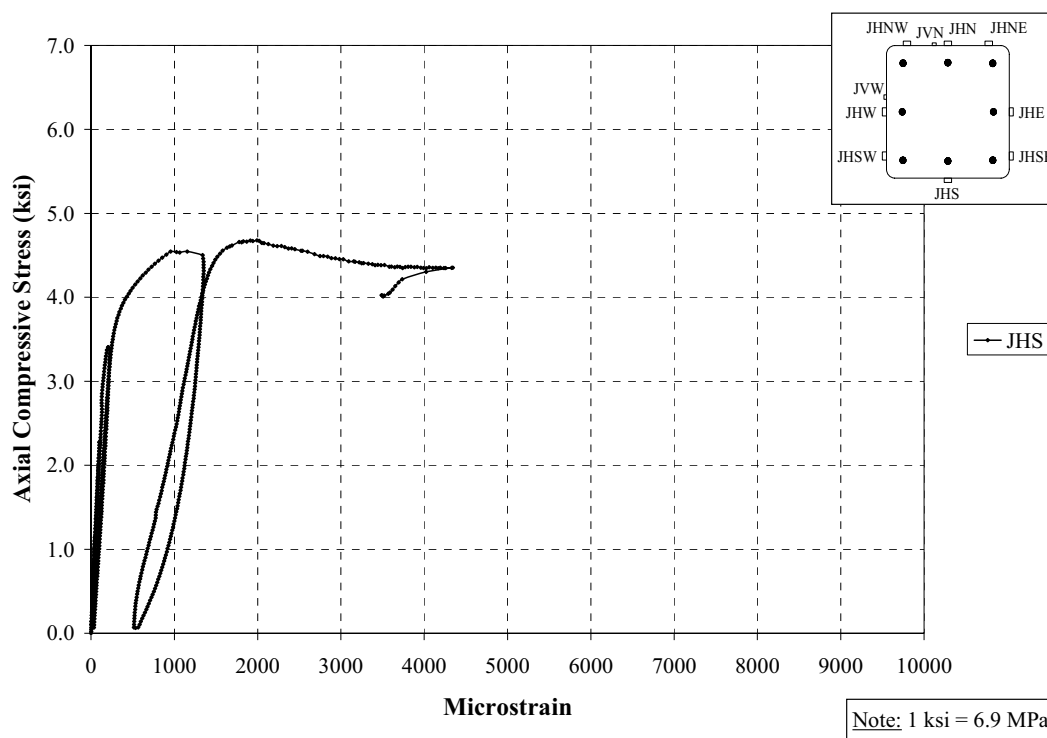
**Figure D59. Axial Stress vs. Transverse Strain on FRP (South); Specimen C2**
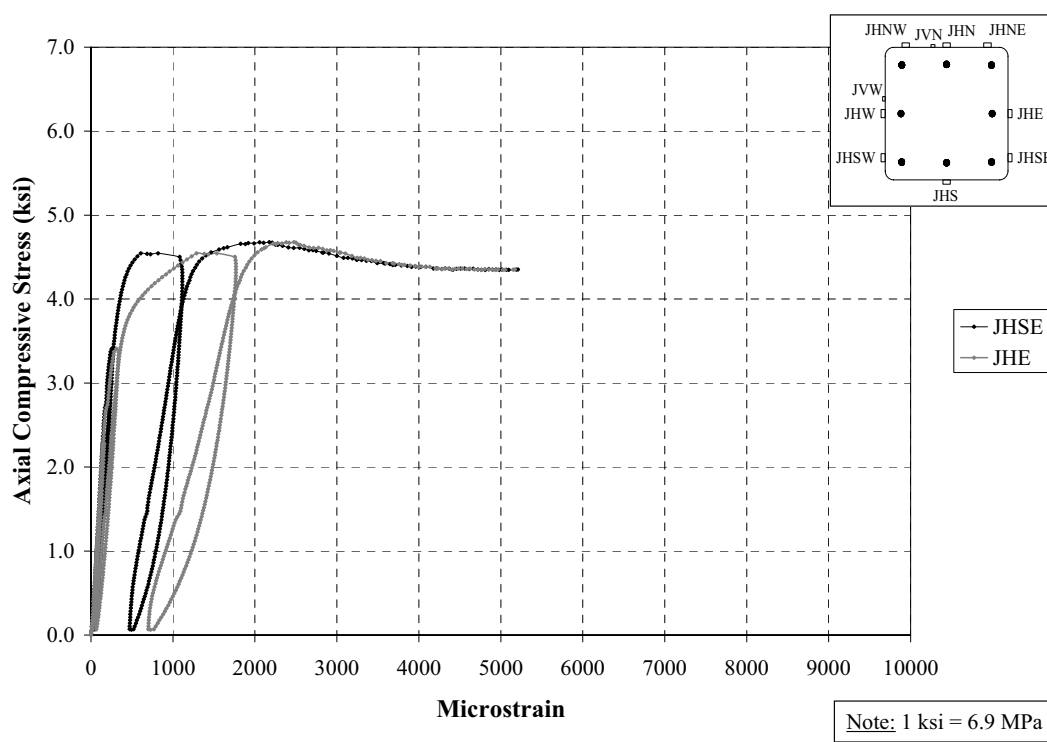


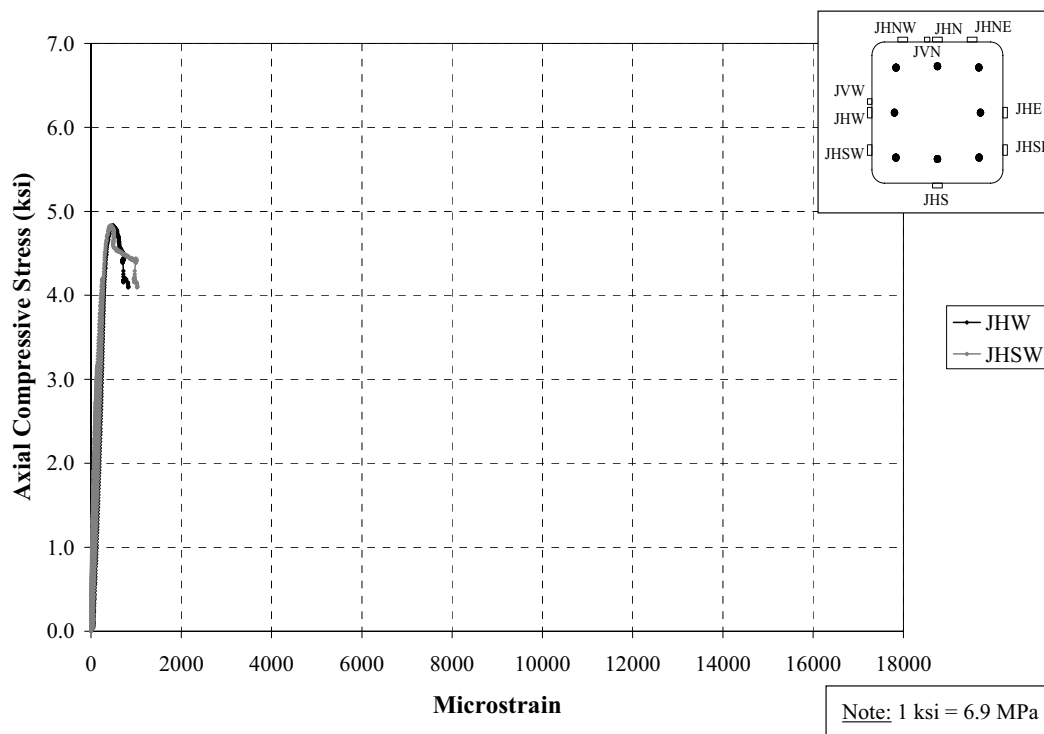**Figure D60. Axial Stress vs. Transverse Strain on FRP (East); Specimen C2**
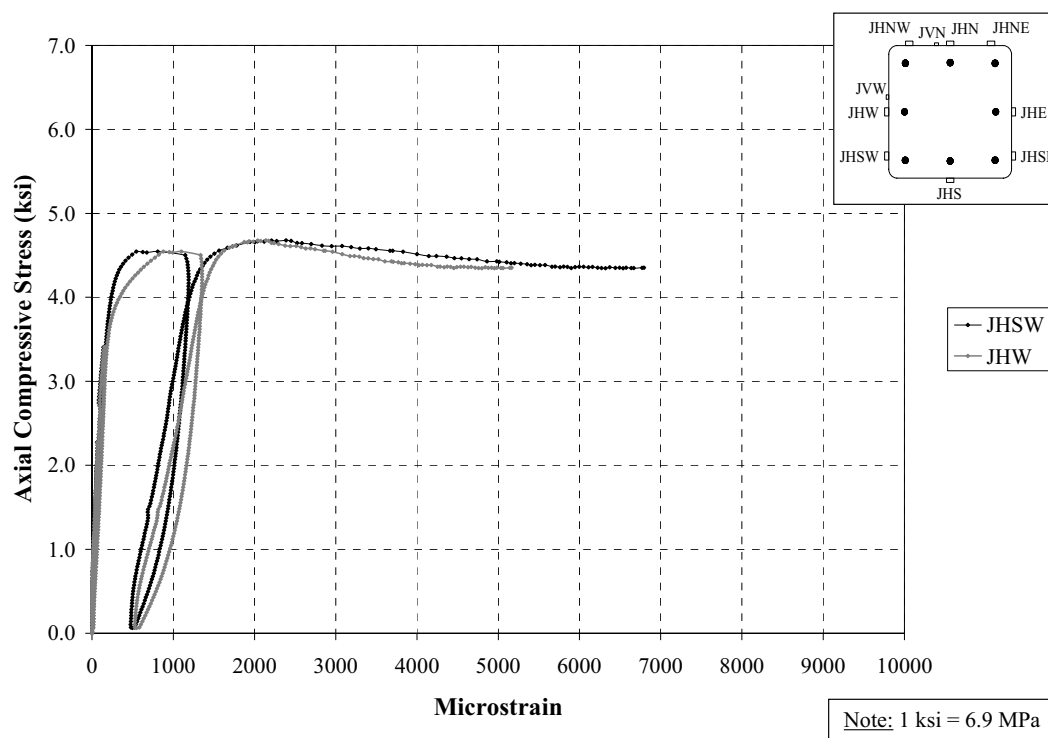
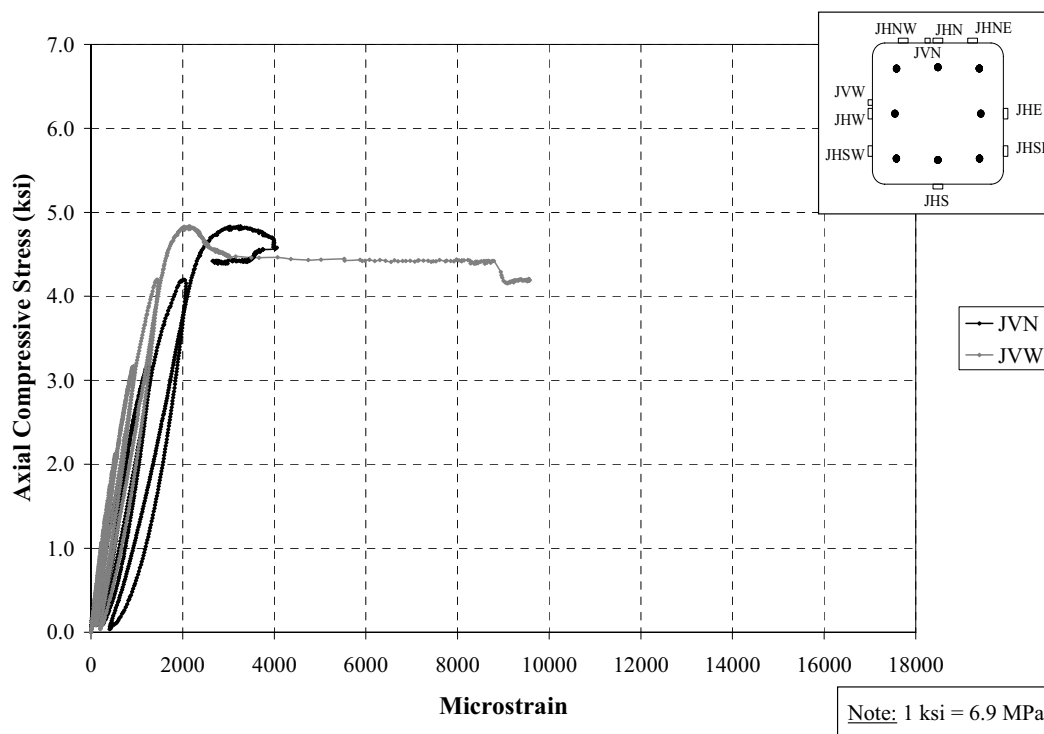**Figure D61. Axial Stress vs. Transverse Strain on FRP (West); Specimen C2**
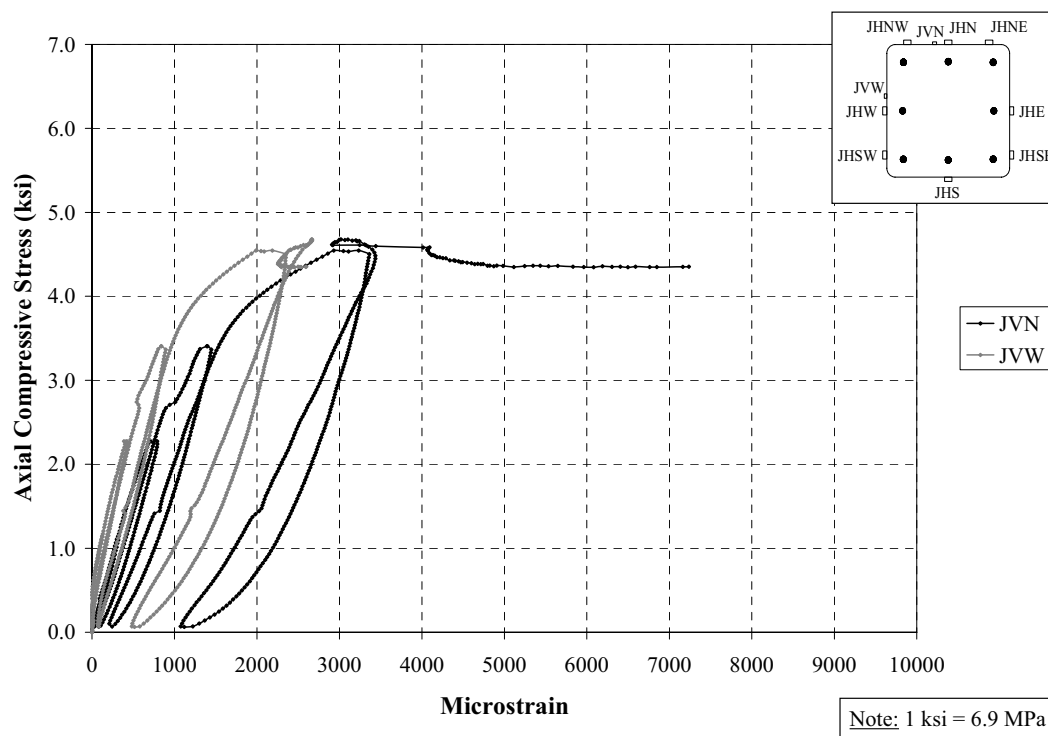


**Figure D62. Axial Stress vs. Axial Strain (Sensors on Vertical Direction); Specimen C2**
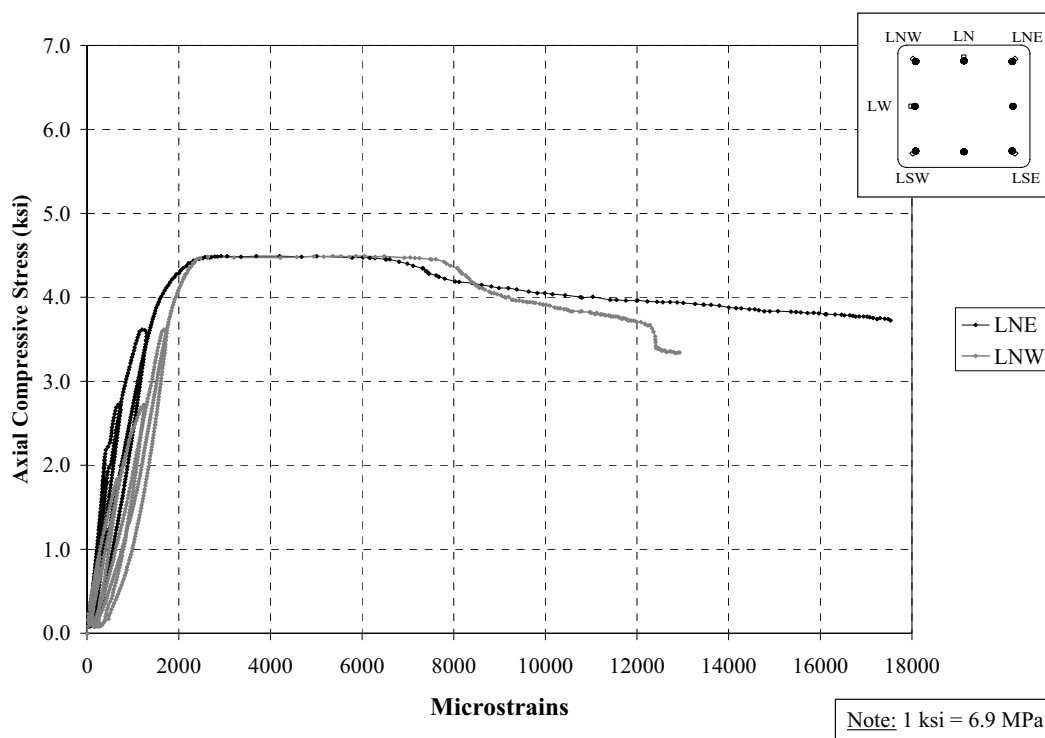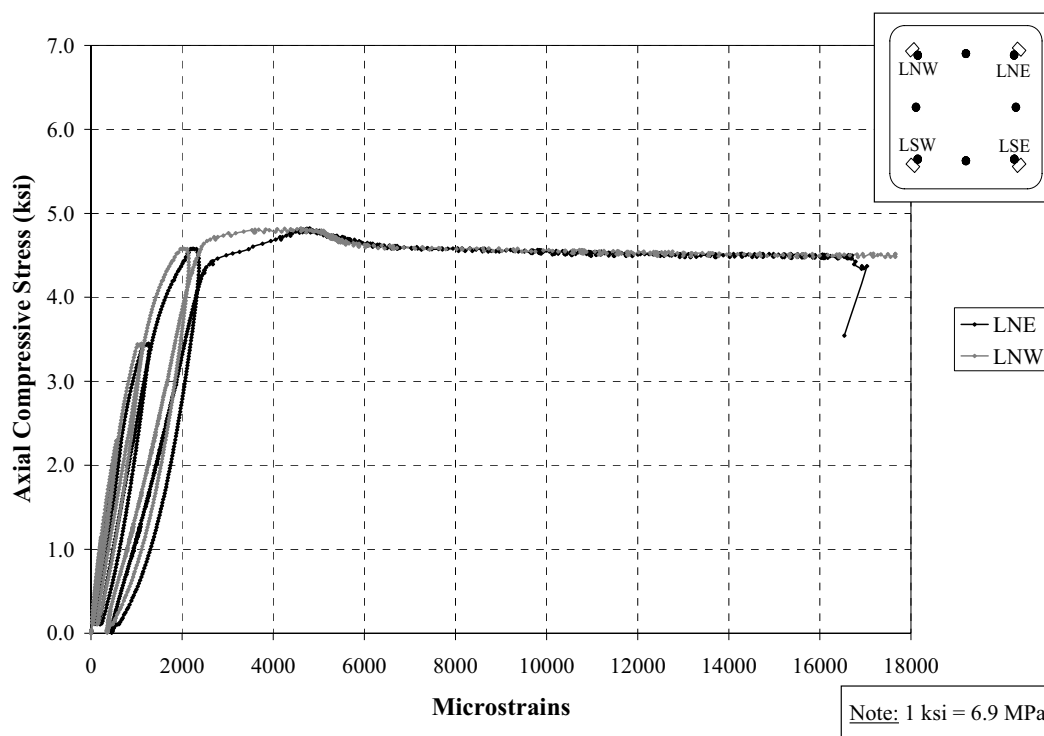
**Figure D63.  Axial Stress vs. Axial Strain on Longitudinal Bars (LNE & LNW); Specimen C3**
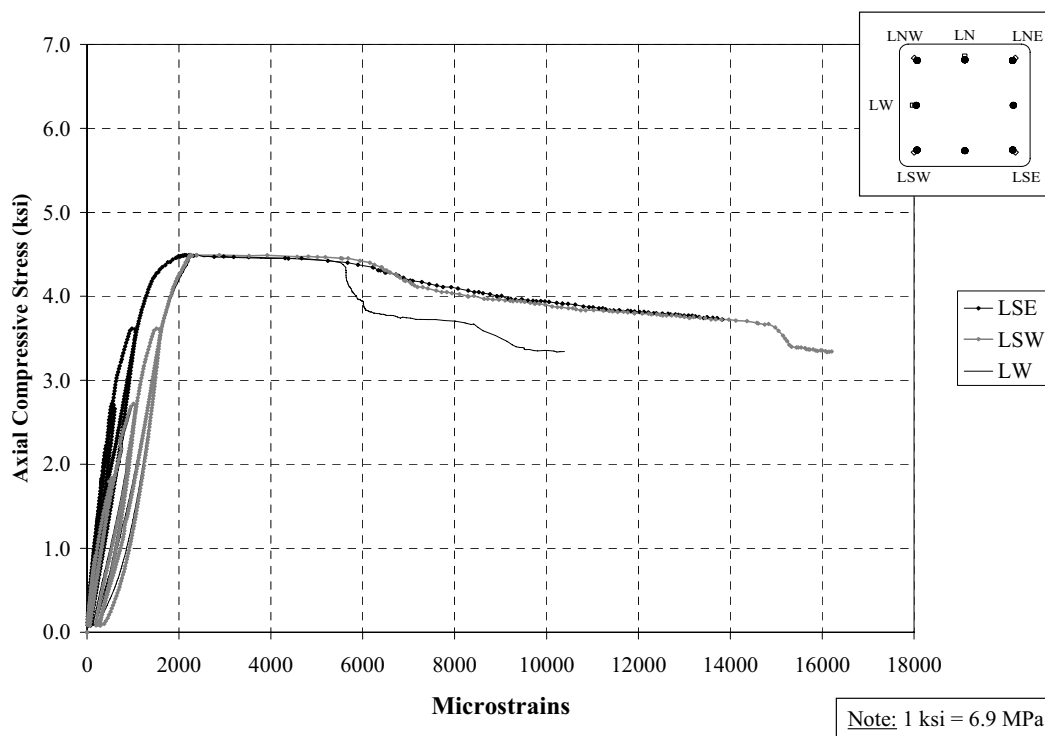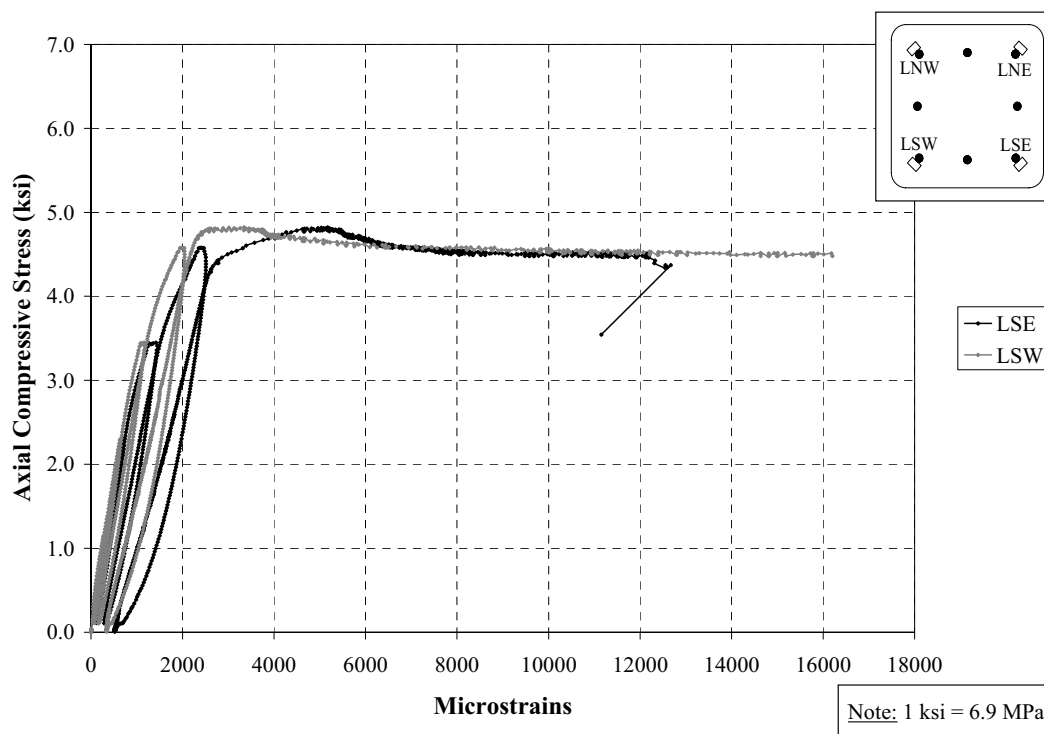


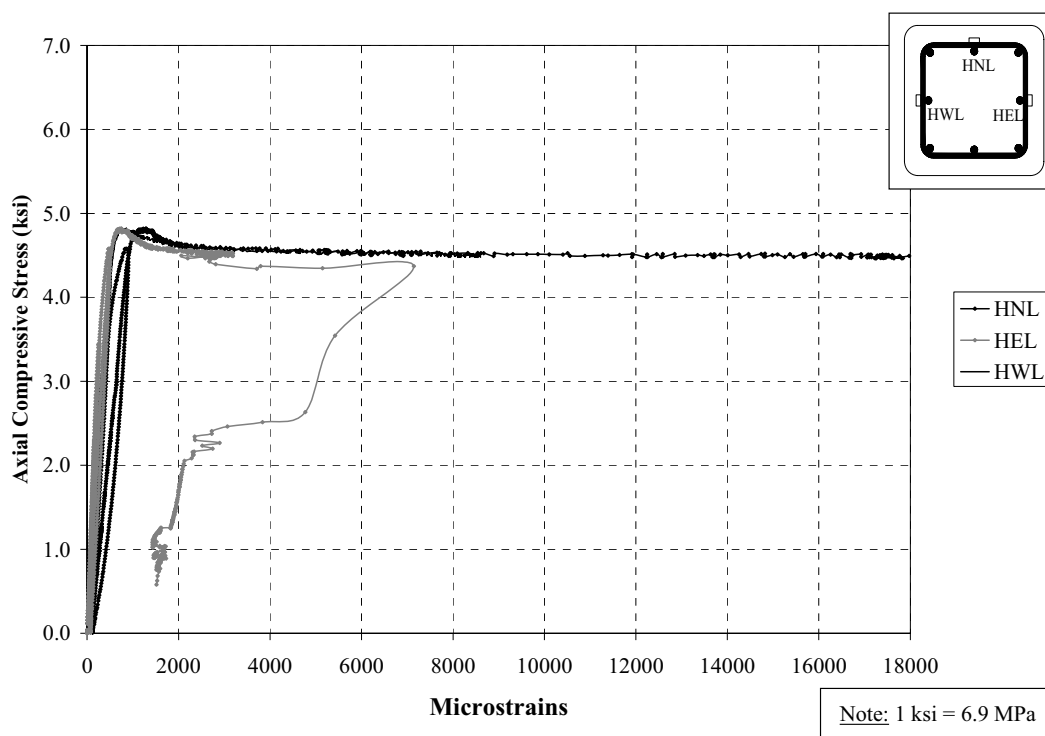**Figure D64.  Axial Stress vs. Axial Strain on Longitudinal Bars (South & LW); Specimen C3**
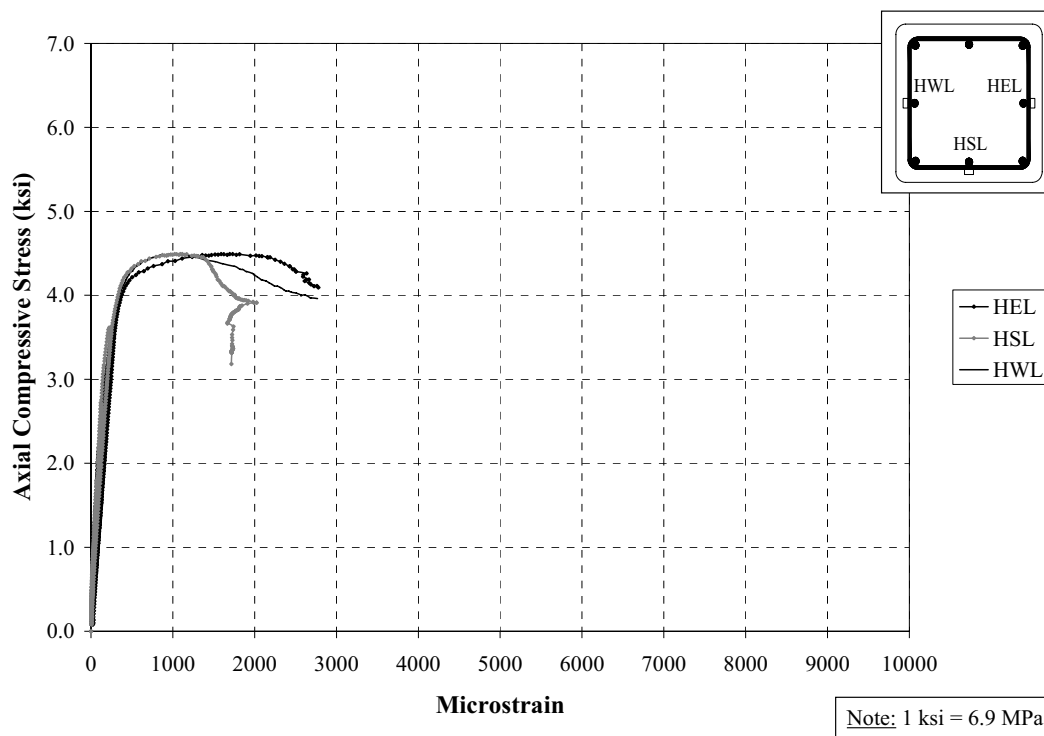
**Figure D65.  Axial Stress vs. Transverse Strain on Lower Tie; Specimen C3**
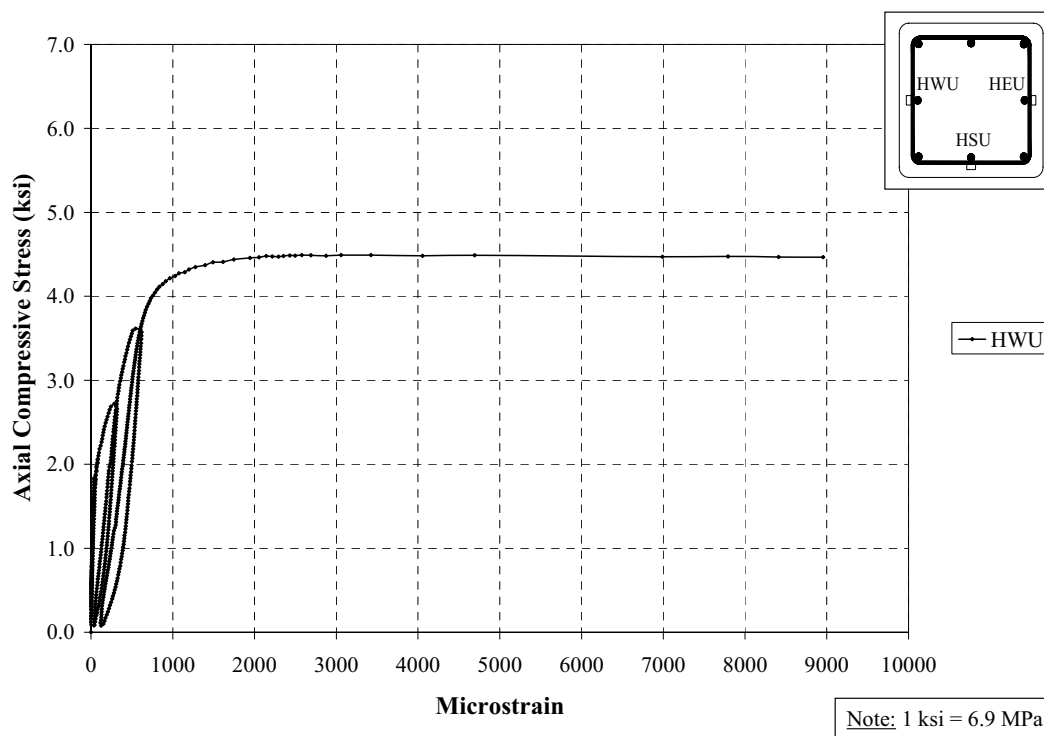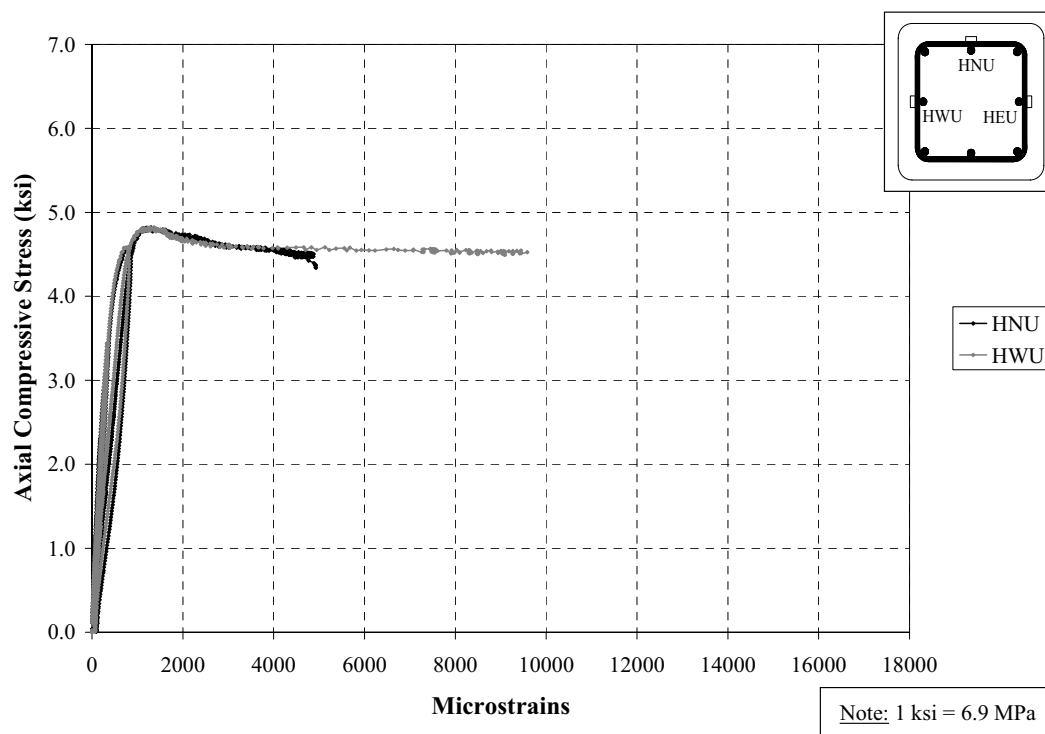


**Figure D66.  Axial Stress vs. Transverse Strain on Upper Tie; Specimen C3**
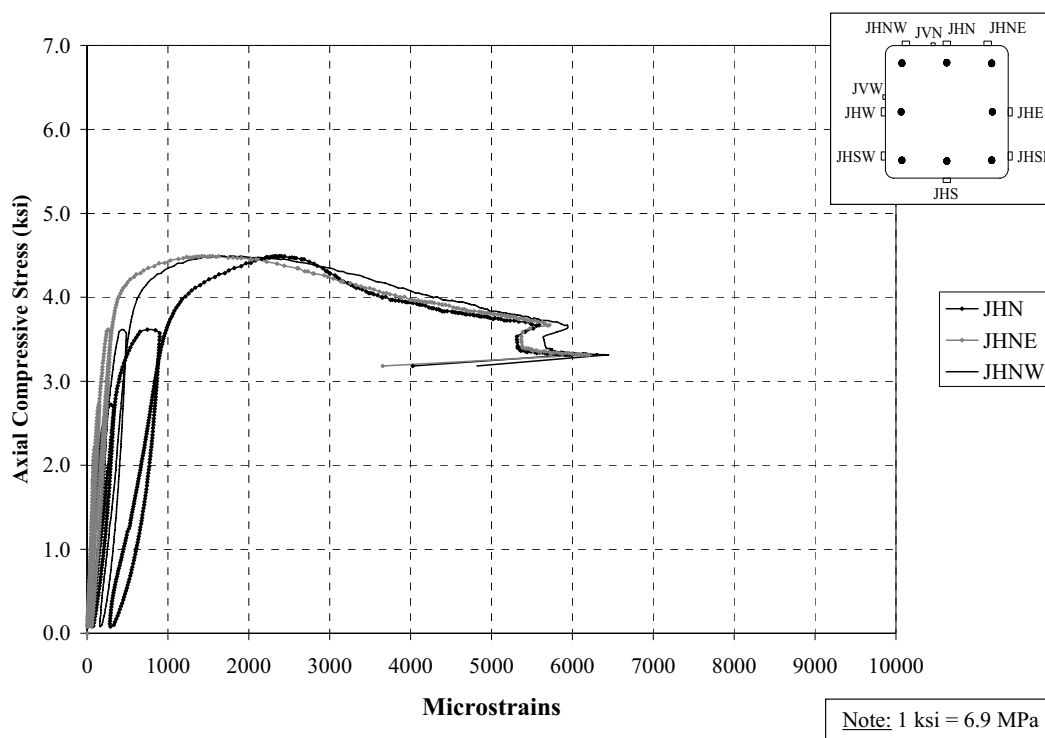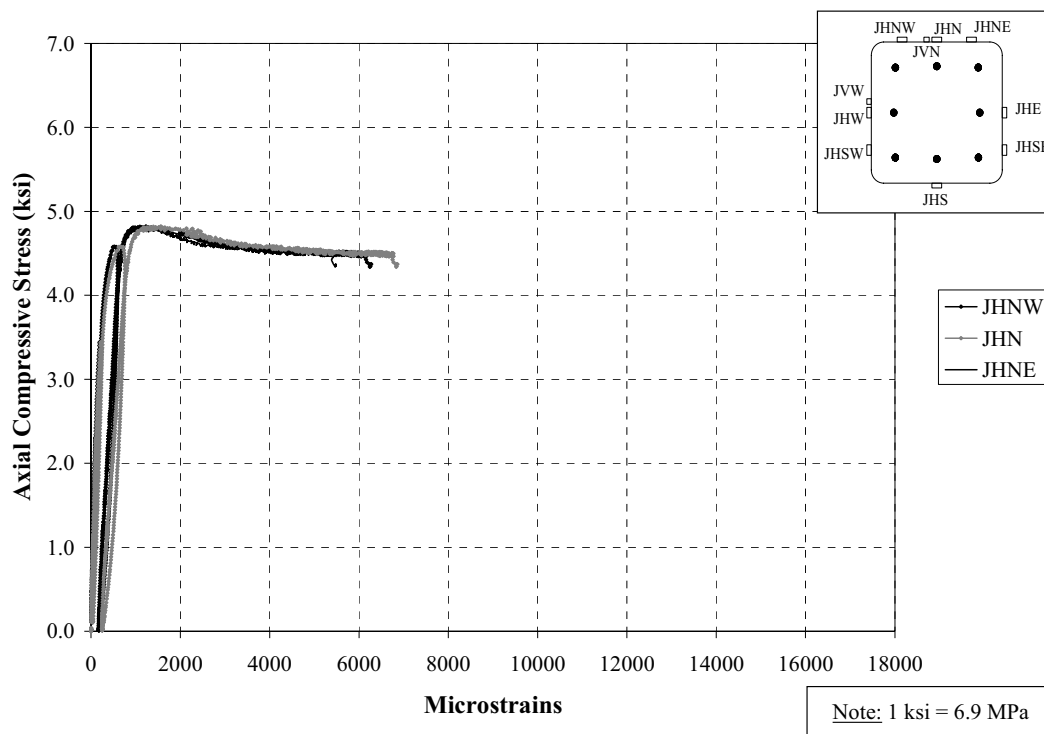
**Figure D67.  Axial Stress vs. Transverse Strain on FRP (North); Specimen C3**
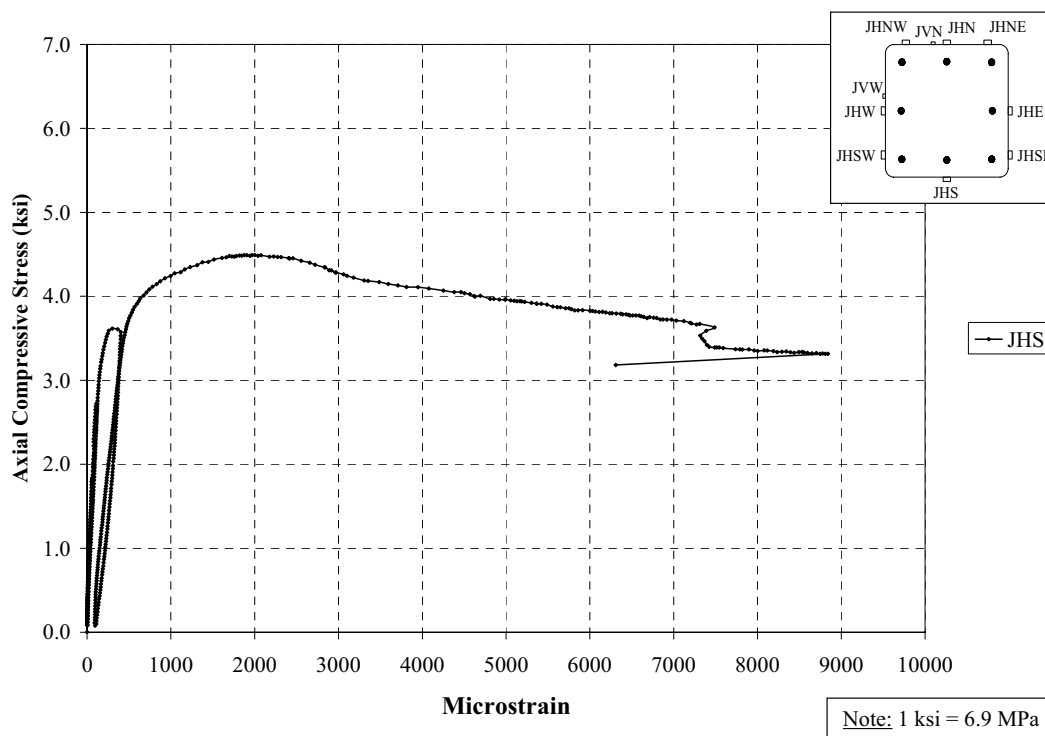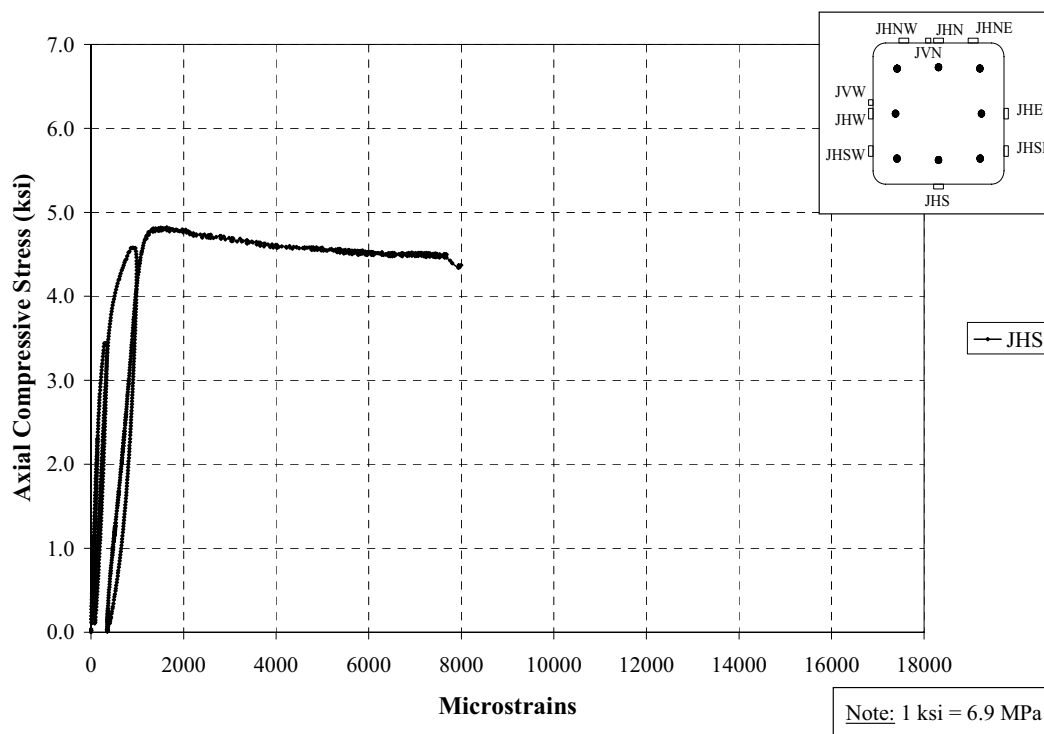


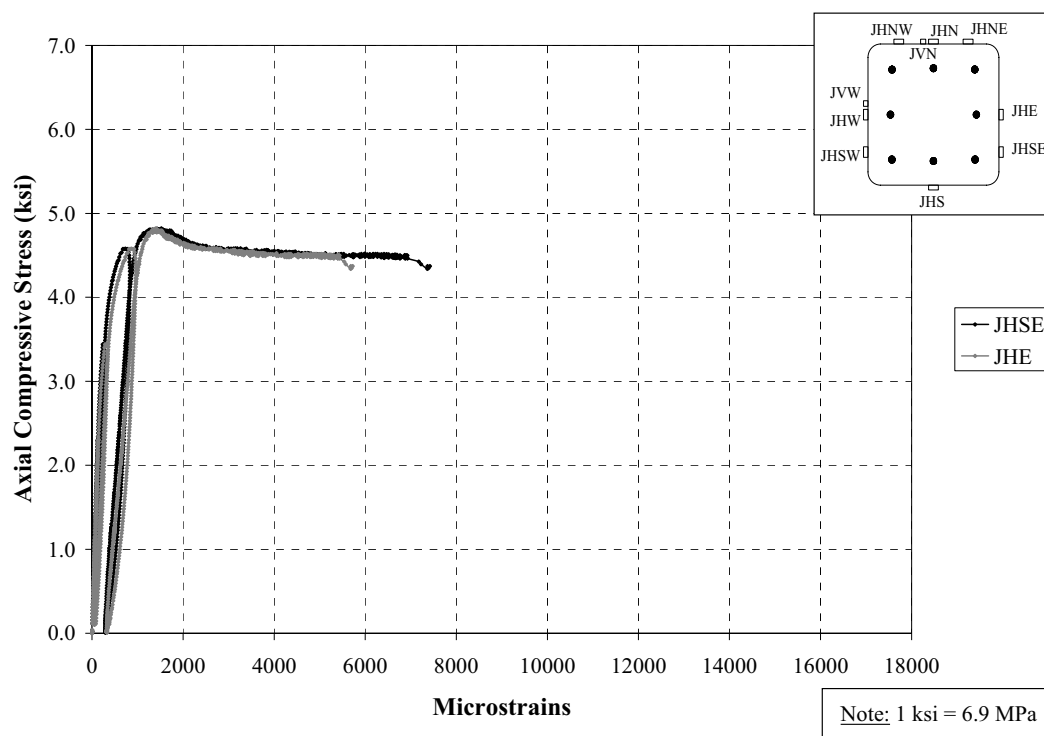**Figure D68.  Axial Stress vs. Transverse Strain on FRP (South); Specimen C3**
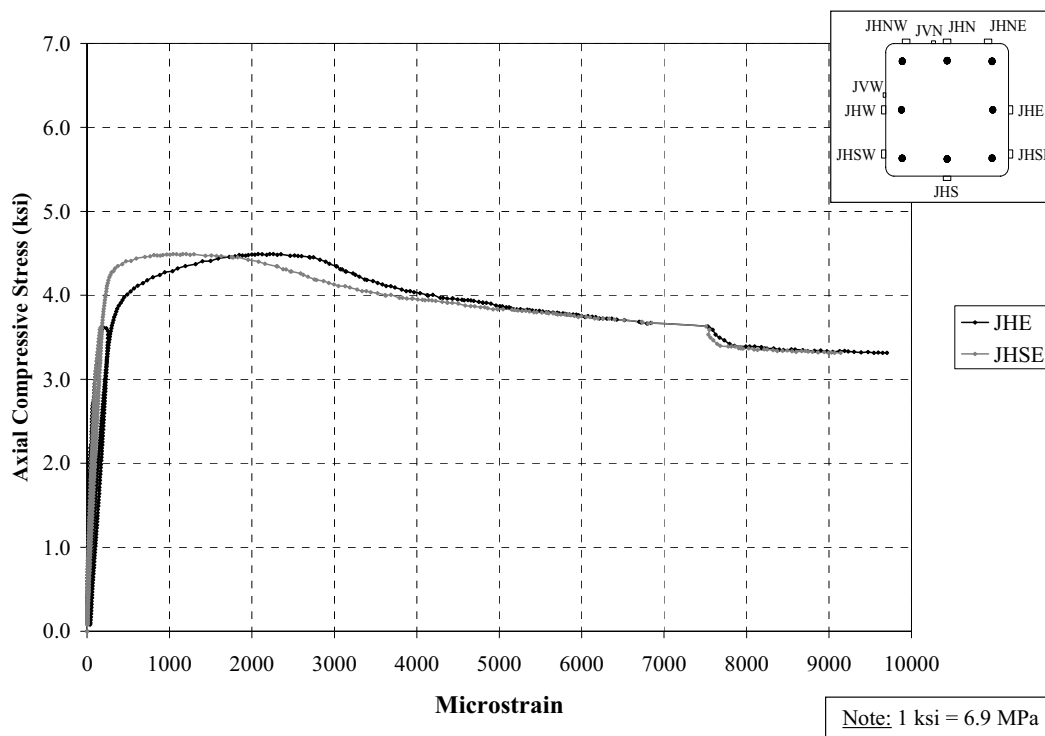
**Figure D69.  Axial Stress vs. Transverse Strain on FRP (East); Specimen C3**
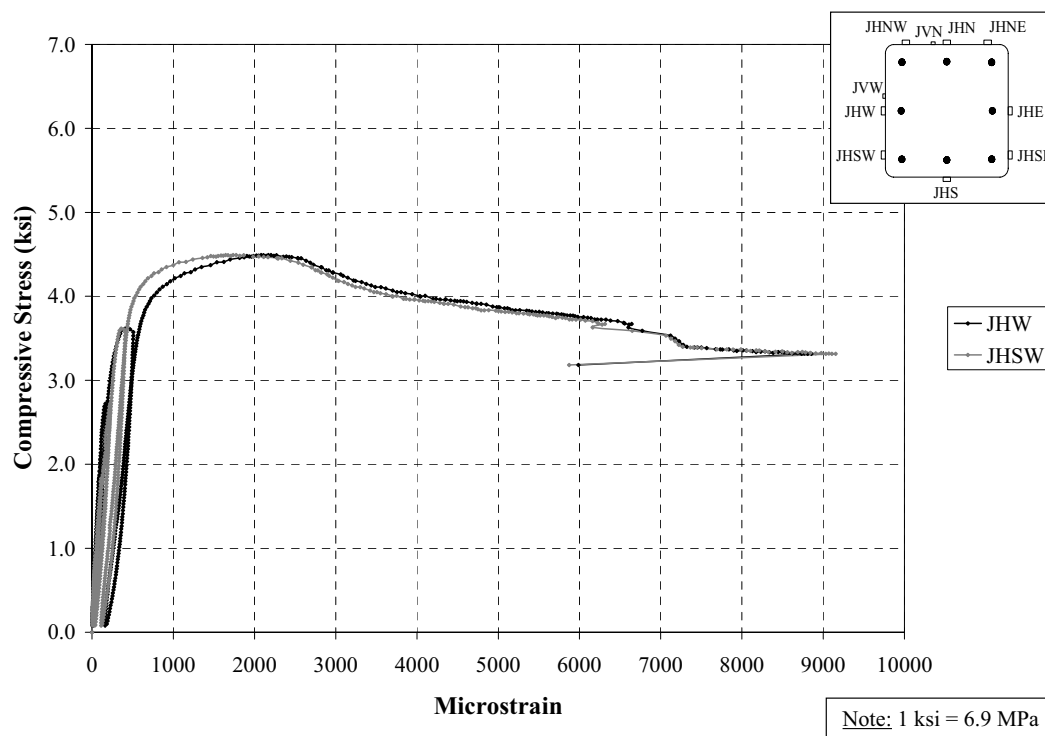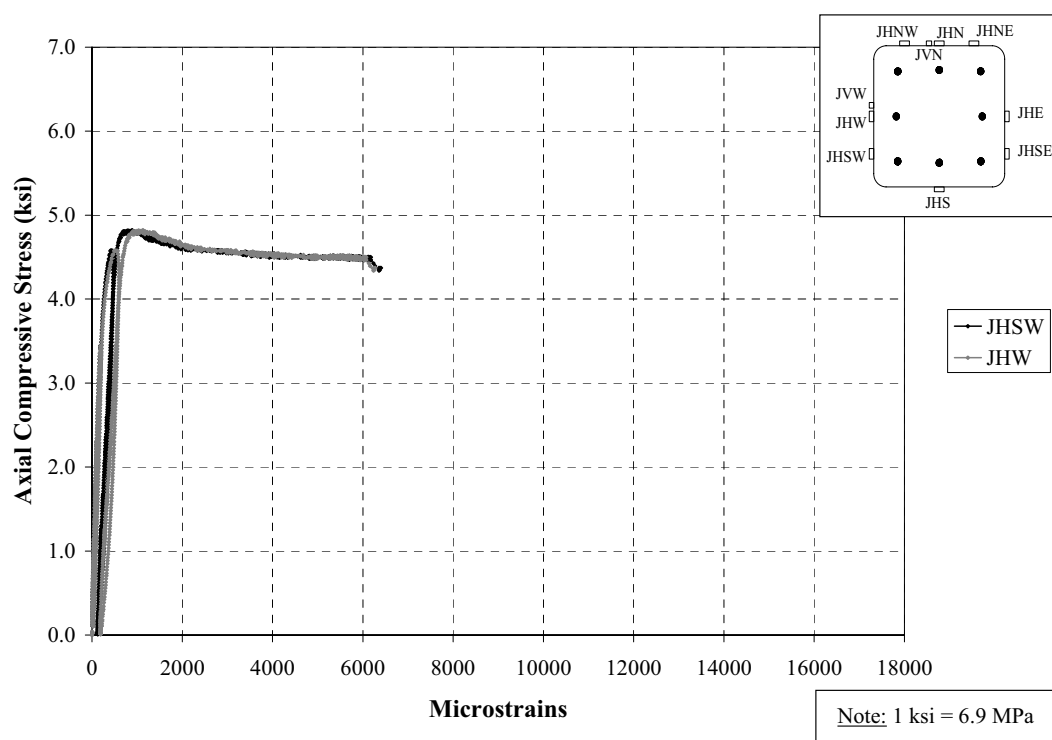


**Figure D70.  Axial Stress vs. Transverse Strain on FRP (West); Specimen C3**
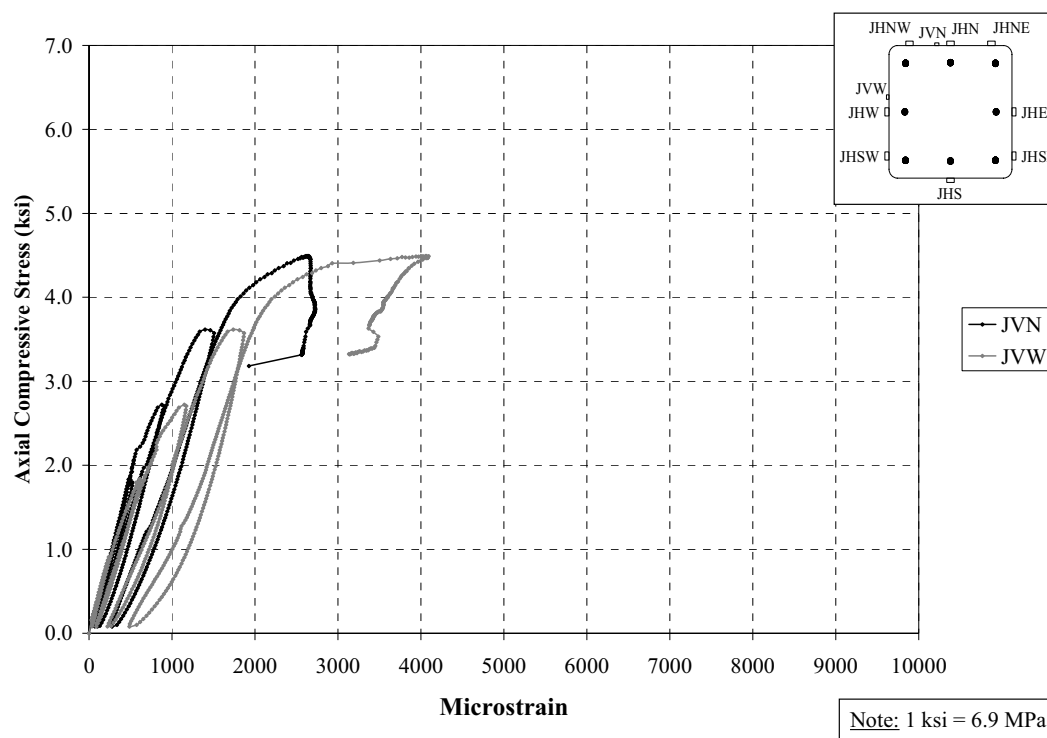
**Figure D71. Axial Stress vs. Axial Strain on FRP (Sensors on Vertical Direction); Specimen C3**
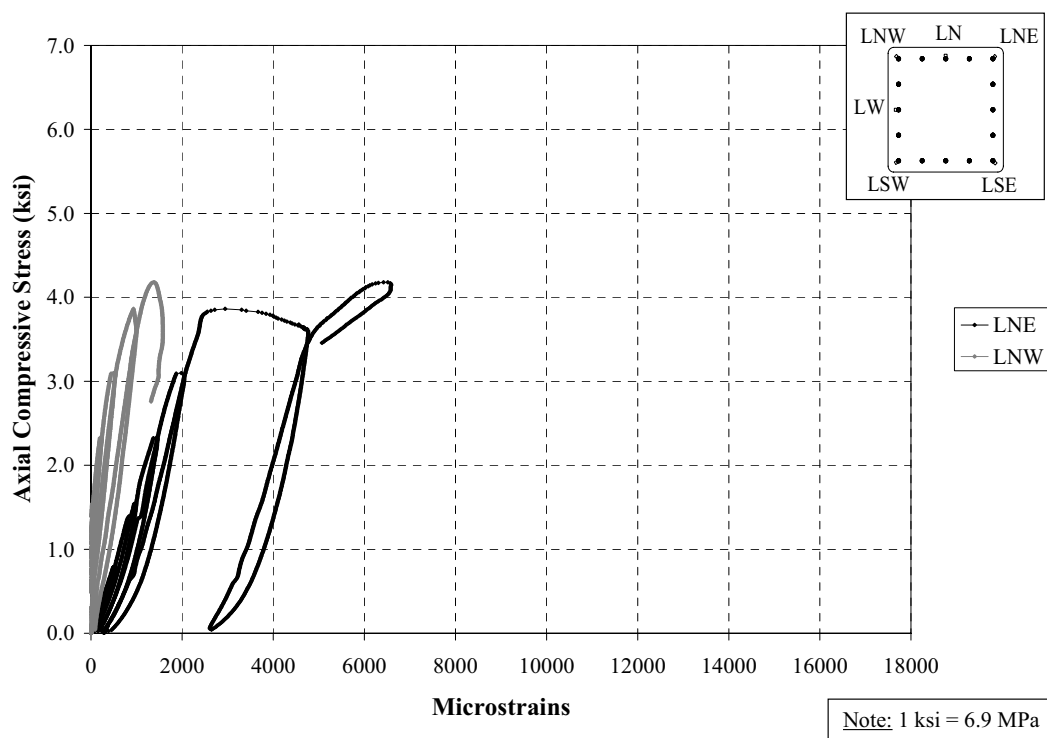
**Figure D72.  Axial Stress vs. Axial Strain on Longitudinal Bars (North-Corners); Specimen D1**
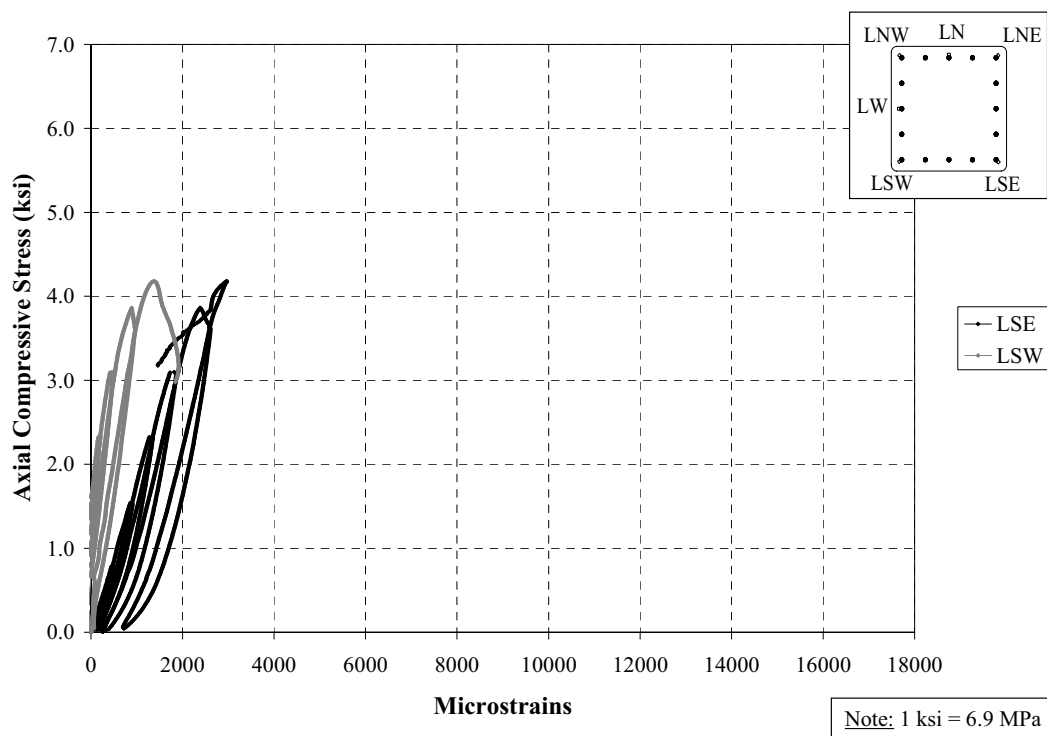


**Figure D73.  Axial Stress vs. Axial Strain on Longitudinal Bars (South-Corners); Specimen D1**
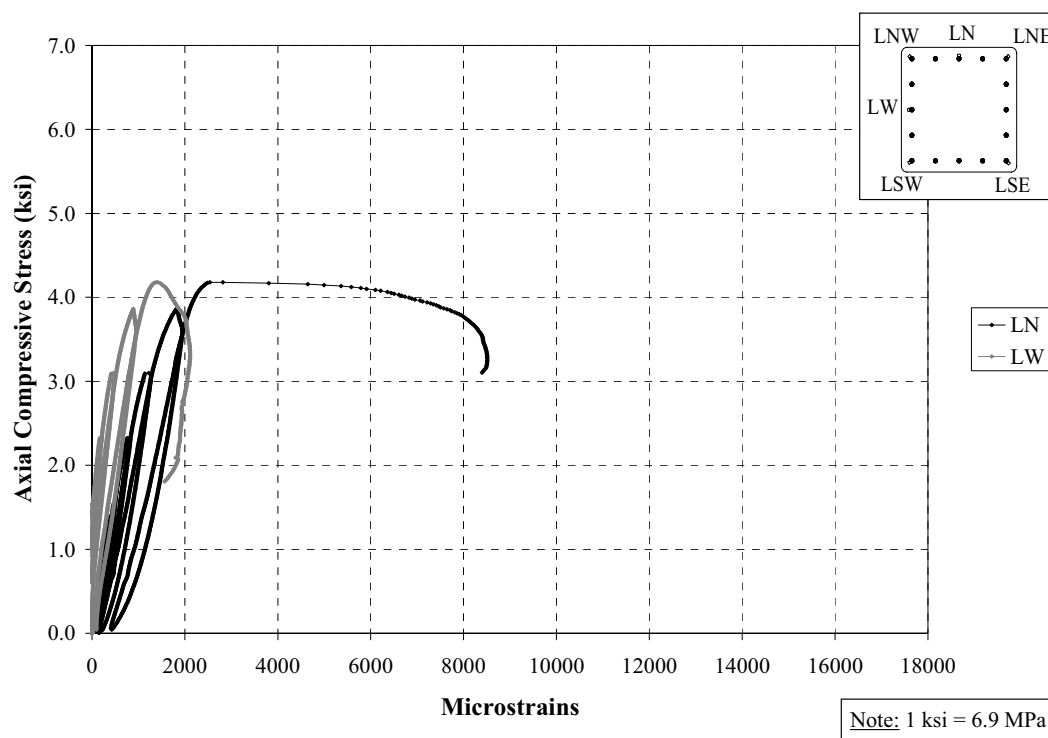
**Figure D74. Axial Stress vs. Axial Strain on Longitudinal Bars (LN & LW); Specimen D1**
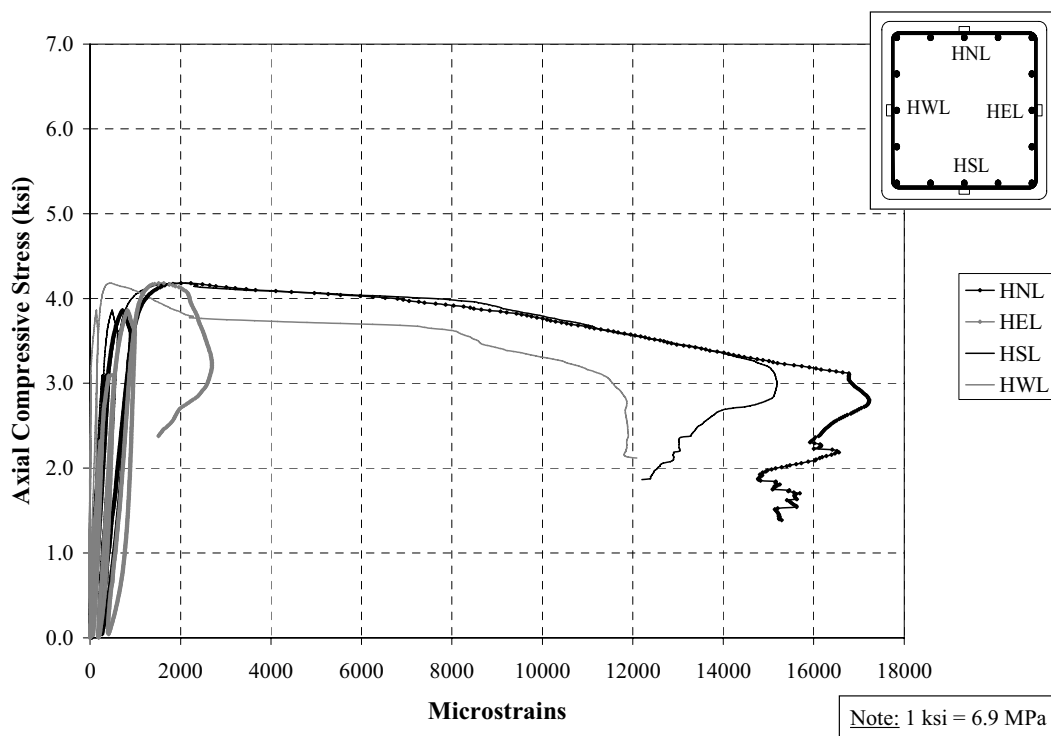


**Figure D75. Axial Stress vs. Transverse Strain on Lower Tie; Specimen D1**
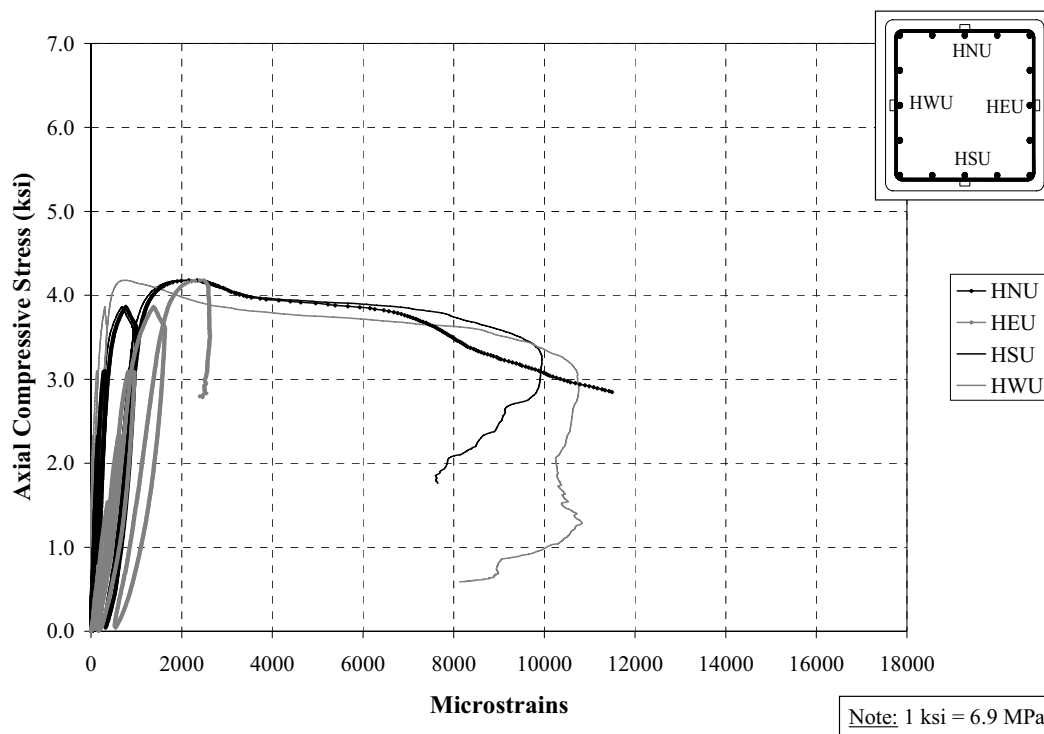
**Figure D76. Axial Stress vs. Transverse Strain on Upper Tie; Specimen D1**
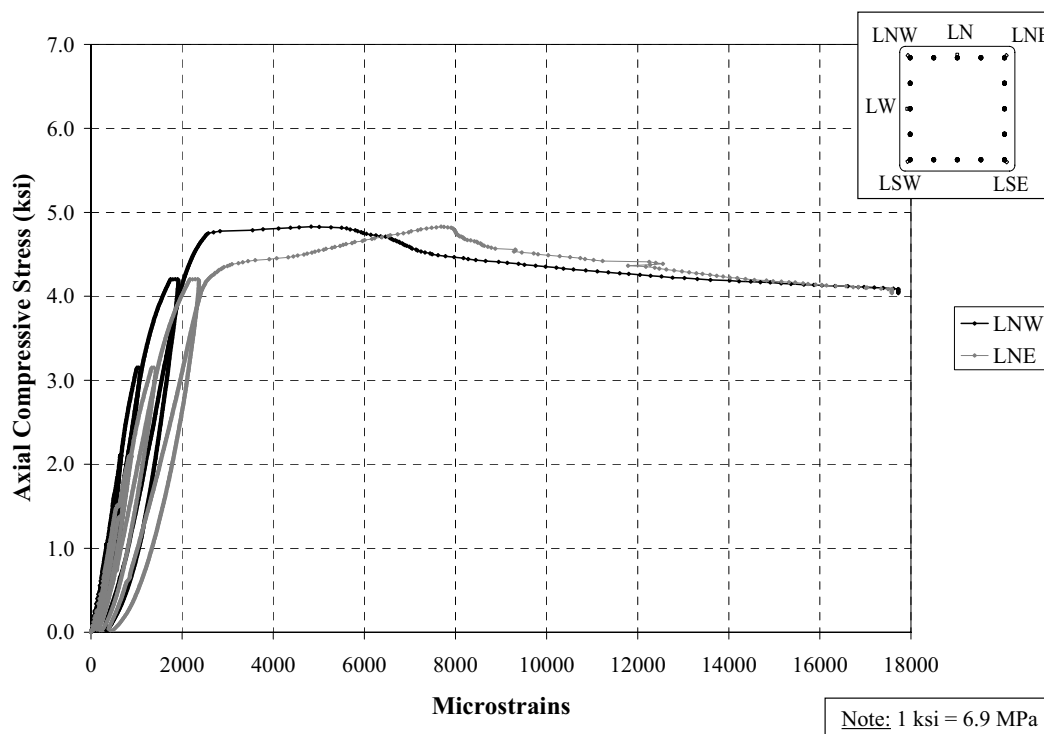


**Figure D77. Axial Stress vs. Axial Strain on Longitudinal Bars (North-Corners); Specimen D2**
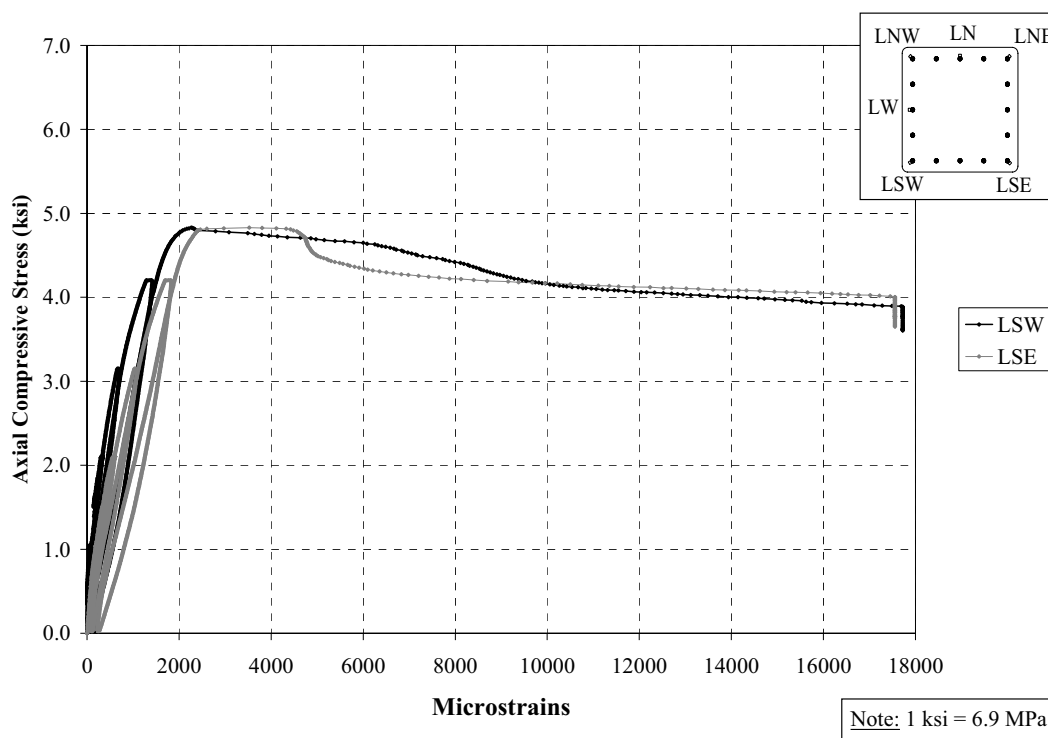
**Figure D78. Axial Stress vs. Axial Strain on Longitudinal Bars (South-Corners); Specimen D2**
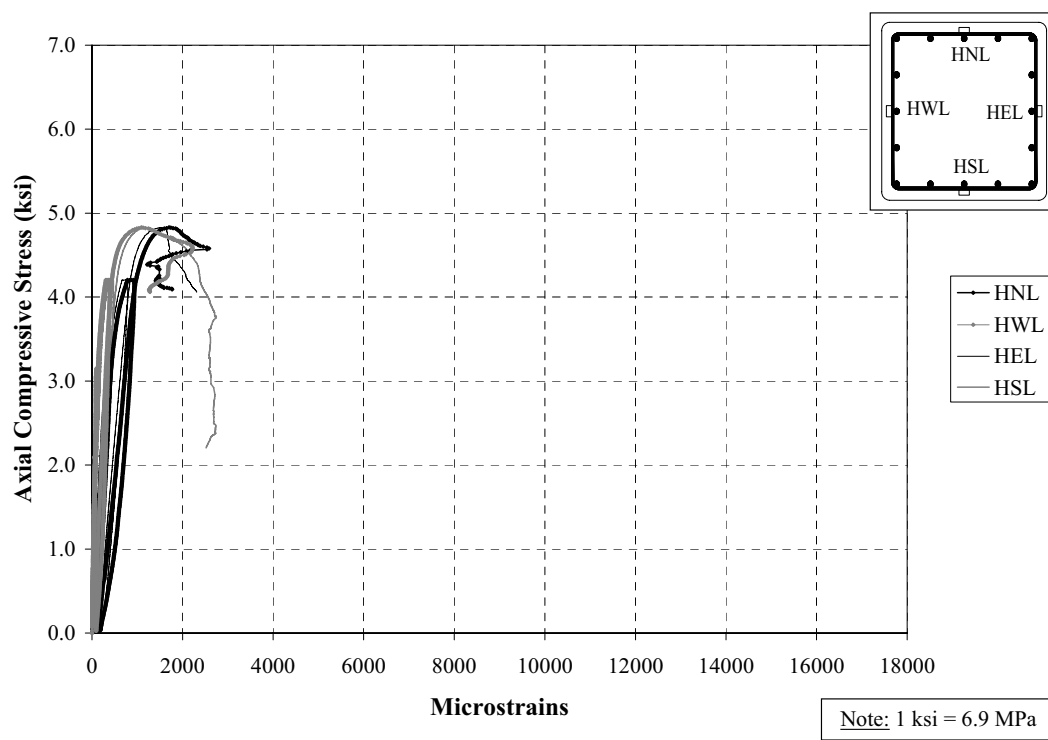


**Figure D79. Axial Stress vs. Transverse Strain on Lower Tie; Specimen D2**
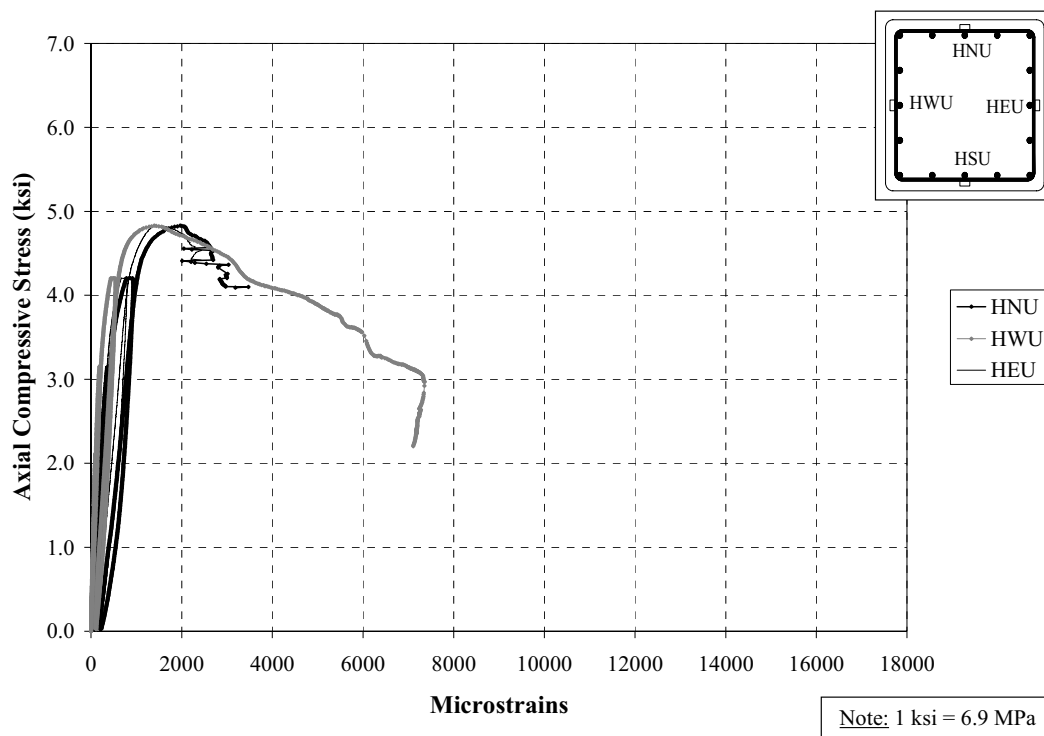
**Figure D80. Axial Stress vs. Transverse Strain on Upper Tie; Specimen D2**
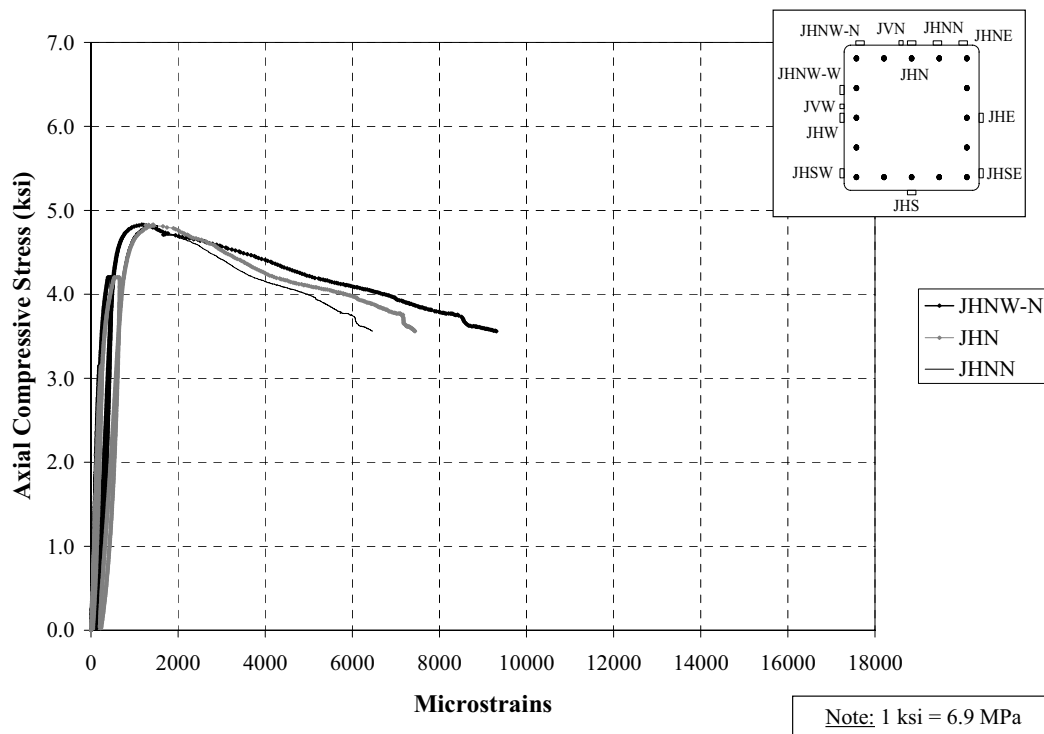


**Figure D81. Axial Stress vs. Transverse Strain on FRP (North); Specimen D2**
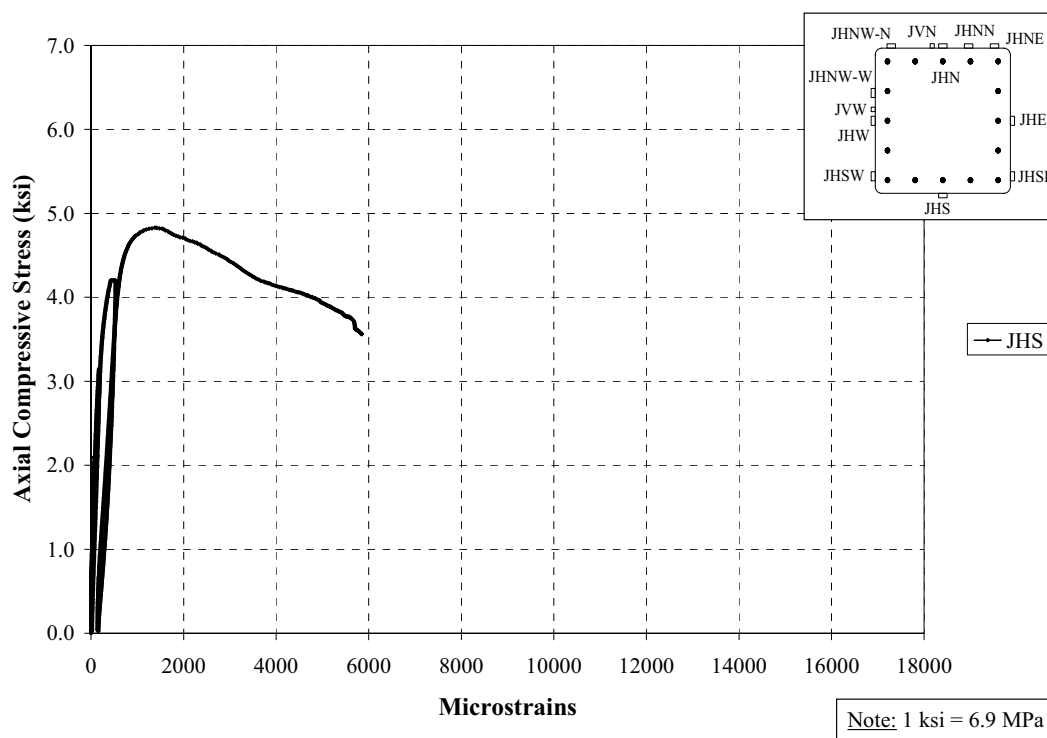
**Figure D82.  Axial Stress vs. Transverse Strain on FRP (South); Specimen D2**
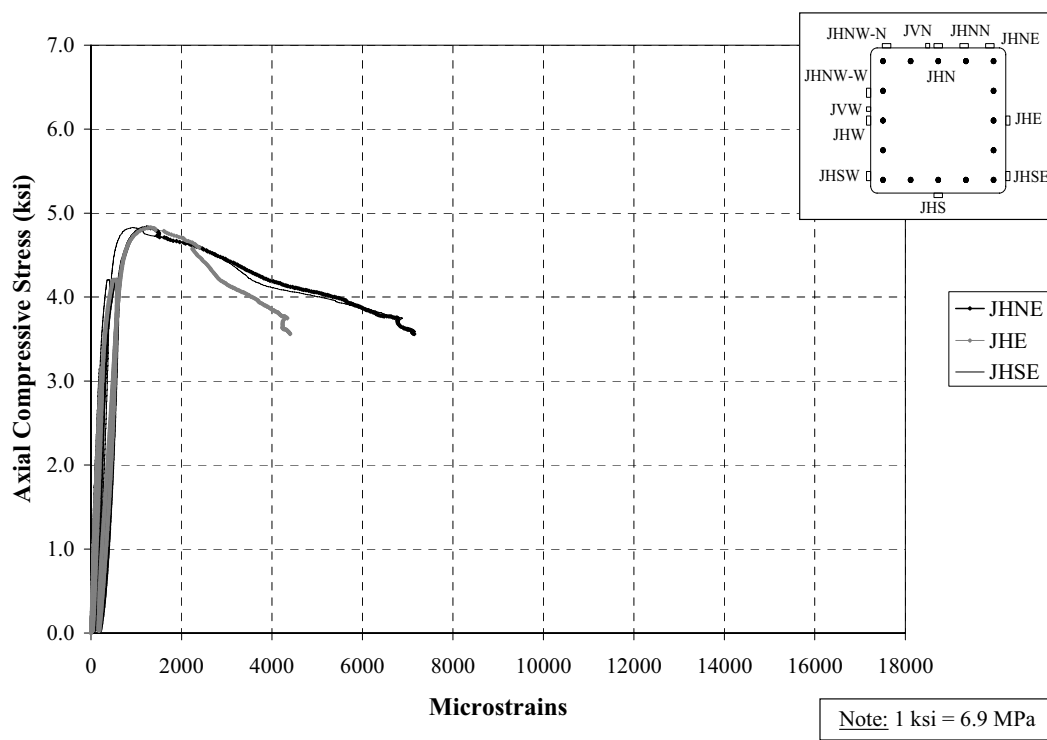


**Figure D83.  Axial Stress vs. Transverse Strain on FRP (East); Specimen D2**
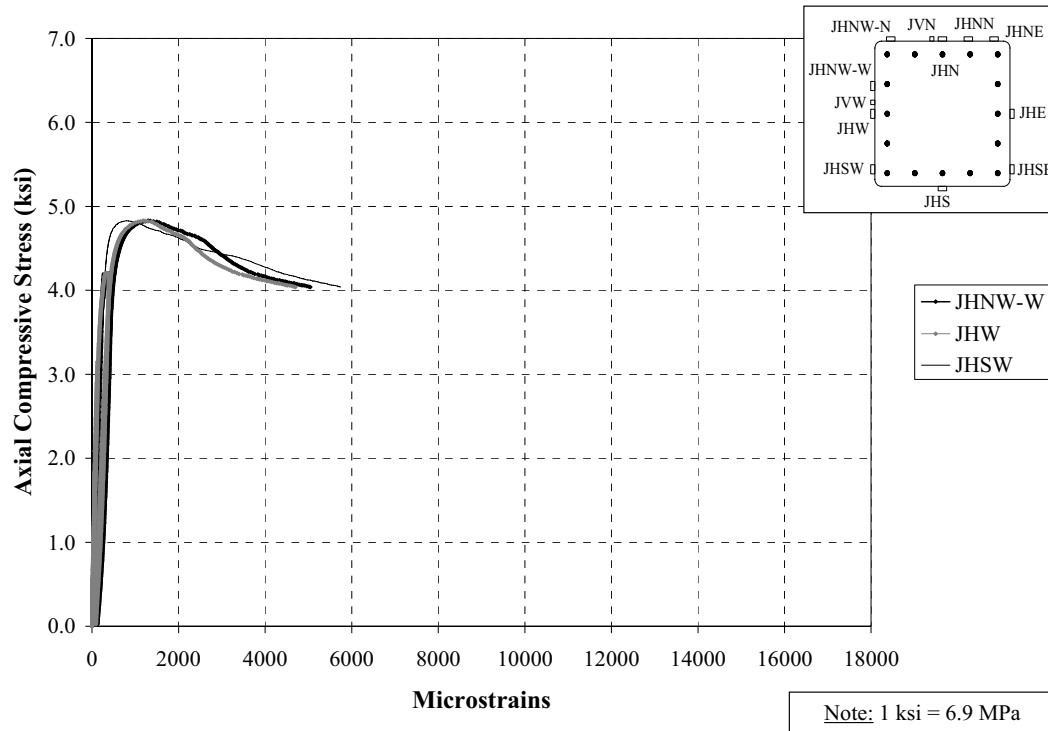
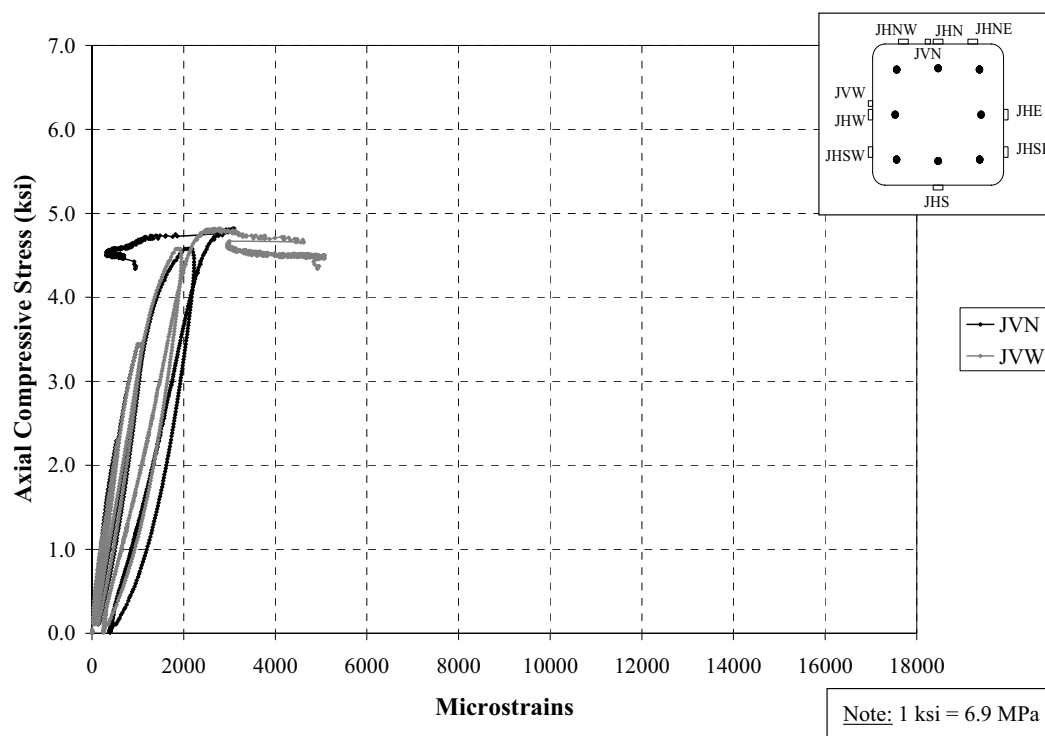**Figure D84. Axial Stress vs. Transverse Strain on FRP (West); Specimen D2**
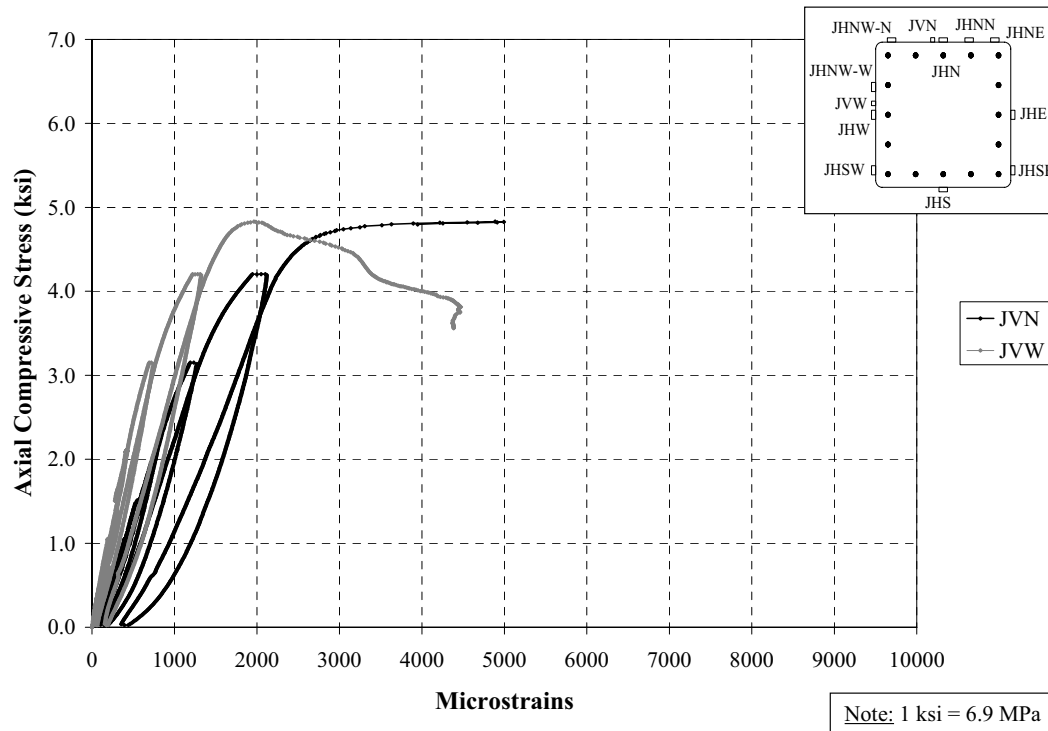


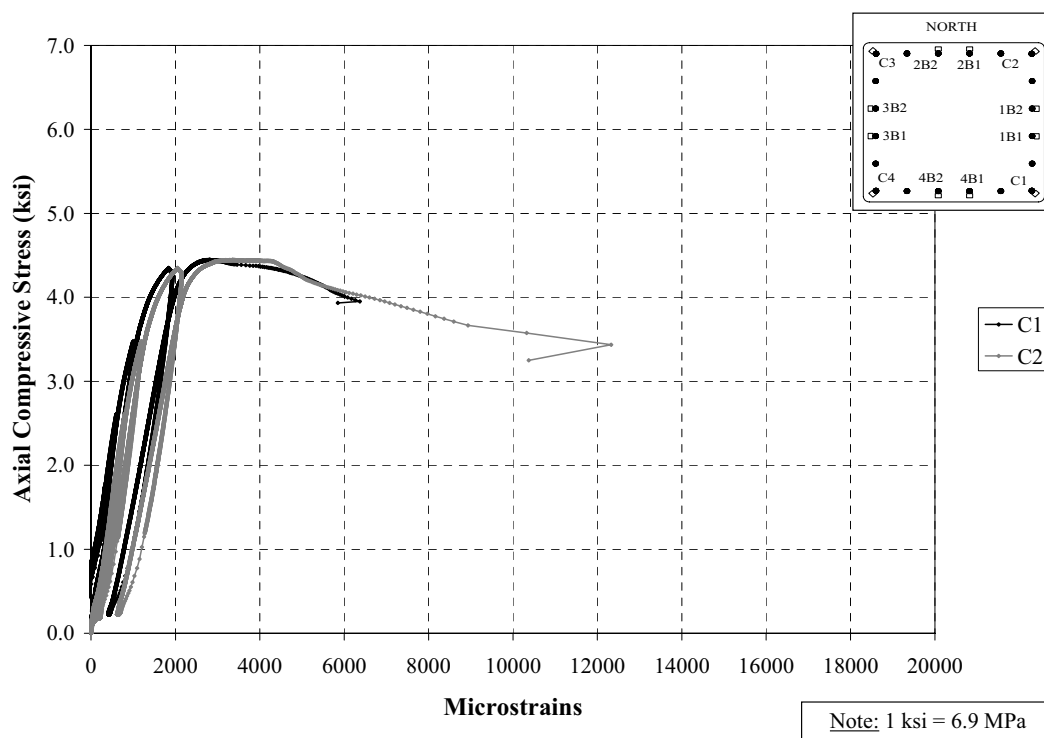**Figure D85. Axial Stress vs. Axial Strain (Sensors on Vertical Direction); Specimen D2**
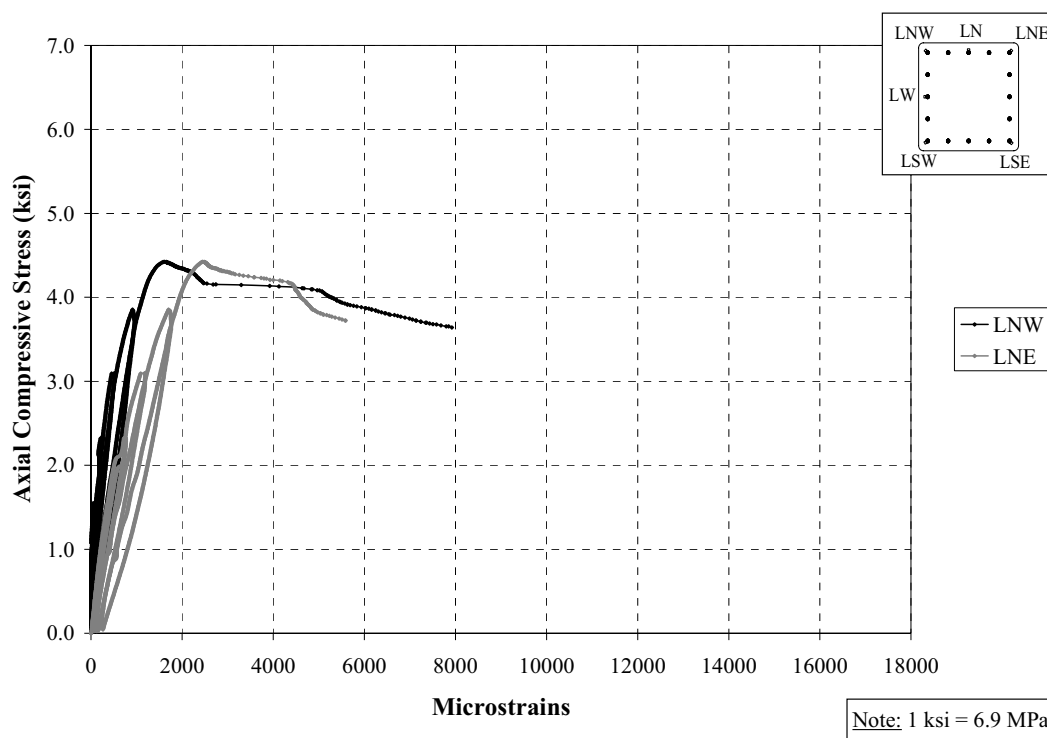
**Figure D86. Axial Stress vs. Axial Strain on Longitudinal Bars (North-Corners); Specimen D3**
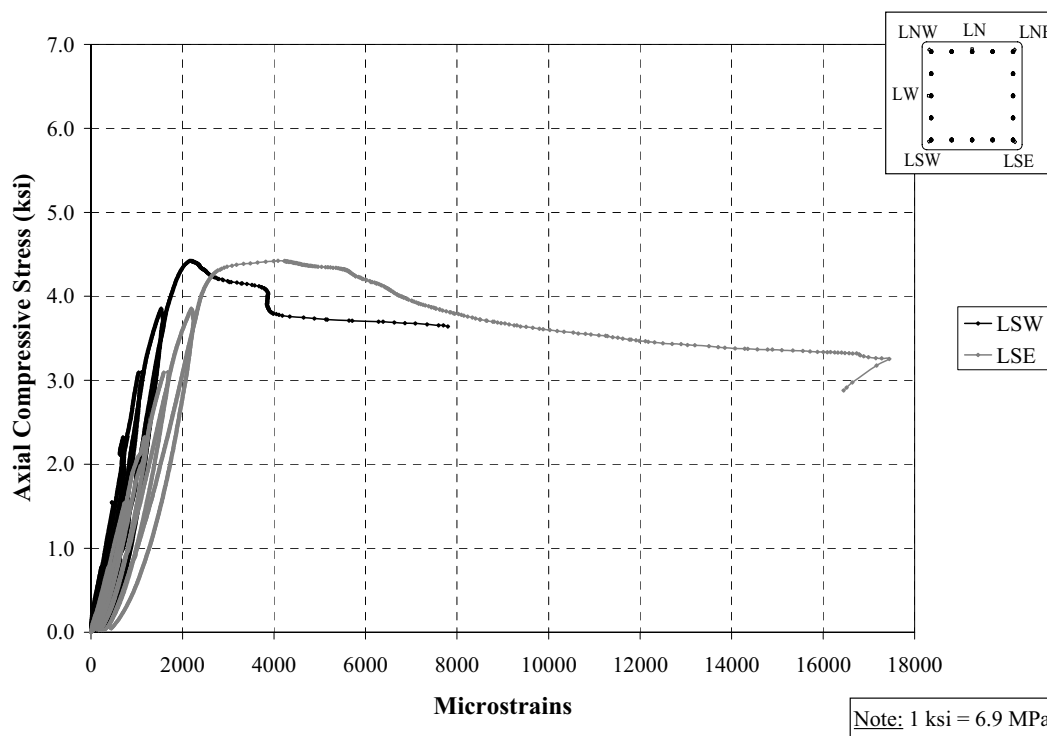


**Figure D87. Axial Stress vs. Axial Strain on Longitudinal Bars (South-Corners); Specimen D3**
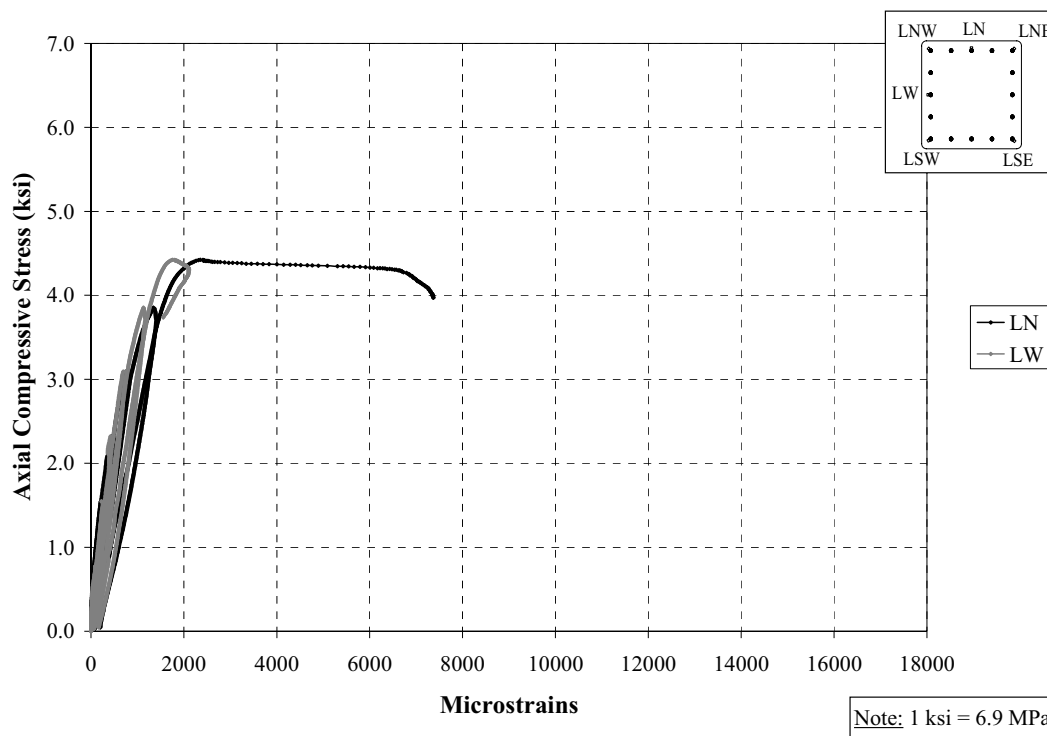
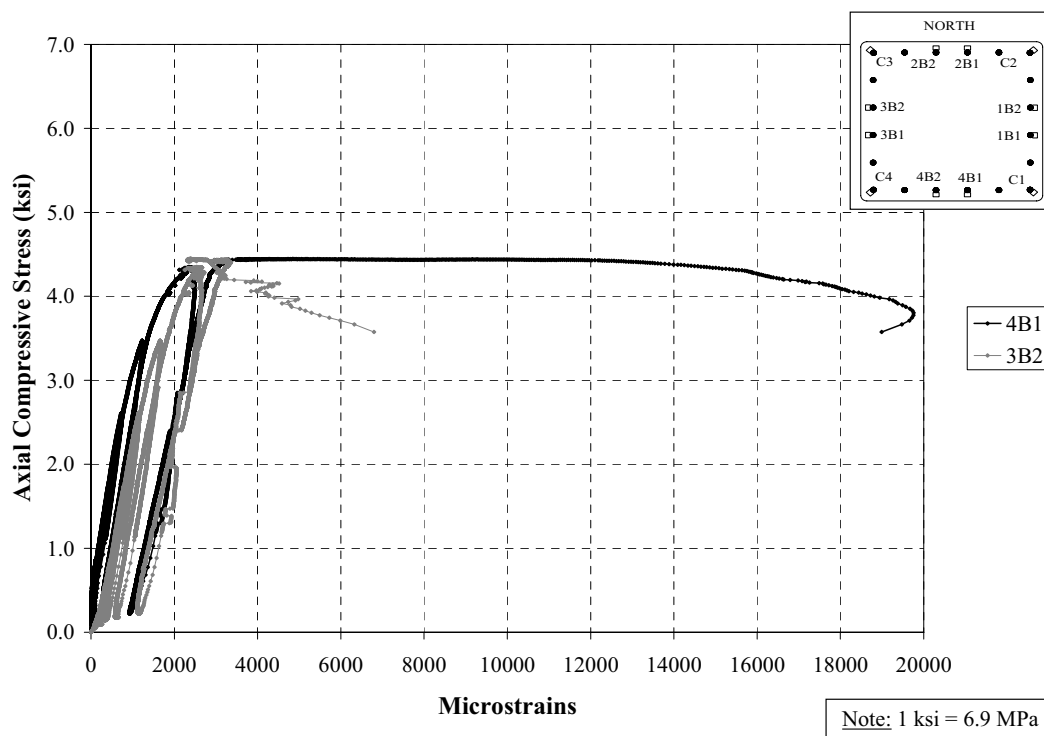**Figure D88.  Axial Stress vs. Axial Strain on Longitudinal Bars (LN & LW); Specimen D3**
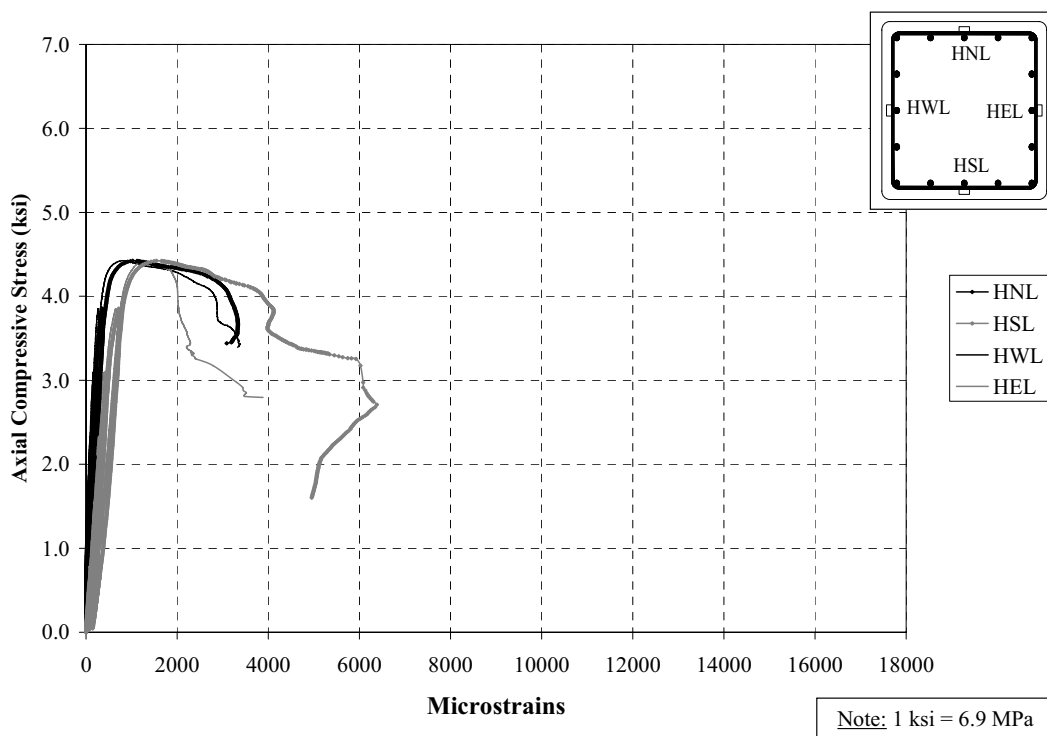


**Figure D89.  Axial Stress vs. Transverse Strain on Lower Tie; Specimen D3**
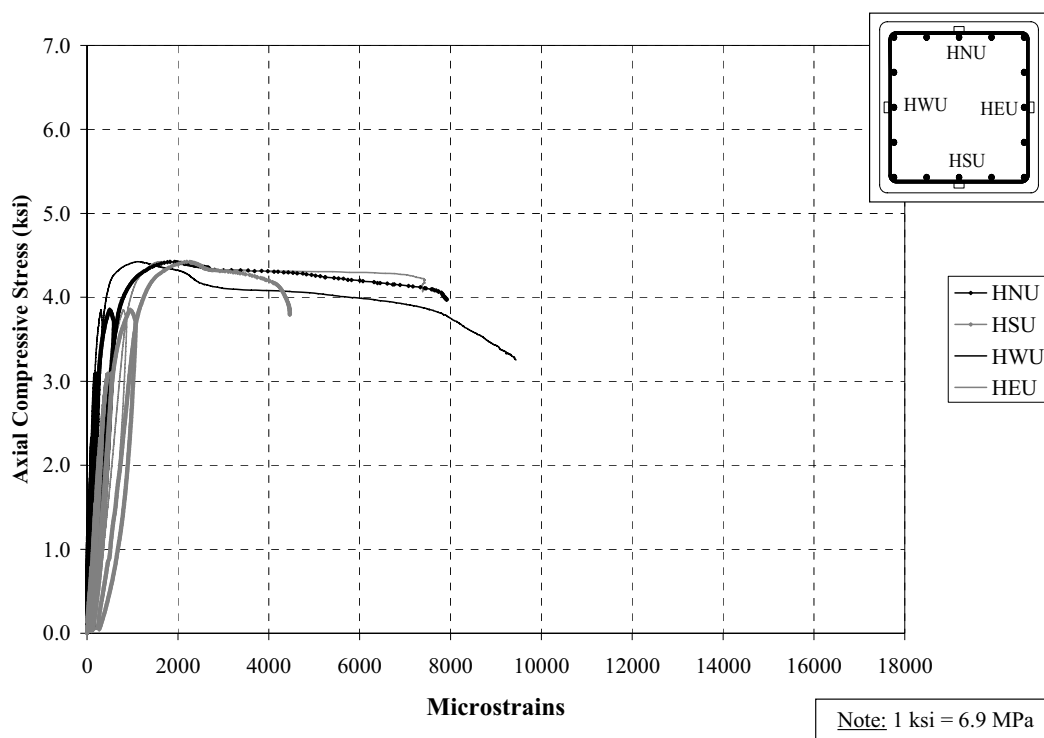
**Figure D90.  Axial Stress vs. Transverse Strain on Upper Tie; Specimen D3**
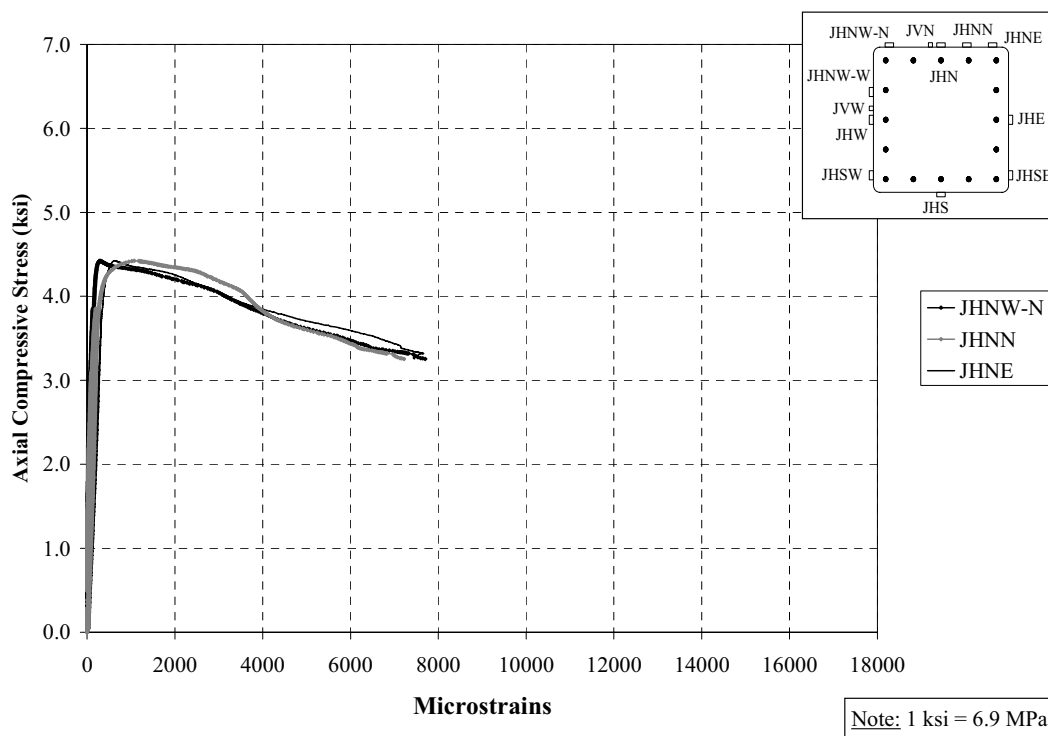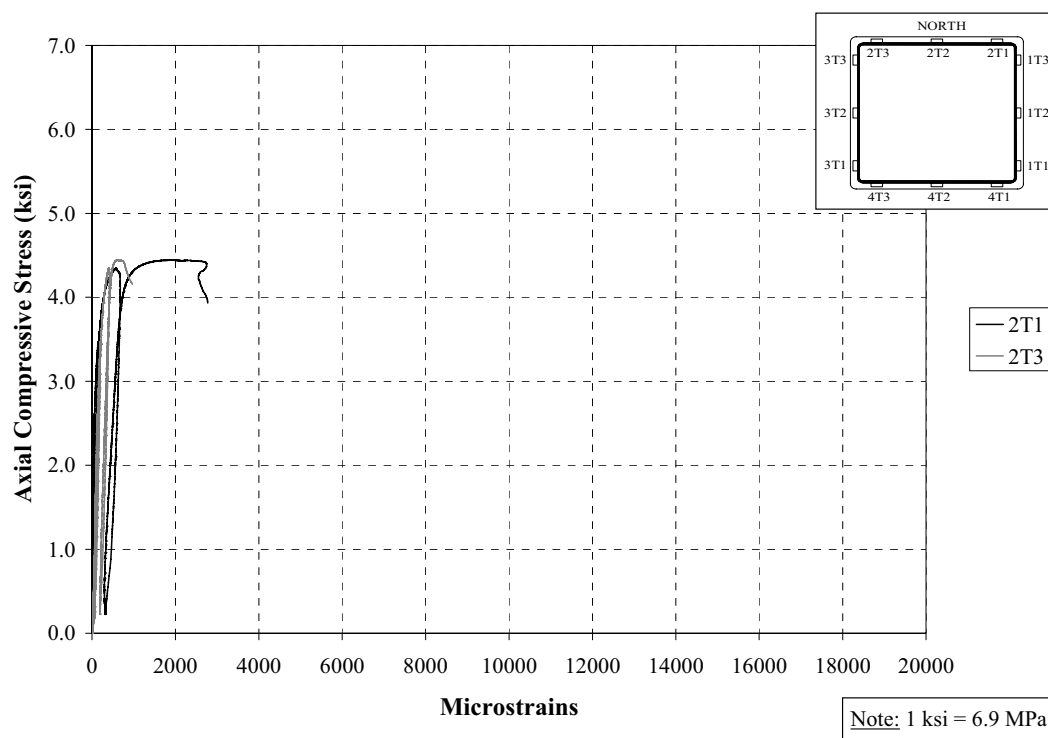


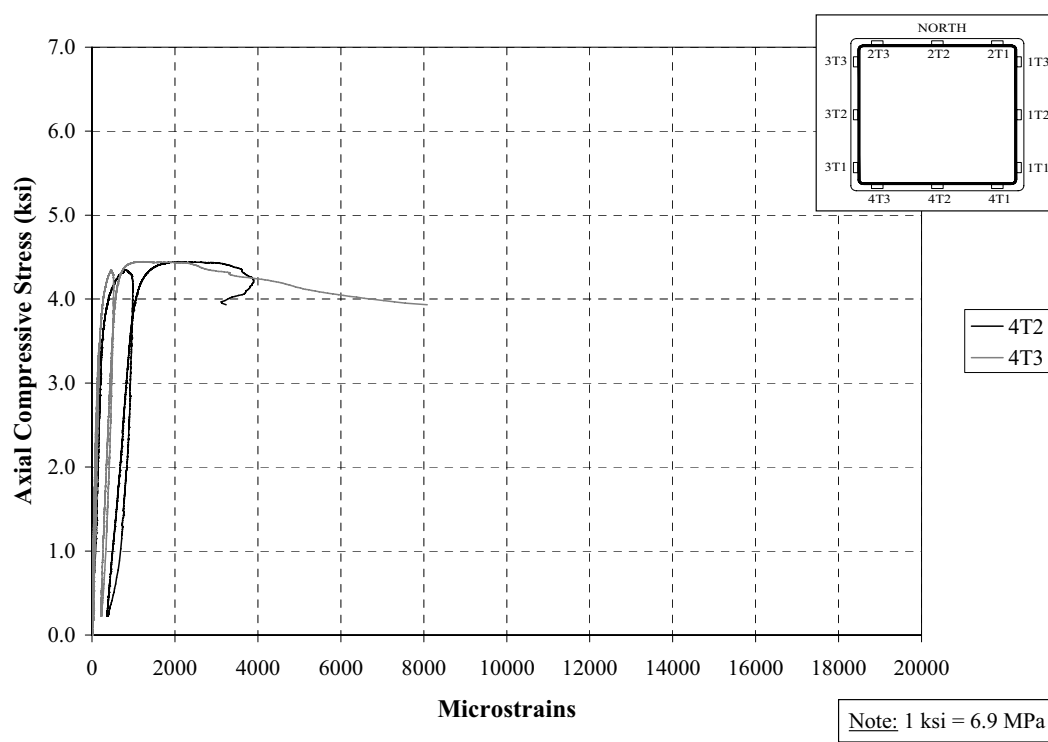**Figure D91.  Axial Stress vs. Transverse Strain on FRP (North); Specimen D3**
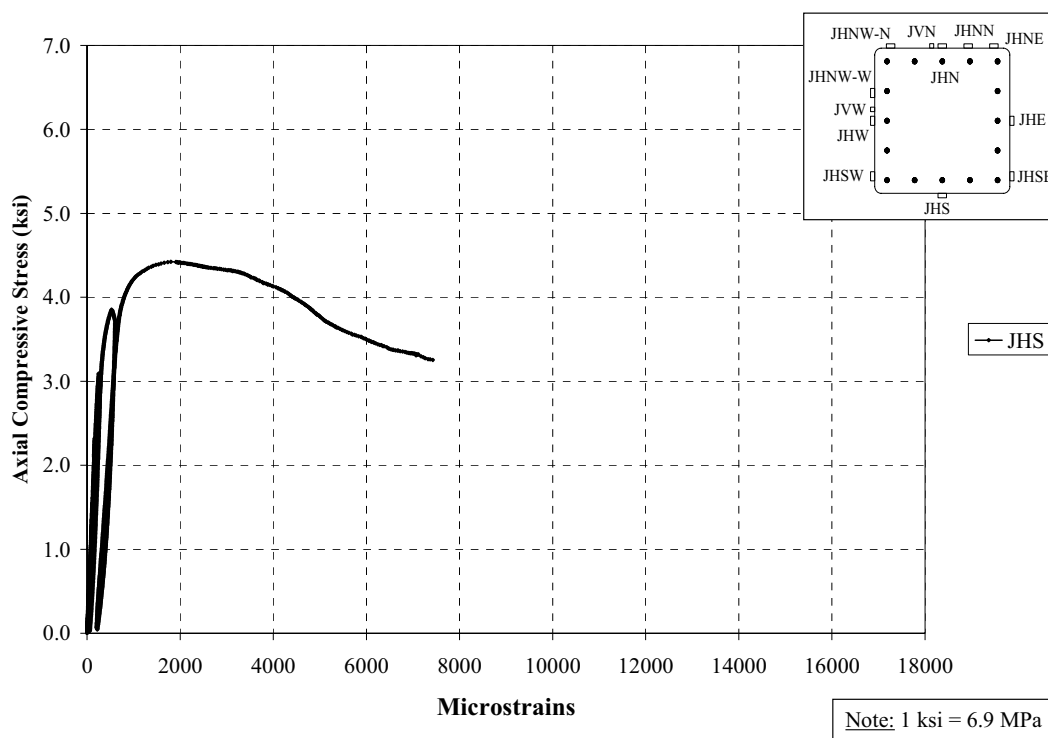
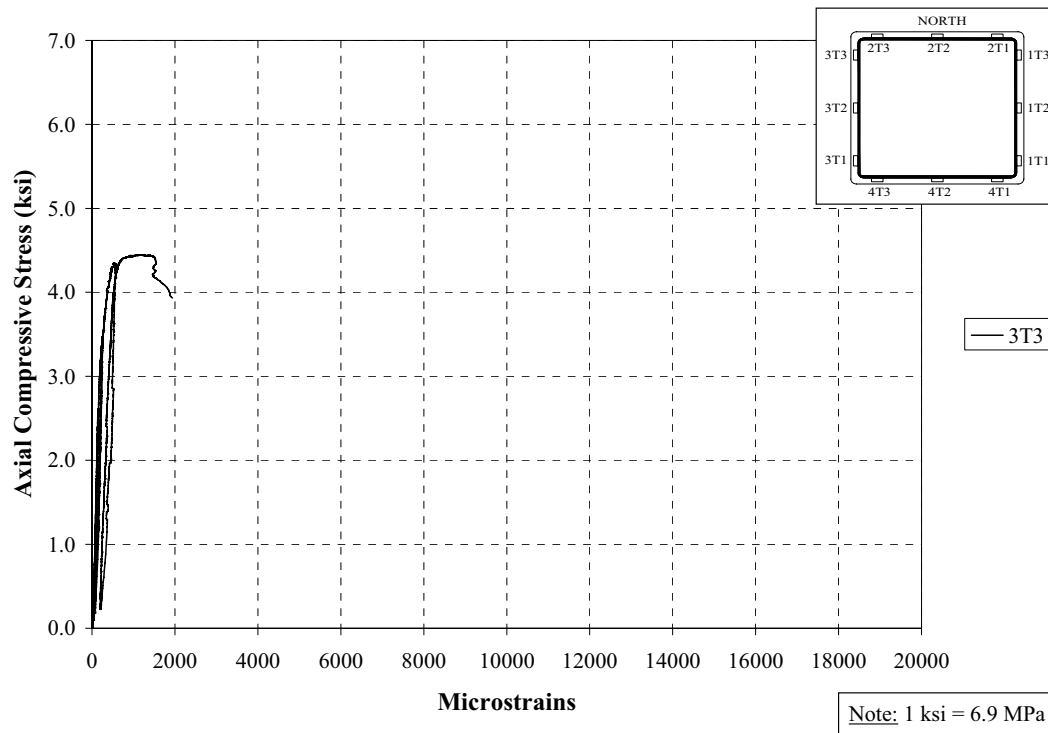Figure D92.  Axial Stress vs. Transverse Strain on FRP (South); Specimen D3
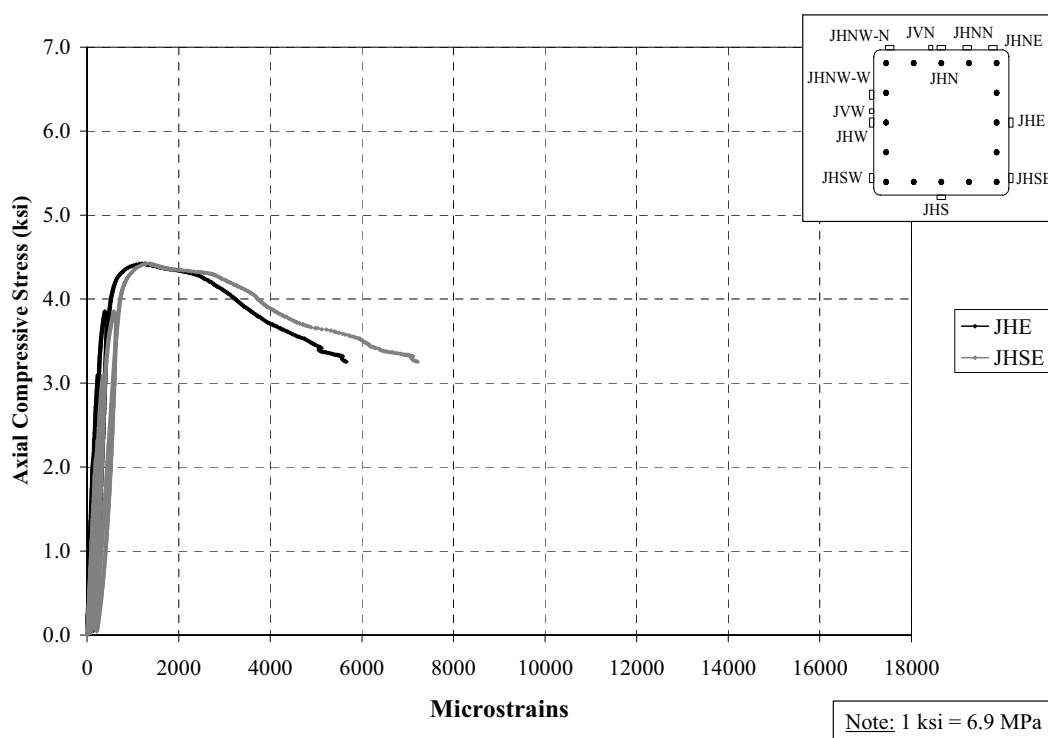


Figure D93.  Axial Stress vs. Transverse Strain on FRP (East); Specimen D3
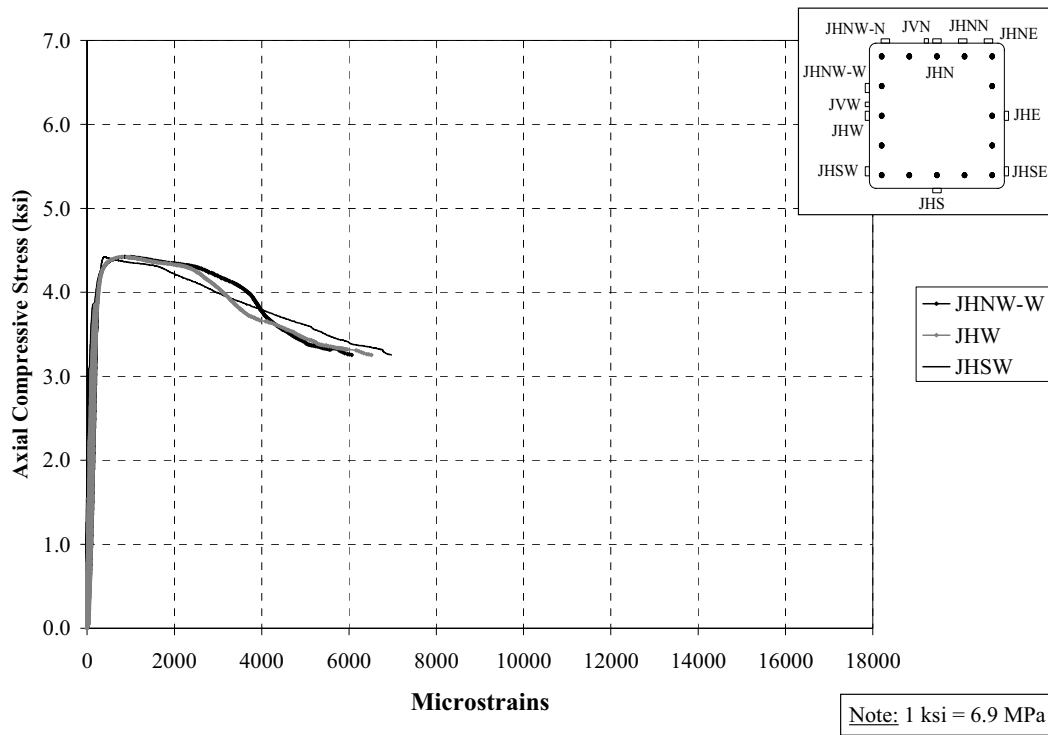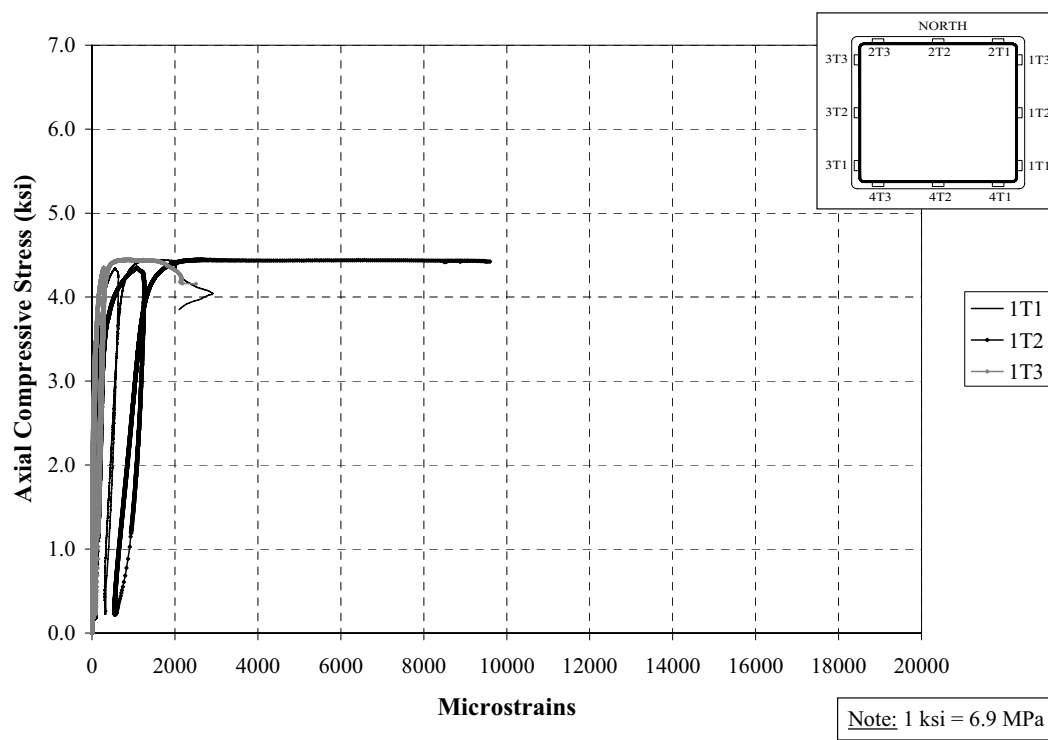
**Figure D94.  Axial Stress vs. Transverse Strain on FRP (West); Specimen D3**
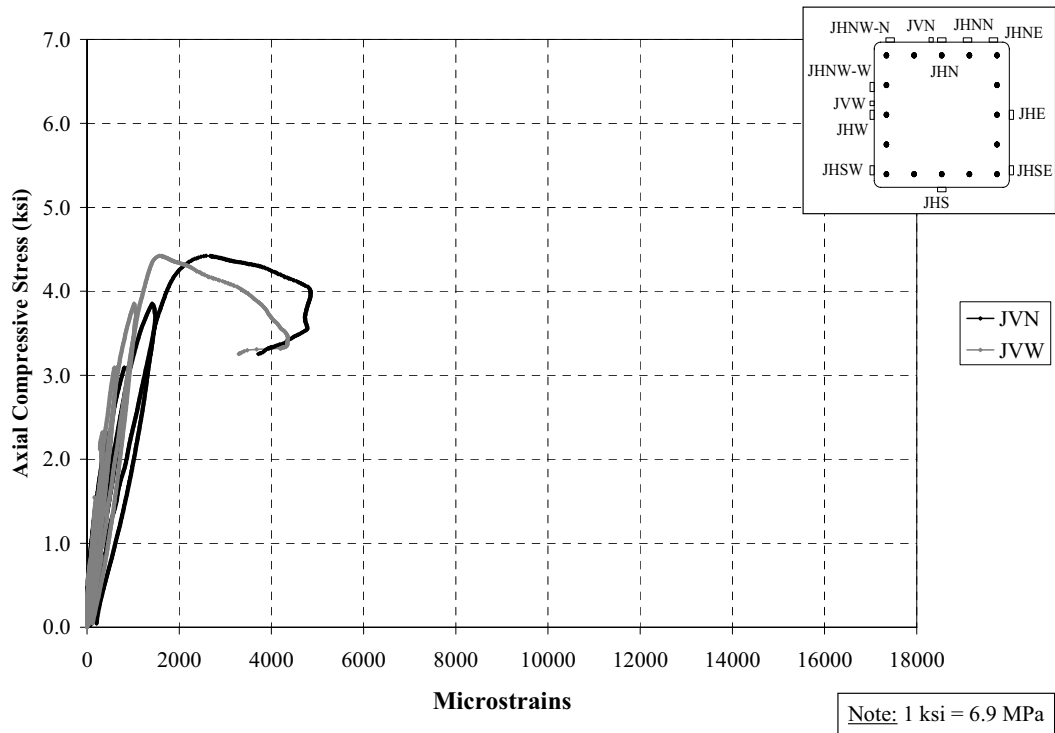


**Figure D95.  Axial Stress vs. Axial Strain on FRP (Sensors on Vertical Direction); Specimen D3**
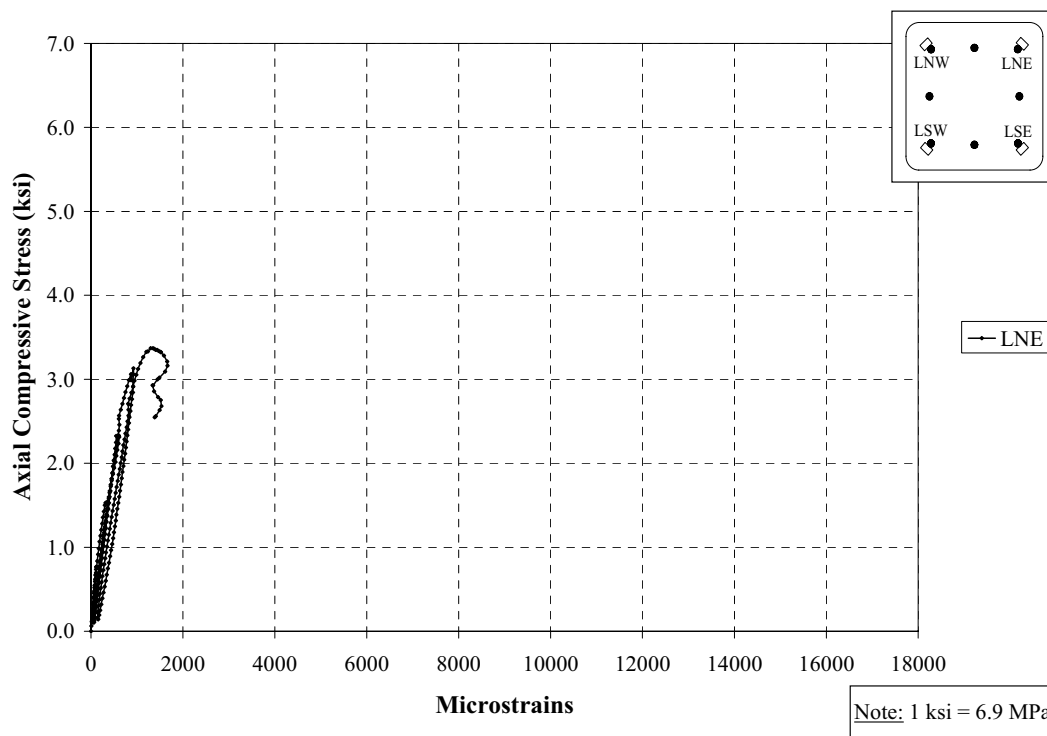
**Figure D96.  Axial Stress vs. Axial Strain on Longitudinal Bars (North); Specimen E1**
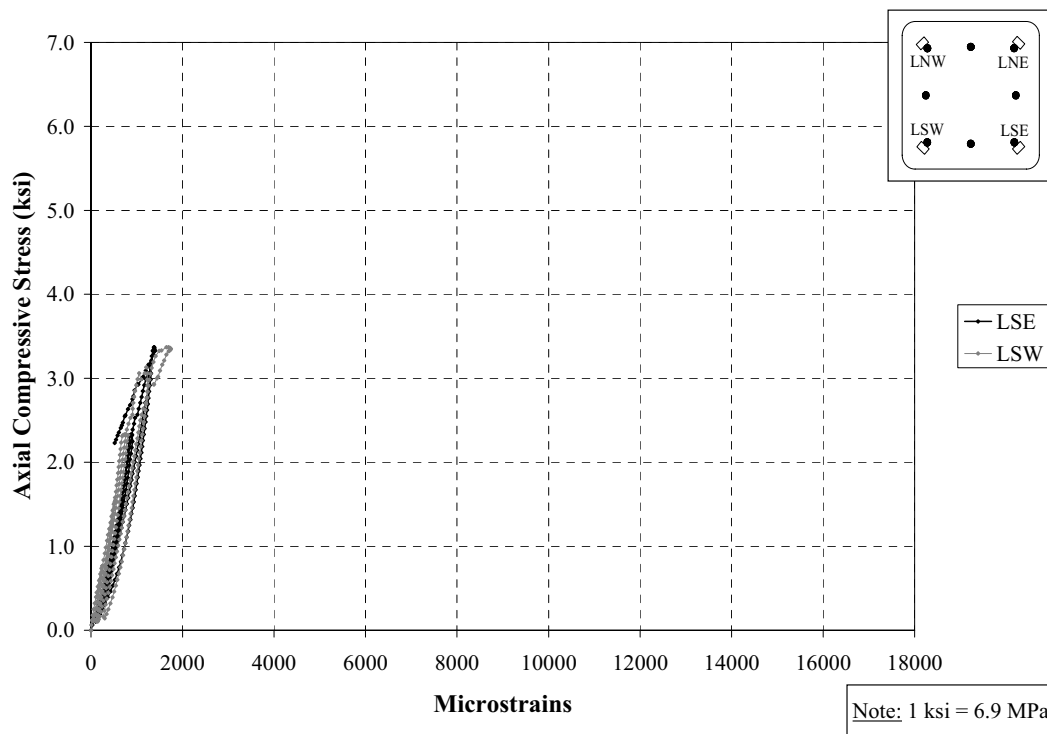


**Figure D97.  Axial Stress vs. Axial Strain on Longitudinal Bars (South); Specimen E1**
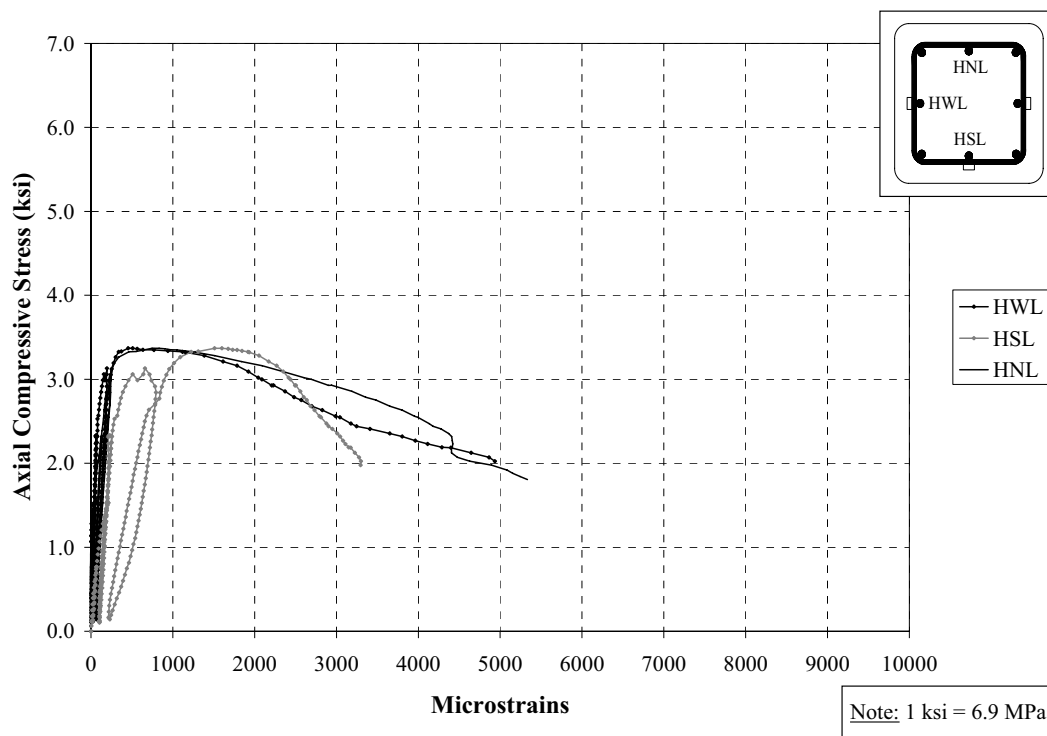
**Figure D98. Axial Stress vs. Transverse Strain on Lower Tie; Specimen E1**
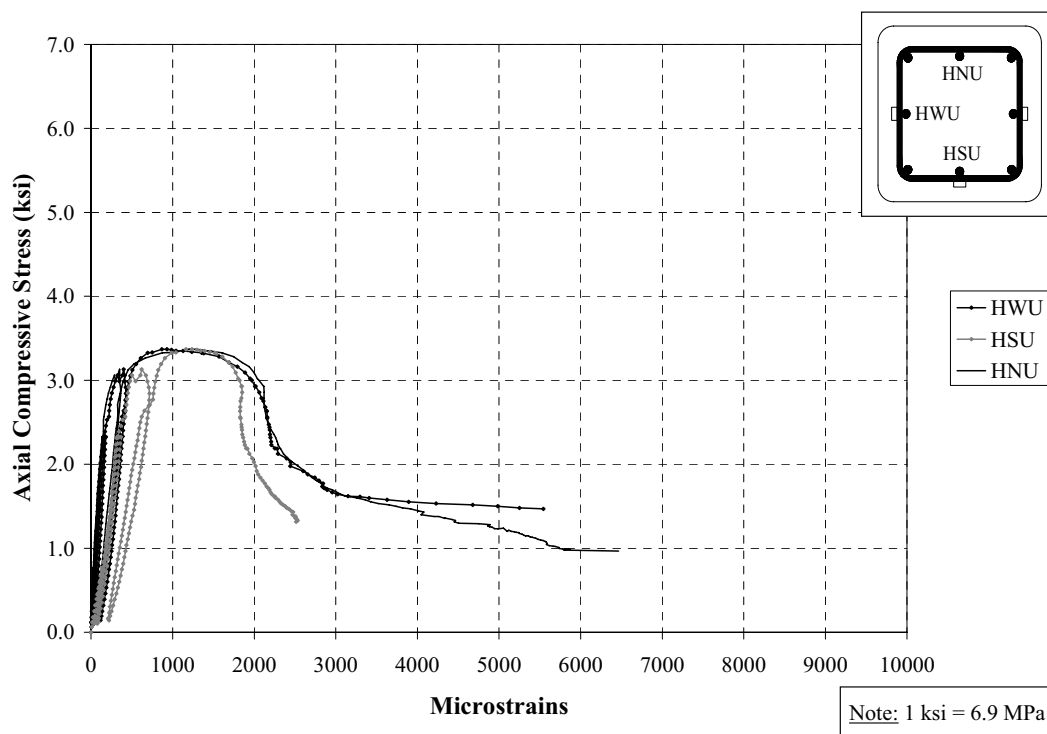


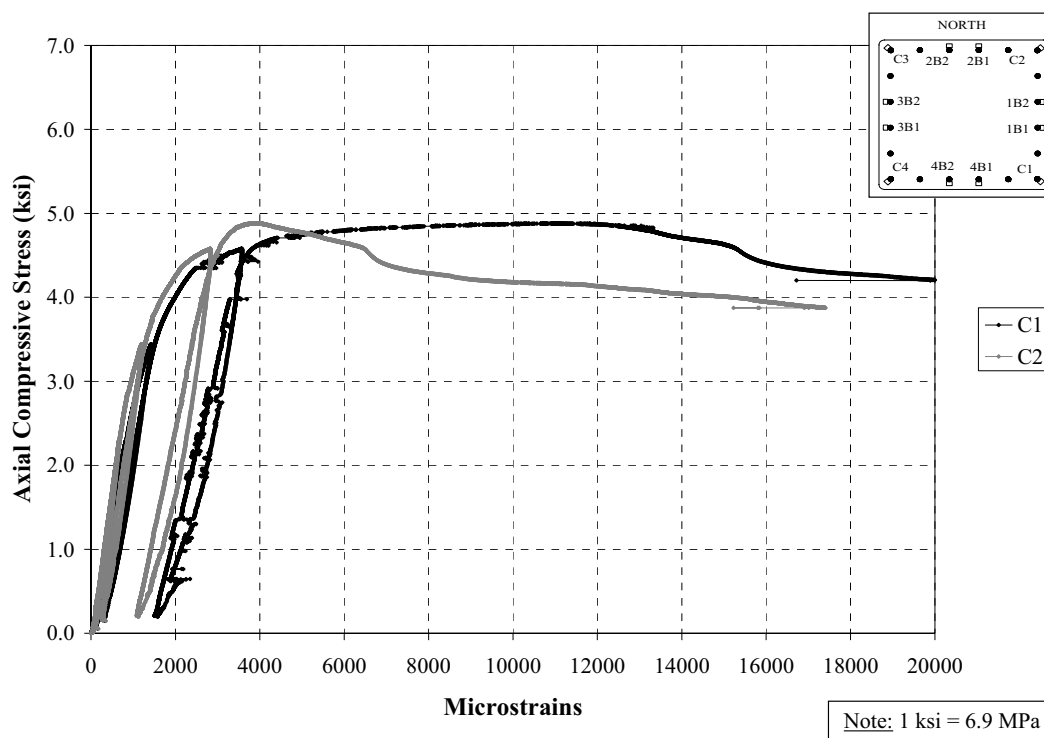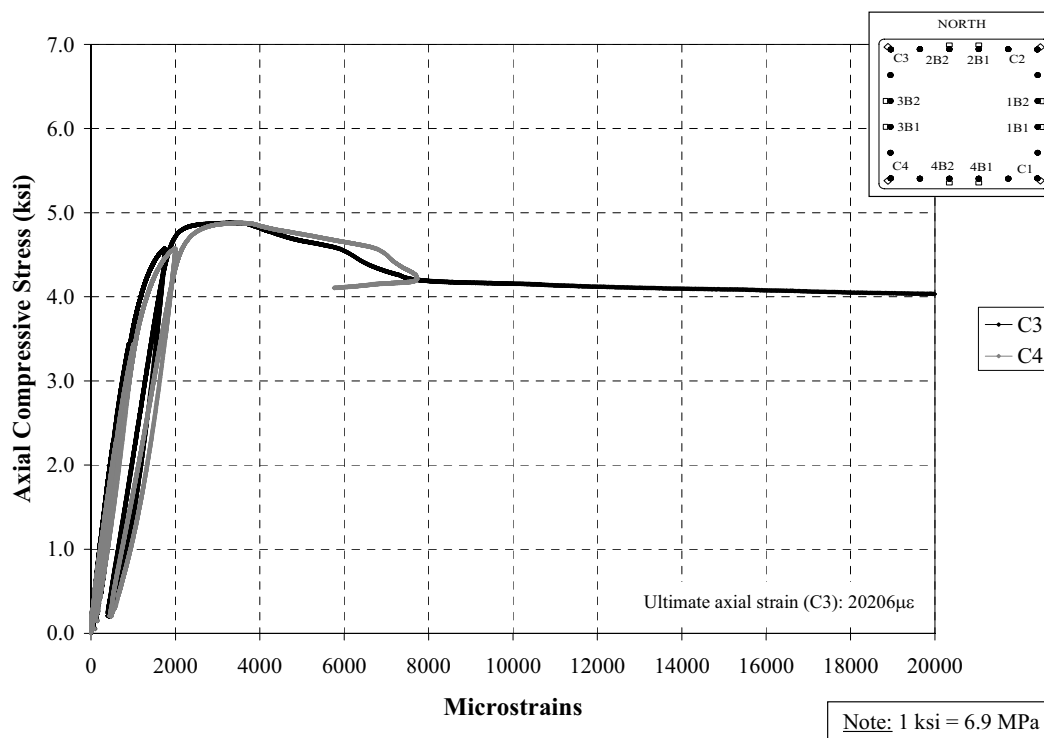**Figure D99. Axial Stress vs. Transverse Strain on Upper Tie; Specimen E1**

**Figure D100. Axial Stress vs. Axial Strain on Longitudinal Bars (North); Specimen E2**



**Figure D101. Axial Stress vs. Axial Strain on Longitudinal Bars (South); Specimen E2**

**Figure D102.  Axial Stress vs. Transverse Strain on Upper Tie; Specimen E2**
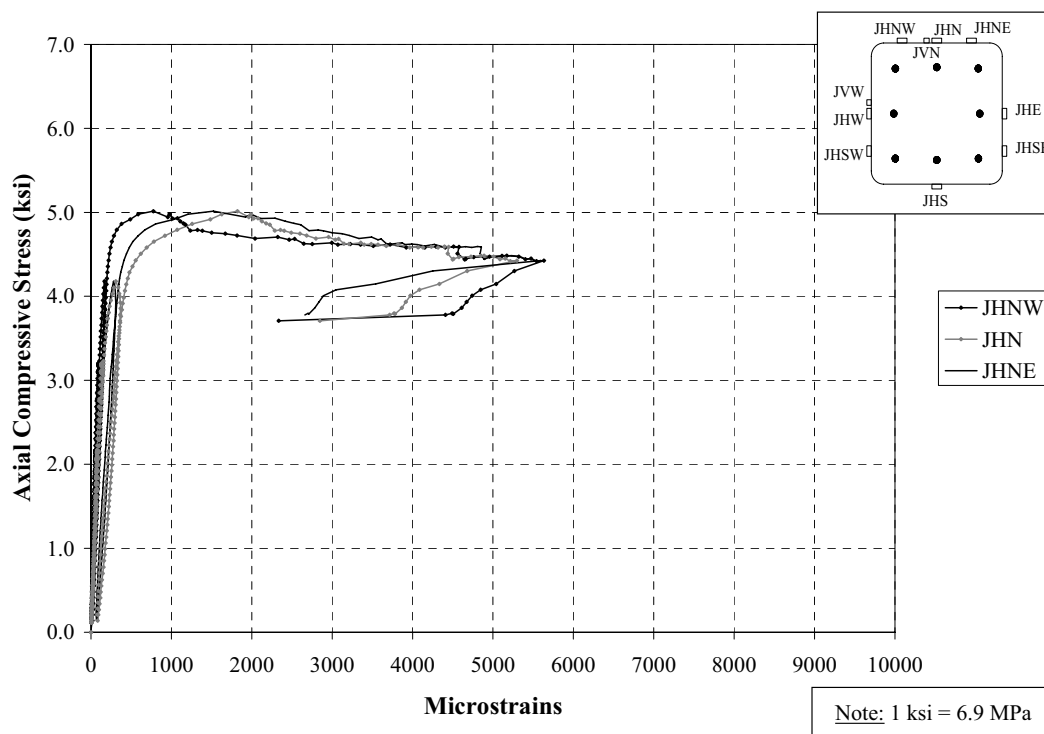


**Figure D103.  Axial Stress vs. Transverse Strain on FRP (North); Specimen E2**
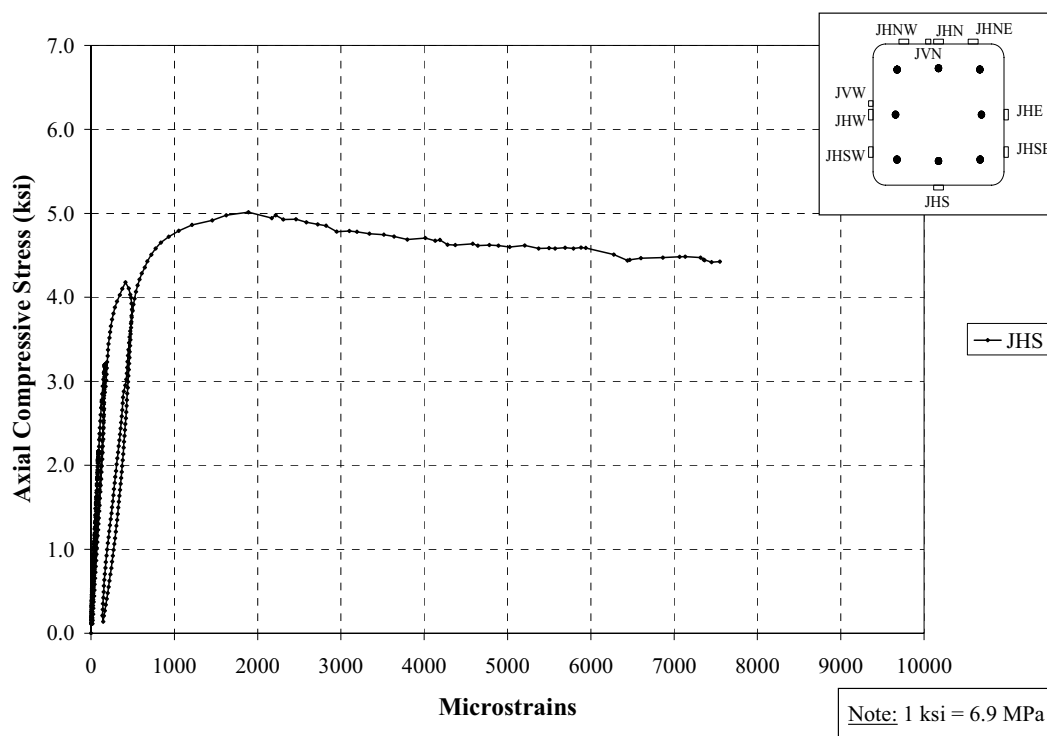
**Figure D104.  Axial Stress vs. Transverse Strain on FRP (South); Specimen E2**
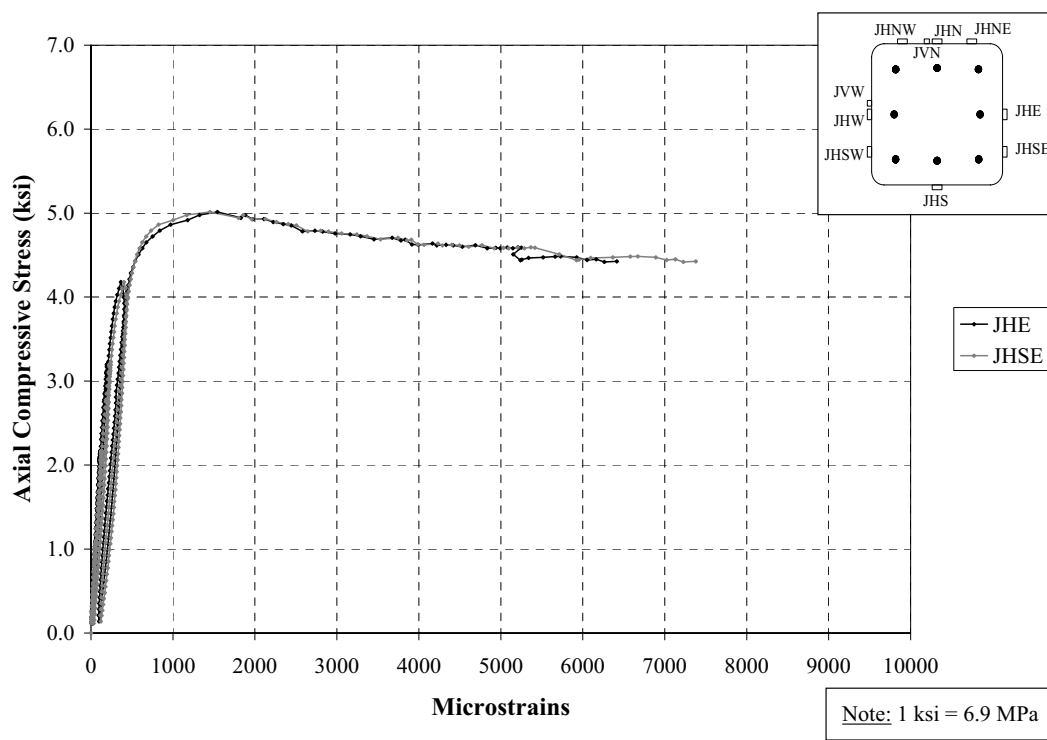


**Figure D105.  Axial Stress vs. Transverse Strain on FRP (East); Specimen E2**
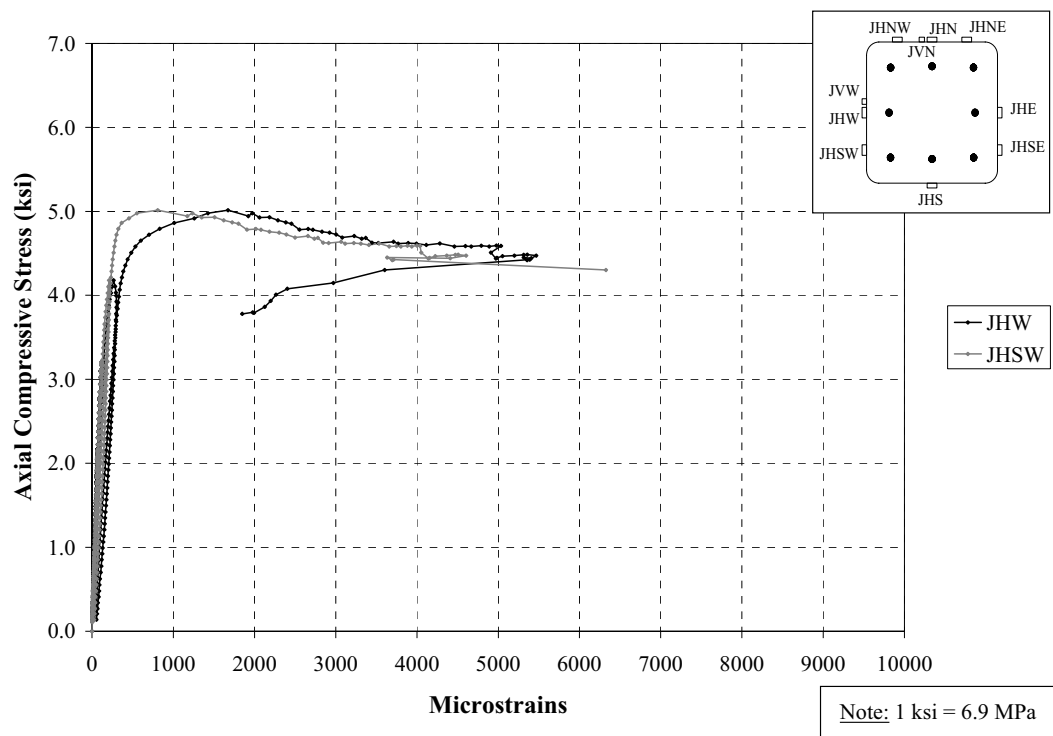
**Figure D106. Axial Stress vs. Transverse Strain on FRP (West); Specimen E2**
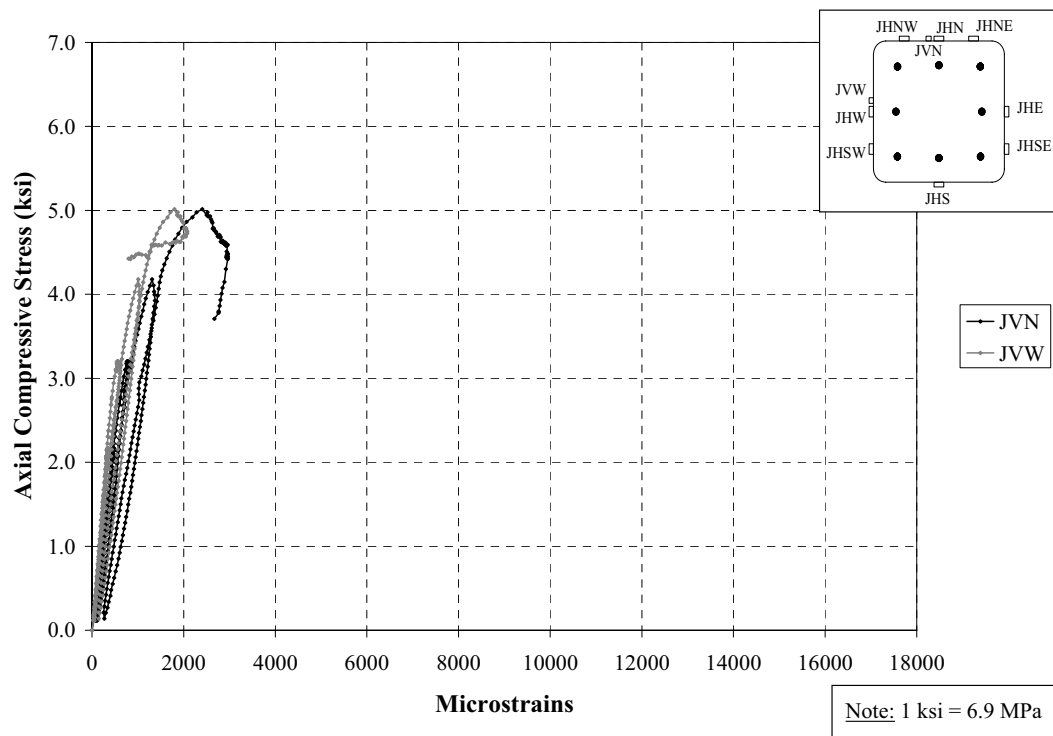


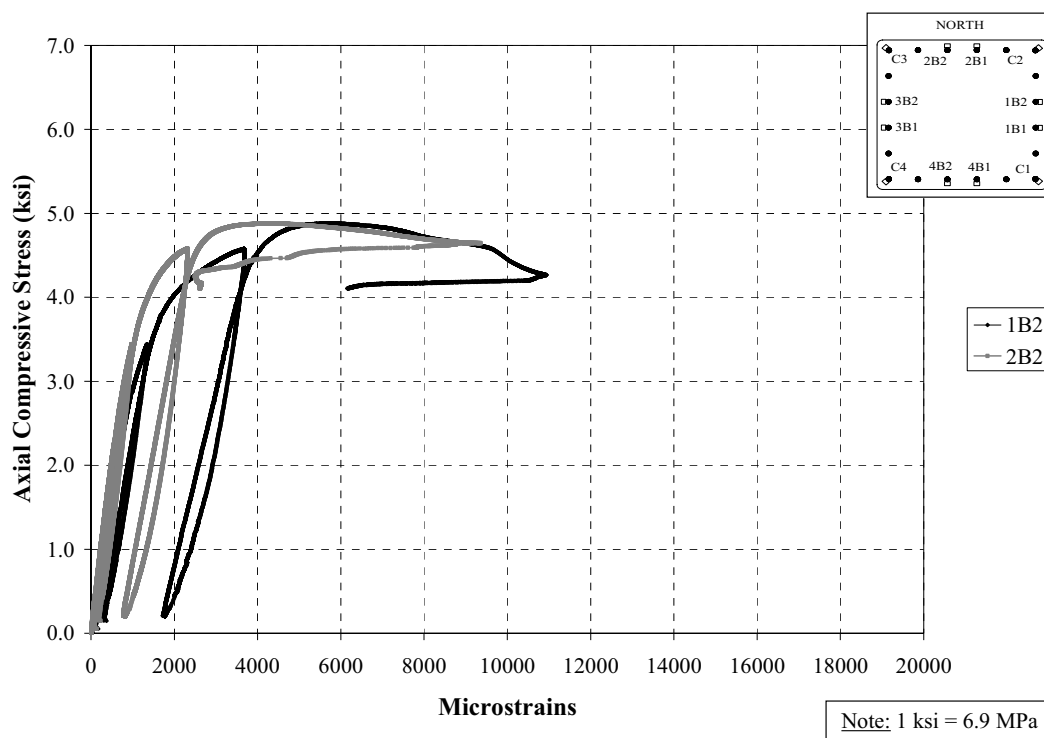**Figure D107. Axial Stress vs. Axial Strain (Sensors on Vertical Direction); Specimen E2**

**Figure D108.  Axial Stress vs. Axial Strain on Longitudinal Bars (North); Specimen E3**



**Figure D109.  Axial Stress vs. Axial Strain on Longitudinal Bars (South-Corners);
Specimen E3**

**Figure D110.  Axial Stress vs. Transverse Strain on Lower Tie; Specimen E3**



**Figure D111.  Axial Stress vs. Transverse Strain on Upper Tie; Specimen E3**
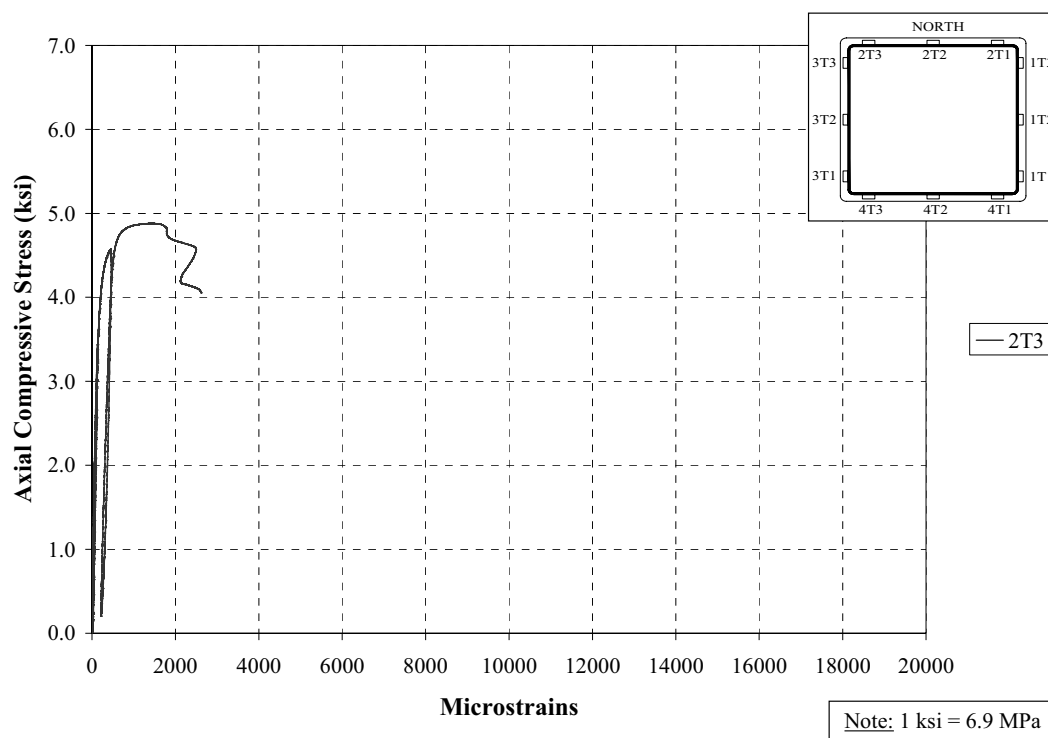
**Figure D112.  Axial Stress vs. Transverse Strain on FRP (North); Specimen E3**
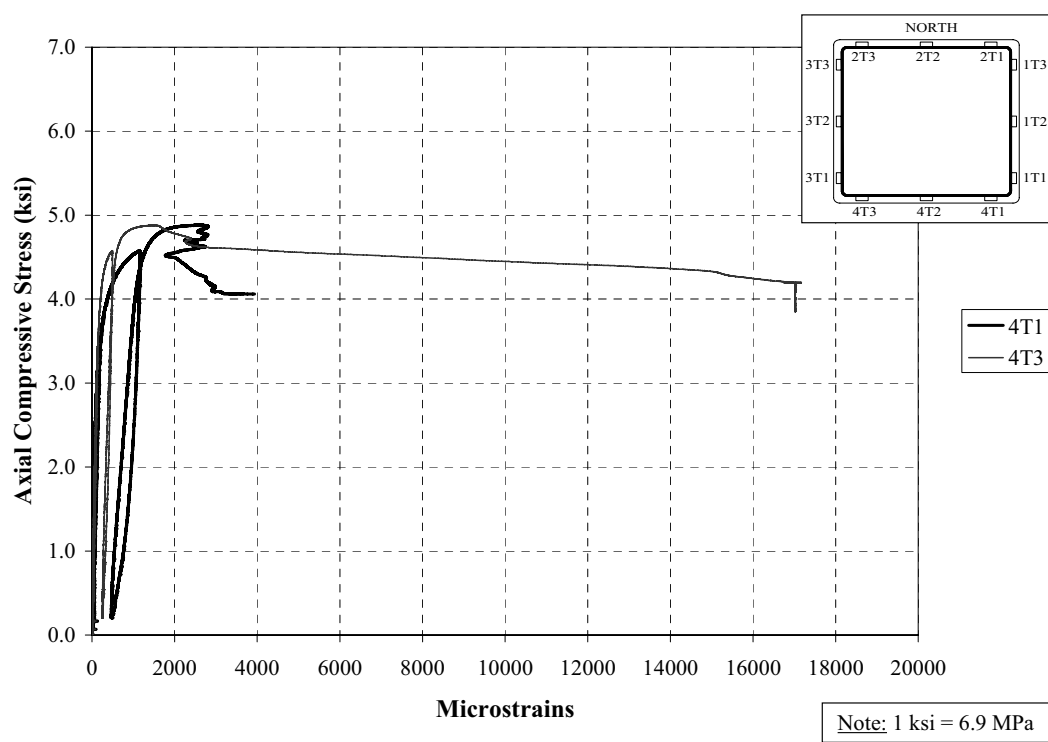


**Figure D113.  Axial Stress vs. Transverse Strain on FRP (South); Specimen E3**
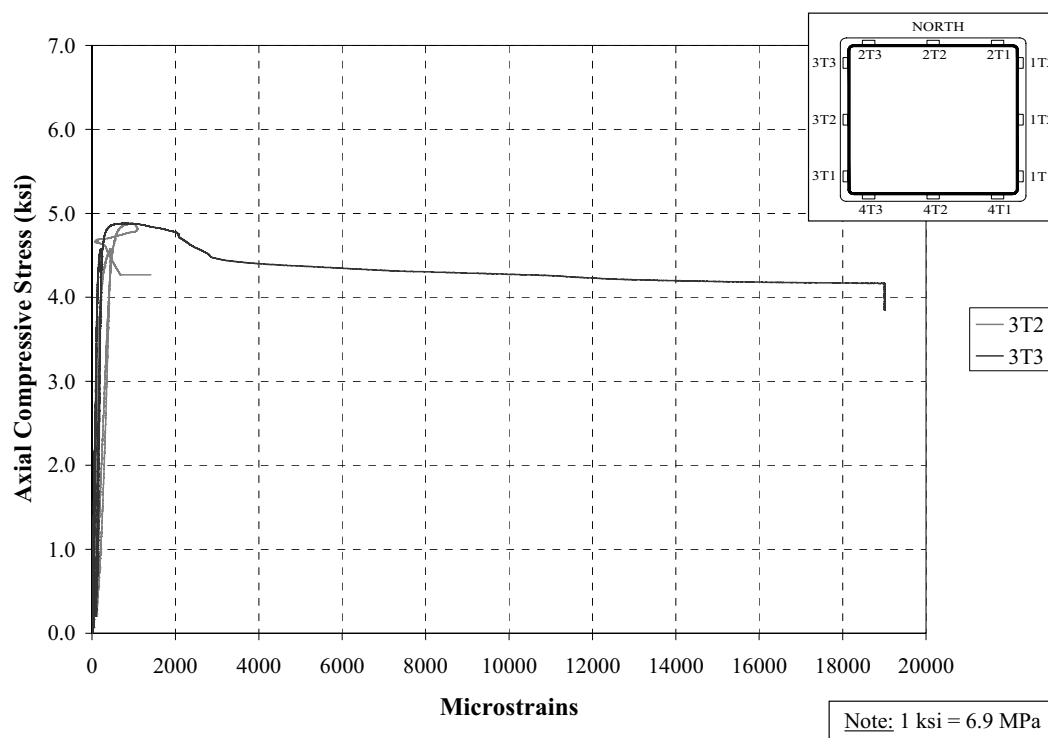
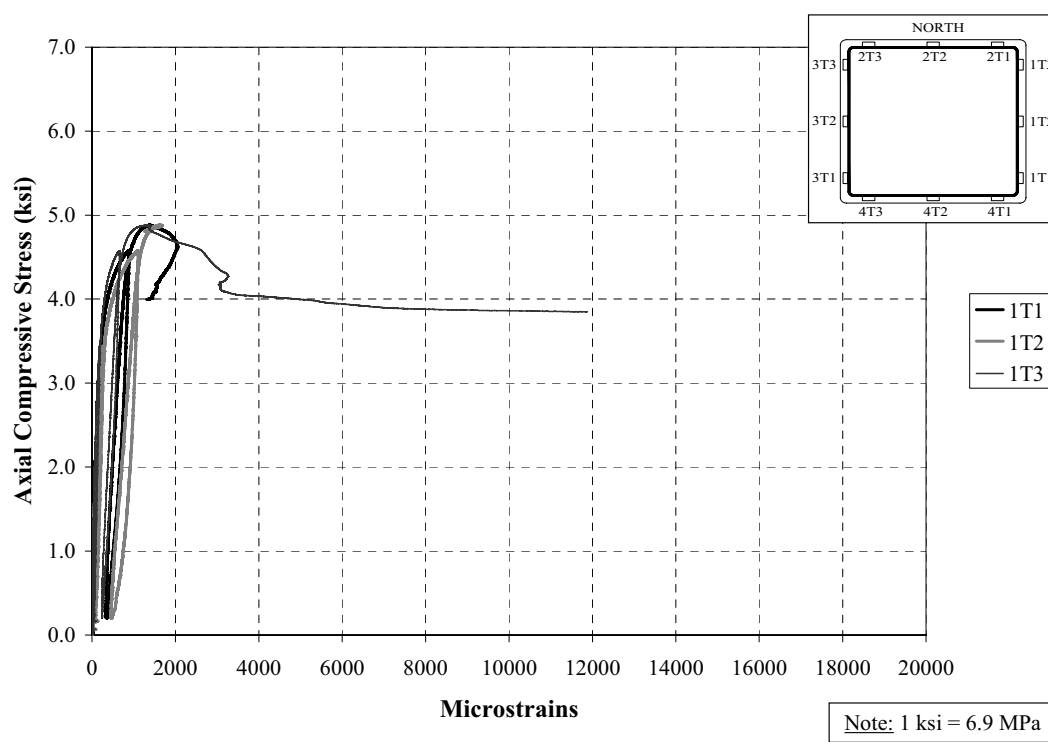**Figure D114.  Axial Stress vs. Transverse Strain on FRP (East); Specimen E3**



**Figure D115.  Axial Stress vs. Transverse Strain on FRP (West); Specimen E3**

**Figure D116. Axial Stress vs. Axial Strain on FRP (Sensors on Vertical Direction); Specimen E3**

**Figure D117. Axial Stress vs. Axial Strain on Longitudinal Bars (North); Specimen F1**



**Figure D118. Axial Stress vs. Transverse Strain on Lower Tie; Specimen F1**

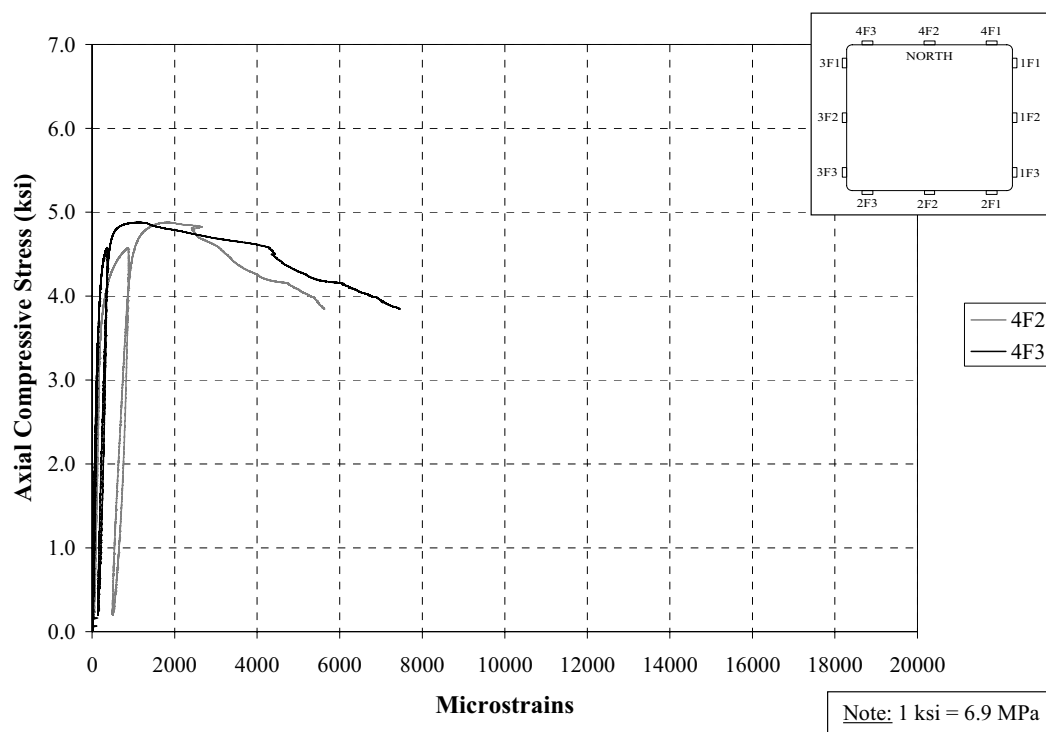**Figure D119.  Axial Stress vs. Transverse Strain on Upper Tie; Specimen F1**



**Figure D120.  Axial Stress vs. Axial Strain on Longitudinal Bars (North); Specimen F2**

**Figure D121.  Axial Stress vs. Axial Strain on Longitudinal Bars (South); Specimen F2**



**Figure D122.  Axial Stress vs. Transverse Strain on Lower Tie; Specimen F2**

**Figure D123.  Axial Stress vs. Transverse Strain on Upper Tie; Specimen F2**



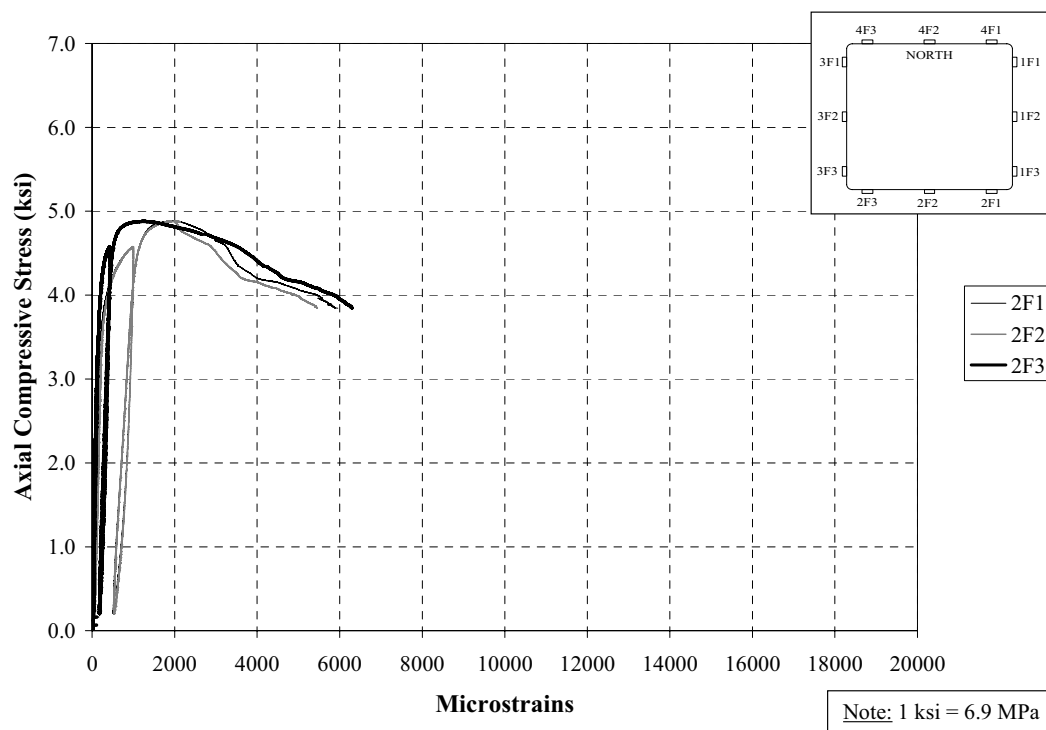**Figure D124.  Axial Stress vs. Transverse Strain on FRP (North); Specimen F2**

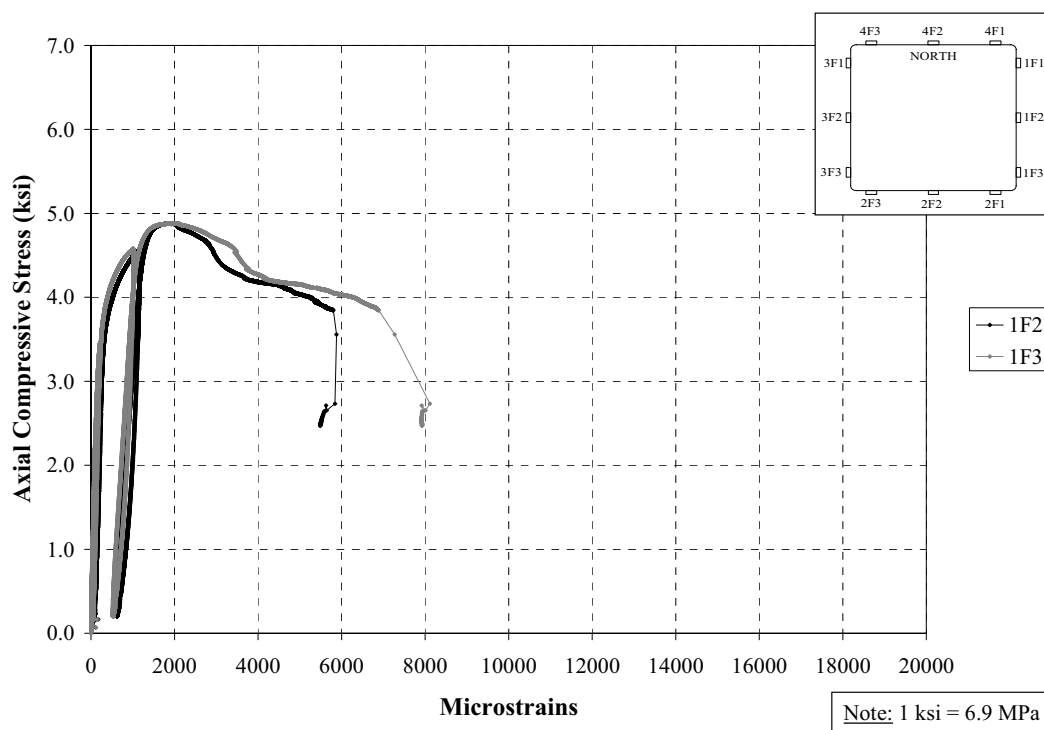**Figure D125.  Axial Stress vs. Transverse Strain on FRP (South); Specimen F2**
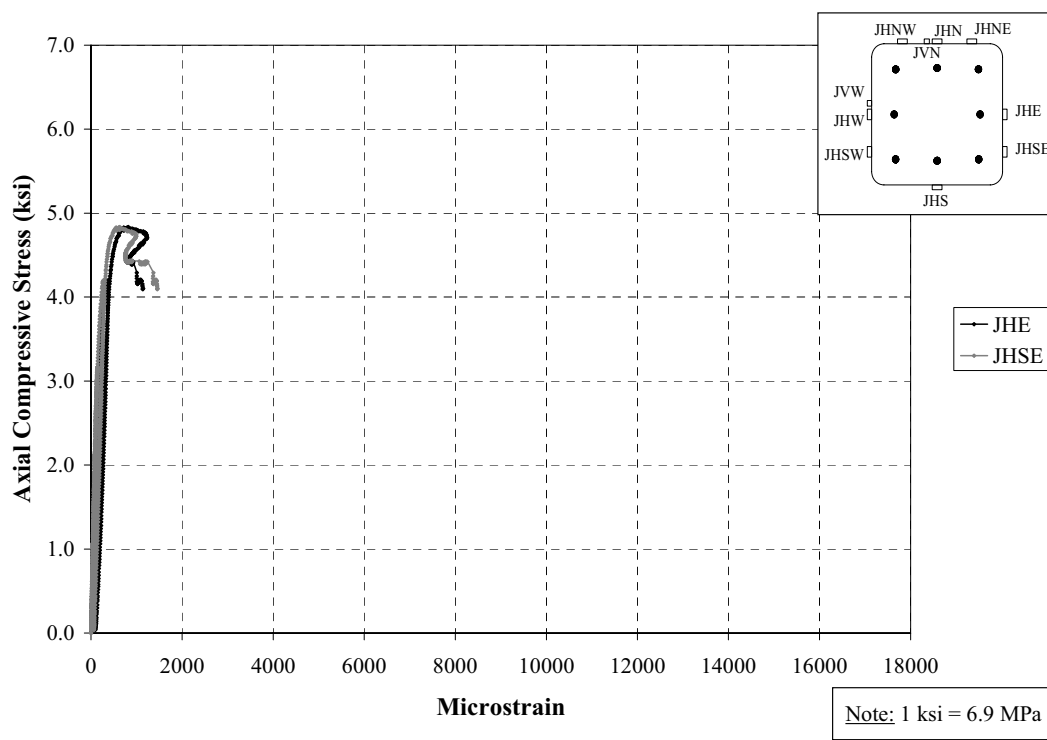


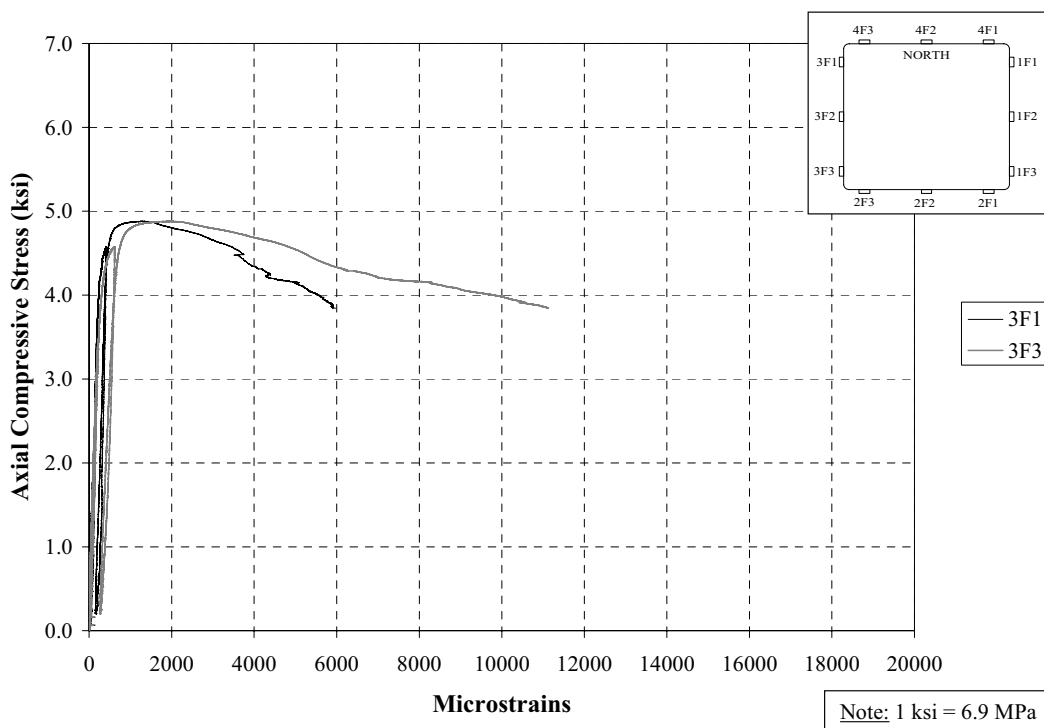**Figure D126.  Axial Stress vs. Transverse Strain on FRP (East); Specimen F2**

**Figure D127. Axial Stress vs. Transverse Strain on FRP (West); Specimen F2**



**Figure D128. Axial Stress vs. Axial Strain (Sensors on Vertical Direction); Specimen F2**

**Figure D129. Axial Stress vs. Axial Strain on Longitudinal Bars (North); Specimen F3**



**Figure D130. Axial Stress vs. Axial Strain on Longitudinal Bars (South); Specimen F3**

**Figure D131.  Axial Stress vs. Transverse Strain on Lower Tie; Specimen F3**



**Figure D132.  Axial Stress vs. Transverse Strain on Upper Tie; Specimen F3**

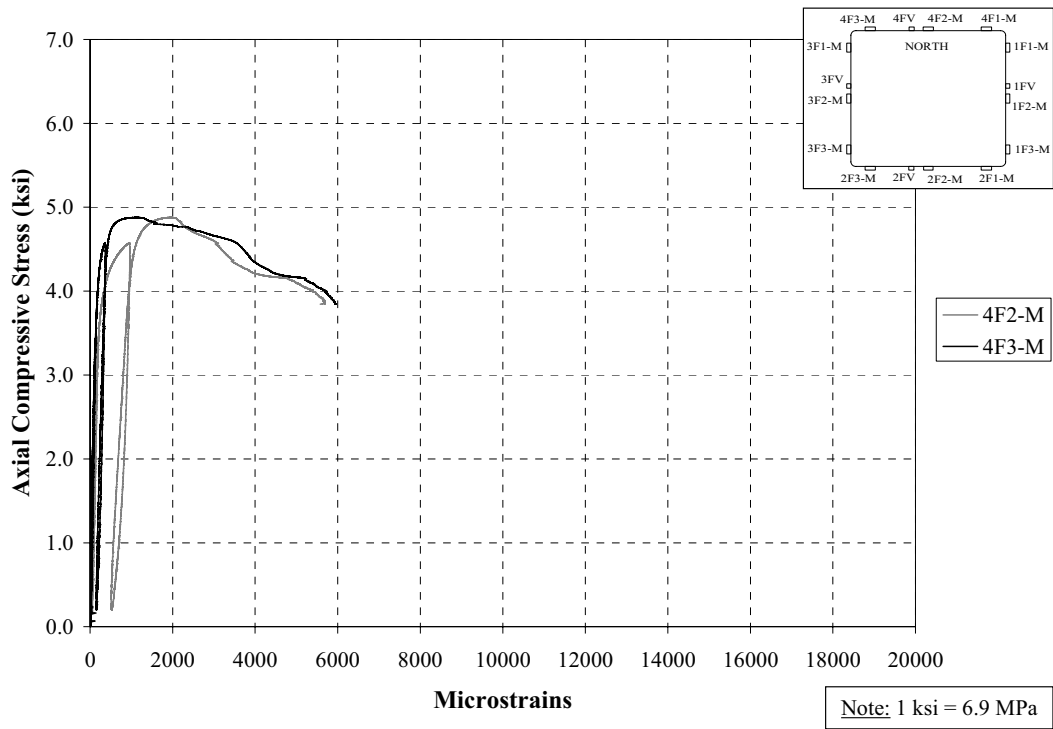**Figure D133. Axial Stress vs. Transverse Strain on FRP (North); Specimen F3**



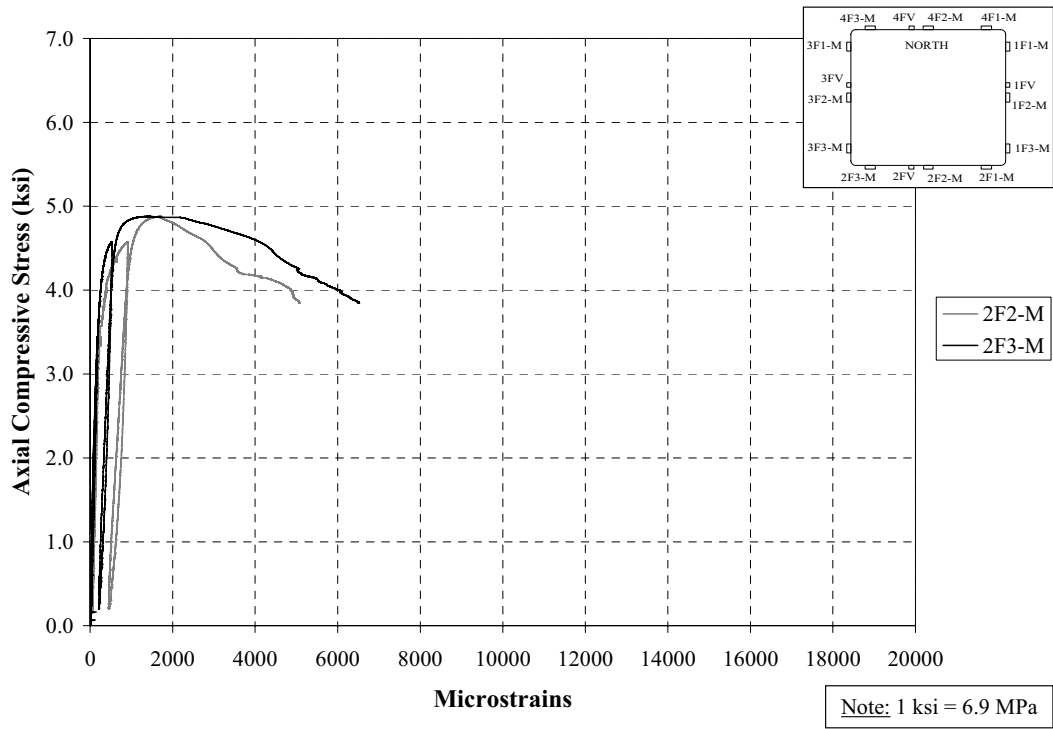**Figure D134. Axial Stress vs. Transverse Strain on FRP (South); Specimen F3**

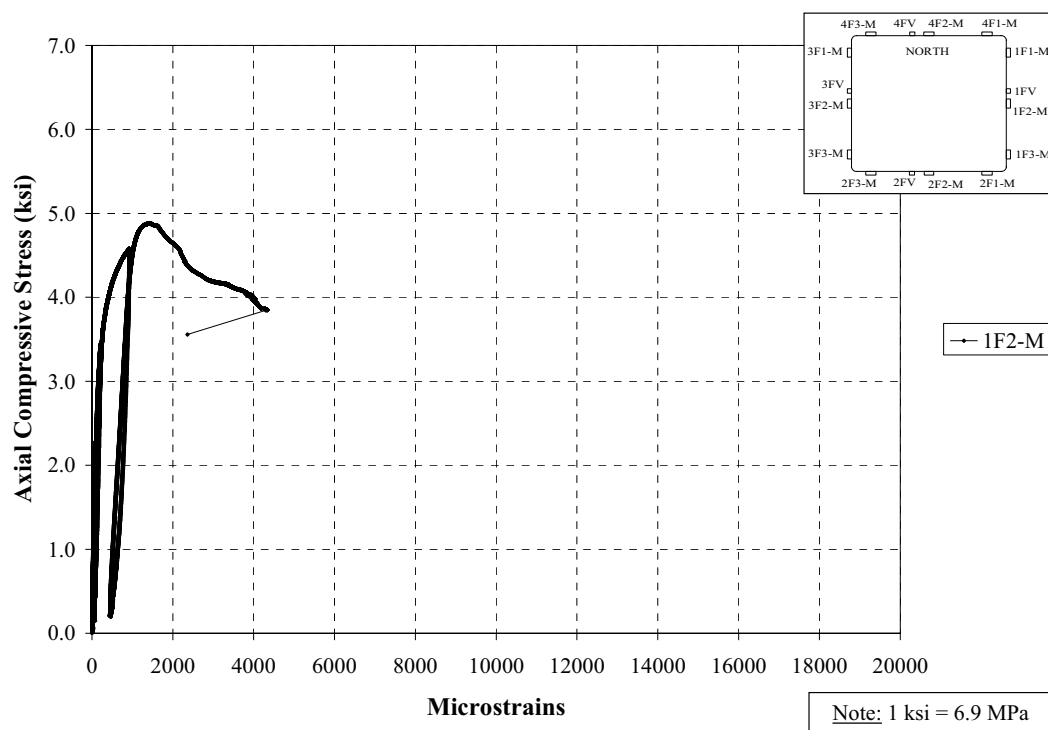**Figure D135.  Axial Stress vs. Transverse Strain on FRP (East); Specimen F3**



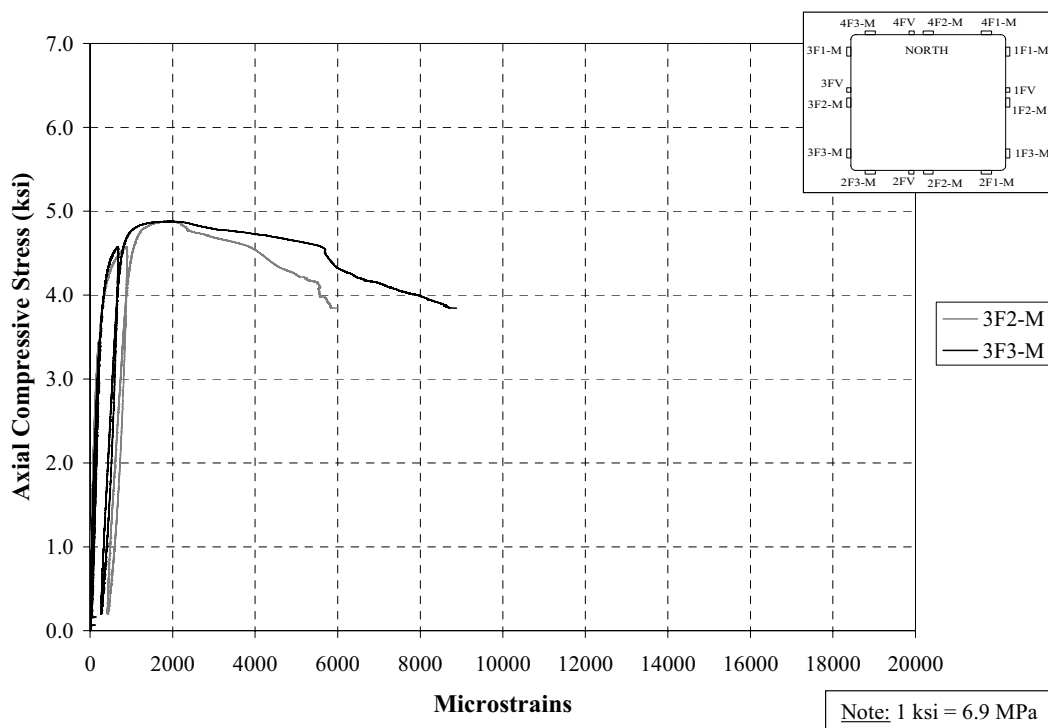**Figure D136.  Axial Stress vs. Transverse Strain on FRP (West); Specimen F3**
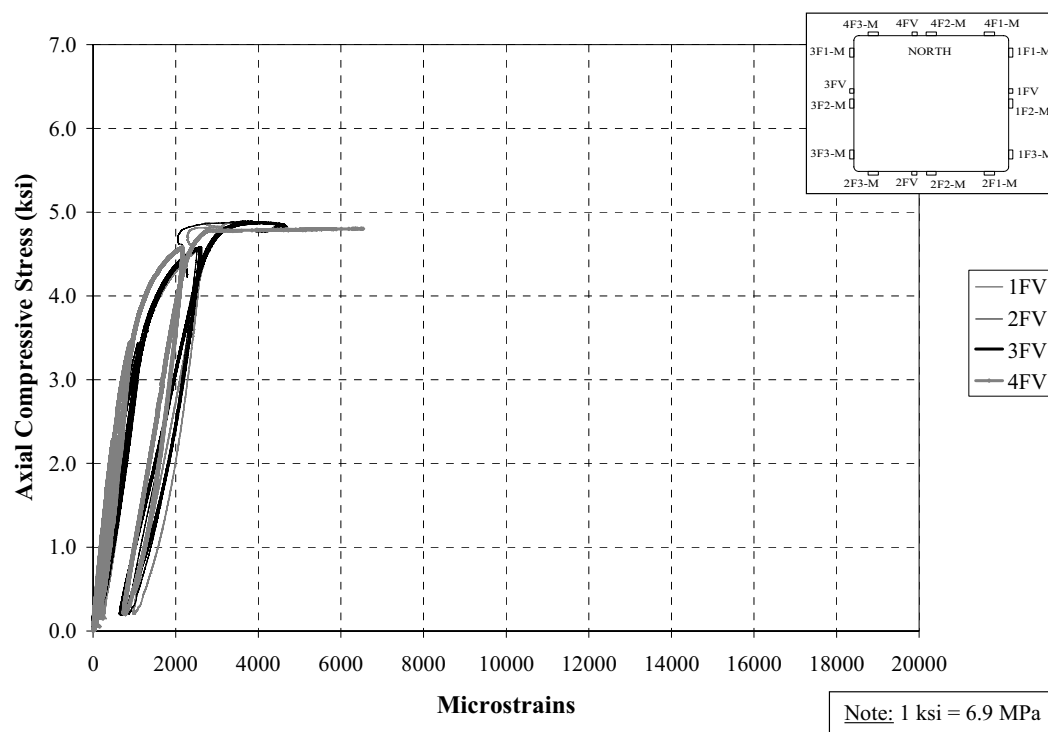
**Figure D137. Axial Stress vs. Axial Strain on FRP (Sensors on Vertical Direction); Specimen F3**
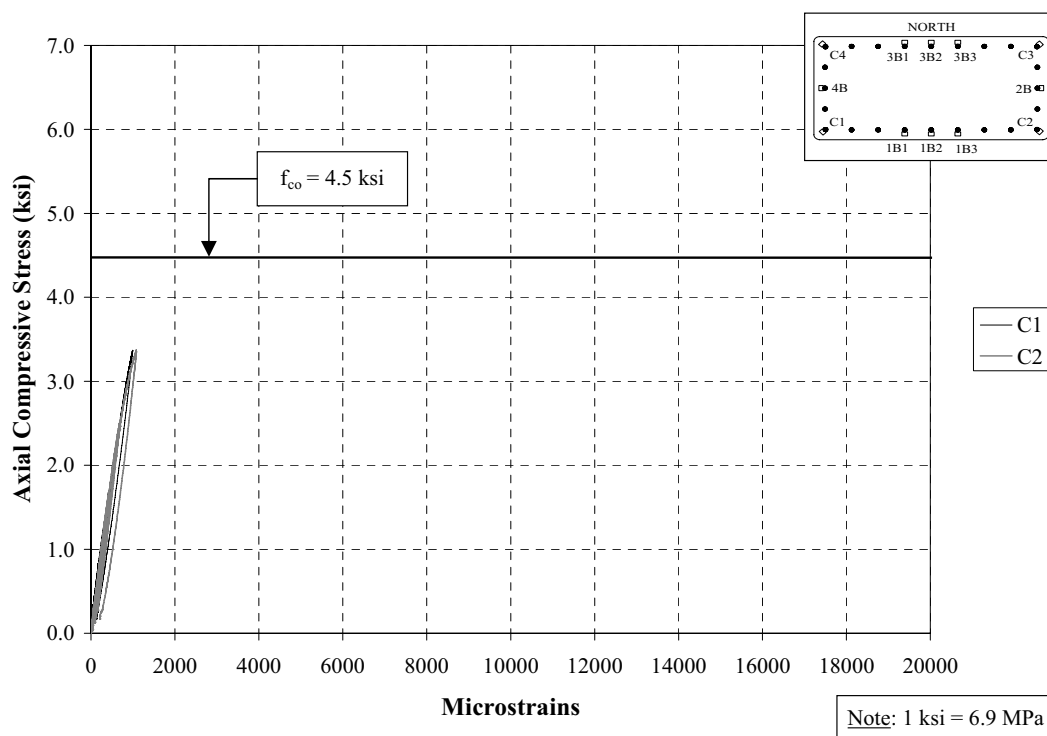
**Figure D138. Axial Stress vs. Axial Strain on Longitudinal Corner Bars C1 & C2; Specimen G1**
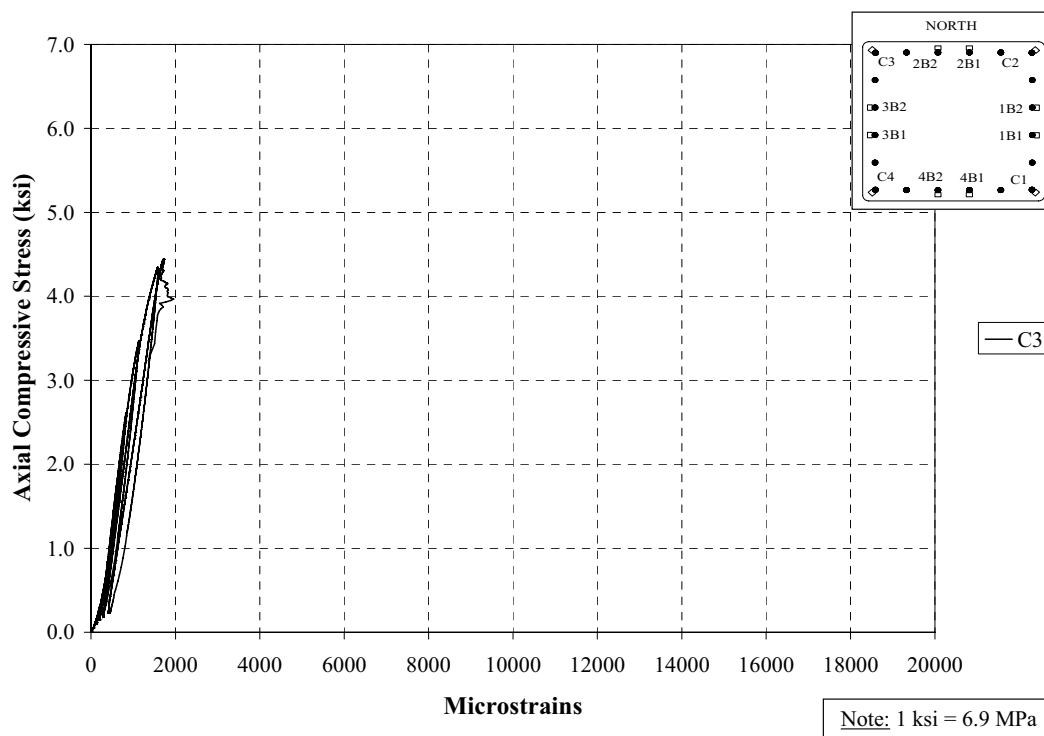


**Figure D139. Axial Stress vs. Axial Strain on Longitudinal Corner Bar C3; Specimen G1**
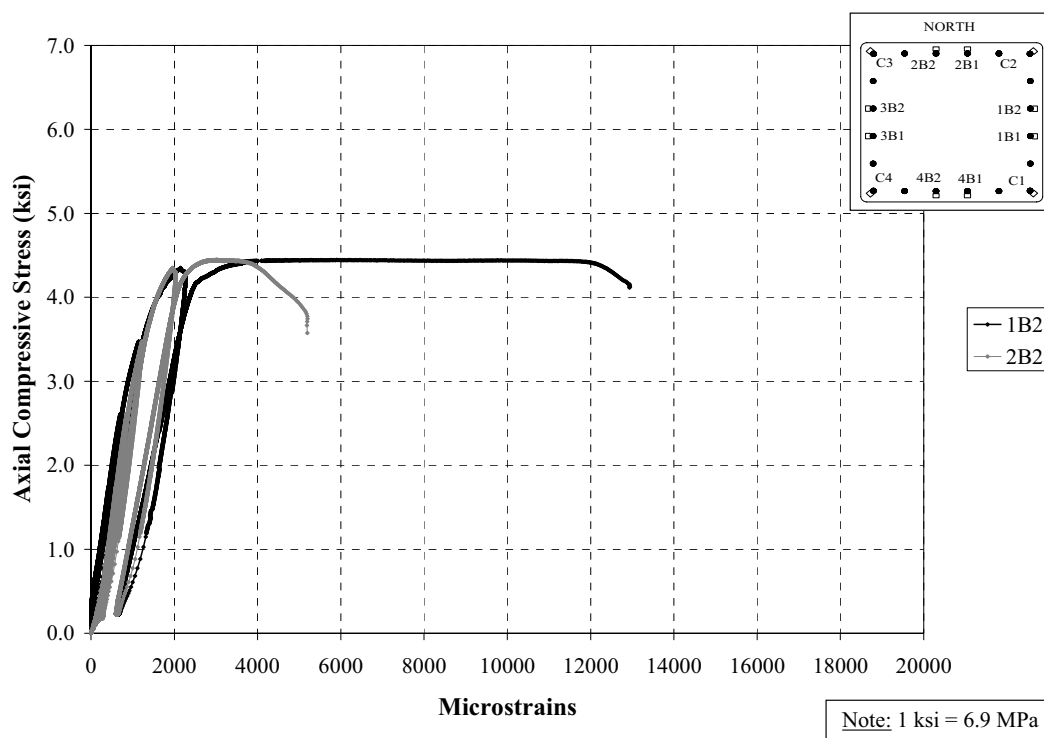
**Figure D140.  Axial Stress vs. Axial Strain on Longitudinal Central Bars (1B2 & 2B2);
Specimen G1**



**Figure D141.  Axial Stress vs. Axial Strain on Longitudinal Central Bars (4B1 & 3B2);
Specimen G1**

**Figure D142.  Axial Stress vs. Transverse Strain on Tie (North); Specimen G1**



**Figure D143.  Axial Stress vs. Transverse Strain on Tie (South); Specimen G1**

**Figure D144.  Axial Stress vs. Transverse Strain on Tie (East); Specimen G1**



**Figure D145.  Axial Stress vs. Transverse Strain on Tie (West); Specimen G1**

**Figure D146.  Axial Stress vs. Axial Strain on Longitudinal Corner Bars (C1 & C2); Specimen G2**
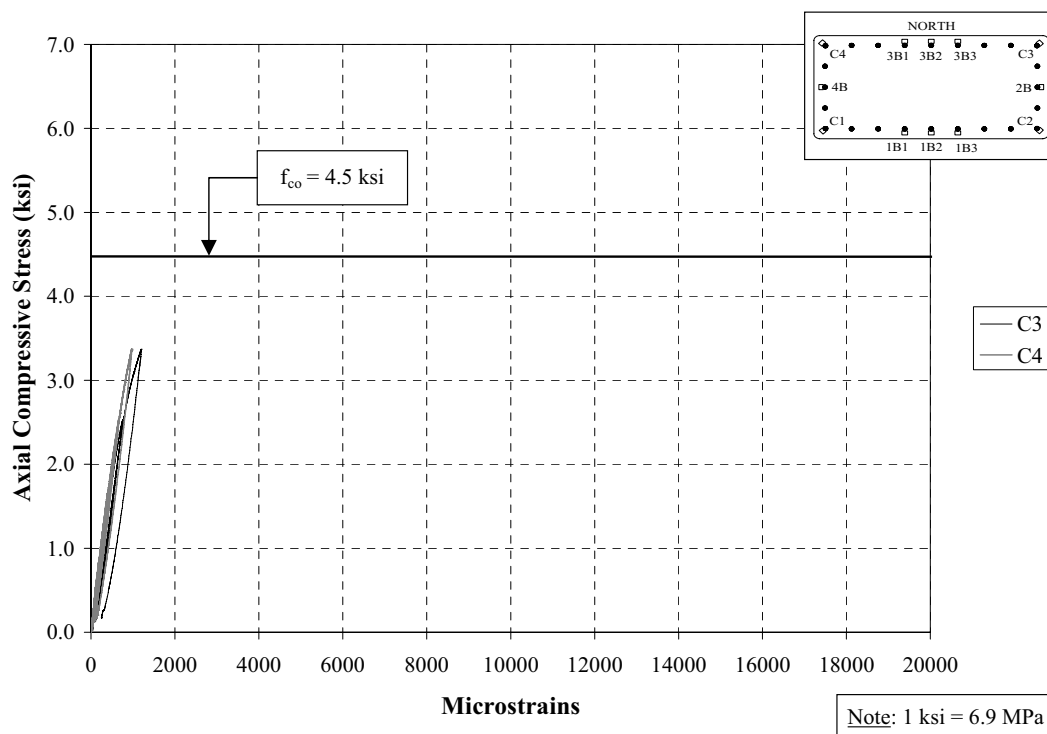


**Figure D147.  Axial Stress vs. Axial Strain on Longitudinal Corner Bars (C3 & C4); Specimen G2**
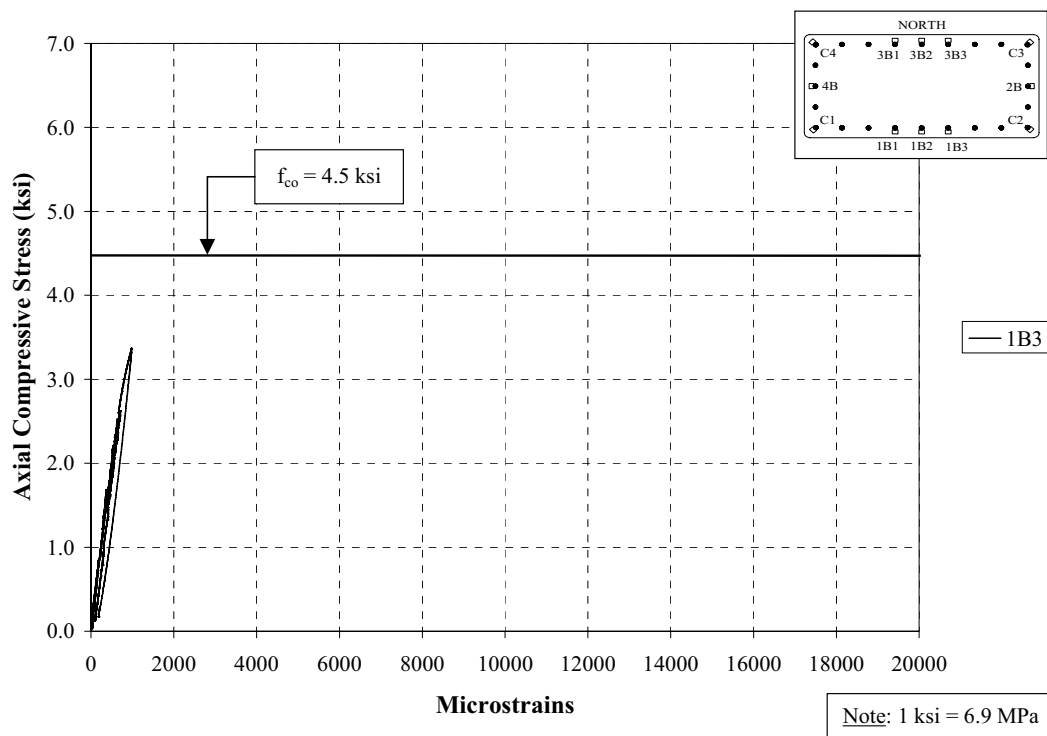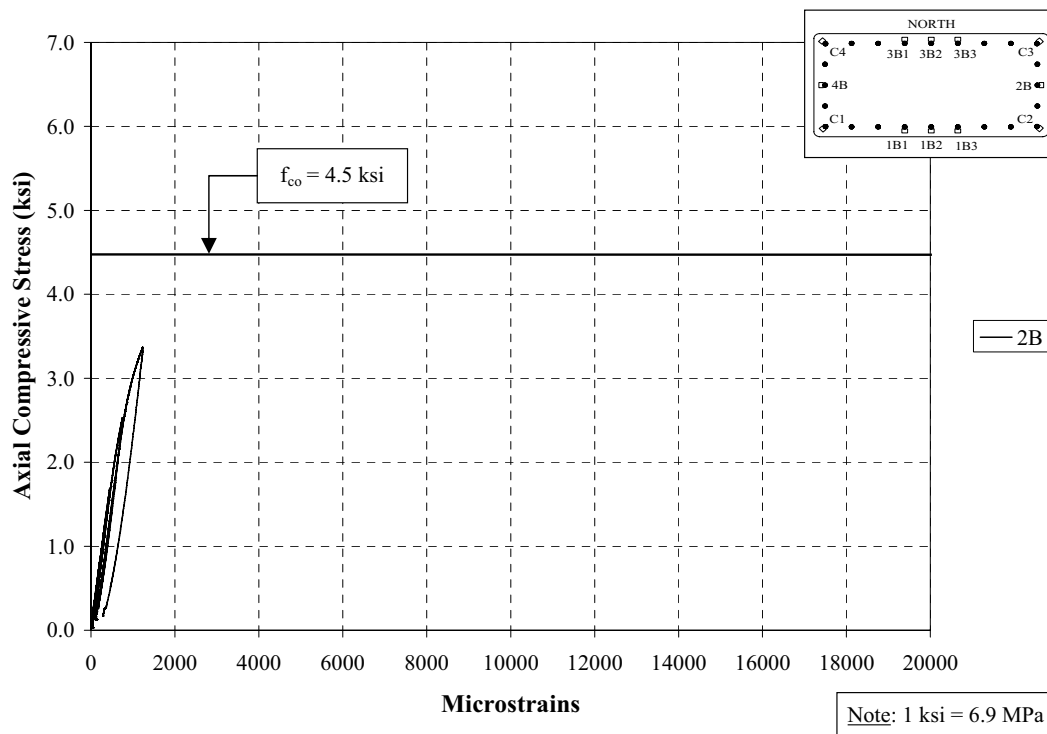
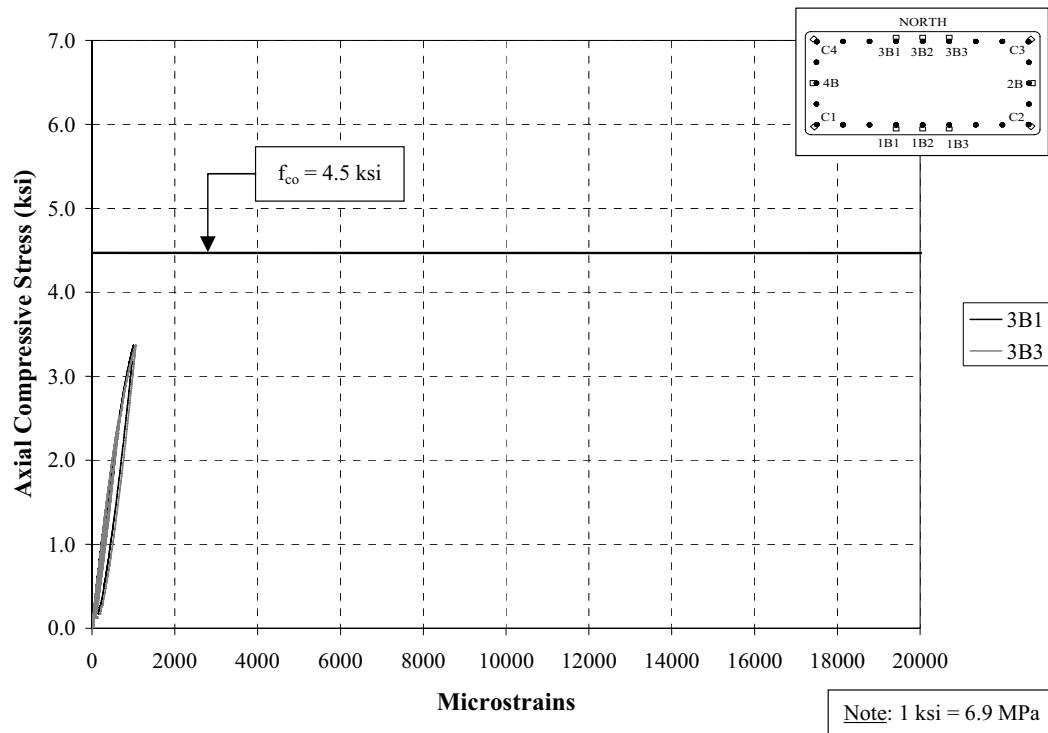**Figure D148. Axial Stress vs. Axial Strain on Longitudinal Central Bars (1B2 & 2B2); Specimen G2**
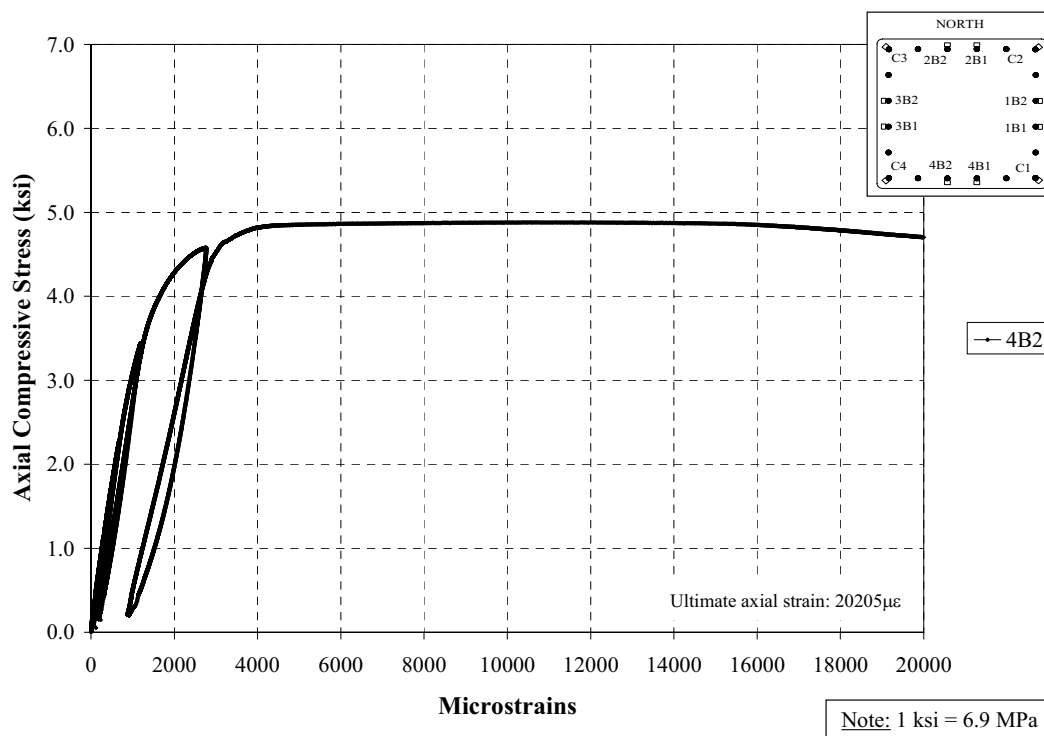


**Figure D149. Axial Stress vs. Axial Strain on Longitudinal Central Bar (4B2); Specimen G2**
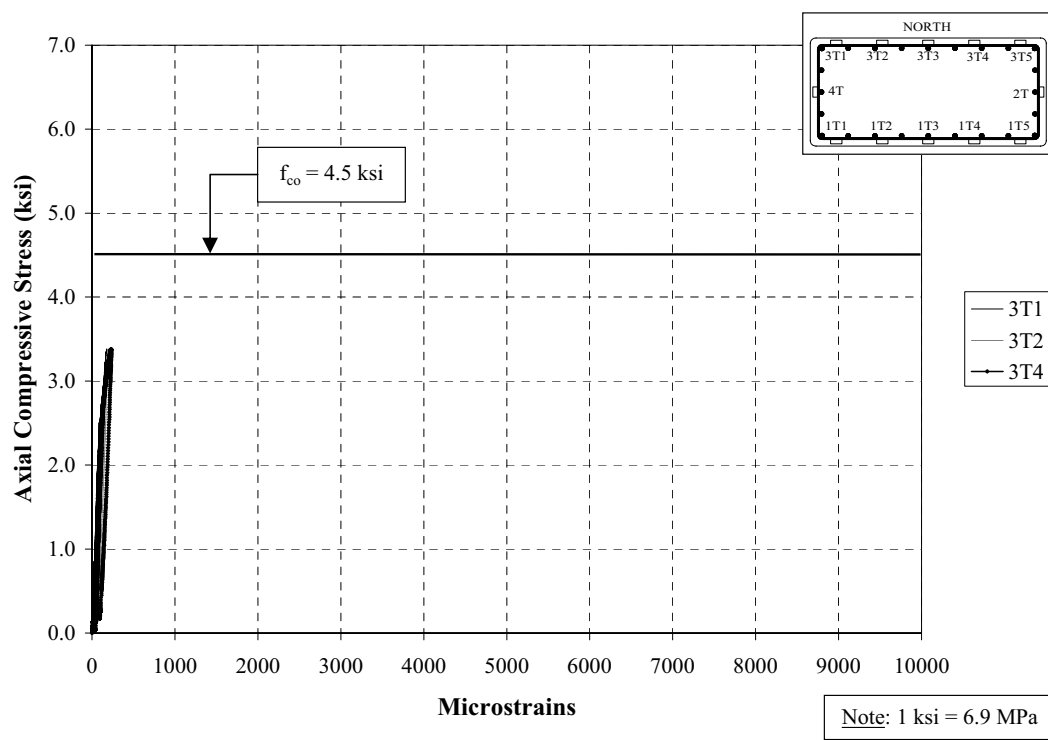
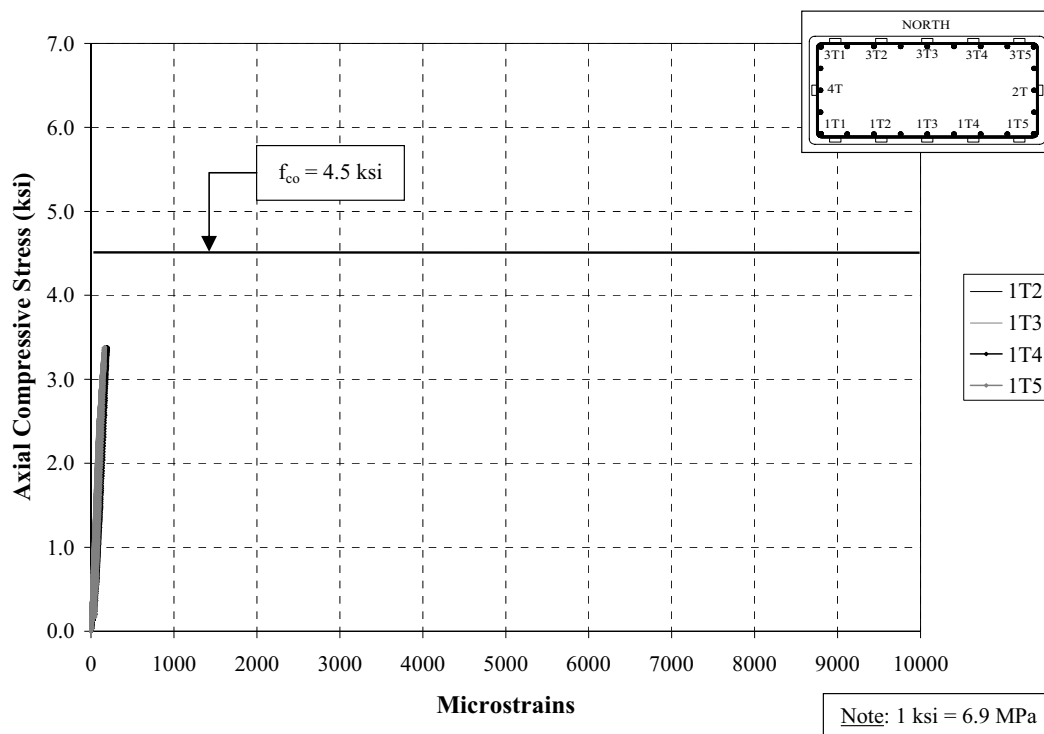**Figure D150. Axial Stress vs. Transverse Strain on Tie (North); Specimen G2**



**Figure D151. Axial Stress vs. Transverse Strain on Tie (South); Specimen G2**

**Figure D152.  Axial Stress vs. Transverse Strain on Tie (West); Specimen G2**



**Figure D153.  Axial Stress vs. Transverse Strain on Tie (East); Specimen G2**
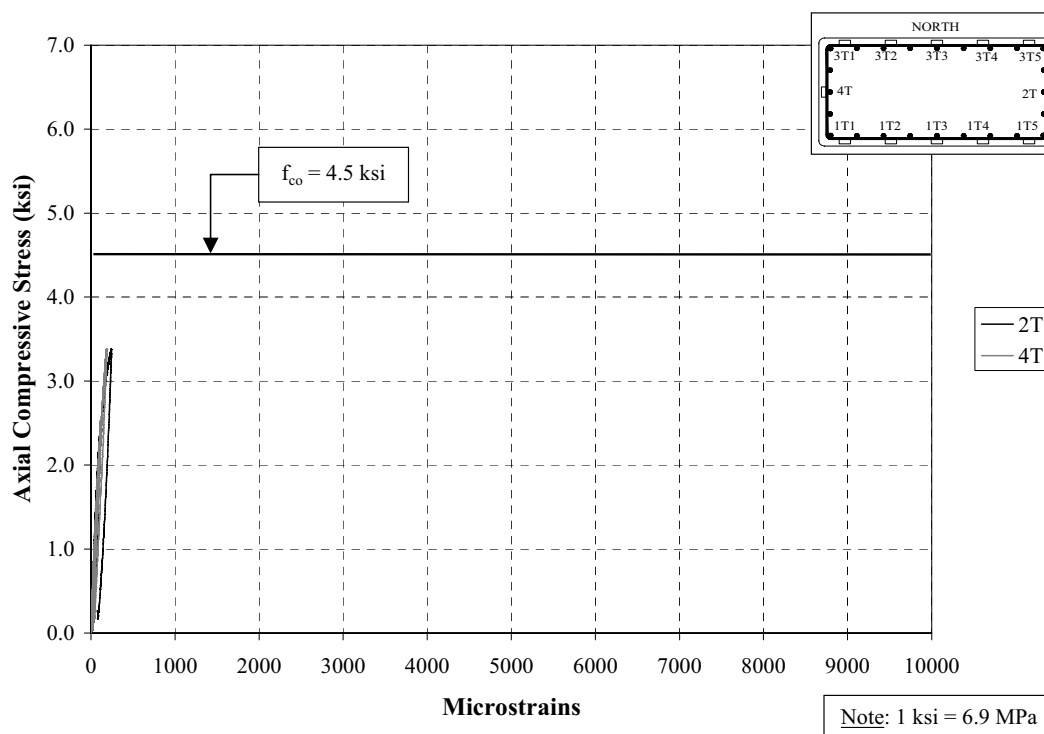
**Figure D154.  Axial Stress vs. Transverse Strain on FRP at 48 in from Bottom (North); Specimen G2**



**Figure D155.  Axial Stress vs. Transverse Strain on FRP at 48 in from Bottom (South); Specimen G2**

**Figure D156. Axial Stress vs. Transverse Strain on FRP at 48 in from Bottom (East); Specimen G2**



**Figure D157. Axial Stress vs. Transverse Strain on FRP at 48 in from Bottom (West); Specimen G2**

**Figure D158.  Axial Stress vs. Transverse Strain on FRP at Mid-height (North); Specimen G2**



**Figure D159.  Axial Stress vs. Transverse Strain on FRP at Mid-height (South); Specimen G2**

**Figure D160.  Axial Stress vs. Transverse Strain on FRP at Mid-height (East); Specimen G2**



**Figure D161.  Axial Stress vs. Transverse Strain on FRP at Mid-height (West); Specimen G2**

**Figure D162.  Axial Stress vs. Axial Strain on FRP (Sensors on Vertical Direction); Specimen G2**
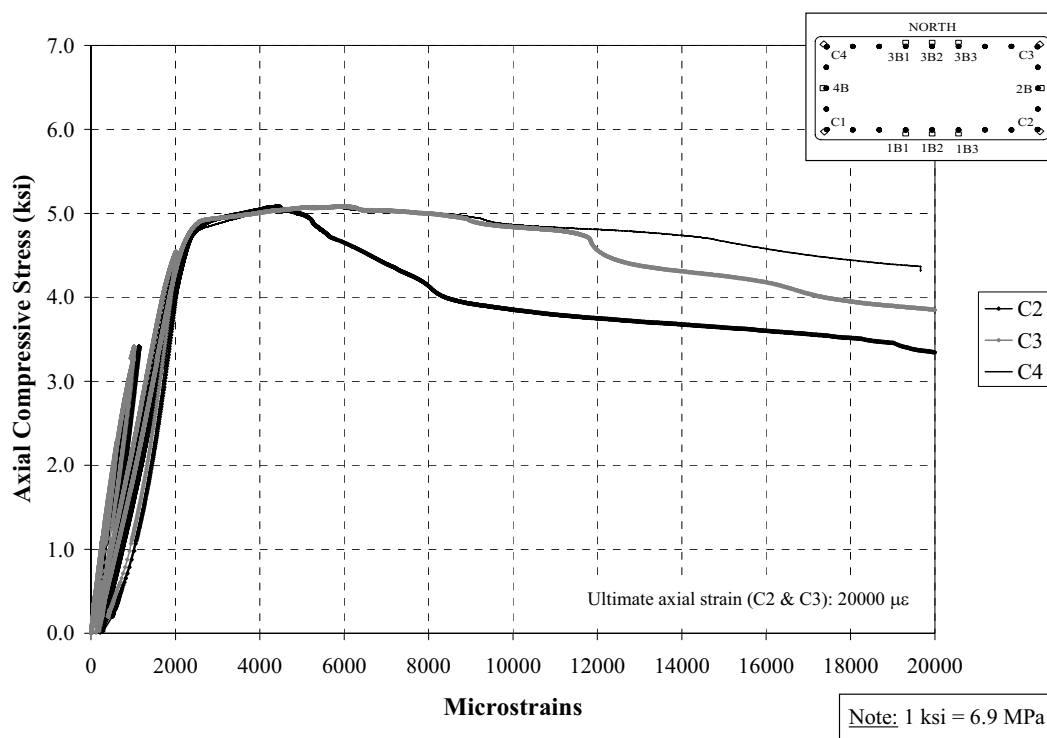
**Figure D163. Axial Stress vs. Axial Strain on Longitudinal Corner Bars C1 & C2; Specimen H1**



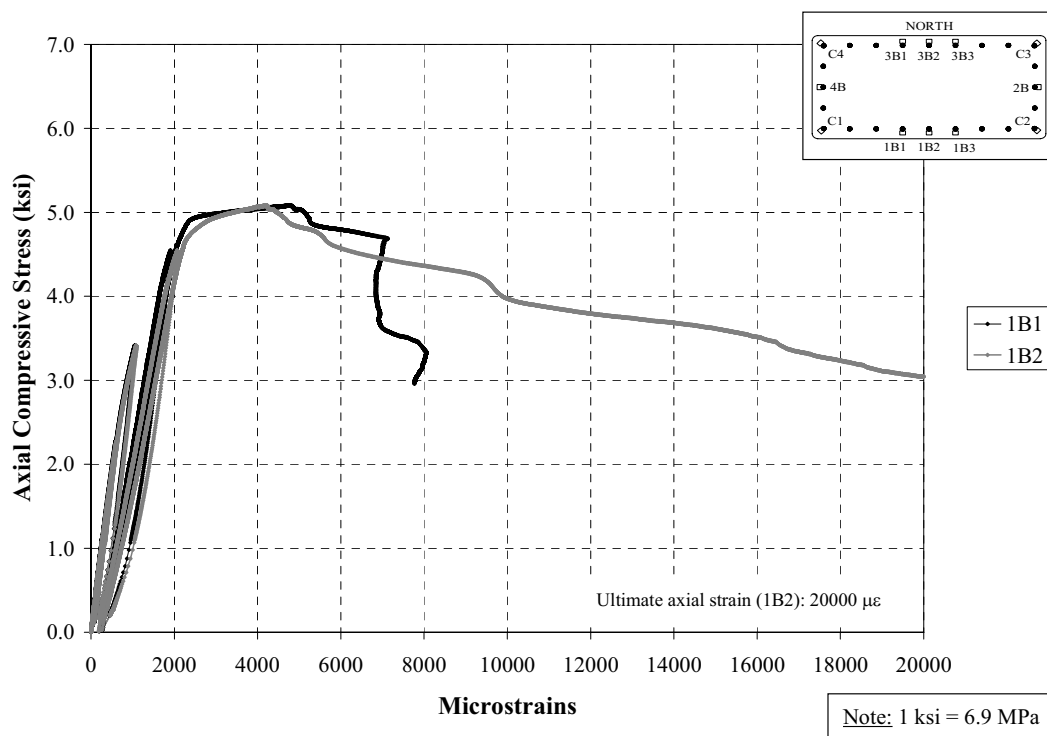**Figure D164. Axial Stress vs. Axial Strain on Longitudinal Corner Bars C3 & C4; Specimen H1**

**Figure D165.  Axial Stress vs. Axial Strain on Longitudinal Central Bar (1B3); Specimen H1**



**Figure D166.  Axial Stress vs. Axial Strain on Longitudinal Central Bars (2B); Specimen H1**
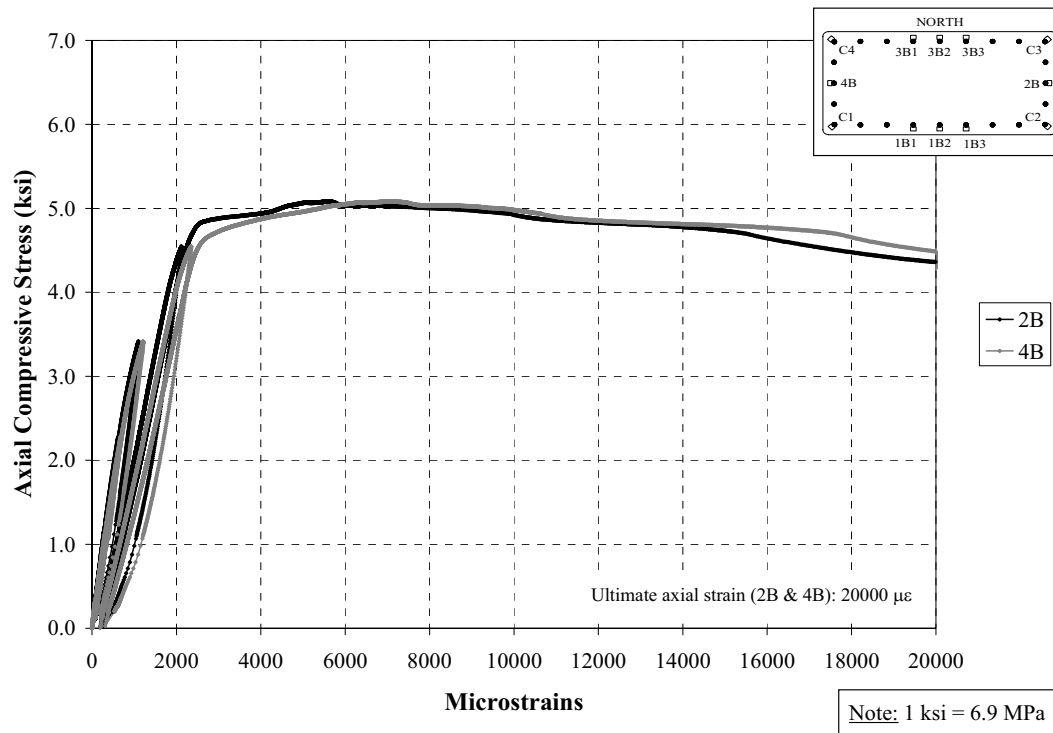
**Figure D167.  Axial Stress vs. Axial Strain on Longitudinal Central Bars (3B1 & 3B3); Specimen H1**
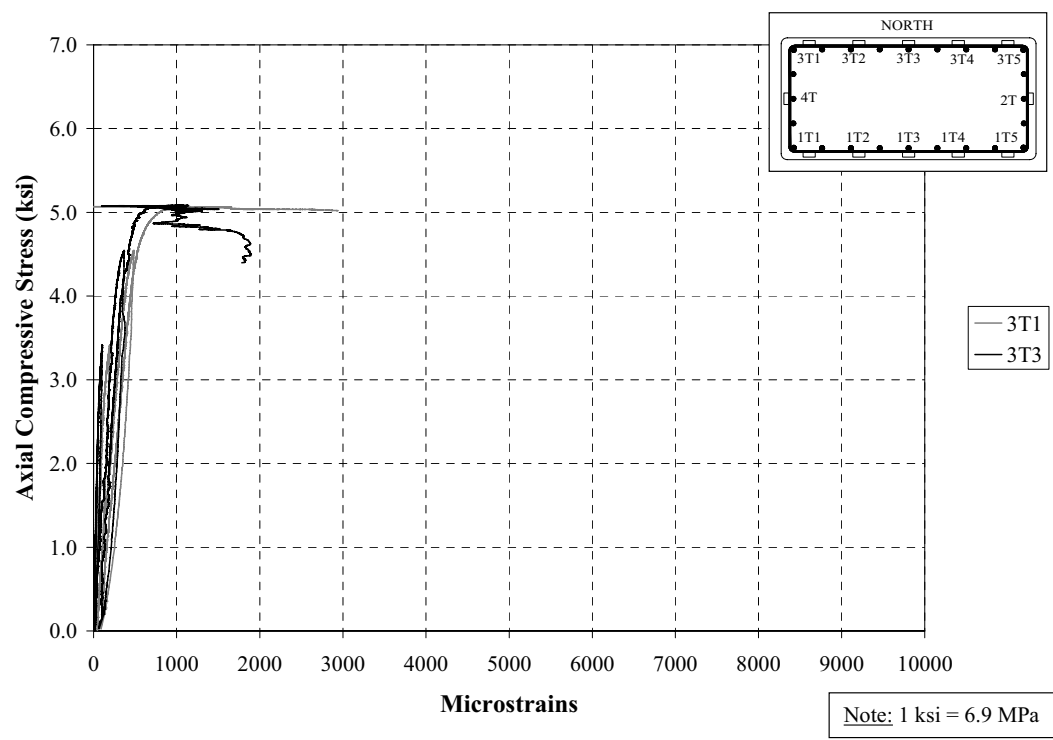


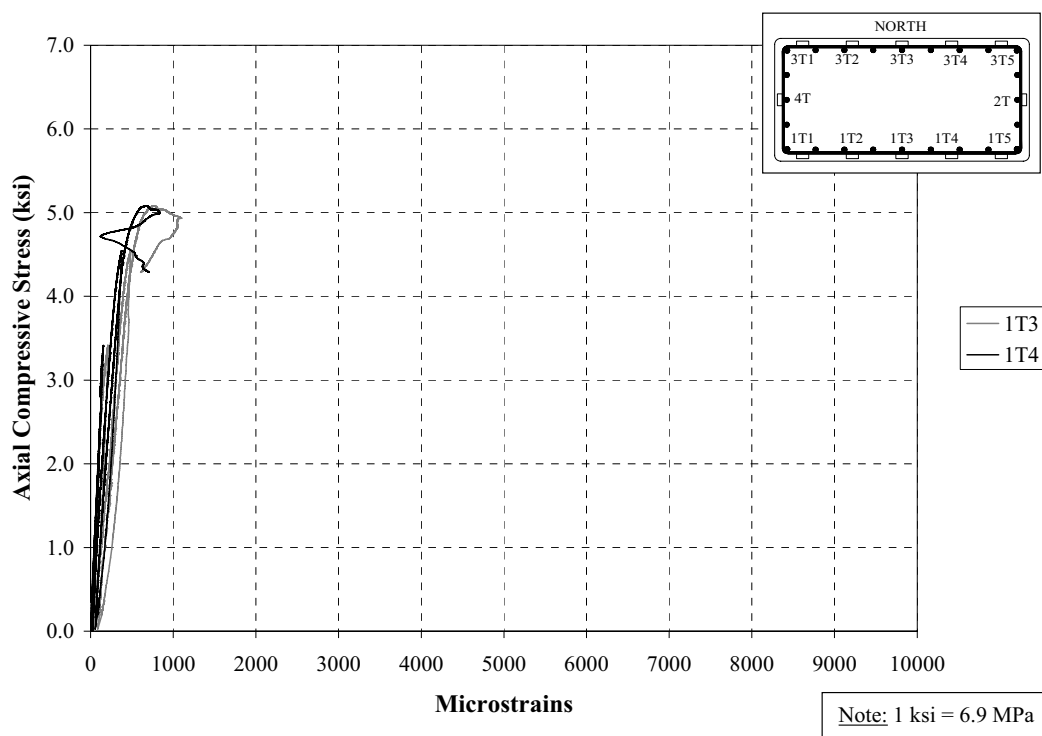**Figure D168.  Axial Stress vs. Transverse Strain on Tie (North); Specimen H1**

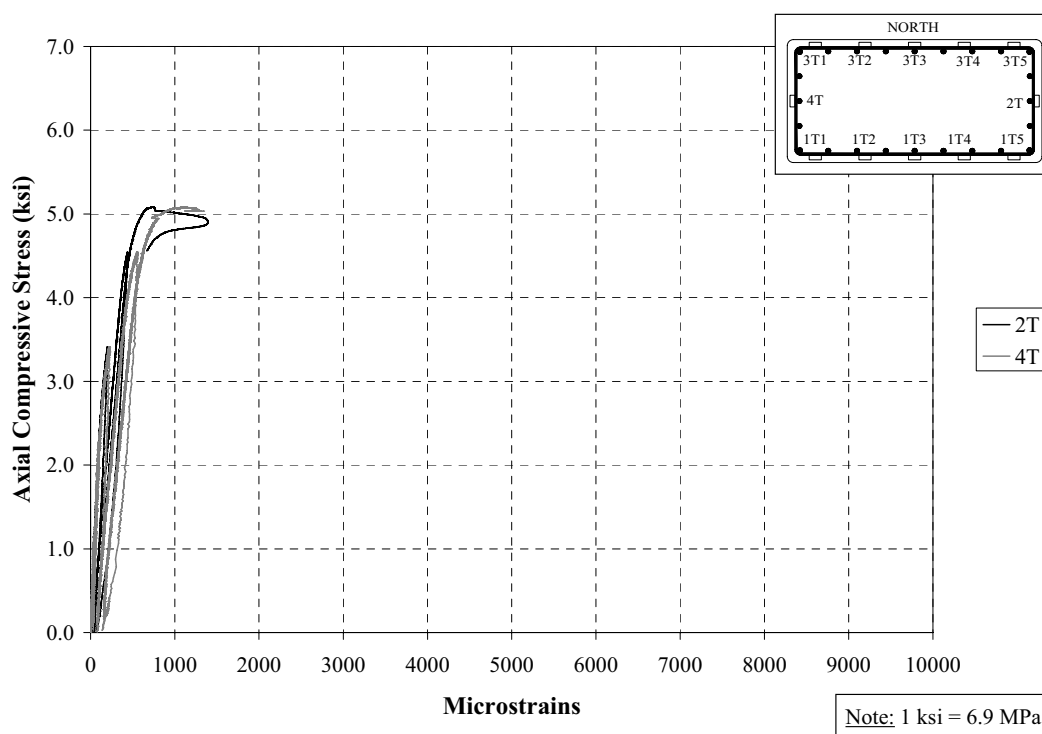**Figure D169.  Axial Stress vs. Transverse Strain on Tie (South); Specimen H1**



**Figure D170.  Axial Stress vs. Transverse Strain on Tie (East & West); Specimen G1**
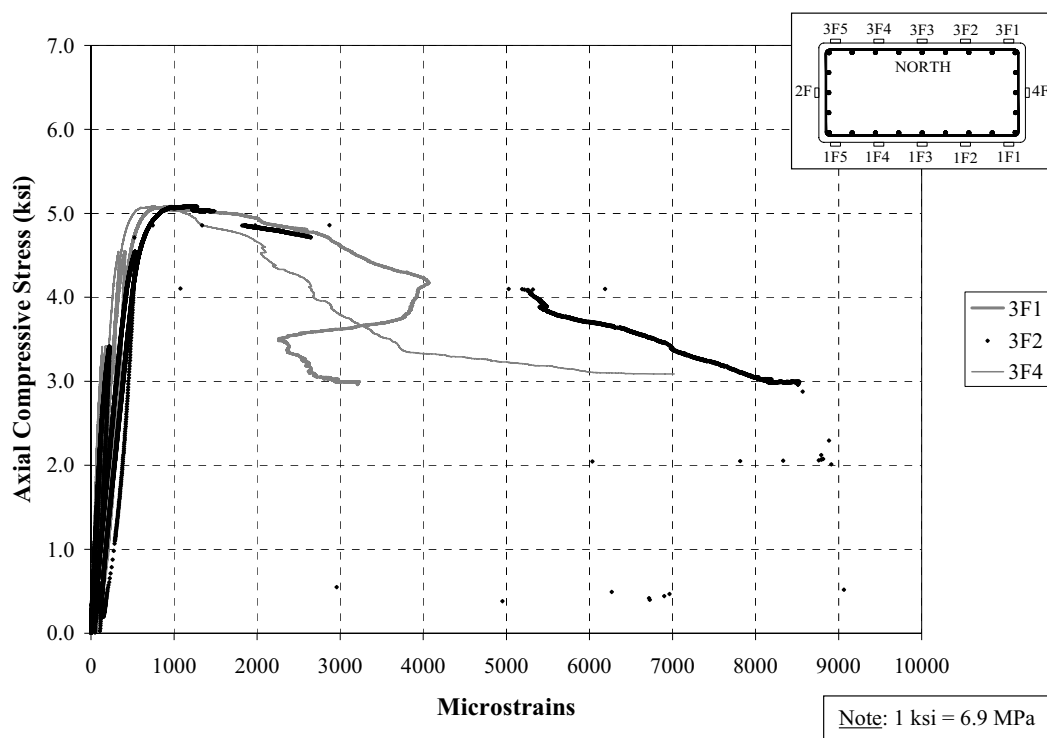
**Figure D171.  Axial Stress vs. Axial Strain on Longitudinal Corner Bars; Specimen H2**



**Figure D172.  Axial Stress vs. Axial Strain on Longitudinal Central Bars (1B2 & 1B2);
Specimen H2**

**Figure D173. Axial Stress vs. Axial Strain on Longitudinal Central Bars (2B & 4B); Specimen H2**



**Figure D174. Axial Stress vs. Transverse Strain on Tie (North); Specimen H2**

**Figure D175.  Axial Stress vs. Transverse Strain on Tie (South); Specimen H2**



**Figure D176.  Axial Stress vs. Transverse Strain on Tie (East & West); Specimen H2**

**Figure D177.  Axial Stress vs. Transverse Strain on FRP at 62 in from Bottom (North); Specimen H2**
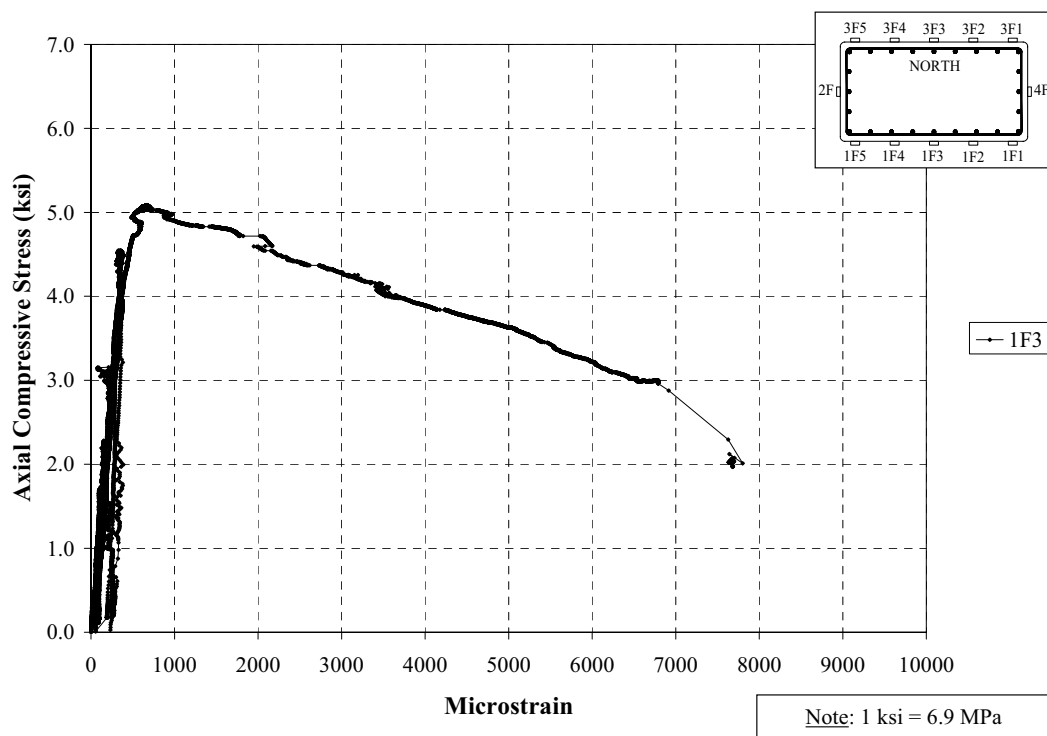


**Figure D178.  Axial Stress vs. Transverse Strain on FRP at 62 in from Bottom (South); Specimen H2**
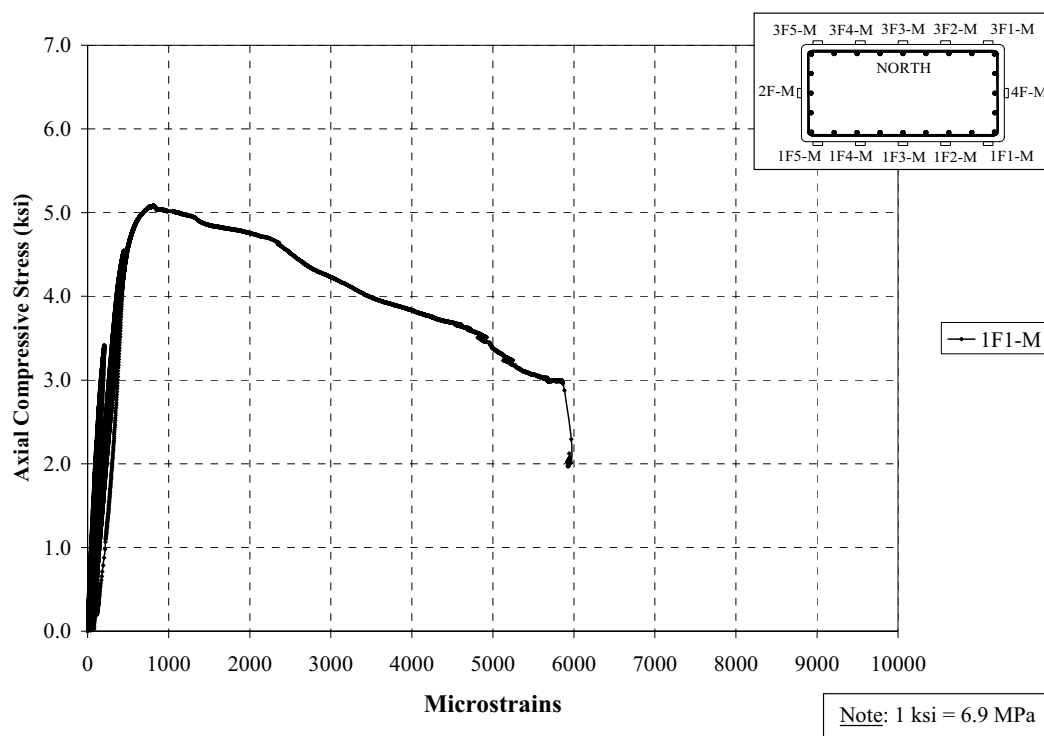
**Figure D179.  Axial Stress vs. Transverse Strain on FRP at Mid-height (South); Specimen H2**
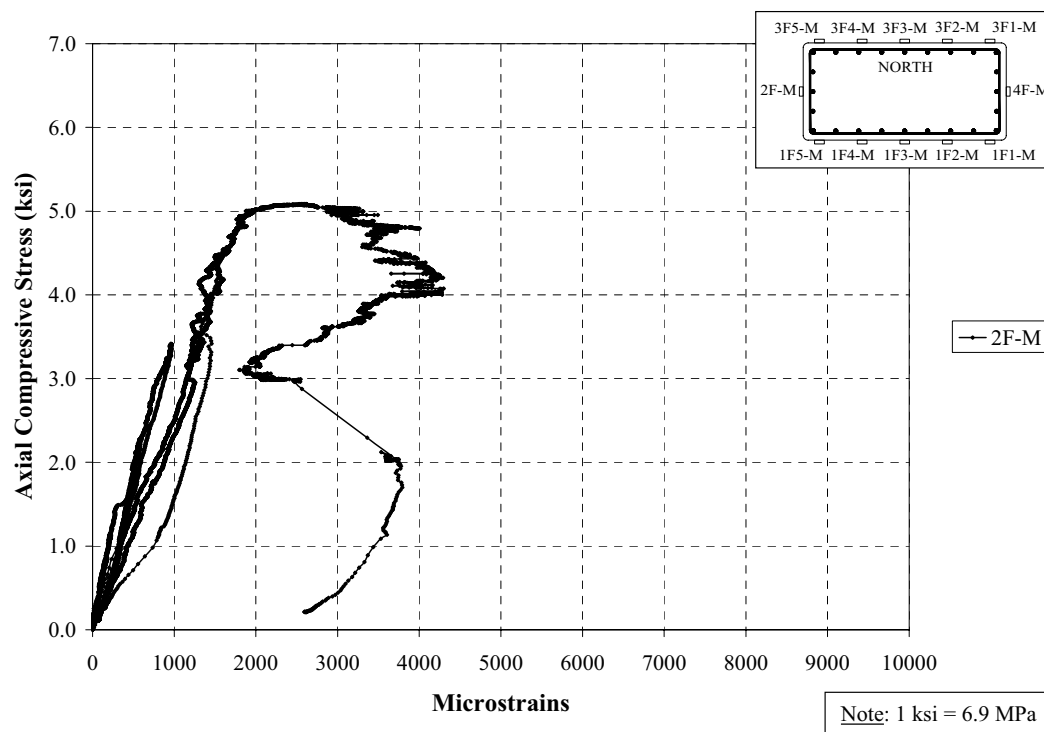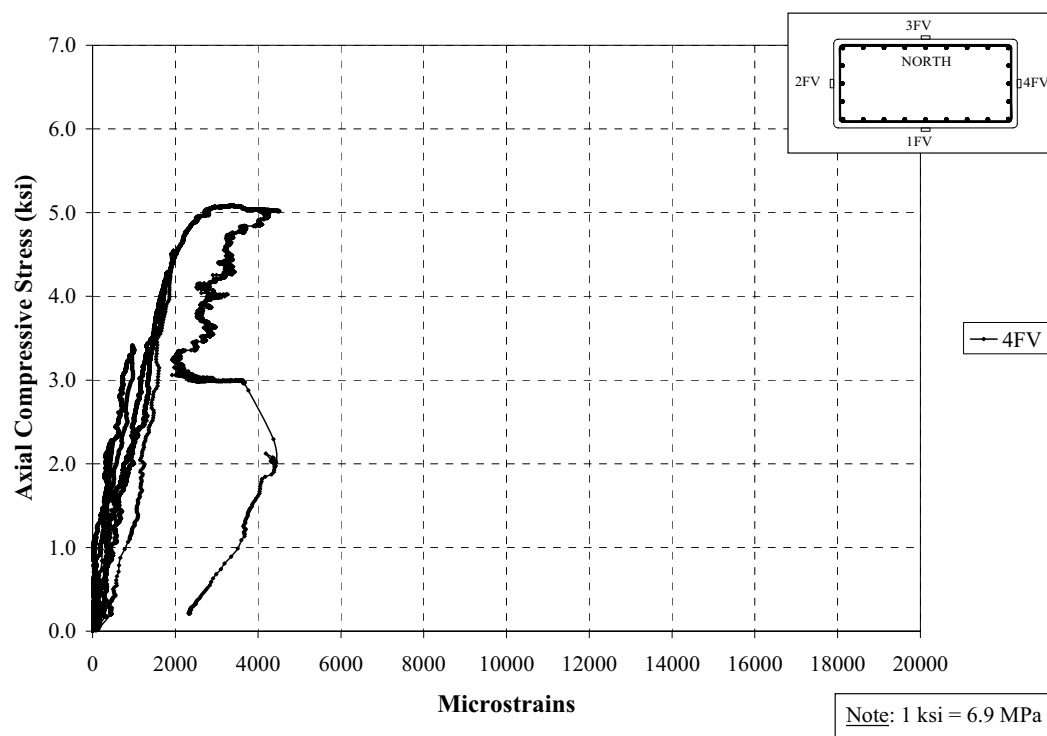


**Figure D180.  Axial Stress vs. Transverse Strain on FRP at Mid-height (West); Specimen H2**

**Figure D181.  Axial Stress vs. Axial Strain on FRP (Sensors on Vertical Direction); Specimen H2**

**APPENDIX E**

**DVD UNIT – VIDEOS OF FAILURE OF SPECIMENS**